UNIVERSITY OF CALIFORNIA SAN DIEGO

SAN DIEGO STATE UNIVERSITY

Atropisomerism as Inspiration Towards the Development of New Chemical Methodologies

A dissertation submitted in partial satisfaction of the
requirements for the degree Doctor of Philosophy

in

Chemistry

by

Sean Michael Maddox

Committee in charge:

University of California, San Diego

Professor John Crowell
Professor Bradley Moore
Professor Emmanuel Theodorakis

San Diego State University

Professor Jeffrey L. Gustafson, Chair
Professor Douglas Grotjahn

2018

The dissertation of Sean Michael Maddox is approved, and it is acceptable in quality and for publication on microfilm and electronically:

_____

_____

_____

_____

_____

Chair

University of California, San Diego

San Diego State University

2018

Dedication

To my family and friends

Table of Contents

List of Figures

List of Tables

List of Schemes

Acknowledgements

I have leaned on several impactful people in my life over the last 5 years, and I owe my appreciation to all of them. I was very lucky to join the Gustafson Lab at San Diego State University (SDSU) for several reasons. First, for SDSU Chemistry and Biochemistry, the drawbridges to every chemistry group in this department were always opened for me. Fellow graduate students in my neighboring groups were always sincere and willing to help me out, and I was met with no less from all professors that I interacted with. For this, I can't thank my colleagues across the halls enough. To Josh F Swider, Braden Silva, and Brian Maniaci; you were the closest friends I could ask for in grad school. We went through a lot together, and I want to thank you for letting me be part of the crew. Furthermore, the groups of students that gravitated to the Gustafson Lab were all very upbeat and hardworking. This provided a work atmosphere that really motivated me and made it easy to come into lab early and stay in lab late. To the first wave of graduate students; Chris Nalbandian, Danae Madrid, Davis Smith, and Mari Gabra, I couldn't have asked for a better group to start a research lab with. To the second wave of graduate students; Dinner, Ninja, Noorby, and Sparkles, we really became a tight-knit group of friends and thank you for the dank memes. Oh, and don't forget Therapy Thursdays. To the final graduate student who joined as I was wrapping up my Ph.D.; Zach Brown, I'm glad you joined the group and had fun with us, good luck man.

The Ph.D. program at San Diego State University offers a unique experience as there is a large population of research-hungry undergraduate students, many of whom I had the pleasure of meeting, training, and building personal relationships with. To Eric Miller, Therapy Thursdays…. and I guess you're O.K. at fantasy football... To Nick Rochester, thank you for being such a consistent and reliable person, both in the lab and out. You have all around made my life much

easier; third time's a charm my man. To Greg Dawson, I had a blast working with you over the last couple of years. Thank you for all your hard work, and have fun at NYU! I would say good luck, but you shouldn't need it.

Finally, I wouldn't be here without the guidance of Professor Jeffrey L. Gustafson. Your energy and teaching style shaped me as a doctoral candidate, and your drive will forever be inspiring. It was an honor to be one the first graduate students to join your lab, and I'm excited to watch the dynasty grow.

I also had a reliable support group outside of SDSU. To my family, thank you all so much for supporting me during this time, I don't thank you nearly enough. I could not have made it thru this program without your generosity. Our times in the spa with dad will never get old… or will they. Grandma, you were such an inspiration throughout as you stay strong and keep your head up in the darkest of times. To the UC Davis crew, you have no idea how much I looked forward to my semi-annual week-long stays with you all. That was always some much-needed R&R. Chris Wilson, my brother, you are one of the most important people in my life, and you will never understand how much the support from you and your family always means to me. To Tito Mar and Tita Carol, I am very grateful to you for accepting me into the family, and I can't wait to create more wonderful memories.

To Arianna… As I read, edit, re-read, and re-edit these acknowledgements up until this point, it becomes blatantly obvious to me how important you have been throughout my graduate career; you have been there nearly every step of the way. Thank you for walking this path with me, and I eagerly look forward to our future together.

The contents in Chapter 2 are a reformatted reprint of the following manuscript, with permission from the American Chemical Society: Maddox, S. M.; Nalbandian, C. J.; Smith, D. E.;

Gustafson, J. L. "A Practical Lewis Base Catalyzed Electrophilic Chlorination of Arenes and Heterocycles." *Org. Lett.* **2015**, *17*, 1042. The dissertation author was the primary researcher for the data presented. Support of this work by San Diego State University is acknowledged.

The contents in Chapter 3 are in part a reformatted reprint of the following manuscript, with permission from the American Chemical Society: Maddox, S. M.; Dinh, A. N.; Armenta, F.; Um, J.; Gustafson, J. L. "The Catalyst-Controlled Regiodivergent Chlorination of Phenols." *Org. Lett.* **2016**, *18*, 5476. The dissertation author was the primary researcher for the data presented. Support of this work by San Diego State University is acknowledged.

Chapter 3 in part contains material that may be used in a future publication. The following are coauthors on the corresponding project: Maddox, S. M.; Dinh, A. N.; Janke, L.; Addison, J. B.; Cooksy, A. L.; Gustafson, J. L. "Experimental and Computational Probes into the Principles Driving Selectivity in the Catalyst-Controlled Regiodivergent Chlorination of Phenols." The dissertation author was the primary researcher for the data presented. Support of this work by the National Science Foundation is acknowledged (CHE-1664565).

The contents in Chapter 4 are a reformatted reprint of the following manuscript, with permission from the American Chemical Society: Maddox, S. M.; Dawson, G. A.; Rochester, N. C.; Ayonon, A. B.; Moore, C. E.; Rheingold, A. L.; Gustafson, J. L. "Atroposelective Dynamic Kinetic Resolution of Aryl-Naphthoquinones via the Addition of Thiophenols" *ACS Catal.* **2018**, *8*, 5443. The dissertation author was the primary researcher for the data presented. Support of this work by the National Institute of General Medical Sciences is acknowledged (R35GM124637).

Vita

2008-2011 Associate of Science, Biology and Natural Sciences, Sierra Community College

2011-2013 Bachelor of Science, Chemistry, University of California Davis

2013-2017 Teaching Assistant, San Diego State University

2017-2018 Graduate Researcher, San Diego State University

2013-2018 Doctor of Philosophy, Chemistry, University of California San Diego and San Diego State University

Publications

1. Dinh, A. N.; Noorbehesht, R. N.; Toenjes, S. T.; Jackson, A. C.; Saputra, M. A.; Maddox, S. M.; Gustafson, J. L. "Towards a Catalytic Atroposelective Synthesis of Diaryl Ethers via C(sp^2)-H Alkylation Using Nitroalkanes" *SYNLETT* **2018**, *submitted*

2. Maddox, S. M.; Dawson, G. A.; Rochester, N. C.; Ayonon, A. B.; Moore, C. E.; Rheingold, A. L.; Gustafson, J. L. "Enantioselective Synthesis of Biaryl Atropisomers via the Addition of Thiophenols into Aryl-Naphthoquinones" *ACS Catal.* **2018**, *8*, 5443

3. Maddox, S. M.; Dinh, A. N.; Armenta F.; Um, J.; Gustafson, J. L. "The Catalyst-Controlled Regiodivergent Chlorination of Phenols" *Org. Lett.* **2016**, *18*, 5476

4. Maddox, S. M.; Hecht, D.; Gustafson, J. L. "Enhancing the selectivity of kinase inhibitors in oncology: a chemical biology perspective" *Future Med. Chem.* **2016**, *8*, 241

5. Luca, O. R.; Gustafson, J. L.; Maddox, S. M.; Fenwick, A. Q.; Smith, D. C. "Catalysis by electrons and holes: formal potential scales and preparative organic electrochemistry" *Org. Chem. Front.*, **2015**, *2*, 823

6. Maddox, S. M.; Nalbandian, C. J.; Smith, D. E.; Gustafson, J. L. "A Practical Lewis Base Catalyzed Electrophilic Chlorination of Arenes and Heterocycles" *Org. Lett.* **2015**, *17*, 1042

Manuscripts in Preparation

1. Maddox, S. M.; Dinh, A. N.; Janke, L.; Cooksy, A. L.; Gustafson, J. L. "Experimental and Computational Probes into the Principles Driving Selectivity in the Catalyst-Controlled Regiodivergent Chlorination of Phenols"

2. Maddox, S. M.; Dawson, G. A.; Gustafson, J. L. "A Mild and Atroposelective Total Synthesis of Dialkylbiaryl Phosphine Ligands for use in Enantioselective Palladium-Catalyzed Coupling Reactions"

Presentations (*Presented by author in bold*):

1. "Atroposelective Dynamic Kinetic Resolution of Aryl-Naphthoquinone Atropisomers via the Addition of Thiophenols: A Proof of Concept Towards the General Synthesis of Diverse Classes of Atropisomers" **S. M. Maddox**, J. L. Gustafson, poster presentation at

the Gordon Research Conference: Stereochemistry, Newport, RI, July 2018

2. "Development of a Nucleophilic Dynamic Kinetic Resolution of Aryl-Naphthoquinone Atropisomers" **S. M. Maddox**, J. L. Gustafson, oral presentation at the 255th National Meeting of the American Chemical Society, New Orleans, LA, March, 2018, abstract #: ORGN 238

3. "Atroposelective Dynamic Kinetic Resolution of Aryl-Naphthoquinones" **S. M. Maddox**, oral presentation at SDSU Student Research Symposium, San Diego State University, March 2018, abstract #: 393

4. "The Catalyst-Controlled Regiodivergent Chlorination of Phenols Towards Drug Discovery Efforts" **S. M. Maddox**, A. N. Dinh, J. L. Gustafson, poster presentation at the 30th Annual CSU Biotechnology Symposium, Santa Clara, CA, January 2018

5. "The Catalyst-Controlled Chlorination of Arenes and Heterocycles" **S. M. Maddox**, A. N. Dinh, J. L. Gustafson, poster presentation at the Gordon Research Conference: Organic Reactions and Processes, Easton, MA, July 2017

6. "A Nucleophilic Dynamic Kinetic Resolution of Aryl-Naphthoquinone Atropisomers" **S. M. Maddox**, G. A. Dawson, J. L. Gustafson, poster presentation at the 45th National Organic Chemistry Symposium (ACS), Davis, CA, June 2017

7. "Nucleophilic Dynamic Kinetic Resolution of Atropisomeric Naphthoquinones Towards the Synthesis of Unique Chiral Scaffolds" **S. M. Maddox**, J. L. Gustafson, oral presentation at SDSU Student Research Symposium, San Diego State University, March 2017

8. "Atroposelective Synthesis of Common Structural Motifs in Medicinal Chemistry" **S. M. Maddox**, A. B. Ayonon, J. L. Gustafson, poster presentation at the 29th Annual CSU Biotechnology Symposium, Santa Clara, CA, January 2017

9. "Dynamic Kinetic Resolution of Atropisomeric Biaryls and Diaryl Ethers via Chiral Cation-Directed Catalysis" **S. M. Maddox**, A. N. Dinh, J. L. Gustafson, poster presentation at the Gordon Research Conference: Stereochemistry, Newport, RI, 2016

10. "Lewis-Base Catalyzed Regioselective Chlorination of Activated Aromatic Small Molecules" **S. M. Maddox**, J. L. Gustafson, oral presentation at the 30th Annual CSU Student Research Competition, Bakersfield, CA, April 2016

11. "Lewis-base Catalyzed Regioselective Chlorination of Activated Aromatic Compounds" **S. M. Maddox**, J. L. Gustafson, poster presentation at the 75th San Diego ACS Anniversary Symposium, San Diego, CA, April 2016

12. "Lewis-base Catalyzed Regioselective Chlorination of Activated Aromatic Compounds" **S. M. Maddox**, J. L. Gustafson, poster presentation at the 251st National Meeting and

Exposition of the American Chemical Society, March 2016, abstract #: ORGN-718

13. "Lewis-Base Catalyzed Regioselective Chlorination of Activated Aromatic Small Molecules" **S. M. Maddox**, J. L. Gustafson, oral presentation at SDSU Student Research Symposium, San Diego, CA, March 2016

14. "Atropisomer Selective Synthesis of Pyrrolopyrimidine Scaffolds to Increase Seectivity in Kinase Inhibition" **S. M. Maddox**, J. L. Gustafson, poster presentation at the 28th Annual CSU Biotechnology Symposium, Anaheim, CA, January 2016

15. "Bcl-2 inhibitor analogs that are preorganized along an axis of chirality; the effect of atropisomerism on protein binding" **M. Gabra**, **S. M. Maddox**, J. L. Gustafson, poster presentation at the 26th Annual CSU biotechnology Symposium, Santa Clara, CA, January 2014

Honors and Awards

Achievement Rewards for College Scientists (ARCS) Foundation Award (2015-2018)

Harry E. Hamber Memorial Scholarship (2017)

SDSU Student Research Symposium – President's Award (2016)

Major Field of Study

Major Field: Chemistry (Organic)

Development of Regio- and Enantioselective Organocatalytic Chemical Methodology

Professor Jeffrey L. Gustafson

Abstract of the Dissertation

Atropisomerism as Inspiration Towards the Development of New Chemical Methodologies

by

Sean Michael Maddox

Doctor of Philosophy in Chemistry

University of California San Diego, 2018

San Diego State University, 2018

Professor Jeffrey L. Gustafson, Chair

Atropisomerism represents a form of chirality that is often swept under the rug in medicinal chemistry and drug development. Nonetheless, our lab has demonstrated that atropisomerism can in fact be exploited to increase the target selectivity of kinase inhibitors, with subsequent perspectives and reports leveraging our findings as a "call to arms" to invoke atropisomerism as a design element in drug discovery efforts. As atroposelective methodology remains a relatively underdeveloped niche in chemistry, we focused our efforts to develop new chemical methodology to move the field of atropisomer synthesis forward. Rigidifying the atropisomeric axis of known kinase inhibitor scaffolds remained a challenging task until we developed a Lewis base catalyzed

chlorination of arenes and heterocycles, which is discussed in Chapter 2. We then extended this mode of catalysis towards a regiodivergent chlorination of phenols presented in Chapter 3. The ability to control the site of electrophilic aromatic chlorination by choice of catalyst has been utilized in the synthesis of several natural products and drug-like molecules. Lastly, Chapter 4 discloses a proof of concept towards a first-in-class enantioselective synthesis of diverse atropisomeric scaffolds with the potential for unparalleled access to several different functional groups proximal to the atropisomeric axis. We expect these developed methodologies to make an impact beyond our own research program, hopefully with implications in drug discovery efforts.

Chapter 1: Introduction

1.1 The Impact of Chirality on the Treatment of Disease

In 1957, racemic thalidomide was introduced to the world as a prescription sedative that was commonly used to treat morning sickness in pregnant women. Shortly thereafter, in 1961, thalidomide was removed from the market due to unforeseen teratogenic effects of the drug. These teratogenic effects caused thousands of children to be born with major deformities of their extremities. Luckily, thalidomide was never approved by the United States Food and Drug Association, thus only a handful of children with thalidomide-induced malformations were born in the United States.[1] Nonetheless, in response to the thalidomide tragedy, the Kefauver-Harris Drug Amendments were passed, ensuring that drug manufacturers had to not only prove that a drug was safe, but also effective. This includes evaluating the pharmacokinetics and pharmacological activities of each enantiomer *in vivo*.[2]

Aside from the influence thalidomide had on drug regulations in the United States, its pharmacokinetic profile[3] has had a profound lasting impact on how modern pharmaceutical companies approach chirality during preclinical drug development. Even though thalidomide was prescribed as a racemic mixture of two enantiomers, the pharmacological activities of each enantiomer wasn't fully understood when it first reached the market. It wasn't realized until much later that only the (*R*)-enantiomer of thalidomide was responsible for its sedative effects, while the (*S*)-enantiomer contributed to the observed teratogenic side effects.[4] Moreover, it was shown that even if thalidomide was administered as a pure enantiomer (e.g. (*R*)-thalidomide), the enantiopure drug quickly racemized *in-vivo* (racemization $t_{1/2}$ = 2-6 hours; elimination $t_{1/2}$ = 3-8 hours),[5,6]

precluding its use as a safe and effective anti-nausea drug. Nowadays, the safety and effectiveness of each enantiomer of every chiral drug must be examined and fully understood before being considered for approval by the FDA for the drug to enter the market. However, it could be argued that one form of chirality, *atropisomerism*, has effectively evaded this regulation thus far.

1.2 Atropisomerism

The concept of chirality is generally introduced in undergraduate level organic chemistry via point chirality. With point chirality, a molecule is considered chiral if it contains a stereogenic center (often a carbon atom) which has four different substitutions, resulting in a molecule that is not superimposable with its mirror image (Figure 1.2.1A). However, chirality can exist beyond point chirality (*i.e.* inherent chirality, axial chirality, and planar chirality; Figure 1.2.1B-D), yet such modes of chirality aren't commonly introduced in an academic setting until the graduate level.

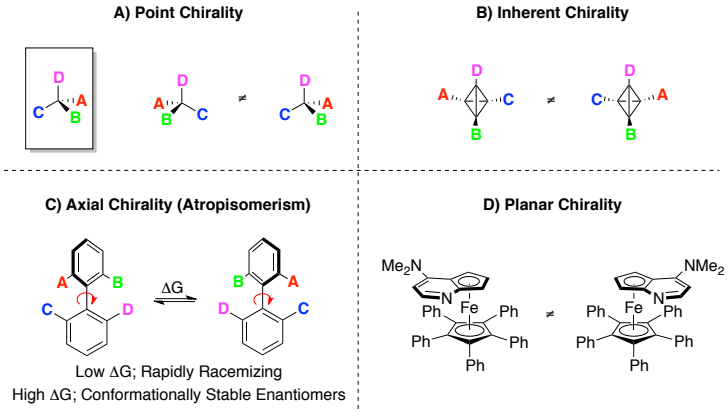

Figure 1.2.1. The Various Forms of Chirality in Chemistry

Atropisomerism is an example of planar chirality that specifically arises from the hindered rotation about a non-symmetrical axis, typically a bond between two sp^2-hybridized atoms (Figure 1.2.1C). Like point chiral molecules, enantiomers of atropisomers are mirror images of each other which are non-superimposable. However, while point chiral molecules can only racemize via

breaking and forming chemical bonds (chemical control), atropisomers can racemize simply via rotation of the atropisomeric sigma bond (thermal control). If the substituents proximal to the atropisomeric axis are small, the bond can freely rotate at mild temperatures. However, as you increase the size of the substituents proximal to the atropisomeric axis, rotation about that bond can slow down enough to eliminate interconversion, resulting in two separable rotational isomers, or enantiomers.

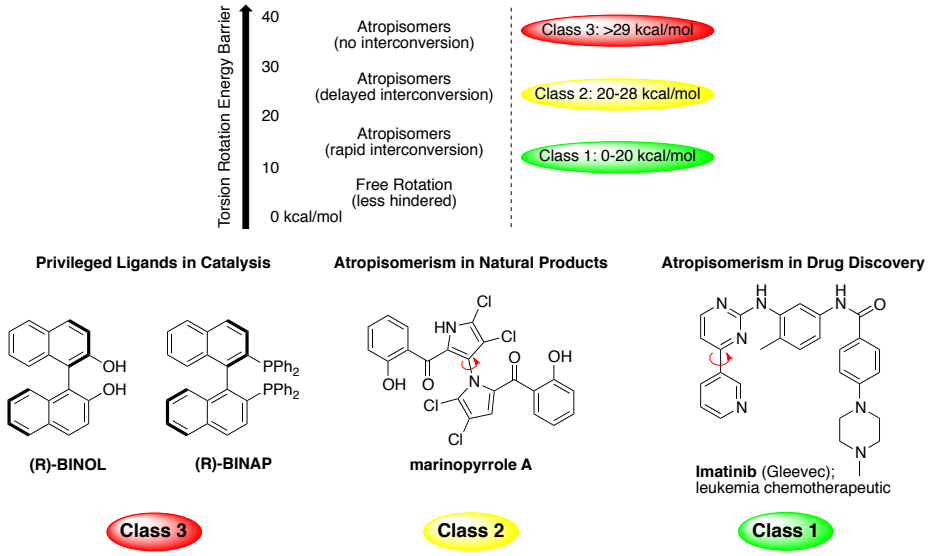

Figure 1.2.2. Classifying Atropisomers by Stereochemical Stability

Atropisomers can be classified into one of three groups. Class 3 atropisomers exhibit a barrier to rotation of over 29 kcal/mol, which corresponds to a half-life to racemization of about a year at physiological temperatures. However, many Class 3 atropisomers are known to be stereochemically stable for millions of years at room temperature. Such high stereochemical stability is exemplified by the ligands BINOL and BINAP (Figure 1.2.2), which also represent two of the most used chiral scaffolds in enantioselective catalysis.[7] Class 2 atropisomers represent those with barriers to rotation ranging from 20-29 kcal/mol. The enantiomers in this class can be separated and characterized, however they will racemize within a relatively short period of time at

mild temperatures. Marinopyrrole A[8] is a well-studied example of a Class 2 atropisomer (Figure 1.2.2), albeit at the more stable end of Class 2 atropisomers. Atropisomers with barriers to rotation of <20 kcal/mol are considered to be Class 1 atropisomers.[9] Several FDA approved small molecule drugs belong to this class of atropisomers, and as they rapidly interconvert in solution at room temperature, they are generally treated as achiral molecules.

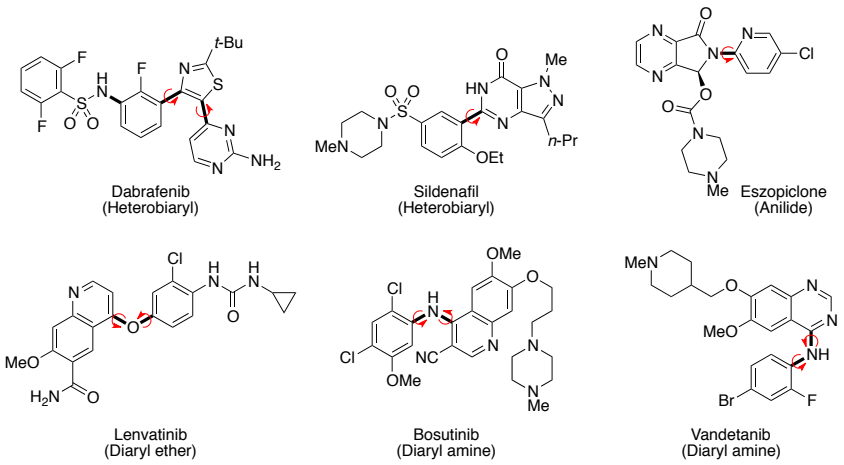

Figure 1.2.3. Drugs Exhibiting Class 1 Atropisomerism

In fact, a recent review from our lab examined every small molecule kinase inhibitor from the United States FDA Drug Bank, finding that since 2011, 30% of all drugs have one or more interconverting axes of chirality, and some classes of drugs (*i.e.* kinase inhibitors) are almost entirely comprised of Class 1 atropisomers (Figure 1.2.3).[10] This is perhaps due to the finding that several of the most utilized reactions in medicinal chemistry have the potential to give rise to an atropisomeric axis.[11] In fact, four of the top ten reactions in medicinal chemistry by occurrence can result in forming an atropisomeric axis. These classes of reactions include amide bond formation, nucleophilic aromatic substitution, Suzuki-Miyaura cross coupling, and heterocycle syntheses (bonds potentially formed via these reactions bolded in Figure 1.2.3). However, while such rapidly racemizing atropisomeric drugs are treated as achiral molecules, it has been shown

that the active sites of the corresponding biological targets have an innate preference for one atropisomer over the other.[12]

1.3 The Problem of Selectivity in Kinase Inhibition

Unregulated kinase activity is implicated in many chronic diseases such as cancer, autoimmune disorders, and diabetes.[13] As such, kinases have become common therapeutic targets in the development of new medicines. Most small molecule kinase inhibitors are classified as Type-I inhibitors, meaning they competitively bind to the ATP binding site of the kinase. However, the kinase active site is highly conserved across the human kinome. As a result of this, selectivity is a major unmet challenge in the design of small molecule kinase inhibitors. Non-selective kinase inhibitor drugs often give rise to negative side effects that can lower the quality of life due to off-target activity. This lack of selectivity largely limits the use of kinases as therapeutic targets to life threatening diseases (such as cancer) where the negative side effects are only tolerated in order to extended the patient's life. Lastly, while kinase inhibitor chemical probes on the market are often advertised as "selective inhibitors," this is not necessarily the case. For example, PP1 is sold as a Src inhibitor,[14] however it exhibits significant activity towards several other wild-type kinases.[15] This false sense of selectivity further convolutes experimental design and can ultimately invalidate the conclusions reached by studies which utilize such non-selective chemical probes.

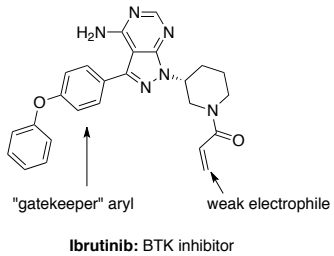

Figure 1.3.1. Ibrutinib Utilizes Both Covalent Targeting and Gatekeeper Selectivity Filters

One strategy to increase the selectivity of a lead kinase inhibitor is to covalently target non-conserved nucleophilic residues (such as cysteine) in or around the active site of the kinase with a *weak electrophile* (Figure 1.3.1).[16] When applicable, this strategy often results in very potent and selective kinase inhibitors,[17] however it relies on the rare occurrence of non-conserved cysteine residues, rendering this approach ineffective for most kinases. Furthermore, it is has been shown that the use of this covalent strategy can lead to drug resistance via a single point mutation of the targeted residue.[18] A second strategy exploits the gatekeeper residue, which consists of a single amino acid within the active site that can either block or allow access to a nearby hydrophobic pocket, depending on the size of the gatekeeper side chain. If the gatekeeper residue of a target kinase is small, a large substituent (such as a *"gatekeeper" aryl*) can be incorporated into the lead inhibitor to increase selectivity by causing steric clash with the large gatekeeper residues of off-target kinases (Figure 1.3.1). However, while this can weed out kinases with large gatekeeper residues,[19] it does little to weed out the other 100+ kinases with a small gatekeeper, so selectivity is arguably still an issue. To address this currently unsolved problem of selectivity in kinase inhibition, a general selectivity filter that can span the entire kinome, rather than just a small fraction of kinases, needs to be developed.

1.4 Atropisomerism as a Selectivity Filter in Kinase Inhibition

For the reasons mentioned in Section 1.1, stable atropisomerism is typically avoided in modern drug discovery efforts.[20] However, as atropisomerism is ubiquitous in kinase inhibitors[10] and as selectivity remains a largely unsolved problem in kinase inhibition, our lab hypothesized that we could leverage a target kinase's atropisomer preference as a general selectivity filter in kinase inhibition. As biology is inherently chiral, we felt this strategy held the potential to be amenable across the entire human kinome, representing a benchmark that had not been met at the time.

Table 1.4.1. Exploiting Atropisomerism to Improve the Target Selectivity of Kinase Inhibitors

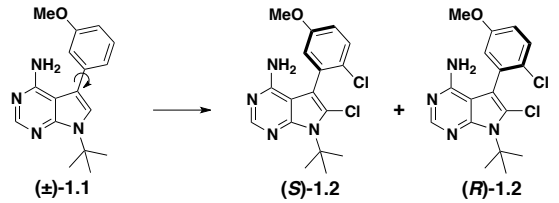

(±)-1.1 (*S*)-1.2 (*R*)-1.2

Kinase	IC_{50} 1.1	IC_{50} (S)-1.2	IC_{50} (R)-1.2
Src	151±9	1193±170	5570±970
EGFR	641±54	>10 000	>10 000
Yes	92±11	727±177	895±90
Ret	128±3	7659±754	1857±482
Abl	245±19	1432±210	>10,000

To test this hypothesis, my colleague Davis Smith synthesized atropisomerically stable analogues of rapidly interconverting and non-selective tyrosine kinase inhibitor **1.1**. The parent inhibitor and its corresponding atropisomer analogues, **(*S*)-1.2** and **(*R*)-1.2**, were tested across a subset of tyrosine kinases to assess their activity towards the panel of kinases. The reported results represented the first example of exploiting atropisomerism as a selectivity filter in kinase inhibition.[15] Not only were **(*S*)-1.2** and **(*R*)-1.2** more selective than the parent inhibitor **1.1**, but

rigidifying the atropisomeric axis effectively decoupled the activity of each rotational conformer (Table 1.4.1). While **(*S*)-1.2** and **(*R*)-1.2** were shown to be about an order of magnitude less potent than the parent compound, you don't necessarily lose potency by rigidifying the atropisomeric axis of a rapidly interconverting drug-like atropisomer. In fact, recent examples in literature have shown that rigidifying the atropisomeric axis of drug-like compounds can indeed improve selectivity without an observable loss in potency (Figure 1.4.1).[21,22] Ongoing work in our lab by Sean Toenjes continues to map the landscape of atropisomerism as a design element to improve the selectivity and potency of small molecule kinase inhibitors towards the development of state-of-the-art chemical probes.

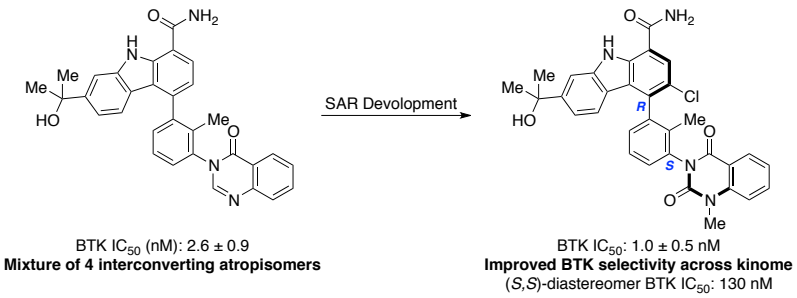

Figure 1.4.1. Atropisomerism as a Selectivity Filter in BTK Selectivity Without Loss in Potency

Synthesis of the reported atropisomerically stable analogues was no trivial task. At the time, there were no known methodologies to directly install functional groups proximal to the rapidly interconverting axis in inhibitor **1.1** in a mild fashion. As a young lab, we were keenly interested in developing new chemical methods to address some of the shortcomings in the regio- and enantioselective syntheses of stereochemically stable atropisomers. As such, with atropisomerism as inspiration, we have since reported on the discovery of new chemical reactions which carry the potential to have a profound impact beyond our own research program, particularly in the design of atropisomeric and pro-atropisomeric bioactive compounds. The following chapters

outline our endeavors towards the development of Lewis base catalytic methodology (Chapter 2) and its application in regiodivergent transformations (Chapter 3). Finally, a proof of concept towards the development of a general enantioselective synthesis of diverse classes of atropisomers with unparalleled functional group diversity proximal to the atropisomeric axis is also discussed (Chapter 4).

Chapter 2: A Practical Lewis Base Catalyzed Chlorination of Arenes and Heterocycles

2.1 Copyright

2.2 Introduction

Towards modern medicinal chemistry efforts, academic and industrial research institutions, alike, are increasingly expending resources for the development of chemical transformations that can directly modify lead bioactive compounds.[23,24] In particular, the direct electrophilic chlorination of arenes and heterocycles represents a powerful transformation in chemical synthesis, as chloride substitution is capable of modulating the electronic and physical properties of molecules and can partake in inter- and intramolecular electrostatic interactions.[25–27]

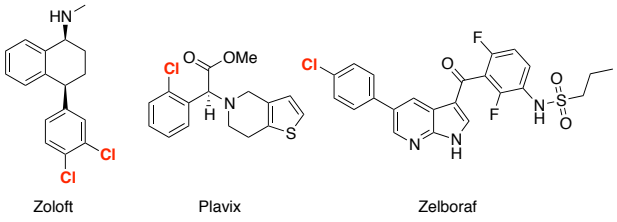

Figure 2.2.1. Blockbuster Drugs that Contain Chlorinated Arenes

Because of these properties, aryl chlorides are ubiquitous throughout drug discovery with numerous chlorinated small molecule pharmaceuticals, including blockbuster drugs Zoloft, Plavix, and Zelboraf (Figure 2.2.1).[28] Moreover, the myriad unique methods to functionalize aryl

chlorides, (i.e. nucleophilic aromatic substitution, modern cross coupling chemistries, metal-halogen exchanges, and more) renders them versatile synthetic intermediates in modern medicinal chemistry.[29]

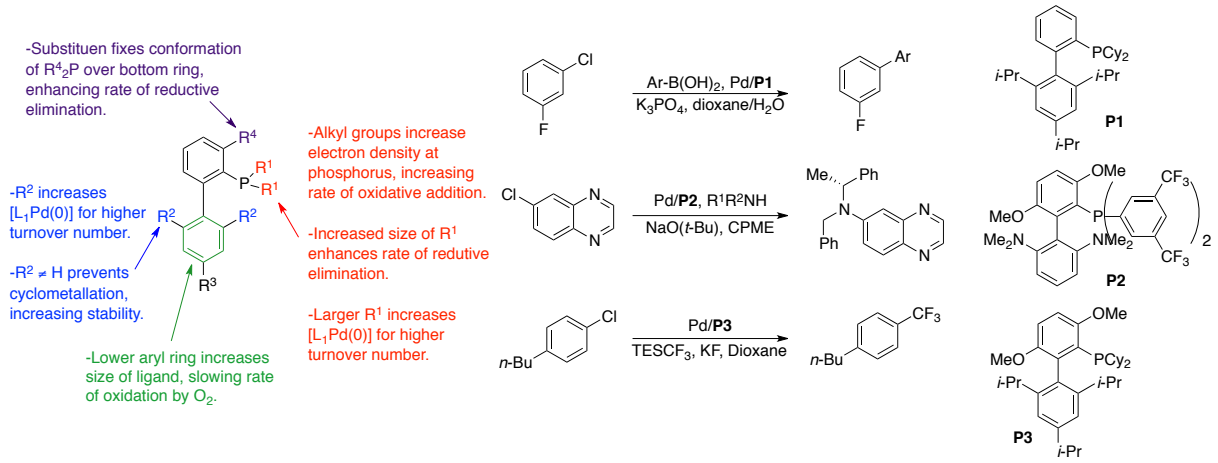

Figure 2.2.2. The Design of Dialkylbiaryl Phosphine Ligands and Exemplary Applications in Aryl Chloride Coupling Reactions.

Of particular importance are the recent developments in the ligand structure of canonical cross coupling reactions which have allowed for mild C-C, C-N, and C-O bond formation from aryl chloride starting materials. Professor Stephen L. Buchwald,[30–32] Professor Gregory C. Fu,[33,34] and Professor Matthias Beller[35] are perhaps two of the most prominent pioneers in modern C-Cl bond functionalization reactions. Buchwald led the way in the design of dialkylbiaryl phosphine ligands, which are utilized in state-of-the-art transformations toward C-C and C-N bond-forming reactions throughout medicinal chemistry settings.[36,37] Dialkylbiaryl phosphines are effective ligands in cross coupling reactions due to their increased electron density at the phosphine center (aids in oxidation addition, which is often regarded as the rate determining step) and the increased steric bulk around the phosphine (aids in reductive elimination), as shown in Figure 2.2.2 (reformatted from an excellent review by Buchwald[31]). These findings represent a major

breakthrough in the field of transition metal catalyzed coupling chemistry and serve as a call to arms to develop mild and site-selective direct chlorinations of arenes and heterocycles.

Classical electrophilic aromatic halogenations often suffer from severe drawbacks. For example, canonical Friedel-Crafts electrophilic aromatic halogenations involve the activation of diatomic halogen by strong Lewis acid catalysts. However, the presence of Lewis basic functionality on the aromatic substrate often limits the effectiveness of Lewis acid catalysts as they tend to form acid-base adducts, largely quenching the catalyst's activity. Alternatively, the *in-situ* oxidation of halide ions to form electrophilic intermediates possesses several practical advantages. However, this traditionally requires stoichiometric amounts of harsh oxidants, which can have deleterious effects on the substrate arene or heterocycle. New methodologies that implement milder oxidants[38,39] hold promise as greener alternatives, yet thus far require elevated temperatures for chlorination on activated arenes. Lewis has recently demonstrated the synthetic utility of the halogenase RebH as an enzymatic catalyst towards the regioselective chlorination of tryptophan.[40] In a follow up publication, it was shown that they can control the site of chlorination via directed evolution.[41] Albeit, the application of this seminal work on larger scales is currently held back due to low enzyme stability.[42]

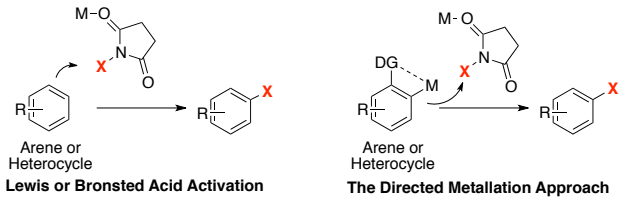

Figure 2.2.3. Previous Catalytic Electrophilic Halogenations Using NXS

Electrophilic aromatic halogenation using preformed halogen source such as *N*-halosuccinimides is one of the most common methods to make aryl halides[43–45] however often suffers from low reactivity, particularly when dealing with less reactive reagents such as *N*-

chlorosuccinimide (NCS). While it is known that Lewis or Brønsted acids are able to activate NXS (Figure 2.2.3), many conditions rely on activated substrates and high temperatures, or super acidic conditions to effect efficient conversions.[46,47]

Recently, Yamamoto[48] has developed a $ZrCl_4$ catalyzed halogenation of electronically activated aromatic compounds. Inspired by his work, later studies have implemented catalytic Lewis[48–50] or Brønsted[51] acids to activate *N*-bromosuccinimide (NBS) towards regio- or enantioselective brominations; however most of these studies have not been extended to chlorination due to the lower inherent reactivity of NCS. The field of directed C-H functionalization has also turned attention to regioselective halogenation with numerous examples of functional-group directed halogenations (Figure 2.2.3), many of which invoke a dual activation of both the arene and NXS.[52–57] Recently, Baran[58] and Xiao[59] have disclosed new stoichiometric chlorinating reagents chloro-bis(methoxycarbonyl)-guanidine (CBMG) and 1-chloro-1,2-benziodoxol-3-one, respectively. Both reagents display increased reactivity while maintaining selectivity compared to classical chlorinating reagents, perhaps representing the current state-of-the-art stoichiometric reagents in the field, albeit at a higher price.

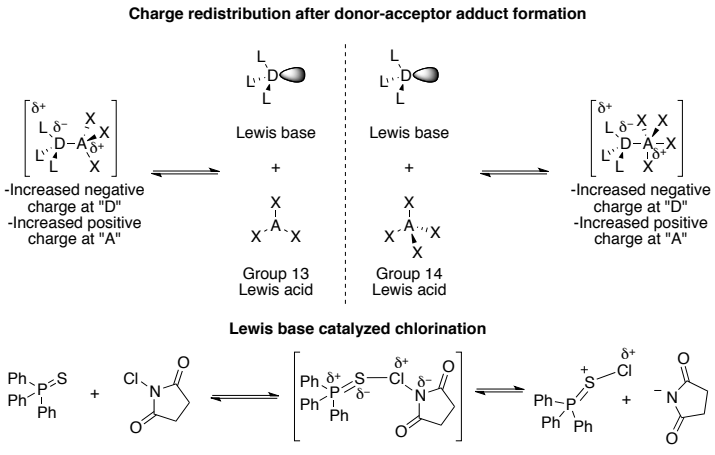

Figure 2.2.4. Charge Redistribution in Lewis Base Catalysis

While there is significant precedence for the use of Lewis acids as catalysts for electrophilic aromatic substitution, Lewis bases had not yet been explored in this realm at the time. As shown in Figure 2.2.3, Lewis acids act to remove electron density from the electrophile via acid-base coordination, thereby increasing the electrophilicity of the reacting species. Unlike Lewis acid activation, Lewis bases act as an electron donor which acts to decrease the electron density at the electrophilic atom via what is informally termed as a "spillover" effect that arises from a donor-acceptor interaction. As a general example, the donor-acceptor interaction shown in Figure 2.2.4 (reformatted from an eloquent review by Prof. Scott Denmark at the University of Illinois)[60] ultimately results in a net increase of electron density at the donor atom and a net decrease of electron density at the acceptor atom. This contradicts the usual assumption that the net change in formal charge localizes on the donor (positive charge) and acceptor (negative charge). Such modes of charge redistribution arise from Gutmann's[61] observations of the changes in the bond lengths of the corresponding donor-acceptor adducts due to charge density variations, where the bonds adjacent to the donor and acceptor will either contract or elongate to compensate for the change in electron density at the donor and acceptor. Albeit, while Lewis base catalysts had been reported to affect the electrophilic halofunctionalization of alkenes,[62] nobody at the time had disclosed utilizing catalytic Lewis base in an electrophilic aromatic substitution setting.

2.3 Discussion

Stimulated by seminal work in Lewis base catalysis[60,62,63] we postulated that NCS activation with an appropriate Lewis base would represent a mild and efficient catalytic strategy

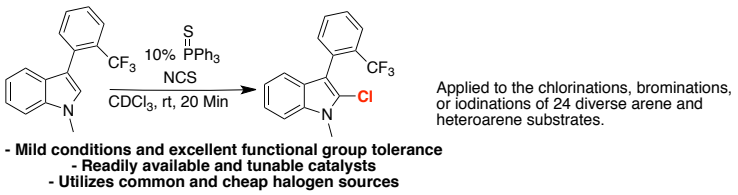

Figure 2.3.1. This Work: Lewis Basic Phosphine Sulfide Catalyzed Electrophilic Aromatic Halogenation of Arenes and Heterocycles

that could overcome many of the current shortcomings (Figure 2.3.1). As a proof of concept, we initially investigated the electrophilic chlorination of the *C*-2 position of 3-substituted 7-azaindoles (i.e. **2.1**), a class of molecules ubiquitous throughout medicinal chemistry, that possesses no reactivity toward NCS in the absence of catalyst at room temperature (Table 2.3.1, entries 1 and 2), and attenuated activity toward Yamamoto's Lewis acid catalyzed conditions (Table 2.3.1, entry 9), possibly due to adduct formation between the Lewis acid and the Lewis basic heterocyclic nitrogen. Lewis basic triphenylphosphine sulfide proved an excellent catalyst with a 20% catalytic loading, providing 84% conversion in 18 hours at room temperature (Table 2.3.1, entry 3). Other Lewis bases proved to be much less efficient; for example, triphenylphosphine oxide possessed no catalytic activity (Table 2.3.1, entry 5) whereas triphenylphosphine selenide displayed reduced activity (Table 2.3.1, entry 6).

Table 2.3.1. Evaluation of Chlorination Catalysts

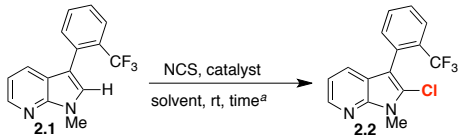

entry	catalyst	solvent	time (h)	yield[b]
1	none	$CDCl_3$	24	0
2	none	CD_2Cl_2	22	0
3	$Ph_3P{=}S$ (**2.3**)	$CDCl_3$	18	84
4	$Ph_3P{=}S$	CD_2Cl_2	22	44
5	$Ph_3P{=}O$ (**2.4**)	$CDCl_3$	24	0
6	$Ph_3P{=}Se$ (**2.5**)	$CDCl_3$	24[c]	54
7	$S(n\text{-}Bu)_2$ (**2.6**)	$CDCl_3$	24[c]	81
8	$(n\text{-}Bu)_3P{=}S$ (**2.7**)	$CDCl_3$	12	94
9	$ZrCl_4$	$CDCl_3$	24[c]	27[d]

[a]Reactions were performed at room temperature by the addition of 0.03 mmol **2.1**, 0.006 mmol catalyst, and 600 μL solvent into an NMR tube, followed by the addition of 0.040 mmol NCS. [b]Percent conversions by NMR represent an average of three trials using tetramethylsilane as internal standard. [c]NMR showed incomplete conversion of NCS. [d]Reaction was performed dry in an argon atmosphere; percent conversion by NMR represents an average of two trials using tetra(trimethylsilyl)silane as internal standard; 0.0015 mmol $ZrCl_4$ was used.

Motivated by Snyder's[64] work with halosulfonium salts, as well as recent work by Yeung,[64–67] we investigated butyl sulfide (**2.6**), which proved a capable catalyst, however presented less opportunity to modulate electronically from a catalyst design perspective (Table 2.3.1, entry 7). We next theorized that electron rich phosphine sulfides would be better Lewis base catalysts, thus we tested tributylphosphine sulfide (**2.7**) and found it to be noticeably more active. To illustrate the utility of this chemistry, we chose to focus primarily on commercially available catalyst **2.3** to define its scope, however, the superiority of **2.7** suggests that further catalyst modifications will be fruitful. Notably, CBMG proved remarkably effective at chlorinating azaindoles, going to full conversion in minutes (Scheme 2.3.1).

Scheme 2.3.1. Chlorination of Heterocycles

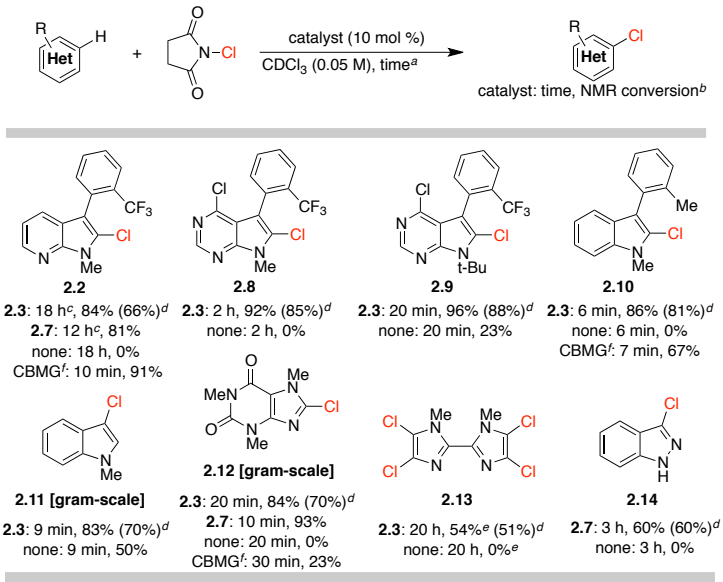

[a]Reactions were performed at room temperature by the addition of 0.03 mmol substrate, 0.003 mmol catalyst, and 600 μL $CDCl_3$ into an NMR tube, followed by the addition of 0.040 mmol NCS. [b]Percent conversions by NMR represent an average of three trials using tetramethylsilane as an internal standard. [c]0.006 mmol catalyst was used. [d]Isolated yield represents an average of three trials (isolated yield on the gram-scale represents an average of two trials [See Supporting Information for gram-scale procedure]). [e]0.126 mmol NCS was used. [f]CBMG was used as the stoichiometric chlorine source instead of NCS, and no catalyst was added to the reaction.

In general, we found 10% **2.3** to catalyze the rapid chlorination of diverse heterocycles, many of which represent privileged scaffolds in drug discovery (Scheme 2.3.1). For example, 3-substituted pyrrolopyrimidines, a well-known kinase inhibitor scaffold[68] that possesses little or no background reactivity, rapidly chlorinated to **2.8** or **2.9** (92% conversion to **2.8** in 2 hours and 96% conversion to **2.9** within 20 minutes). These results highlight the utility of Lewis base catalysis in the context of electrophilic aromatic chlorination. To the best of our knowledge there are no literature precedence for the direct *C*-2 chlorination of azaindoles and only scarce patent precedence for pyrrolopyrimidines.[69] 3-Substituted indoles, a privileged scaffold class in medicinal chemistry,[70] also proved to be amenable substrates, chlorinating at the *C*-2 position with large rate accelerations compared to without catalyst (86% conversion to **2.10** in 6 minutes, with

little to no conversion observed in the absence of a catalyst at that time point), while also offering a noticeable improvement to CBMG under comparable non-catalyzed conditions.

Cleaner conversion was also observed for the *C*-3 chlorination of *N*-methylindole to afford **2.11** (83% in 9 minutes), while avoiding the use of DMF, the literature standard solvent for halogenation due to the ability of DMF to affect the reactivity of NXS.[43] Caffeine also smoothly chlorinated at the *C*-8 position, converting to **2.12** in minutes with no observable background reaction. Even greater rate acceleration was observed in the presence of **2.7** (93% in 10 minutes), representing a marked improvement over CBMG (23% conversion at 30 minutes). We also found this system adept at chlorination other heterocycles such as imidazole (i.e. perchlorination of bis-imidazole to give **2.13** in 50% conversion after 20 hours) and indazole (60% conversion to **2.14** in 3 hours with no observed reaction in the absence of **2.7**). To further demonstrate the potential utility of this chemistry, we applied these conditions on the gram scale to access **2.11** and **2.12** with results comparable to those on the NMR scale.

Scheme 2.3.2. Chlorination of Arenes

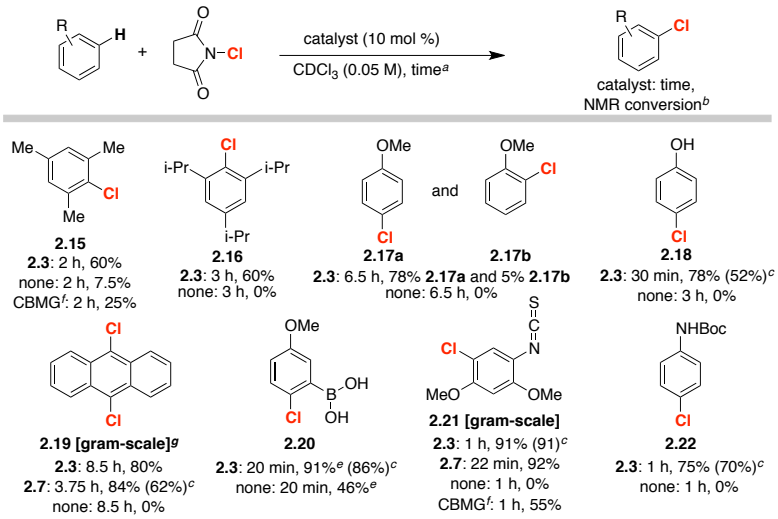

[a]Reactions were performed at room temperature by the addition of 0.03 mmol substrate, 0.003 mmol catalyst, and 600 μL $CDCl_3$ into an NMR tube, followed by the addition of 0.040 mmol NCS. [b]Percent conversions by NMR represent an average of three trials using tetramethylsilane as an internal standard. [c]Isolated yield represents an average of three trials (isolated yield on the gram-scale represents an average of two trials [See Supporting Information for gram-scale procedure]). [e]A 9:1 mixture of $CDCl_3$:CD_3OD was used as the solvent. [f]CBMG was used as the stoichiometric chlorine source instead of NCS, and no catalyst was added to the reaction. [g]2.4 equiv of NCS was used.

We next evaluated the chlorination of simple arenes (Scheme 2.3.2). Mesitylene gave monochlorinated **2.15** in 60% conversion after 2 hours, with the attenuated yield being due to the formation of dichlorinated product, offering a noticeable improvement over CBMG (25% conversion to **2.15** at 2 hours albeit with minimal dichlorinated product observed). 1,3,5-Triisopropylbenzene gave similar results converting to 57% **2.16** after 3 hours. Phosphine sulfide catalysis also proved efficient toward chlorinating anisole, resulting in 83% conversion to monochlorinated derivatives **2.17a** and **2.17b** (15:1 mixture of *para*- to *ortho*- by NMR) after 6.5 hours with no observable background reaction. This represents a striking yield and selectivity compared to other literature precedents. In comparison, CBMG required elevated temperatures or the action of a strong acid to chlorinate anisole with comparable yields and selectivity. Phenol also rapidly chlorinated at the *para*- position to give **2.18** in good yield after 30 minutes. Anthracene, which Borhan has recently predicted to have high affinity toward halenium ions, also proved to be

an excellent substrate, reaching full conversion to 9,10-dichloroanthracene (**2.19**) in 3.5 hours with catalyst **2.7** (no observable background after 8.5 hours). To demonstrate the mild nature of Lewis base catalysis, we investigated arene substrates with electrophilic functional groups, finding each substrate to convert to a monochlorinated product. This included chlorination of 3-methoxyphenylboronic acid (**2.20**, 86% conversion after 1 hour) and 2,4-dimethoxyphenyl isothiocyanate (**2.21**, 91% conversion at 1 hour with **2.3**; 92% conversion with **2.7** at 22 minutes). Notably, comparable results were obtained on gram scale. *N*-Boc-aniline also chlorinated at the *para*- position with no background reaction, affording **2.22** in 70% isolated yield with the acid-sensitive protecting group still intact. These results demonstrate the functional group tolerance of this system.

Scheme 2.3.3. Bromination and Iodination of Arenes and Heterocycles

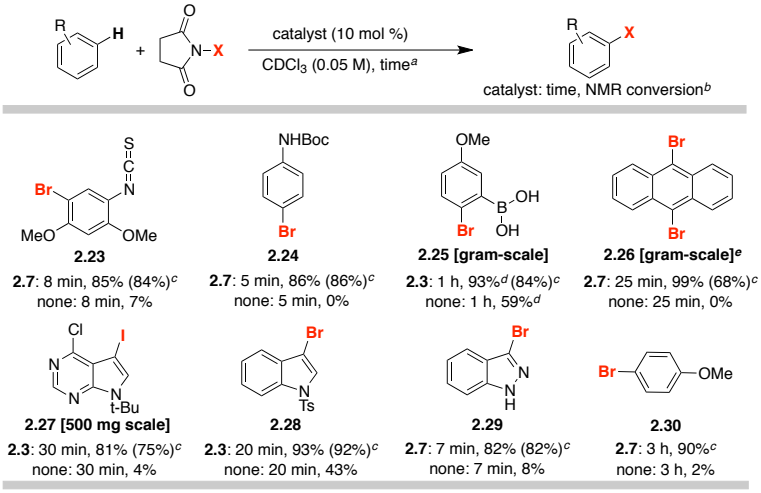

[a]Reactions were performed at room temperature by the addition of 0.03 mmol substrate, 0.003 mmol catalyst, and 600 μL $CDCl_3$ into an NMR tube, followed by the addition of 0.040 mmol NXS (X = Br or I). [b]Percent conversions by NMR represent an average of three trials using tetramethylsilane as internal standard. [c]Isolated yield represents an average of three trials (isolated yield on the gram-scale represents an average of two trials [See Supporting Information for gram-scale procedure]). [d]A 9:1 mixture of $CDCl_3$:CD_3OD was used as the solvent. [e]2.4 equiv of NBS was added used.

As mentioned throughout the text, we also compared our results side by side with stoichiometric CBMG, observing noticeable improvements across several substrates (i.e. indole

2.10, caffeine, mesitylene, phenol, and 2,4-dimethoxyphenyl isothiocyanate). However, 7-azaindoles (i.e. **2.2**), which required increased reaction times and catalytic loadings toward phosphine sulfide catalysis, possessed striking activity toward CBMG, rapidly going to completion in minutes (Scheme 2.3.1). Overall, these data suggest phosphine sulfide catalyzed chlorination with NCS are complementary, and in many cases more efficient than those with CBMG.

We then investigated more reactive halogen sources such as NBS and NIS (Scheme 2.3.3), observing excellent activities, often on preparative scales. With catalyst **2.7**, we were able to mono-brominate 2,4-dimethoxyphenyl isothiocyanate and *N*-Boc-aniline to afford **2.23** and **2.24**, respectively, in over 80% yield within minutes, with little to no observable background reaction. 3-Methoxyphenylboronic acid smoothly brominated to give **2.25** in 93% conversion at 1 hour with catalyst **2.3**, while the yield was attenuated in the absence of catalyst. The dibromination of anthracene completed in 25 minutes to yield **2.26** at 99% conversion by NMR. *N*-(*t*-Bu)-substituted pyrrolopyrimidine cleanly iodinated at the *C*-3 position to give **2.27**, resulting in 81% conversion after 30 minutes, while only observing 4% conversion without **2.3**.

While a number of these reactions had marked background reactions, we generally found the catalytic conditions to be cleaner and higher yielding. This is exemplified by *N*-tosylindole, which smoothly brominated in 20 minutes to yield **2.28** in 93% yield in the presence of **2.3**. The non-catalyzed reaction was also rapid; however, it only yielded 43% of the *C*-3 brominated indole along with at least two other prevalent side products by NMR. Indazole also cleanly brominated at the *C*-3 position, converting to **2.29** in 82% yield, with highly attenuated reactivity in the absence of **2.7**. Finally, anisole selectively brominated at the *para*- position to give **2.30** in excellent yields (91% at 3 hours) with little to no reaction in the absence of Lewis base catalyst.

In summary, we developed a practical, inexpensive, and highly reactive Lewis basic catalytic system to improve the chlorination, and more generally halogenation, of diverse arenes and heterocycles, with many examples validated on gram scales. The dependence of this chemistry on the presence of catalysts opens the possibility to design next generation phosphine sulfide catalysts that effect enantio- or regioselective chlorinations. Our endeavors towrad the Lewis base-catalyzed regioselective chlorination of phenols are discussed in the next chapter.

2.4 Experimental Section

2.4.1 General Information

^{1}H, ^{13}C, and ^{31}P NMR spectra were recorded on Varian VNMRS 400 MHz, Varian Inova 500 MHz and Varian VNMRS 600 MHz spectrometers at 24 ^{o}C. All chemical shifts were reported in parts per million (δ) and were internally referenced to residual protio solvents. ^{19}F spectra were referenced to an external TFA standard. Spectral data were reported as follows: chemical shift (multiplicity [singlet (s), doublet (d), triplet (t), quartet (q), pentet (p), and multiplet (m)], coupling constants [Hz], integration). Carbon spectra were recorded with complete proton decoupling. Conventional mass spectra were either obtained using an Agilent 6200 series TOF LC/MS ESI ([M+H]), a Thermo Finnigan TSQ 7000 with EI probe ([M]), or Thermo Finnigan LCQ Deca XP MS/MS. *N*-chlorosuccinimide and *N*-bromosuccinimide were recrystallized from water or acetic acid. For cross-coupling reactions, 1,4-dioxane and deionized H_2O were degassed with nitrogen three times by freeze-pump-thaw method before use; for the synthesis of tributylphosphine sulfide catalyst, dichloromethane was also degassed with nitrogen 3 times using the freeze-pump-thaw method. All other chemicals used were purchased from Sigma Aldrich, TCI, Frontier Scientific, Acros Organics, Strem, Oakwood, Cambridge Isotope Laboratories, or Fisher and were used as received without further purification. All flash column chromatography (FCC) was performed using Grade 60 Silica Gel (230-400 mesh) purchased from Fisher Scientific.

2.4.2 General Preparation of Phosphine Sulfides

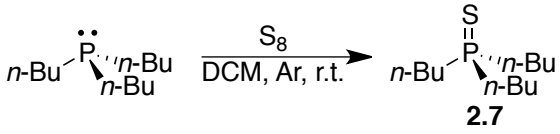

2.7

Scheme 2.4.1. Synthesis of Tributylphosphine Sulfide (2.7)

Tributylphosphine sulfide (**2.7**): 820 μL (3.29 mmol, 1.0 equiv.) of tributylphosphine was added to a 50 ml round-bottom flask equipped with stir bar, and the flask was evacuated and backfilled with argon (2x) followed by the addition of 32 ml degassed dichloromethane. 243 mg (6.58 mmol, 2.0 equiv.) ground elemental sulfur was then added to the flask under an argon counter flow (bubbles formed immediately). Upon completion of reaction (<2 hours), the solvent was removed by rotovap and the resultant oil was purified by flash column chromatography (hexanes:ethyl acetate: 1:0 to 9:1) to yield 693 mg (90% yield) tributylphosphine sulfide (**2.7**) as clear oil. ^{1}H NMR (400 MHz, $CDCl_3$) δ 1.84-1.74 (m, 6H), 1.62-1.50 (m, 6H), 1.42 (h, 6H), 0.94 (t, 9H); ^{13}C NMR (101 MHz, $CDCl_3$) δ 30.75 (d, J = 50 Hz), 24.61 (d, J = 4 Hz), 24.14 (d, J = 15 Hz), 13.80; ^{31}P NMR (162 MHz, $CDCl_3$) δ 49.32 (referenced to external H_3PO_4 standard); MS (ESI): Calculated $C_{12}H_{28}PS^+$ [M+H] 235.1644. Found: 235.1654 m/z.

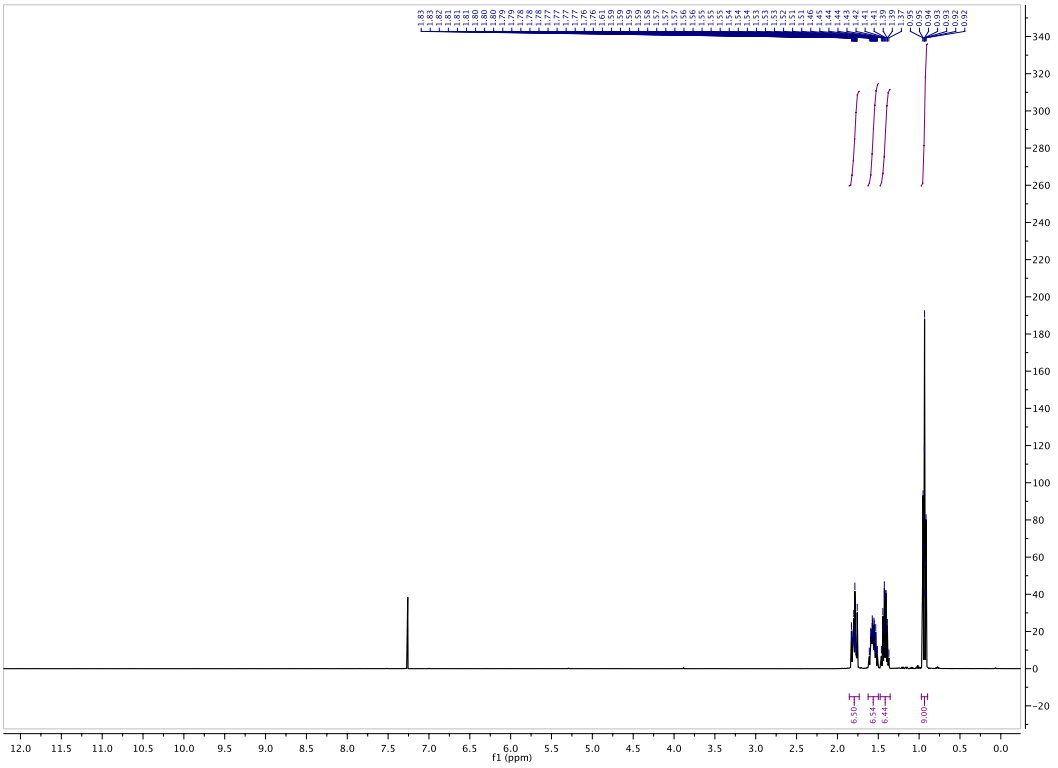

Figure 2.4.1. ^{1}H of 2.7

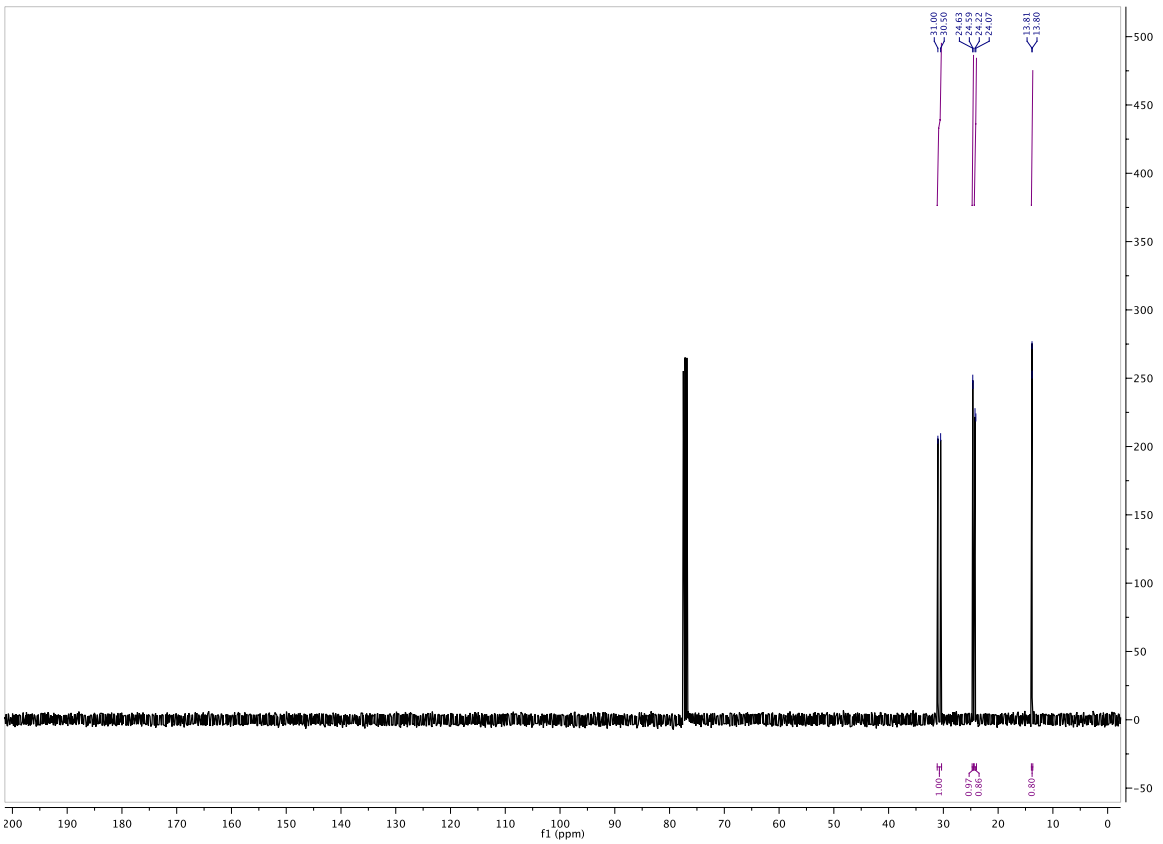

Figure 2.4.2. ^{13}C of 2.7

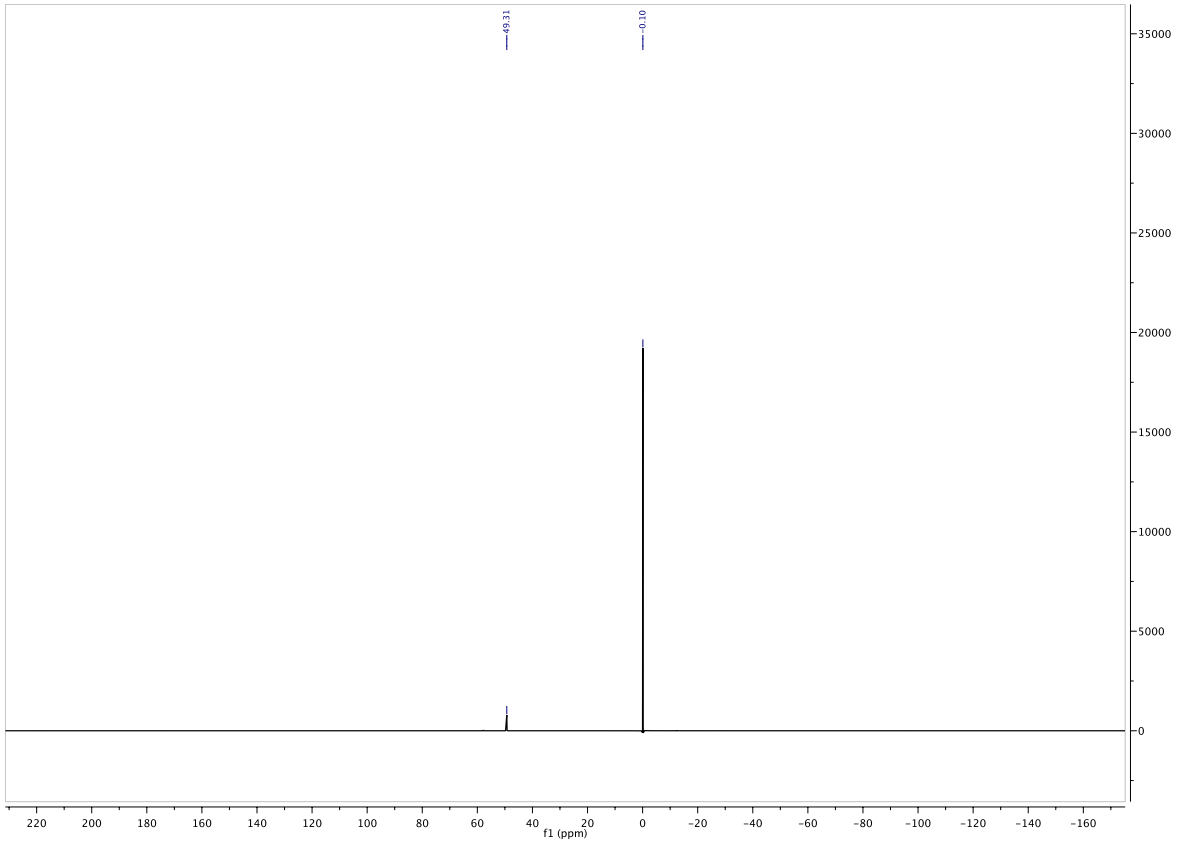

Figure 2.4.3. ^{31}P of 2.7

2.4.3 Substrate Preparation

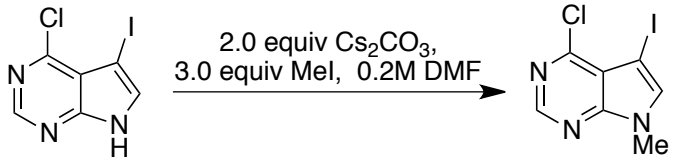

Scheme 2.4.2. Synthesis of 4-chloro-5-iodo-7-methylpyrrolopyrimidine

To 4-chloro-5-iodo-pyrrolopyrimidine (456 mg, 1.55 mmol, 1.0 equiv.) was charged Cs_2CO_3 (800 mg, 3.2 mmol) and 3 mL DMF. The mixture was cooled to 0 ^oC in an ice bath and iodomethane added (300 μL, 4.81 mmol). The mixture was warmed to room temperature and left stir for 14 hours. At this time, the mixture was cooled in an ice bath and 5 mL cold water was added. The formed solid was filtered by vacuum filtration to yield 390 mg 4-chloro-5-iodo-7-methylpyrrolopyrimidine (51% yield) as beige solid. ^1H NMR (599 MHz, $CDCl_3$) δ 8.63 (S, 1H), 7.36 (S, 1H), 3.88 (S, 3H).

General Procedure for the Syntheses of 6-chloro-7-aryl-deazapurines (Cross Coupling):

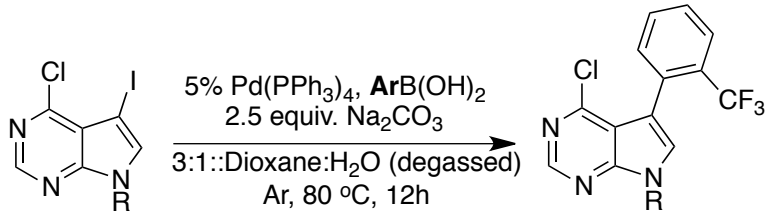

Scheme 2.4.3. General Cross Coupling Protocol

To 7-substituted-4-chloro-5-iodo-pyrrolopyrimidine (1.0 equiv.) in a 6-dram vial was added aryl boronic acid (1.5 equiv.), $Pd(PPh_3)_4$ (0.05 equiv.), and Na_2CO_3 (2.5 equiv.). The mixture was thoroughly purged with argon and then dissolved in a 3:1 mixture of degassed dioxane and degassed water until the mixture was 0.2 M in pyrrolopyrimidine. The mixture was then let stir for 18 h at 80 ^oC at which time the mixture was partitioned between 5 mL water and 5 mL

ethyl acetate. The organic layers were separated, and the aqueous layer was extracted two more times with ethyl acetate. The organic layers were combined, dried with Na_2SO_4, and concentrated down to yield a crude oil which was purified by FCC (hexanes:ethyl acetate: 40:1 to 8:1) to yield pure product.

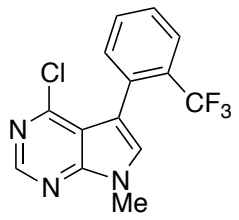

Figure 2.4.4. Substrate for 2.8

4-chloro-7-methyl-5-(2-trifluoromethyl)phenylpyrrolopyrimidine (Substrate for **2.8**): 67% isolated yield as a pale white powder. R_f: 0.18 (4:1 hexanes:ethyl acetate); ^{1}H NMR (500 MHz, $CDCl_3$) δ 8.67 (s, 1H), 7.77 (d, J = 7.8 Hz, 1H), 7.57 (t, J = 7.3 Hz, 1H), 7.52 (t, J = 7.3 Hz, 1H), 7.42 (d, J = 7.4 Hz, 1H), 7.20 (s, 1H), 3.94 (s, 3H); ^{13}C NMR (125 MHz, $CDCl_3$) δ 150.0, 151.0, 150.8, 134.2, 131.5, 130.8, 130.3 (q, J = 30 Hz.), 129.4, 128.0, 125.7 (q, J = 6.5 Hz.), 124.0 (q, J = 274 Hz.), 116.0, 112.1, 31.5; ^{19}F NMR (376 MHz, $CDCl_3$) δ -57.16 (referenced to an external trifluoroacetic acid standard); MS (EI): Calculated $C_{14}H_9ClF_3N_3$ [M] 311.044. Found: 311.027 m/z.

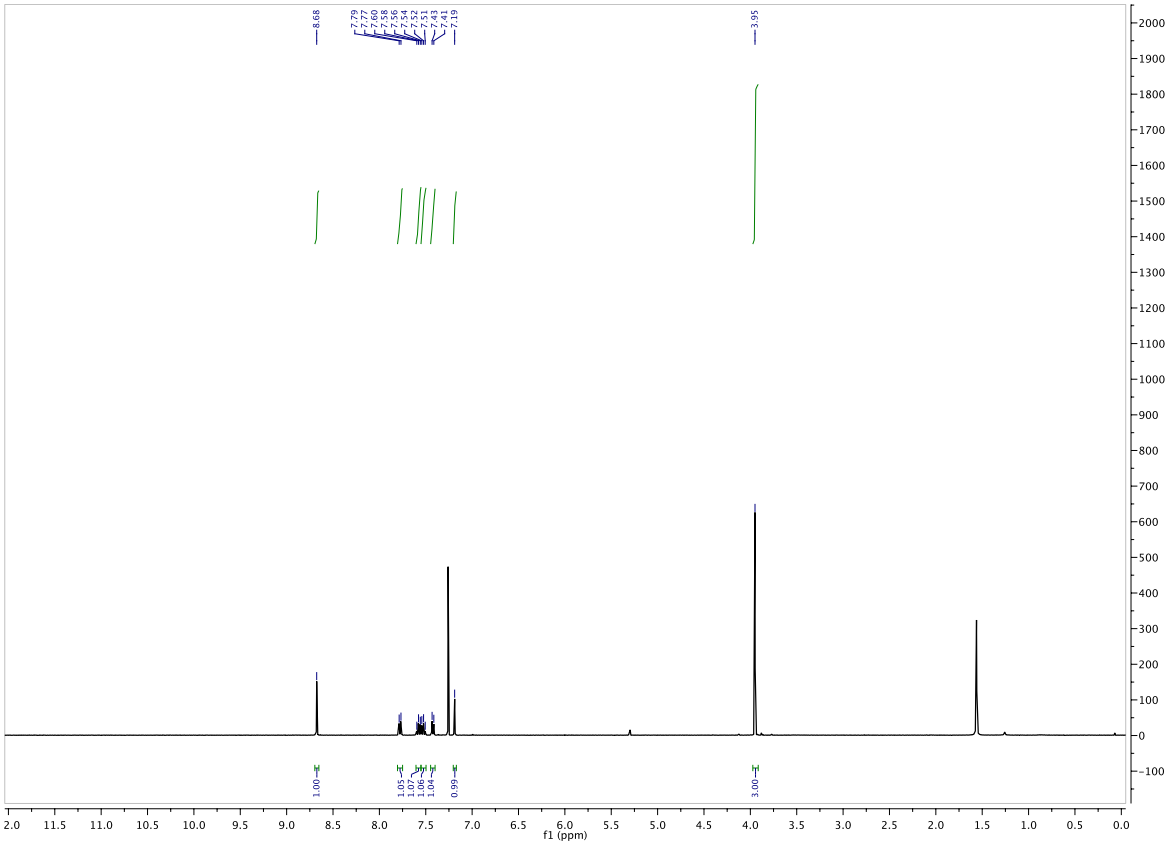

Figure 2.4.5. ^{1}H of Substrate for 2.8

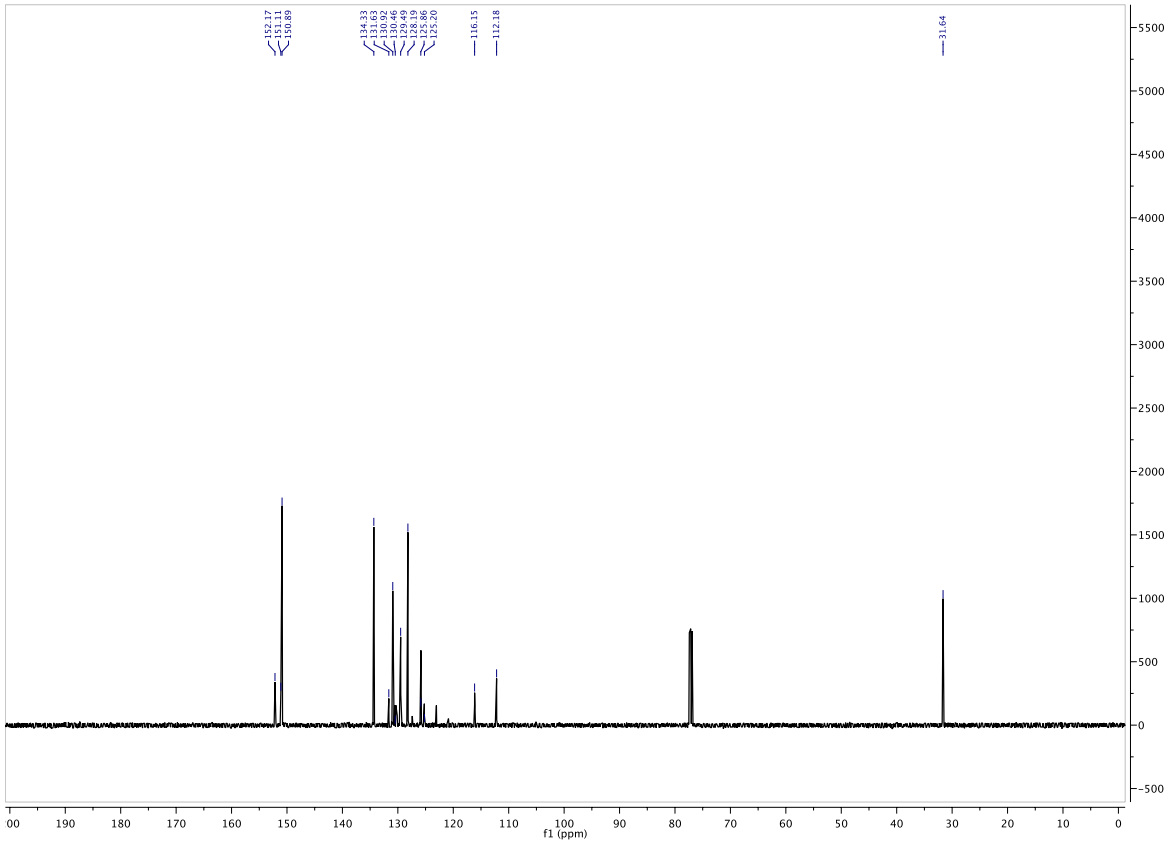

Figure 2.4.6. ^{13}C of Substrate for 2.8

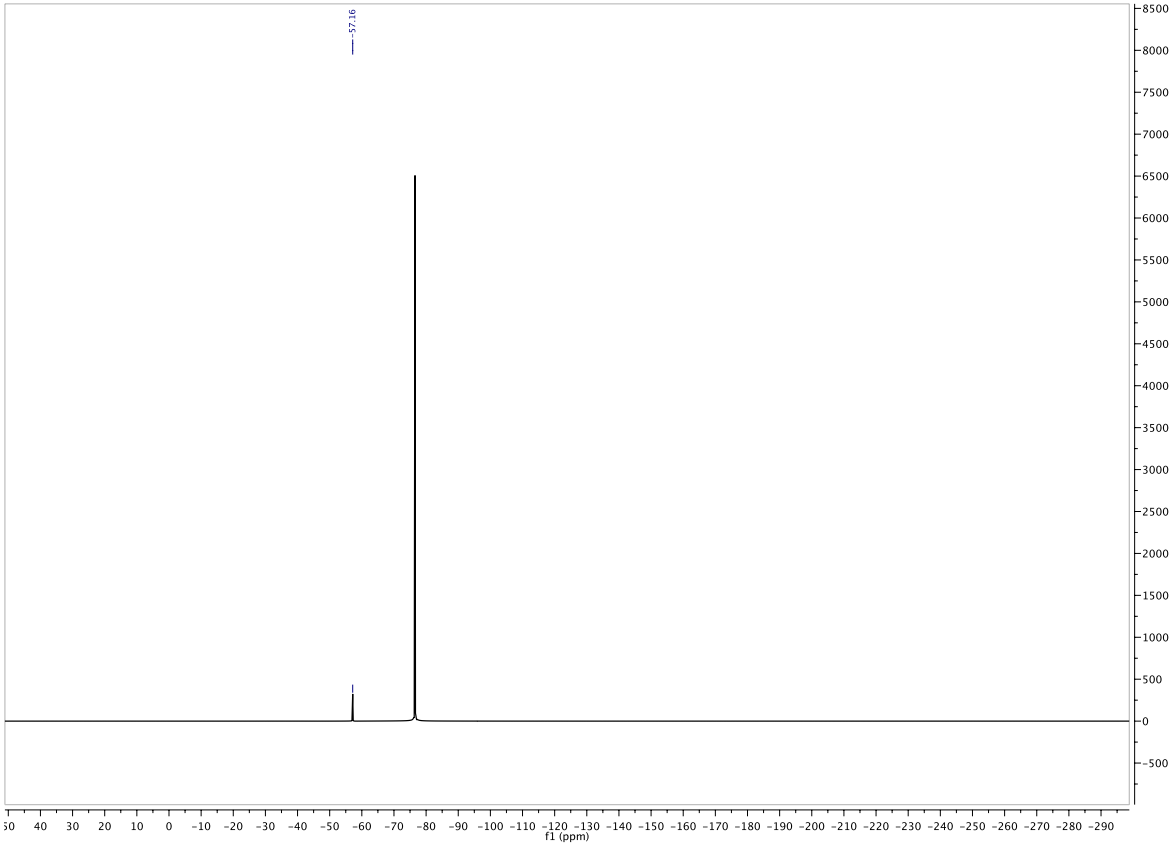

Figure 2.4.7. ^{19}F of Substrate for 2.8

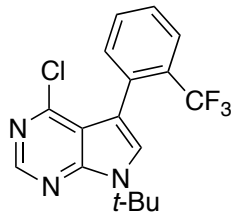

Figure 2.4.8. Substrate for 2.9

7-(tert-butyl)-4-chloro-5-(2-trifluoromethyl)phenylpyrrolopyrimidine (Substrate for **2.9**): 76% isolated yield as a yellow oil. R_f: 0.30 (9:1 hexanes:ethyl acetate); ^{1}H NMR (599 MHz, $CDCl_3$) δ 8.65 (s, 1H), 7.77 (d, J = 7.8 Hz, 1H), 7.57 (t, J = 7.5 Hz, 1H), 7.51 (t, J = 7.8 Hz, 1H), 7.44 (d, J = 7.3 Hz, 1H), 7.36 (s, 1H), 1.83 (s, 9H); ^{13}C NMR (126 MHz, $CDCl_3$) δ 152.10, 150.95, 149.58, 134.48, 132.38 (q, J = 1.7 Hz), 130.84, 130.58 (q, J = 29 Hz), 128.03, 126.70, 125.88 (q, J = 5.2 Hz), 124.57 (q, J = 274 Hz), 117.43, 110.76, 58.18, 29.43; ^{19}F NMR (376 MHz, $CDCl_3$) δ -57.20 (referenced to an external trifluoroacetic acid standard); MS (ESI): Calculated $C_{17}H_{16}ClF_3N_3^+$ [M+H] 354.0979. Found: 354.0976 m/z.

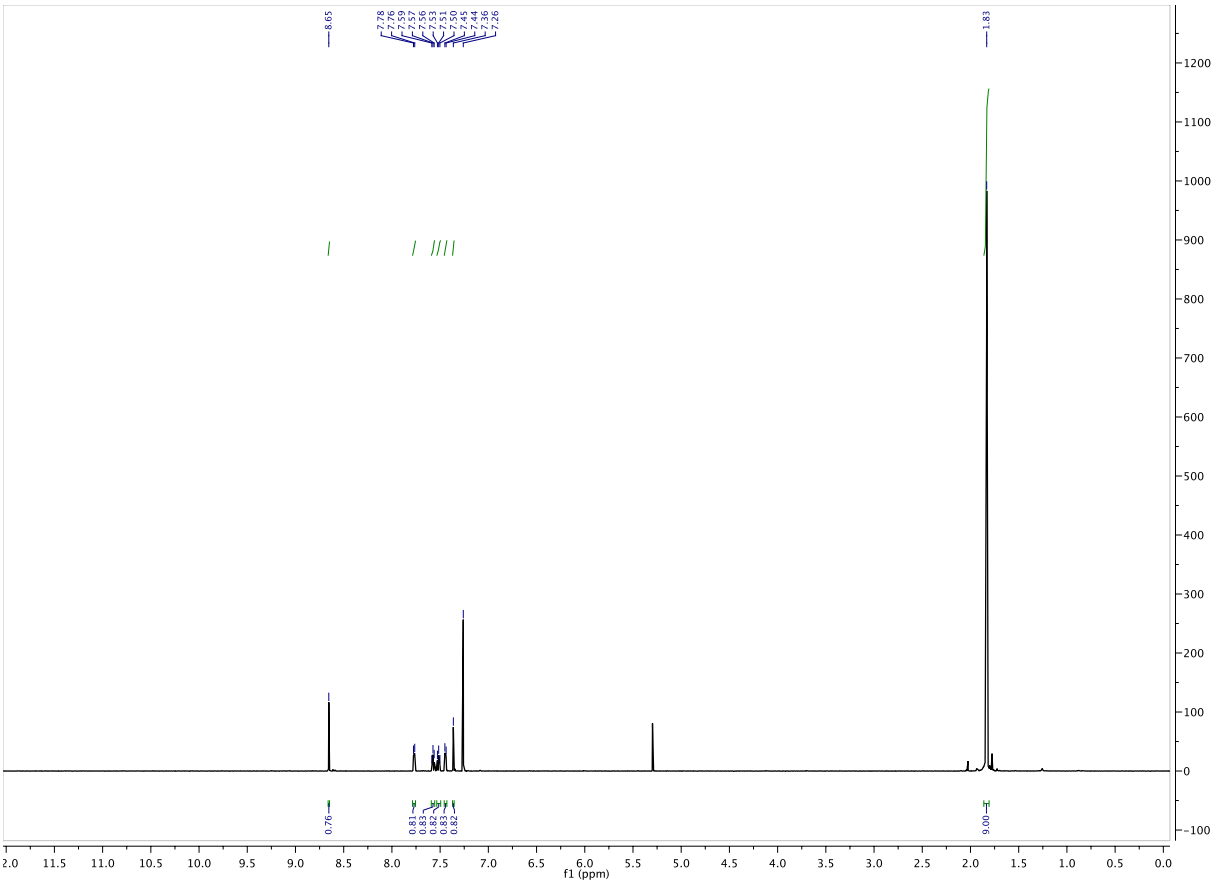

Figure 2.4.9. ^{1}H of Substrate for 2.9

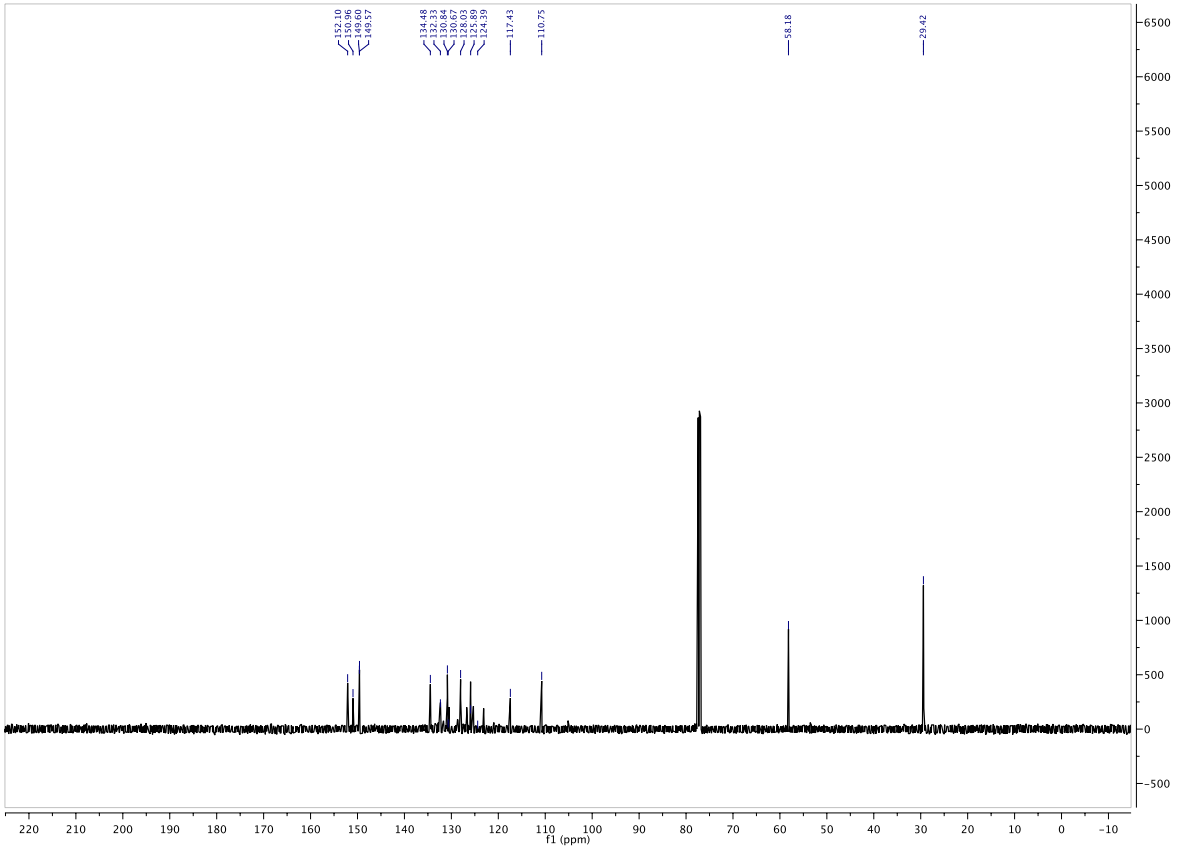

Figure 2.4.10. ^{13}C of Substrate for 2.9

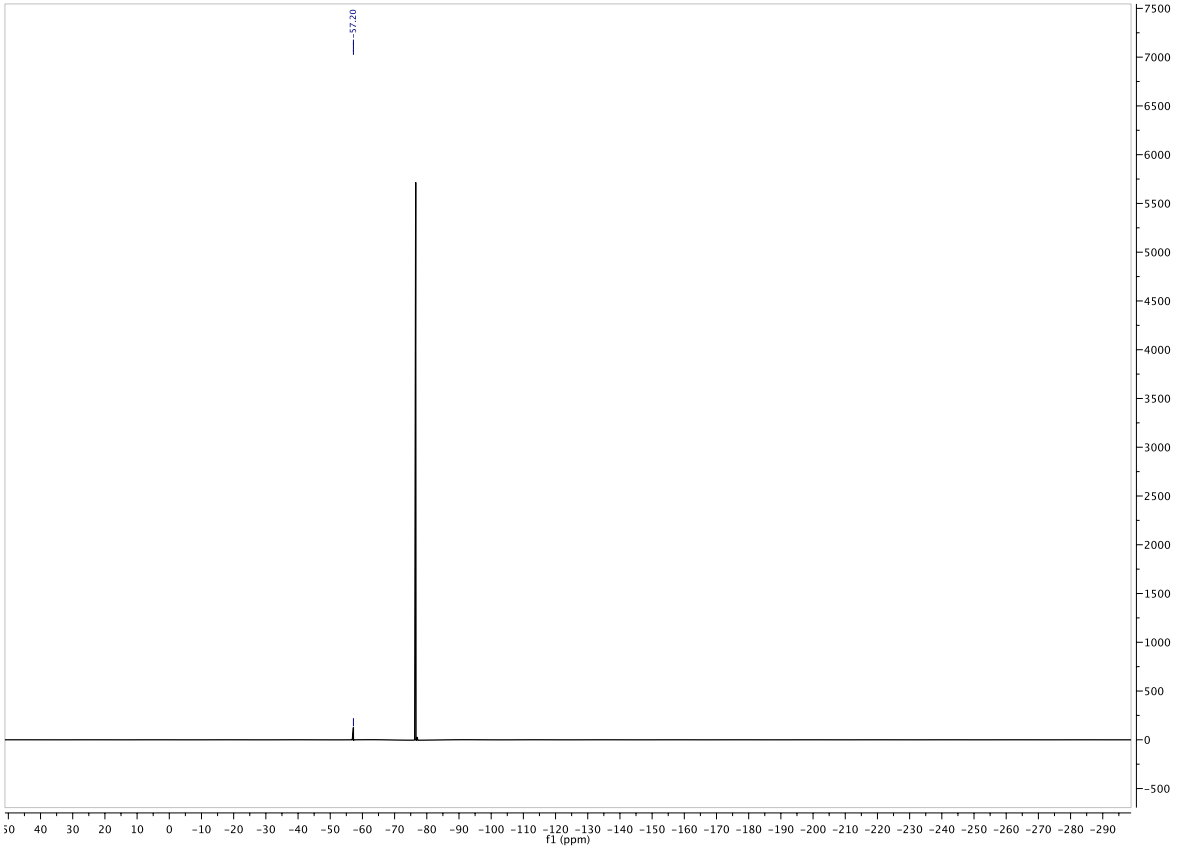

Figure 2.4.11. ^{19}F of Substrate for 2.9

Preparation of Indole and Azaindole Substrates:

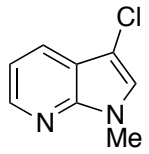

Figure 2.4.12. *N*-methyl-3-chloro-7-azaindole

N-methyl-3-chloro-7-azaindole: *N*-methyl-7-azaindole (1.0 g, 1.0 equiv.) and **2.3** (0.10 equiv.) were added to a 250 mL round bottom flask followed by the addition of dichloromethane (0.10 M in indole). *N*-chlorosuccinimide (1.2 equiv.) was added to the stirring reaction mixture at room temperature, and the reaction was followed by TLC. Upon completion, solvent was evaporated by rotovap, and the crude solid was washed in ethyl acetate (100 mL) with brine (40 mL) 3x. The organic layer was dried over anhydrous sodium sulfate and evaporated by rotovap to yield a crude oil. The crude oil was purified by FCC (97:3 hexanes:ethyl acetate) to yield 3-chloro-1-methyl-7-azaindole. 74% isolated yield as an orange oil. ^{1}H NMR (400 MHz, $CDCl_3$) δ 8.37 (d, J = 4.7 Hz, 1H), 7.69 (d, J = 7.9 Hz, 1H), 7.14 (s, 1H), 7.12 (dd, J = 7.9 Hz, 4.7 Hz, 1H), 3.86 (s, 3H); ^{13}C (101 MHz, $CDCl_3$) 146.50, 144.14, 126.78, 125.57, 118.50, 116.13, 103.20, 31.34; MS (ESI): Calculated $C_8H_8ClN_2^+$ [M+H] 167.0371. Found: 167.0371 m/z.

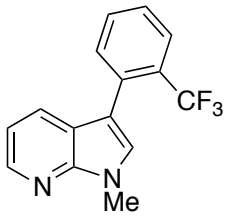

Figure 2.4.13. 1-methyl-3-(2-(trifluoromethyl)phenyl)-7-azaindole (2.1)

1-methyl-3-(2-(trifluoromethyl)phenyl)-7-azaindole (**2.1**): A 20 mL scintillation vial equipped with a stir bar was charged with 3-chloro-1-methyl-7-azaindole (1.0 equiv.), (*o*-

trifluoromethyl)phenylboronic acid (1.5 equiv.), potassium phosphate tribasic (2.0 equiv.), palladium (II) acetate (0.02 equiv.), and XPhos (0.04 equiv.). The vial was then evacuated and backfilled with argon (3x) followed by the addition of a 3:1 mixture of degassed dioxane and degassed water until mixture was 0.2 M in 7-azaindole. The mixture was stirred at 80 ^{o}C for 8 hours. Upon completion by TLC, the reaction mixture was cooled to room temperature and filtered thru a thick pad of celite. The filtrate was concentrated, and the crude oil was purified by FCC (hexanes:ethyl acetate:: 15:1 to 8:1) to obtain the cross-coupled product in 63% isolated yield as an orange solid. R_f: 0.29 (4:1 hexanes:ethyl acetate); ^{1}H NMR (400 MHz, $CDCl_3$) δ 8.39 (d, J = 4.7 Hz, 1H), 7.80 (d, J = 7.9 Hz, 2H), 7.58 (t, J = 7.4 Hz, 1H), 7.52 (d, J = 7.5 Hz, 1H), 7.44 (t, J = 7.6 Hz, 1H), 7.28 (s, 1H), 7.08 (dd, J = 7.9, 4.7 Hz, 1H), 3.96 (s, 3H); ^{13}C NMR (101 MHz, $CDCl_3$) δ 147.61, 143.33, 133.43 (q, J = 2 Hz), 133.13, 131.49, 129.34 (q, J = 28 Hz), 128.18 (q, J = 3 Hz), 127.72, 126.98, 126.62 (q, J = 5.6 Hz), 124.54 (q, J = 274 Hz), 120.54, 31.34; ^{19}F NMR (376 MHz, $CDCl_3$) δ -58.53 (referenced to an external trifluoroacetic acid standard); MS (ESI): Calculated: $C_{15}H_{12}F_3N_2^+$ [M+H] 277.0947. Found: 277.0942 m/z.

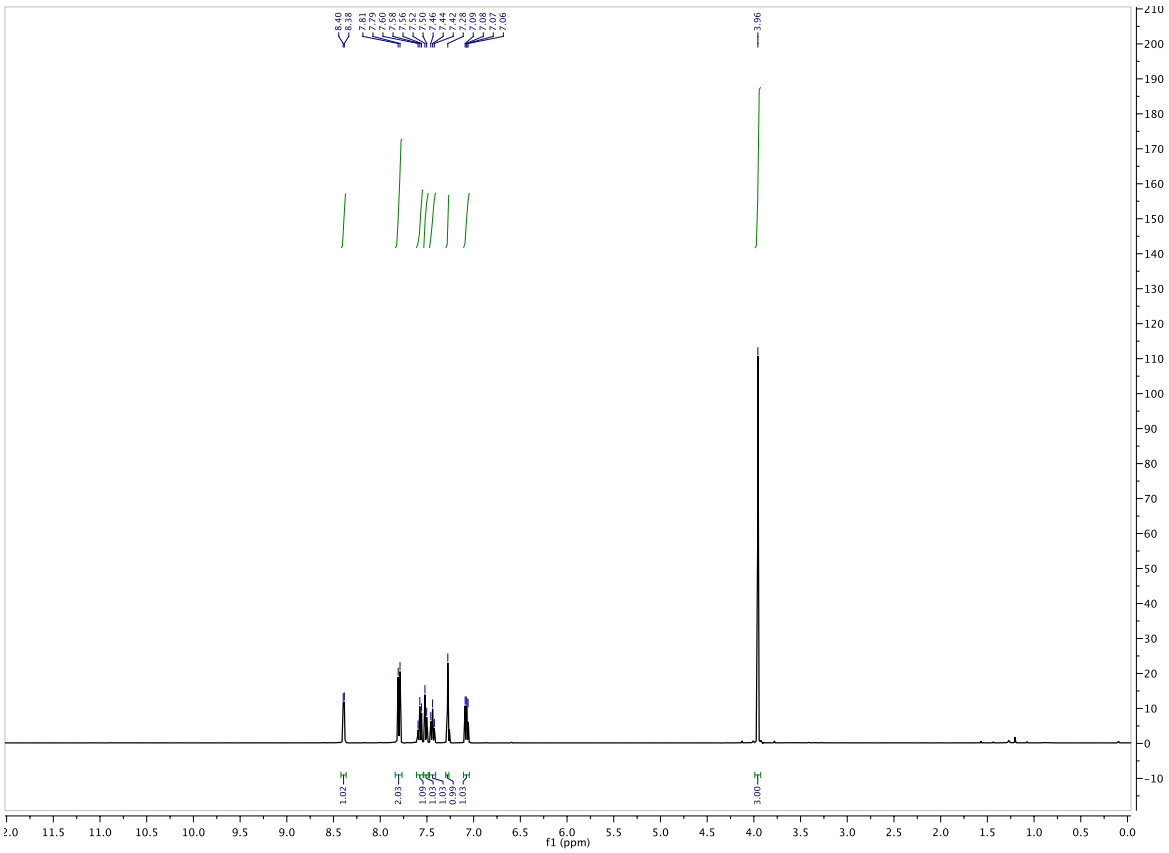

Figure 2.4.14. ^{1}H of 2.1

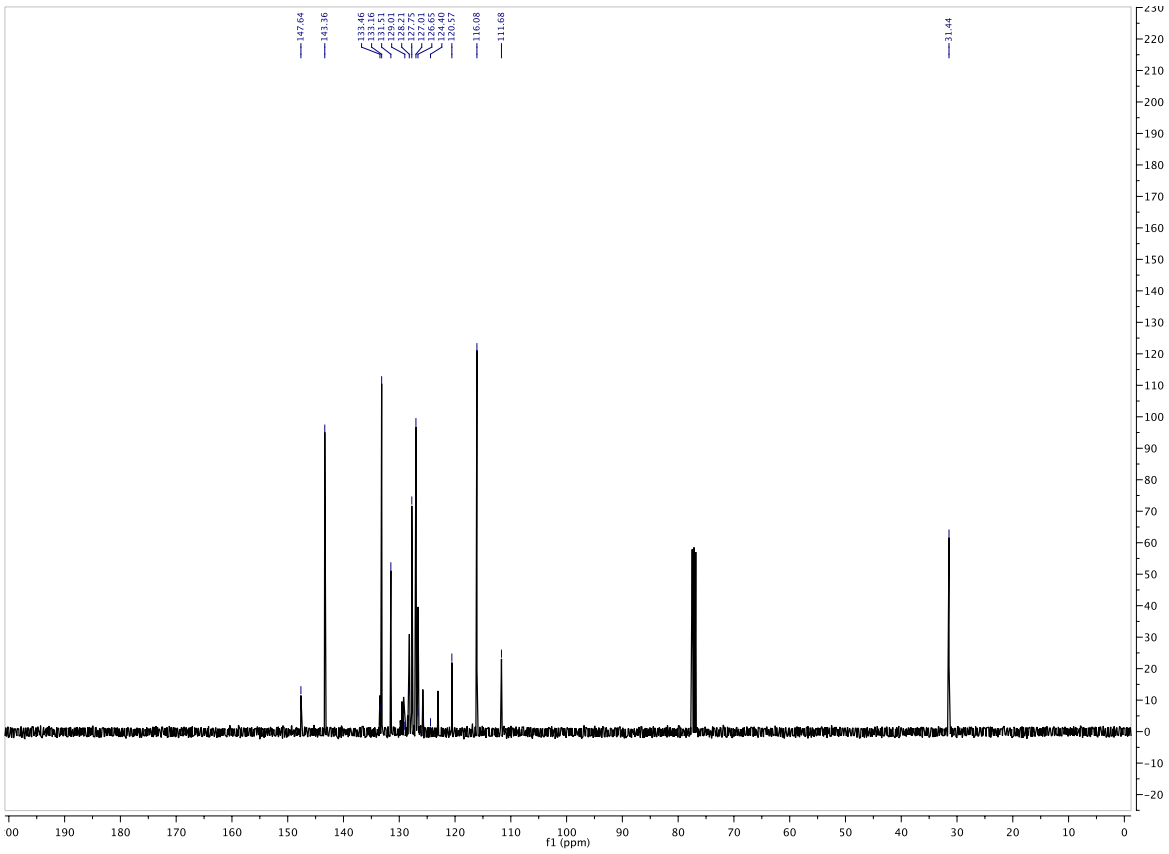

Figure 2.4.15. ^{13}C of 2.1

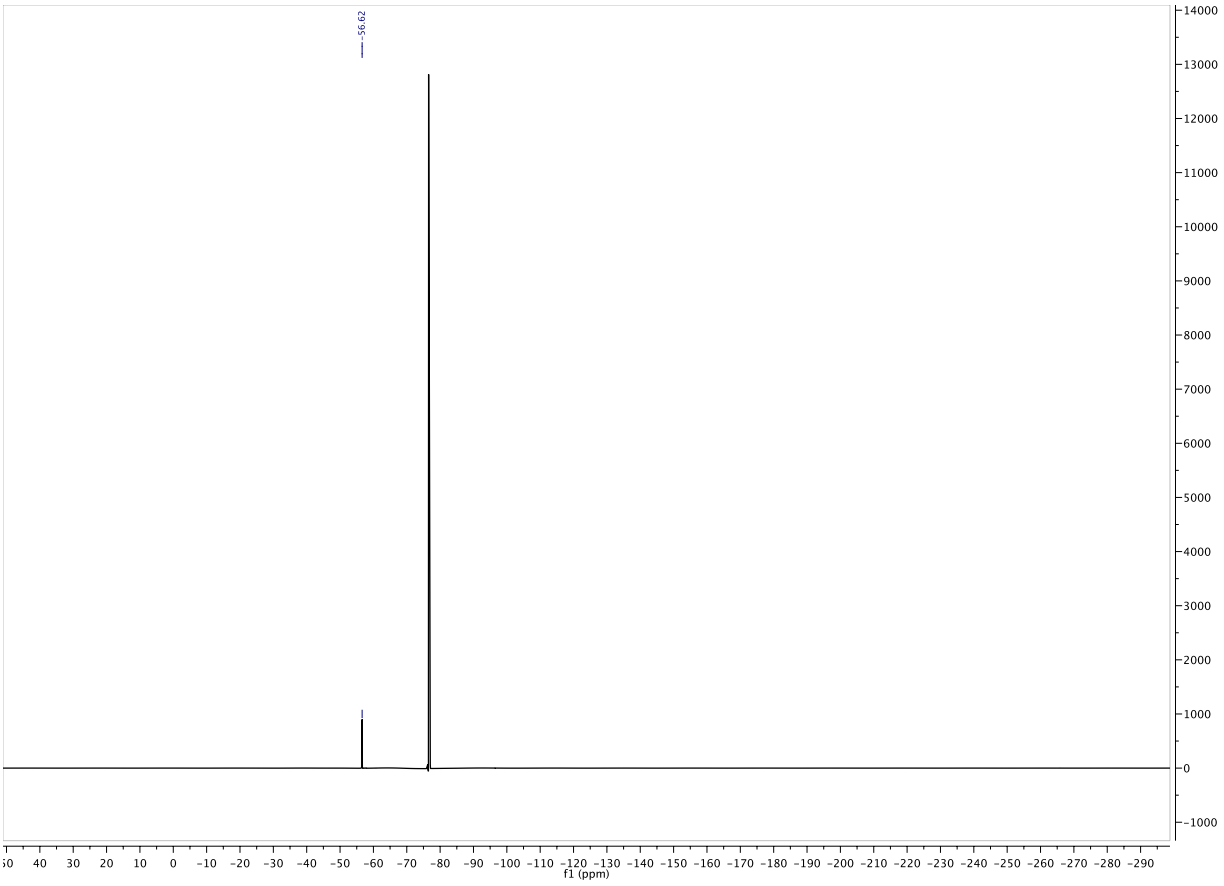

Figure 2.4.16. ^{19}F of 2.1

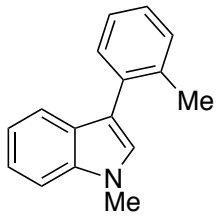

Figure 2.4.17. Substrate for 2.10

1-methyl-3-(*o*-tolyl)indole (Substrate for **2.10**): 3-chloro-1-methylindole (1.0 equiv.), (2-methyl)phenylboronic acid (1.3 equiv.), potassium phosphate tribasic (2.0 equiv.), palladium (II) acetate (0.1 equiv.), and XPhos (0.2 equiv.) were added to a 20 mL scintillation vial equipped with a stir bar. The vial was evacuated and backfilled with argon (3x) followed by the addition of degassed dioxane and degassed water (3:1 dioxane:water) until the mixture was 0.2 M in indole, and the reaction was let stir under argon at 80 ^{o}C for 12 hours. Upon completion, the mixture was filtered thru a thick pad of celite, followed by the removal of solvents by rotovap. The crude solid with purified by FCC (hexanes:ethyl acetate: 1:0 to 50:1) to afford the product 81% isolated yield as a clear oil. ^{1}H NMR (400 MHz, $CDCl_3$) δ 7.54 (d, J = 7.9 Hz, 1H), 7.44-7.42 (m, 1H), 7.39 (d, J = 8.2 Hz, 1H), 7.35-7.32 (m, 1H), 7.30-7.24 (m, 3H), 7.14 (t, J = 7.0 Hz, 1H), 7.06 (s, 1H), 3.87 (s, 3H), 2.35 (s, 3H); ^{13}C NMR (126 MHz, $CDCl_3$) δ 136.86, 134.70, 131.03, 130.46, 127.74, 127.65, 127.61, 126.69, 125.72, 121.86, 120.41, 119.56, 116.15, 109.42, 32.98, 20.95. MS (ESI): Calculated $C_{16}H_{15}N^{+}$ [M+H] 222.1277. Found: 222.1277 m/z.

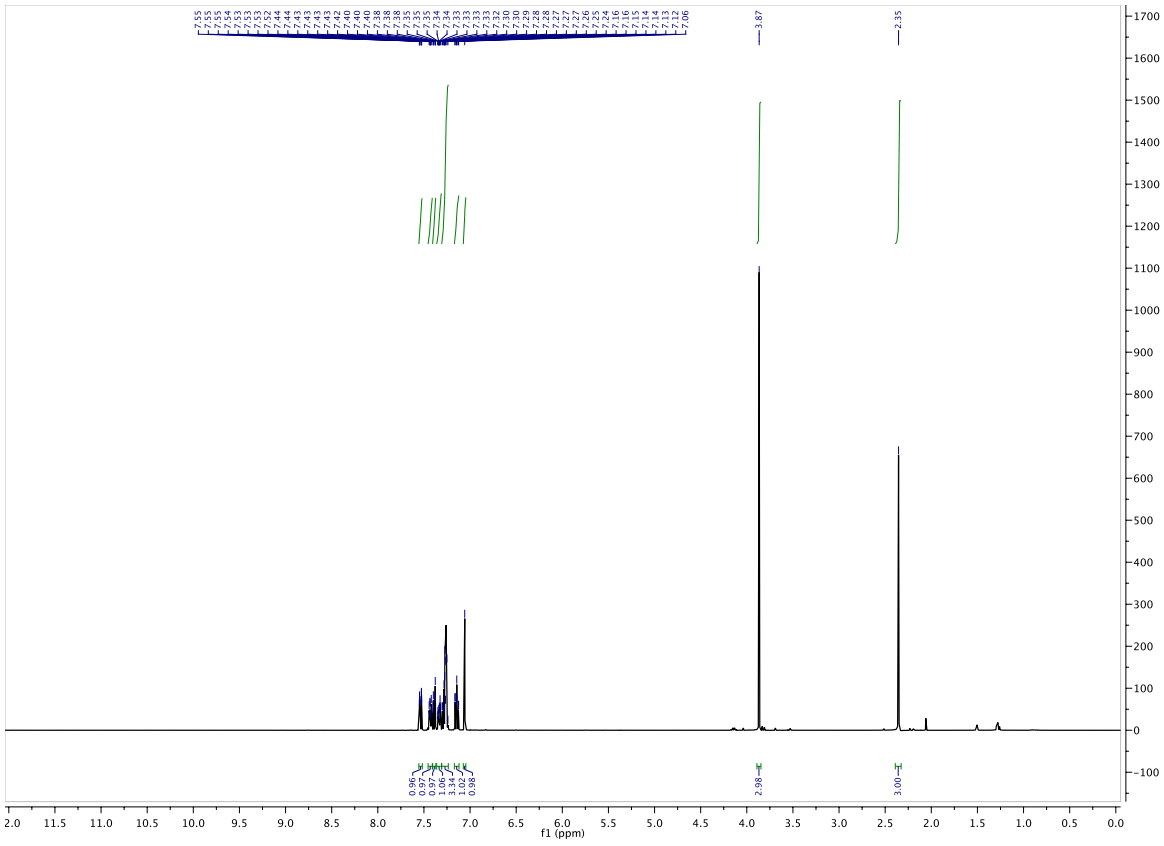

Figure 2.4.18. ^{1}H of Substrate for 2.10

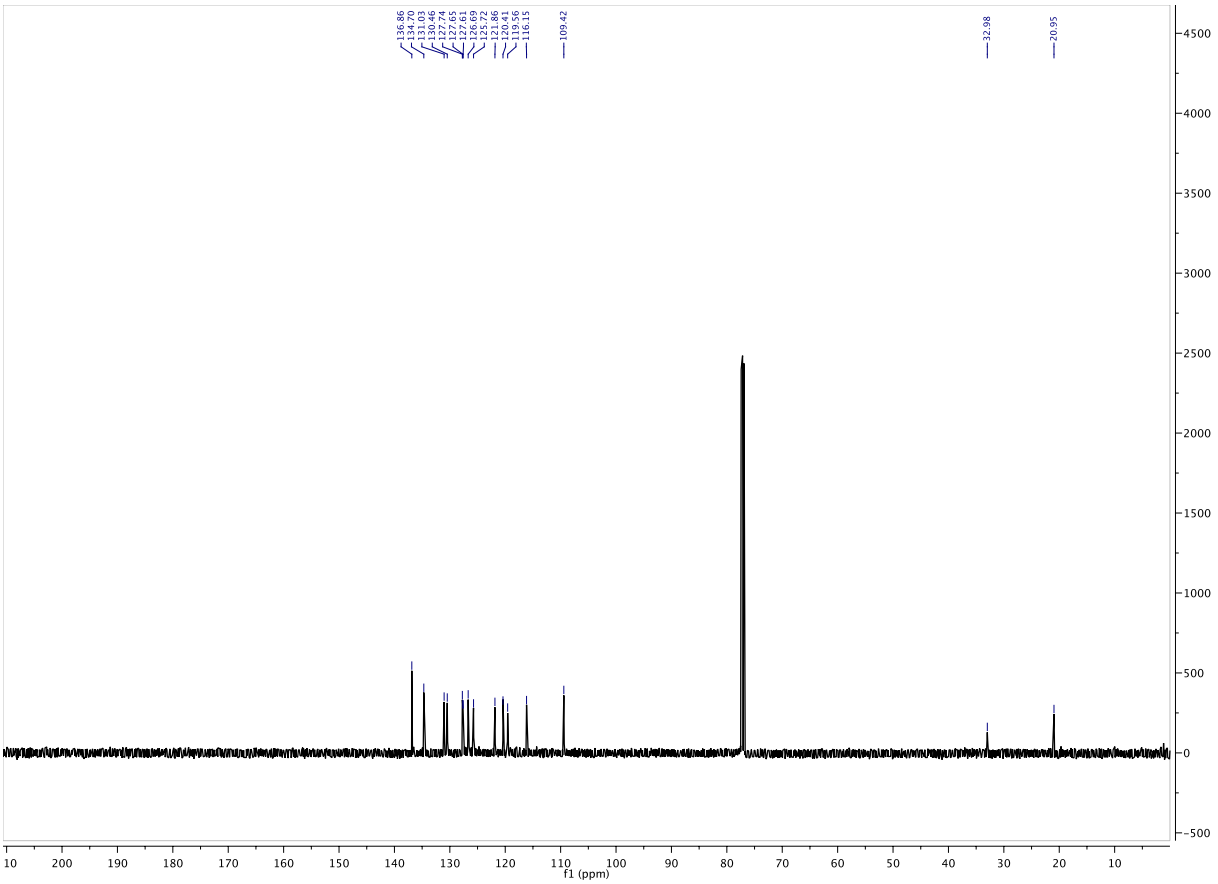

Figure 2.4.19. ^{13}C of Substrate for 2.10

2.4.4 General Chlorination Procedure

To a 5mm, 7", 100MHz NMR sample tube was added arene or heterocycle (0.03 mol, 1.0 equiv.), catalyst (0.003-0.006 mol, 0.10-0.20 equiv.), chloroform-D (600 μL, 0.05 M in substrate), and one drop tetramethylsilane (as internal standard). After obtaining a zero-point NMR, *N*-chlorosuccinimide, *N*-bromosuccinimide, or *N*-iodosuccinimide (0.033-0.051 mol, 1.2-4.2 equiv.) was added to the mixture and the reaction monitored by NMR until completion. Gram-scale reactions were performed by the addition of arene or heterocycle (1.0 g, 1.0 equiv.), catalyst (0.10 equiv.), and dichloromethane (0.10 M in substrate) into a 250 mL round bottom flask equipped with stir bar. NXS (1.2-2.4 equiv.) was then added to the stirring mixture at room temperature, and the reaction was monitored by TLC. Unless otherwise stated, isolated yields were obtained by the removal of solvent by rotovap upon reaction completion and purification of the crude mixture by FCC to yield halogenated product. Quoted NMR yields were determined using tetramethylsilane as the internal standard.

2.4.5 Characterization of Halogenated Products

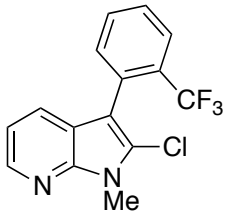

Figure 2.4.20. Product 2.2

2-chloro1-methyl-3-(2-(trifluoromethyl)phenyl)-7-azaindole (**2.2**): 84% conversion by NMR, and 66% isolated yield as a white solid. R_f: 0.41 (4:1 hexanes:ethyl acetate); ^{1}H NMR (400 MHz, $CDCl_3$) δ 8.34 (d, J = 4.8 Hz, 1H), 7.83 (d, J = 7.8 Hz, 1H), 7.62 (t, J = 7.5 Hz, 1H), 7.56 (t, J = 7.7 Hz, 1H), 7.52 (d, J = 7.4 Hz, 1H), 7.37 (d, J = 7.5 Hz, 1H), 7.05 (dd, J = 7.9, 4.7 Hz, 1H),

3.93, (s, 3H); ^{13}C NMR (101 MHz, $CDCl_3$) δ 143.20, 134.06, 131.82 (q, J = 1.1 Hz), 131.29 (q, J = 2.1 Hz), 131.26 (q, J = 30.0 Hz), 128.48, 127.19, 126.52 (q, J = 5.1 Hz), 126.27, 123.82 (q, J = 274.0 Hz), 121.01, 116.88, 109.29, 28.92; ^{19}F NMR (376 MHz, $CDCl_3$) δ -59.14 (referenced to an external trifluoroacetic acid standard); MS (ESI) Calculated: $C_{15}H_{11}ClF_3N_2^+$ [M+H] 311.0557. Found: 311.0563 m/z.

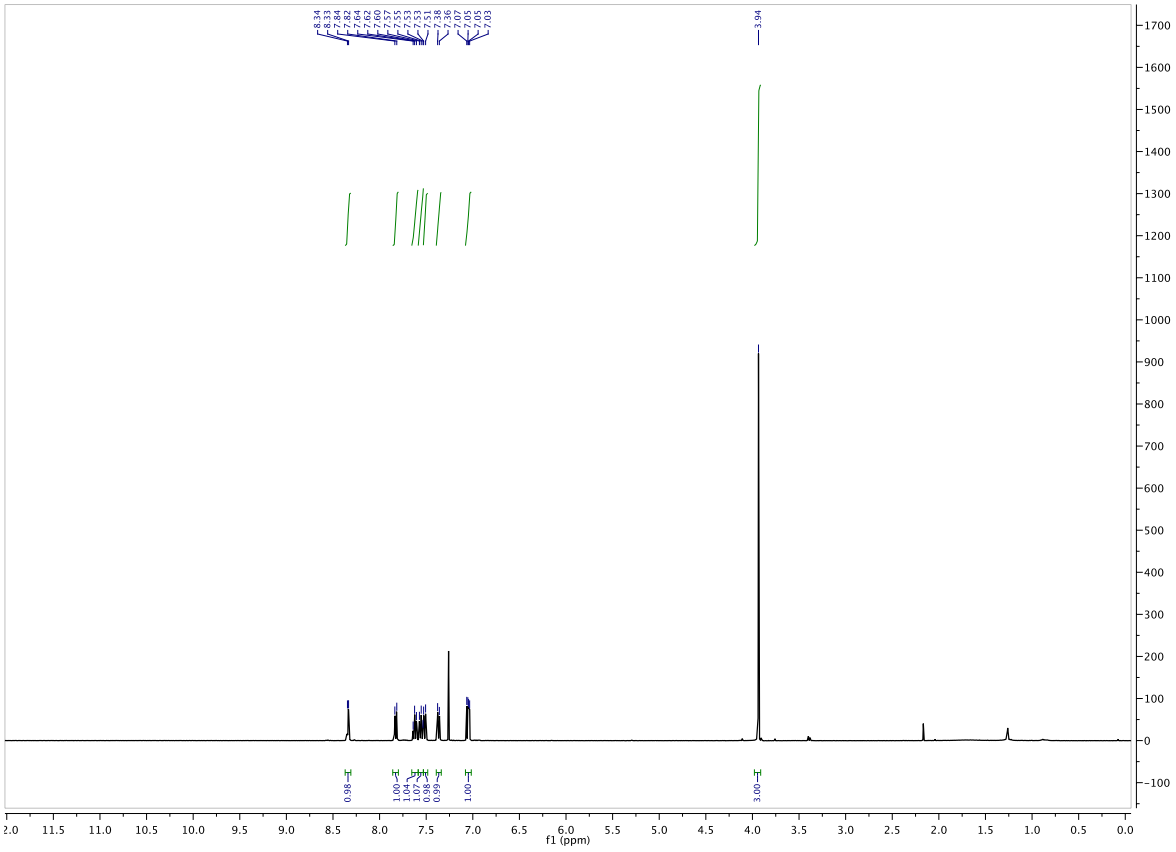

Figure 2.4.21. ^{1}H of 2.2

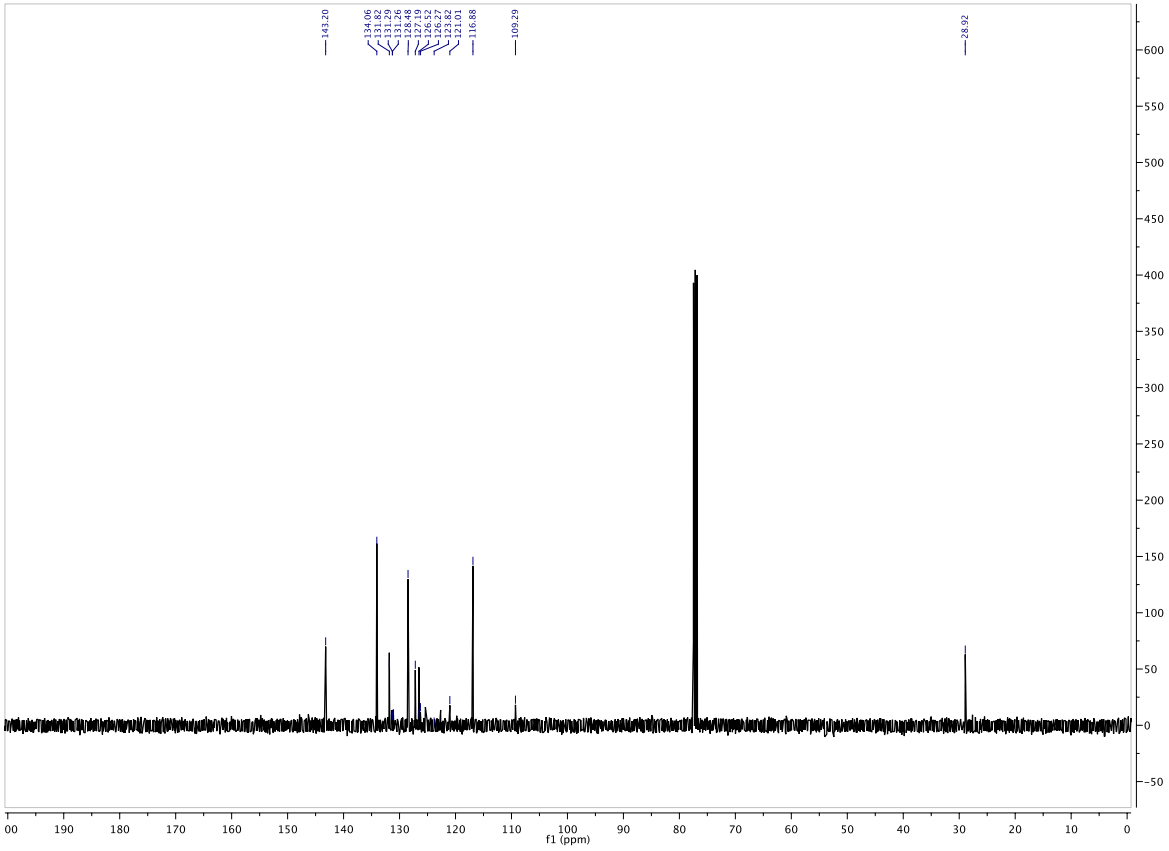

Figure 2.4.22. ^{13}C of 2.2

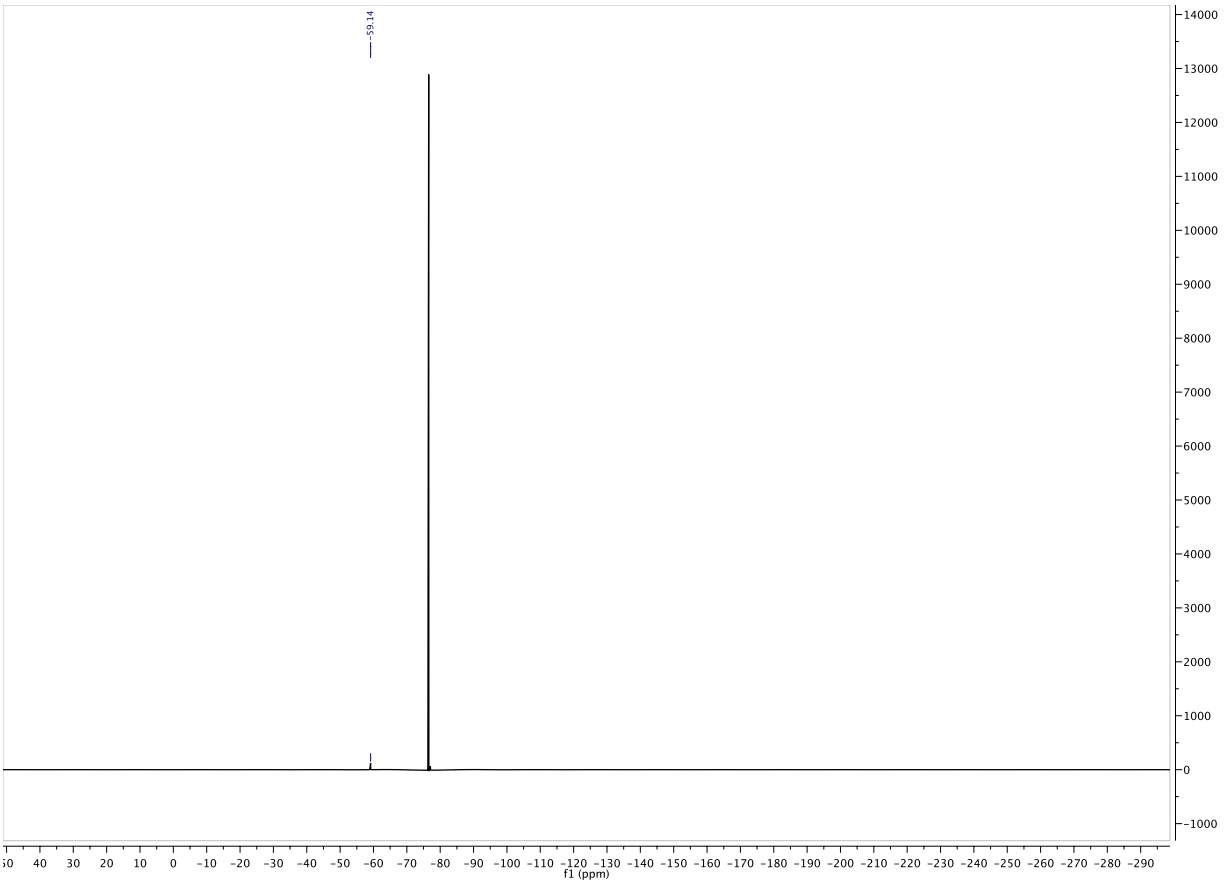

Figure 2.4.23. ^{19}F of 2.2

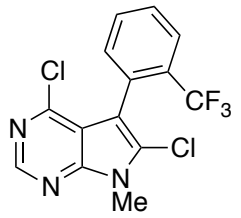

Figure 2.4.24. Product 2.8

4,6-chloro-7-methyl-5-(2-(trifluoromethyl)phenyl)pyrrolopyrimidine (**2.8**): 92% conversion by NMR, and 85% isolated yield as a white solid. R_f: 0.33 (4:1 hexanes:ethyl acetate); ^{1}H NMR (599 MHz, $CDCl_3$) δ 8.64 (s, 1H), 7.81 (d, J = 7.8 Hz, 1H), 7.62 (t, J = 8.5 Hz, 1H), 7.57 (t, J = 7.7 Hz, 1H), 7.37 (d, J = 7.4 Hz, 1H), 3.91 (s, 3H); ^{13}C NMR (151 MHz, $CDCl_3$) δ 150.9 150.8, 150.1, 133.5, 131.4, 131.0 (q, J = 31 Hz.), 129.8 (q, J = 1.8 Hz.), 128.9, 128.5, 126.1 (q, J = 5.2 Hz.), 123.7 (q, J = 273 Hz.), 116.2, 109.0, 29.3; ^{19}F NMR (376 MHz, $CDCl_3$) δ -59.51 (referenced to an external trifluoroacetic acid standard); MS (EI): Calculated $C_{14}H_8Cl_2F_3N_3$ [M] 345.004. Found: 345.007 m/z.

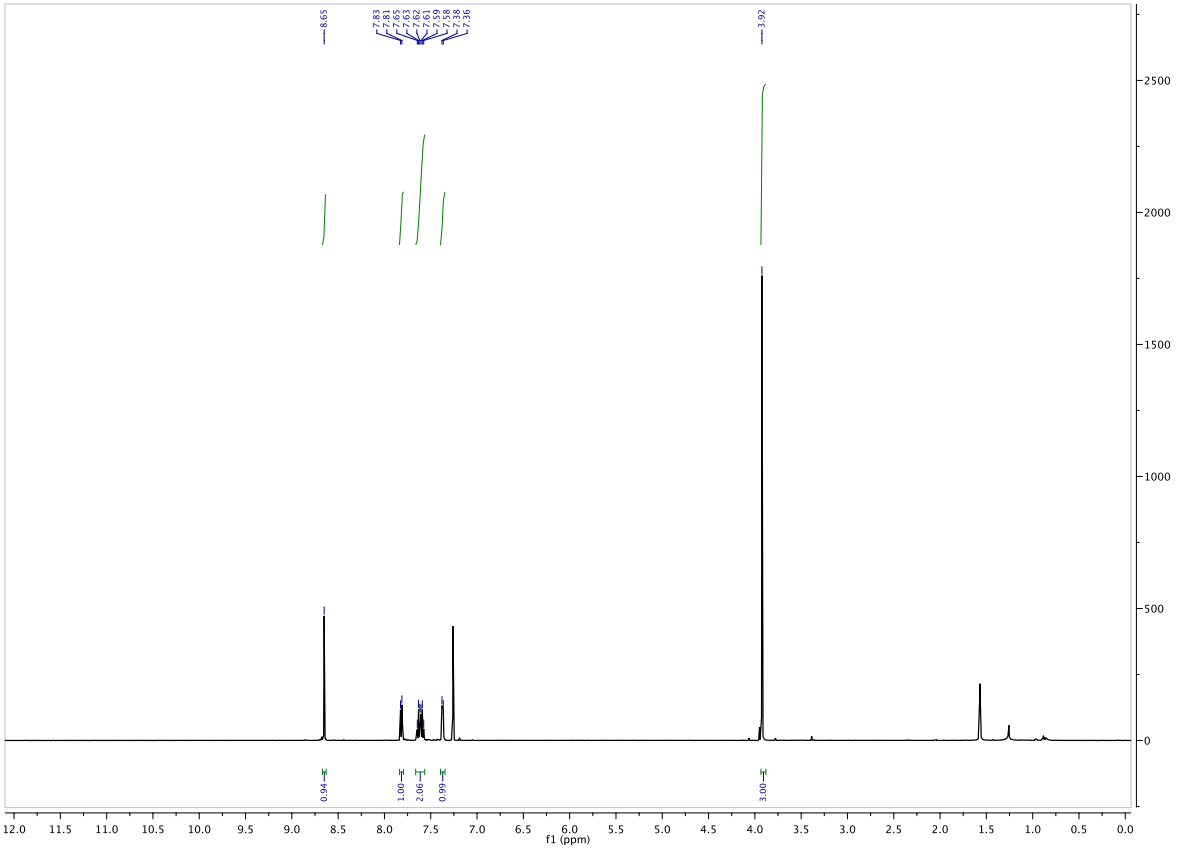

Figure 2.4.25. ^{1}H of 2.8

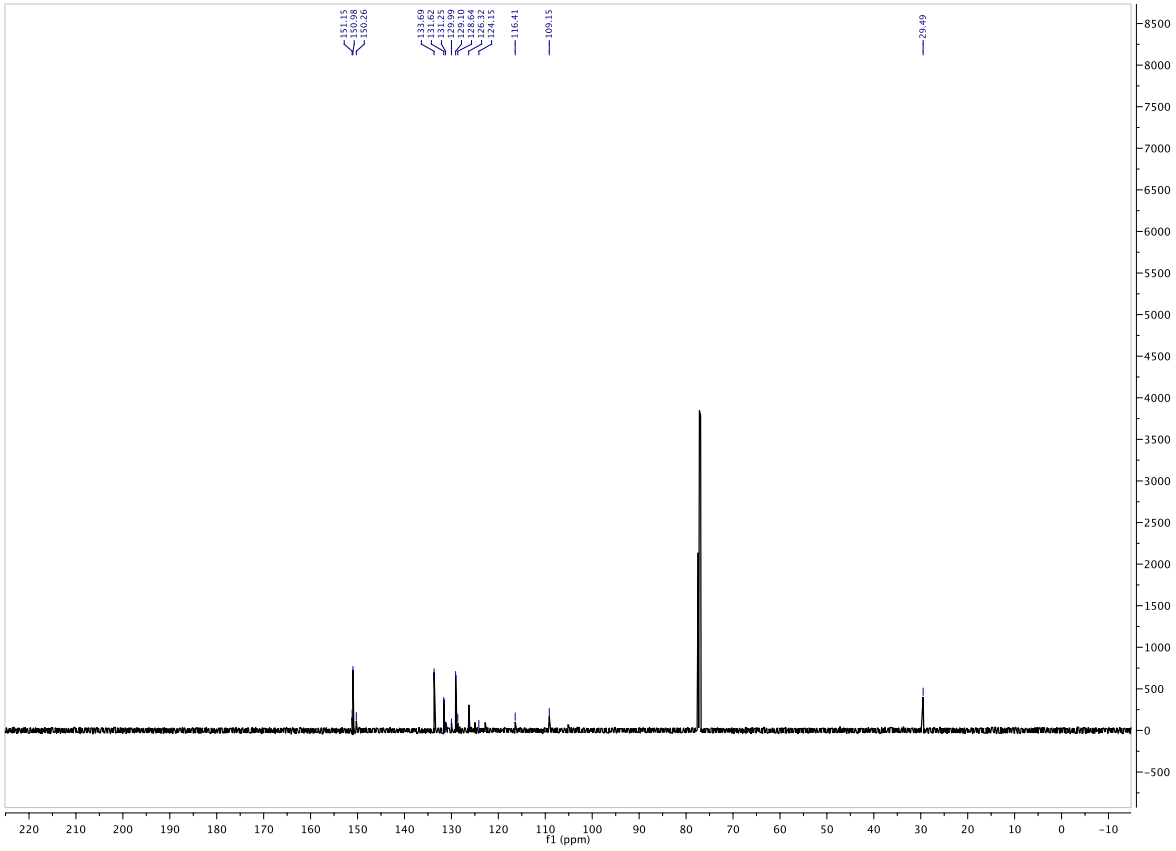

Figure 2.4.26. ^{13}C of 2.8

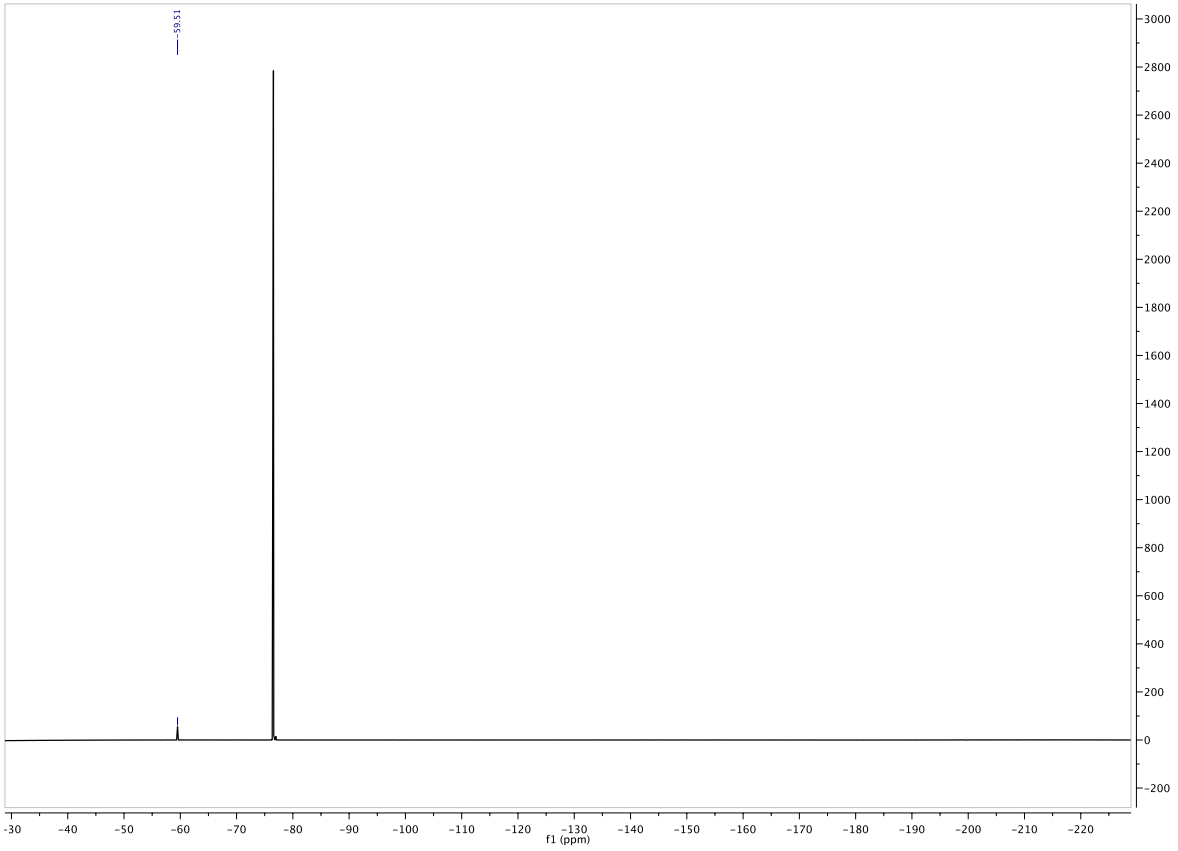

Figure 2.4.27. ^{19}F of 2.8

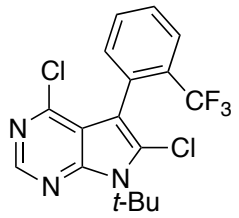

Figure 2.4.28. Product 2.9

7-(tert-butyl)-4,6-dichloro-5-(2-(trifluoromethyl)phenyl)pyrrolopyrimidine (**2.9**): 96% conversion by NMR, and 88% isolated yield as a clear oil. R_f: 0.37 (9:1 hexanes:ethyl acetate); ^{1}H NMR (500 MHz, $CDCl_3$) δ 8.59 (s, 1H), 7.80 (d, J = 7.6 Hz, 1H), 7.62 (t, J = 7.2 Hz, 1H), 7.57 (t, J = 7.4 Hz, 1H), 7.37 (d, J = 7.4 Hz, 1H), 2.03 (s, 9H); ^{13}C (126 MHz, $CDCl_3$) δ 151.50, 150.97, 149.44, 133.59, 131.57, 131.16 (q, J = 30 Hz), 130.96 (q, J = 2.0 Hz), 128.88, 128.73, 126.28 (q, J = 5.2 Hz), 124.06 (q, J = 274 Hz), 116.59, 111.63, 63.74, 31.38; ^{19}F NMR (376 MHz, $CDCl_3$) δ -59.86 (referenced to an external trifluoroacetic acid standard); MS (ESI): Calculated $C_{17}H_{15}Cl_2F_3N_3^+$ [M+H] 388.0590. Found: 388.0604 m/z.

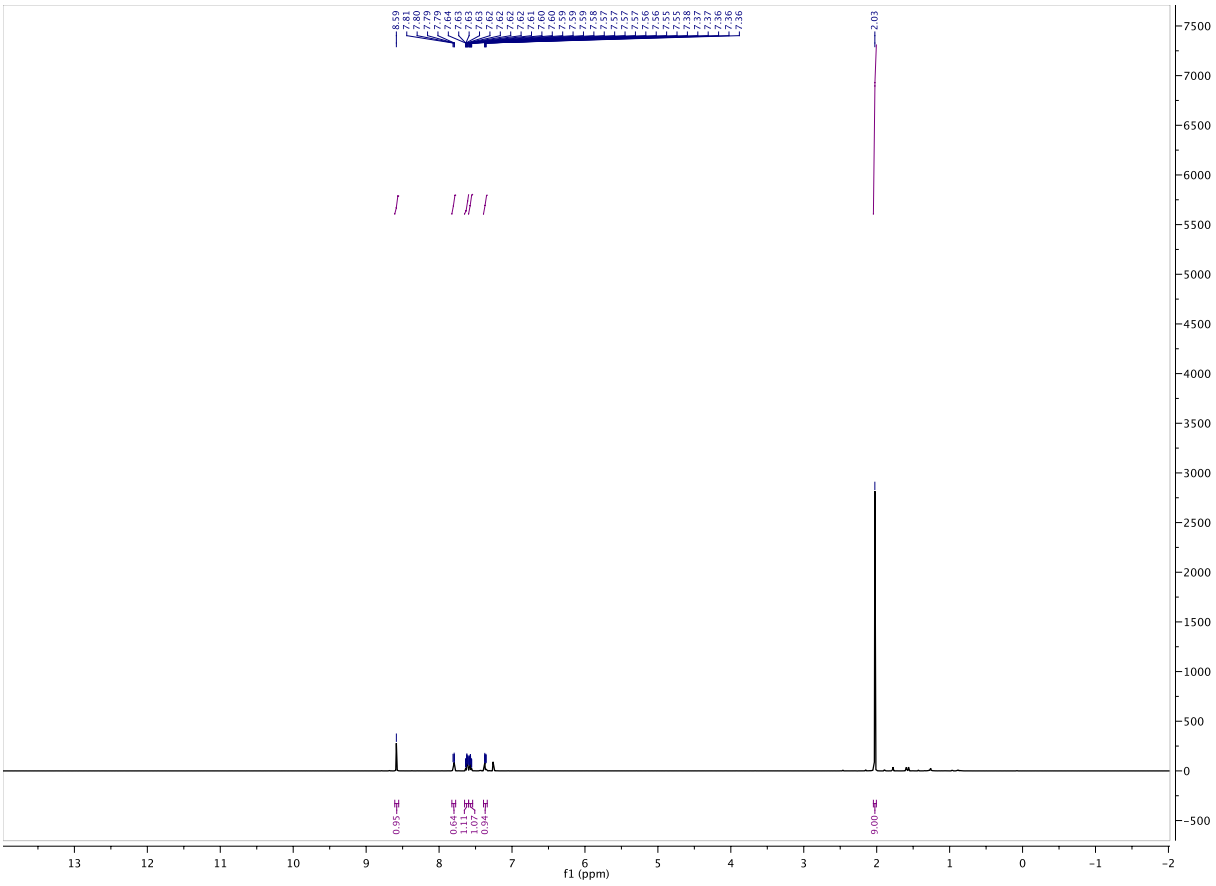

Figure 2.4.29. ^{1}H of 2.9

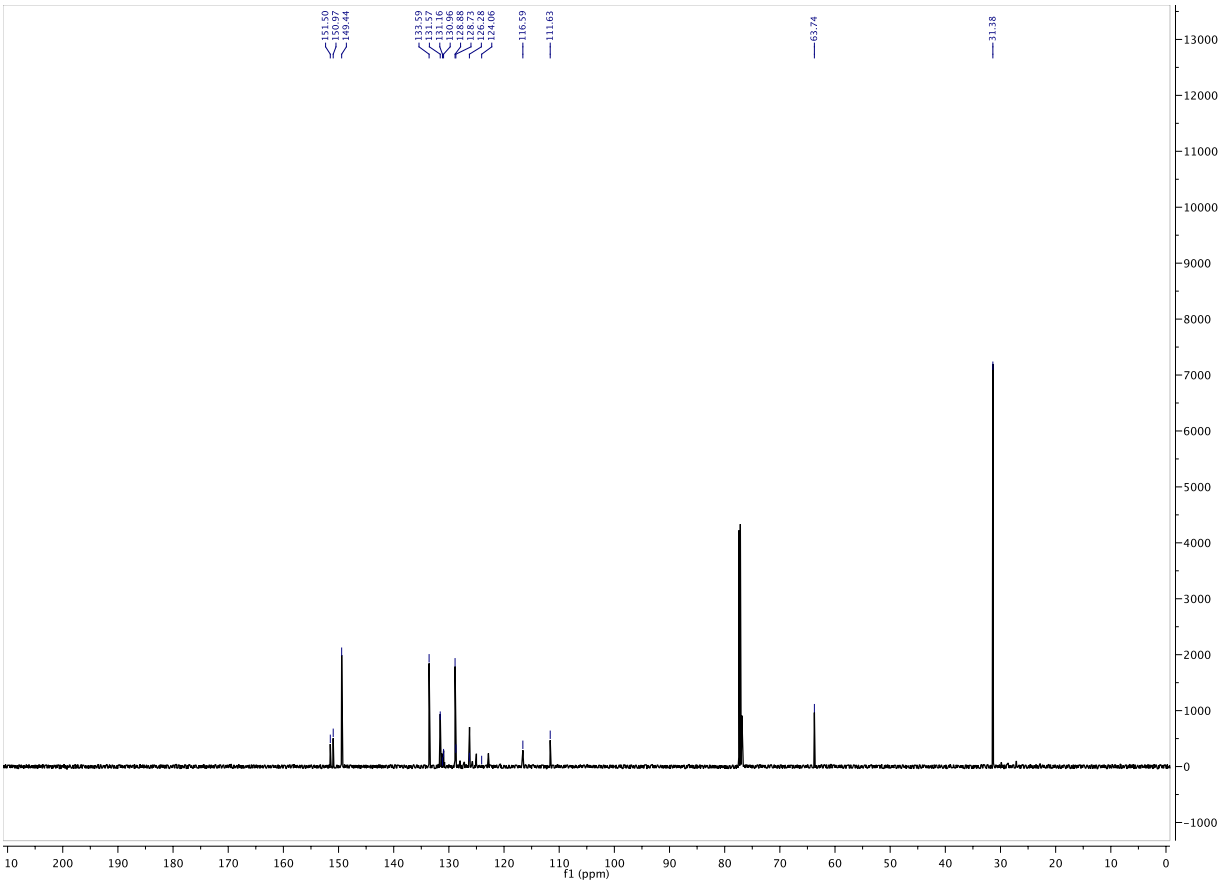

Figure 2.4.30. ^{13}C of 2.9

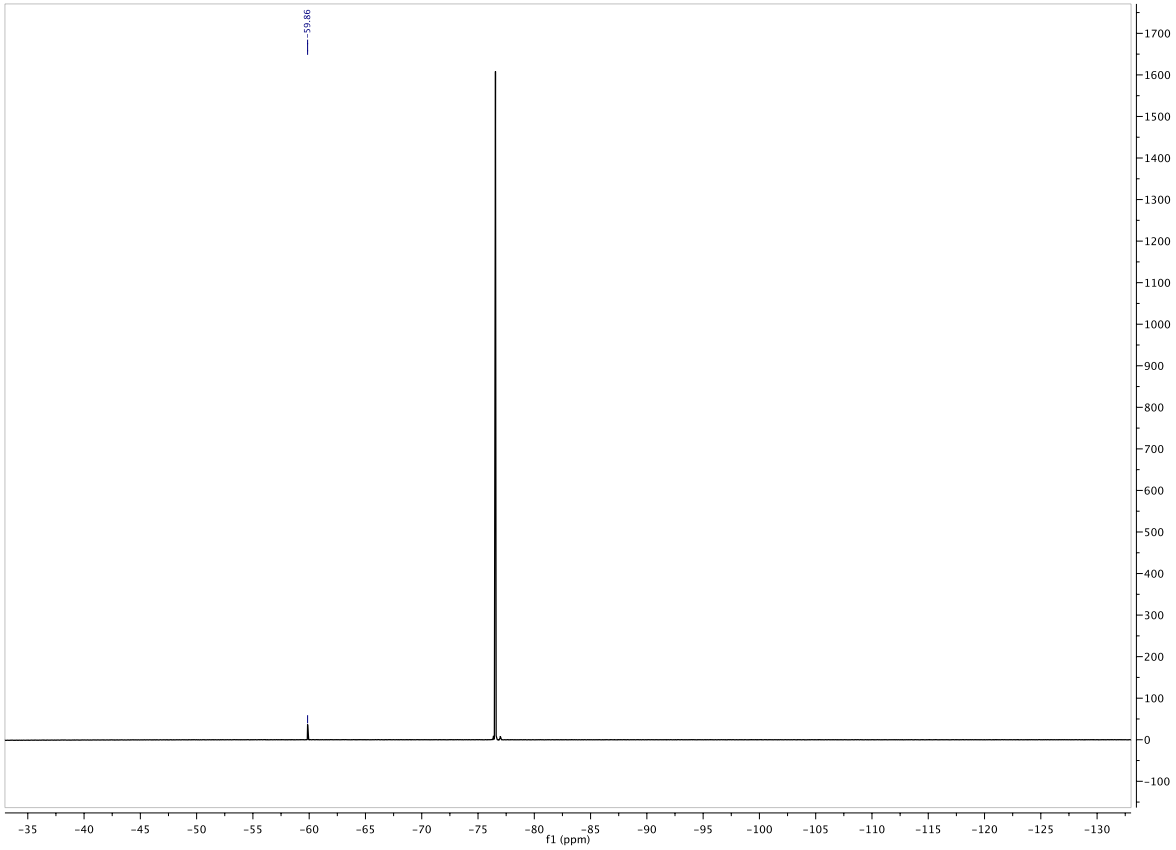

Figure 2.4.31. ^{19}F of 2.9

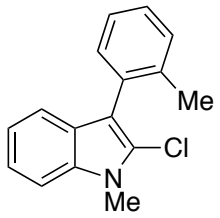

Figure 2.4.32. Product 2.10

2-chloro-3-(2-methylphenyl)-1-methylindole (**2.10**): 86% conversion by NMR, and 81% isolated yield as a clear oil. R_f: 0.40 (95:3 hexanes:ethyl acetate); ^{1}H NMR (599 MHz, $CDCl_3$) δ 7.35-7.24 (m, 7H), 7.11 (t, J = 7.1 Hz, 1H), 3.82 (s, 3H), 2.21 (2, 3H); ^{13}C NMR (126 MHz, $CDCl_3$) δ 138.14, 135.76, 132.55, 131.61, 130.31, 127.74, 127.03, 125.69, 124.04, 122.14, 120.30, 119.52, 113.17, 109.24, 30.17, 20.29; MS (ESI): Calculated $C_{16}H_{15}ClN^+$ [M+H] 256.0888. Found: 256.0897 m/z.

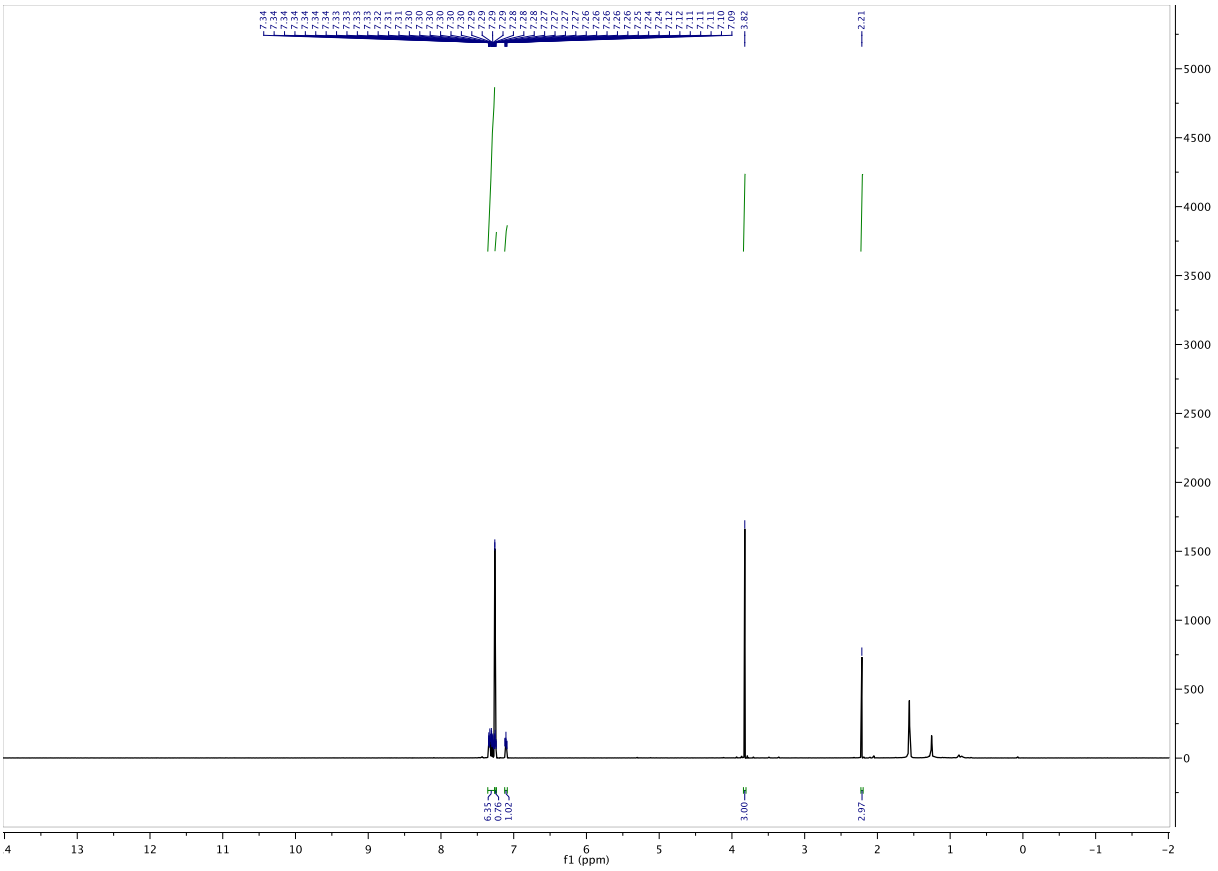

Figure 2.4.33. ^{1}H of 2.10

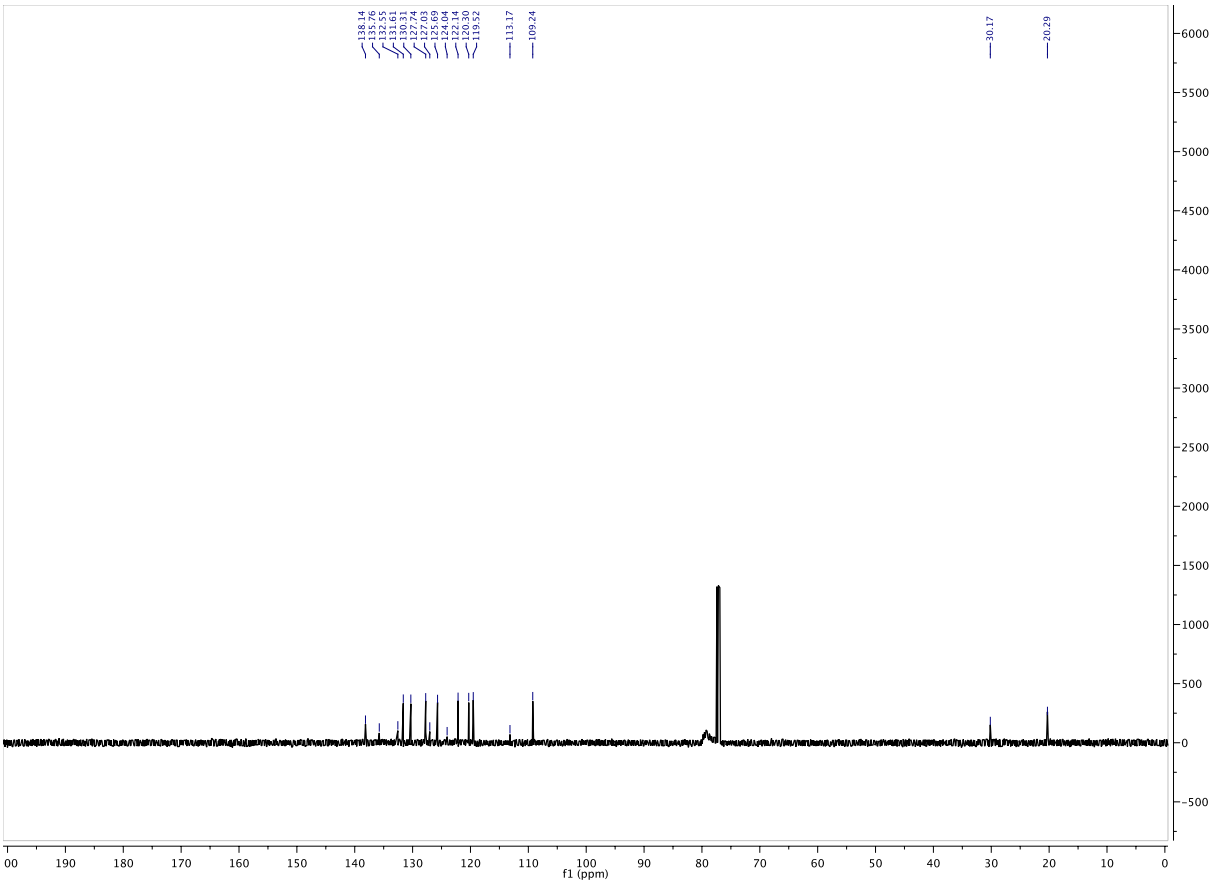

Figure 2.4.34. ^{13}C of 2.10

Figure 2.4.35. Product 2.11

3-chloro-1-methylindole (**2.11**): 83% conversion by NMR, and 70% isolated yield as a yellow oil. R_f: 0.46 (9:1 hexanes:ethyl acetate); ^{1}H NMR (500 MHz, $CDCl_3$) δ 7.63 (d, J = 8.0 Hz, 1H), 7.33-7.26 (m, 2H), 7.19 (t, J = 8.0 Hz, 1H), 7.03 (s, 1H), 3.76 (s, 3H); ^{13}C (126 MHz, $CDCl_3$) δ 136.00, 125.89, 125.36, 122.74, 120.03, 118.51, 109.60, 104.59, 33.07; MS (ESI): Calculated $C_9H_9ClN^+$ [M+H] 166.0418. Found: 166.0415 m/z.

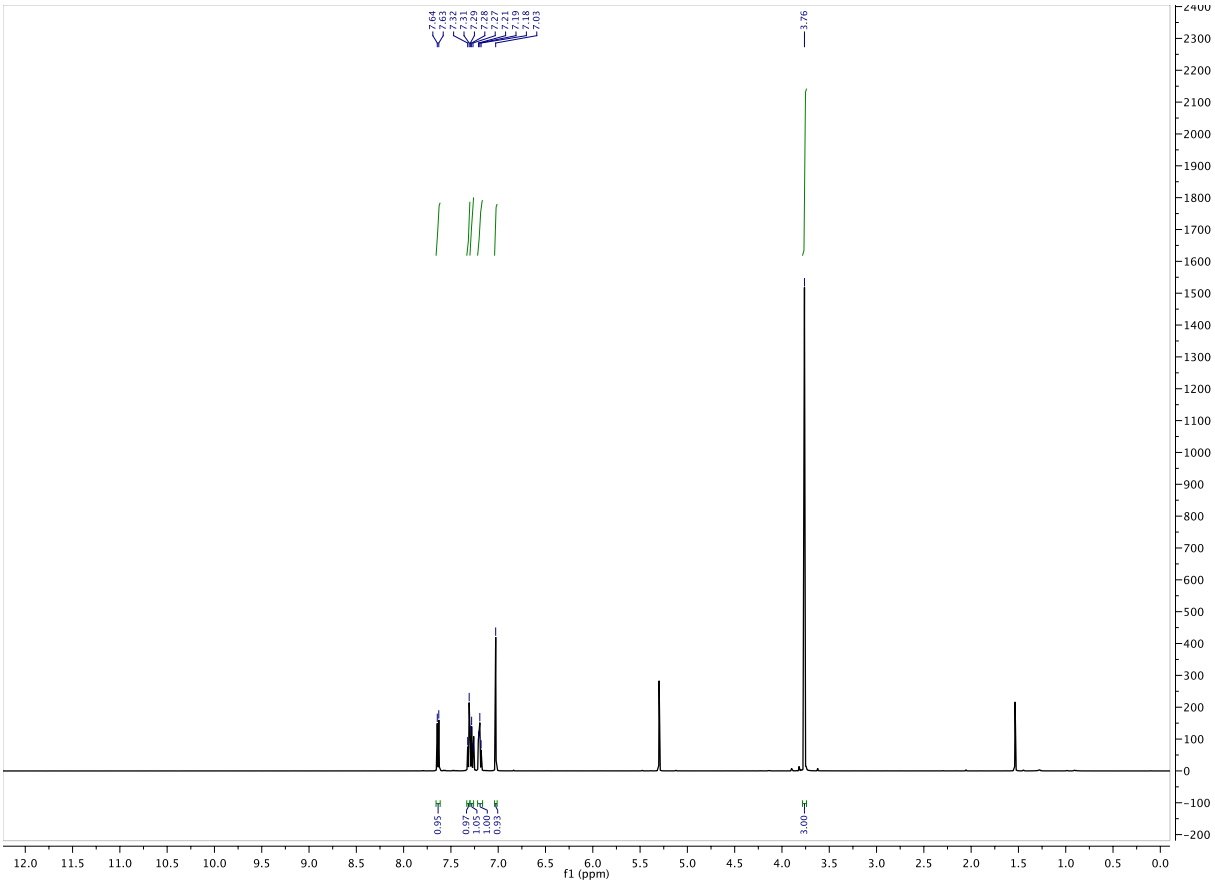

Figure 2.4.36. ^{1}H of 2.11

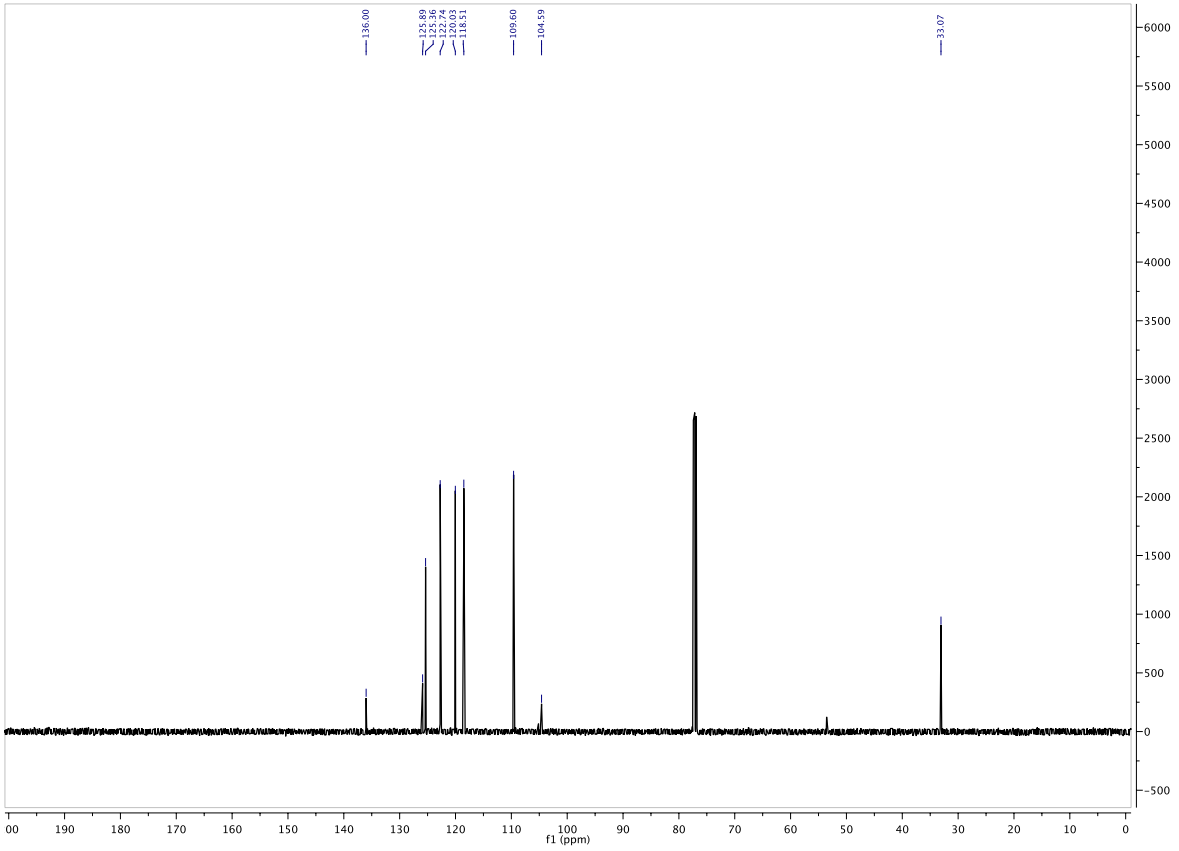

Figure 2.4.37. ^{13}C of 2.11

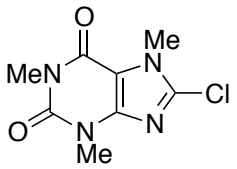

Figure 2.4.38. Product 2.12

8-chloro-1,3,7-trimethylpurinedione (**2.12**): 84% conversion by NMR, and 70% isolated yield as a white solid. R_f: 0.07 (4:1 hexanes:ethyl acetate); ^{1}H NMR (400 MHz, $CDCl_3$:CD_3OD::9:1) δ 3.94 (s, 3H), 3.53 (s, 3H), 3.38 (s, 3H); ^{13}C NMR (101 MHz, $CDCl_3$:CD_3OD: 9:1) δ 154.70, 151.42, 147.19, 139.12, 108.38, 32.82, 29.96, 28.13. MS (ESI): Calculated $C_8H_9ClN_4O_2^+$ [M+H] 229.0487. Found: 229.0487 m/z.

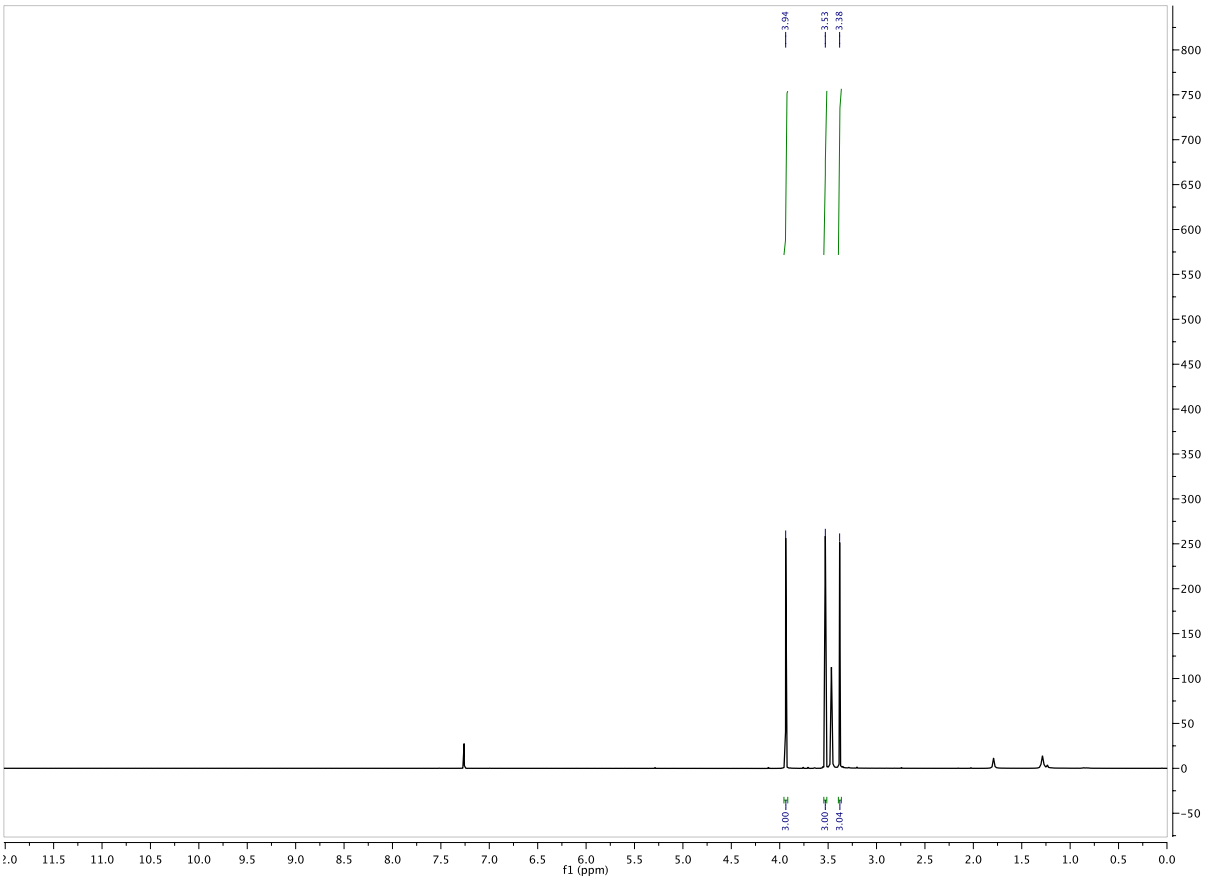

Figure 2.4.39. ^{1}H of 2.12

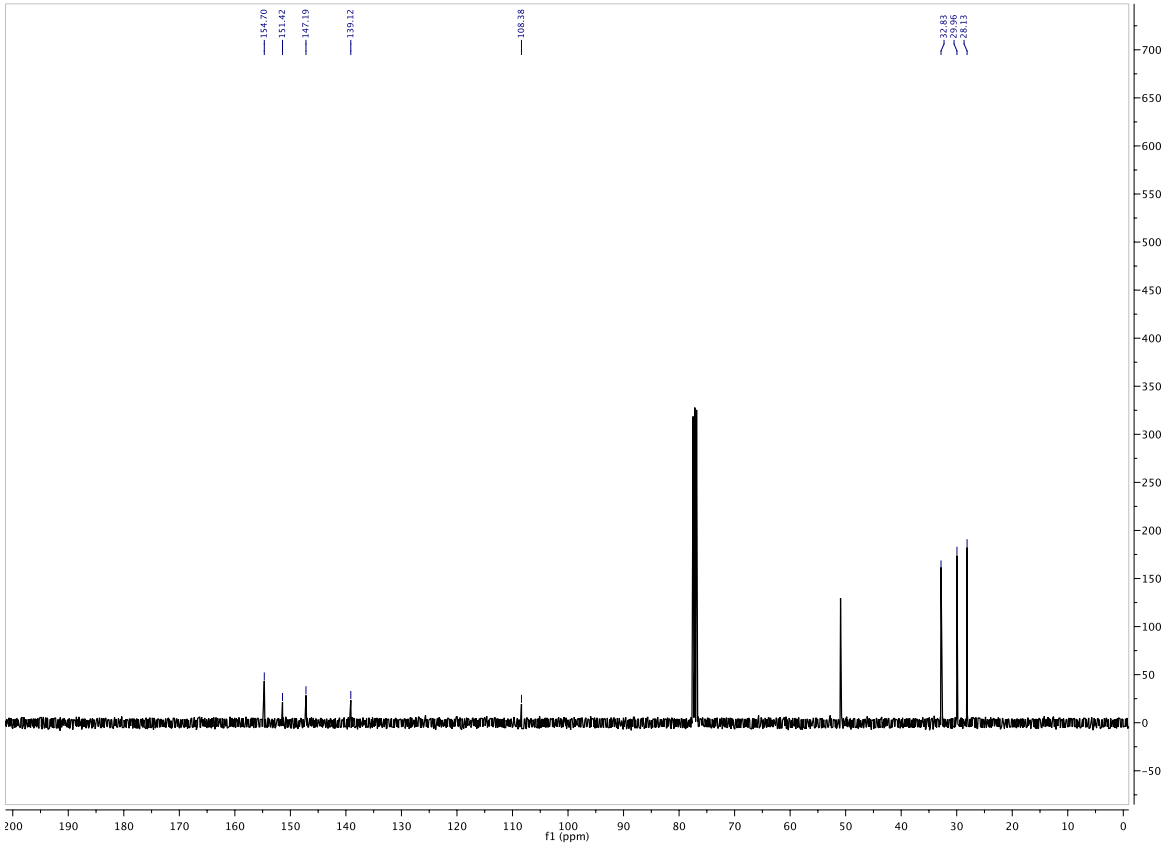

Figure 2.4.40. ^{13}C of 2.12

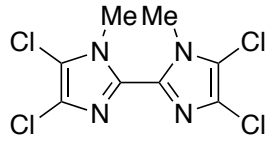

Figure 2.4.41. Product 2.13

4,4',5,5'-tetrachloro-1,1'-dimethyl-2,2'-biimidazole (**2.13**): 4.2 equiv. of NCS was used instead of 1.2 equiv. 54% conversion by NMR, and 51% isolated yield as a white solid. R_f: 0.47 (9:1 hexanes:ethyl acetate); ^{1}H NMR (400 MHz, $CDCl_3$) δ 3.96 (s, 6H); ^{13}C NMR (101 MHz, $CDCl_3$) δ 134.77, 125.61, 116.60, 22.96. MS (ESI): Calculated $C_8H_6Cl_4N_4^+$ [M+H] 298.9419. Found: 298.9420 m/z.

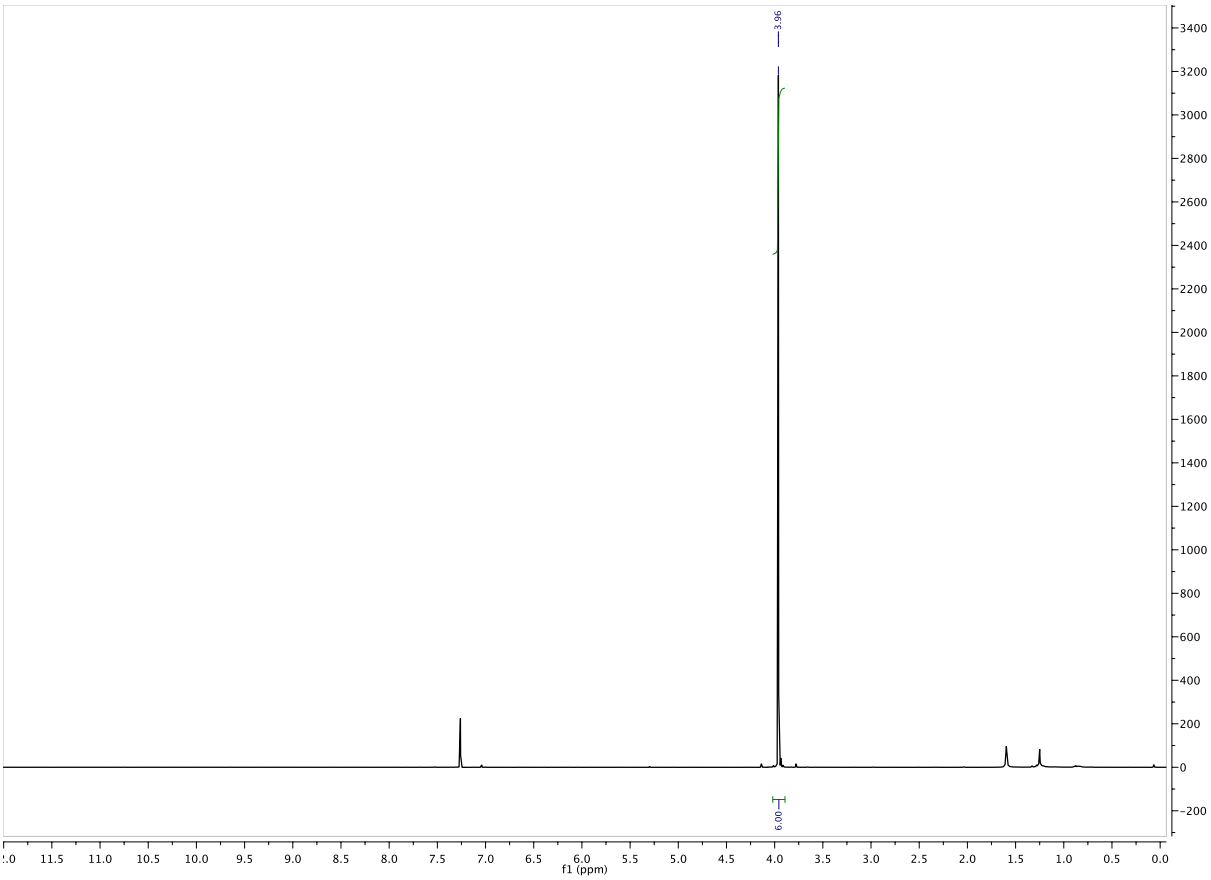

Figure 2.4.42. ^{1}H of 2.13

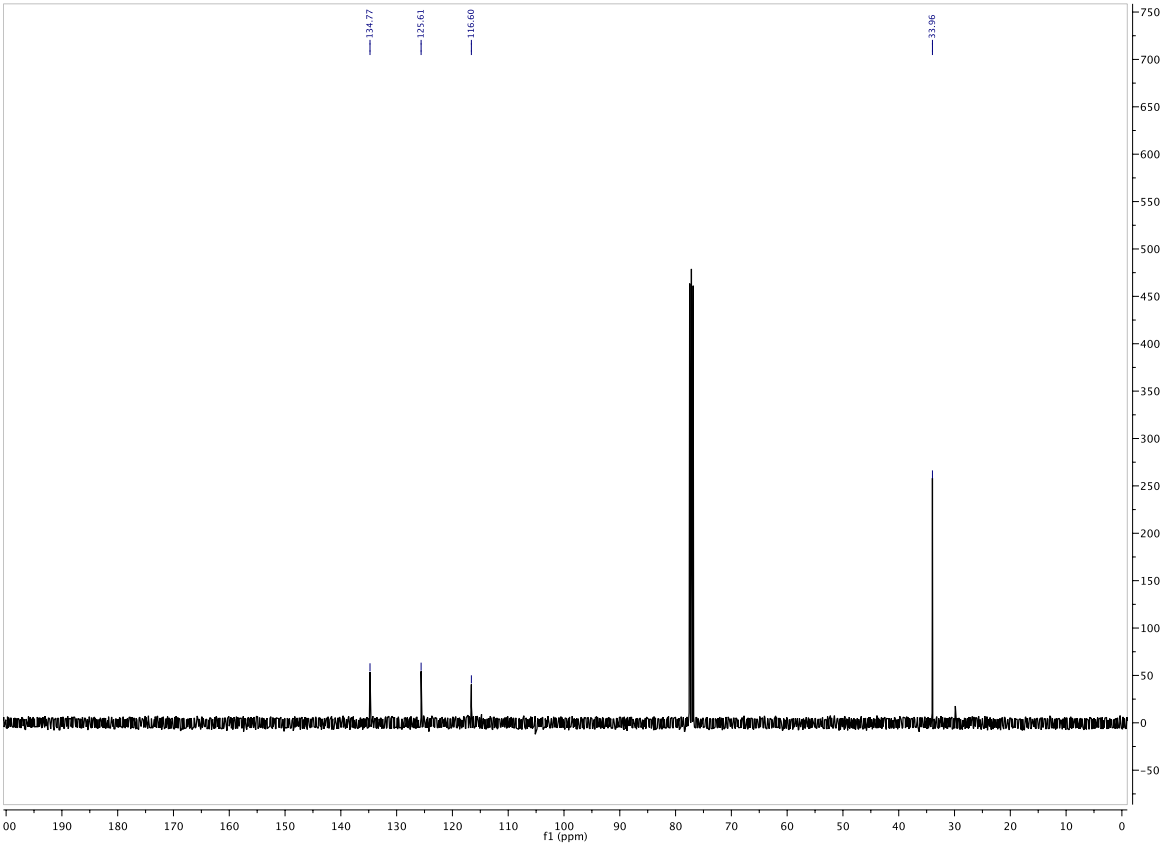

Figure 2.4.43. ^{13}C of 2.13

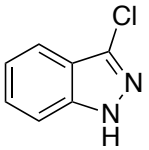

Figure 2.4.44. Product 2.14

3-chloroindazole (**2.14**): 60% conversion by NMR, and 60% isolated yield as a white solid. R_f: 0.23 (4:1 hexanes:ethyl acetate). NMR data match standard available from Sigma Aldrich.

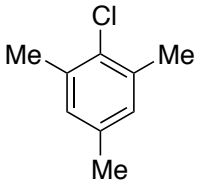

Figure 2.4.45. Product 2.15

2-chloro-1,3,5-trimethylbenzene (**2.15**): 60% conversion by NMR. NMR data match the data reported in literature: Prebil, R.; Laali, K.K.; Stavber, S. Org. Lett. 2013, Vol. 15, No. 9, 2108-2111.

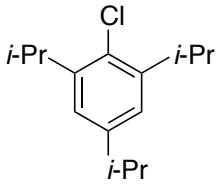

Figure 2.4.46. Product 2.16

2-chloro-1,3,5-triisopropylbenzene (**2.16**): 60% conversion by NMR. NMR data match the data reported in literature: Muraki, T.; Togo, H; Yokoyama, M. J. Org. Chem. 1999, 64, 2883-2889.

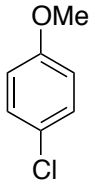

Figure 2.4.47. Product 2.17a

4-chloroanisole (**2.17a**): 78% conversion by NMR. NMR data match the data reported in literature: Molander, G.A.; Cavacanti, L.N. J. Org. Chem. 2011, 76, 7195-7203.

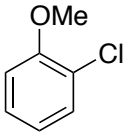

Figure 2.4.48. Product 2.17b

2-chloroanisole (**2.17b**): 5% conversion by NMR. NMR data match the data reported in literature: Wu, H.; Hynes, J. Jr. Org. Lett., 2010, Vol. 12, No. 6, 1192-1195.

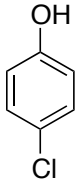

Figure 2.4.49. Product 2.18

4-chlorophenol (**2.18**): 78% conversion by NMR, and 52% isolated yield as a white solid. NMR data match the data reported in literature: Lavery, C.B.; Rotta-Loria, N.L.; McDonald, R.; Stradiotto *Adv. Syn. Cat.* **2013**, *355*, 981-987.

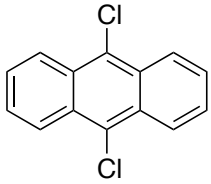

Figure 2.4.50. Product 2.19

9,10-dichloroanthracene (**2.19**): 84% conversion by NMR, and 62% isolated yield as a yellow fibrous solid. R_f: 0.58 (100% hexanes); NMR data match the data reported in literature: Kuwahara, Y.; Zhang, A.; Soma, H.; Tsuda, A. *Org. Lett.* **2013**, *15*, 3376-3379.

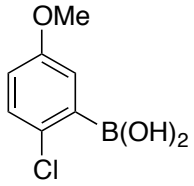

Figure 2.4.51. Product 2.20

(2-chloro-5-methoxyphenyl)boronic acid (**2.20**): A 9:1 mixture of chloroform-D:methanol-D was used as the solvent. 91% conversion by NMR, and 86% isolated yield as a white solid. R_f: 0.21 (4:1 hexanes:ethyl acetate); NMR data are identical to NMR spectra obtained from a standard purchased from Sigma Aldrich.

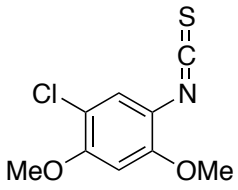

Figure 2.4.52. Product 2.21

1-chloro-5-isothiocyanato-2,4-dimethoxybenzene (**2.21**): 91% conversion by NMR, and 91% isolated yield as a white solid. R_f: 0.21 (9:1 hexanes:ethyl acetate); ^{1}H NMR (599 MHz, $CDCl_3$) δ 7.11 (s, 1H), 6.48 (s, 1H), 3.92 (s, 3H), 3.91 (s, 3H); ^{13}C NMR (151 MHz, $CDCl_3$) δ

155.98, 154.91, 140.40, 126.41, 113.73, 113.61, 96.97, 56.66, 56.54. MS (ESI): Calculated nominal mass [M+H] 230. Found: 230. m/z. It should be noted, while the nominal mass of 230 was observed (230:232 = 3:1 due to chlorine's isotopic ratio) significant parent molecule-solvent by-products and fragmentation patterns were observed using methanol as the solvent.

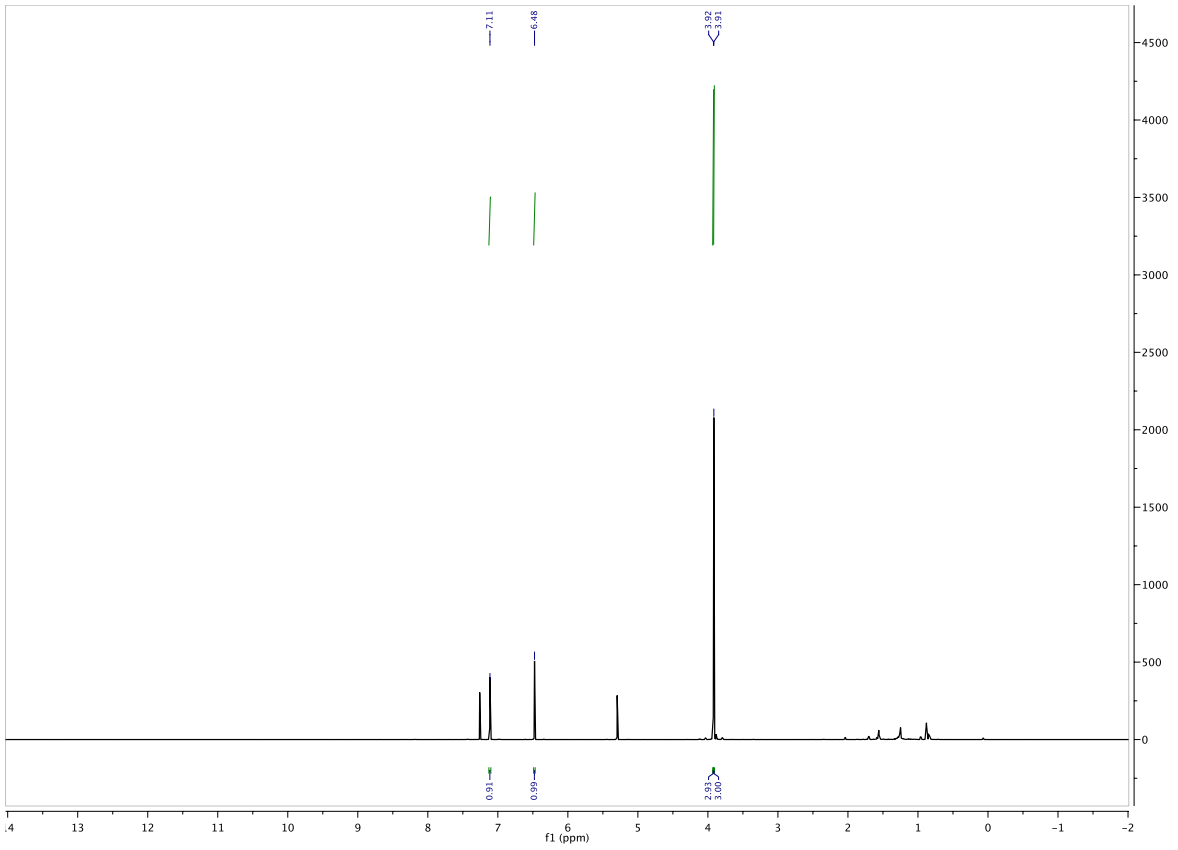

Figure 2.4.53. ^{1}H of 2.21

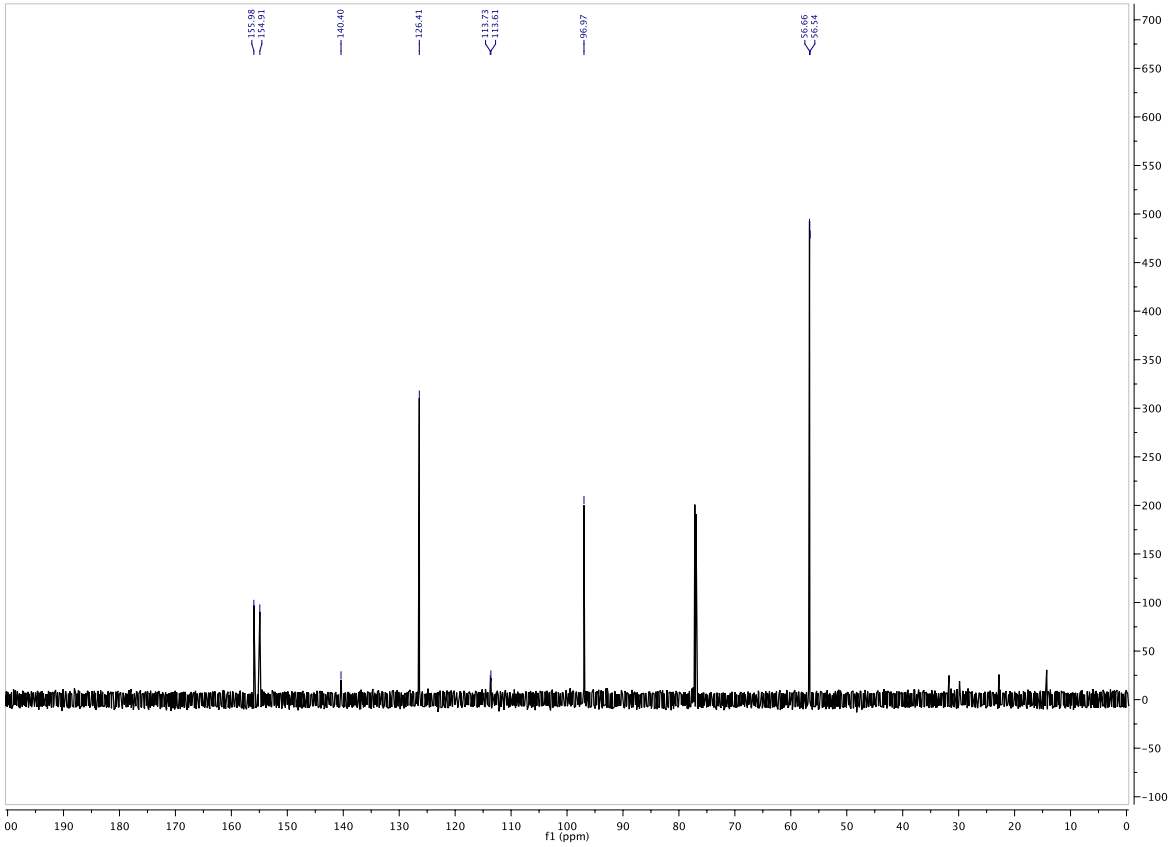

Figure 2.4.54. ^{13}C of 2.21

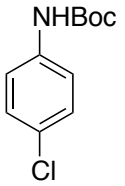

Figure 2.4.55. Product 2.22

tert-butyl (4-chlorophenyl)carbamate (**2.22**): 75% conversion by NMR, and 70% isolated yield as a white solid. R_f: 0.35 (9:1 hexanes:ethyl acetate). NMR data match the data reported in literature: Sarkar, A.; Roy, S.R.; Parikh, N.; Chakraborti, A.K. *J. Org. Chem.* **2011**, *76*, 7132-7140.

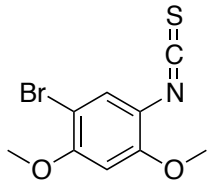

Figure 2.4.56. Product 2.23

1-bromo-5-isothiocyanato-2,4-dimethoxybenzene (**2.23**): 85% conversion by NMR, and 84% isolated yield as a white solid. R_f: 0.21 (9:1 hexanes:ethyl acetate); ^{1}H NMR (500 MHz, $CDCl_3$) δ 7.28 (s, 1H), 6.47 (s, 1H), 3.92 (s, 3H), 3.91 (s, 3H); ^{13}C NMR (126 MHz, $CDCl_3$) δ 156.62, 155.91, 140.44, 129.34, 114.40, 101.56, 96.92, 56.78, 56.53. NMR data was compared to that of **2.21**.

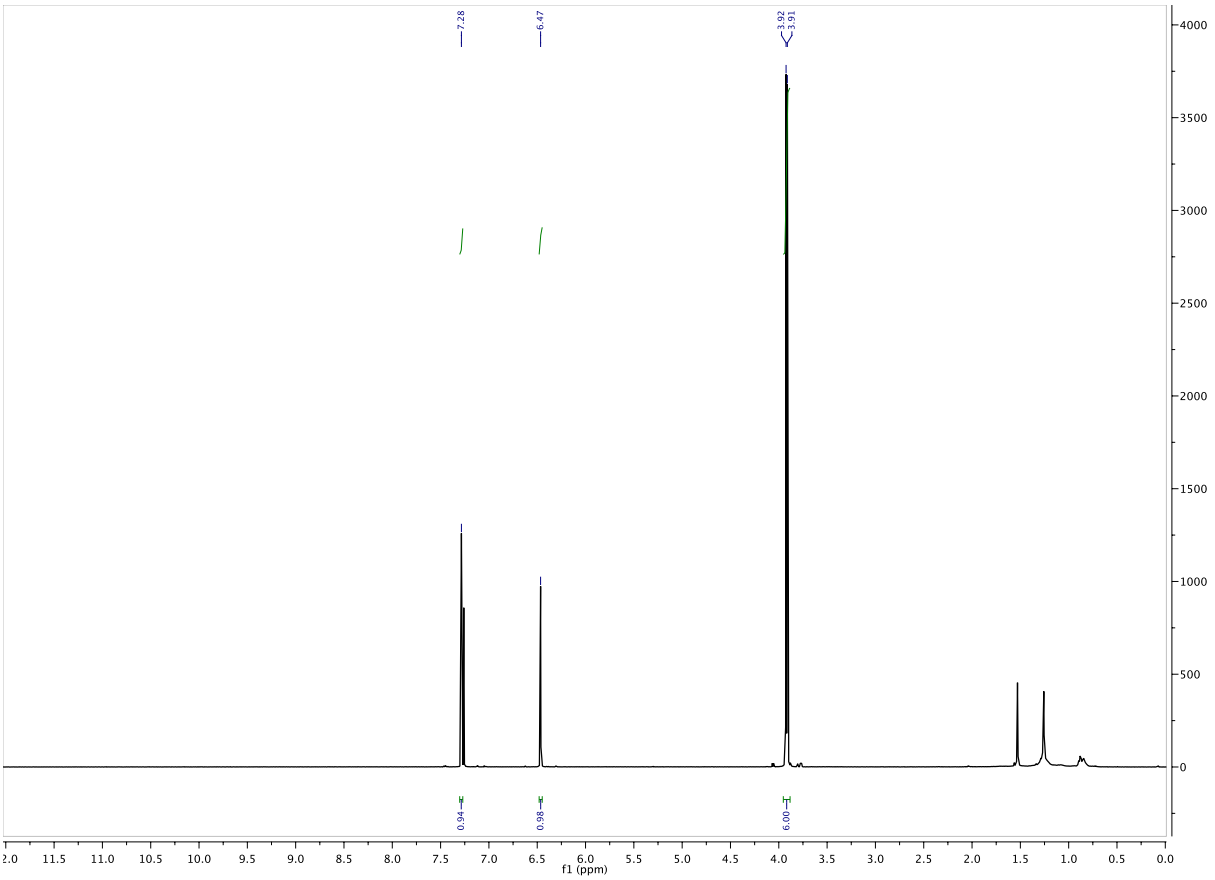

Figure 2.4.57. ^{1}H of 2.23

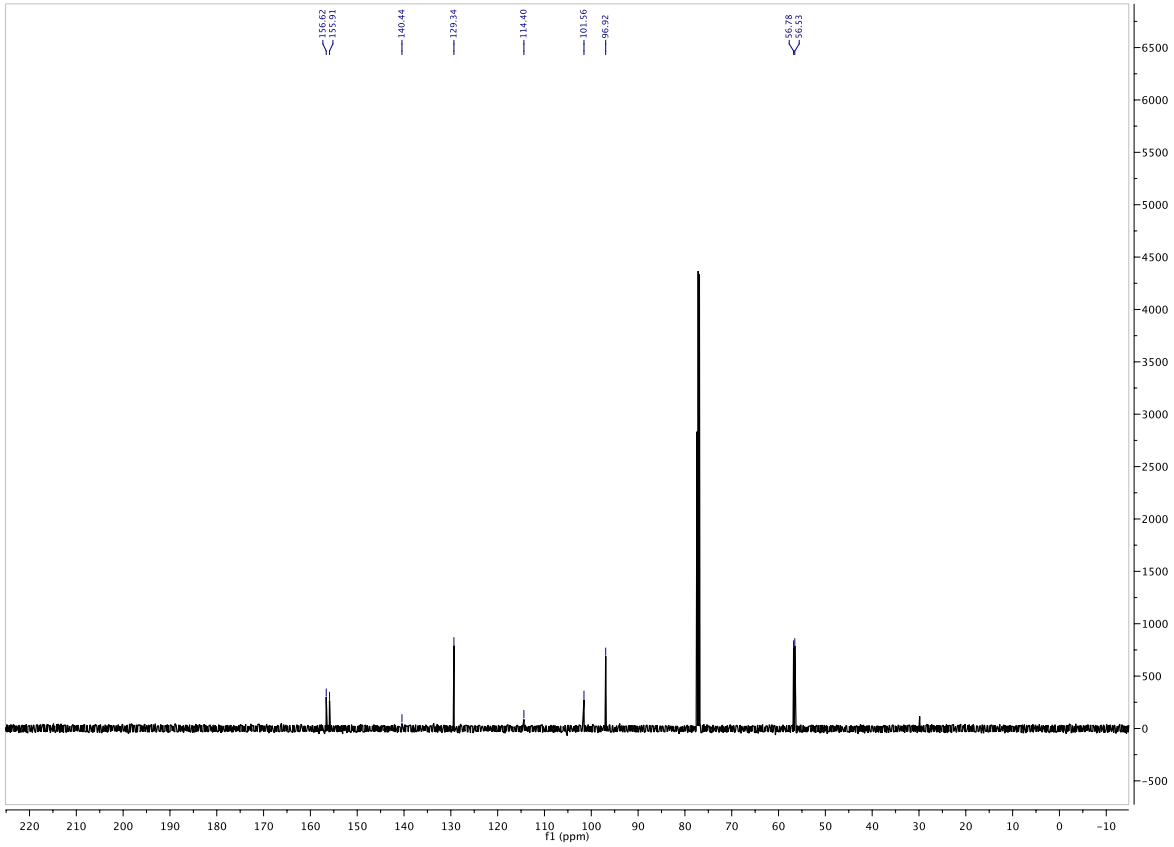

Figure 2.4.58. ^{13}C of 2.23

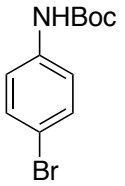

Figure 2.4.59. Product 2.24

tert-butyl (4-bromophenyl)carbamate (**2.24**): 86% conversion by NMR, and 86% isolated yield as a white solid. R_f: 0.37 (9:1 hexanes:ethyl acetate); NMR data match the data reported in literature: Roosen, P.C.; Kallepalli, V.A.; Chattopadhyay, B.; Singleton, D.A.; Maleczka, R.E. Jr.; Smith, M.R. III *J. Am. Chem. Soc.* **2012**, *134*, 11350-11353.

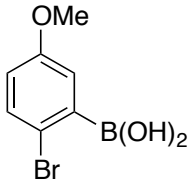

Figure 2.4.60. Product 2.25

(2-bromo-5-methoxyphenyl)boronic acid (**2.25**): A 9:1 mixture of chloroform-D:methanol-D was used as the solvent. 93% conversion by NMR, and 84% isolated yield as a white solid. R_f: 0.29 (4:1 hexanes:ethyl acetate); ^{1}H NMR (500 MHz, d6-DMSO) δ 8.27 (s, 2H), 7.39 (d, J = 8.7 Hz, 1H), 6.89 (d, J = 3.1 Hz, 1H), 6.83 (dd, J = 8.7 Hz, 3.1 Hz, 1H), 3.73 (s, 3H); ^{13}C NMR (126 MHz, d6-DMSO) δ 157.75, 132.30, 118.86, 115.95, 115.41, 55.27. ^{11}B NMR (160 MHz, $CDCl_3$) δ 29.10. ^{11}B Spectra referenced to external BF_3-Et_2O standard. Regioselectivity was determined by analogy to **2.20** (analysis of coupling constants).

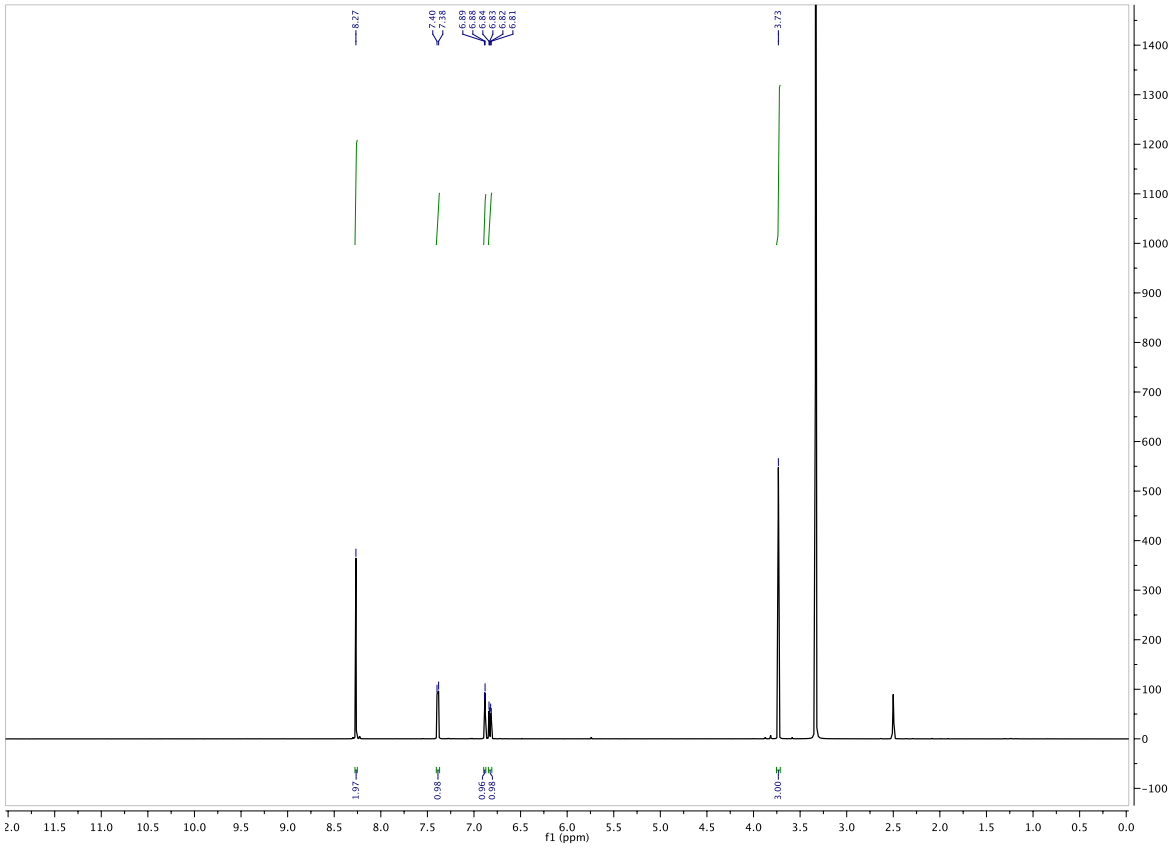

Figure 2.4.61. ^{1}H of 2.25

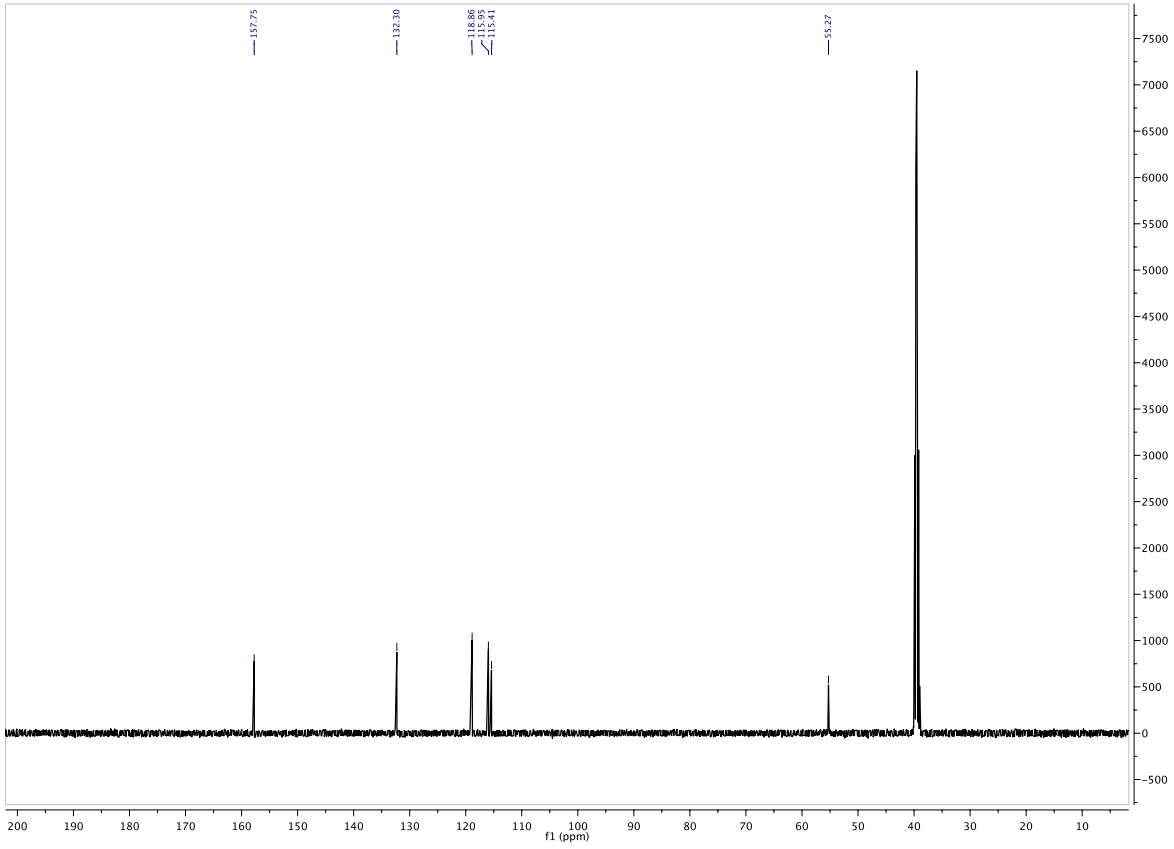

Figure 2.4.62. ^{13}C of 2.25

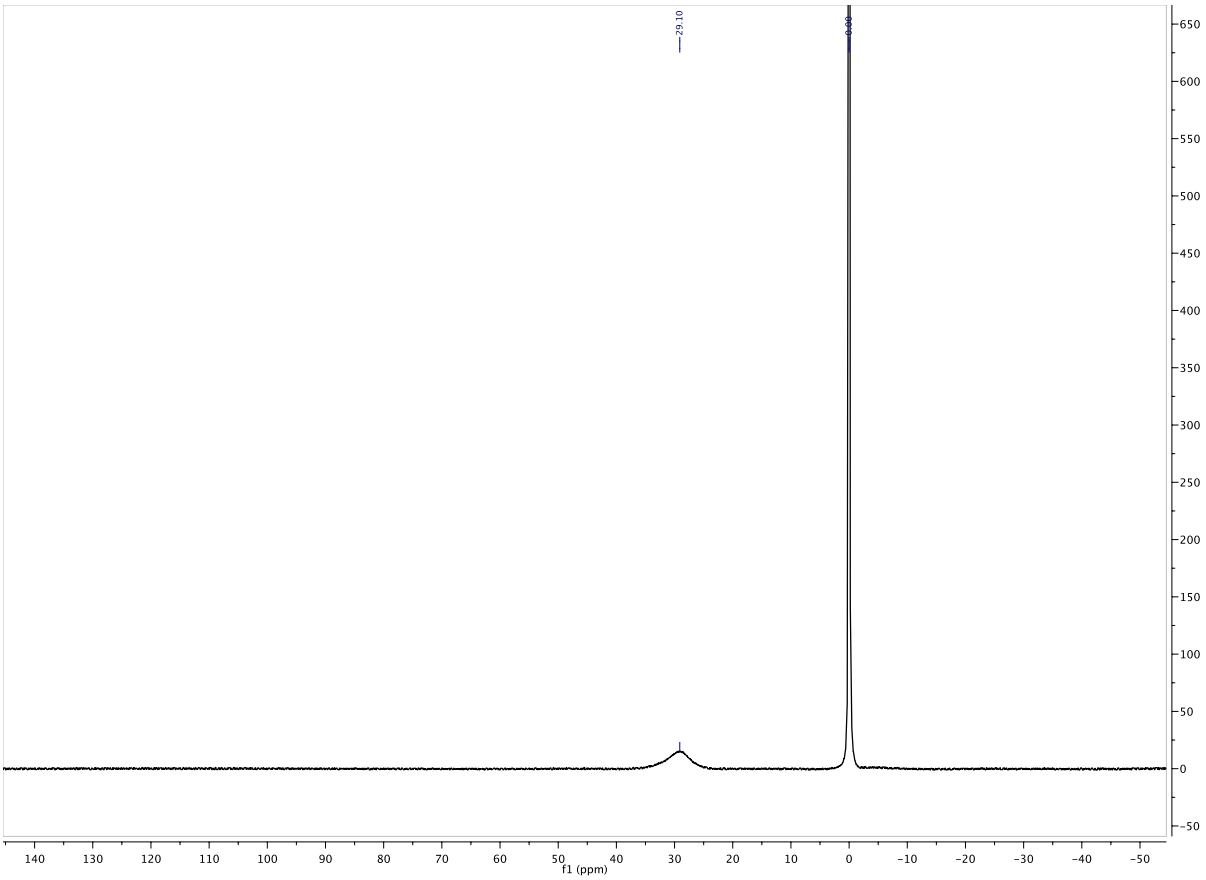

Figure 2.4.63. ^{11}B of 2.25

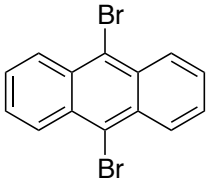

Figure 2.4.64. Product 2.26

9,10-dibromoanthracene (**2.26**): 99% conversion by NMR, and 68% isolated yield as a yellow fibrous solid. R_f: 0.62 (100% hexanes). NMR data match the data reported in literature: Chien, W.-L.; Yang, C.-M.; Chen, T.-L.; Li, S.-T.; Hong, J.-L. *RSC Adv.* **2013**, *3*, 6930-6938.

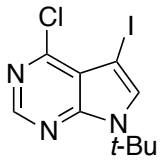

Figure 2.4.65. Product 2.27

7-(*tert*-butyl)-4-chloro-5-iodopyrrolopyrimidine (**2.27**): *N*-iodosuccinimide was used instead of N-chlorosuccinimide. 81% conversion by NMR, and 75% isolated yield as a yellow oil. R_f: 0.31 (9:1 hexanes:ethyl acetate); ^{1}H NMR (600 MHz, $CDCl_3$) δ 8.58 (s, 1H), 7.48 (s, 1H), 1.76 (s, 9H); ^{13}C NMR (151 MHz, $CDCl_3$) δ 152.55, 150.77, 149.53, 132.88, 118.15, 58.94, 49.39, 29.29; MS (ESI): Calculated $C_{10}H_{12}ClIN_3^+$ [M+H] 335.97. Found: 335.93 m/z.

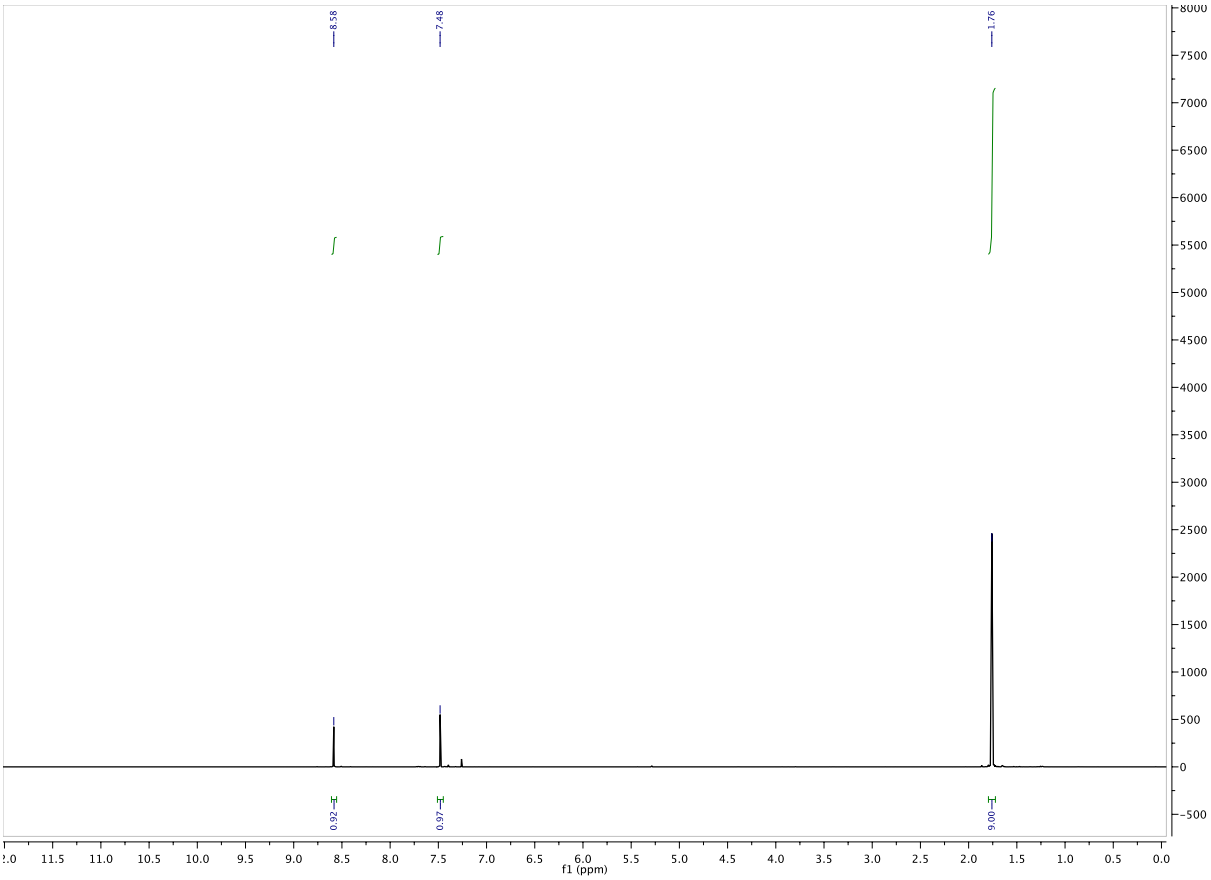

Figure 2.4.66. ^{1}H of 2.27

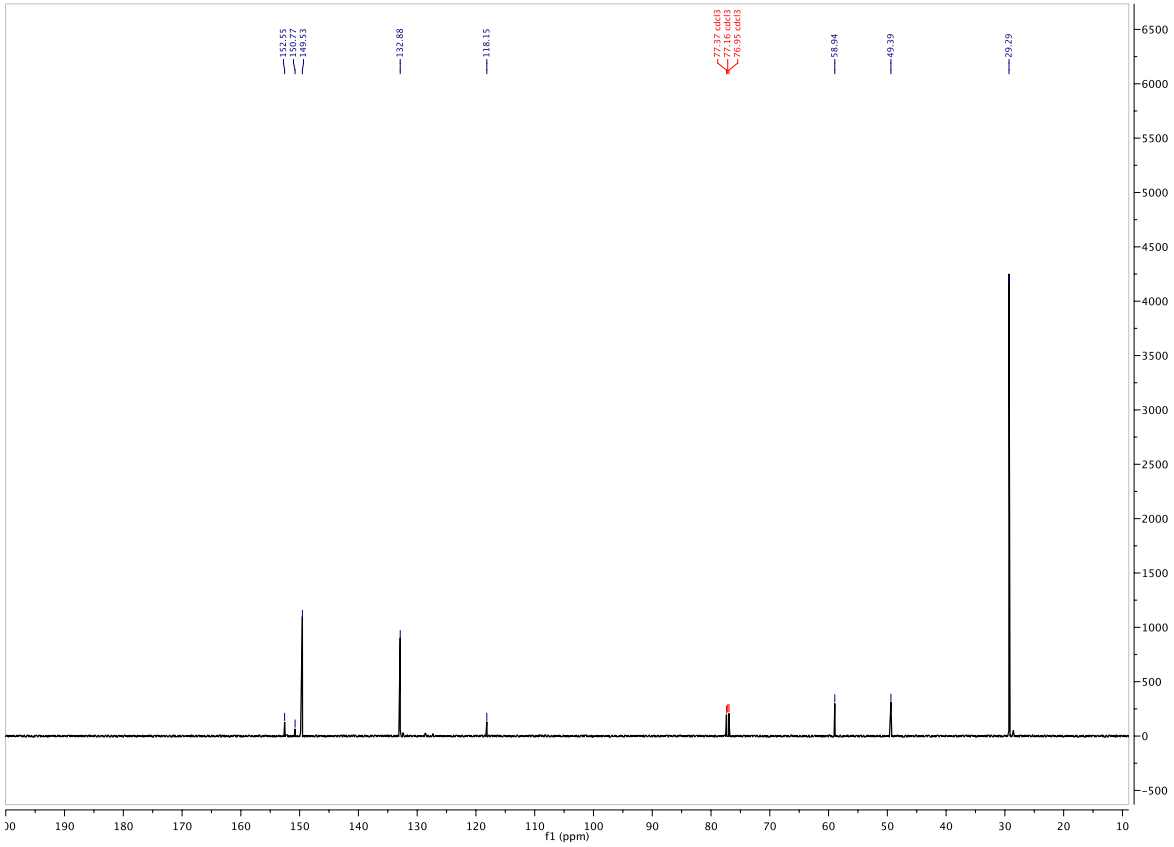

Figure 2.4.67. ^{13}C of 2.27

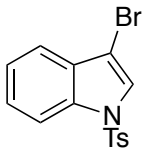

Figure 2.4.68. Product 2.28

3-bromo-1-tosylindole (**2.28**): 93% conversion by NMR, and 92% isolated yield as a white solid. R_f: 0.70 (4:1 hexanes:ethyl acetate); ^{1}H NMR (599 MHz, $CDCl_3$) δ 7.99 (d, J = 8.3 Hz, 1H), 7.77 (d, J = 8.4 Hz, 2H), 7.62 (s, 1H), 7.49 (d, J = 7.8 Hz, 1H), 7.37 (t, J = 7.0 Hz, 1H), 7.31 (t, J = 6.9 Hz, 1H), 7.23 (d, J = 8.6, Hz, 2H), 2.35 (s, 3H); ^{13}C NMR (126 MHz, $CDCl_3$) δ 145.48, 135.09, 134.46, 130.17, 129.93, 127.07, 125.88, 124.95, 124.02, 120.20, 113.76, 99.74, 21.73; MS (ESI): Calculated $C_{15}H_{13}BrNO_2S^+$ [M+H] 349.9845. Found: 349.9848 m/z.

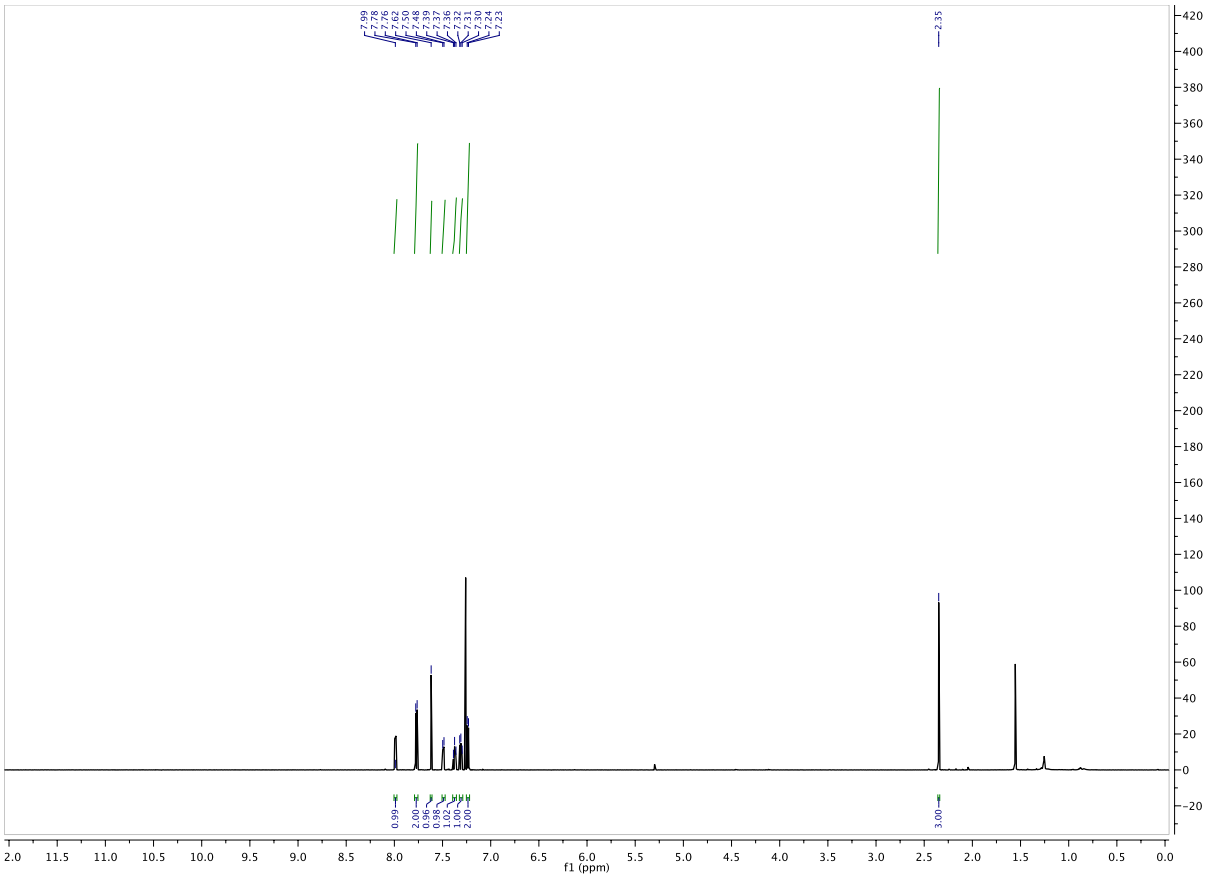

Figure 2.4.69. ^{1}H of 2.28

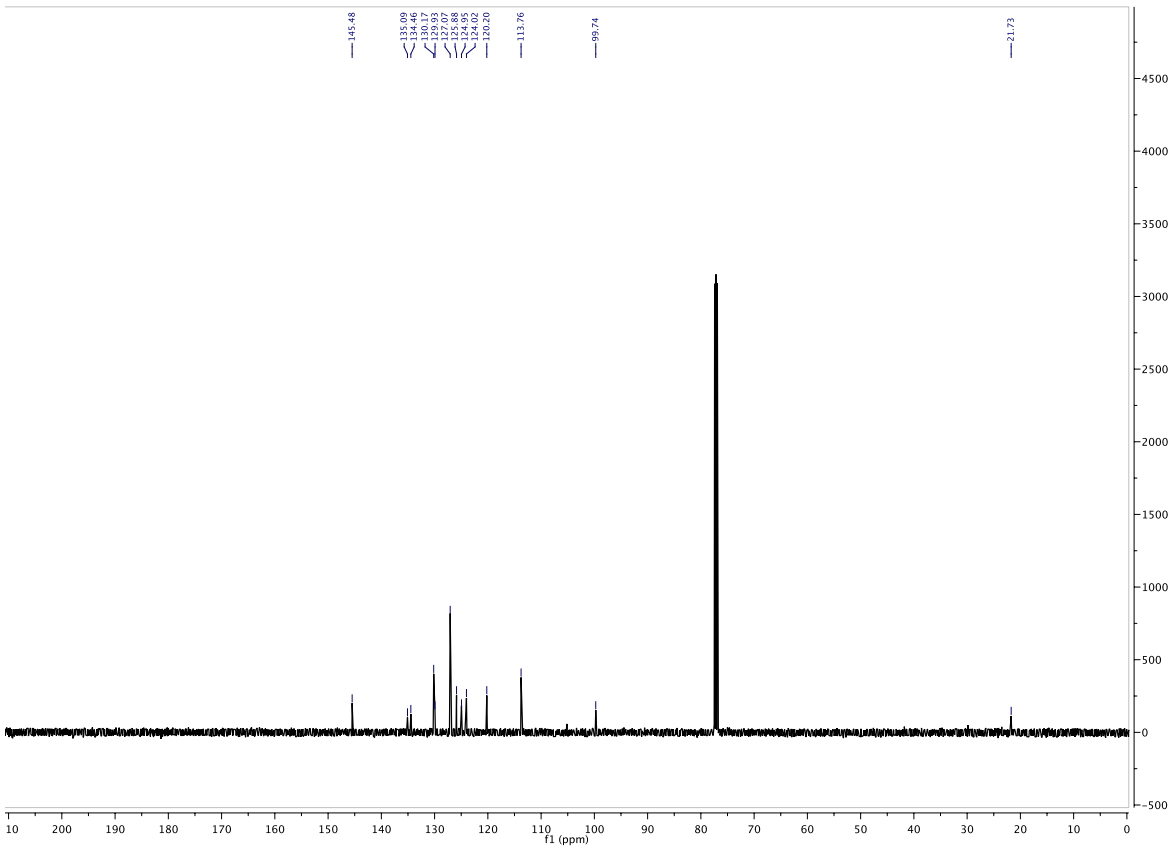

Figure 2.4.70. ^{13}C of 2.28

Figure 2.4.71. Product 2.29

3-bromoindazole (**2.29**): 82% conversion by NMR, and 82% isolated yield as a white solid. R_f: 0.20 (4:1 hexanes:ethyl acetate); NMR data match the data reported in U.S. pantent: Civiello, R.L.; Combrick, K.D.; Gulgeze, H.B.; Meanwell, N.; Pearce, B.C.; Sin. N.; Thuring, J.W.; Venables, B.L.; Wang, X.; Yin, Z.; et al. Heterocyclic Substituted 2-Methyl-Benzimidazole Antiviral Agents, 2002, Application Number: PCT/US2001/045149.

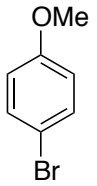

Figure 2.4.72. Product 2.30

4-bromoanisole (2.30): 90% conversion by NMR. NMR data match the data reported in literature: Bose, A.; Mal, P. *Tet. Lett.* **2014**, *55*, 2154-2156.

2.5 Acknowledgements

The contents in Chapter 2 are a reformatted reprint of the following manuscript, with permission from the American Chemical Society: Maddox, S. M.; Nalbandian, C. J.; Smith, D. E.; Gustafson, J. L. "A Practical Lewis Base Catalyzed Electrophilic Chlorination of Arenes and Heterocycles." *Org. Lett.* **2015**, *17*, 1042. The dissertation author was the primary researcher for the data presented. Support of this work by San Diego State University is acknowledged.

Chapter 3: The Catalyst-Controlled Regiodivergent Chlorination of Phenols

3.1 ACS Copyright

3.2 Introduction

Electrophilic aromatic substitution represents a broadly utilized route to access aryl chlorides. Traditional electrophilic halogenations[71–73] suffer from several drawbacks such as a reliance on harsh reaction conditions, reduced reactivity towards electron poor arenes, and a lack of regioselectivity across many substrate classes. While recent advances[48,58,59,74–79] have largely addressed the first two issues, regioselectivity is still an unsolved problem as current electrophilic halogenations rely on substrate-controlled regioselectivity (Figure 3.2.1), often resulting in a mixture of constitutional isomers. On the other hand, it becomes a synthetic challenge to obtain a non-favored isomer when the substrate possesses a strong innate reaction preference toward electrophilic aromatic chlorination.

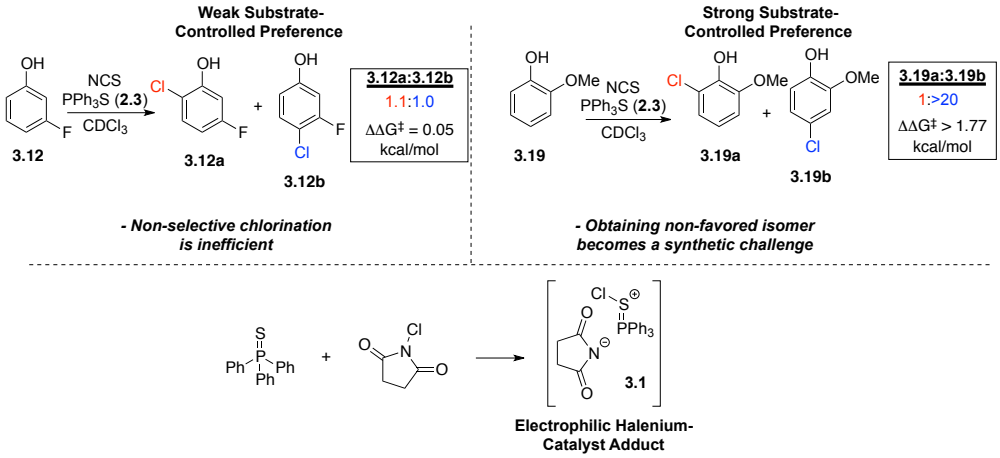

Figure 3.2.1. Substrate-Controlled Reactivities in Electrophilic Chlorination with Catalyst 2.3

There are relatively few examples of catalyst-controlled regioselectivities in the arena of electrophilic aromatic substitution (Figure 3.2.2). Seminal work by Miller[80,81] exploits the design of low molecular weight peptides mimicking the known Vancomycin binding regions of the $_D$Ala-$_D$Ala segments of the bacterial cell wall, in order to affect the site selective bromination of Vancomycin.

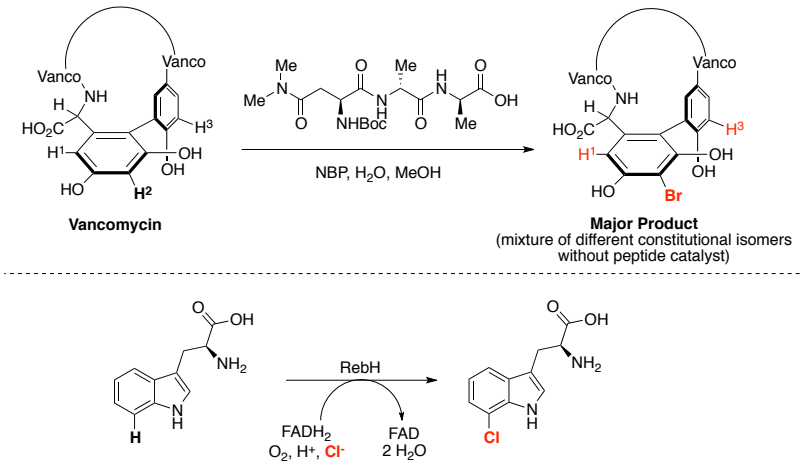

Figure 3.2.2. Seminal Work in Regioselective Electrophilic Halogenation

Alternatively, Lewis[40,41] has engineered mutants of the enzyme RebH to overcome the innate regioselectivity of tryptophan chlorination. Herein, we disclose a novel approach to address

these issues, in which we demonstrate the ability of different catalysts to control the regioselectivity of phenol halogenation in a divergent fashion.

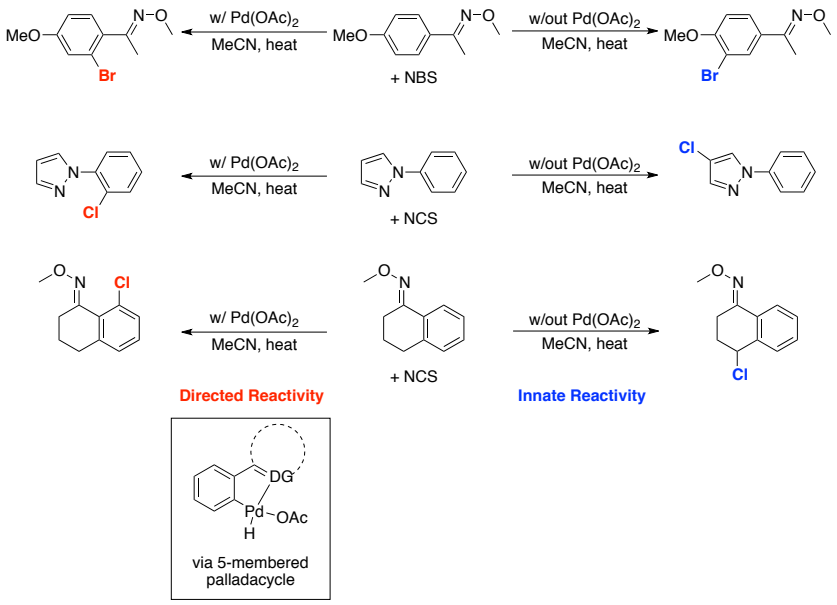

Figure 3.2.3. Metal-Directed Halogenations via 5-Membered Palladacycle[55]

Beyond electrophilic aromatic substitution, metal-directed halogenations represent atom-efficient approaches towards the site-selective functionalization of arenes and heterocycles.[82] In 2006, Sanford[55] reported a series of examples wherein the site of halogenation was directly influenced by the presence or absence of the associating metal (Figure 3.2.3), with the overall metal-directed reaction proceeding first-order in $Pd(OAc)_2$ and zeroth order in both NXS and substrate. Metal-directed halogenations are believed proceed via a 5-membered cyclopalladation (also 5-membered palladacycles for many alkyl C-H bond functionalizations[83]) before the C-X bond-forming step. These palladacycle intermediates allow for precise control of the site of C-H functionalization. It should be noted that tridentate directing groups have been shown to stabilize 6-membered palladacycles as well.[84]

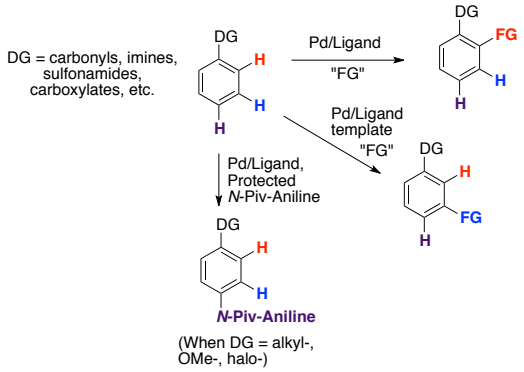

Figure 3.2.4. Ligand- and Template-Enabled Directed C-H Functionalizations.

Professor Jin-Quan Yu (Scripps) is arguably one of the most impactful leaders in this frontier of directed C-H functionalization,[53,54,85,86] because his group has exhibited the potential ability to add any functional group imaginable proximal to a carbonyl moiety.[87] Furthermore, Yu's work in directed C-H functionalization expands beyond *ortho*- functionalization to include *meta*-[88–90] and *para*-directed[91] C-H functionalizations (Figure 3.2.4). However, while these transformations will indeed find utility within the scope of directed functionalizations, they currently rely on the presence of strongly coordinating imine/carbonyl moieties, heterobiaryl functionality, molecular templates, tedious ligand design, or a combination thereof. Nonetheless, these studies have all but shown that with the appropriate combination of ligand design and existing functionality, you may be able to, in principle, selectively functionalize any bioactive small molecule during the late stages of drug design.

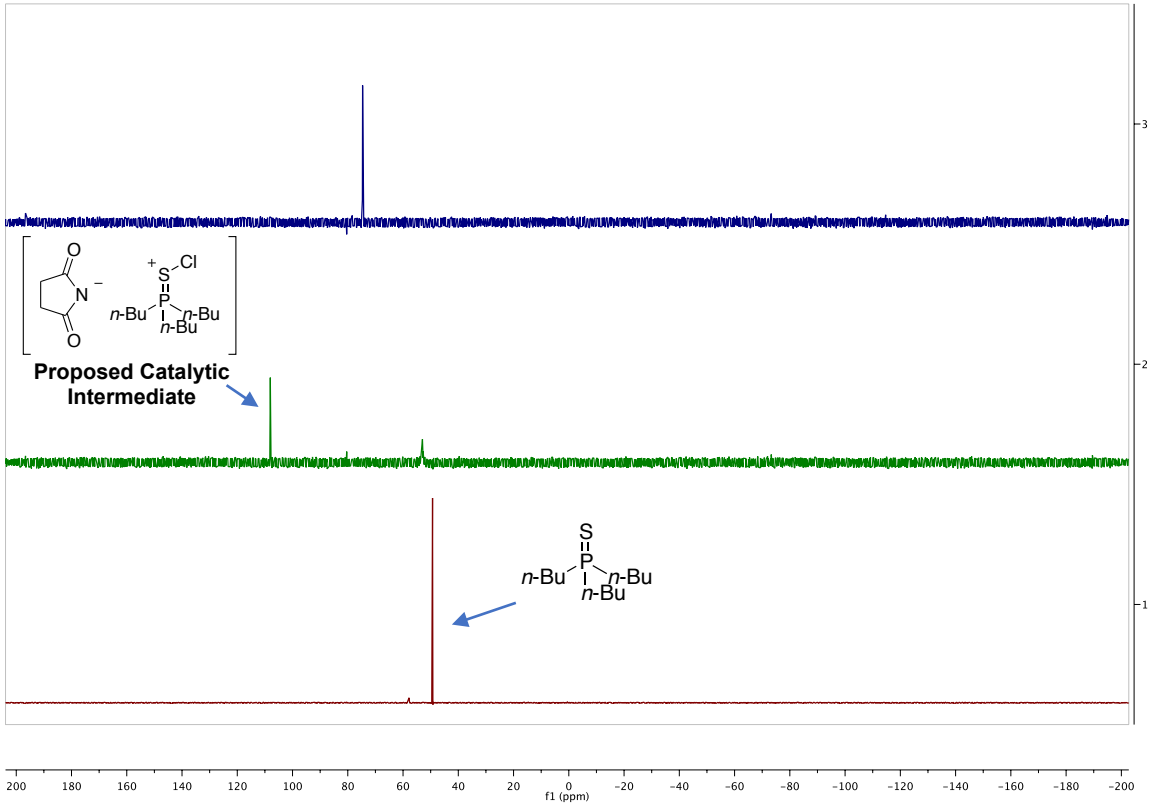

Figure 3.2.5. Following Lewis Base Catalyzed Chlorination by ^{31}P NMR. ($CDCl_3$ was used as solvent. The blue spectrum was obtained after addition of 10 equiv. of caffeine {the molecular structure of the resulting compound is unknown})

To overcome some of the potential drawbacks of metal-directed functionalizations, our lab was interested in developing a mild Lewis base catalyzed directed halogenation of arenes with weakly coordinating directing groups (i.e. phenol). Chapter 2[77] discusses a mild catalytic electrophilic halogenation of arenes and heterocycles using catalytic Lewis bases[62,63,65,66,92–94] (i.e. phosphine sulfide **2.3**) to activate *N*-halosuccinimides. These catalysts were able to affect the chlorination of diverse arenes according to the innate preference of the substrate with regioselectivity closely following those reported in literature.[58,78,79] Monitoring the course of the reaction by ^{31}P NMR (Figure 3.2.5) suggested the formation of an intermediate with a large degree of phosphonium character,[95] which would be expected if the chemistry proceeded through a

catalyst-halenium adduct[62,96] such as **3.1** (Figure 3.2.1). This observation was corroborated by DFT (Figure 3.2.6) studies that predict halogenation to proceed through such an intermediate.

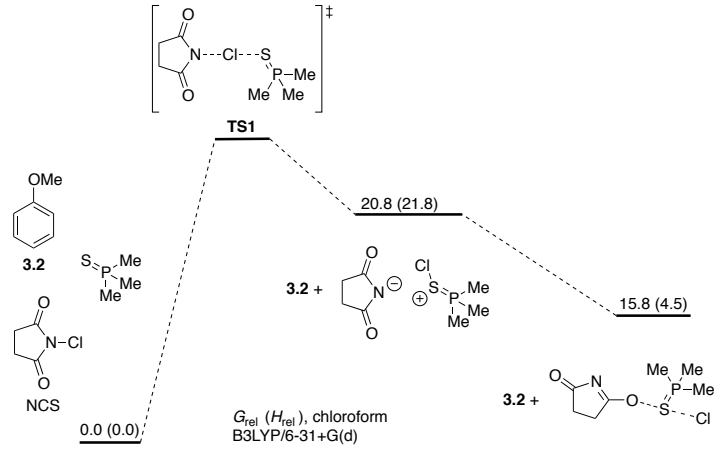

Figure 3.2.6. DFT Calculations of Potential Catalytic Intermediates in Lewis Base Catalyzed Chlorination

As these data suggest the activated halenium is associated with the catalyst, we hypothesized that the Lewis base catalyst structure can alter the reaction outcome in the site-selectivity of electrophilic aromatic halogenation. As a proof of concept, we chose to test this in the context of the *ortho*-chlorination of phenols. Phenols represent an important class of arenes that typically display a moderate to high *para*-preference (Figure 3.2.1). While bulky amines are known to affect the *ortho*-chlorination of phenols,[73,97] these reactions operate under fairly harsh conditions (sulfuryl chloride at 70 ^{o}C) and have been shown to have limited substrate scope.[98] Since our report, Yeung has shown the *ortho*- electrophilic functionalization of phenols can proceed smoothly with the use of ammonium salt catalyst.[99] Other commonly employed routes to *ortho*-chlorinated phenols involve multistep processes that include arene oxidation,[100,101] dehalogenation,[102,103] or *O*-methoxymethyl (MOM) directed lithiation.[104,105] A catalytic room temperature *ortho*-selective electrophilic chlorination would represent a more desirable approach

that could be performed in one step with few precautions. lending it several practical advantages over current routes.

3.3 Discussion

Table 3.3.1. Catalyst Exploration Towards the *ortho*- Chlorination of Phenol

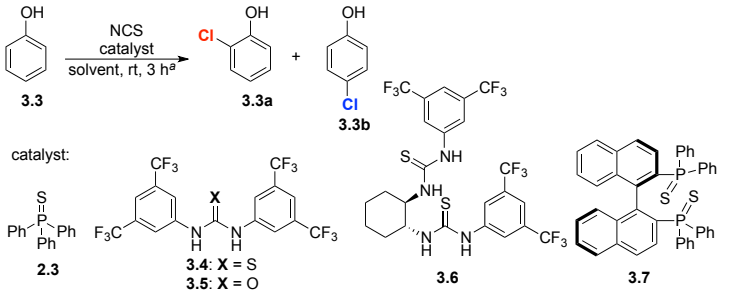

entry	catalyst (%)	solvent (molarity)[b]	conversion to **3.3a** (%)[c]	**3.3a**:**3.3b**[d]	ΔΔG‡ (kcal/mol)[f]
1	**2.3** (10)	$CDCl_3$ (0.05)	23	1.0:4.0	0
2	**3.4** (10)	$CDCl_3$ (0.025)	33	1.0:2.0	0.41
3	**3.5** (10)	$CDCl_3$ (0.025)	14	1.0:1.1	0.76
4	**3.6** (10)	$CDCl_3$ (0.05)	67	5.4:1.0	1.82
5	**3.6** (10)	$CDCl_3$ (0.05)	48	3.2:1.0	1.49
6	**3.6** (10)	C_6D_6 (0.05)	55	6.4:1.0	1.92
7	**3.6** (5)	C_6D_6 (0.025	75	6.9:1.0	1.96
8	**3.6** (10)	$CDCl_3$ (0.025)	83	27:1.0	2.77
9	**3.6** (5)	$CDCl_3$ (0.025)	82	12:1.0	2.29
10	**2.3** (10)	$CDCl_3$ (0.025)	20	1.0:3.0	0.17
11	**3.7** (10)	$CDCl_3$ (0.05)	13	1.0:7.1	-0.33
12	**3.6** (10)	CD_2Cl_2 (0.025)	64	4.7:1.0	1.73
13	**3.7** (10)	CD_2Cl_2 (0.05)	16	1.0:5.0	-0.13

[a]All reactions were performed by addition of catalyst, solvent, and 0.03 mmol **3.3** at rt, followed by the addition of 0.036 mmol NCS. [b]Molarity of the reaction is in reference to **3.3**. [c]Percent conversion to **3.3a** was determined by ^{1}H NMR and represents an average of three trials using tetramethylsilane or tetrakis(trimethylsilyl)methane as an internal standard. [d]Isomeric ratios were determined by ^{1}H NMR and represent an average of three trials. [e]We observed only minor decreases in selectivities with CD_2Cl_2 as the solvent, allowing us to reliably use DCM as our solvent upon scale-up to mitigate loss of volatile products. [f]$\Delta\Delta G^{\ddagger} = \Delta\Delta G^{\ddagger}_{\textbf{entry\#}} - \Delta\Delta G^{\ddagger}_{\textbf{entry 1}}$, with *ortho*-selectivity defined as positive $\Delta\Delta G^{\ddagger}$ and *para*-selectivity defined as negative $\Delta\Delta G^{\ddagger}$.

We began these studies by evaluating several privileged[7] catalyst structures that also possessed Lewis basic functional groups that are known to activate NXS.[63] Schreiner's thiourea[106,107] (**3.4**) efficiently catalyzed this reaction and yielded a 1.0:2.0 **3.3a**:**3.3b** ratio (Table 3.3.1, Entry 2). While **3.4** still favored **3.3b**, we were intrigued by the moderate increase (compared to **2.3**) in *ortho*- isomer **3.3a** formed and decided to evaluate other thioureas. A slight increase in the selectivity for **3.3a** was observed with urea **3.5**, albeit at the expense of significantly reduced

reactivity. We found that Nagasawa's bis-thiourea[108] (**3.6**) overcame the substrate's innate preference, yielding a 5.4:1.0 mixture of isomers favoring **3.3a** (Table 3.3.1, Entry 4). This ratio could be improved to 27:1.0 by diluting the reaction concentration (Table 3.3.1, Entry 8). This noticeable effect on the regioselectivity is likely due to a decrease in catalyst aggregation at lower concentration and is consistent with recent work by Seidel.[109] To put the efficiency of catalyst **3.6** into perspective, the $\Delta\Delta\Delta G^{\ddagger}$ between catalyst **3.6** and **2.3** towards *ortho*-chlorination is 2.77 kcal/mol, which corresponds to approximately 98% *ee* in the realm of enantioselective catalysis.

Scheme 3.3.1. *ortho*-Selective Chlorination of Substituted Phenols

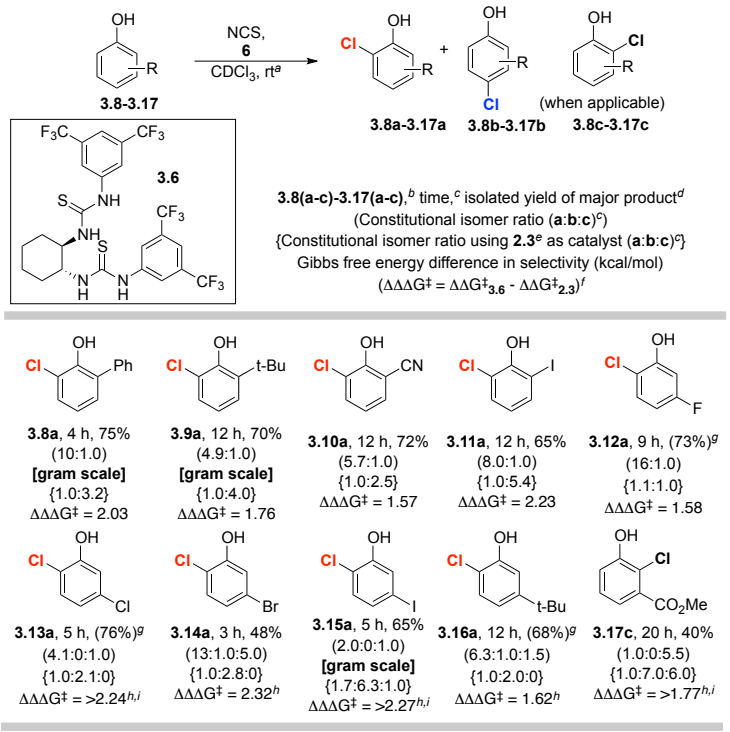

[a]Optimized reaction conditions were used with respect to the catalyst (See Table 3.1). [b]Only the major product is shown. [c]Reaction times and constitutional isomer ratios were determined by ^{1}H NMR and represent an average of two trials using tetramethylsilane or tetakis(trimethylsilyl)methane (TTMSM) as an internal standard. [d]Isolated yields were determined on the 50-1,000 mg scale, using DCM as the solvent (due to volatility), and represent an average of two trials. [e]The selectivities observed with catalyst **2.3** are included for comparison. [f]*ortho*-selectivity defined as positive $\Delta\Delta G^{\ddagger}$ and *para*-selectivity defined as negative $\Delta\Delta G^{\ddagger}$. [g]Due to product volatility, an isolated yield could not be reported, therefore % conversion was reported as determined by ^{1}H NMR using TTMSM as an internal standard. [h]Both *ortho* products (**a** and **c**) combined to simplify calculation. [i]Assuming >20:1 *ortho*:*para* with **3.6**.

To define the generality of this catalyst-controlled *ortho*-chlorination, we applied catalyst **3.6** across a series of differentially substituted phenols, observing predominantly *ortho*-chlorination across the substrate set (Scheme 3.3.1). This was in contrast to catalyst **2.3**, which predominantly yielded *para*-chlorination. For example, **3.6** effected the chlorination of phenol **3.8** to give an *ortho*:*para* ratio (**3.8a**:**3.8b**) of 10:1.0, with **3.8a** being isolated in 75% yield. We observed a decrease in *ortho*-selectivity for 2-*tert*-butyl substituted **3.9** (*ortho*:*para* ratio of 3:1), perhaps due to the bulky substituent interfering with a catalyst-substrate interaction. Nonetheless, we were able to isolate **3.9a** with a 70% yield. Nitrile-containing **3.10** and 2-iodophenol (**3.11**) also proved good substrates, affording *ortho*:*para* ratios of 5.7:1 and 8:1, respectively.

The chlorination of *meta*-substituted phenols also proceeded with *ortho*-selectivity in the presence of **3.6**. For example, the chlorination of 3-fluorophenol (**3.12**) yielded an excellent 16.0:1.0 **12a**:**12b** ratio. Substrates with less electronically withdrawing *meta*-substituents were also chlorinated *ortho*- to the phenol by **3.6**, however now varying degrees of chlorination at the more hindered *ortho*-position was observed in line with expected electronic trends (see substrates **3.13**-**3.16** in Scheme 3.3.1). **3.17** possessed particularly interesting selectivity as **3.6** primarily effected chlorination at the more hindered *ortho*-position to give predominantly **17c** (1.0:0:5.5 ratio of **3.17a**:**3.17b**:**3.17c**). From an energetic perspective, catalyst **3.6** was less effective on these substrates than phenol, however the $\Delta\Delta\Delta G^{\ddagger}$ between catalyst **3.6** and catalyst **2.3** were still quite good, corresponding to a range of 85% to 96% *ee* when an analogy to enantioselective catalysis is made.

With an *ortho*-selective catalyst in hand, we then turned our attention to catalysts that augment the innate *para*-selectivity of phenols, finding that bis(diphenylphosphino)-1,1'-

binaphthyl (BINAP)-derived phosphine sulfide **3.7** could improve upon the innate *para*-selectivity of this reaction, yielding a **3.3a**:**3.3b** ratio of 1.0:7.1 (Table 3.3.1, Entry 11).

Scheme 3.3.2. Augmenting the Innate Chlorination of Phenol

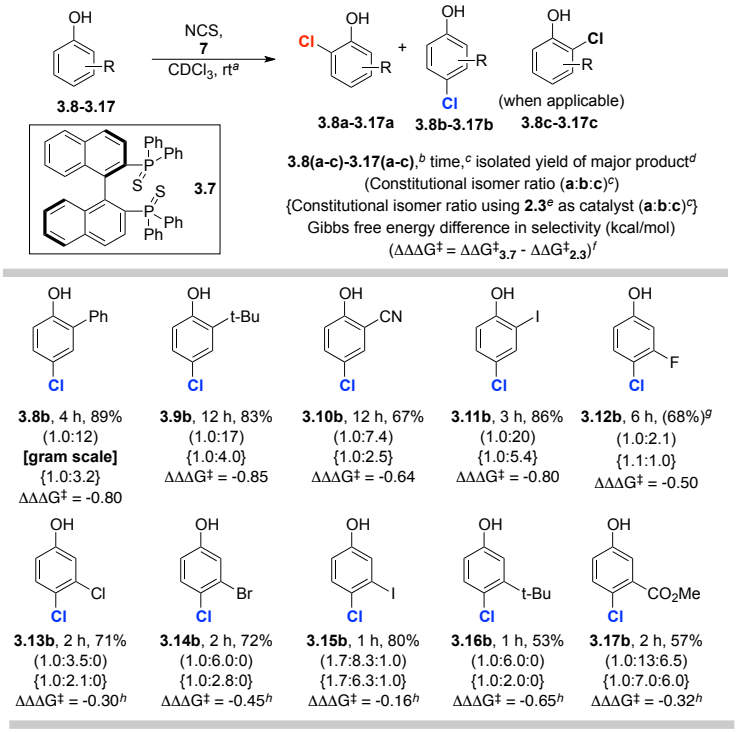

[a]Optimized reaction conditions were used with respect to the catalyst (See Table 3.1). [b]Only the major product is shown. [c]Reaction times and constitutional isomer ratios were determined by ^{1}H NMR and represent an average of three trials using tetramethylsilane or tetakis(trimethylsilyl)methane as an internal standard. [d]Isolated yields were determined on the 50-1,000 mg scale, using DCM as the solvent (due to volatility), and represent an average of two trials. [e]The selectivities observed with catalyst **2.3** are included for comparison. [f]*ortho*-selectivity defined as positive ΔΔG‡ and *para*-selectivity defined as negative ΔΔG‡. [g]Due to product volatility, an isolated yield could not be reported, therefore % conversion was reported as determined by ^{1}H NMR using TTMSM as in internal standard. [h]Both *ortho* products (**a** and **c**) combined to simplify calculation.

We then evaluated catalyst **3.7** across the same set of substrates (Scheme 3.3.2). In general, **3.7** was found to yield markedly improved *para*-selectivities compared to those of **2.3**. For example, **3.7** effected the chlorination of phenols **3.8** and **3.9** with *ortho*:*para* ratios of 1.0:12 (compared to 1.0:3.2 and 1.0:4.0, respectively, by **2.3**). We also observed a similar degree of *para*-augmentation with **3.7** for nitrile-containing **3.10** (**3.10a**:**3.10b** of 1.0:7.4 vs. 1.0:2.5 with **2.3**), and

2-iodophenol (**3.11**) (*ortho*:*para* ratio of 1.0:20 vs. 1:5.4). Catalyst **3.7** also augmented the *para*-selectivity of *meta*-substituted phenols when compared to catalyst **2.3**. For example, while fluorophenol **3.12** gave a ratio of **3.12a**:**3.12b** as 1.1:1.0 with catalyst **2.3**, chlorination of **3.12** with catalytic **3.7** altered the reaction outcome to give *para*-chlorinated **3.12b** as the major product (ratio of **3.12a**:**3.12b** as 1.0:2.1). **3.7** also resulted in increases in *para*-selectivity of 2-3 fold for phenols **3.14**, **3.16**, and **3.17**. It should be noted that for some phenols, such as **3.13** and **3.15**, catalyst **3.7** increased selectivity minimally. Finally, the chlorination of ester-containing **3.17** was seemingly unselective with catalyst **2.3**, resulting in a mixture of **3.17a**:**3.17b**:**3.17c** as 1.0:7.0:6.0, yet in the presence of **3.7**, the chlorination proceeded to yield a *para*-favoring mixture of **3.17a**:**3.17b**:**3.17c** as 1.0:13:6.5. While the increase in *para*-selectivities when using catalyst **3.7** over catalyst **2.3** complements the catalyst-directed *ortho*-chlorinations in Scheme 3.1, and serves as another proof of concept that catalyst structure can both augment (as with **3.7**) or override (as with **3.6**) innate regioselectivities.

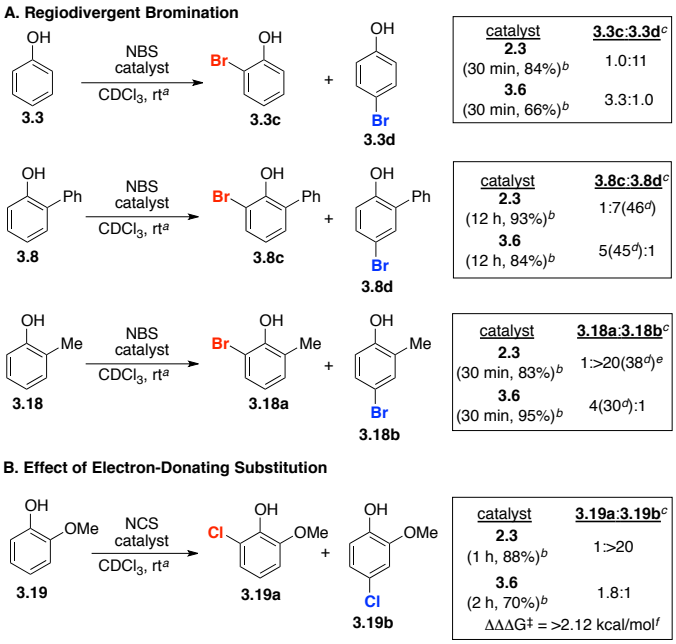

[a]Optimized reaction conditions were used with respect to the catalyst (See Table 1). [b]Reaction times and conversions to mono-brominated products were determined by ^{1}H NMR and represent an average of two trials using tetramethylsilane or tetrakis(trimethylsilyl)methane as an internal standard. [c]Ratios were determined by ^{1}H NMR and represent an average of three trials. [d]Isolated yields in parentheses were determined on the 50-100 mg scale, using DCM as the solvent (due to volatility), and represent an average of two trials (See SI). [e]Ratio could not be determined by ^{1}H NMR, however **3.18b** was the predominant isomer (See SI). [f]*ortho*-selectivity defined as positive ΔΔG‡ and *para*-selectivity defined as negative ΔΔG‡ (ΔΔΔG‡ = $\Delta\Delta G^{\ddagger}_{3.6}$ - $\Delta\Delta G^{\ddagger}_{2.3}$).

Figure 3.3.1. Regiodivergent Bromination and the *o*-Chlorination of Guaiacol.

We next probed whether these catalysts could also affect regioselective brominations. While there are robust conditions for *ortho*-bromination, catalyst-controlled bromination might find utility in late-stage functionalization. In these studies, we found little difference between catalysts **2.3** and **3.7**, with both yielding predominantly *para*-brominated products, however as with chlorination, **3.6** overcame this innate *para*-preference to give mostly *ortho*-brominated products. For example, phenol **3.3** yielded excellent regioselectivities (**3.3c**:**3.3d** ratio of 1.0:11, Figure 3.3.1), albeit with a significant amount of polybromination, while **3.6** gave an observed **3.3c**:**3.3d** ratio of 3.3:1.0. *Ortho*-substituted phenols **3.8** and **3.18** proceeded more smoothly, with **2.3** yielding predominantly *para*-brominated **3.8d** and **3.18b**, and catalyst **3.6** favoring bromination *ortho*- to the hydroxy group each time (**3.8c**:**3.8d** ratio of 5:1; **3.18a**:**3.18b** ratio of

4:1). It should be noted that when using 1.2 equiv. NBS we observed some dibromination which complicated purification and resulted in isolated yields that were lower than observed NMR conversions.

We also evaluated the chlorination of substrates that possessed multiple directing groups such as guaiacol (**3.19**), finding catalyst **2.3** to effect chlorination exclusively *para*- to the hydroxy group, giving **3.19b** in high yields. Interestingly, catalyst **3.6** could overcome this large substrate preference to yield *ortho*-chlorinated **3.19a** as the major product, however with a more modest ratio than other substrates in Scheme 3.1. It is worth mentioning that this modest selectivity is due to the large innate *para*-preference of **3.19**, as from an energetic perspective, catalyst **3.6** overcomes roughly 2.1 kcal/mol, comparable, if not better than many of the substrates in Scheme 3.3.1.

In conclusion, we have demonstrated that the catalyst structure of Lewis bases can influence the regioselectivity of the electrophilic halogenation of phenols. A particularly exciting aspect of this work is the observed reversal of regioselectivity by Nagasawa's bis-thiourea **3.6**, presumably through a mechanism in the one thiourea interacts with the phenol hydroxy group, and the other activates NCS through Lewis basic (analogous to that depicted in Figure 3.3.1) or a Brönsted acidic manifold (H-bonding with NCS carbonyl). Mechanistic studies to understand how this chemistry works are ongoing. These results represent a novel and facile route to access arene substitution patterns that are not currently readily available. More broadly, these results represent a key proof of concept that a catalyst can indeed alter the reaction outcome of electrophilic halogenation.

3.4 Experimental Section

3.4.1 Initial Mechanistic Investigations (Figures 3.2.5 and 3.2.6)

Results in Figure 3.2.5 were obtained as follows: 2.4 mg (0.01 mmol, 1.0 equiv.) of tributylphosphinesulfide (**2.3**) was added to an NMR tube followed by the addition of 600 μL $CDCl_3$. A ^{31}P NMR spectrum was obtained, represented as the bottom spectrum in red (Figure 3.2.5). 6.7 mg (0.05 mmol, 5.0 equiv.) NCS was then added to the NMR tube and shaken vigorously for 3 minutes. A second ^{31}P NMR spectrum was obtained, represented by the middle spectrum in green (Figure 3.2.5). Immediately after obtaining the second ^{31}P spectrum, 9.7 mg (0.5 mmol, 5.0 equiv.) of caffeine was added to the NMR tube and left for 30 minutes with 4 equally spaced out short periods of mixing. After the 30 minutes was up, a third ^{31}P NMR spectrum was obtained, represented by the blue spectrum (Figure 3.2.5). While the blue spectrum in Figure 3.2.5 is a different species than the starting catalyst by ^{31}P NMR, sequential additions of NCS followed by caffeine continued to effect catalytic chlorination. Mass spectral analysis of the reaction after chlorination revealed an observed mass of 437.5 m/z, suggesting the formation of a resting-state catalyst such as **3.20** (calculated mass of protonated **3.20** is 437.3 m/z).

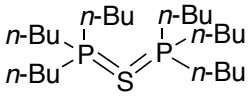

3.20

Figure 3.4.1. Proposed Resting-State Catalyst 3.20

As a control, 2.4 mg (0.01 mmol, 1.0 equiv.) of tributylphosphinesulfide (**2.3**) was added to an NMR tube, followed by the addition of succinimide and 8-chlorocaffeine. The ^{31}P NMR spectrum of the control mixture was analogous to that of the **2.3** alone (red spectrum, Figure 3.2.5).

Scheme 3.4.1. Energies from Figure 3.2.6

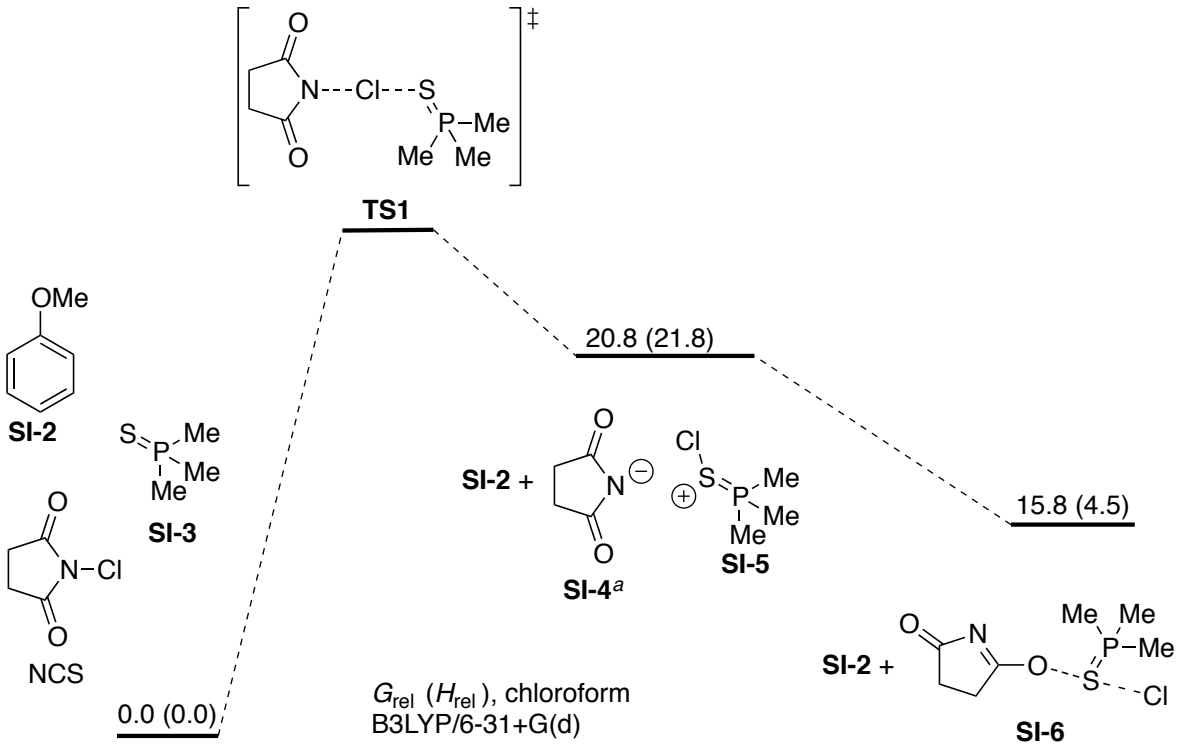

Scheme 3.4.1 is a reformatted version of Figure 3.2.6. The energies given for **SI-4** and **SI-5** represent the *separated* ions with implicit solvent calculations. Explicit solvation may result in a lower energy ion pair. All attempts to locate ion-pair type interactions between **SI-4** and **SI-5** in the gas phase resulted in convergence to intermediate **SI-6** or higher energy species.

3.4.2 General Information

^{1}H and ^{13}C NMR spectra were recorded on Varian VNMRS 400 MHz, Varian Inova 500 MHz, Varian VNMRS 600 MHz, and Bruker Avance III 600 MHz spectrometers at 25 ^{o}C. All chemical shifts were reported in parts per million (δ) and were internally referenced to residual protio solvents unless otherwise noted. ^{19}F NMR spectra were referenced to an external TFA standard. Spectral data were reported as follows: chemical shift (multiplicity [singlet (s), doublet (d), triplet (t), quartet (q), pentet (p), and multiplet (m)], coupling constants [Hz], integration). Carbon spectra were recorded with complete proton decoupling. Conventional mass spectra were obtained using Advion Expression^{s} CMS (APCI, ASAP). *N*-chlorosuccinimide was recrystallized from acetic acid, and *N*-bromosuccinimide was recrystallized from water. For the synthesis of **3.7**, toluene was degassed prior to use via the freeze-pump-thaw method. All other chemicals used were purchased from Sigma Aldrich, TCI, Frontier Scientific, Acros Organics, Strem, Oakwood, Matrix Scientific, Cambridge Isotope Laboratories, or Fisher and were used as received without further purification, unless specifically noted. All normal phase flash column chromatography (FCC) was performed using Grade 60 Silica Gel (230-400 mesh) purchased from Fisher Scientific. Reverse phase flash chromatography was performed on a Biotage Isolera One with a Biotage SNAP cartridge (KP-C18-HS 12g). Preparative Thin Layer Chromatography (TLC) plates contained grade 60 silica gel coated with fluorescent indicator F_{254}. Catalysts were either purchased (**2.3**), prepared from known literature procedures (**3.4**,[110] **3.5**,[110] **3.6**,[111]) or synthesized (**3.7**).

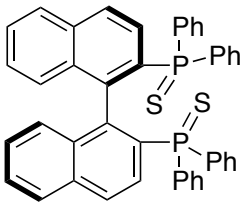

Figure 3.4.2. Catalyst 3.7

(*R*)-[1,1'-binaphthalene]-2,2'-diylbis(diphenylphosphine sulfide) (**3.7**): (*R*)-BINAP (1.0 g, 1.61 mmol, 1.0 equiv.) and ground elemental sulfur (210 mg, 6.42 mmol, 4.0 equiv.) was added to a round bottom (rb) flask equipped with a stir bar. The flask was evacuated and backfilled with nitrogen (1x), followed by the addition of degassed toluene (3.2 mL, 0.5 M). The flask was attached to a reflux condenser and a nitrogen line. The reaction was refluxed overnight at 120 ^{o}C under nitrogen. Upon reaction completion (determined by ^{31}P NMR), the solvent was removed by rotovap; and the remaining sulfur was removed via flash column chromatography. The fractions containing **3.7** were collected, dried over sodium sulfate, and evaporated by rotovap. The relatively pure material was then dissolved in a 2-dram vial with hot toluene (~3 mL), capped, and placed in the freezer for 24 hours. The resulting crystals were filtered, and washed with minimal cold toluene to afford **3.7** as off-white solid crystals (592 mg, 54%). **^{1}H NMR** (500 MHz, $CDCl_3$) δ 7.78 (dd, *J* = 8.7, 2.0 Hz, 2H), 7.75-7.61 (m, 10H), 7.46 (dd, *J* = 12.3, 8.7 Hz, 2H), 7.41-7.35 (m, 2H), 7.34-7.27 (m, 4H), 7.25-7.20 (m, 8H), 6.72 (d, *J* = 8.5 Hz, 2H), 6.63 (t, *J* = 7.4 Hz, 2H); **^{13}C NMR** (126 MHz, $CDCl_3$) δ 140.65 (dd, *J* = 8.2, 5.2 Hz), 135.83 (d, *J* = 86 Hz), 134.12 (d, *J* = 2.5 Hz), 133.57 (d, *J* = 11.5 Hz), 132.95 (d, *J* = 10 Hz), 132.30 (d, *J* = 11 Hz), 131.59, 130.97 (d, *J* = 3.0 Hz), 130.69 (d, *J* = 3.0 Hz), 129.49 (d, *J* = 12 Hz), 128.74 (d, *J* = 85 Hz), 128.11 (d, *J* = 13 Hz), 128.10 (d, *J* = 12 Hz), 127.95 (d, *J* = 13 Hz), 127.80, 127.56, 127.38 (d, *J* = 1.0 Hz), 125.81 (d, *J* = 1.0 Hz); **^{31}P NMR** (202 MHz, $CDCl_3$) δ 43.12 (referenced to external H_3PO_4 standard); **MS (APCI)**: **Calculated for** $C_{44}H_{33}P_2S_2$ $[M+H]^+$ 687.2. **Found:** 687.2 m/z.

3.4.3 General Regiodivergent Halogenation Procedure

Substrate (0.030 mmol, 1 equiv.), catalyst (0.0030 mmol, 0.1 equiv.), and $CDCl_3$ (600 μL or 1200 μL) were added to an NMR tube followed by the addition of either tetramethylsilane (TMS) or tetrakis(trimethylsilyl)methane (TTMSM) as an internal standard (when necessary). A ^1H spectrum of the reaction mixture was then obtained with a relaxation delay of 5.00 sec (number of scans = 4), representing the reaction mixture at time = 0. *N*-Halosuccinimide (0.036 mmol, 1.2 equiv.) was then added to the NMR tube, and the reaction was monitored by ^1H NMR. The reaction was considered complete once the substrate conversion had ceased. Isomeric ratios were determined via integration of the aromatic peaks of each product. Conversion to mono-Cl products represents the sum of the conversions of all identified mono-chlorinated products, and the value was determined via integration of mono-chlorinated products with respect to either the residual protio solvent or TMS. Isomeric ratios determined by analysis of non-obscure peaks. When necessary, clear coupling patterns were partially integrated, and full integration value was extrapolated from the partial integration. If multiple peaks were clear, the average of those peaks were used to determine the isomeric ratio. Each experiment was performed in triplicate, and the reported ratios are the average of the three trials. An example from each set is reported with the Spectral Data. Each example was zoomed in for clear visualization of each isomer.

Isolated yields were determined on a 50-1,000 mg scale using dichloromethane (DCM) as the reaction solvent instead of $CDCl_3$, due to the low boiling points of many of the products; all reagents and solvent were scaled equally, omitting TMS (or TTMSM). When catalyst **3.6** was used on these scales, the concentration with respect to the substrate was adjusted to 0.05 M to avoid using unnecessary volumes of solvent; the catalyst loading was subsequently adjusted to 0.025 mol% to avoid catalyst aggregation. Upon reaction completion, as determined by Thin-Layer

Chromatography (TLC), the reaction was filtered through a short normal phase silica plug with DCM to remove succinimide. The solvent was then removed by rotovap, and, for almost all substrates, the resulting crude mixture was purified by Flash Column Chromatography (FCC) on normal phase silica gel, eluting with hexanes and ethyl acetate (hexanes:ethyl acetate::100:0 → 99:1 → 98:2 → 97:3 → 95:5), unless otherwise noted. Many of the isolated products had low boiling points, thereby negatively affecting the isolated yield upon being exposed to strong

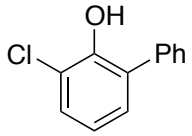

vacuums for extended periods of time. For the chlorination and bromination of phenol (**3.3**), spectra were compared to literature precedents (**3.3a**,[112] **3.3b**,[77] **3.3c**,[113] **3.3d**[113]) to determine isomeric ratios. For the chlorination of guaiacol (**3.19**), spectra were compared to literature precedents (**3.19a**[114]) and the Spectral Database for Organic Compounds (**3.19b**).

Figure 3.4.3. Product 3.8a

3-chloro-[1,1'-biphenyl]-2-ol (**3.8a**): Prepared according to the general procedure on a 1.0 g scale, using **3.6** as catalyst. 902 mg (75% yield) of **3.8a** was isolated as a white solid. **^{1}H NMR** (599 MHz, $CDCl_3$) δ 7.54 (dd, *J* = 7.8, 1.4 Hz, 2H), 7.46 (t, *J* = 7.5 Hz, 2H), 7.39 (tt, *J* = 7.4, 1.2 Hz, 1H), 7.33 (dd, *J* = 8.0, 1.6 Hz, 1H), 7.23 (dd, *J* = 7.8, 1.4 Hz, 1H), 6.95 (t, *J* = 7.9 Hz, 1H), 5.70 (s, 1H); **^{13}C NMR** (151 MHz, $CDCl_3$) δ 148.55, 137.19, 129.84, 129.56, 129.29, 128.66, 128.43, 127.89, 121.22, 120.81; **MS (APCI)**: **Calculated for** $C_{12}H_{10}ClO$ $[M+H]^+$ 205.0. **Found:** 205.0 m/z.

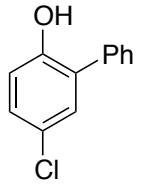

Figure 3.4.4. Product 3.8b

5-chloro-[1,1'-biphenyl]-2-ol (**3.8b**): Prepared according to the general procedure on a 1.0 g scale, using **3.7** as catalyst. 1.081 g (89% yield) of **3.8b** was isolated as a white solid. **^{1}H NMR** (400 MHz, $CDCl_3$) δ 7.54 – 7.47 (m, 2H), 7.47 – 7.40 (m, 3H), 7.24 – 7.19 (m, 2H), 6.95 – 6.90 (m, 1H), 5.17 (bs, 1H); **^{13}C NMR** (126 MHz, $CDCl_3$) δ 151.25, 135.97, 129.91, 129.66, 129.62, 129.07, 129.03, 128.57, 125.70, 117.32; **MS (APCI)**: **Calculated for** $C_{12}H_{10}ClO$ $[M+H]^+$ 205.0. **Found:** 205.0 m/z.

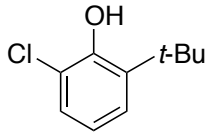

Figure 3.4.5. Product 3.9a

2-(*tert*-butyl)-6-chlorophenol (**3.9a**): Prepared according to the general procedure on a 1.0 g scale, using **3.6** as catalyst. 861 mg (70%) of **3.9a** was recovered as an orange oil. **^{1}H NMR** (500 MHz, $CDCl_3$) δ 7.21 – 7.17 (m, 2H), 6.80 (t, J = 7.9 Hz, 1H), 5.85 (bs, 1H), 1.41 (s, 9H); **^{13}C NMR** (126 MHz, $CDCl_3$) δ 149.83, 137.75, 126.61, 125.85, 121.05, 120.43, 35.34, 29.47; **MS (APCI)**: **Calculated for** $C_{10}H_{14}ClO$ $[M+H]^+$ 185.1. **Found:** 185.1 m/z.

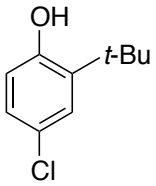

Figure 3.4.6. Product 3.9b

2-(*tert*-butyl)-4-chlorophenol (**3.9b**): Prepared according to the general procedure on a 500 mg scale, using **3.7** as catalyst. 514 mg (83% yield) of **3.9b** was isolated as an orange oil. **^{1}H NMR** (500 MHz, $CDCl_3$) δ 7.22 (d, *J* = 2.6 Hz, 1H), 7.02 (dd, *J* = 8.4, 2.6 Hz, 1H), 6.59 (d, *J* = 8.4 Hz, 1H), 4.79 (s, 1H), 1.39 (s, 9H); **^{13}C NMR** (126 MHz, $CDCl_3$) δ 152.90, 138.18, 127.45, 126.67, 125.57, 117.73, 34.89, 29.48; **MS (APCI)**: **Calculated for** $C_{10}H_{14}ClO$ $[M+H]^+$ 185.1. **Found:** 185.1 m/z.

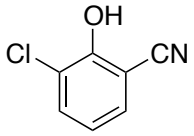

Figure 3.4.7. Product 3.10a

3-chloro-2-hydroxybenzonitrile (**3.10a**): Prepared according to the general procedure (except for purification) on a 100 mg scale, using **3.6** as catalyst. Upon reaction completion, the solvent was evaporated by rotovap, and the resulting crude material was immediately purified by FCC with an isocratic elution of 100% dichloromethane to obtain 93 mg (72% yield) of **3.10a** as a white solid. **^{1}H NMR** (500 MHz, $CDCl_3$) δ 7.56 (dd, *J* = 8.1, 1.5 Hz, 1H), 7.48 (dd, *J* = 7.8, 1.5 Hz, 1H), 6.97 (t, *J* = 7.9 Hz, 1H), 6.23 (s, 1H); **^{13}C NMR** (126 MHz, $CDCl_3$) δ 153.91, 133.87, 132.23, 121.69, 121.26, 115.16, 101.40; **MS (APCI)**: **Calculated for** C_7H_5ClNO $[M+H]^+$ 154.0. **Found:** 154.0 m/z.

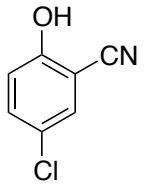

Figure 3.4.8. Product 3.10b

5-chloro-2-hydroxybenzonitrile (**3.10b**): Prepared according to the general procedure (except for purification) on a 100 mg scale, using **3.7** as catalyst. Upon reaction completion, the solvent was evaporated by rotovap, and the resulting crude material was immediately purified by FCC with an isocratic elution of 100% dichloromethane to obtain 86 mg (67% yield) of **3.10b** as a white solid, which consistently included about 12% starting material that could not be removed by available chromatography methods. **^{1}H NMR** (500 MHz, acetone-D6) δ 10.09 (s, 1H), 7.65 (d, *J* = 2.7 Hz, 1H), 7.52 (dd, *J* = 8.9, 2.7 Hz, 1H), 7.12 (d, *J* = 8.9 Hz, 1H); **^{13}C NMR** (126 MHz, acetone-D6) δ 159.59, 135.30, 133.18, 124.92, 118.74, 115.86, 102.30; **MS (APCI)**: **Calculated for** C_7H_5ClNO $[M+H]^+$ 154.0. **Found:** 154.1 m/z.

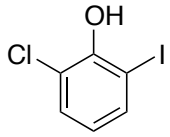

Figure 3.4.9. Product 3.11a

2-chloro-6-iodophenol (**3.11a**): Prepared according to the general procedure on a 100 mg scale, using **3.6** as catalyst. 75 mg (65% yield) of **3.11a** was isolated as a white solid. **^{1}H NMR** (599 MHz, $CDCl_3$) δ 7.62 (d, *J* = 8.0 Hz, 1H), 7.31 (d, *J* = 8.0 Hz, 1H), 6.63 (t, *J* = 8.0 Hz, 1H), 5.93 (s, 1H); **^{13}C NMR** (151 MHz, $CDCl_3$) δ 151.01, 137.92, 129.80, 122.98, 119.39, 83.63; **MS (APCI)**: **Calculated for** C_6H_4ClIO $[M]^+$ 253.9. **Found:** 254.0 m/z.

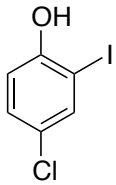

Figure 3.4.10. Product 3.11b

4-chloro-2-iodophenol (**3.11b**): Prepared according to the general procedure on a 100 mg scale, using **3.7** as catalyst. 99 mg (86% yield) of **3.11b** was isolated as a white solid. **^{1}H NMR** (500 MHz, $CDCl_3$) δ 7.63 (d, *J* = 2.4 Hz, 1H), 7.22 (dd, *J* = 8.7, 2.4 Hz, 1H), 6.92 (d, *J* = 8.7 Hz, 1H), 5.28 (s, 1H); **^{13}C NMR** (126 MHz, $CDCl_3$) δ 153.93, 137.28, 130.29, 126.24, 115.82, 85.58; **MS (APCI)**: **Calculated for** C_6H_4ClIO $[M]^+$ 253.9. **Found:** 253.9 m/z.

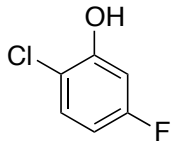

Figure 3.4.11. Product 3.12a

2-chloro-5-fluorophenol (**3.12a**): 5.0 g (44.6 mmol, 1.0 equiv.) of 3-fluorophenol was added to a 100 mL 2-necked round bottom flask, equipped with a stir bar, followed by the addition of 45 mL of dichloromethane. 131 mg (0.446 mmol, 0.01 equiv.) of **2.3** was subsequently added to the reaction mixture while stirring at room temperature. After five minutes, 6.6 g (49.1 mmol, 1.1 equiv.) of *N*-chlorosuccinimide was added to the stirring reaction at room temperature in 3 equal portions over the span of 10 minutes. After 24 hours stirring, 40 mL of hexanes was added to the reaction. Solid succinimide crashed out of solution and was filtered via vacuum filtration. The solid was disposed of, and the collected organic layer was purified via fractional distillation. **3.12a** and **3.12b** could not be isolated on this scale via distillation, however the fractions containing the highest purity of each isomer were collected for spectral analysis (spectra are provided). No isolated yield is reported. **3.12a** distilled at a lower temperature (90-150 ^{o}C), and significant amounts of hexane were present in the purest fraction. Constitutional isomer was assigned by contrast from spectra obtained from **3.12b**. **^{1}H NMR** (500 MHz, $CDCl_3$) δ 7.26 (dd, *J* = 8.9, 5.7

Hz, 1H), 6.77 (dd, J = 9.6, 2.9 Hz, 1H), 6.62 (ddd, J = 9.0, 8.0, 2.9 Hz, 1H), 5.65 (d, J = 1.5 Hz, 1H); **^{13}C NMR** (126 MHz, $CDCl_3$) δ 162.41 (d, J = 246 Hz), 152.45 (d, J = 12.8 Hz), 129.57 (d, J = 9.9 Hz), 115.22 (d, J = 3.5 Hz), 108.70 (d, J = 23.4 Hz), 104.17 (d, J = 26.5 Hz); **MS (APCI)**: **Calculated for** C_6H_4ClFO $[M]^+$ 146.0. **Found:** 145.9 m/z.

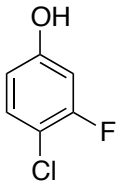

Figure 3.4.12. Product 3.12b

4-chloro-3-fluorophenol (**3.12b**): 5.0 g (44.6 mmol, 1.0 equiv.) of 3-fluorophenol was added to a 100 mL 2-necked round bottom flask, equipped with a stir bar, followed by the addition of 45 mL of dichloromethane. 131 mg (0.446 mmol, 0.01 equiv.) of **2.3** was subsequently added to the reaction mixture while stirring at room temperature. After five minutes, 6.6 g (49.1 mmol, 1.1 equiv.) of *N*-chlorosuccinimide was added to the stirring reaction at room temperature in 3 equal portions over the span of 10 minutes. After 24 hours stirring, 40 mL of hexanes was added to the reaction. Solid succinimide crashed out of solution and was filtered via vacuum filtration. The solid was disposed of, and the collected organic layer was purified via fractional distillation. **3.12a** and **3.12b** could not be isolated on this scale via distillation, however the fractions containing the highest purity of each isomer were collected for spectral analysis (spectra are provided). No isolated yield is reported. In later fractions, where **3.12b** distilled (120-200 ^{o}C), significant amounts of succinimide began to distill with the product. Spectral data matched the data provided by Sigma Aldrich. **^{1}H NMR** (500 MHz, $CDCl_3$) δ 7.21 (t, *J* = 8.6 Hz, 1H), 6.67 (dd, *J* = 10.3, 2.8 Hz, 1H), 6.58 (ddd, *J* = 8.8, 2.8, 1.3 Hz, 1H); **^{13}C NMR** (126 MHz, $CDCl_3$) δ 158.54 (d, *J* = 248 Hz), 155.68 (d, *J* = 10 Hz), 130.88 (d, *J* = 1.4 Hz), 112.40 (d, *J* = 17.7 Hz), 112.22 (d, *J* = 3.5 Hz), 104.68 (d, *J* = 23.9 Hz); **MS (APCI)**: **Calculated for** C_6H_4ClFO $[M]^+$ 146.0. **Found:** 145.9 m/z.

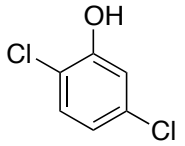

Figure 3.4.13. Product 3.13a

2,5-dichlorophenol (**3.13a**): Prepared according to the general procedure on a 100 mg scale, using **3.6** as catalyst. **3.13a** was isolated as an off-white solid, however the product quickly sublimes under vacuum. No isolated yield was reported, albeit 10 mg of pure material was obtained for spectral analysis. Spectral data matched the data provided by Sigma Aldrich. **^{1}H NMR** (500 MHz, $CDCl_3$) δ 7.24 (d, J = 8.6 Hz, 1H), 7.04 (d, J = 2.4 Hz, 1H), 6.87 (dd, J = 8.6, 2.4 Hz, 1H), 5.58 (s, 1H); **^{13}C NMR** (126 MHz, $CDCl_3$) δ152.05, 133.92, 129.69, 121.74, 118.49, 116.82; **MS (APCI)**: **Calculated for** $C_6H_4Cl_2O$ $[M]^+$ 162.0. **Found:** 161.9 m/z.

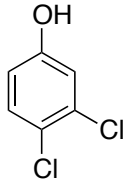

Figure 3.4.14. Product 3.13b

3,4-dichlorophenol (**3.13b**): Prepared according to the general procedure (not purified by FCC) on a 100 mg scale, using **3.7** as catalyst. After filtering reaction mixture through silica plug, solvent was removed under rotovap. The resulting crude material was dissolved in 300 μL of hexane. The resulting solution was purified by preparative TLC (hexane:ethyl acetate::90:10) to afford 90 mg (71% yield) of **3.13b** as a white solid. Spectral data matched the data provided by Sigma Aldrich. **^{1}H NMR** (500 MHz, $CDCl_3$) δ 7.28 (d, J = 8.7 Hz, 1H), 6.96 (d, J = 2.9 Hz, 1H), 6.69 (dd, J = 8.7, 2.9 Hz, 1H), 4.95 (s, 1H); **^{13}C NMR** (126 MHz, $CDCl_3$) δ 154.66, 133.08, 131.05, 124.39, 117.66, 115.38; **MS (APCI)**: **Calculated for** $C_6H_4Cl_2O$ $[M]^+$ 162.0. **Found:** 161.9 m/z.

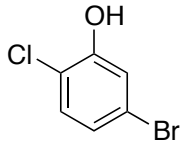

Figure 3.4.15. Product 3.14a

5-bromo-2-chlorophenol (**3.14a**): Prepared according to the general procedure on a 100 mg scale, using **3.6** as catalyst. 57 mg (48% yield) of **3.14a** was isolated as an off-white solid. The structure was assigned by comparison to computationally predicted ^{13}C NMR shifts [B3LYP63-1G+(d,p)]. **^{1}H NMR** (400 MHz, $CDCl_3$) δ 7.19 (d, J = 2.2 Hz, 1H), 7.18 (d, J = 8.6 Hz, 1H), 7.01 (dd, J = 8.5, 2.2 Hz, 1H), 5.56 (s, 1H); **^{13}C NMR** (101 MHz, $CDCl_3$) δ 152.15, 130.02, 124.64, 121.42, 119.68, 119.14; **MS (APCI)**: **Calculated for** $C_6H_4CBrClO$ $[M]^+$ 205.9. **Found:** 205.8 m/z.

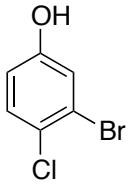

Figure 3.4.16. Product 3.14b

3-bromo-4-chlorophenol (**3.14b**): Prepared according to the general procedure on a 100 mg scale, using **3.7** as catalyst. 86 mg (72% yield) of **3.14b** was isolated as an off-white solid. The structure was assigned by comparison to computationally predicted ^{13}C NMR shifts [B3LYP63-1G+(d,p)]. **^{1}H NMR** (500 MHz, $CDCl_3$) δ 7.29 (d, J = 8.7 Hz, 1H), 7.13 (d, J = 2.9 Hz, 1H), 6.74 (dd, J = 8.7, 2.9 Hz, 1H), 4.90 (s, 1H); **^{13}C NMR** (126 MHz, $CDCl_3$) δ 154.62, 130.87, 126.37, 122.77, 120.80, 116.05; **MS (APCI)**: **Calculated for** $C_6H_4CBrClO$ $[M]^+$ 205.9. **Found:** 205.8 m/z.

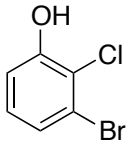

Figure 3.4.17. Product 3.14c

3-bromo-2-chlorophenol (**3.14c**): Prepared according to the general procedure on a 100 mg scale, using **3.6** as catalyst. 17 mg (14% yield) of **3.14c** was isolated as an off-white solid. **^{1}H NMR** (599 MHz, $CDCl_3$) δ 7.20 (dd, *J* = 8.0, 1.1 Hz, 1H), 7.06 (t, *J* = 8.1 Hz, 1H), 6.98 (dd, *J* = 8.2, 1.2 Hz, 1H), 5.66 (s, 1H); **^{13}C NMR** (151 MHz, $CDCl_3$) δ 152.69, 128.78, 125.50, 122.33, 121.00, 115.16; **MS (APCI)**: **Calculated for** $C_6H_4CBrClO$ $[M]^+$ 205.9. **Found:** 205.8 m/z.

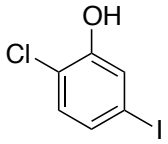

Figure 3.4.18. Product 3.15a

2-chloro-5-iodophenol (**3.15a**): Prepared according to the general procedure on a 1.0 g scale, using **3.6** as catalyst. 750 mg (65% yield) of **3.15a** was isolated as an off-white solid. Spectra obtained from **3.15a** match spectra reported in patent literature.[115] **^{1}H NMR** (400 MHz, $CDCl_3$) δ 7.54 (d, *J* = 2.0 Hz, 1H), 7.36 (dd, *J* = 8.4, 2.0 Hz, 1H), 7.19 (d, *J* = 8.4 Hz, 1H), 5.68 (s, 1H); **^{13}C NMR** (126 MHz, $CDCl_3$) δ 152.13, 130.65, 130.36, 125.56, 120.25, 92.16; **MS (APCI)**: **Calculated for** C_6H_4CClIO $[M]^+$ 253.9. **Found:** 254.0 m/z.

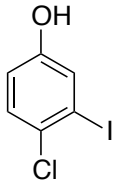

Figure 3.4.19. Product 3.15b

4-chloro-3-iodophenol (**3.15b**): Prepared according to the general procedure on a 50 mg scale, using **3.7** as catalyst. 46 mg (80% yield) of **3.15b** was isolated as a white solid. Constitutional isomer was assigned by contrast to spectra obtained from **3.15a**. **^{1}H NMR** (400 MHz, $CDCl_3$) δ 7.35 (d, *J* = 2.9 Hz, 1H), 7.28 (d, *J* = 8.7 Hz, 1H), 6.78 (dd, *J* = 8.7, 2.9 Hz, 1H), 4.87 (s, 1H); **^{13}C NMR** (126 MHz, $CDCl_3$) δ 154.33, 130.50, 129.66, 126.99, 117.01, 98.04; **MS (APCI)**: **Calculated for** C_6H_4CClIO $[M]^+$ 253.9. **Found:** 254.0 m/z.

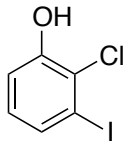

Figure 3.4.20. Product 3.15c

2-chloro-3-iodophenol (**3.15c**): Prepared according to the general procedure on a 1.0 g scale, using **3.6** as catalyst. 320 mg (28% yield) of **3.15c** was isolated as a white solid. **^{1}H NMR** (400 MHz, $CDCl_3$) δ 7.42 (dd, *J* = 7.8, 1.5 Hz, 1H), 7.00 (dd, *J* = 8.2, 1.5 Hz, 1H), 6.92 (t, *J* = 8.0 Hz, 1H), 5.59 (s, 1H); **^{13}C NMR** (126 MHz, $CDCl_3$) δ 151.80, 132.02, 129.60, 124.81, 116.15, 97.41; **MS (APCI)**: **Calculated for** C_6H_4CClIO $[M]^+$ 253.9. **Found:** 254.0 m/z.

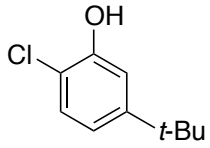

Figure 3.4.21. Product 3.16a

5-(*tert*-butyl)-2-chlorophenol (**3.16a**): Prepared according to the general procedure on a 100 mg scale, using **3.6** as catalyst. 44 mg of **3.16a** was isolated as an orange oil, however approximately 10% impurities were present that could not be removed using available purification techniques (*i.e.* FCC, preparative TLC, etc.). No isolated yield was reported, but the slightly impure material was used for spectral analysis in order to elucidate the structure of **3.16a** (2D

NMR spectra are provided). **^{1}H NMR** (599 MHz, $CDCl_3$) δ 7.22 (d, *J* = 8.4 Hz, 1H), 7.06 (d, *J* = 2.3 Hz, 1H), 6.90 (dd, *J* = 8.4, 2.3 Hz, 1H), 5.52 (bs, 1H), 1.29 (s, 9H); **^{13}C NMR** (151 MHz, $CDCl_3$) δ 152.43, 150.94, 128.42, 118.73, 116.83, 113.63, 34.76, 31.34; **MS (APCI)**: **Calculated for** $C_{10}H_{14}ClO$ $[M+H]^+$ 185.1. **Found:** 185.1 m/z.

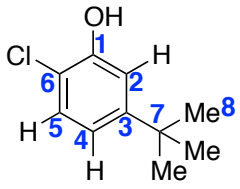

3.16a

no.	δ_H (mult, *J* in Hz)	δ_C	HMBC (H->C)
1		150.9	H-5, H-2, H-4
2	7.06 (d, *J* = 2.3)	113.6	H-5, H-4
3		152.4	H-5, H-2, H-4, Me-8
4	6.90 (dd, *J* = 8.4, 2.3)	118.7	H-2
5	7.22 (d, *J* = 8.4)	128.4	H-4
6		116.8	H-5, H-2, H-4
7		34.8	H-2, H-4
8	1.29 (s)	31.3	

Figure 3.4.22. Multiple Bond Correlations of Product 3.16a

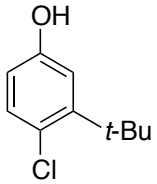

Figure 3.4.23. Product 3.16b

3-(*tert*-butyl)-4-chlorophenol (**3.16b**): Prepared according to the general procedure on a 100 mg scale, using **3.7** as catalyst. 65 mg (53% yield) of **3.16b** was isolated as an orange oil. The constitutional isomer was verified using 2-dimensional NMR analysis. **^{1}H NMR** (599 MHz, $CDCl_3$) δ 7.18 (d, *J* = 8.5 Hz, 1H), 6.91 (d, *J* = 3.0 Hz, 1H), 6.61 (dd, *J* = 8.5, 3.0 Hz, 1H), 1.45 (s,

9H); **^{13}C NMR** (151 MHz, $CDCl_3$) δ 154.12, 148.13, 132.77, 125.20, 115.25, 113.92, 36.13, 29.55; **MS (APCI)**: **Calculated for** $C_{10}H_{14}ClO$ $[M+H]^+$ 185.1. **Found:** 185.1 m/z.

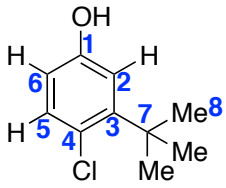

3.16b

no.	δ_H (mult, *J* in Hz)	δ_C	HMBC (H->C)
1		154.1	H-2, H-5, H-6
2	6.91 (d, *J* = 3.0)	115.3	H-5, H-6
3		148.1	H-5, Me-8
4		125.2	H-2, H-5, H-6
5	7.18 (d, *J* = 8.5)	132.8	
6	6.61 (dd, *J* = 8.5, 3.0)	113.9	H-2
7		36.1	H-2, H-5
8	1.45 (s)	29.6	

Figure 3.4.24. Multiple Bond Correlations of Product 3.16b

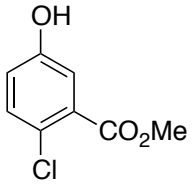

Figure 3.4.25. Product 3.17b

Methyl 2-chloro-5-hydroxybenzoate (**3.17b**): Prepared according to the general procedure on a 100 mg scale, using **3.7** as catalyst. 70 mg (57% yield) of **3.17b** was isolated as a clear oil, which settled to clear thin crystals shortly after. The constitutional isomer was verified using 2-dimensional NMR analysis. **^{1}H NMR** (500 MHz, $CDCl_3$) δ 7.34 (d, *J* = 3.1 Hz, 1H), 7.30 (d, *J* = 8.7 Hz, 1H), 6.93 (dd, *J* = 8.7, 3.1 Hz, 1H), 5.82 (s, 1H), 3.93 (s, 3H); **^{13}C NMR** (126 MHz, $CDCl_3$)

δ 166.56, 154.37, 132.29, 130.50, 125.06, 120.32, 118.28, 52.85; **MS (APCI)**: **Calculated for** $C_8H_8ClO_3$ $[M+H]^+$ 187.0. **Found:** 187.0 m/z.

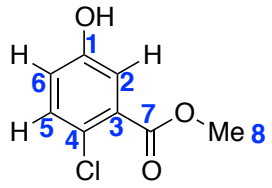

3.17b

no.	δ_H (mult, *J* in Hz)	δ_C	HMBC (H->C)
1		154.1	H-2, H-5, H-6
2	7.34 (d, *J* = 3.1)	118.3	H-6
3		130.5	H-5, Me-8
4		125.1	H-2, H-5, H-6
5	7.30 (d, *J* = 8.7)	132.3	
6	6.93 (dd, *J* = 8.7, 3.1)	120.3	H-2
7		166.6	H-2, H-5, Me-8
8	1.45 (s)	52.9	

Figure 3.4.26. Multiple Bond Correlations of Product 3.17b

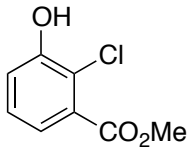

Figure 3.4.27. Product 3.17c

Methyl 2-chloro-3-hydroxybenzoate (**3.17c**): Prepared according to the general procedure (purified using reverse phase FCC) on a 100 mg scale, using **3.6** as catalyst. Upon completion, reaction was filtered thru a short silica plug with DCM. The filtrate was collected, and the solvent was removed by rotovap to afford a crude oil. The crude oil was then dissolved with minimal acetonitrile (50% v/v aqueous). This solution was purified on a Biotage Isolera using a C18 stationary phase SNAP cartridge (water:acetonitrile:: 90:10 → 85:15 → 80:20). Fractions containing the desired compound were combined and extracted with ethyl acetate (3x). The combined organic layers were washed with brine (1x). The organic layer was collected, dried over sodium sulfate, and filtered. The solvent was removed by rotovap to yield 49 mg (40% yield) **3.17c**

as a clear oil. **^{1}H NMR** (599 MHz, $CDCl_3$) δ 7.45 (dd, *J* = 7.6, 1.7 Hz, 1H), 7.24 (t, *J* = 8.0 Hz, 1H), 7.19 (dd, *J* = 8.1, 1.7 Hz, 1H), 5.95 (s, 1H), 3.93 (s, 3H); **^{13}C NMR** (151 MHz, $CDCl_3$) δ 165.88, 152.42, 146.80, 130.13, 127.74, 123.50, 119.56, 52.65; **MS (APCI)**: **Calculated for** $C_8H_8ClO_3$ $[M+H]^+$ 187.0. **Found:** 187.0 m/z.

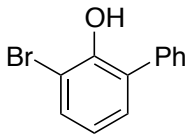

Figure 3.4.28. Product 3.8c

3-bromo-[1,1'-biphenyl]-2-ol (**3.8c**): Prepared according to the general procedure (Purified by preparative TLC) on a 50 mg scale, using **3.6** as catalyst. Upon completion, the reaction was filtered thru a silica plug with DCM. The filtrate was collected, and the solvent was removed by rotovap. The resulting crude material was dissolved in minimal hexane, and the solution was purified by preparative TLC (hexane:ethyl acetate = 90:10) to afford 33 mg (45% yield) of **3.8c** as a white solid. **^{1}H NMR** (500 MHz, $CDCl_3$) δ 7.55 – 7.51 (m, 2H), 7.49 – 7.44 (m, 3H), 7.39 (tt, *J* = 7.4, 1.5 Hz, 1H), 7.26 (dd, *J* = 7.6, 1.6 Hz, 1H), 6.89 (t, *J* = 7.8 Hz, 1H), 5.68 (s, 1H); **^{13}C NMR** (126 MHz, $CDCl_3$) δ 149.38, 137.33, 131.59, 130.30, 129.83, 129.30, 128.69, 127.93, 121.82, 111.15; **MS (APCI)**: **Calculated for** $C_{12}H_{10}BrO$ $[M+H]^+$ 249.0. **Found:** 248.8 m/z.

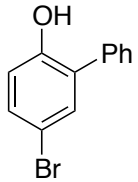

Figure 3.4.29. Product 3.8d

5-bromo-[1,1'-biphenyl]-2-ol (**3.8d**): Prepared according to the general procedure on a 100 mg scale, using **2.3** as catalyst. 68 mg (46% yield) of **3.8d** was isolated as a white solid. **^{1}H NMR**

(500 MHz, $CDCl_3$) δ 7.52 – 7.47 (m, 2H), 7.45 – 7.40 (m, 3H), 7.38 – 7.33 (m, 2H), 6.88 (d, *J* = 8.7 Hz, 1H), 5.19 (s, 1H); **^{13}C NMR** (126 MHz, $CDCl_3$) δ 151.78, 135.84, 132.78, 131.97, 130.20, 129.62, 129.07, 128.59, 117.79, 112.91; **MS (APCI)**: **Calculated for** $C_{12}H_{10}BrO$ $[M+H]^+$ 249.0. **Found:** 248.9 m/z.

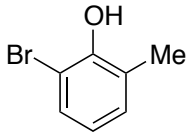

Figure 3.4.30. Product 3.18a

2-bromo-6-methylphenol (**3.18a**): Prepared according to the general procedure on a 50 mg scale, using **3.6** as catalyst. 26 mg (31% yield) of **3.18a** was isolated as a white solid. The yield was severely affected by the presence of dibromination product, which eluted in a similar manner to **3.18a** on normal phase silica gel. **^{1}H NMR** (500 MHz, $CDCl_3$) δ 7.29 (dd, *J* = 8.1, 1.1 Hz, 1H), 7.09 – 7.04 (m, 1H), 6.71 (t, *J* = 7.8 Hz, 1H), 5.54 (s, 1H), 2.30 (s, 3H); **^{13}C NMR** (126 MHz, $CDCl_3$) δ 150.52, 130.52, 129.49, 126.07, 121.35, 110.29, 16.75; **MS (APCI)**: **Calculated for** C_7H_7BrO $[M]^+$ 186.0. **Found:** 185.9 m/z.

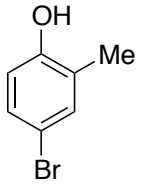

Figure 3.4.31. Product 3.18b

4-bromo-2-methylphenol (**3.18b**): Prepared according to the general procedure on a 50 mg scale, using **2.3** as catalyst. 33 mg (38% yield) of **3.18b** was isolated as a white solid. **^{1}H NMR** (500 MHz, $CDCl_3$) δ 7.24 (d, *J* = 2.0 Hz, 1H), 7.17 (dd, *J* = 8.6, 2.3 Hz, 1H), 6.65 (d, *J* = 8.5 Hz,

1H), 4.68 (s, 1H), 2.22 (s, 3H); **^{13}C NMR** (126 MHz, $CDCl_3$) δ 153.03, 133.67, 129.89, 126.30, 116.67, 112.73, 15.76; **MS (APCI)**: **Calculated for** C_7H_7BrO $[M]^+$ 186.0. **Found:** 185.9 m/z.

3.4.4 Molecular Geometries and Energies for Scheme S1

All structures were optimized in chloroform (CPCM model) using density functional theory, B3LYP/6-31+(d),[I,II] as implemented in the Gaussian 09[III] suite of programs.

SI-2 (anisole)
Number of imaginary frequencies: 0

C	2.2883130	0.3344250	-0.0000630
C	1.3366360	1.3550730	0.0000440
C	-0.0344860	1.0636280	0.0000760
C	-0.4534590	-0.2738530	-0.0000010
C	0.4992610	-1.3063260	-0.0001080
C	1.8583110	-1.0001340	-0.0001380
H	3.3487690	0.5704780	-0.0000870
H	1.6529520	2.3953050	0.0001040
H	-0.7526910	1.8758100	0.0001600
H	2.5861700	-1.8076840	-0.0002210
O	-1.7627840	-0.6732170	0.0000200
C	-2.7813690	0.3262940	0.0001240
H	-3.7277500	-0.2163140	0.0001220
H	-2.7196440	0.9550730	0.8967300
H	-2.7197090	0.9551950	-0.8964000

Energy (0K) = -346.7893763
Energy (0K) + ZPE = -346.656146
Enthalpy (298K) = -346.648318
Free Energy (298K) = -346.687233

***N*-chlorosuccinimide** (NCS)
Number of imaginary frequencies: 0

C	-1.8910590	0.7703380	0.0000190
C	-1.8910590	-0.7703380	0.0000520
C	-0.4306800	-1.1878760	0.0000320
C	-0.4306800	1.1878760	-0.0000160
H	-2.3748120	1.2001160	-0.8823900
H	-2.3747810	1.2001540	0.8824270
H	-2.3748140	-1.2001530	-0.8823380
H	-2.3747800	-1.2001160	0.8824790
N	0.3203470	0.0000000	-0.0000060
Cl	2.0278730	0.0000000	-0.0000380
O	0.0402360	2.3042510	-0.0000470

O	0.0402360	-2.3042510	0.0000450

Energy (0K) = -820.24114
Energy (0K) + ZPE = -820.159520
Enthalpy (298K) = -820.151369
Free Energy (298K) = -820.192270

SI-3 (trimethylphosphine sulfide)
Number of imaginary frequencies: 0

P	0.0000000	0.0000000	-0.1921990
C	0.0000000	1.6836960	-0.9182330
H	-0.8896040	2.2226230	-0.5791860
H	0.8896040	2.2226230	-0.5791860
H	0.0000000	1.6329080	-2.0124860
C	1.4581240	-0.8418480	-0.9182330
H	2.3696500	-0.3408920	-0.5791860
H	1.4800460	-1.8817310	-0.5791860
H	1.4141400	-0.8164540	-2.0124860
C	-1.4581240	-0.8418480	-0.9182330
H	-1.4800460	-1.8817310	-0.5791860
H	-2.3696500	-0.3408920	-0.5791860
H	-1.4141400	-0.8164540	-2.0124860
S	0.0000000	0.0000000	1.8077340

Energy (0K) = -859.3396157
Energy (0K) + ZPE = -859.223656
Enthalpy (298K) = -859.214659
Free Energy (298K) = -859.254473

SI-4
Number of imaginary frequencies: 0

C	-0.7643710	-1.2299740	0.0000160
C	0.7643710	-1.2299740	0.0000570
C	1.1116880	0.2726960	0.0000090
C	-1.1116880	0.2726960	-0.0000250
H	-1.2078630	-1.7065960	-0.8820410
H	-1.2079150	-1.7065640	0.8820640
H	1.2079150	-1.7066160	-0.8819630
H	1.2078630	-1.7065440	0.8821420
N	0.0000000	1.0590930	-0.0000320
O	-2.2873380	0.6812510	-0.0000510
O	2.2873380	0.6812510	0.0000110

Energy (0K) = -360.2074013
Energy (0K) + ZPE = -360.128665
Enthalpy (298K) = -360.122096
Free Energy (298K) = -360.158564

SI-5

Number of imaginary frequencies: 0

P	-0.8463320	0.3697160	0.0000000
C	-1.4025170	2.0967260	0.0000000
H	-1.0445590	2.6089520	0.8966020
H	-1.0445590	2.6089520	-0.8966020
H	-2.4973460	2.0896980	0.0000000
C	-1.4025170	-0.4986530	-1.4910600
H	-1.0765900	0.0503850	-2.3778210
H	-0.9914620	-1.5114930	-1.5094600
H	-2.4958800	-0.5539570	-1.4693150
C	-1.4025170	-0.4986530	1.4910600
H	-0.9914620	-1.5114930	1.5094600
H	-1.0765900	0.0503850	2.3778210
H	-2.4958800	-0.5539570	1.4693150
S	1.2686850	0.5607500	0.0000000
Cl	1.8444510	-1.4348070	0.0000000

Energy (0K) = -1319.33797132
Energy (0K) + ZPE = -1319.219840
Enthalpy (298K) = -1319.209133
Free Energy (298K) = -1319.254998

SI-6
Number of imaginary frequencies: 0

N	-1.8047390	0.0271570	0.5565690
C	-3.1408990	0.1944700	0.9344830
C	-4.0951230	-0.3053340	-0.1605050
H	-4.7158760	-1.1137130	0.2395520
C	-3.1463750	-0.7655280	-1.2737360
C	-1.7873800	-0.5016650	-0.6454570
H	-3.2457200	-0.1959030	-2.2040620
H	-3.2364630	-1.8265490	-1.5292920
H	-4.7665130	0.5054970	-0.4604620
O	-3.4940790	0.6836720	2.0000100
O	-0.7181550	-0.7826550	-1.3241720
Cl	3.0280010	-1.6390220	0.8589800
P	1.5188010	0.9356960	-0.1968220
C	3.1748280	1.2196460	-0.8987550
H	3.3930160	2.2909590	-0.8358100
H	3.9244260	0.6538170	-0.3448940
H	3.1772720	0.9080200	-1.9469310
C	1.4617330	1.4833890	1.5340830
H	2.1583390	0.8885980	2.1287380
H	0.4420190	1.3432550	1.9028730
H	1.7392980	2.5412580	1.5845450
C	0.3746560	1.9626140	-1.1684200
H	0.7710200	2.9836990	-1.1560480
H	0.3250450	1.6046640	-2.1989300
H	-0.6186940	1.9534310	-0.7188830

S 0.9798250 -1.1145540 0.3339730

Energy (0K) = -1679.575544
Energy (0K) + ZPE = -1679.376536
Enthalpy (298K) = -1679.358874
Free Energy (298K) = -1679.421581

Calculation Citations:

(I) (a) Becke, A. D. *J. Chem. Phys.* **1993**, *98,* 5648. (b) Becke, A. D. *J. Chem. Phys.* **1993**, *98,* 1372. (c) Lee, C.; Yang, W.; Parr, R. G. *Phys. Rev. B* **1988**, *98,* 785.

(II) (a) Ditchfield, R.; Hehre, W. J.; Pople, J. A. *J. Chem. Phys.* **1971**, *54*, 724. (b) Hehre, W. J.; Ditchfield, R.; Pople, J. A. *J. Chem. Phys.* **1972**, *56*, 2257. (c) Hariharan, P. C.; Pople, J. A. *Theor. Chim. Acta* **1973**, *28*, 213. (d) Clark, T., J.; Chandrasekhar, C.; Spitznagel, G. W.; Schleyer, P. v. R. *J. Comp. Chem.* **1983**, *4*, 294.

(III) Gaussian 09, Revision D.01. M. J. Frisch, G. W. Trucks, H. B. Schlegel, G. E. Scuseria, M. A. Robb, J. R. Cheeseman, G. Scalmani, V. Barone, B. Mennucci, G. A. Petersson, H. Nakatsuji, M. Caricato, X. Li, H. P. Hratchian, A. F. Izmaylov, J. Bloino, G. Zheng, J. L. Sonnenberg, M. Hada, M. Ehara, K. Toyota, R. Fukuda, J. Hasegawa, M. Ishida, T. Nakajima, Y. Honda, O. Kitao, H. Nakai, T. Vreven, J. A. Montgomery, Jr., J. E. Peralta, F. Ogliaro, M. Bearpark, J. J. Heyd, E. Brothers, K. N. Kudin, V. N. Staroverov, T. Keith, R. Kobayashi, J. Normand, K. Raghavachari, A. Rendell, J. C. Burant, S. S. Iyengar, J. Tomasi, M. Cossi, N. Rega, J. M. Millam, M. Klene, J. E. Knox, J. B. Cross, V. Bakken, C. Adamo, J. Jaramillo, R. Gomperts, R. E. Stratmann, O. Yazyev, A. J. Austin, R. Cammi, C. Pomelli, J. W. Ochterski, R. L. Martin, K. Morokuma, V. G. Zakrzewski, G. A. Voth, P. Salvador, J. J. Dannenberg, S. Dapprich, A. D. Daniels, O. Farkas, J. B. Foresman, J. V. Ortiz, J. Cioslowski, and D. J. Fox, Gaussian, Inc., Wallingford CT, 2013.

3.4.5 Spectral Data for Purified Products

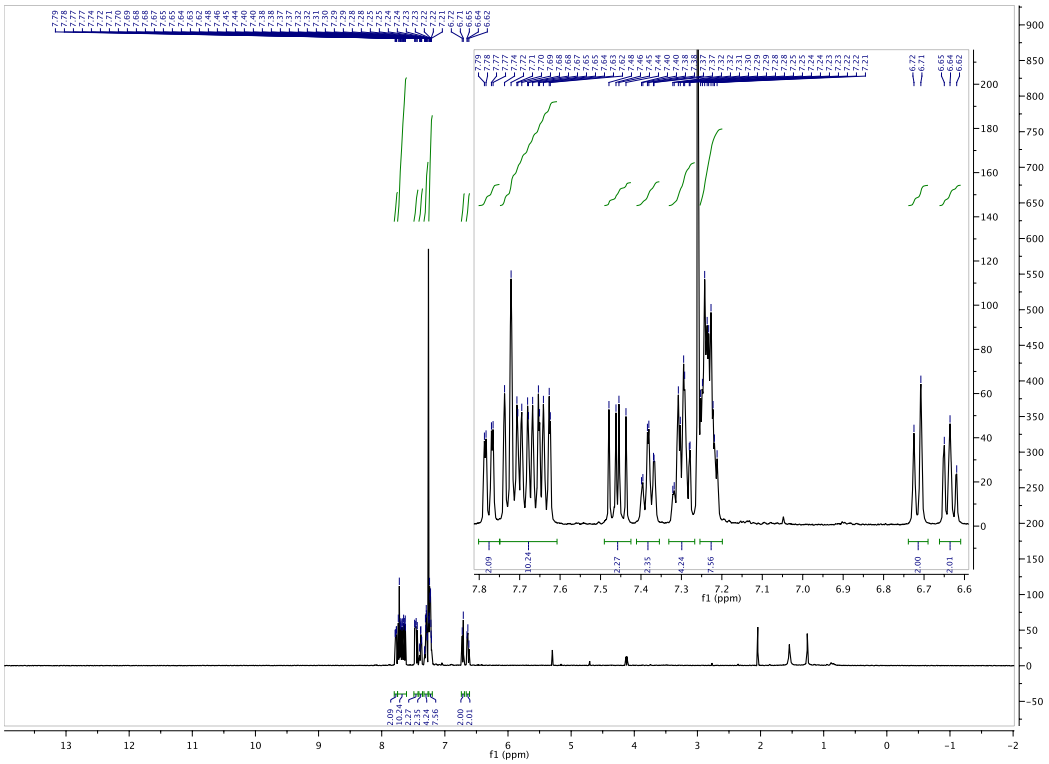

Figure 3.4.32. ^{1}H of 3.7

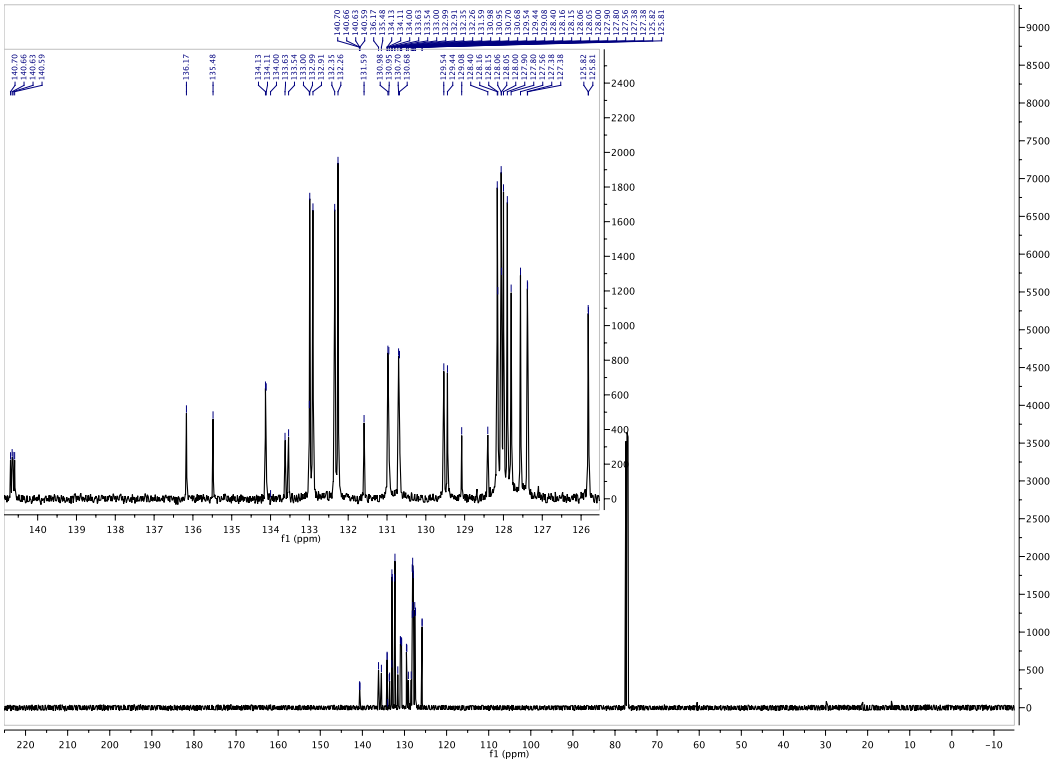

Figure 3.4.33. ^{13}C of 3.7

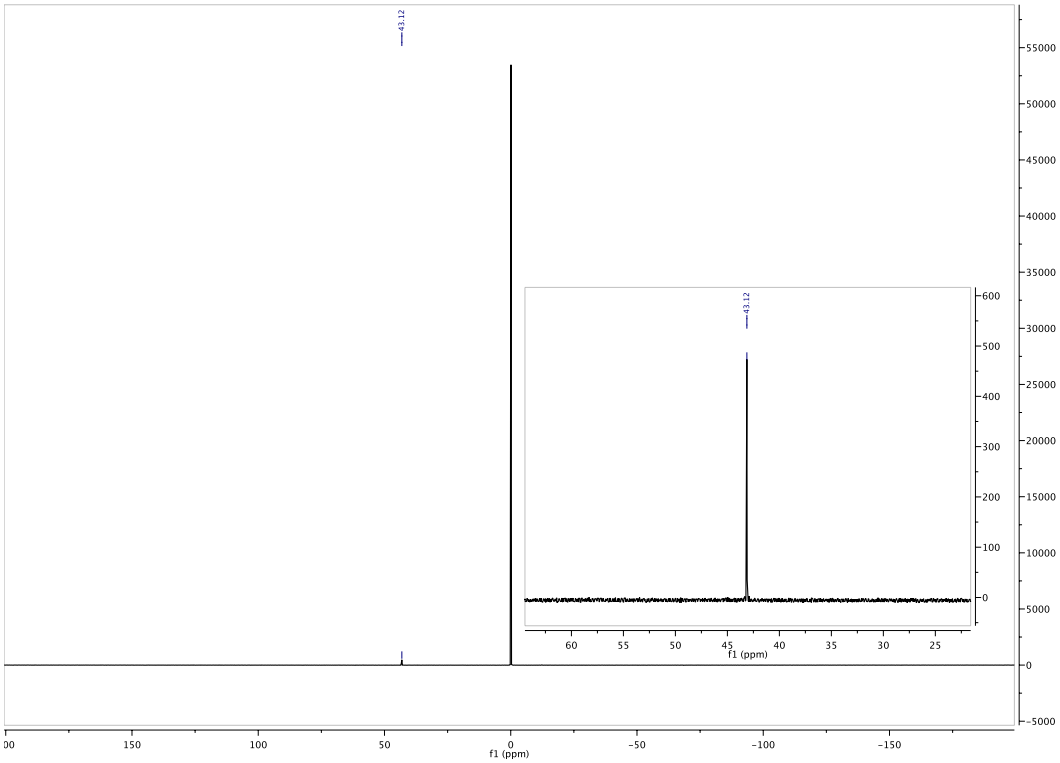

Figure 3.4.34. ^{31}P of 3.7

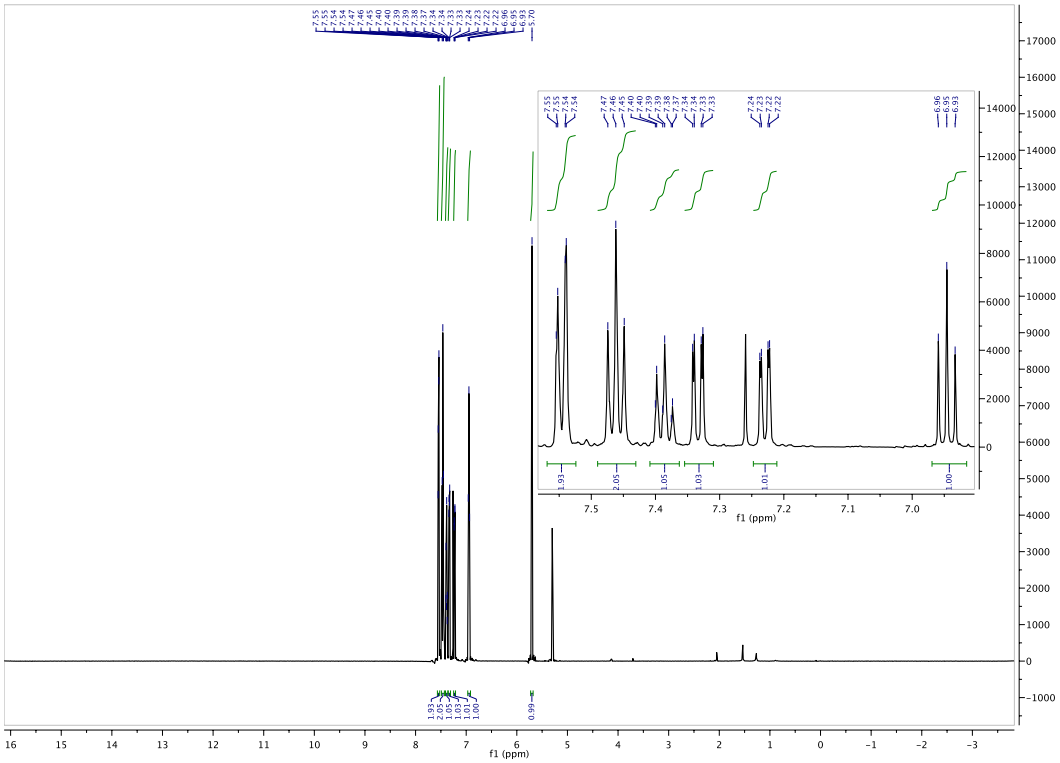

Figure 3.4.35. ^{1}H of 3.8a

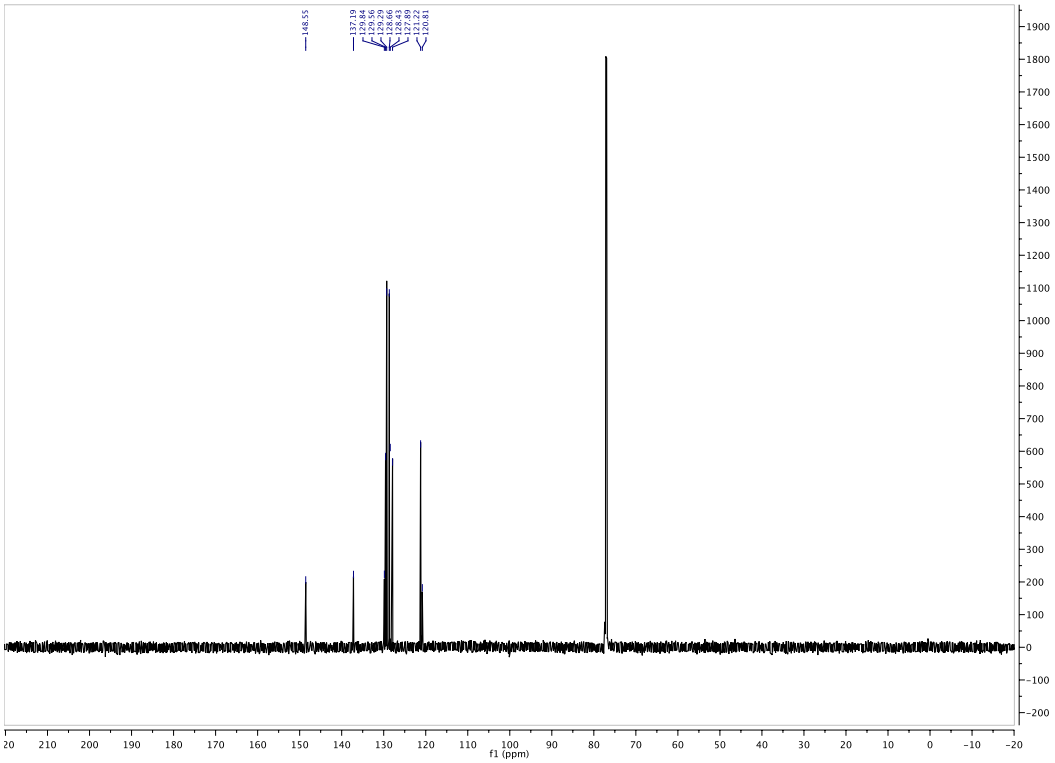

Figure 3.4.36. ^{13}C of 3.8a

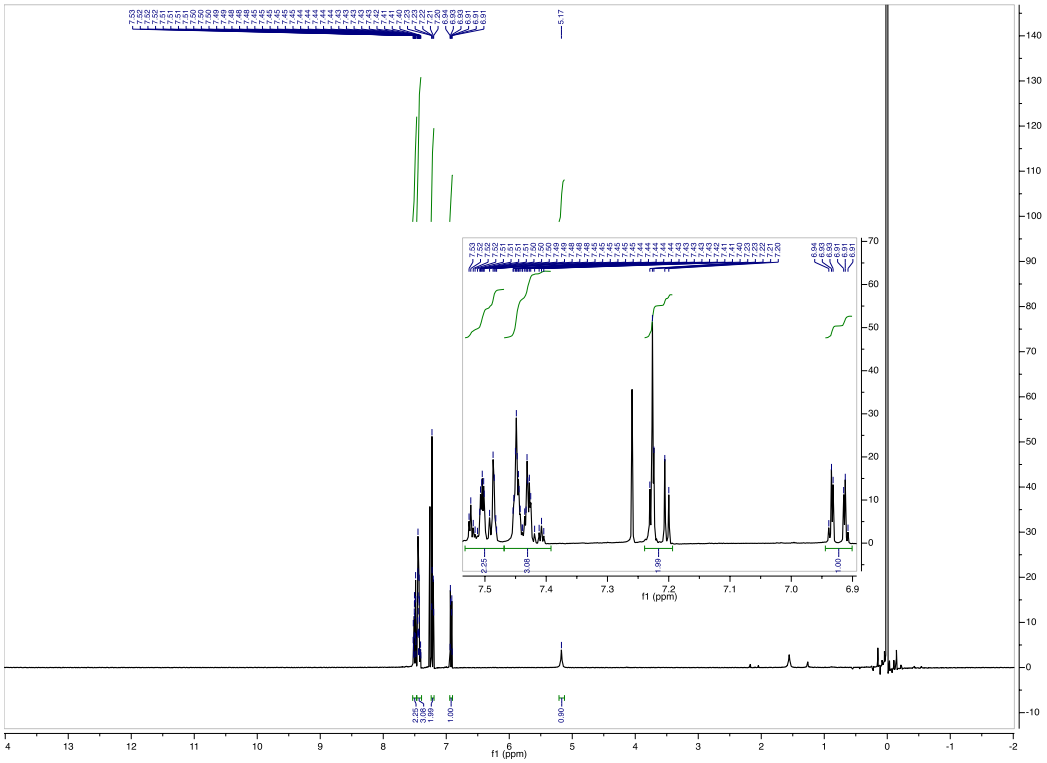

Figure 3.4.37. ^{1}H of 3.8b

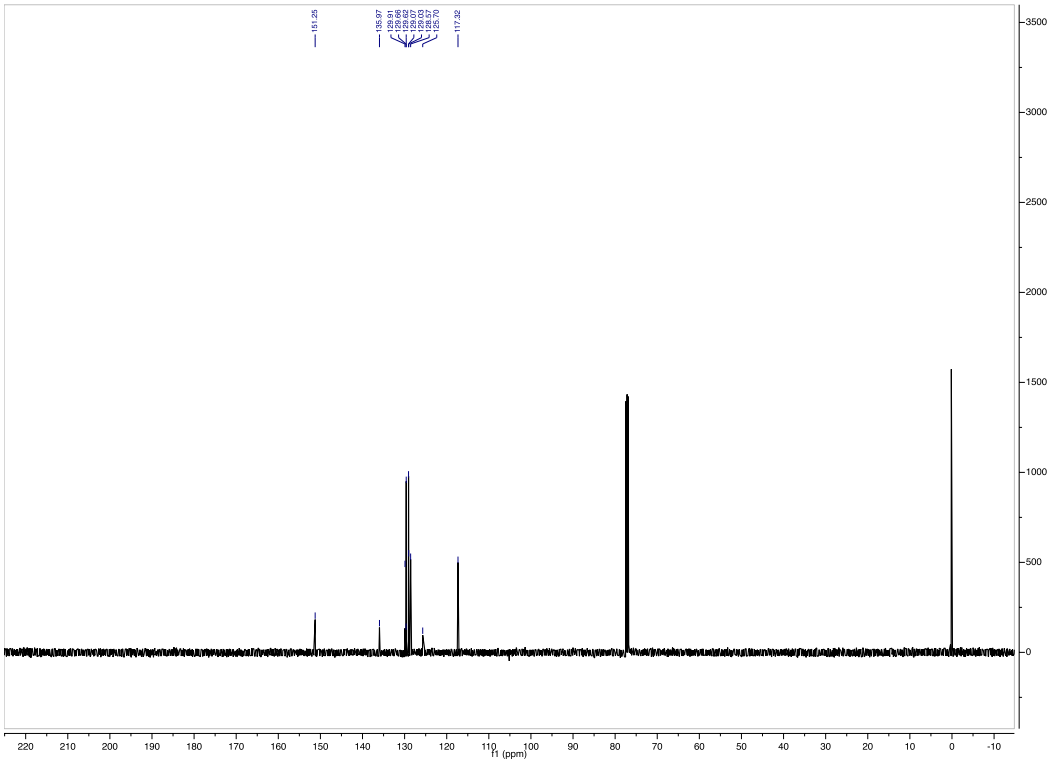

Figure 3.4.38. ^{13}C 3.8b

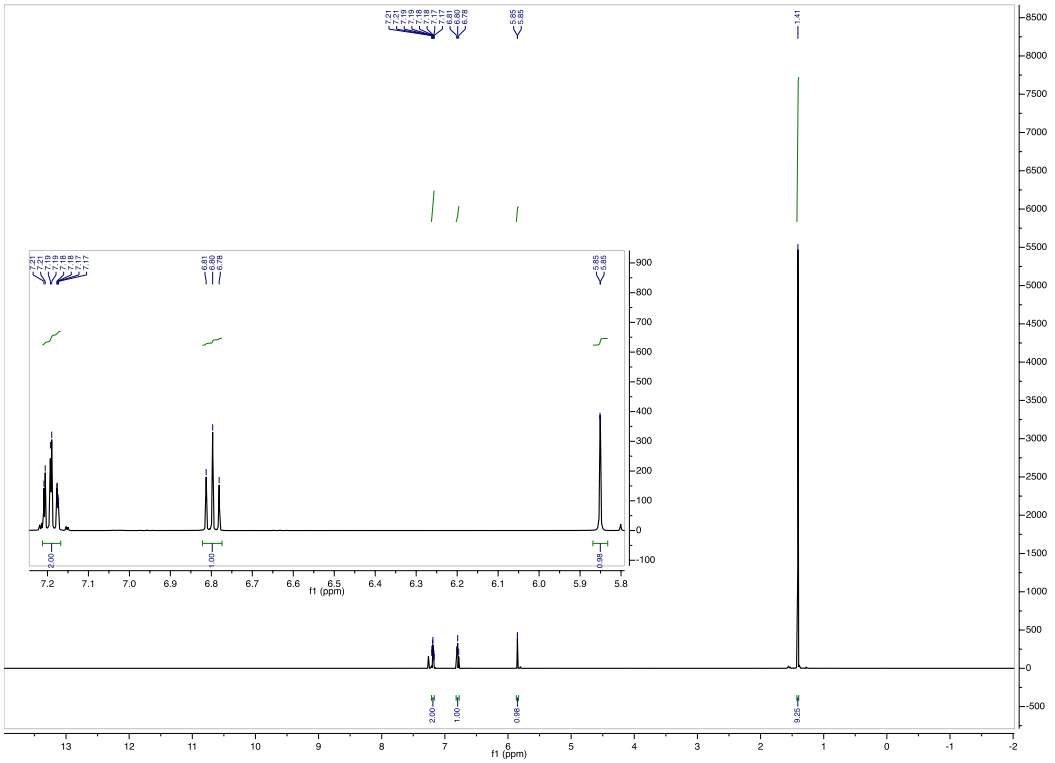

Figure 3.4.39. ^{1}H of 3.9a

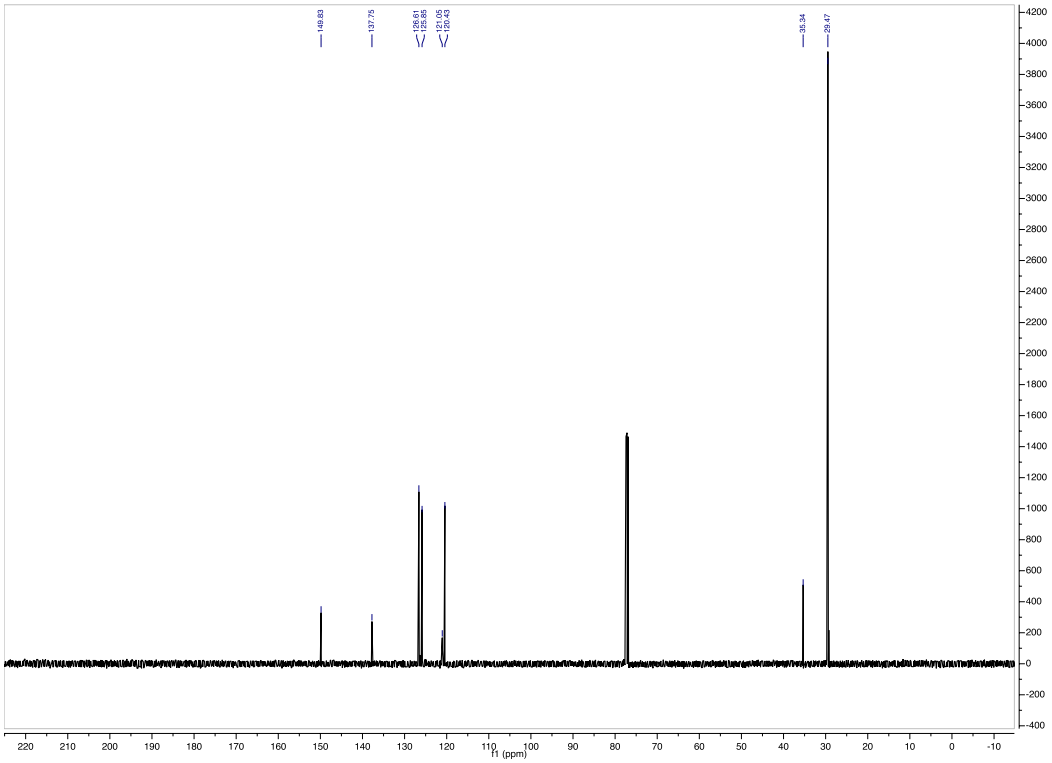

Figure 3.4.40. ^{13}C of 3.9a

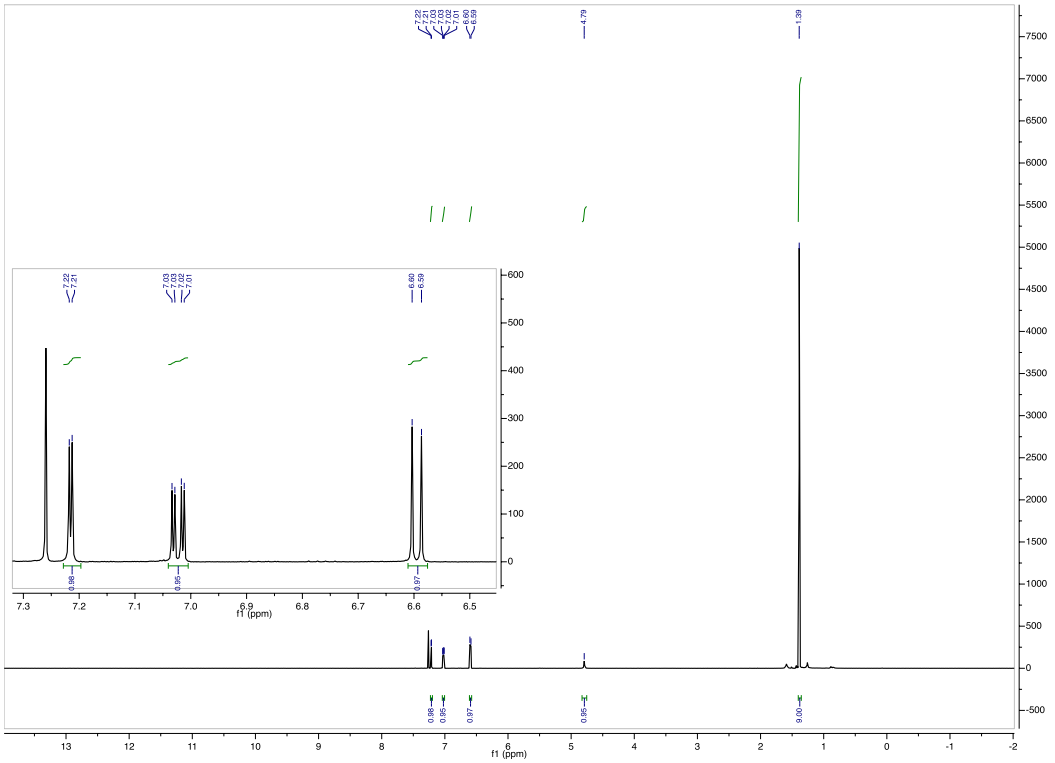

Figure 3.4.41. ^{1}H of 3.9b

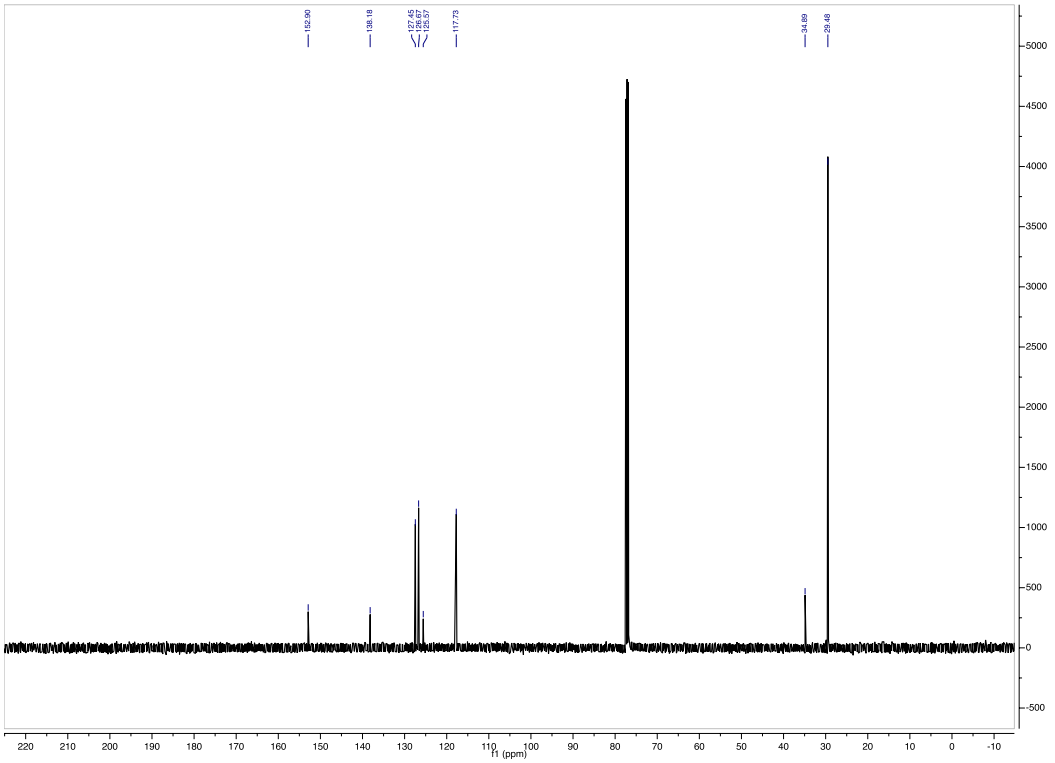

Figure 3.4.42. ^{13}C of 3.9b

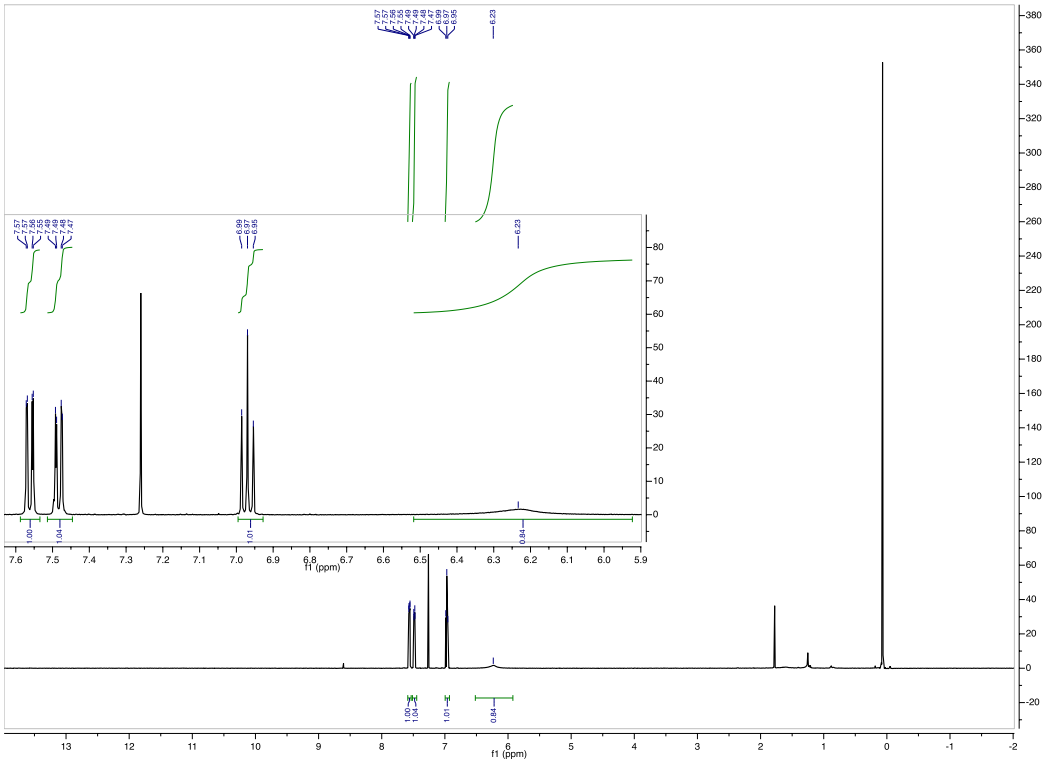

Figure 3.4.43. ^{1}H of 3.10a

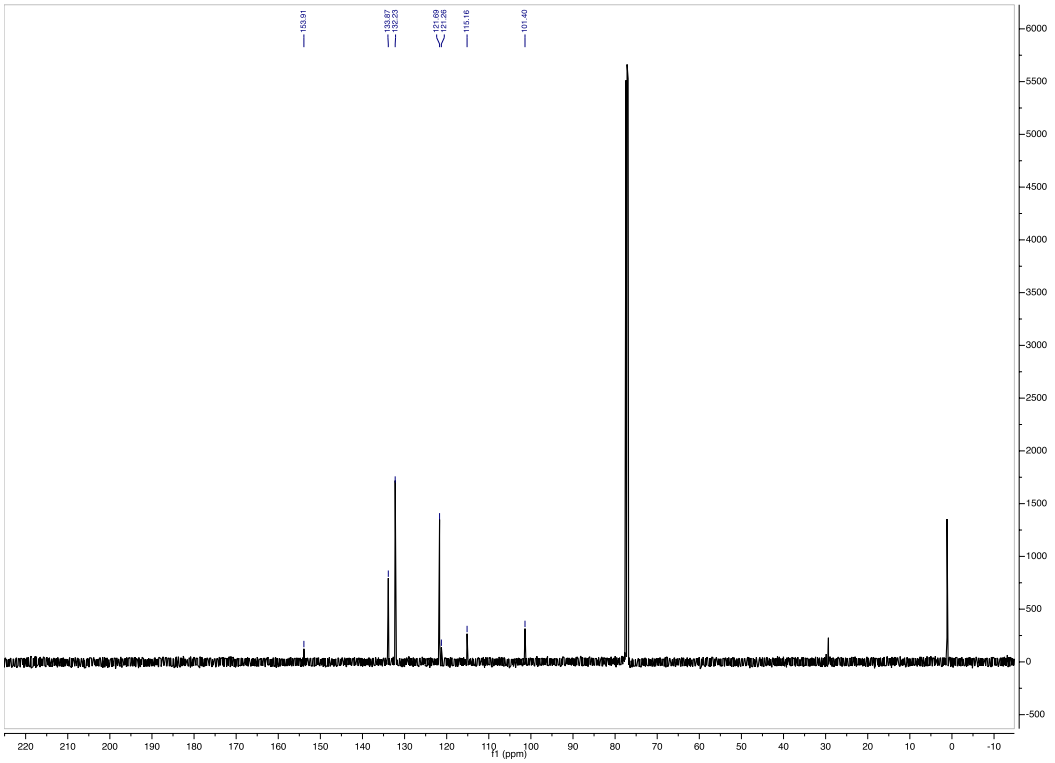

Figure 3.4.44. ^{13}C of 3.10a

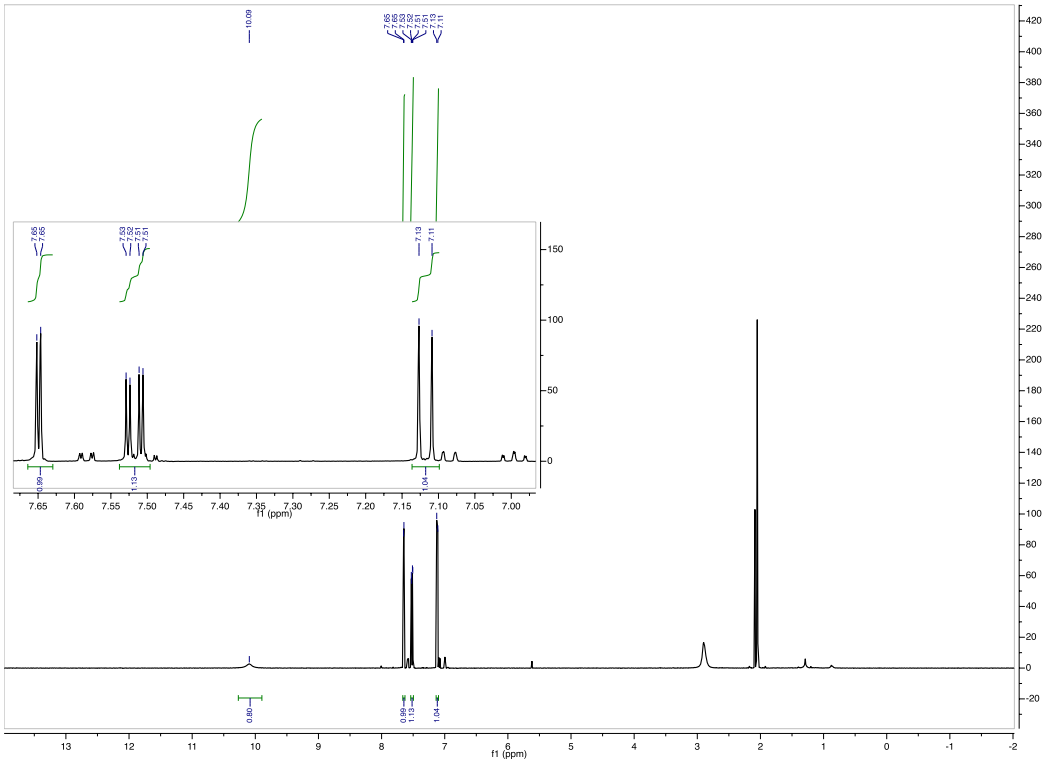

Figure 3.4.45. ^{1}H of 3.10b and ~10% 3.10

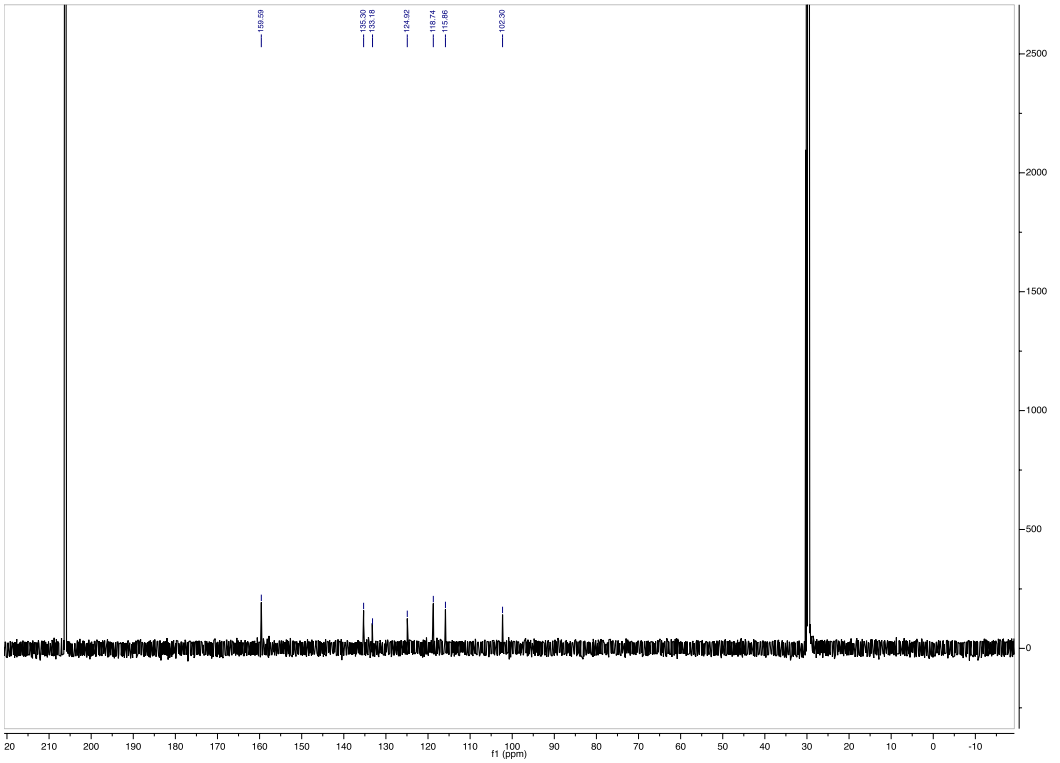

Figure 3.4.46. ^{13}C of 3.10b and ~10% 3.10

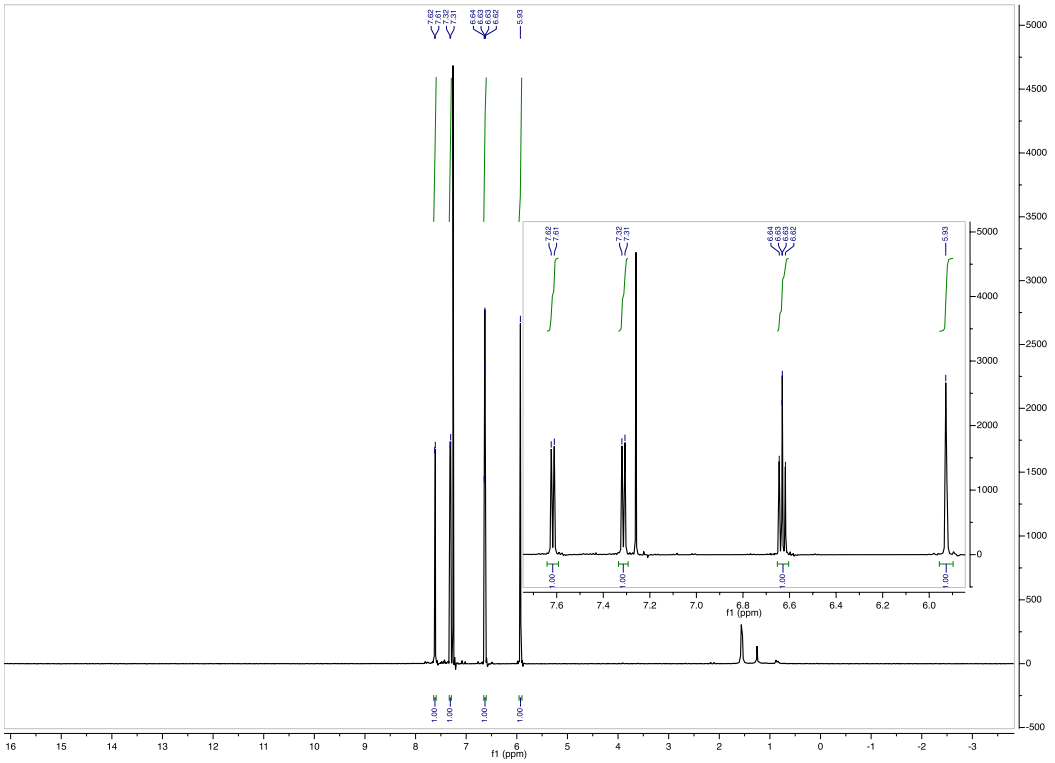

Figure 3.4.47. ^{1}H of 3.11a

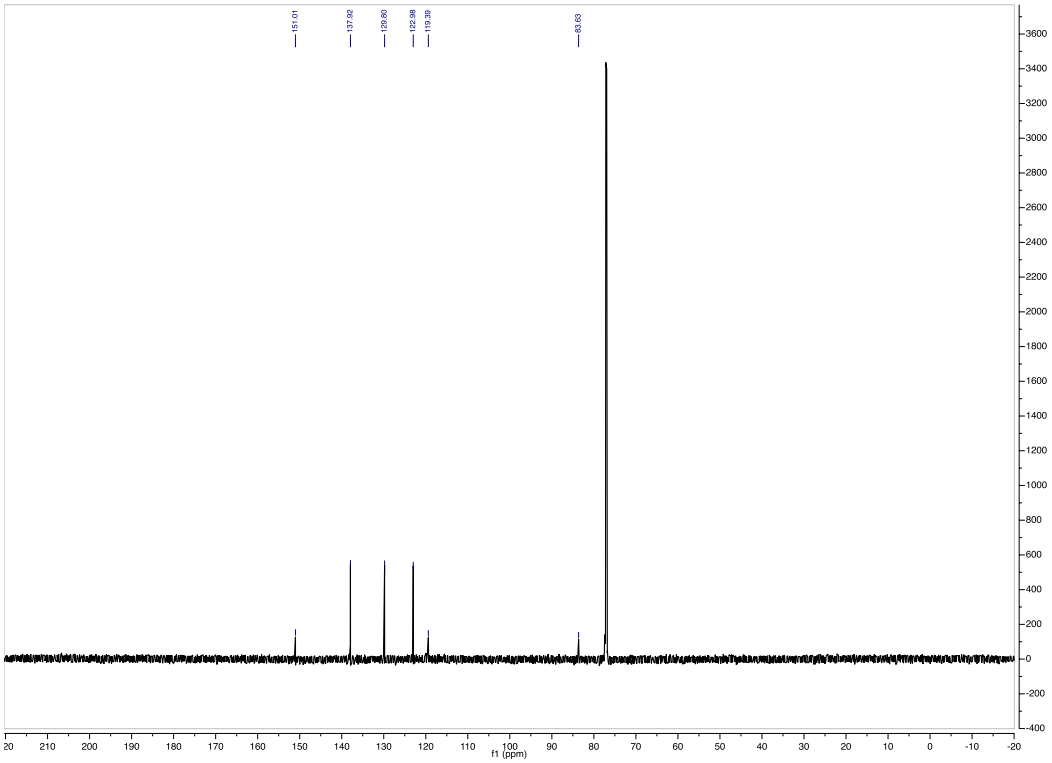

Figure 3.4.48. ^{13}C of 3.11a

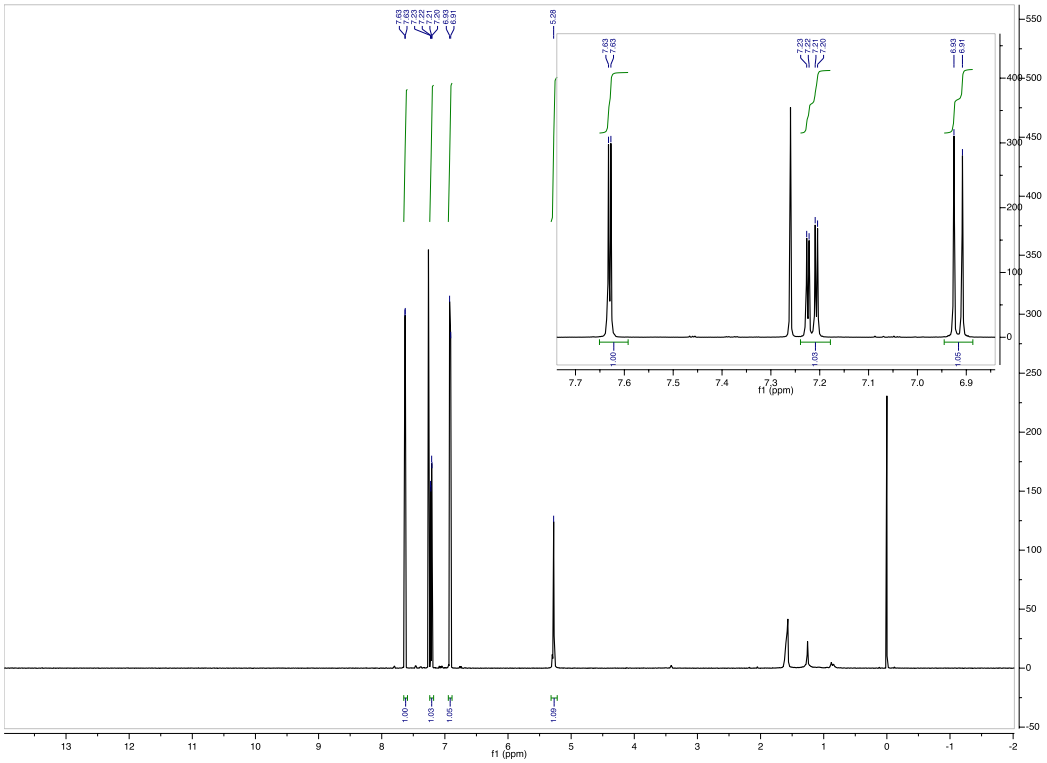

Figure 3.4.49. ^{1}H of 3.11b

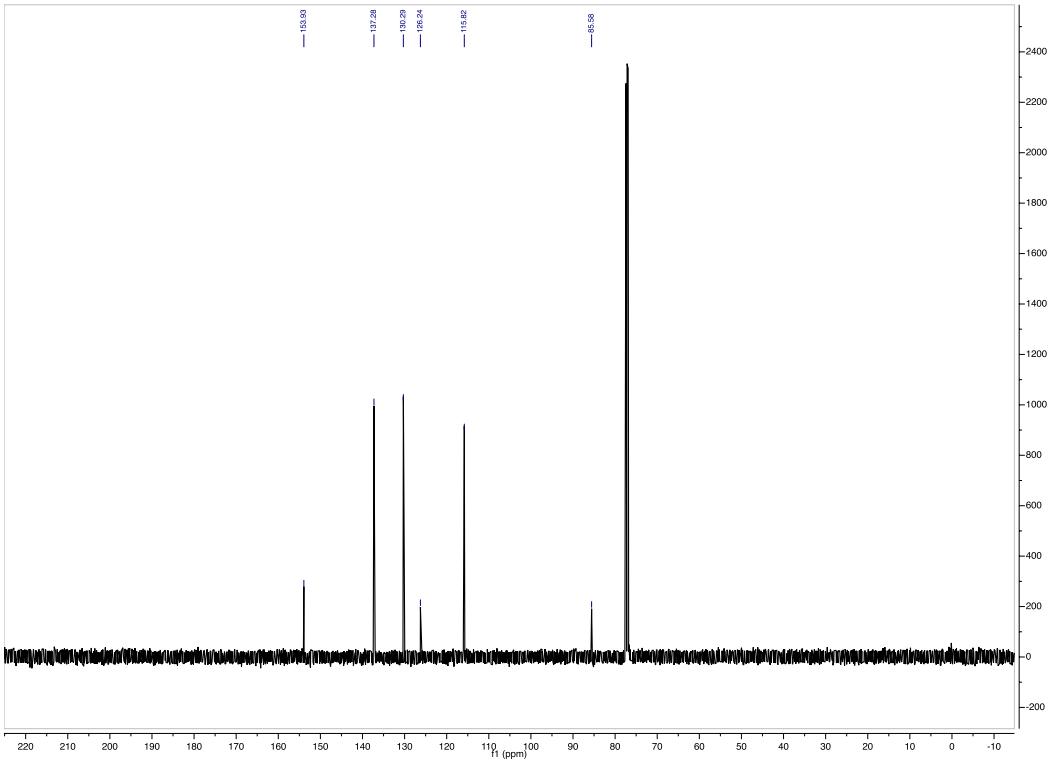

Figure 3.4.50. ^{13}C of 3.11b

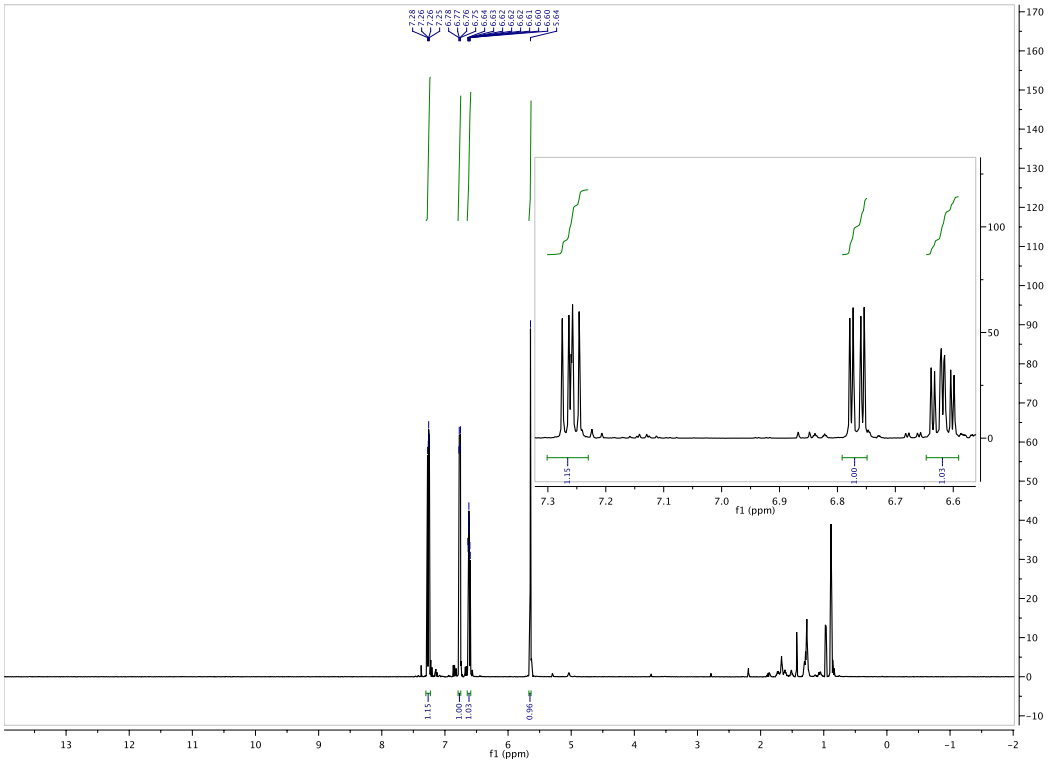

Figure 3.4.51. ^{1}H of 3.12a + impurities

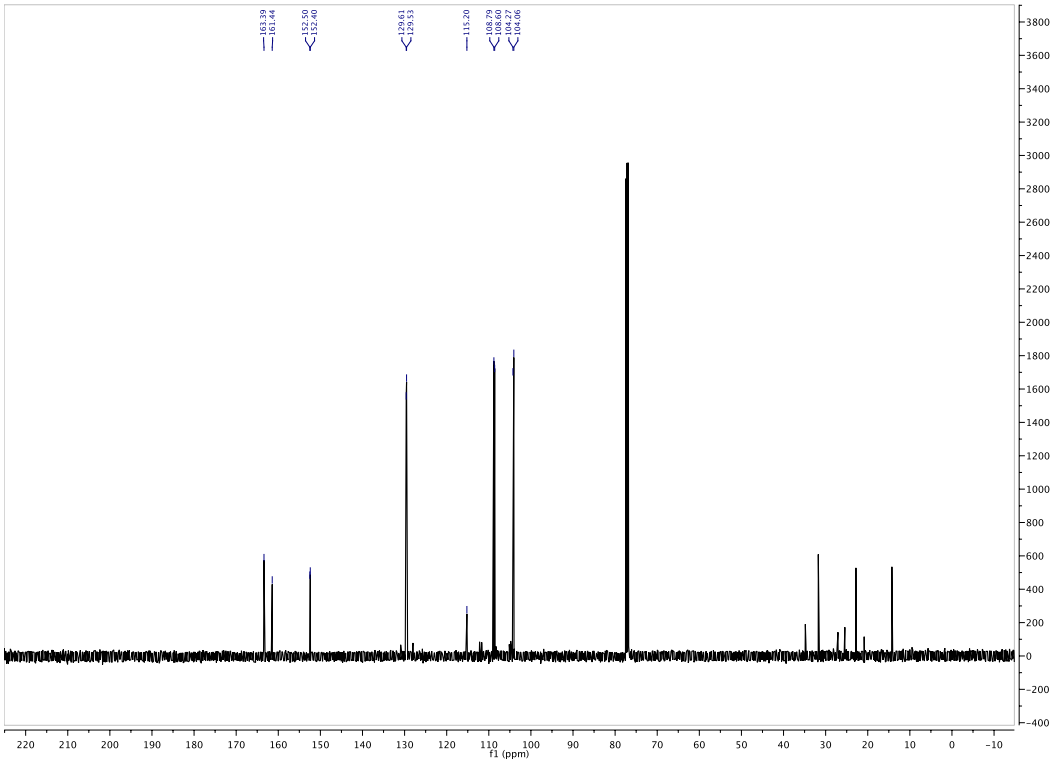

Figure 3.4.52. ^{13}C of 3.12a + impurities

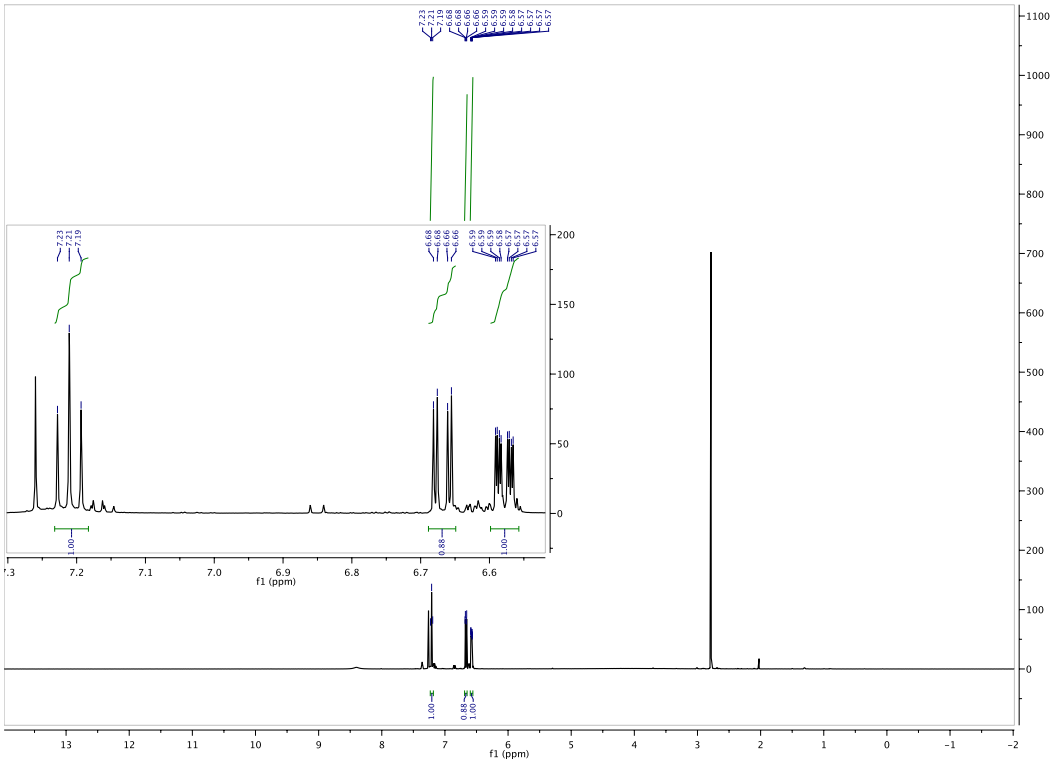

Figure 3.4.53. ^{1}H of 3.12b + impurities

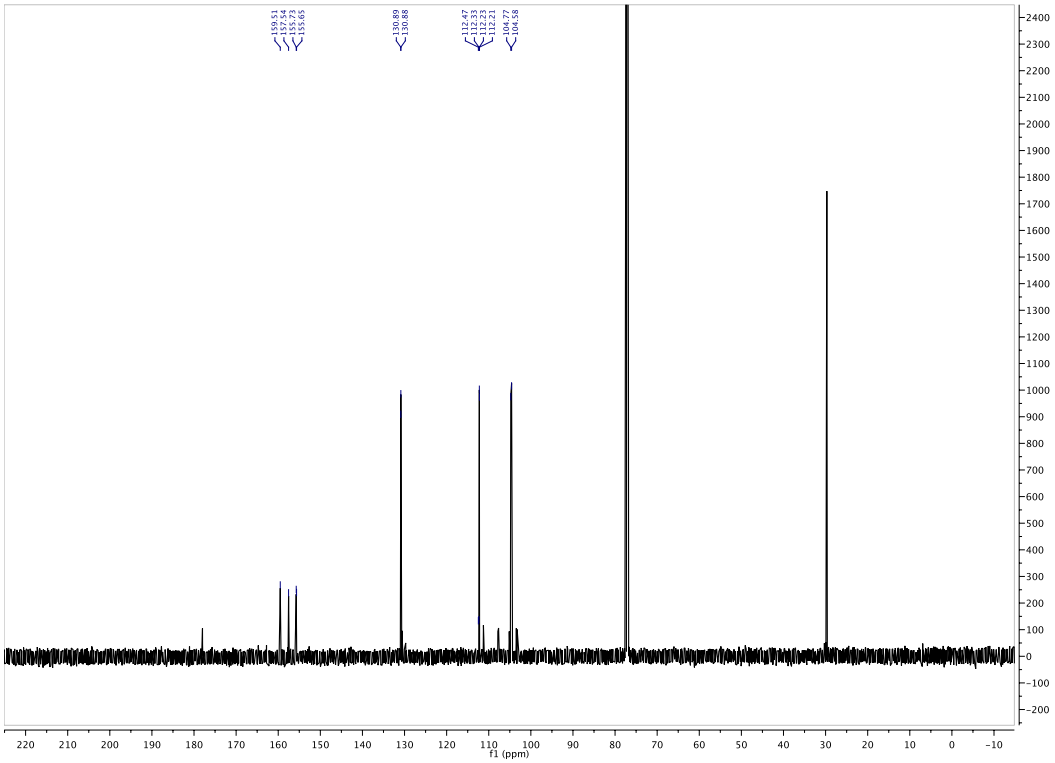

Figure 3.4.54. ^{13}C of 3.12b + impurities

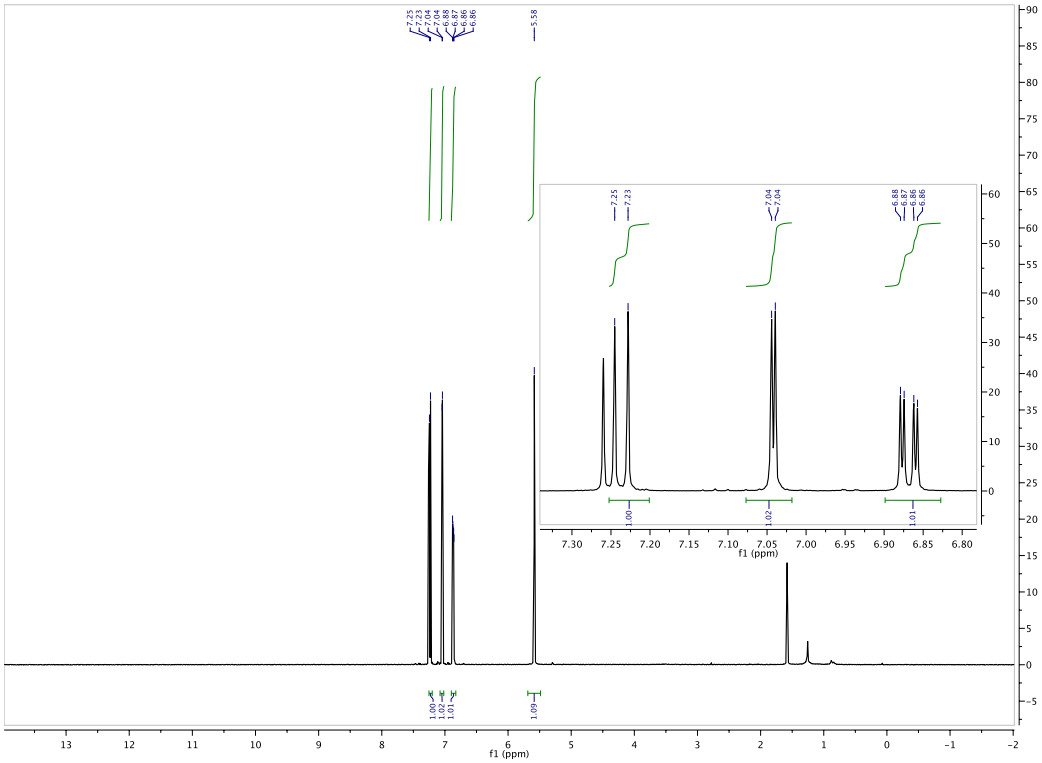

Figure 3.4.55. ^{1}H of 3.13a

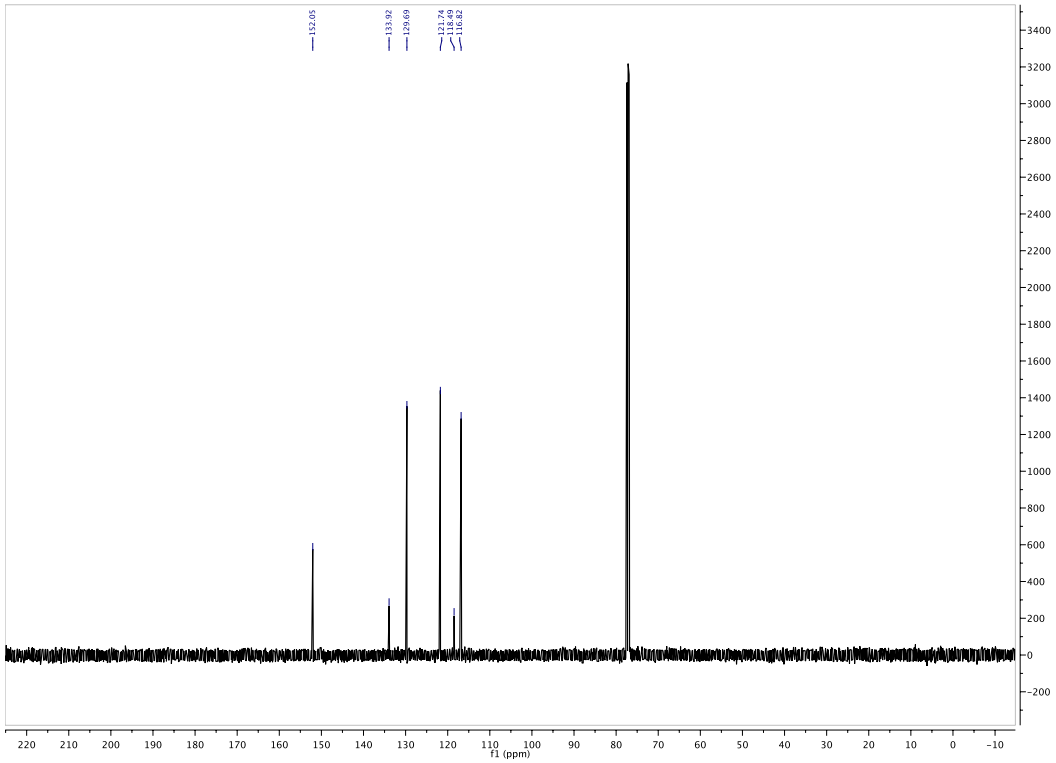

Figure 3.4.56. ^{13}C of 3.13a

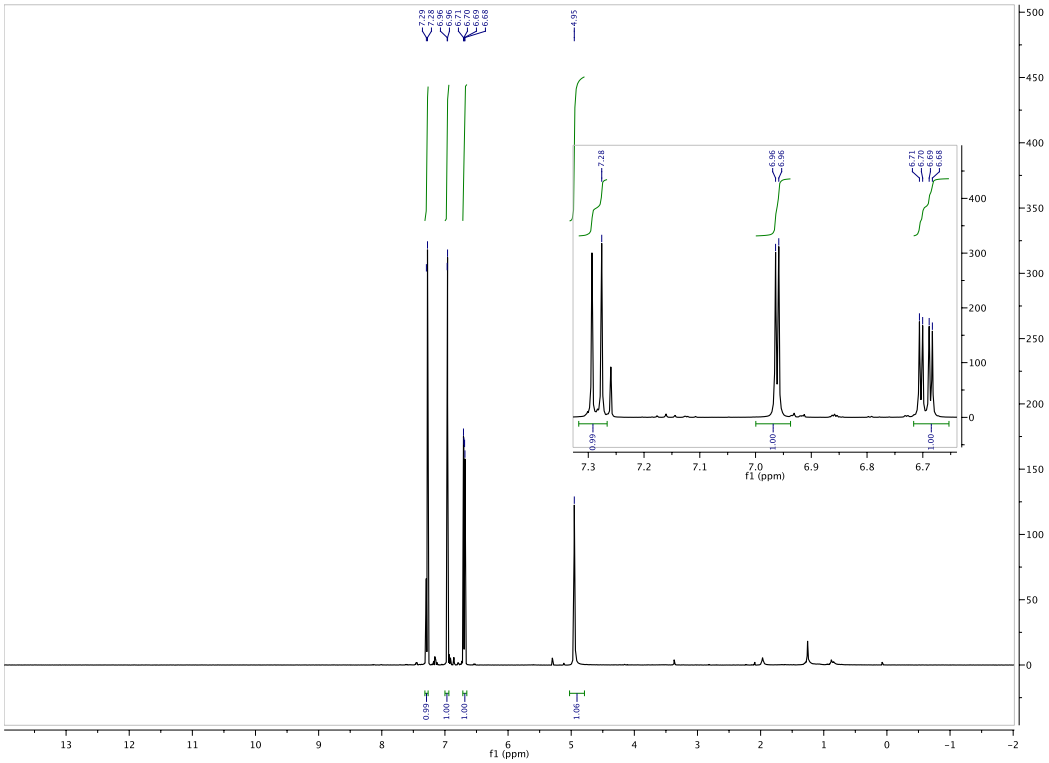

Figure 3.4.57. ^{1}H of 3.13b

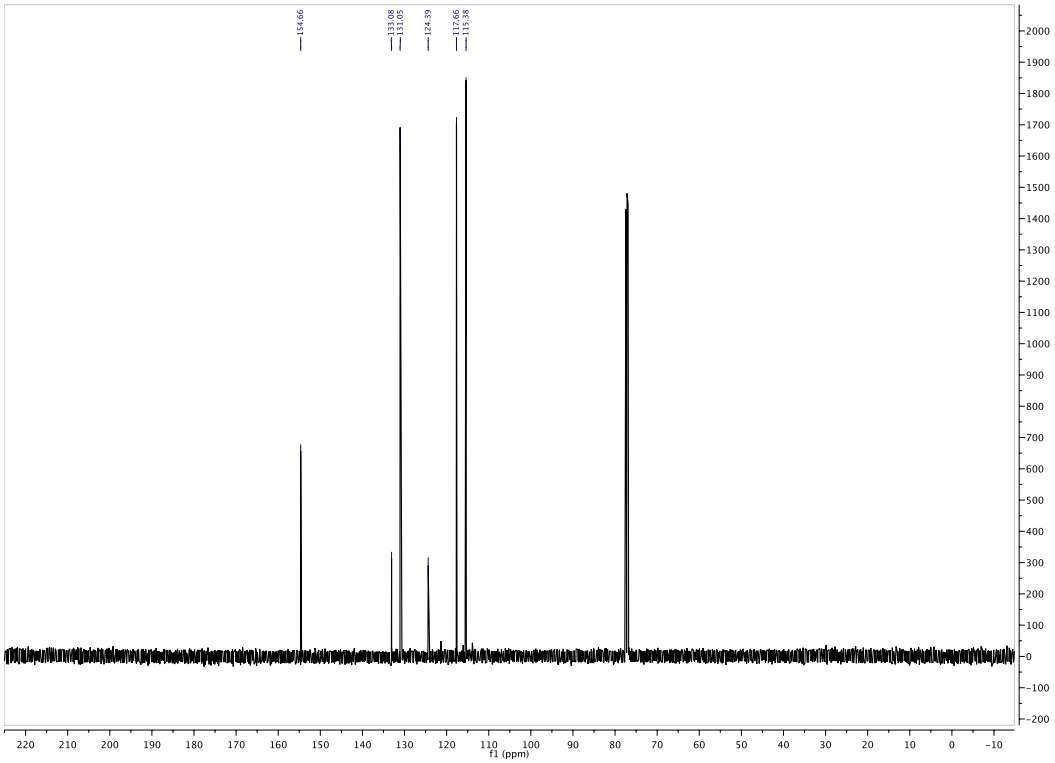

Figure 3.4.58. ^{13}C of 3.13b

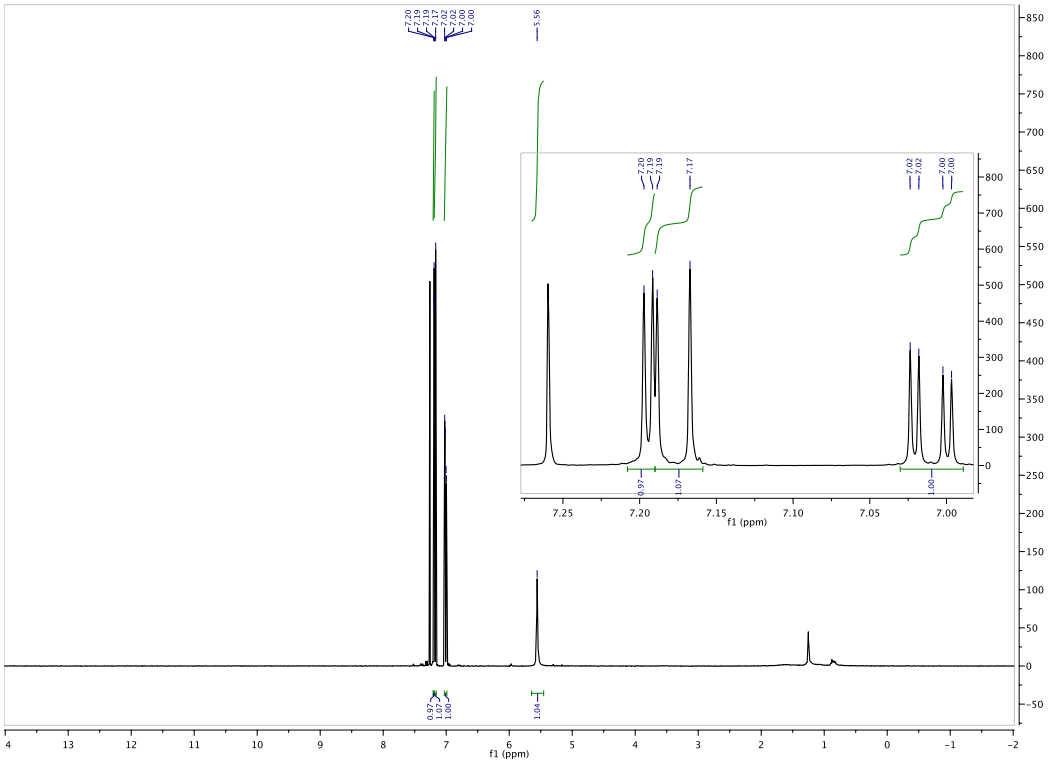

Figure 3.4.59. ^{1}H of 3.14a

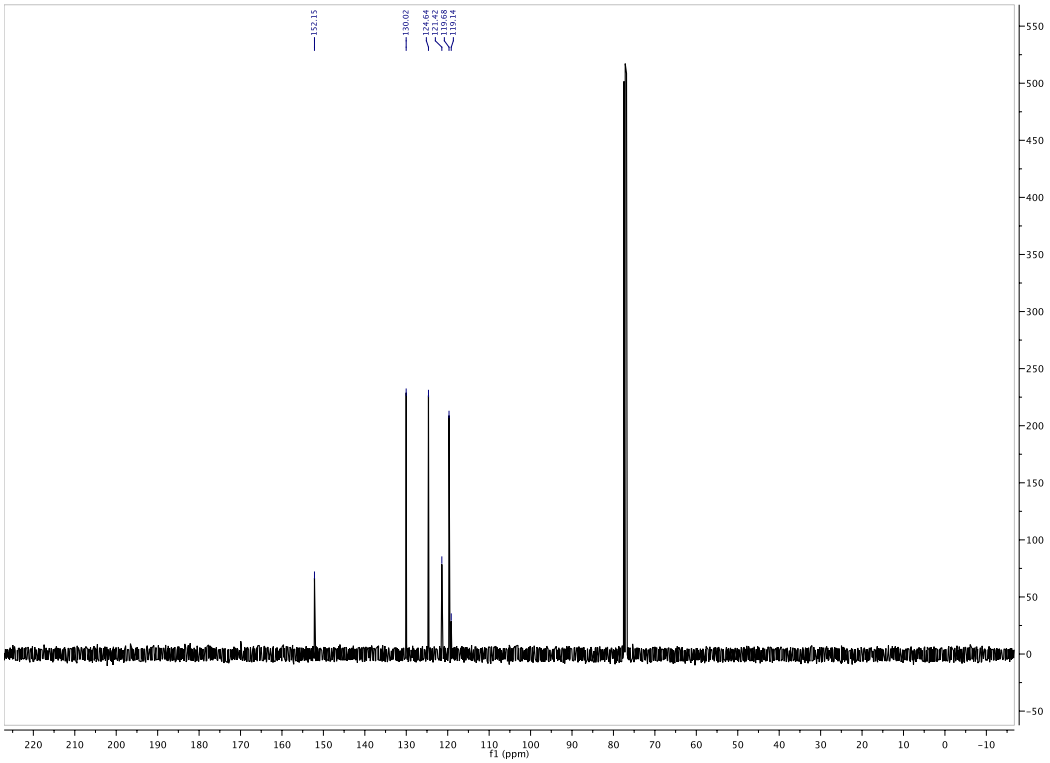

Figure 3.4.60. ^{13}C of 3.14a

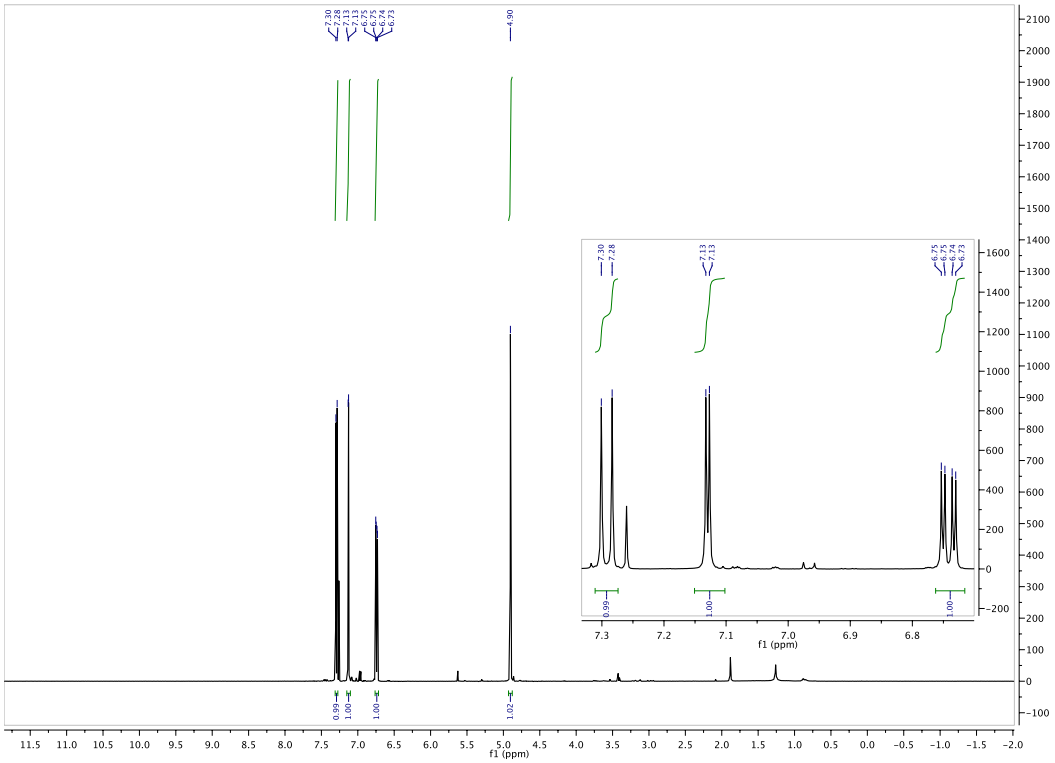

Figure 3.4.61. ^{1}H of 3.14b

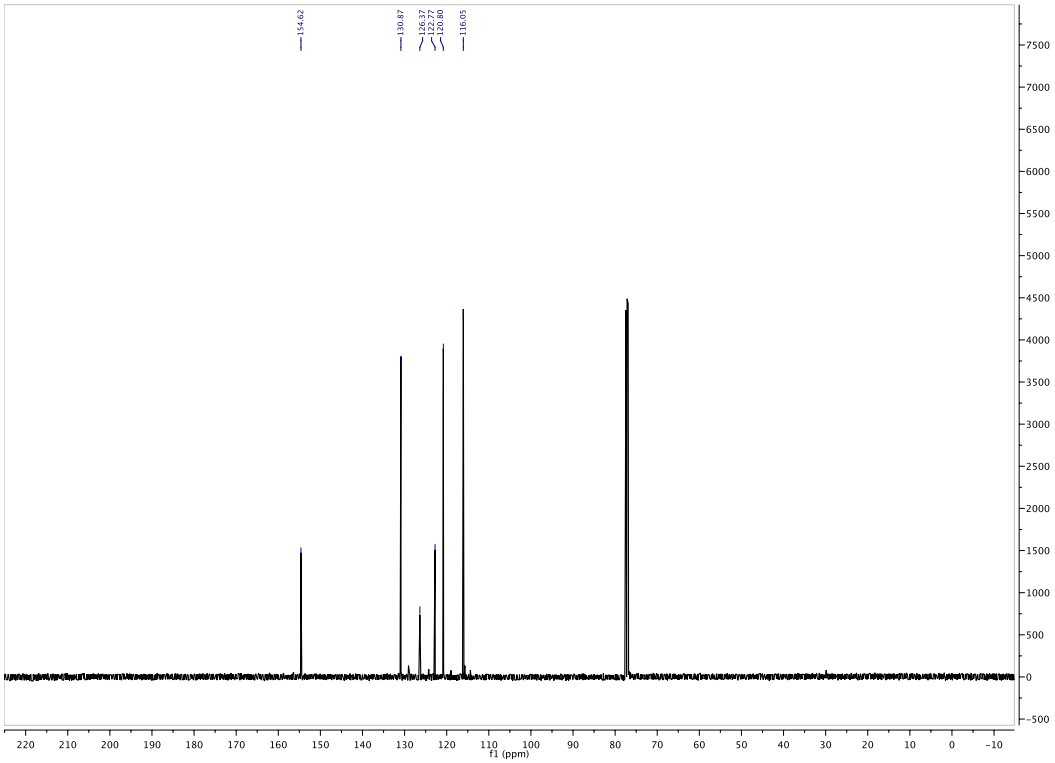

Figure 3.4.62. ^{13}C of 3.14b

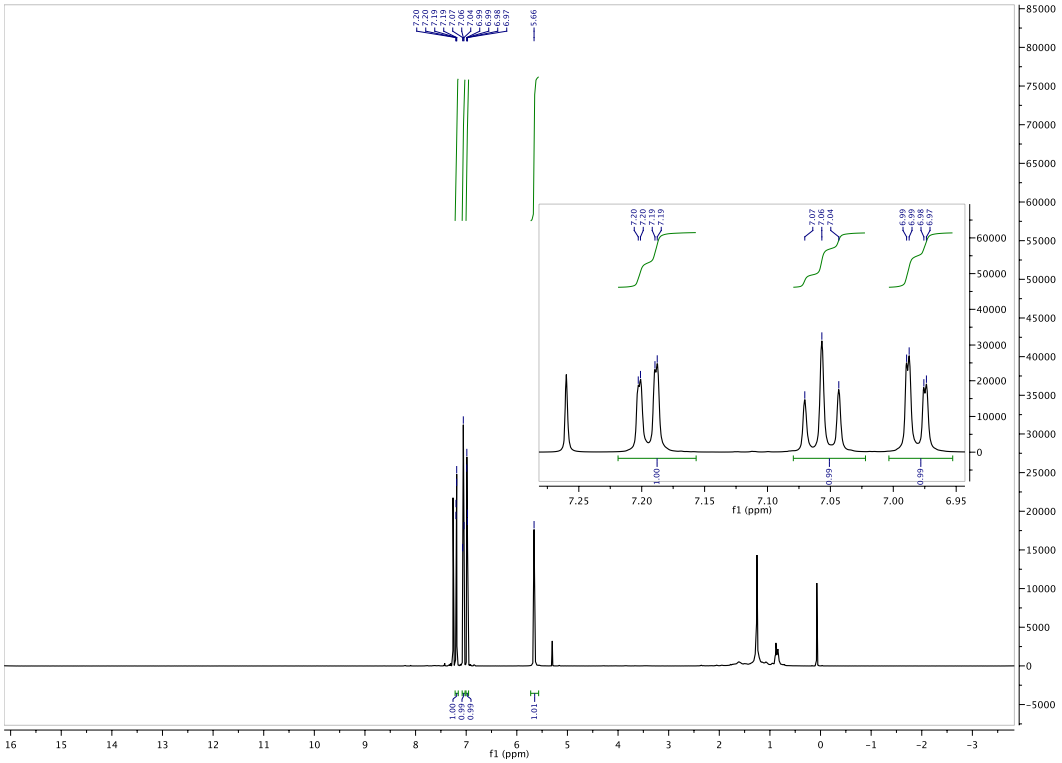

Figure 3.4.63. ^{1}H of 3.14c

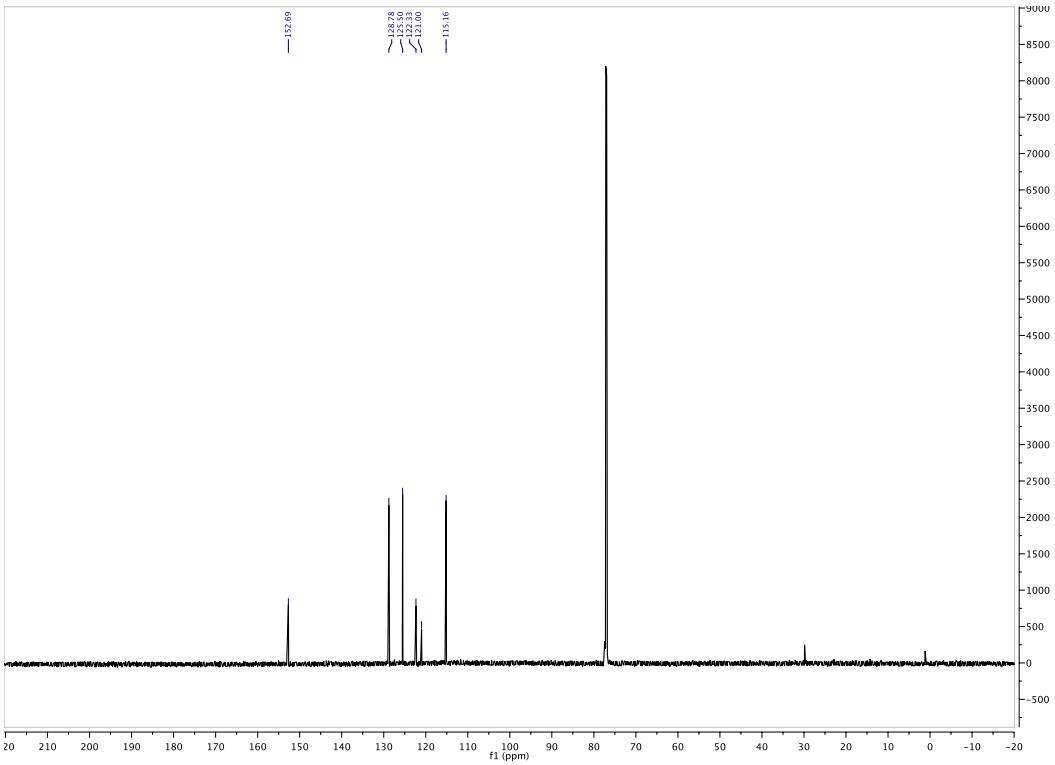

Figure 3.4.64. ^{13}C of 3.14c

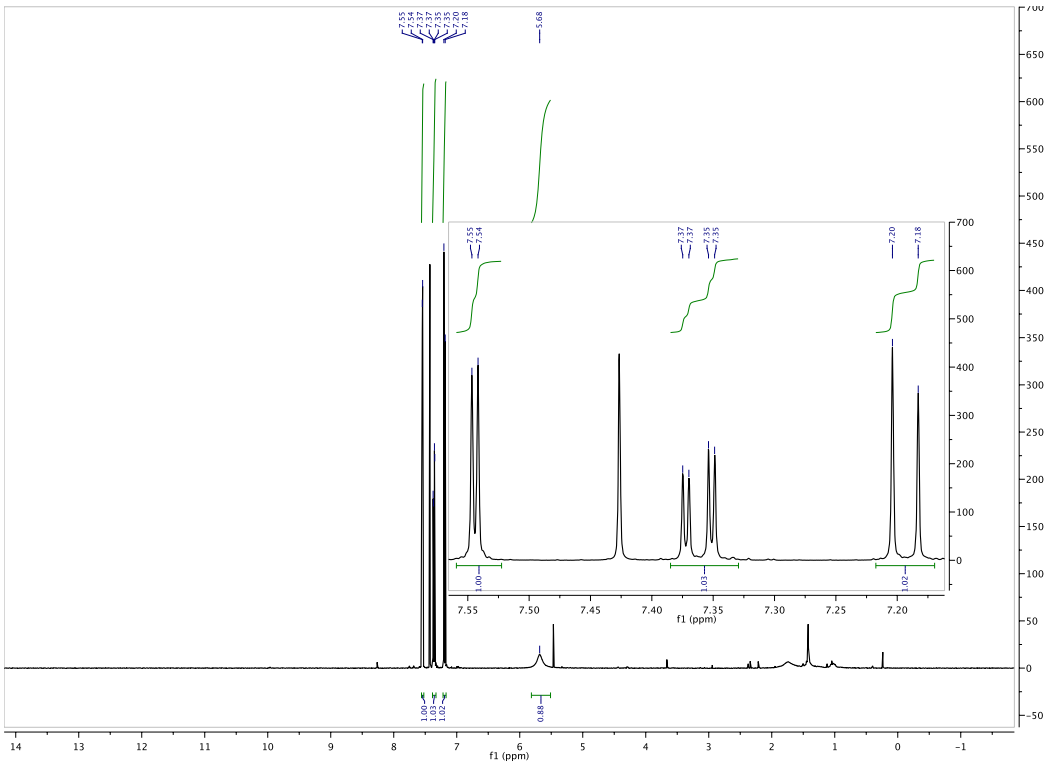

Figure 3.4.65. ^{1}H of 3.15a

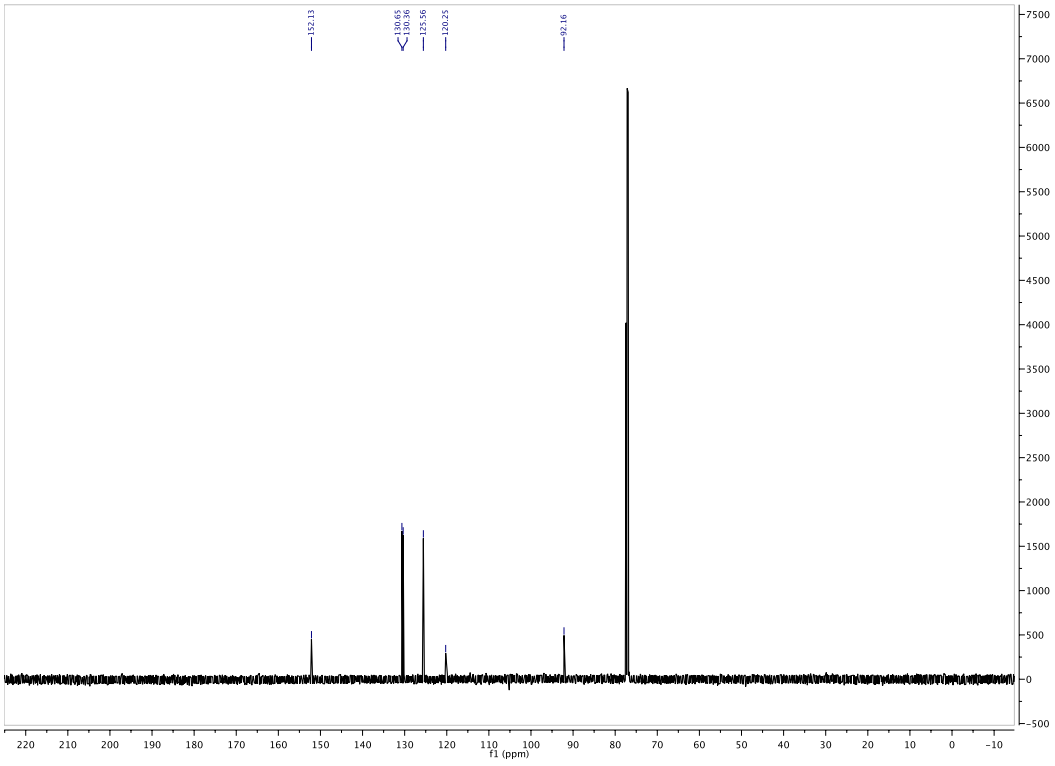

Figure 3.4.66. ^{13}C of 3.15a

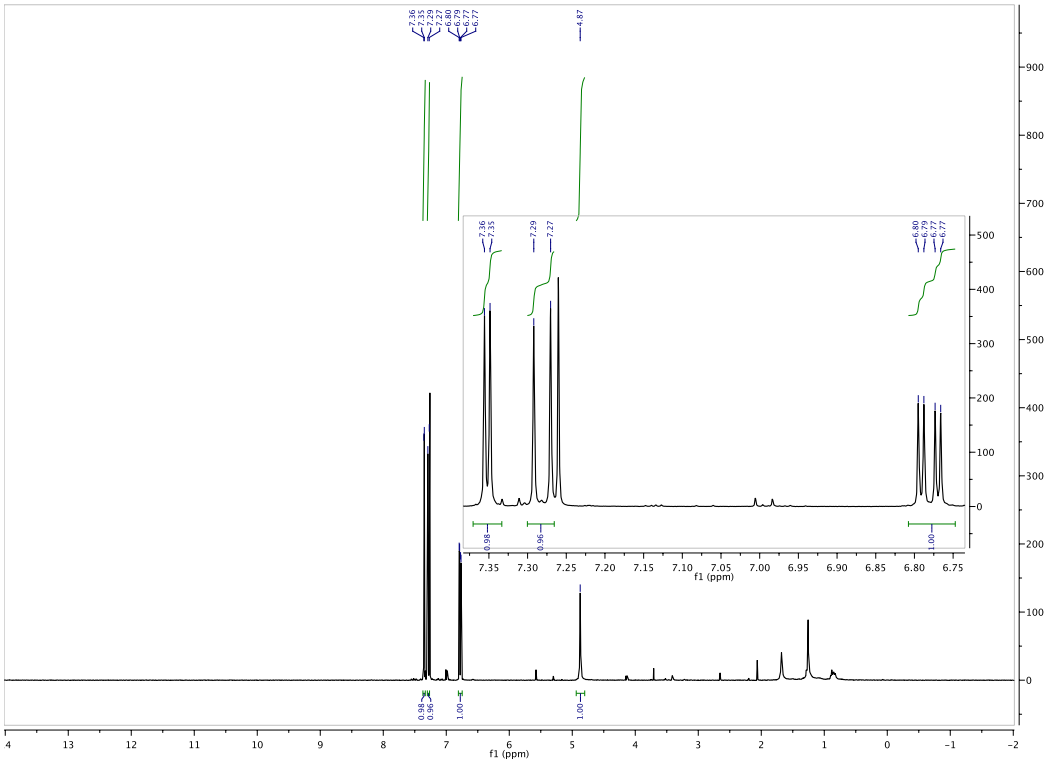

Figure 3.4.67. ^{1}H of 3.15b

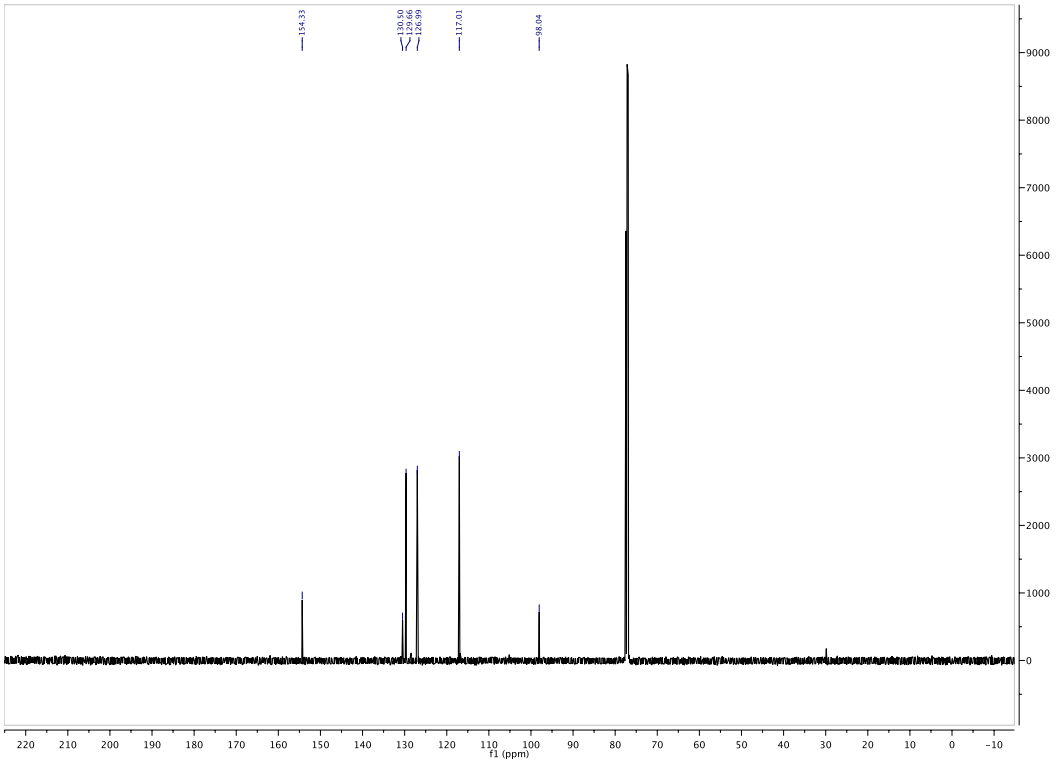

Figure 3.4.68. ^{13}C of 3.15b

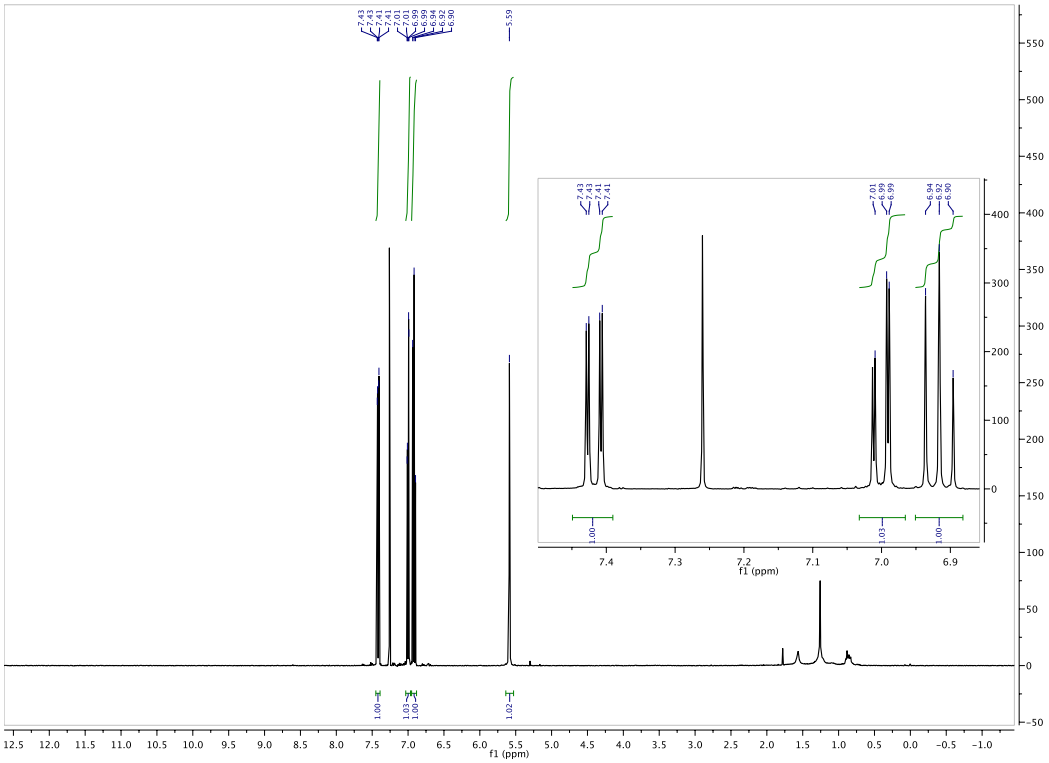

Figure 3.4.69. ^{1}H of 3.15c

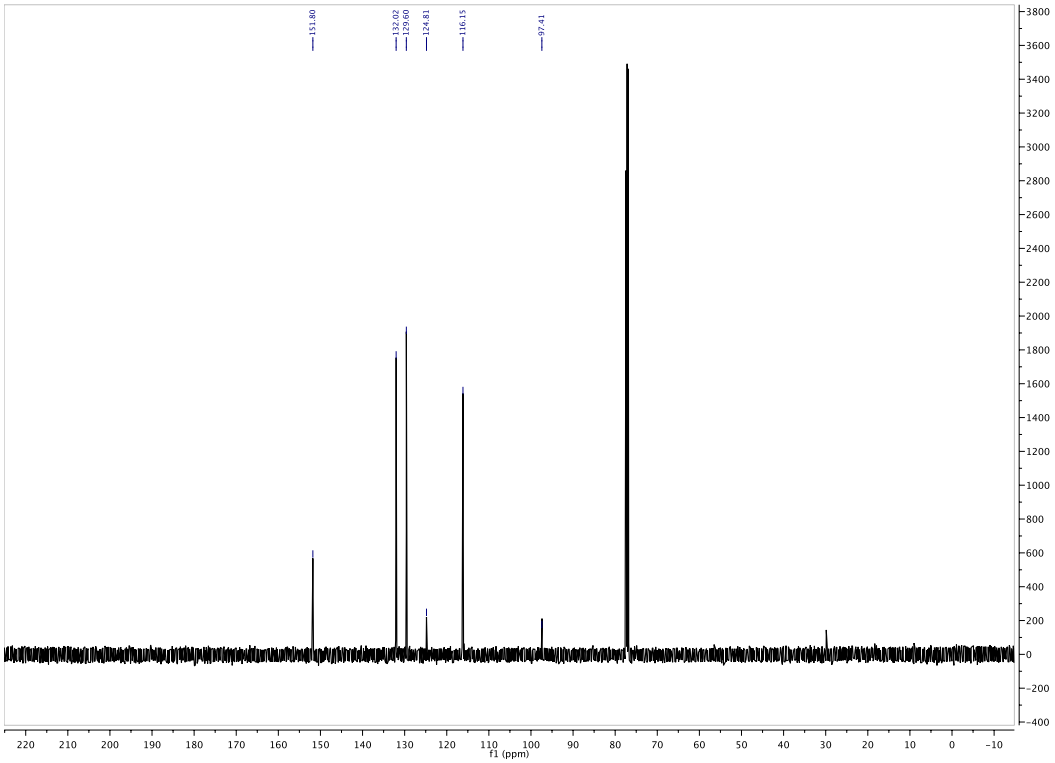

Figure 3.4.70. ^{13}C of 3.15c

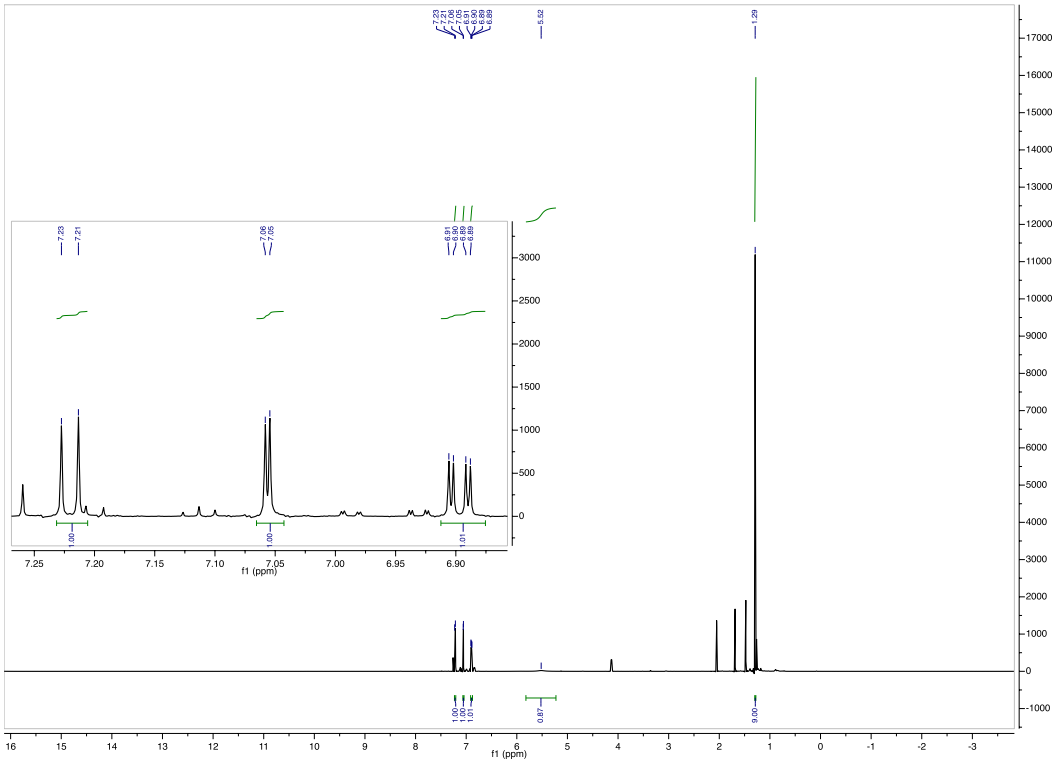

Figure 3.4.71. ^{1}H of 3.16a + impurities

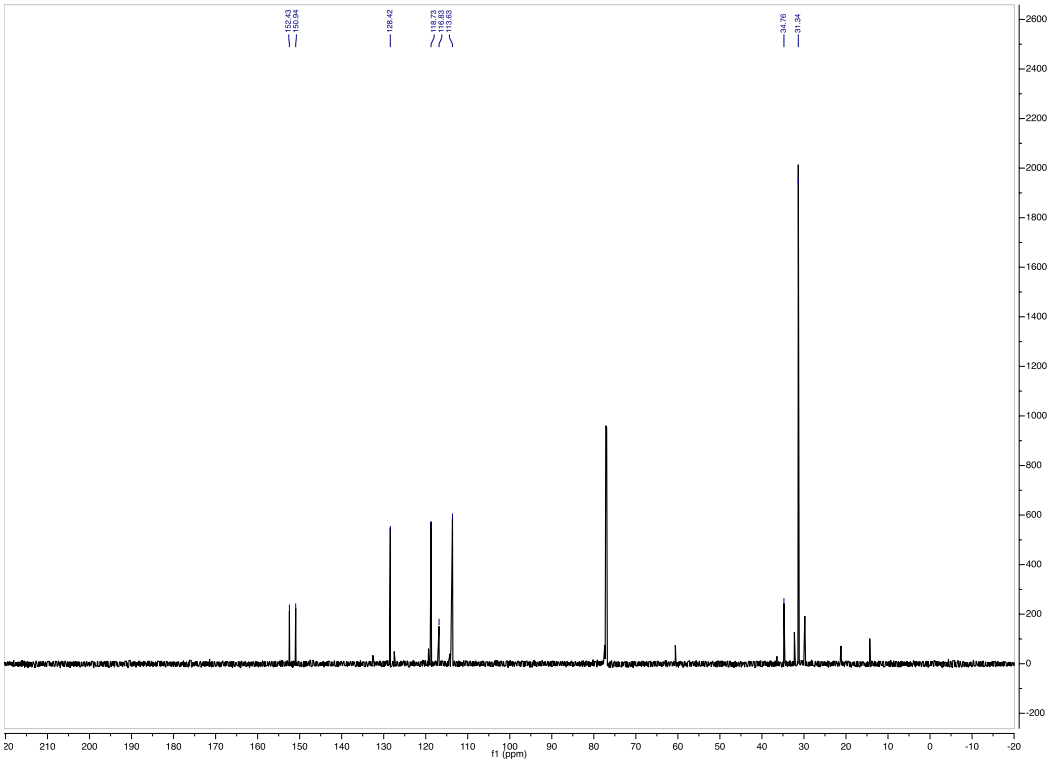

Figure 3.4.72. ^{13}C of 3.16a + impurities

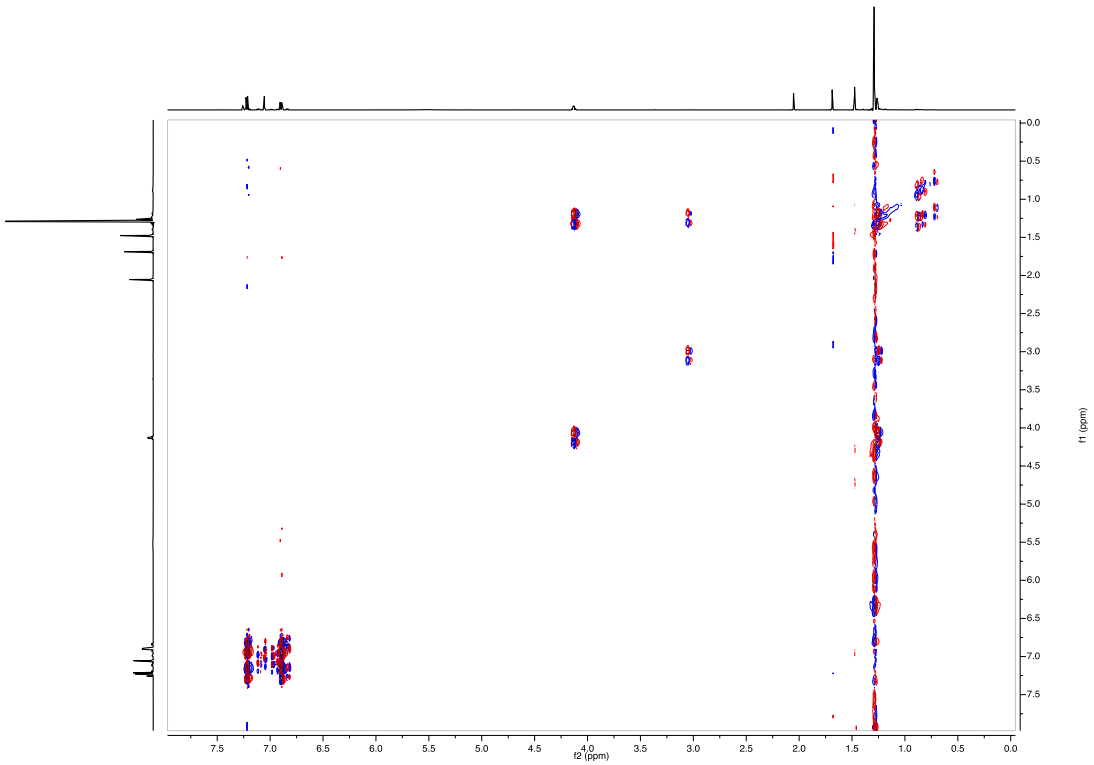

Figure 3.4.73. COSY (^{1}H/^{1}H) of 3.16a + impurities

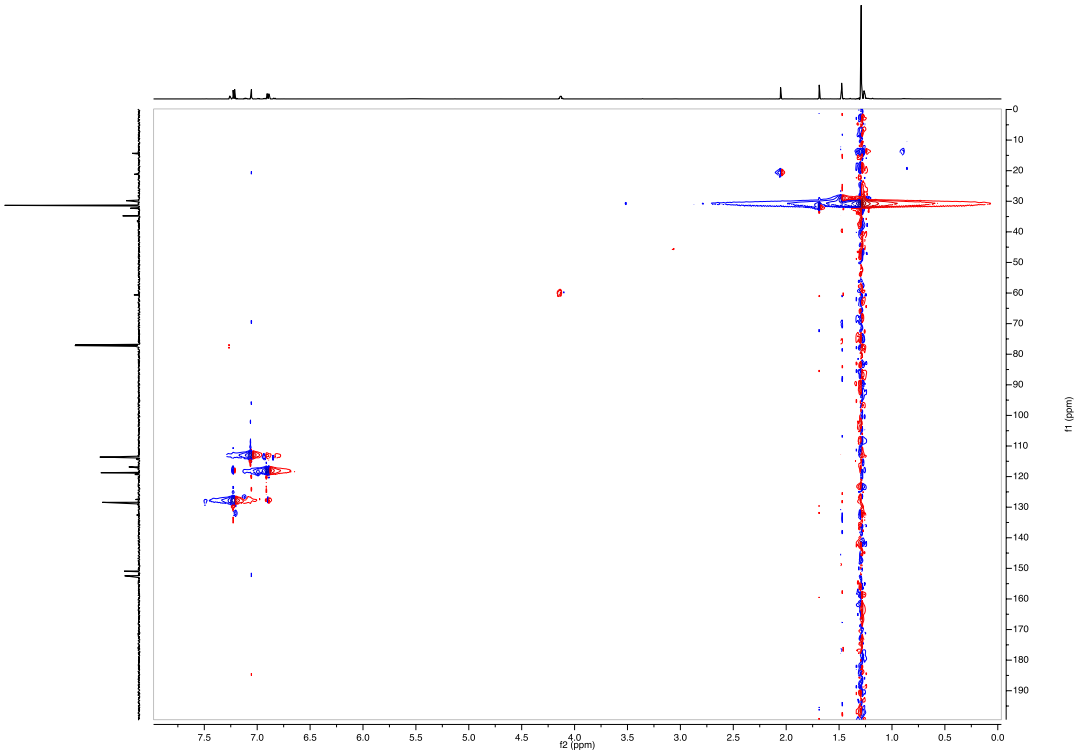

Figure 3.4.74. HSQC ($^{1}H/^{13}C$) of 3.16a + impurities

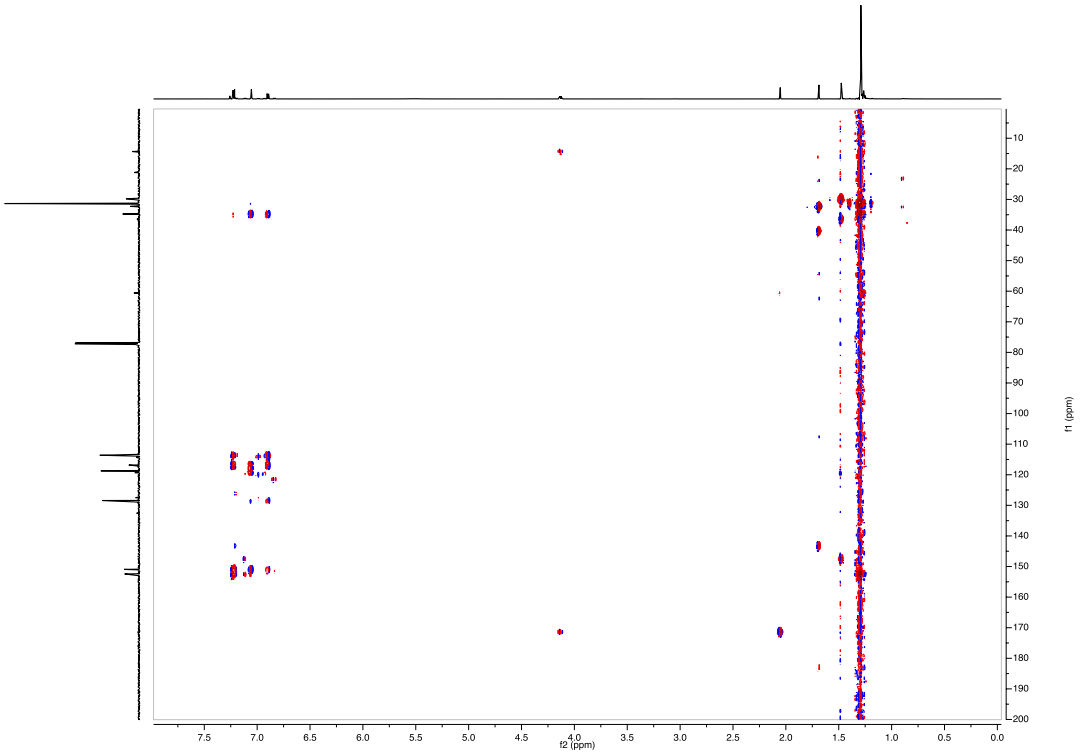

Figure 3.4.75. HMBC ($^{1}H/^{13}C$) of 3.16a + impurities

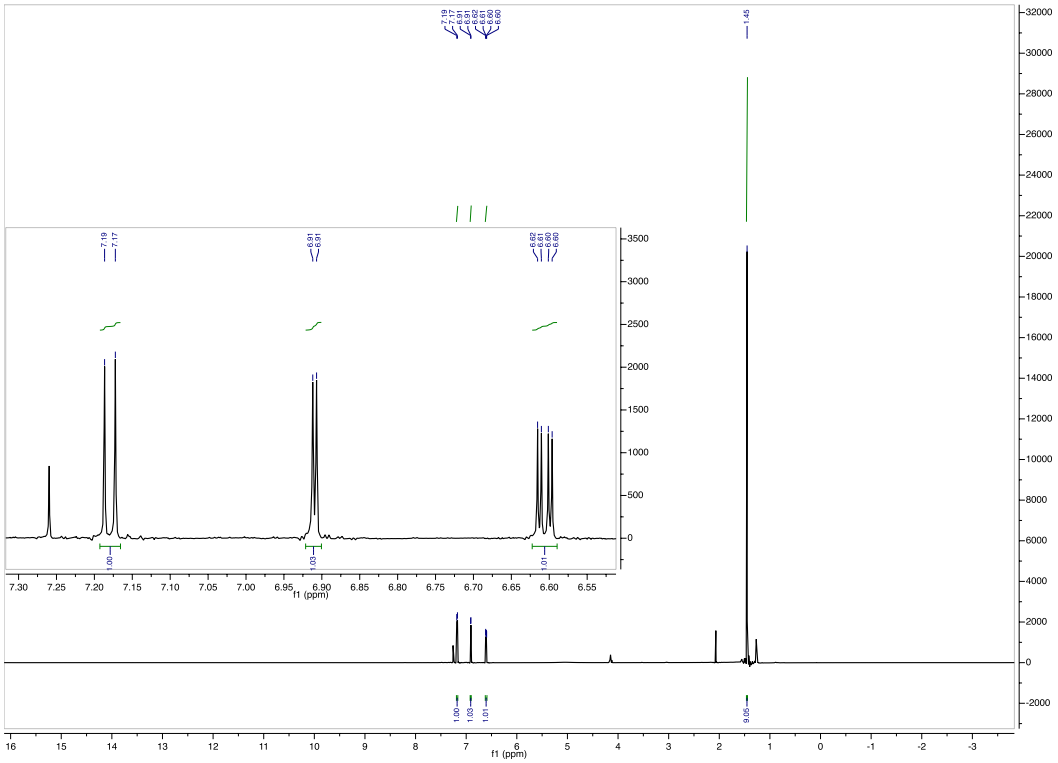

Figure 3.4.76. ^{1}H of 3.16b

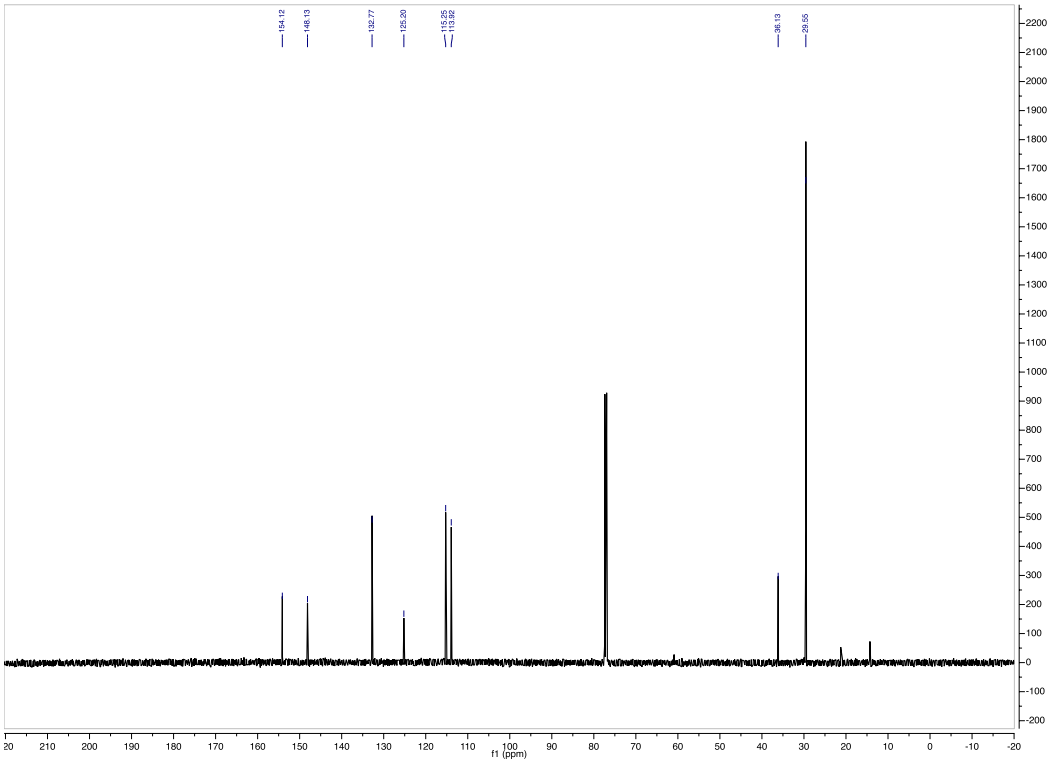

Figure 3.4.77. ^{13}C of 3.16b

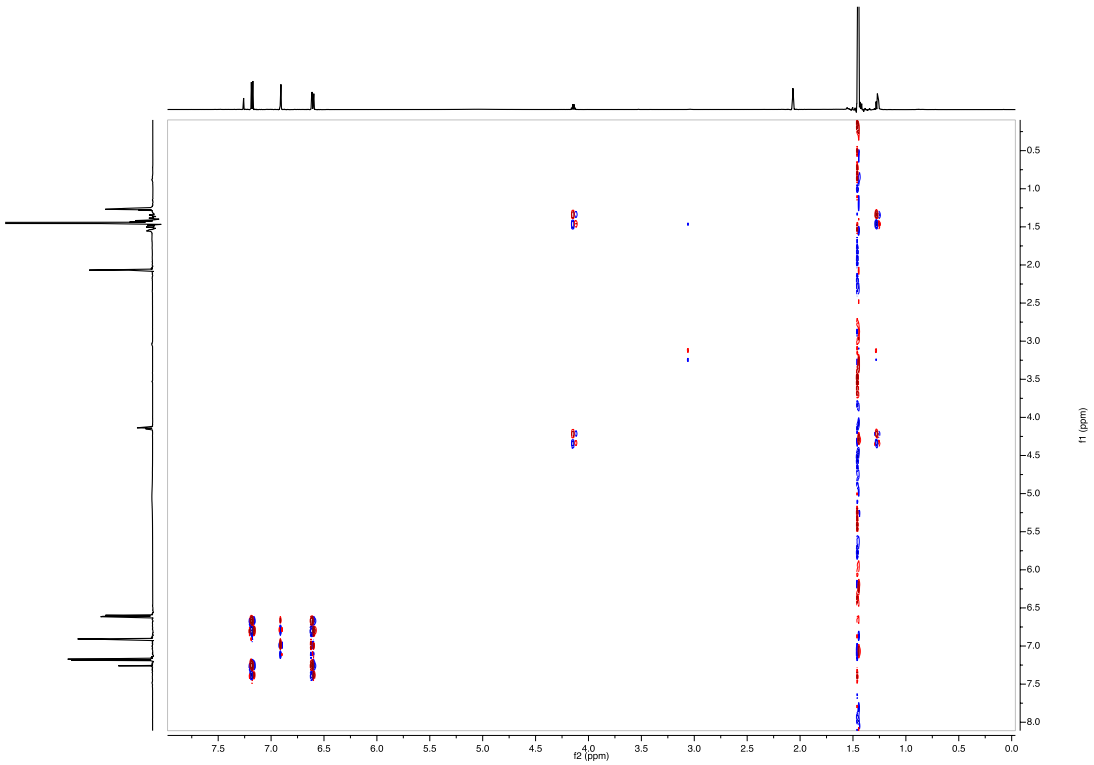

Figure 3.4.78. COSY (^{1}H/^{1}H) of 3.16b

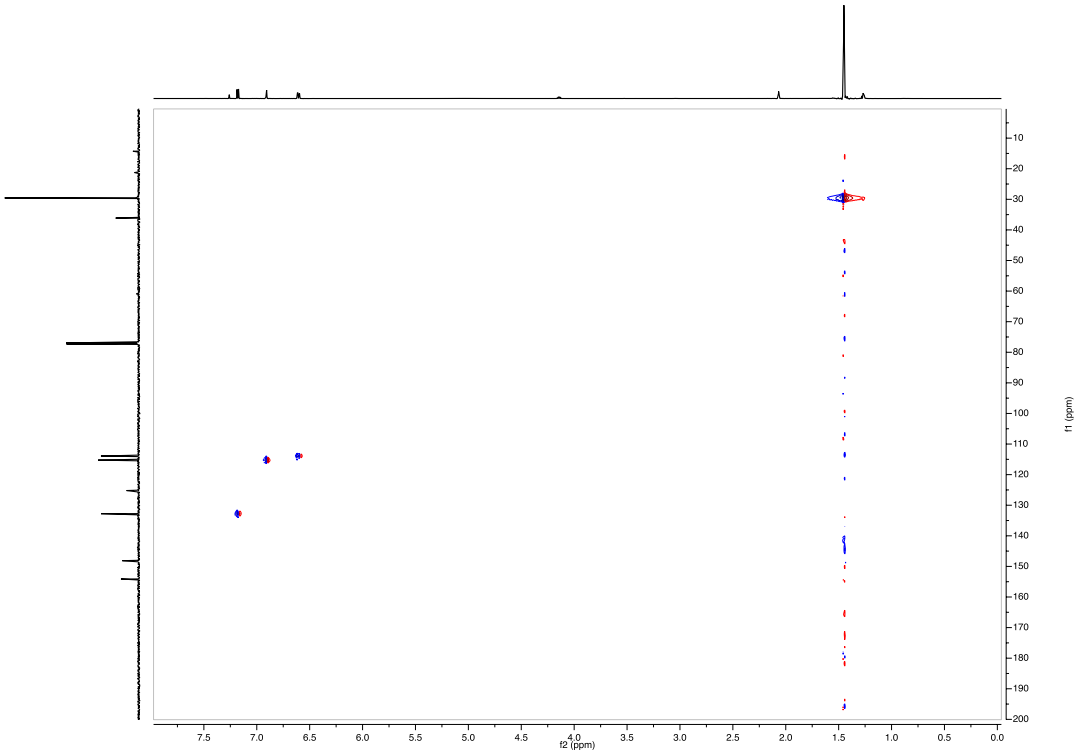

Figure 3.4.79. HSQC ($^{1}H/^{13}C$) of 3.16b

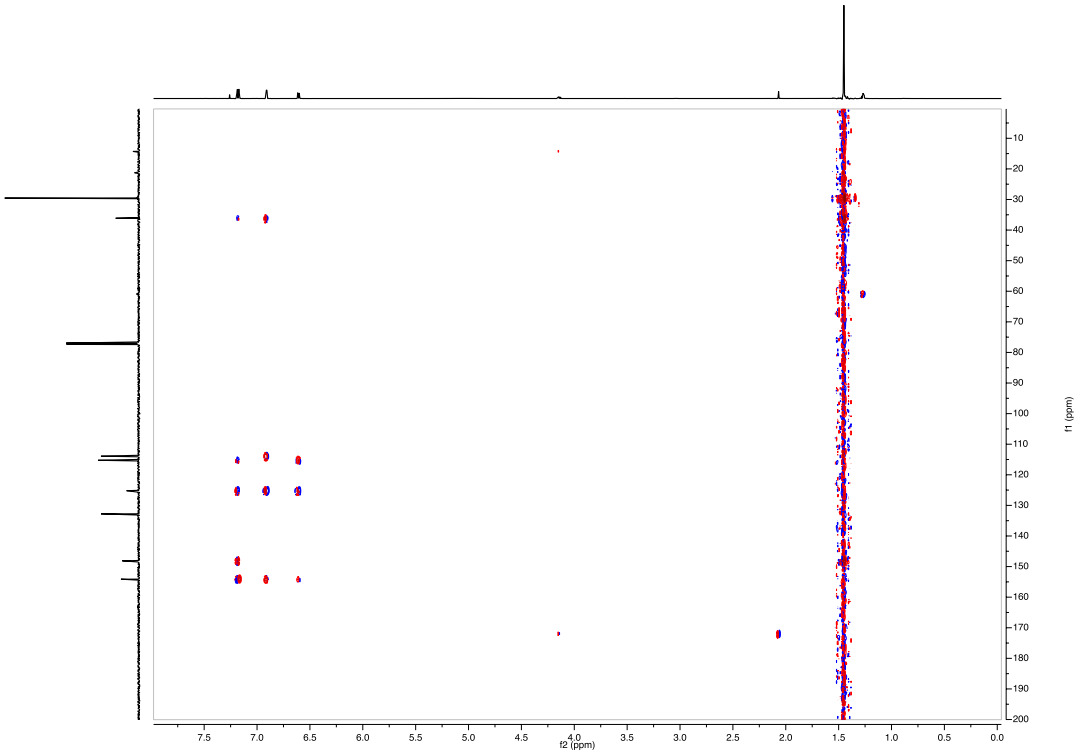

Figure 3.4.80. HMBC ($^{1}H/^{13}C$) of 3.16b

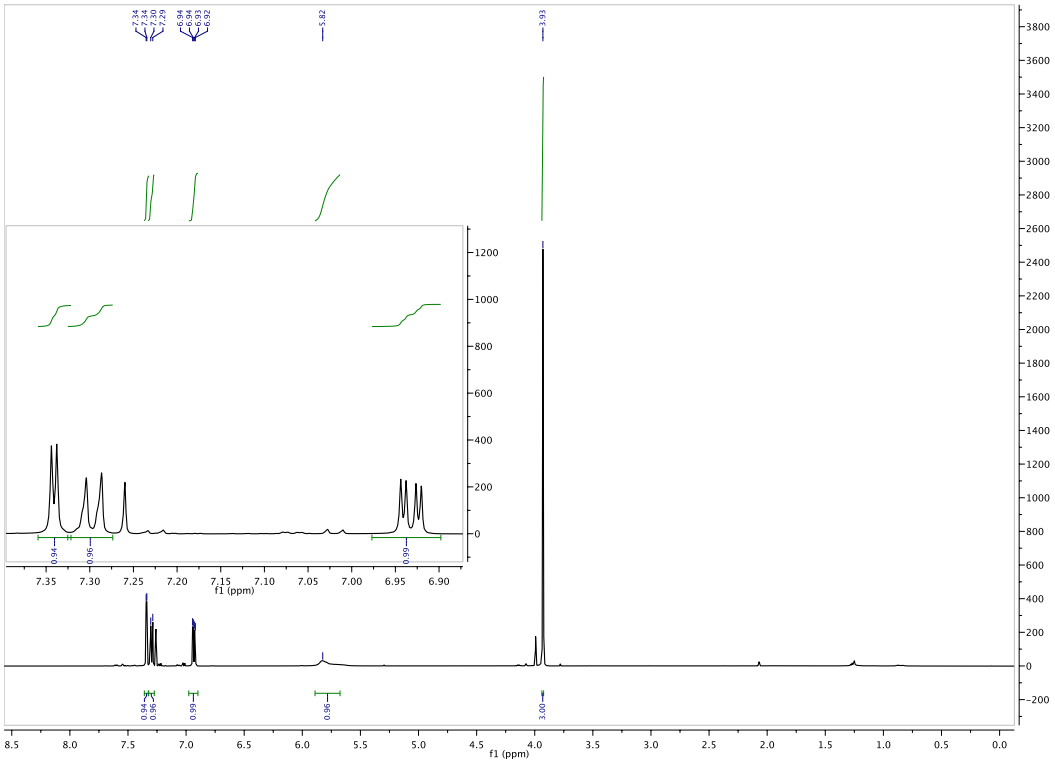

Figure 3.4.81. ^{1}H of 3.17b

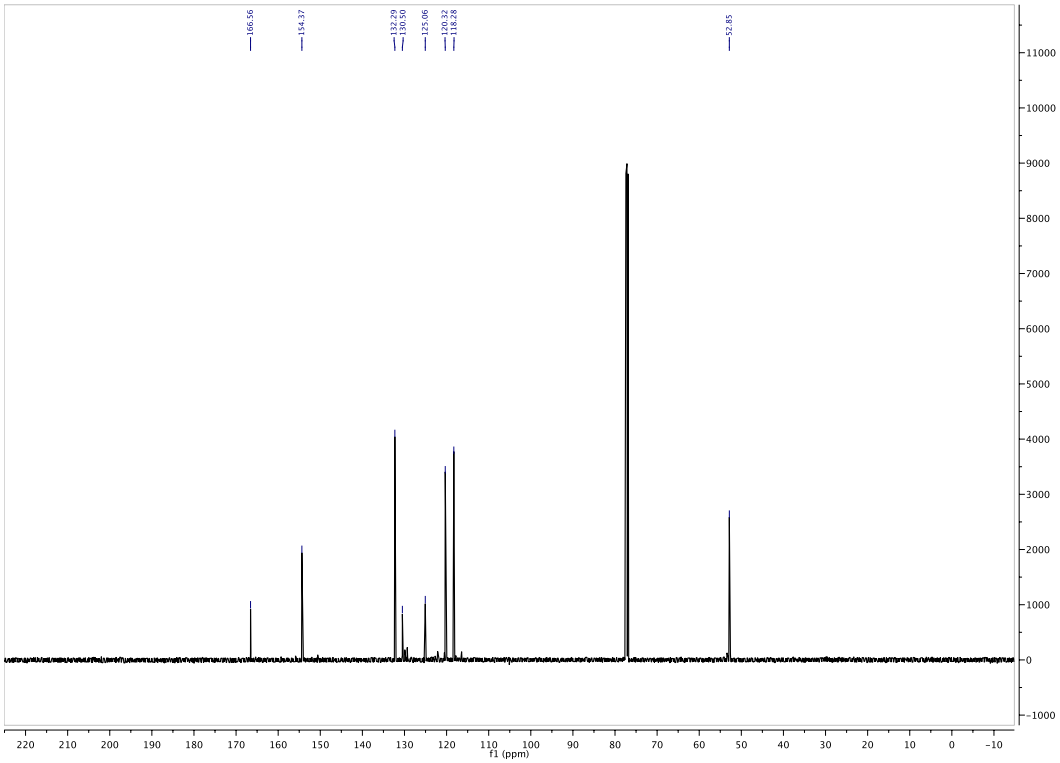

Figure 3.4.82. ^{13}C of 3.17b

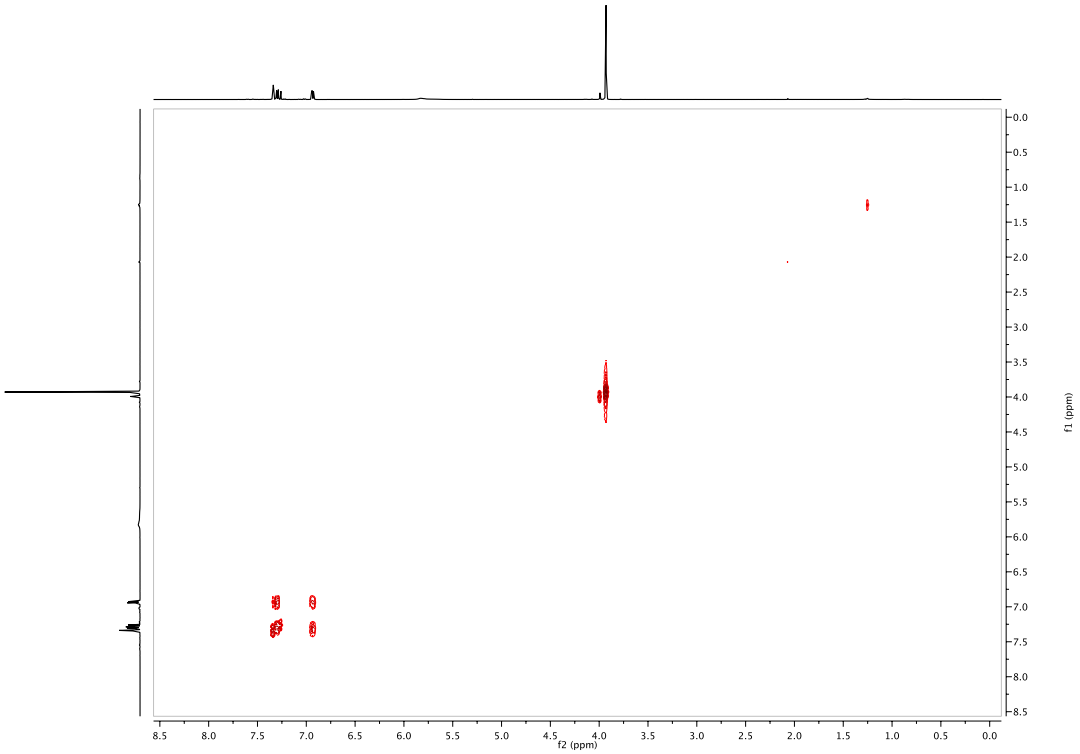

Figure 3.4.83. COSY (^{1}H/^{1}H) of 3.17b

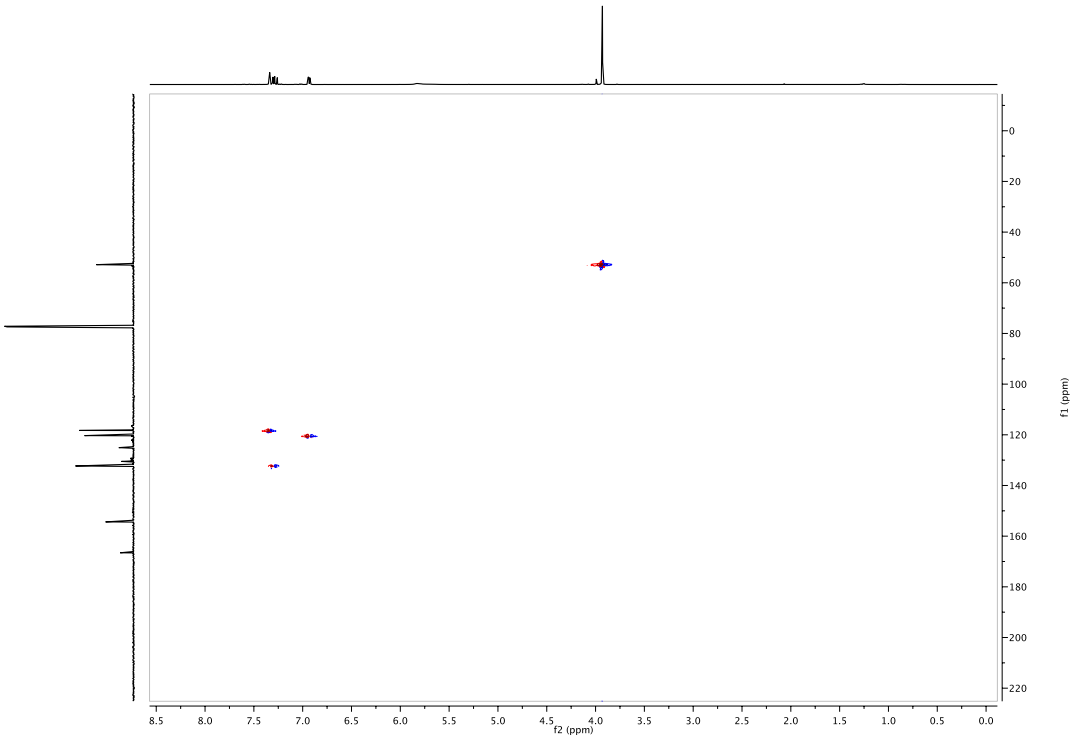

Figure 3.4.84. HSQC ($^{1}H/^{13}C$) of 3.17b

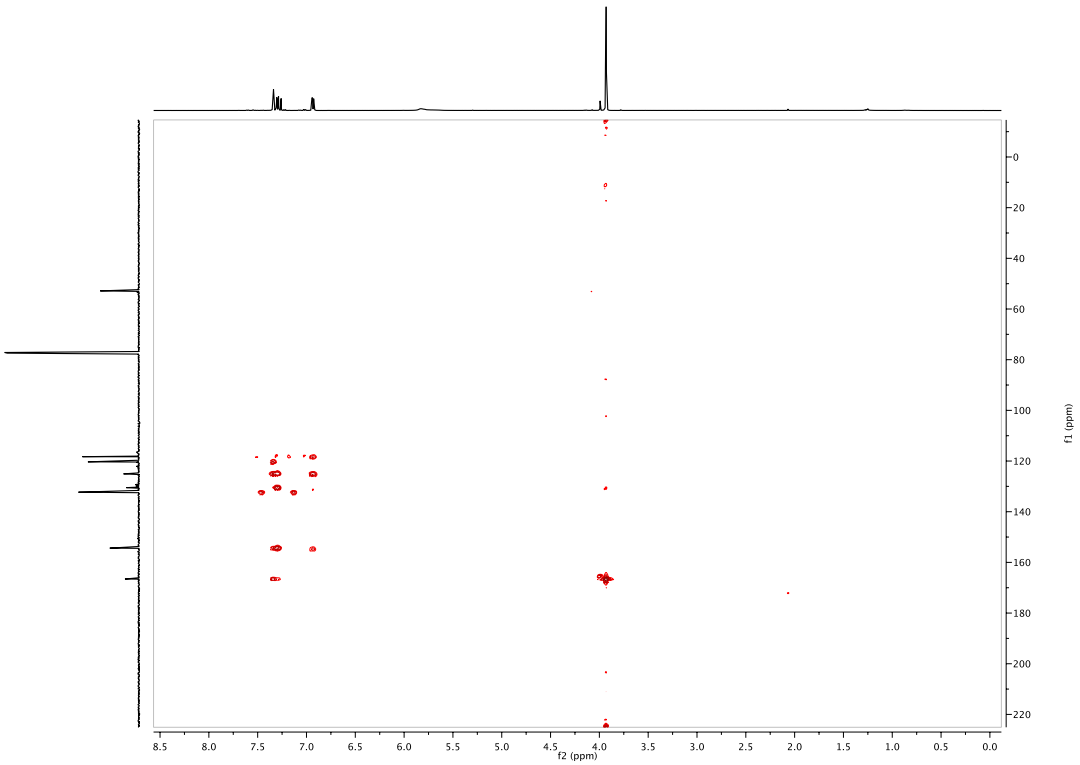

Figure 3.4.85. HMBC ($^{1}H/^{13}C$) of 3.17b

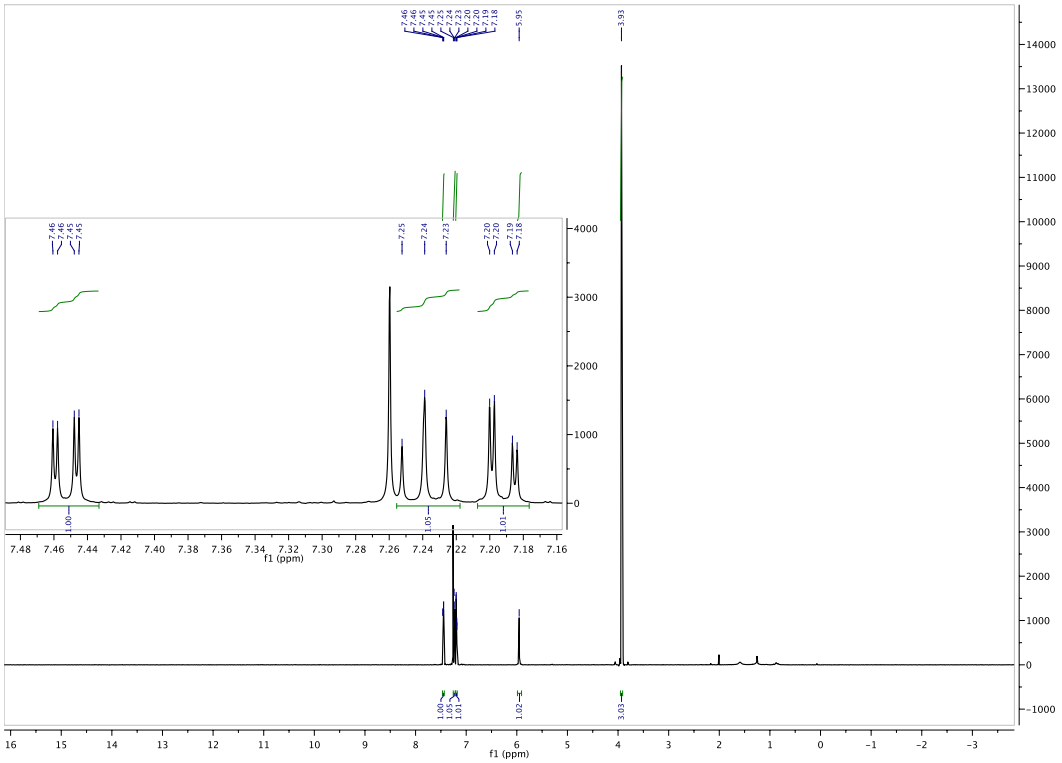

Figure 3.4.86. ^{1}H of 3.17c

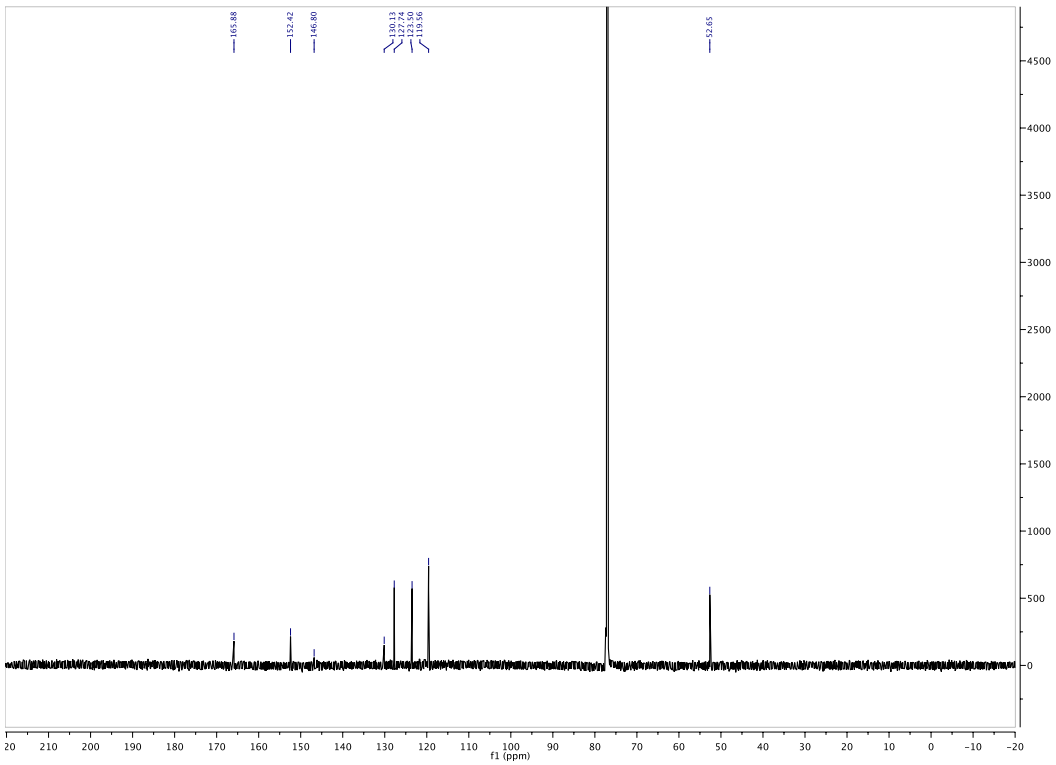

Figure 3.4.87. ^{13}C of 3.17c

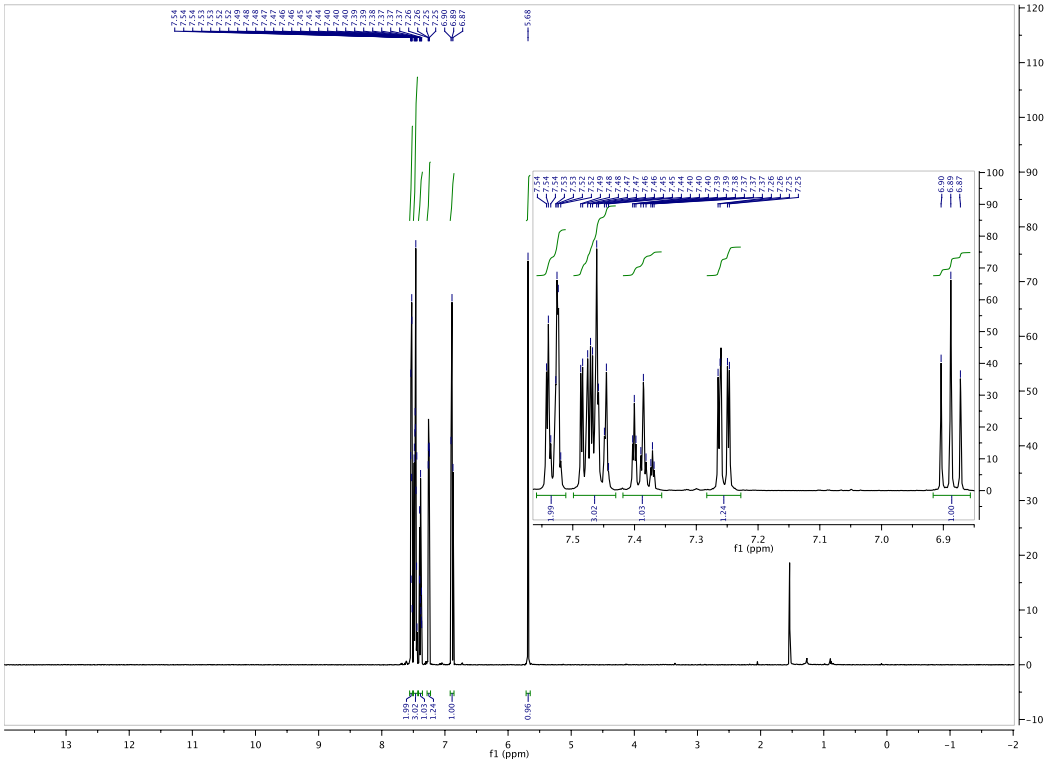

Figure 3.4.88. ^{1}H of 3.8c

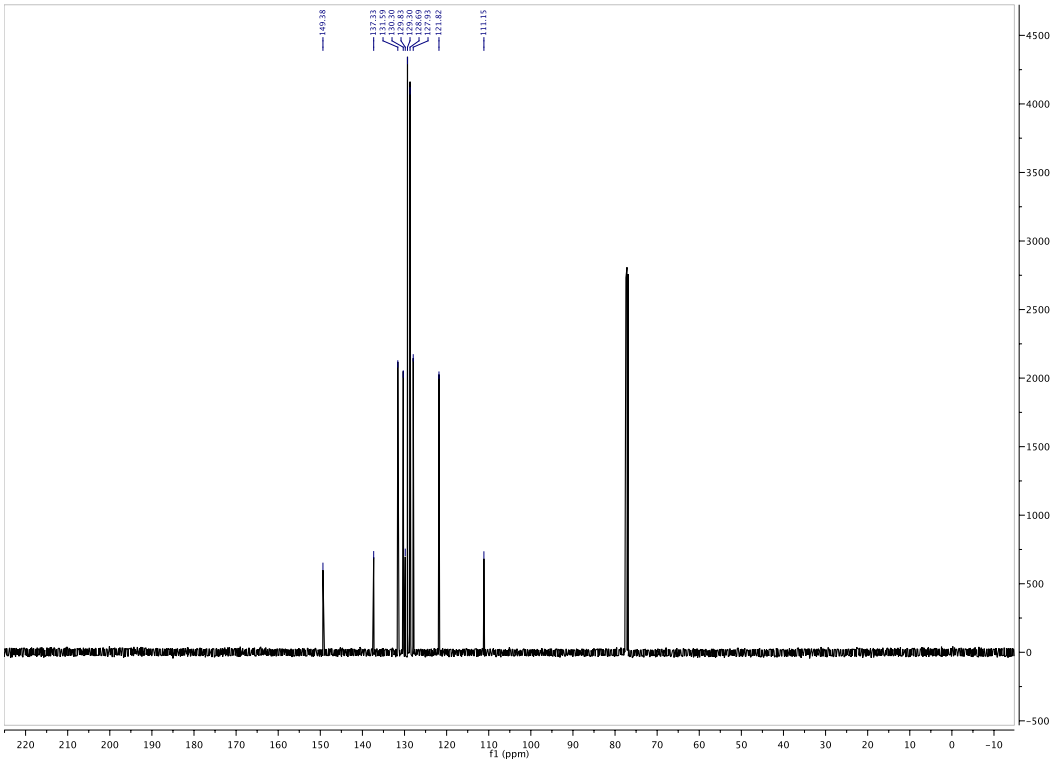

Figure 3.4.89. ^{13}C of 3.8c

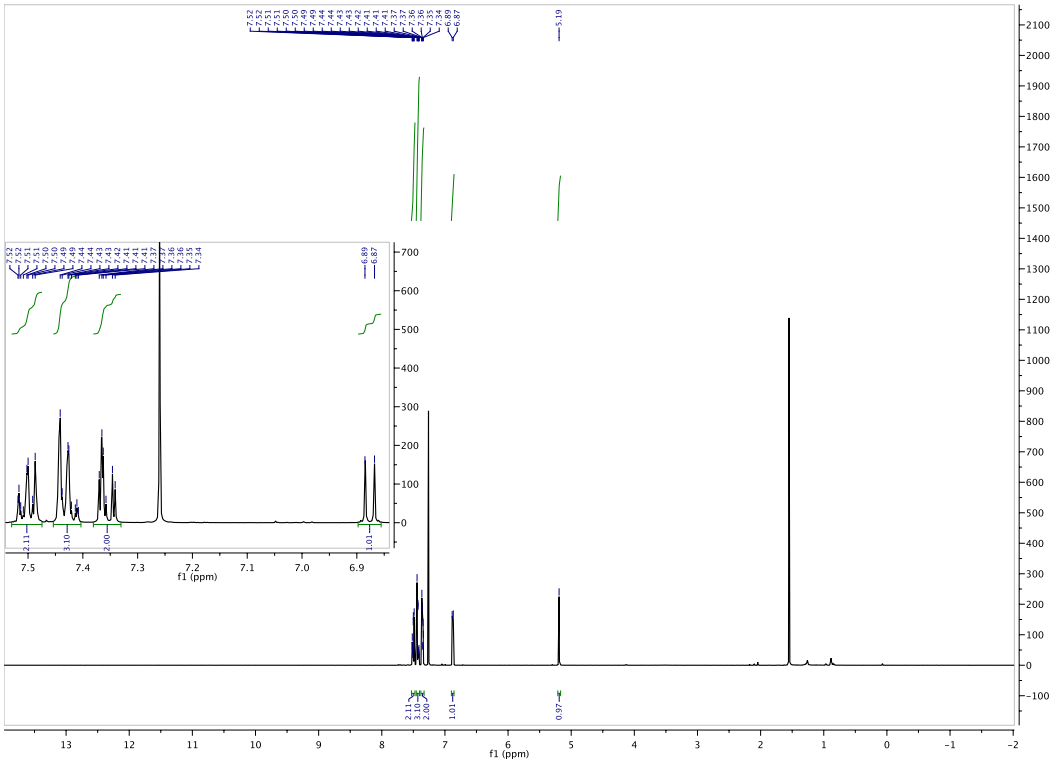

Figure 3.4.90. ^{1}H of 3.8d

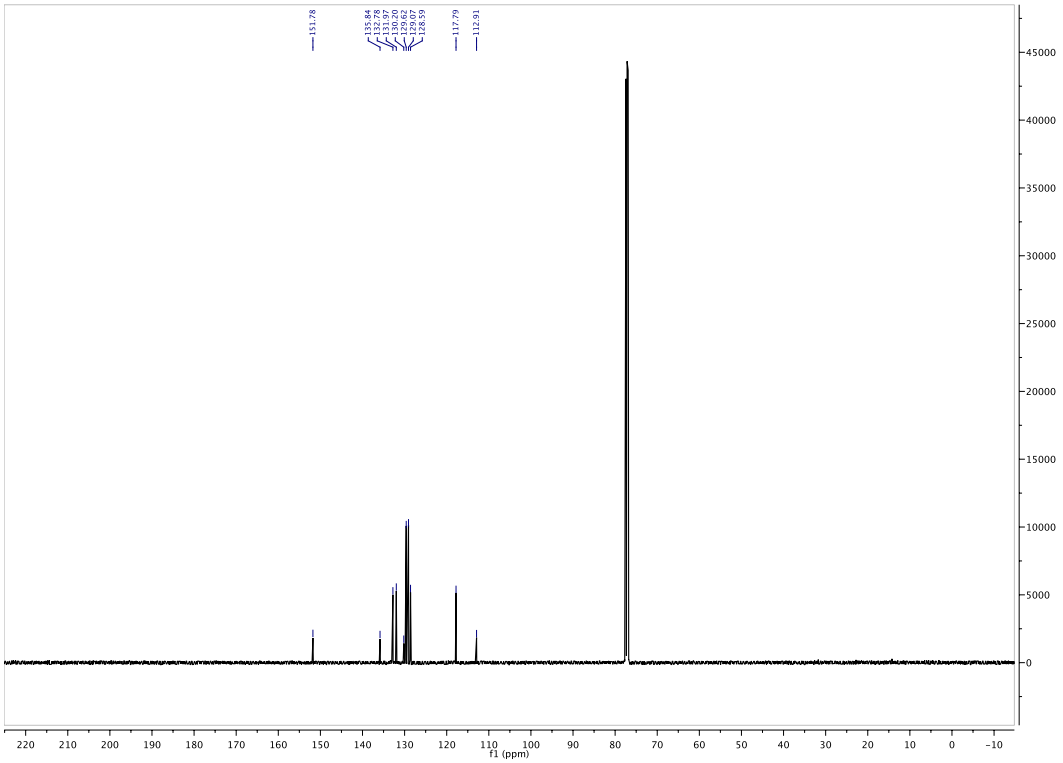

Figure 3.4.91. ^{13}C of 3.8d

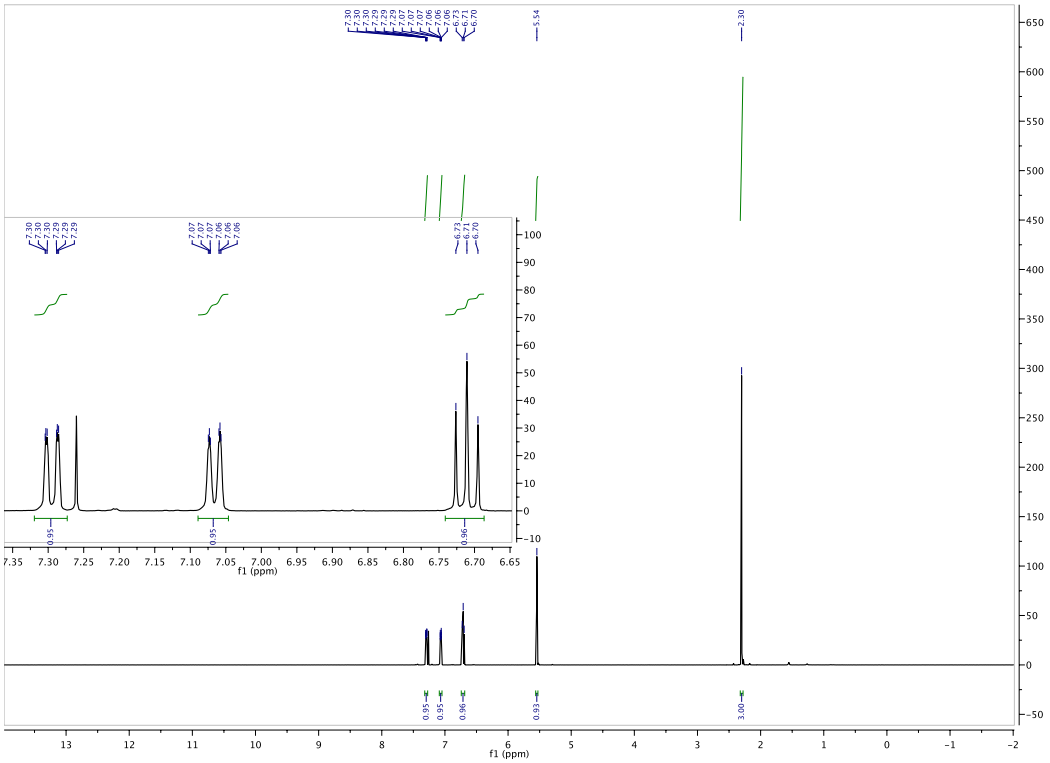

Figure 3.4.92. ^{1}H of 3.18a

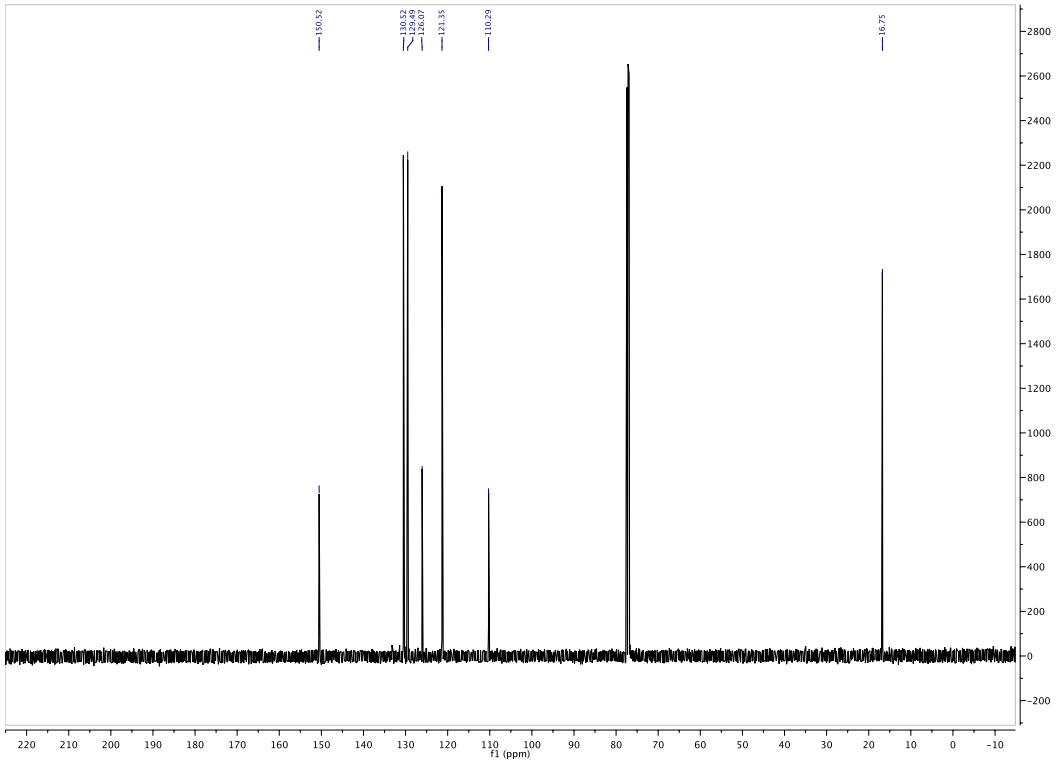

Figure 3.4.93. ^{13}C of 3.18a

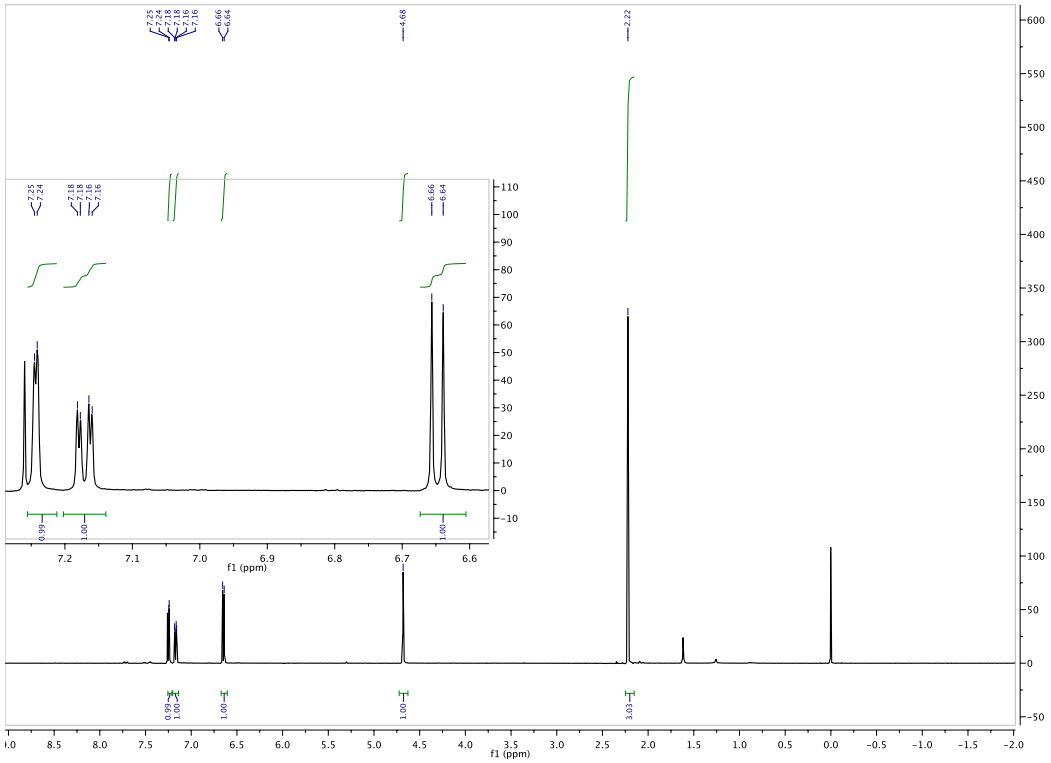

Figure 3.4.94. ^{1}H of 3.18b

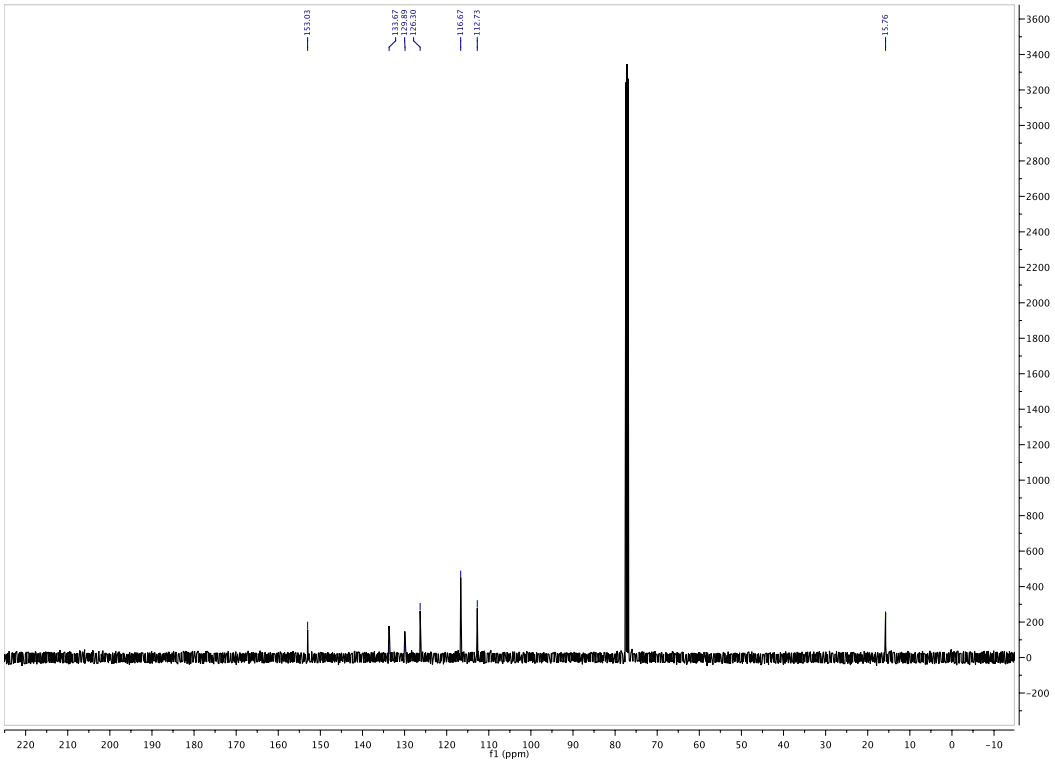

Figure 3.4.95. ^{13}C of 3.18b

3.4.6 Spectral Data Examples for Determination of Ratios for Table 3.3.1

Spectral data examples represent one trial selected from the three trials performed. In the case of phenol exclusively, adding precise equivalents of NCS was crucial, due to over-chlorination. For *ortho*-selective catalyst **3.6**, adding too much NCS resulted in degraded *ortho*-selectivity, and adding too little NCS resulted in improved *ortho*-selectivity. The ratios for all three trials are reported below each of the example NMR spectra.

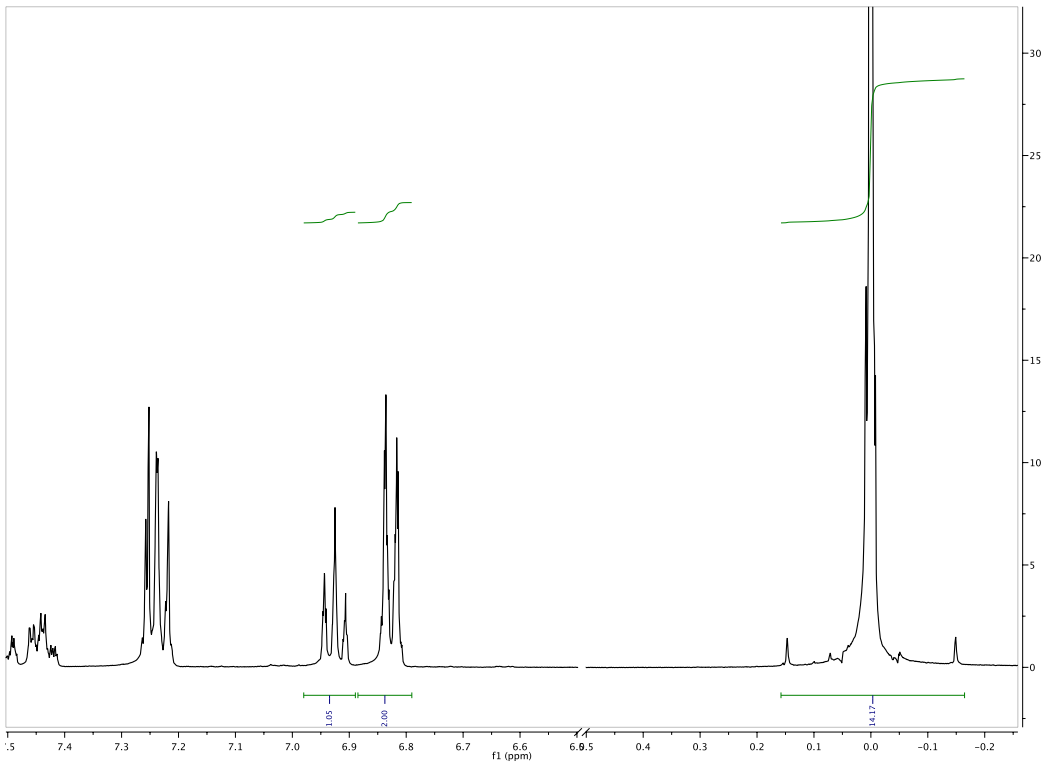

Figure 3.4.96. Example of ^{1}H NMR spectrum for Table 3.3.1, Entry 1; t = 0 h (zoomed in for clear visualization of each isomer)

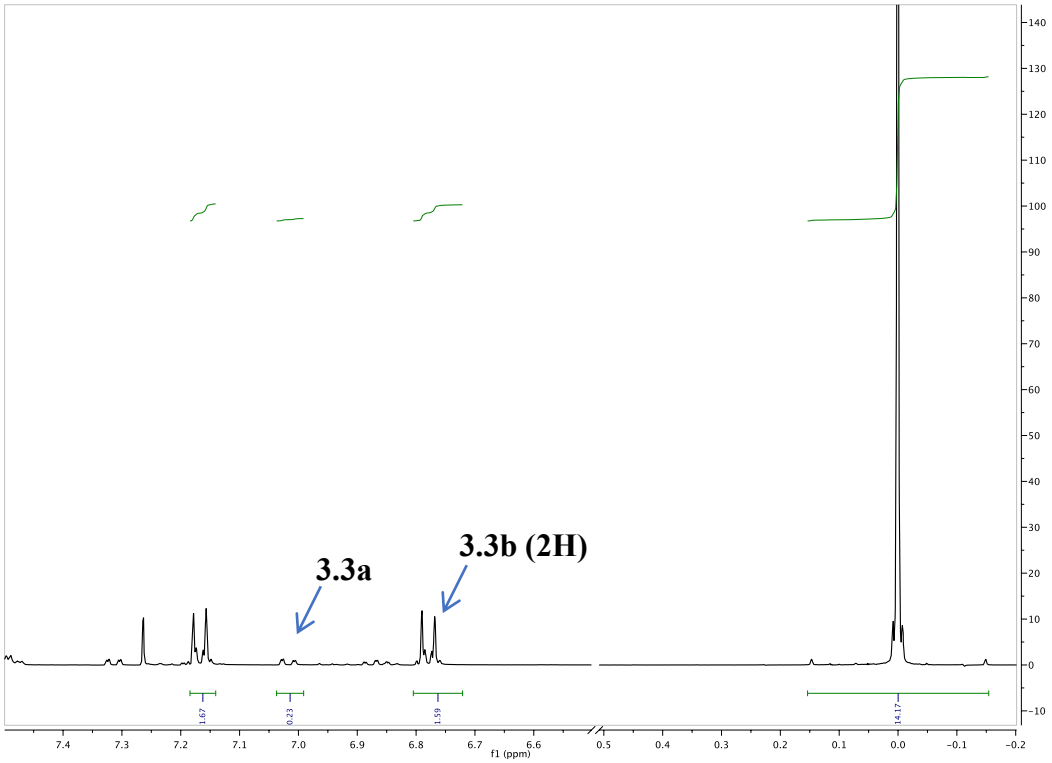

Figure 3.4.97. Example of ^{1}H NMR spectrum for Table 3.3.1, Entry 1; t = 3 h (zoomed in for clear visualization of each isomer)

Trial 1: **3.3a**:**3.3b** as 1.0:5.4
Trial 2: **3.3a**:**3.3b** as 1.0:3.5
Trial 3: **3.3a**:**3.3b** as 1.0:3.1

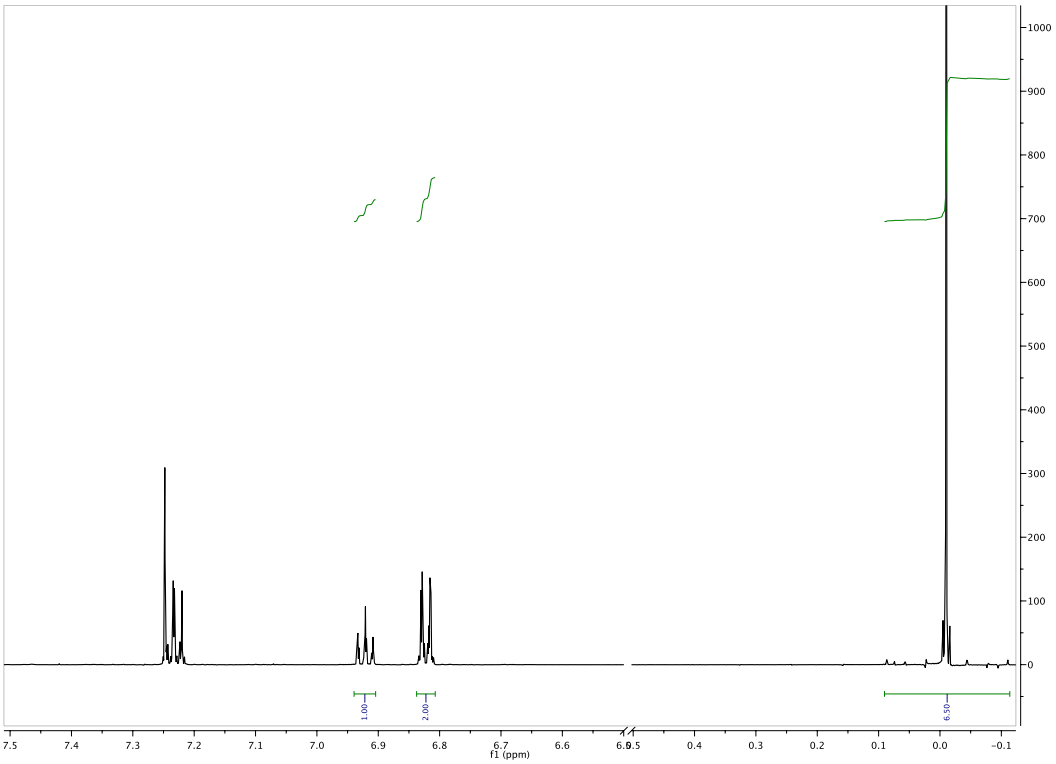

Figure 3.4.98. Example of ^{1}H NMR spectrum for Table 3.3.1, Entry 8; t = 0 h (zoomed in for clear visualization of each isomer)

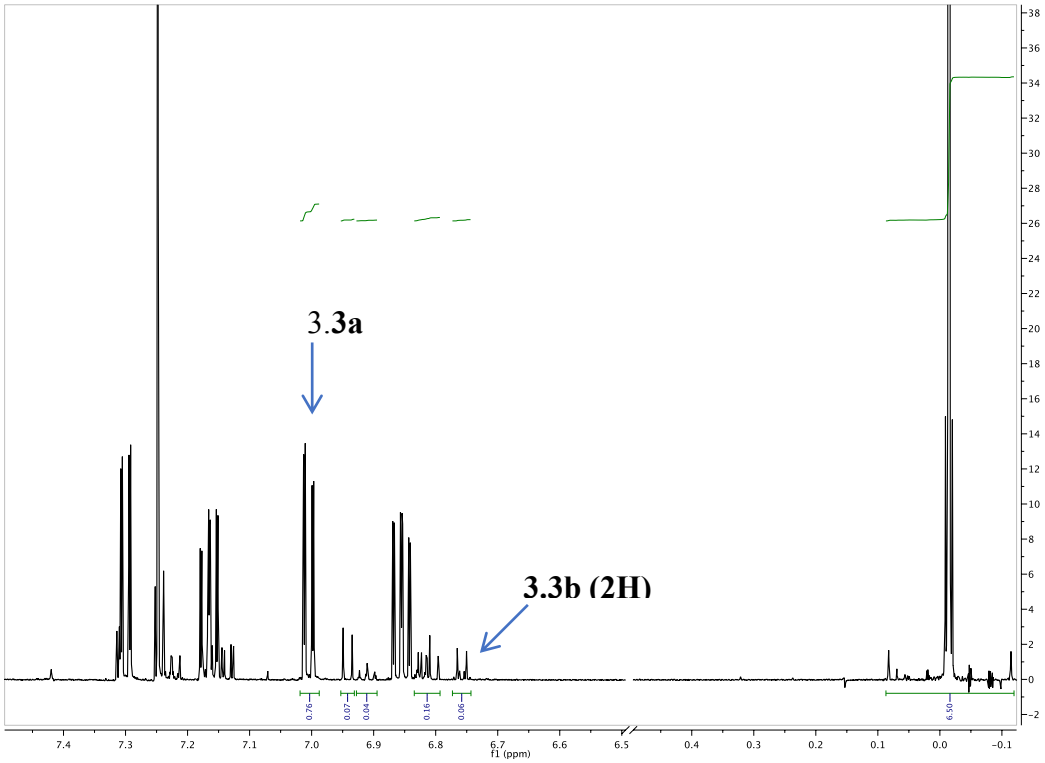

Figure 3.4.99. Example of ^{1}H NMR spectrum for Table 3.3.1, Entry 8; t = 3 h (zoomed in for clear visualization of each isomer)

Trial 1: **3.3a**:**3.3b** as 25:1.0
Trial 2: **3.3a**:**3.3b** as 18:1.0
Trial 3: **3.3a**:**3.3b** as 38:1.0

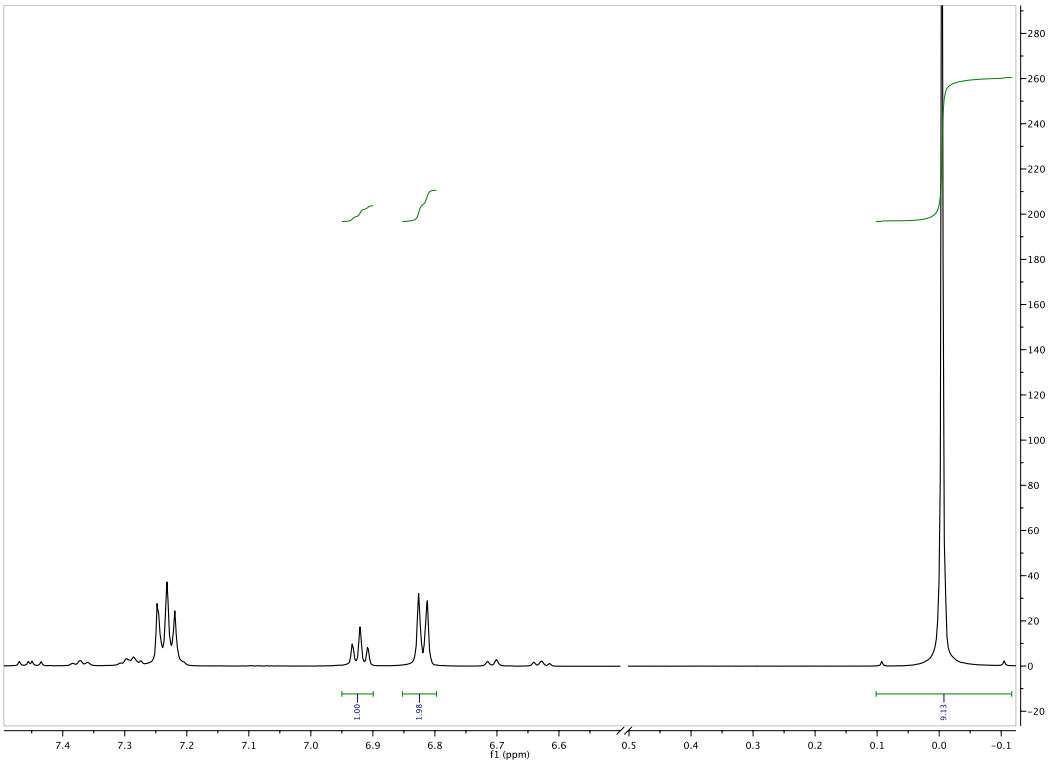

Figure 3.4.100. Example of ^{1}H NMR spectrum for Table 3.3.1, Entry 11; t = 0 h (zoomed in for clear visualization of each isomer)

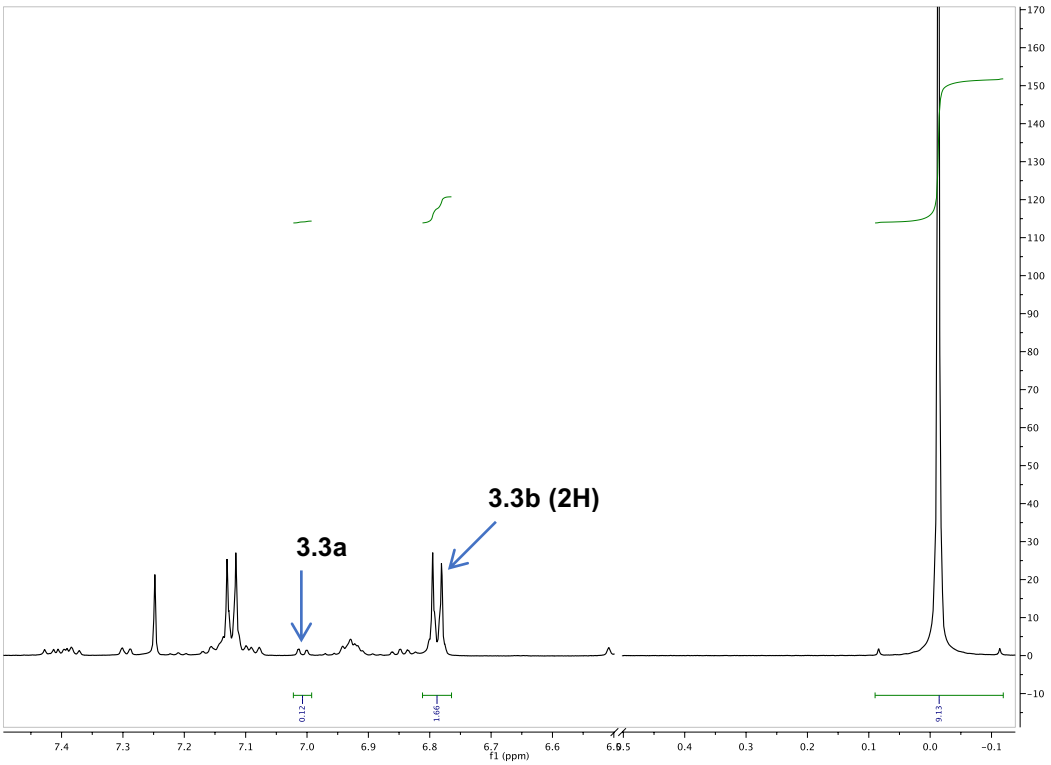

Figure 3.4.101. Example of ^{1}H NMR spectrum for Table 3.3.1, Entry 11; t = 3 h (zoomed in for clear visualization of each isomer)

Trial 1: **3.3a**:**3.3b** as 1.0:6.9
Trial 2: **3.3a**:**3.3b** as 1.0:7.1
Trial 3: **3.3a**:**3.3b** as 1.0:7.4

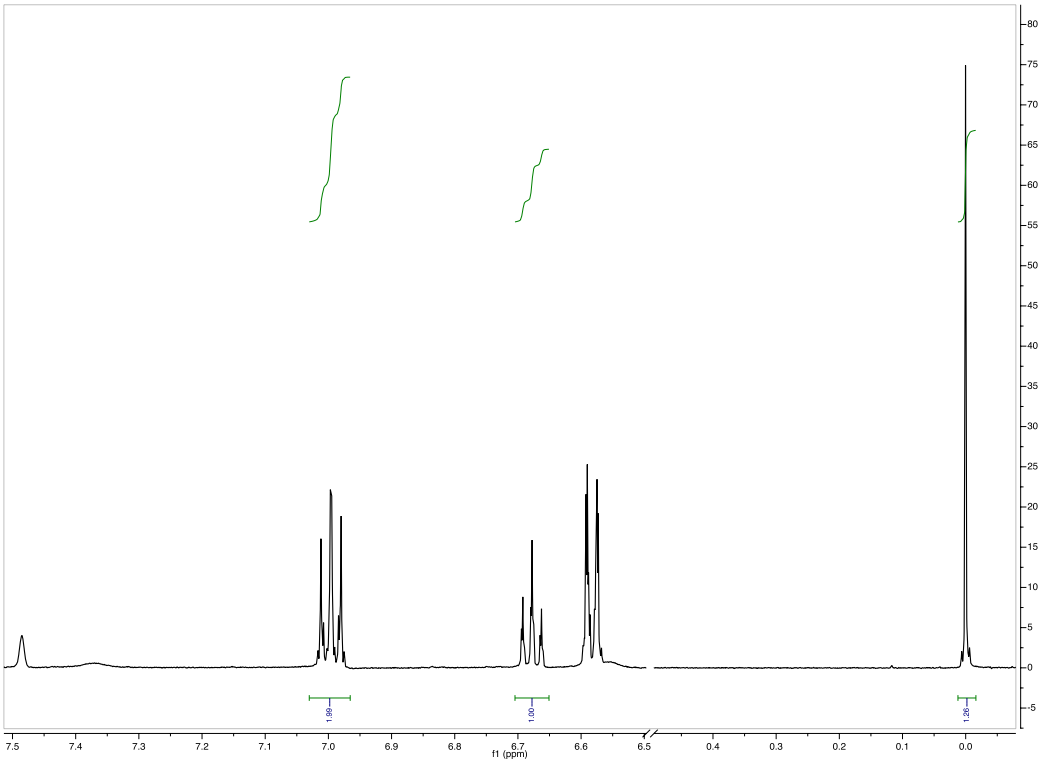

Figure 3.4.102. Example of ^{1}H NMR spectrum for Table 3.3.1, Entry 12; t = 0 h (zoomed in for clear visualization of each isomer)

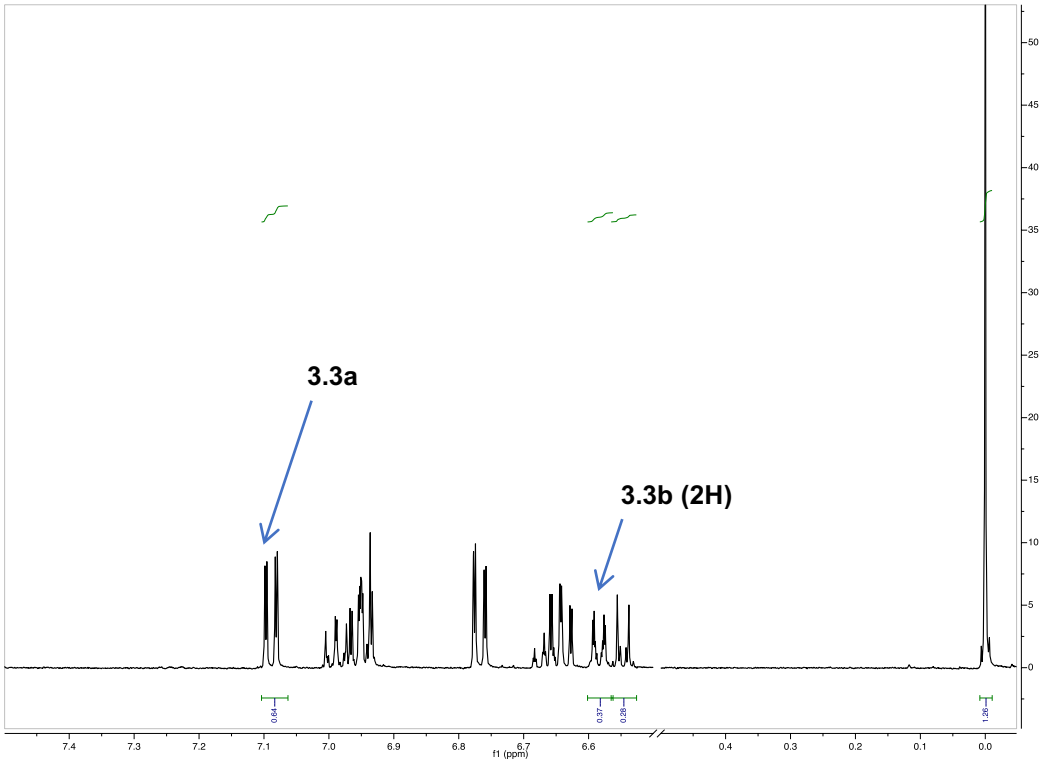

Figure 3.4.103. Example of ^{1}H NMR spectrum for Table 3.3.1, Entry 12; t = 3 h (zoomed in for clear visualization of each isomer)

Trial 1: **3.3a**:**3.3b** as 1.0:4.6
Trial 2: **3.3a**:**3.3b** as 1.0:4.6
Trial 3: **3.3a**:**3.3b** as 1.0:4.8

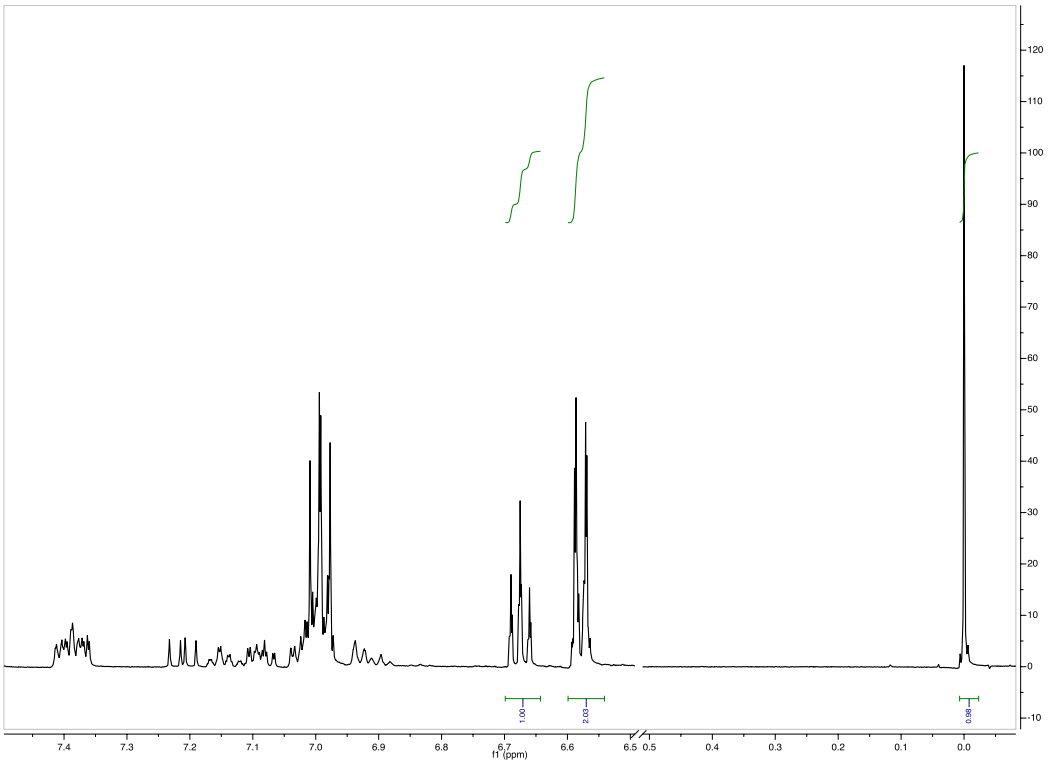

Figure 3.4.104. Example of ^{1}H NMR spectrum for Table 3.3.1, Entry 13; t = 0 h (zoomed in for clear visualization of each isomer)

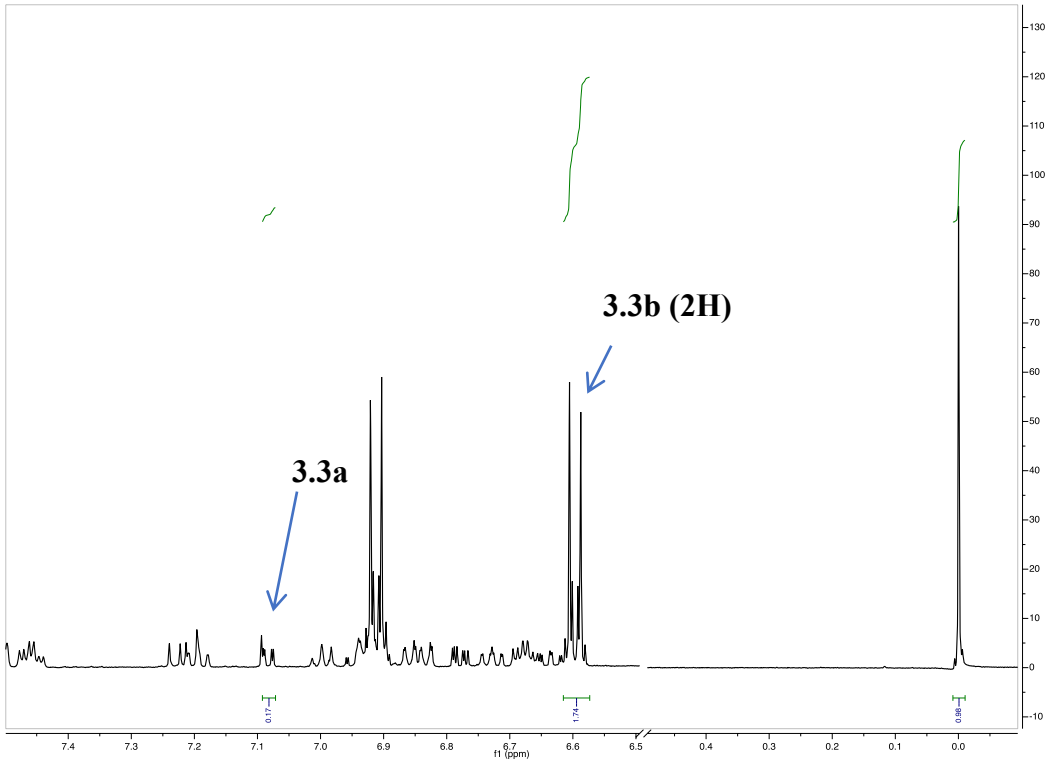

Figure 3.4.105. Example of ^{1}H NMR spectrum for Table 3.3.1, Entry 13; t = 3 h (zoomed in for clear visualization of each isomer)

Trial 1: **3.3a**:**3.3b** as 1.0:5.1
Trial 2: **3.3a**:**3.3b** as 1.0:6.9
Trial 3: **3.3a**:**3.3b** as 1.0:2.9

3.4.7 Example Spectral Data for Determination of Ratios

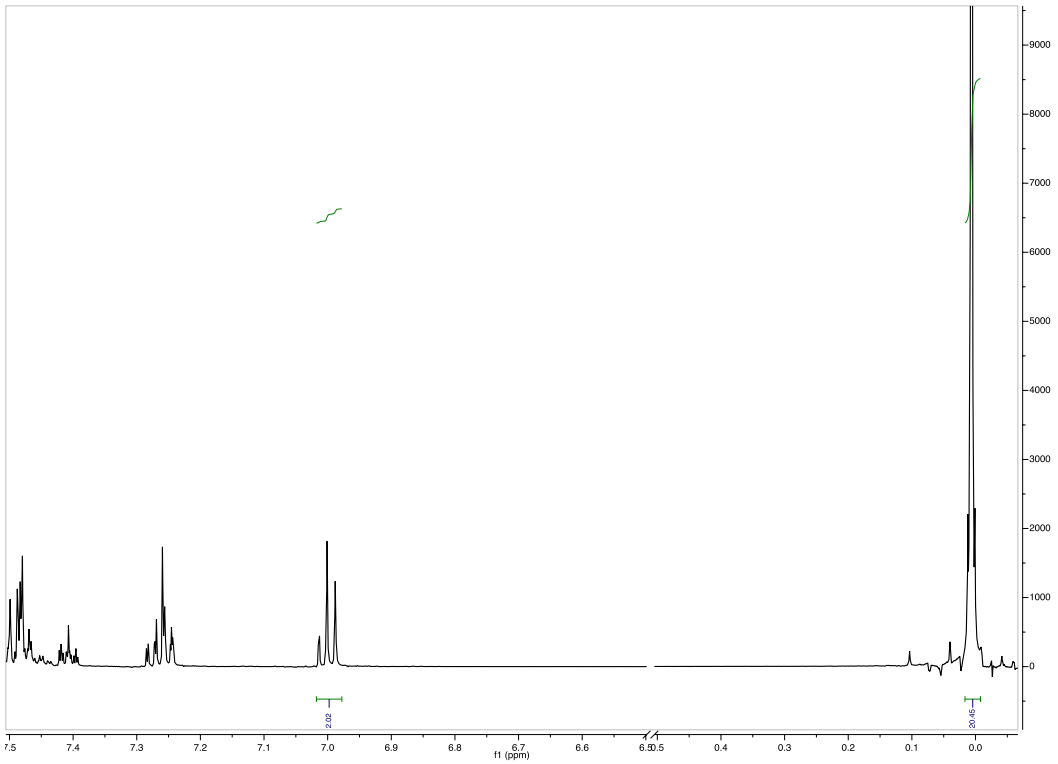

Figure 3.4.106. Example of ^{1}H NMR spectrum for 3.8 + 2.3; t = 0 h (zoomed in for clear visualization of each isomer).

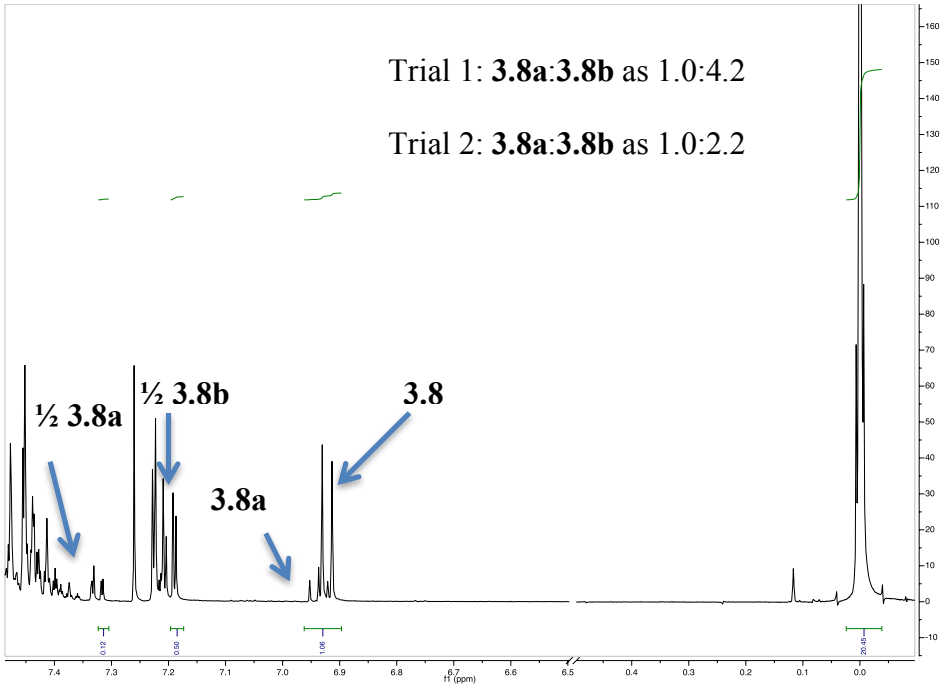

Figure 3.4.107. Example of ^{1}H NMR spectrum for 3.8a + 3.8b + 2.3 + succinimide; t = 4 h after addition of NCS (zoomed in for clear visualization of each isomer).

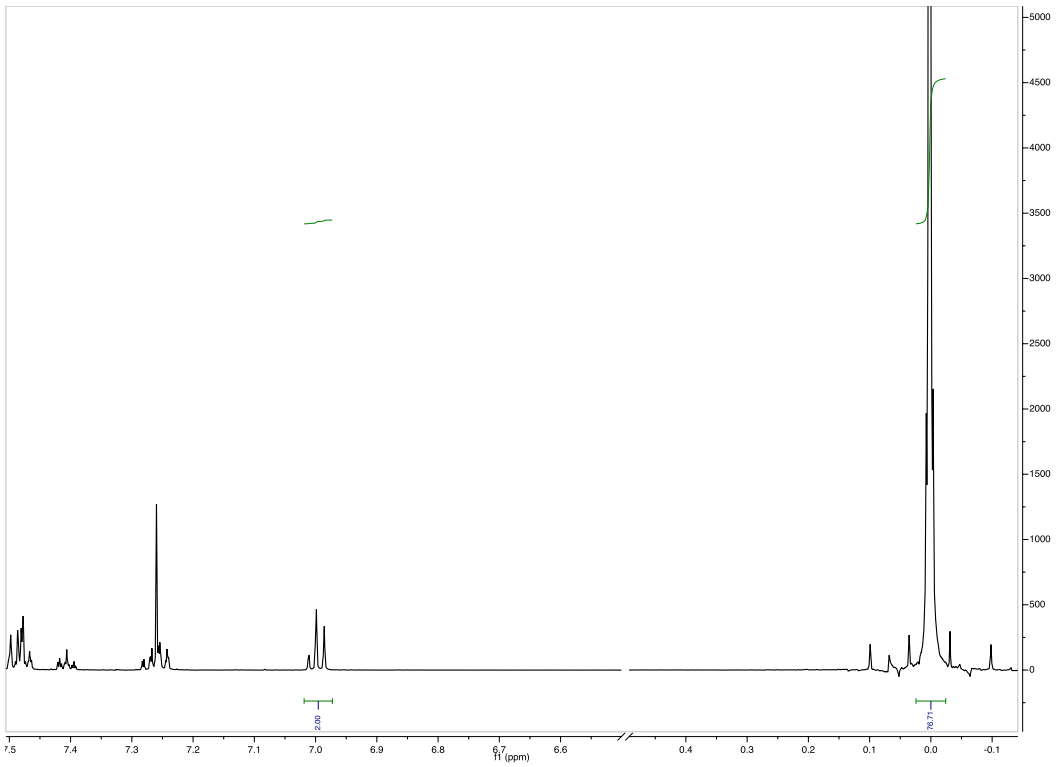

Figure 3.4.108. Example of ^{1}H NMR spectrum for 3.8 + 3.6; t = 0 h (zoomed in for clear visualization of each isomer).

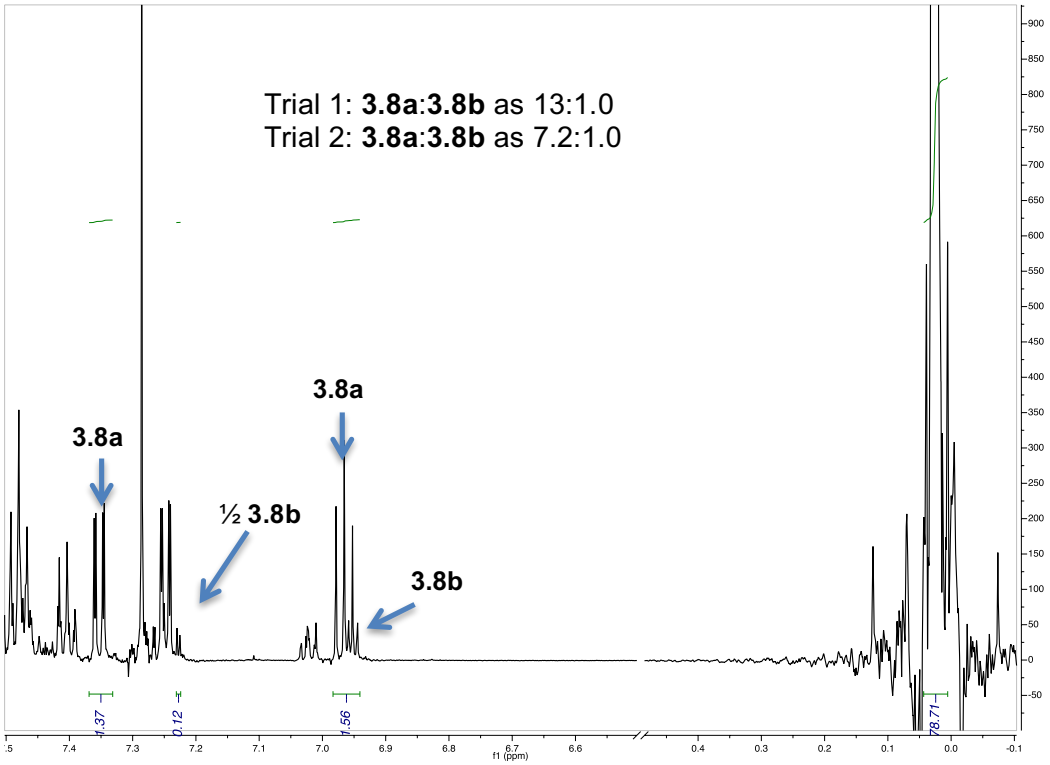

Figure 3.4.109. Example of ^{1}H NMR spectrum for 3.8a + 3.8b + 3.6 + succinimide; t = 4 h after addition of NCS (zoomed in for clear visualization of each isomer).

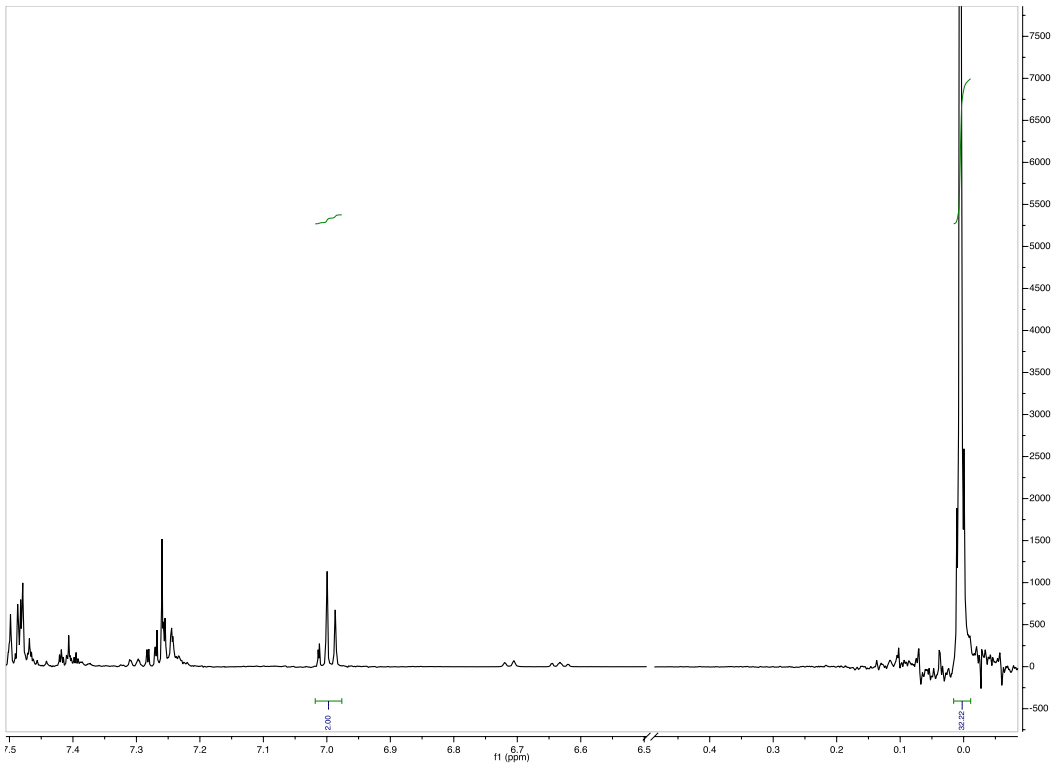

Figure 3.4.110. Example of ^{1}H NMR spectrum for 3.8 + 3.7; t = 0 h (zoomed in for clear visualization of each isomer).

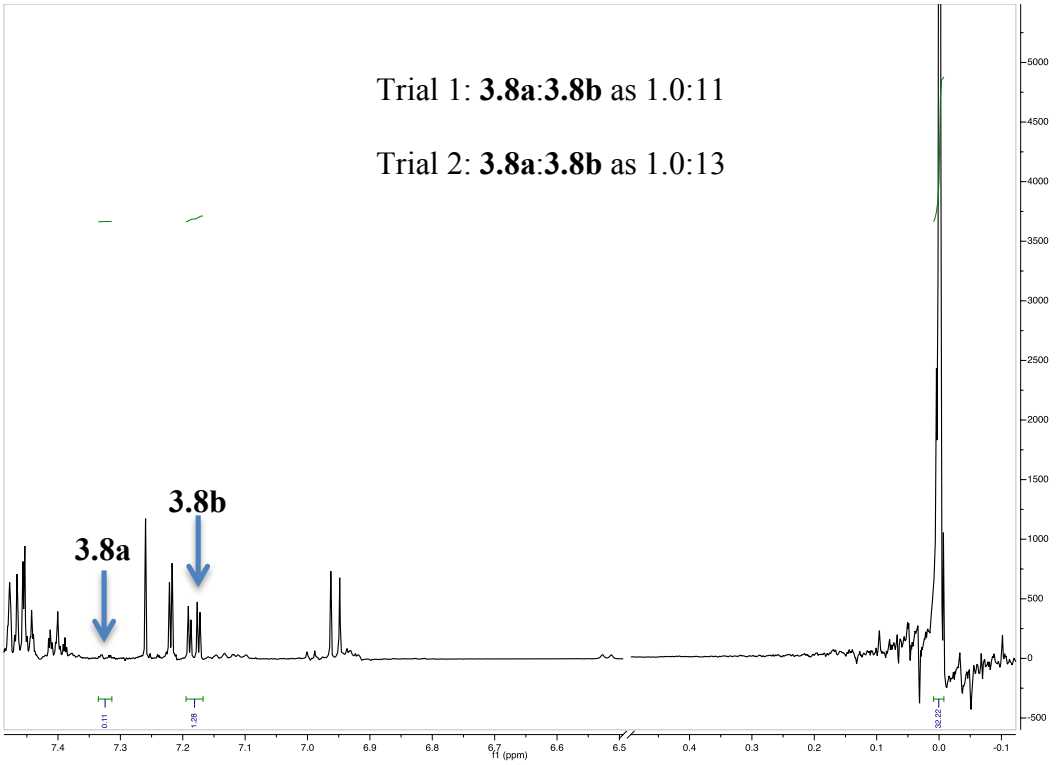

Figure 3.4.111. Example of ^{1}H NMR spectrum for 3.8a + 3.8b + 3.7 + succinimide; t = 4 h after addition of NCS (zoomed in for clear visualization of each isomer).

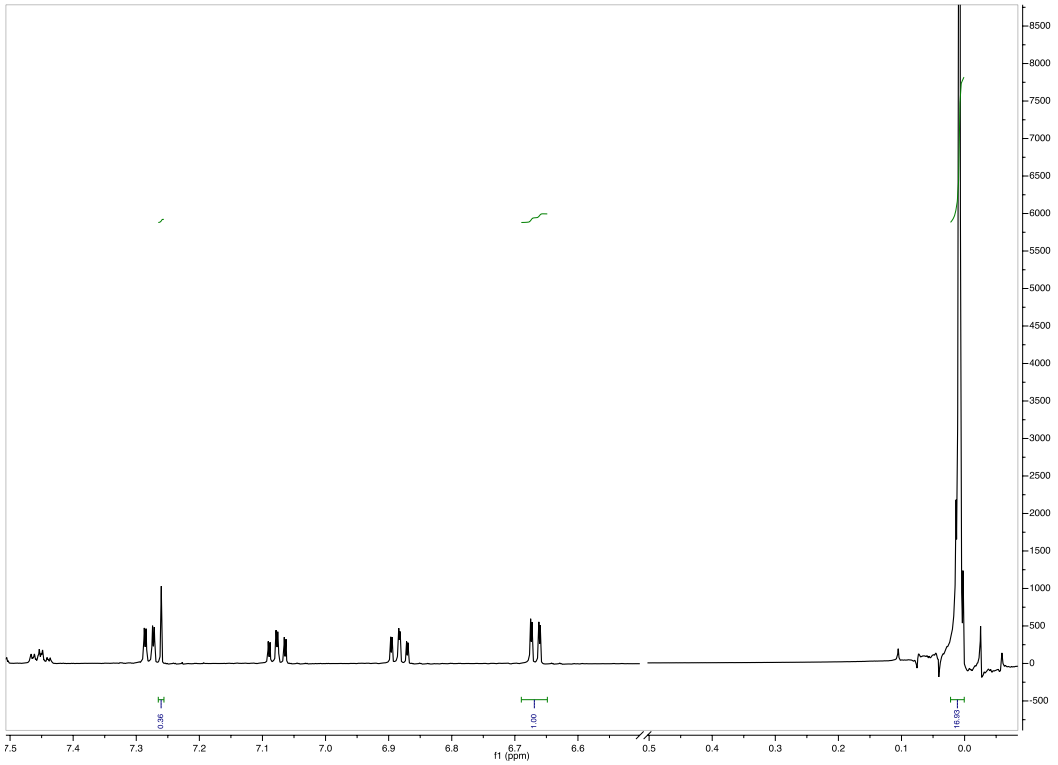

Figure 3.4.112. Example of ^{1}H NMR spectrum for 3.9 + 2.3; t = 0 h (zoomed in for clear visualization of each isomer).

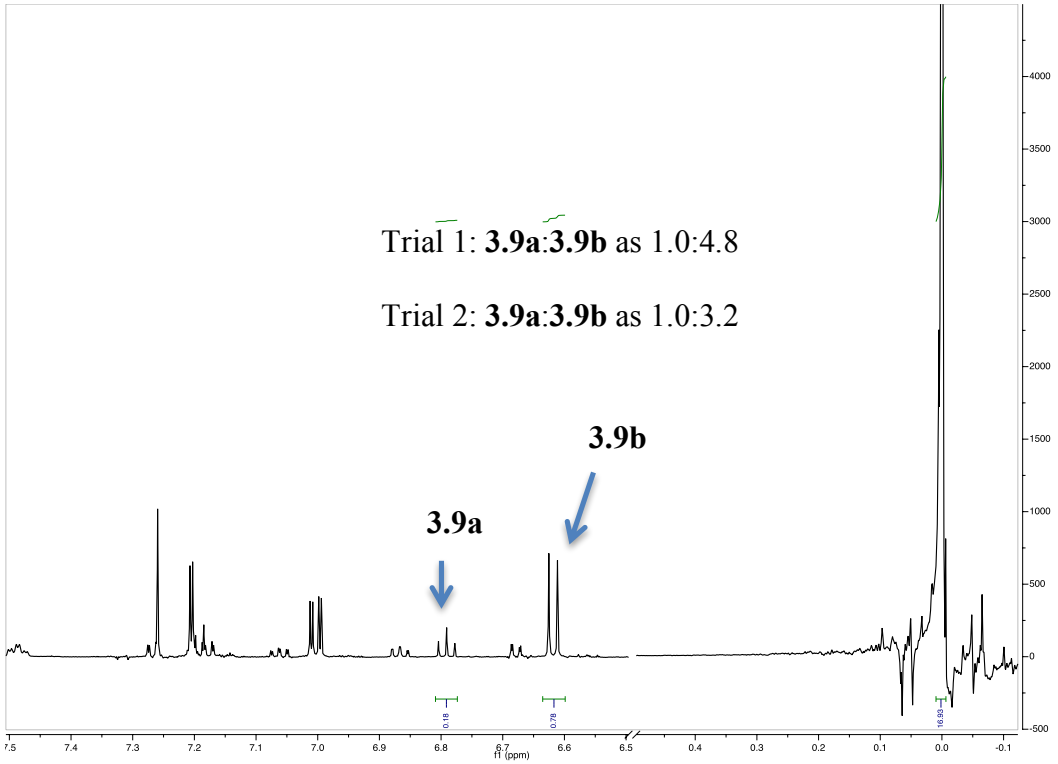

Figure 3.4.113. Example of ^{1}H NMR spectrum for 3.9a + 3.9b + 2.3 + succinimide; t = 12 h after addition of NCS (zoomed in for clear visualization of each isomer).

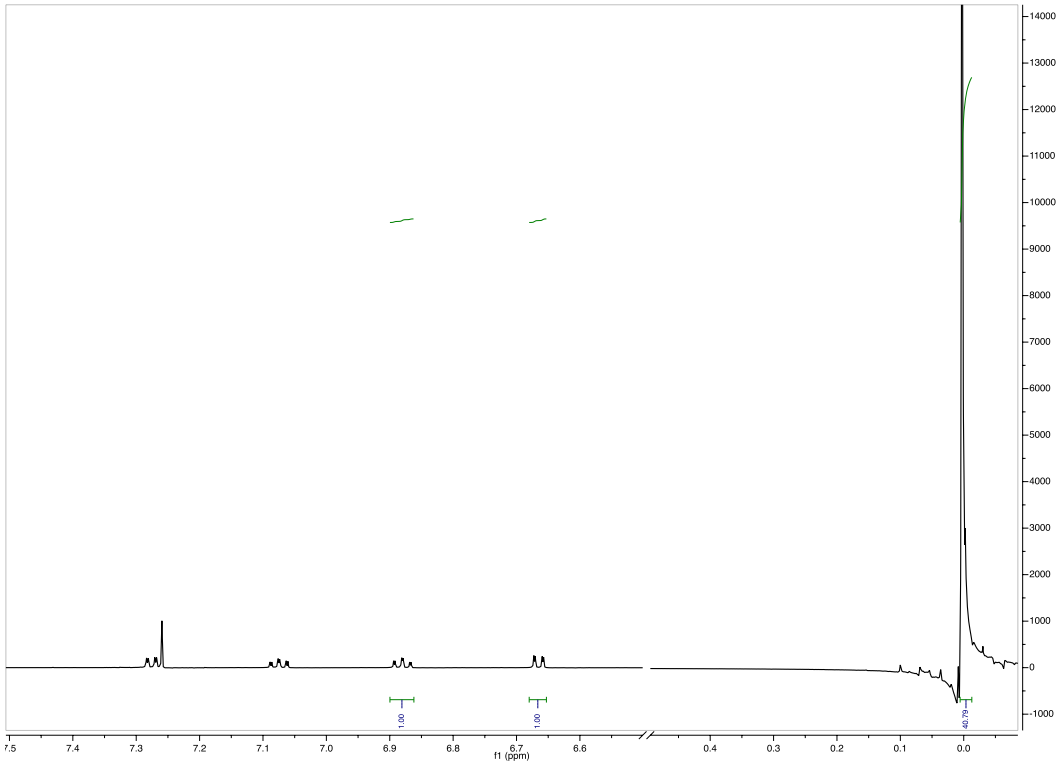

Figure 3.4.114. Example of ^{1}H NMR spectrum for 3.9 + 3.6; t = 0 h (zoomed in for clear visualization of each isomer).

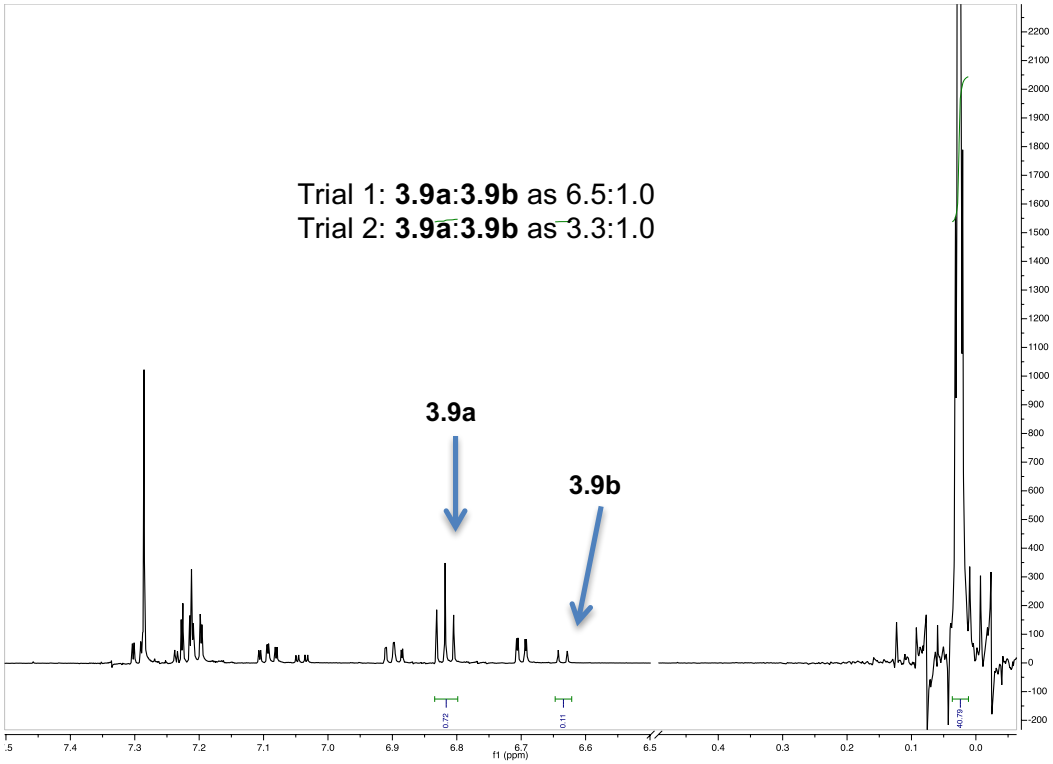

Figure 3.4.115. Example of ^{1}H NMR spectrum for 3.9a + 3.9b + 3.6 + succinimide; t = 12 h after addition of NCS (zoomed in for clear visualization of each isomer).

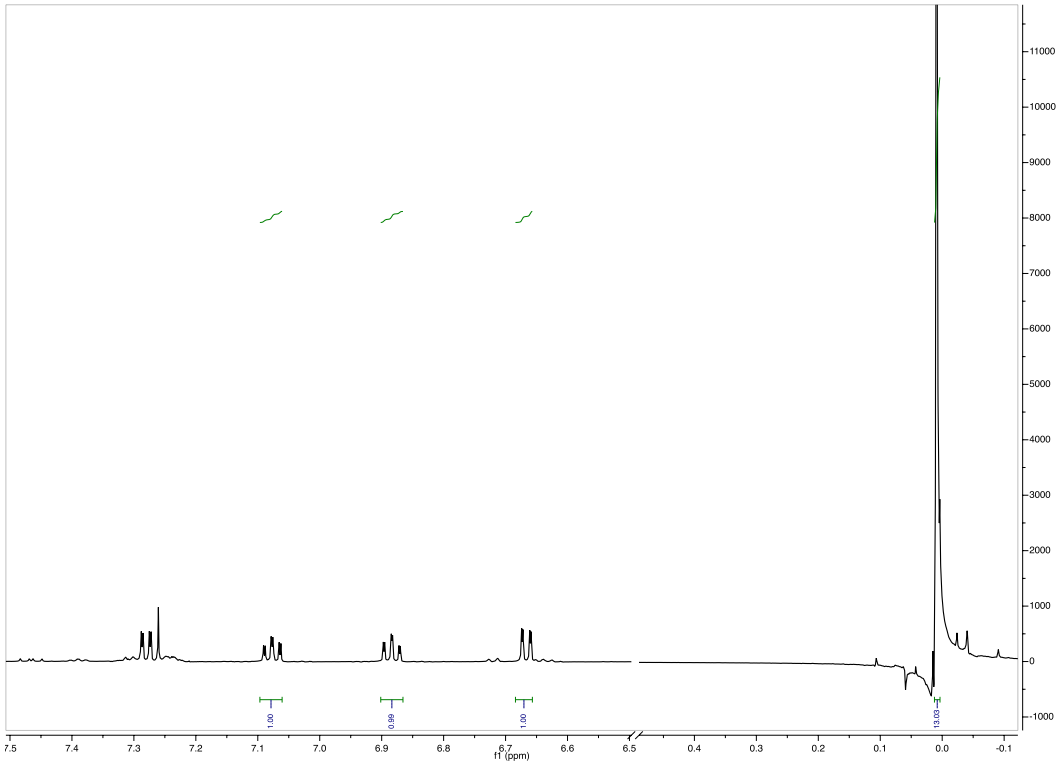

Figure 3.4.116. Example of ^{1}H NMR spectrum for 3.9 + 3.7; t = 0 h (zoomed in for clear visualization of each isomer).

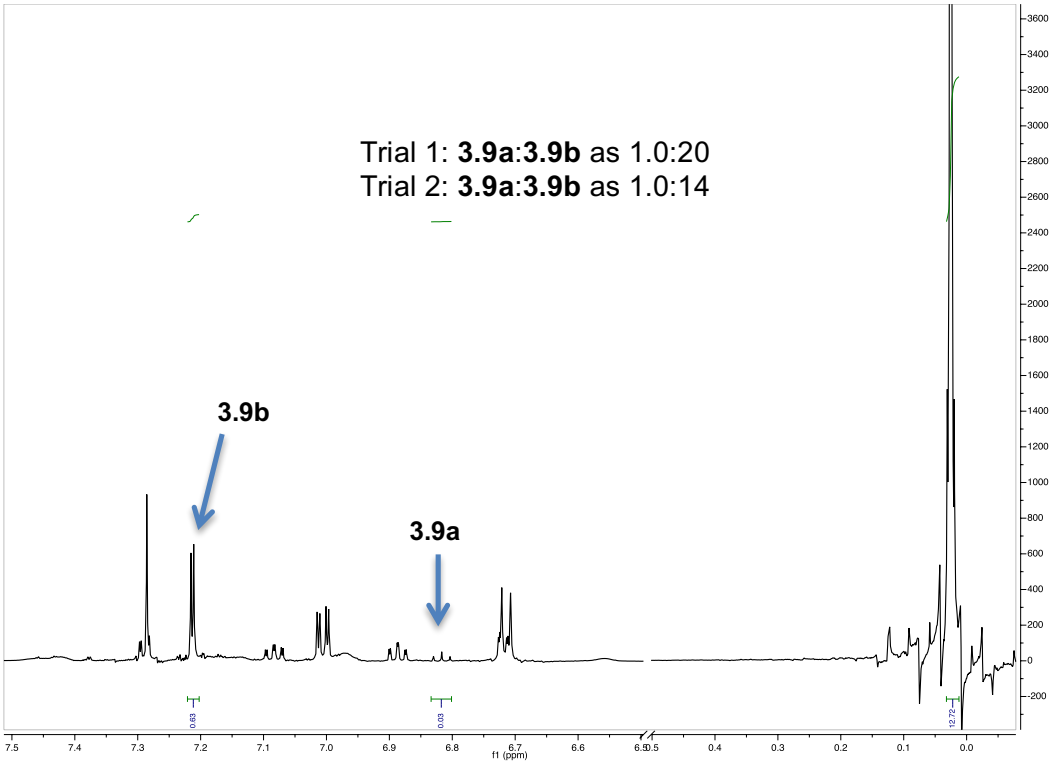

Figure 3.4.117. Example of ^{1}H NMR spectrum for 3.9a + 3.9b + 3.7 + succinimide; t = 12 h after addition of NCS (zoomed in for clear visualization of each isomer).

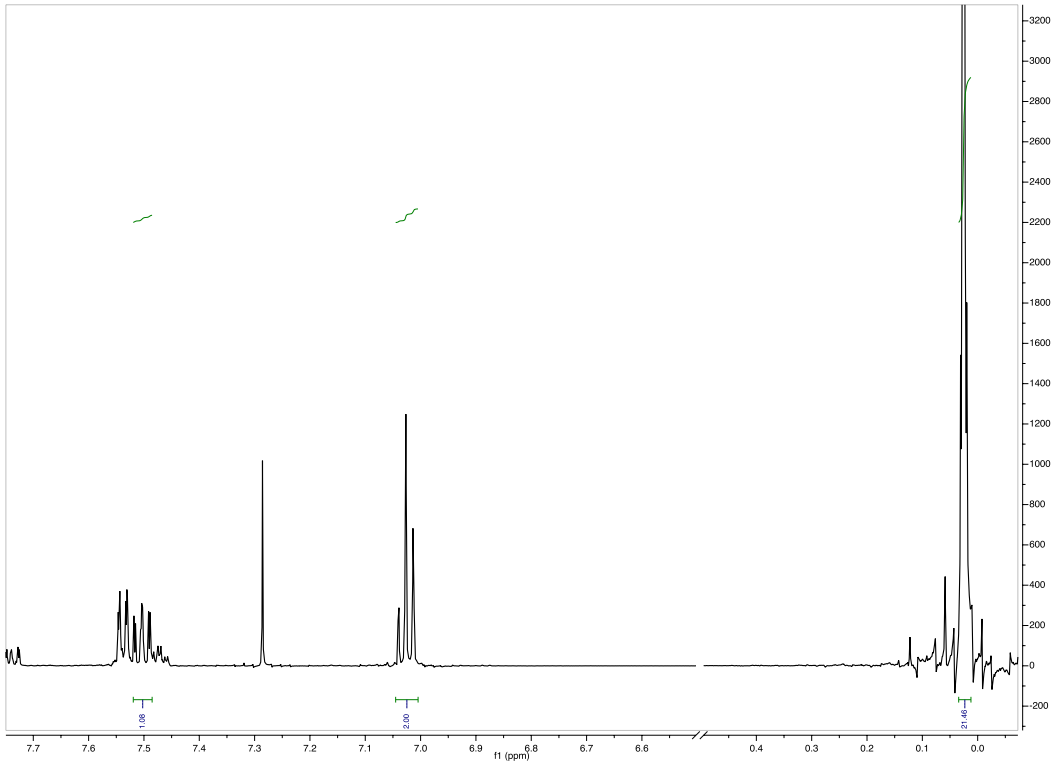

Figure 3.4.118. Example of ^{1}H NMR spectrum for 3.10 + 2.3; t = 0 h (zoomed in for clear visualization of each isomer).

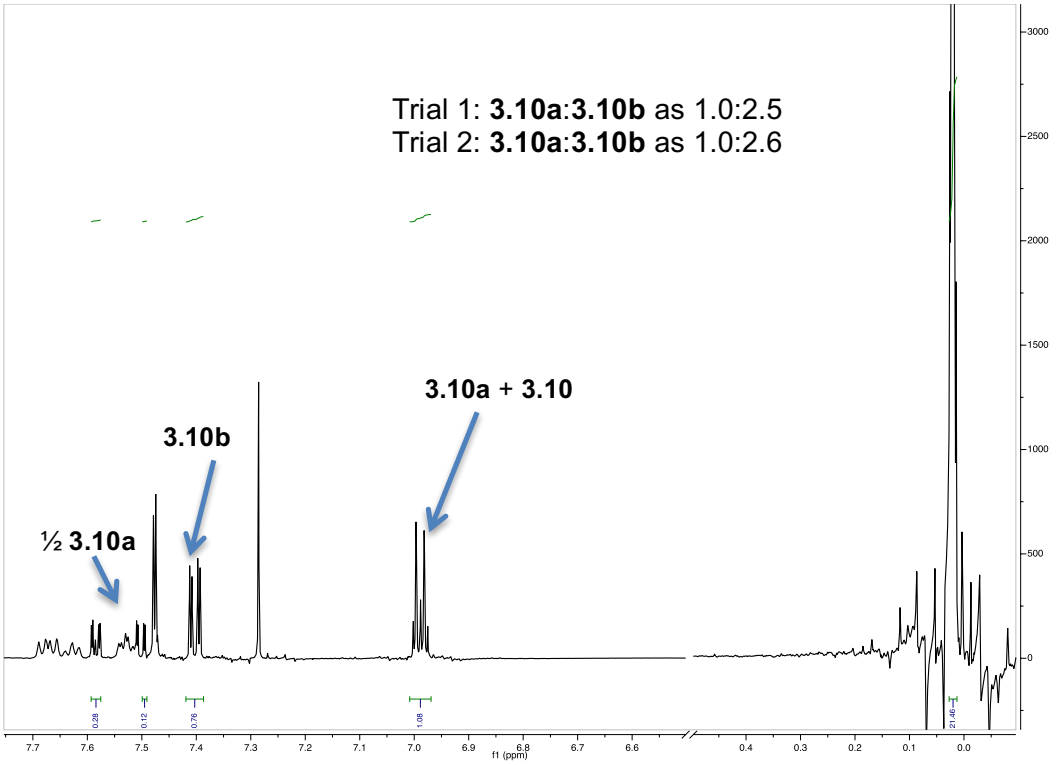

Figure 3.4.119. Example of ^{1}H NMR spectrum for 3.10a + 3.10b + 2.3 + succinimide; t = 12 h after addition of NCS (zoomed in for clear visualization of each isomer).

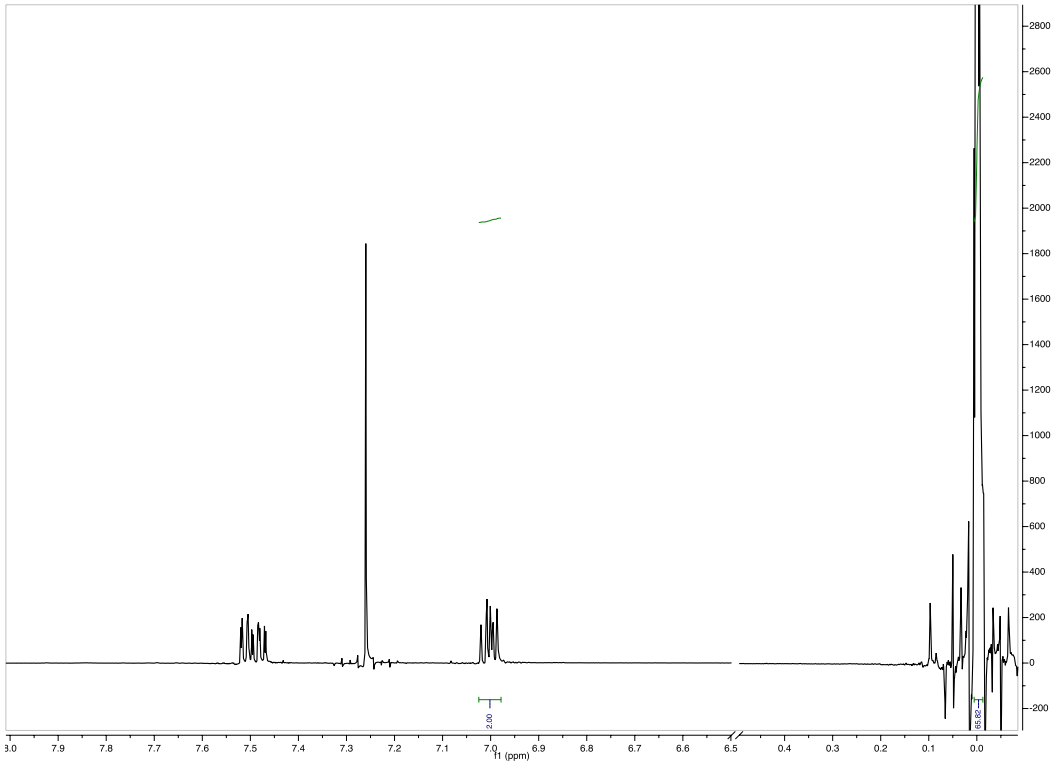

Figure 3.4.120. Example of ^{1}H NMR spectrum for 3.10 + 3.6; t = 0 h (zoomed in for clear visualization of each isomer).

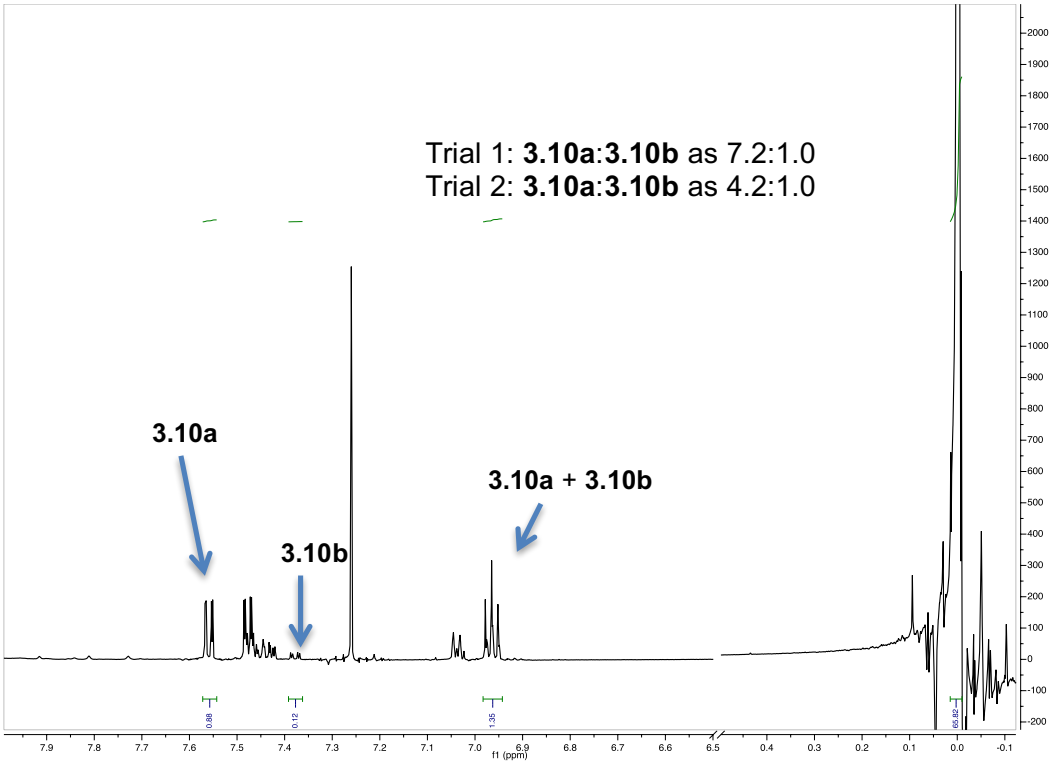

Figure 3.4.121. Example of ^{1}H NMR spectrum for 3.10a + 3.10b + 3.6 + succinimide; t = 12 h after addition of NCS (zoomed in for clear visualization of each isomer).

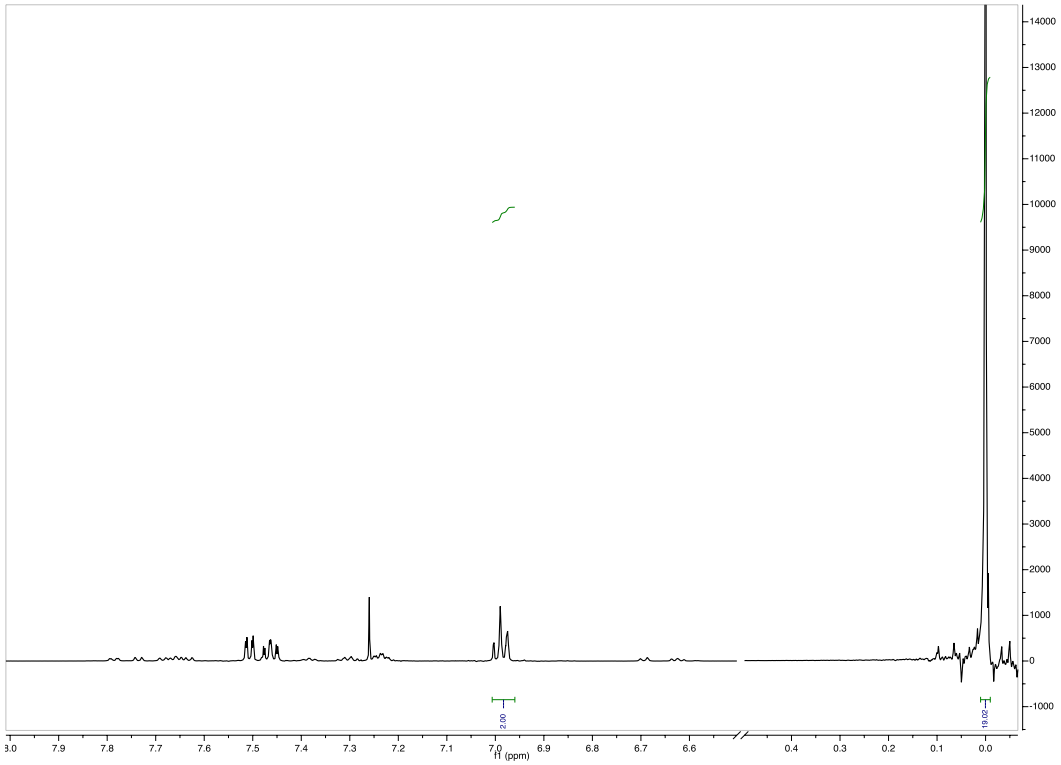

Figure 3.4.122. Example of ^{1}H NMR spectrum for 3.10 + 3.7; t = 0 h (zoomed in for clear visualization of each isomer).

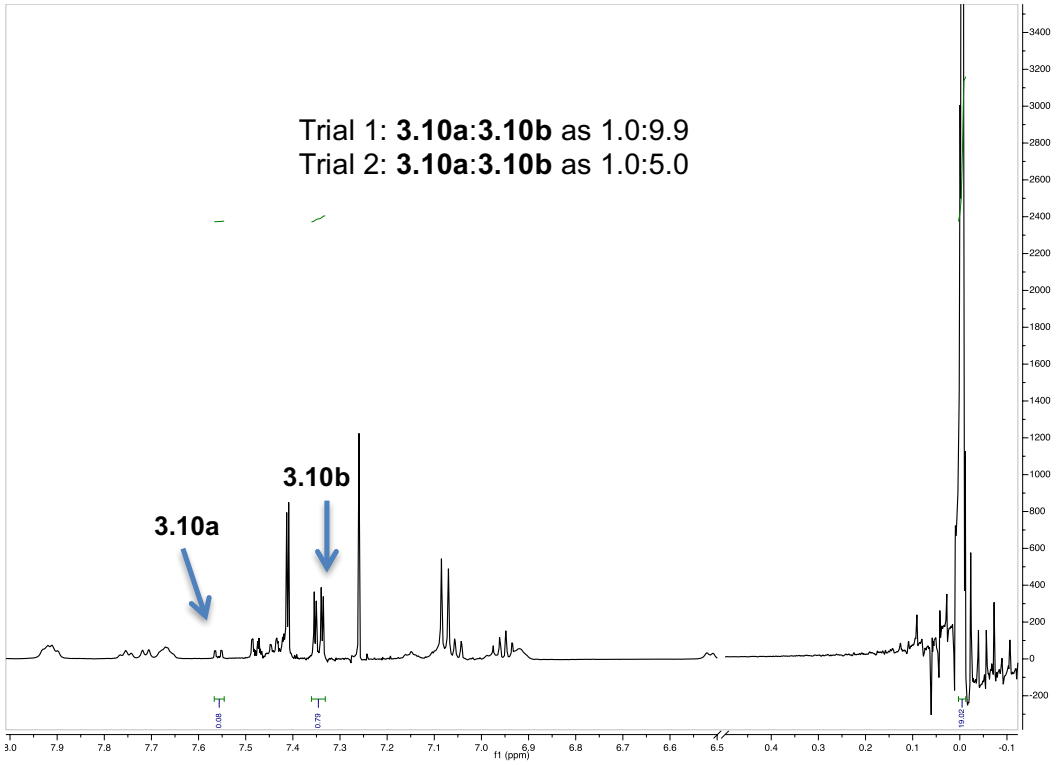

Figure 3.4.123. Example of ^{1}H NMR spectrum for 3.10a + 3.10b + 3.7 + succinimide; t = 12 h after addition of NCS (zoomed in for clear visualization of each isomer).

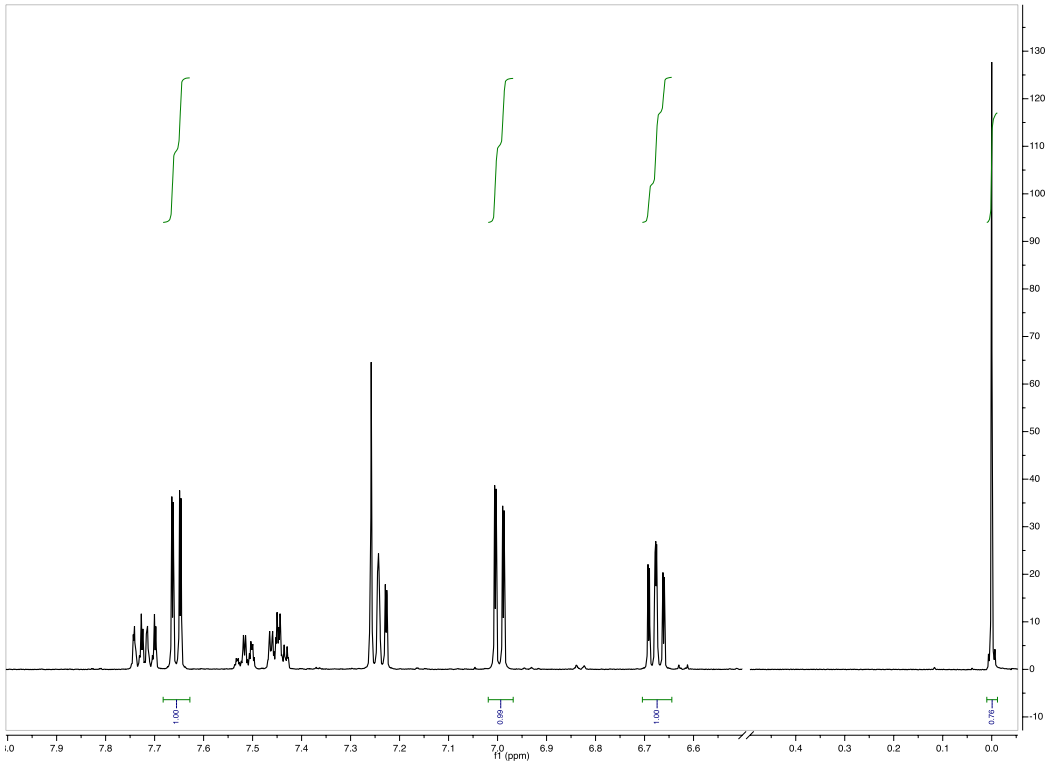

Figure 3.4.124. Example of ^{1}H NMR spectrum for 3.11 + 2.3; t = 0 h (zoomed in for clear visualization of each isomer).

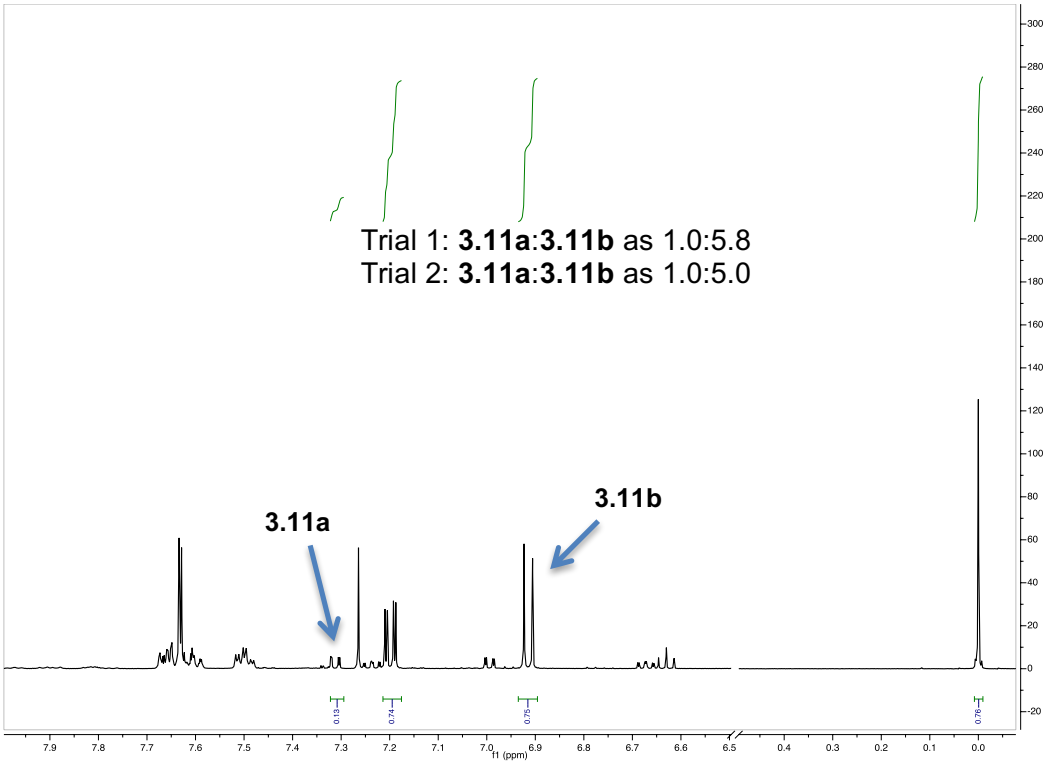

Figure 3.4.125. Example of ^{1}H NMR spectrum for 3.11a + 3.11b + 2.3 + succinimide; t = 12 h after addition of NCS (zoomed in for clear visualization of each isomer).

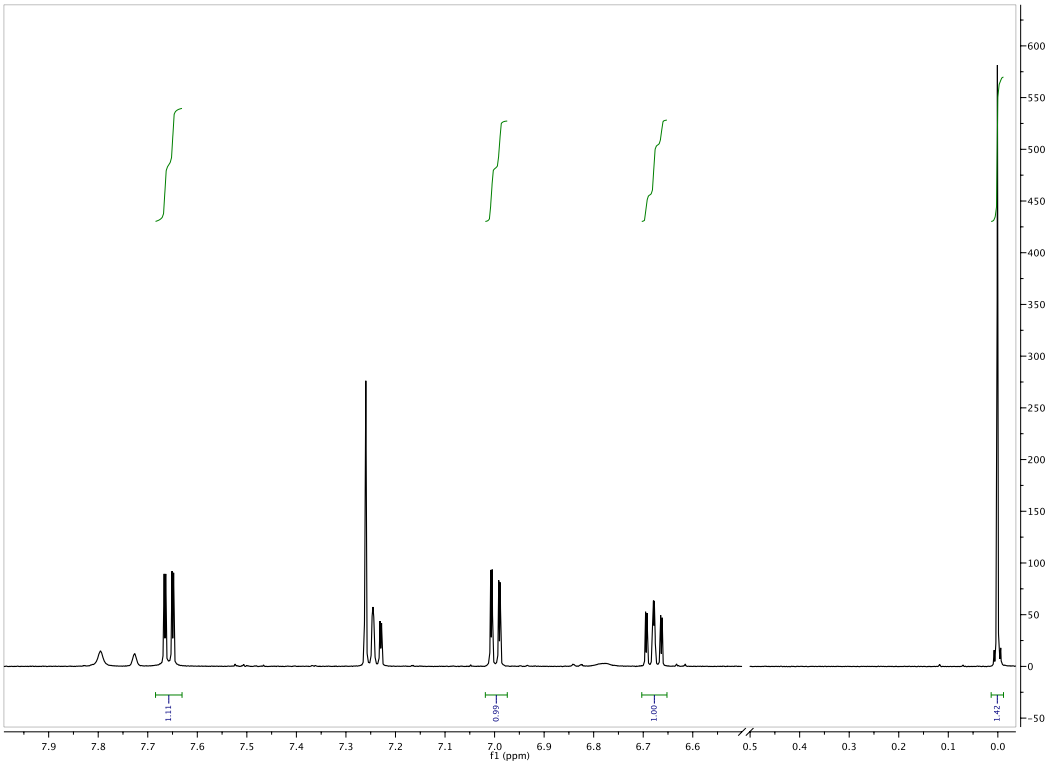

Figure 3.4.126. Example of ^{1}H NMR spectrum for 3.11 + 3.6; t = 0 h (zoomed in for clear visualization of each isomer).

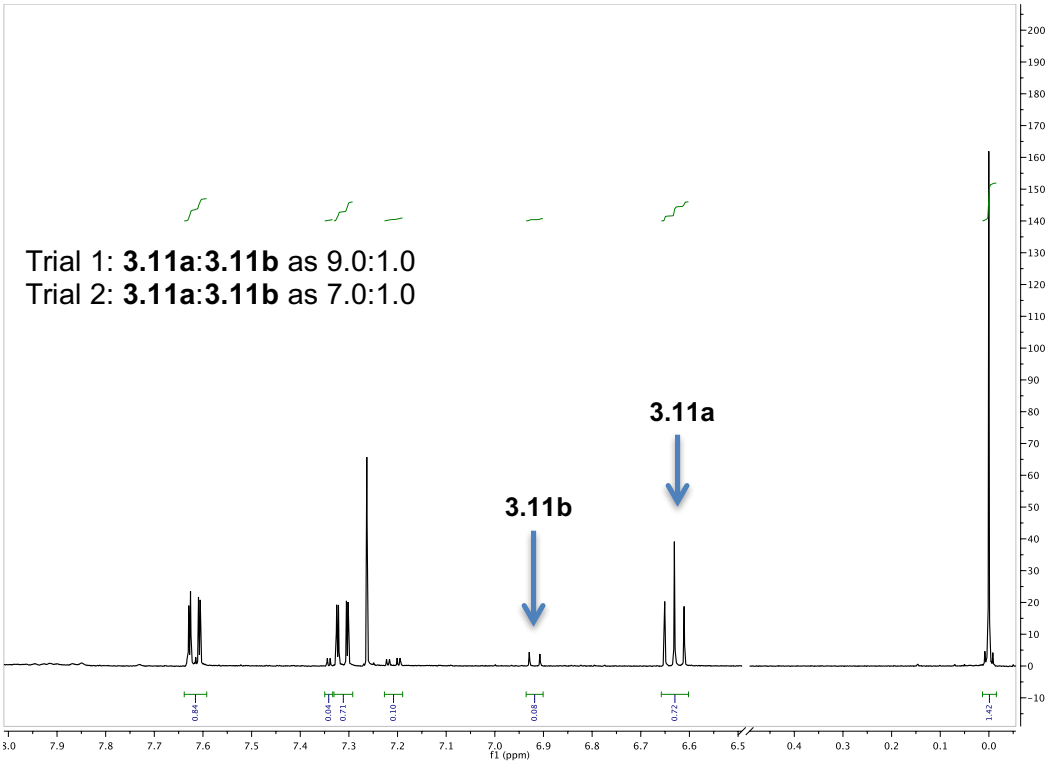

Figure 3.4.127. Example of ^{1}H NMR spectrum for 3.11a + 3.11b + 3.6 + succinimide; t = 12 h after addition of NCS (zoomed in for clear visualization of each isomer).

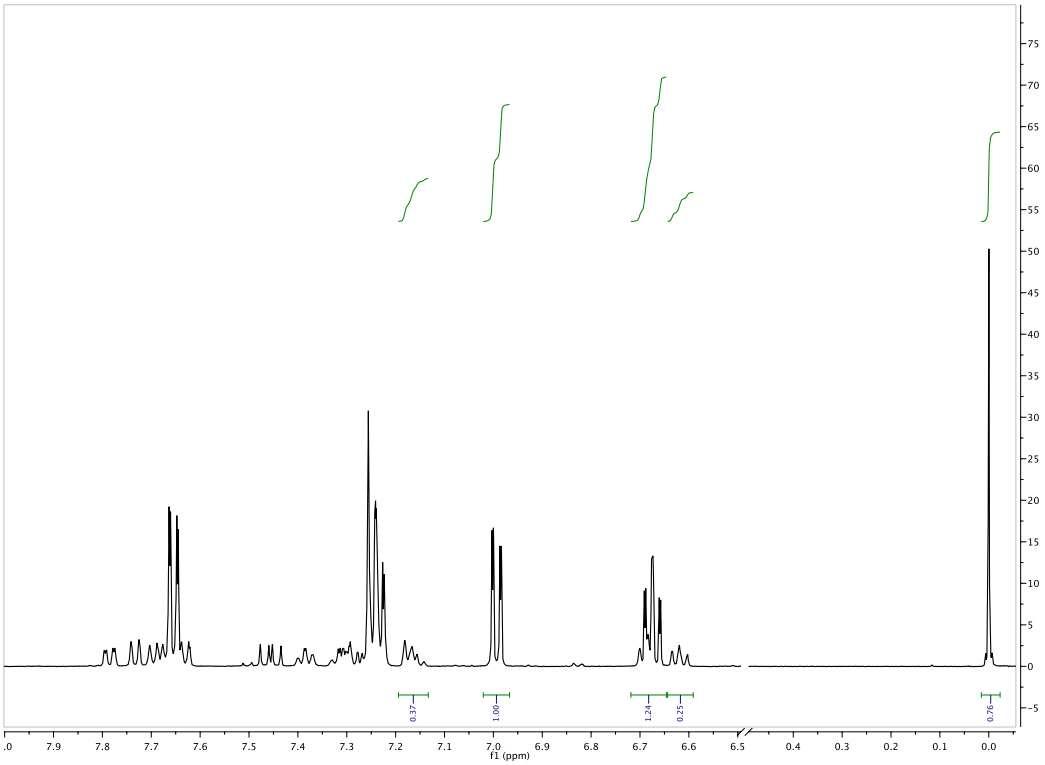

Figure 3.4.128. Example of ^{1}H NMR spectrum for 3.11 + 3.7; t = 0 h (zoomed in for clear visualization of each isomer).

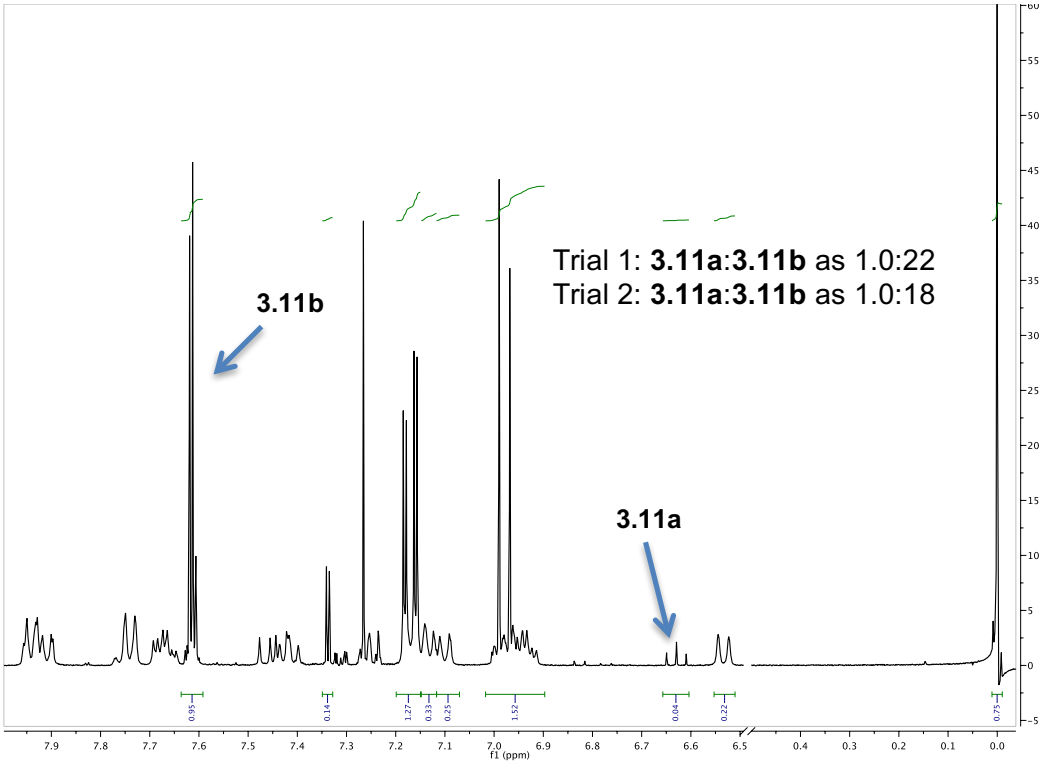

Figure 3.4.129. Example of ^{1}H NMR spectrum for 3.11a + 3.11b + 3.7 + succinimide; t = 12 h after addition of NCS (zoomed in for clear visualization of each isomer).

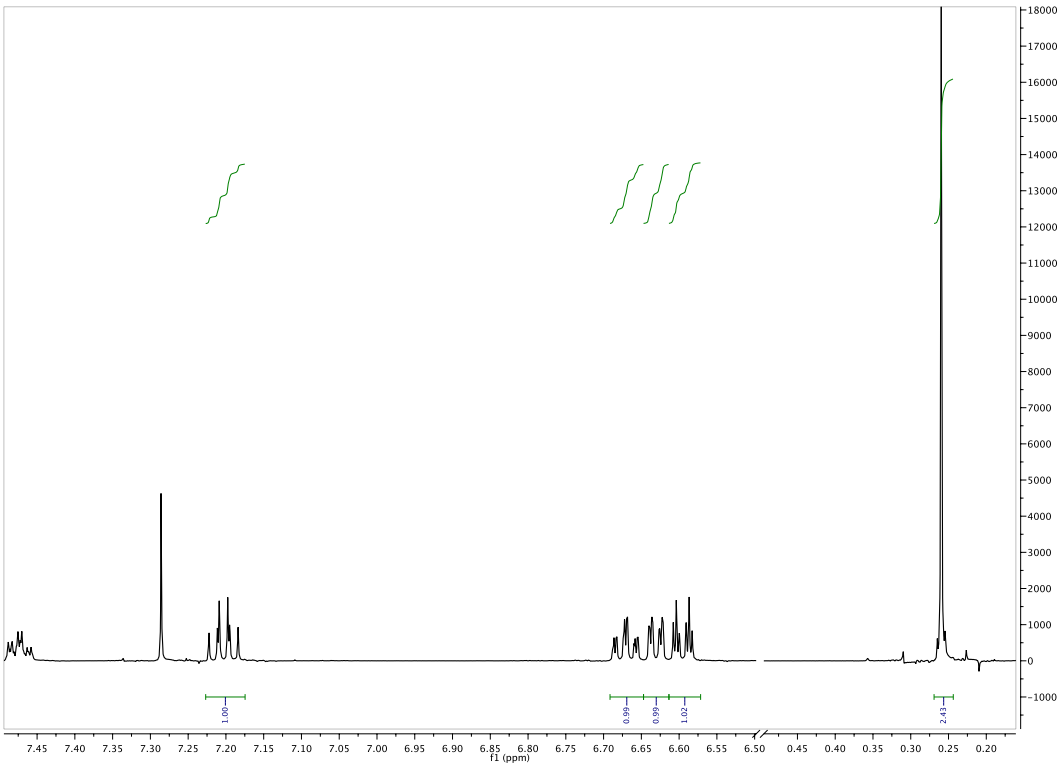

Figure 3.4.130. Example of ^{1}H NMR spectrum for 3.12 + 2.3; t = 0 h (zoomed in for clear visualization of each isomer).

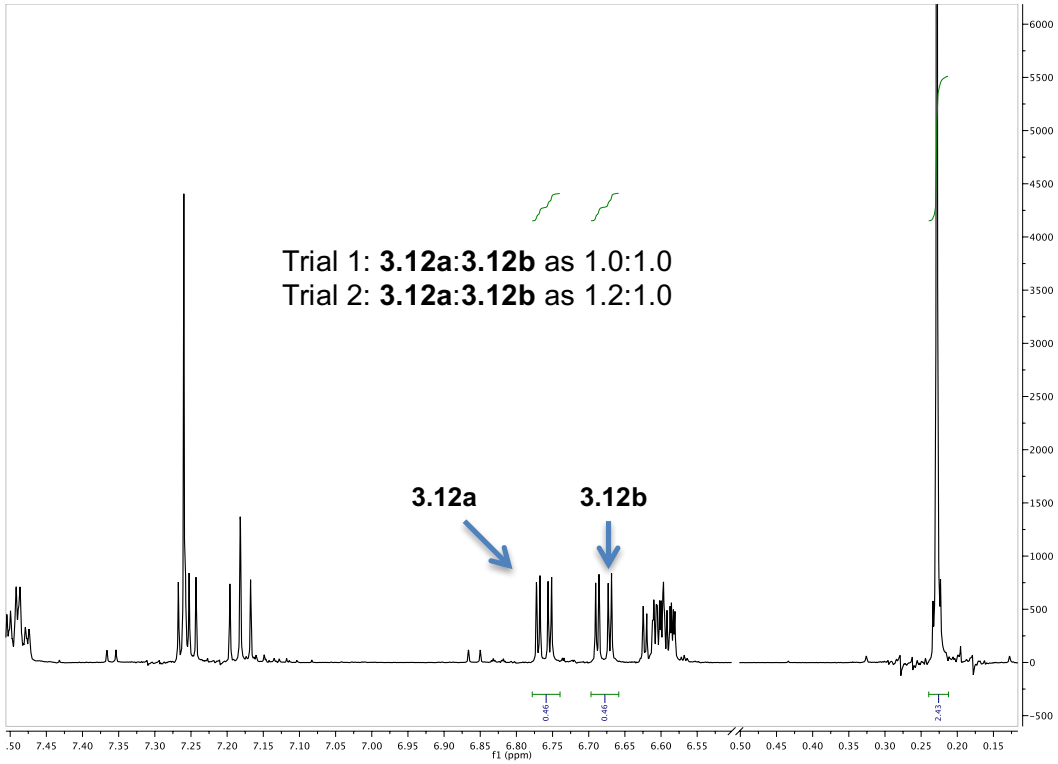

Figure 3.4.131. Example of ^{1}H NMR spectrum for 3.12a + 3.12b + 3.12c + 2.3 + succinimide; t = 9 h after addition of NCS (zoomed in for clear visualization of each isomer).

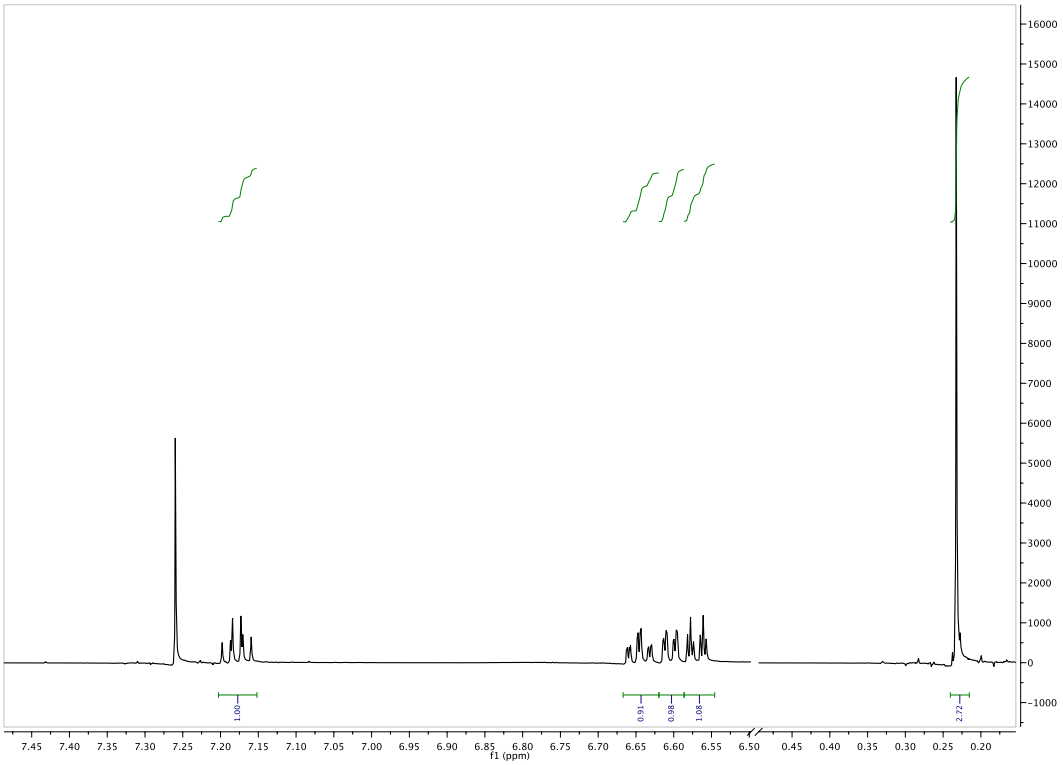

Figure 3.4.132. Example of ^{1}H NMR spectrum for 3.12 + 3.6; t = 0 h (zoomed in for clear visualization of each isomer).

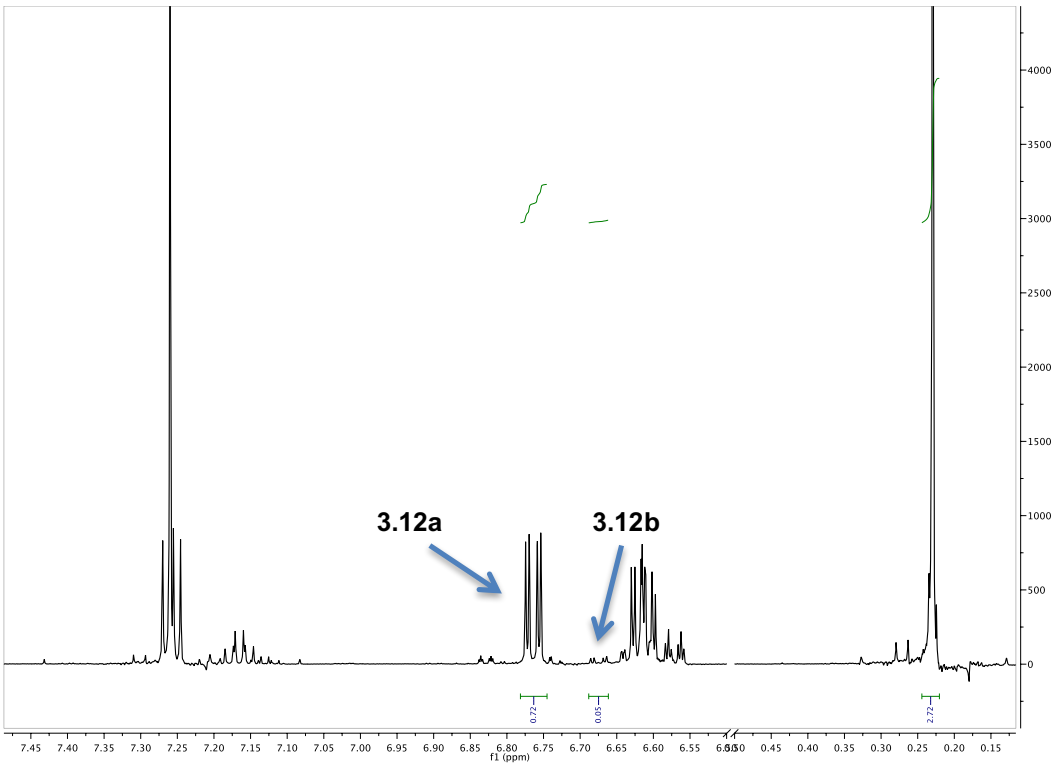

Figure 3.4.133. Example of ^{1}H NMR spectrum for 3.12a + 3.12b + 3.12c + 3.6 + succinimide; t = 9 h after addition of NCS (zoomed in for clear visualization of each isomer).

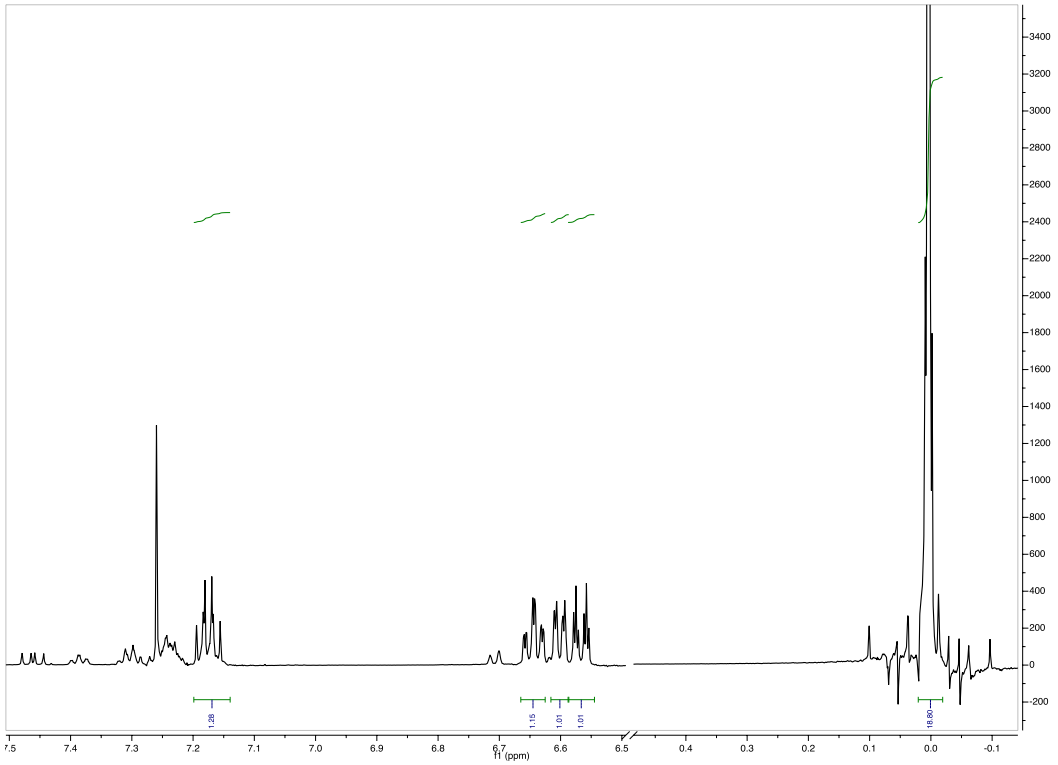

Figure 3.4.134. Example of ^{1}H NMR spectrum for 3.12 + 3.7; t = 0 h (zoomed in for clear visualization of each isomer).

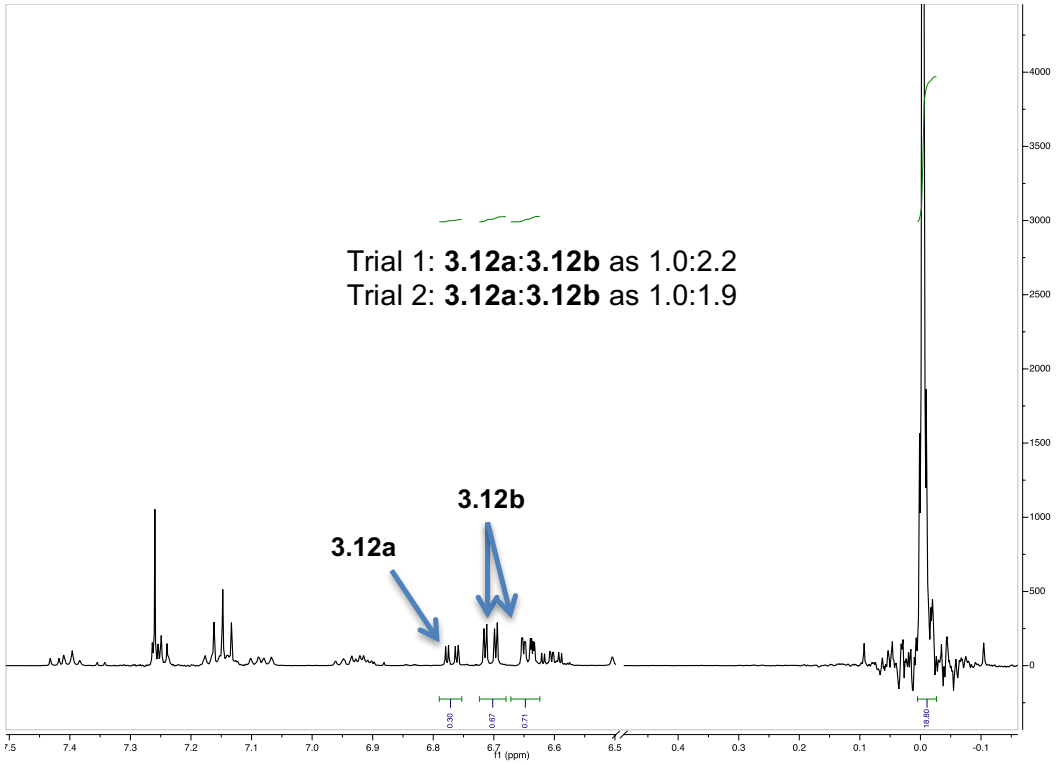

Figure 3.4.135. Example of ^{1}H NMR spectrum for 3.12a + 3.12b + 3.12c + 3.7 + succinimide; t = 6 h after addition of NCS (zoomed in for clear visualization of each isomer).

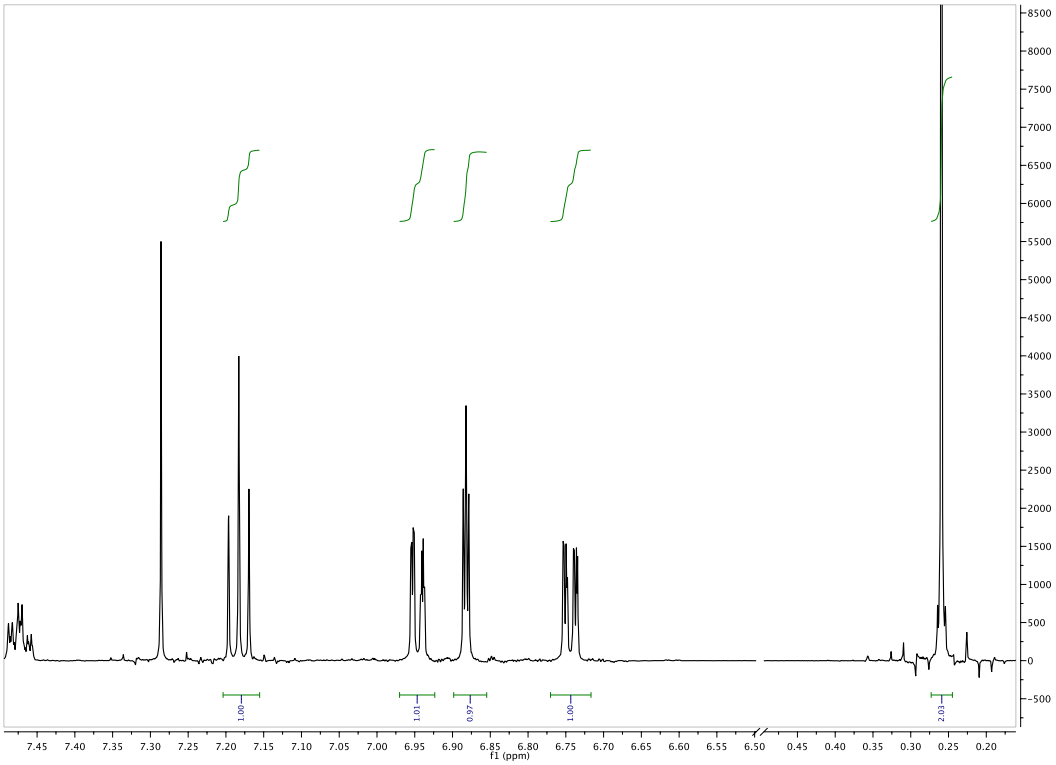

Figure 3.4.136. Example of ^{1}H NMR spectrum for 3.13 + 2.3; t = 0 h (zoomed in for clear visualization of each isomer).

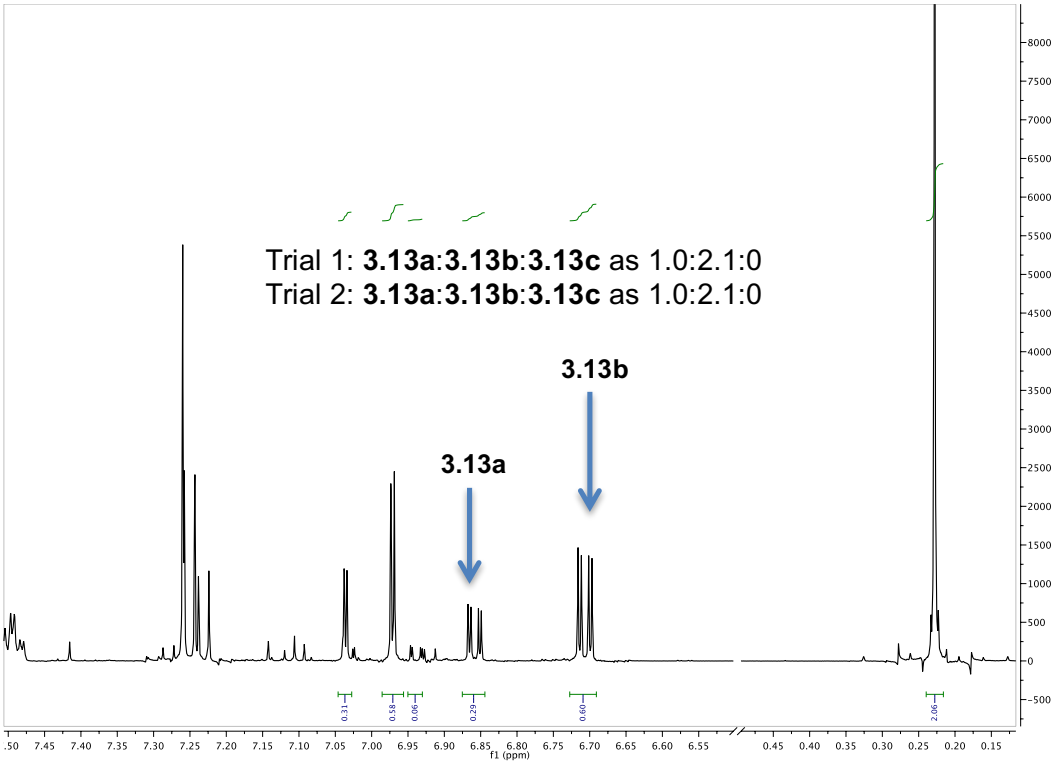

Figure 3.4.137. Example of ^{1}H NMR spectrum for 3.13a + 3.13b + 3.13c + 2.3 + succinimide; t = 5 h after addition of NCS (zoomed in for clear visualization of each isomer).

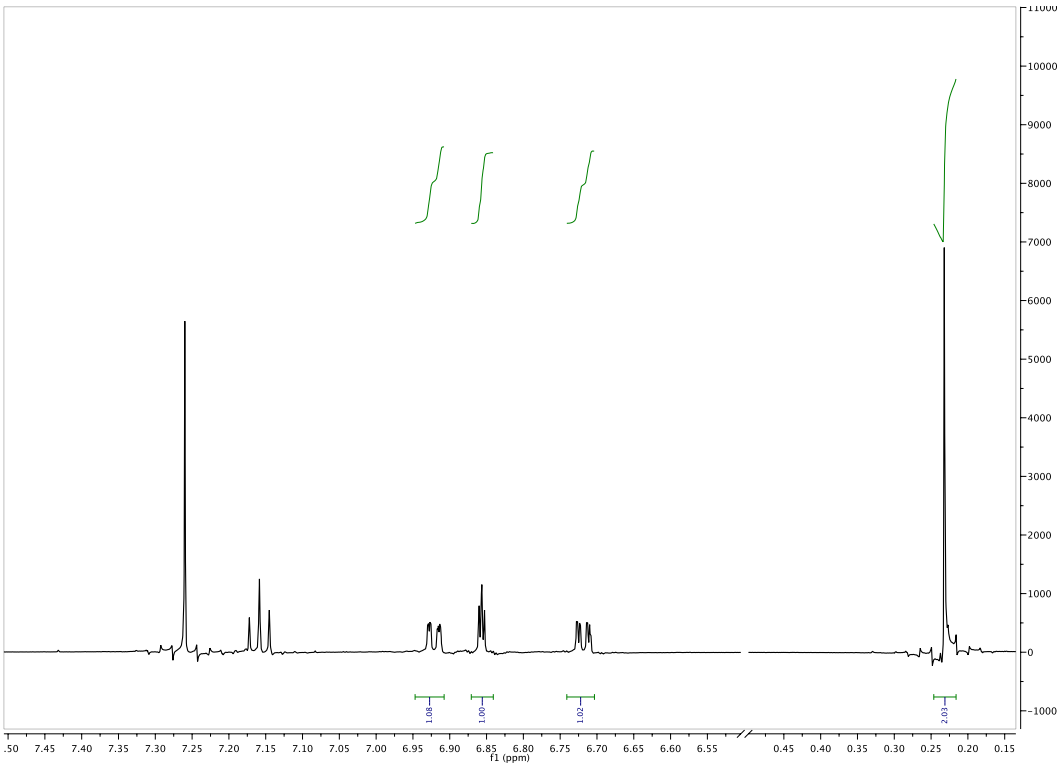

Figure 3.4.138. Example of ^{1}H NMR spectrum for 3.13 + 3.6; t = 0 h (zoomed in for clear visualization of each isomer).

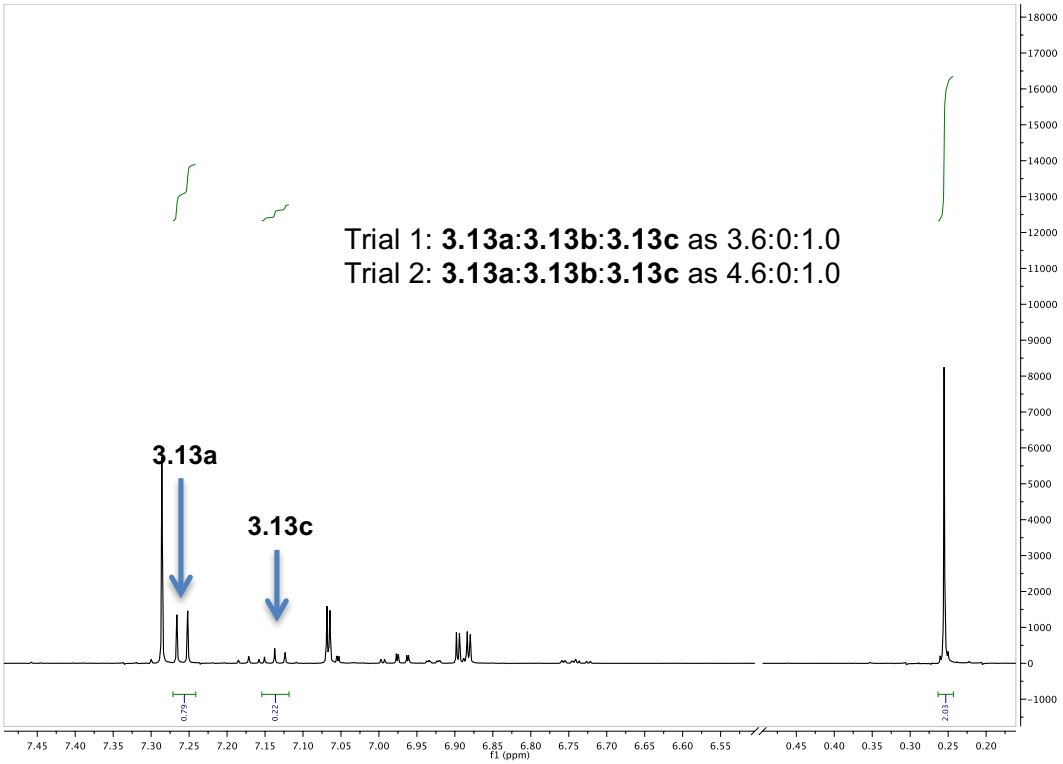

Figure 3.4.139. Example of ^{1}H NMR spectrum for 3.13a + 3.13b + 3.13c + 3.6 + succinimide; t = 5 h after addition of NCS (zoomed in for clear visualization of each isomer).

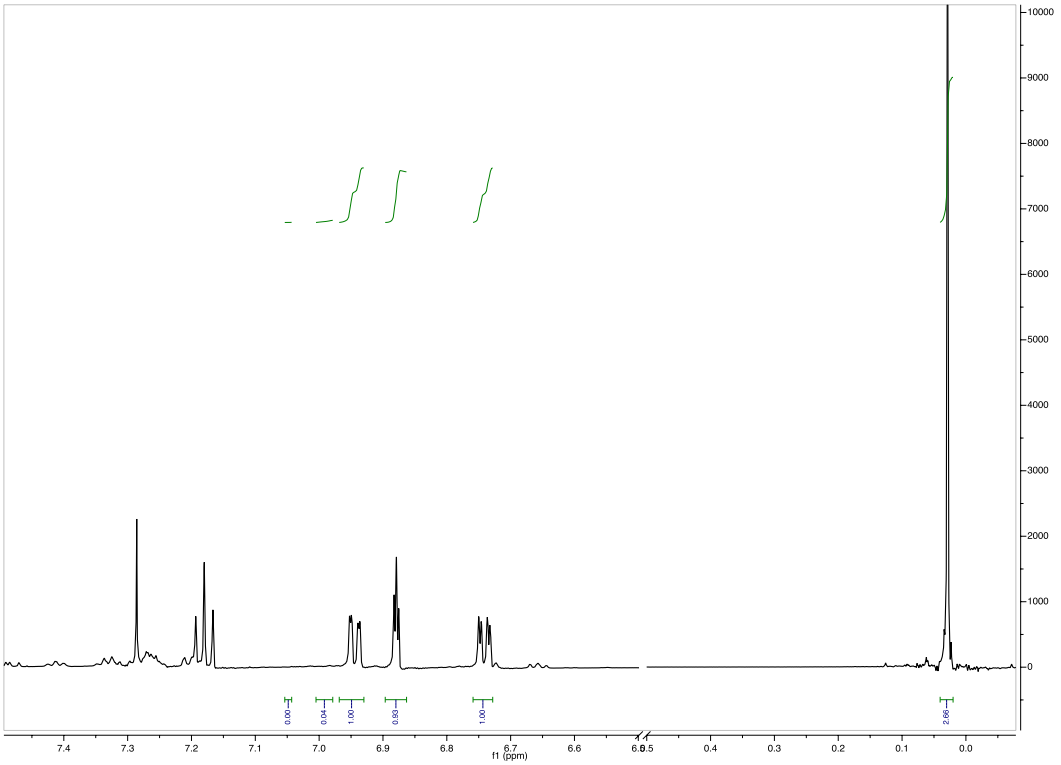

Figure 3.4.140. Example of ^{1}H NMR spectrum for 3.13 + 3.7; t = 0 h (zoomed in for clear visualization of each isomer).

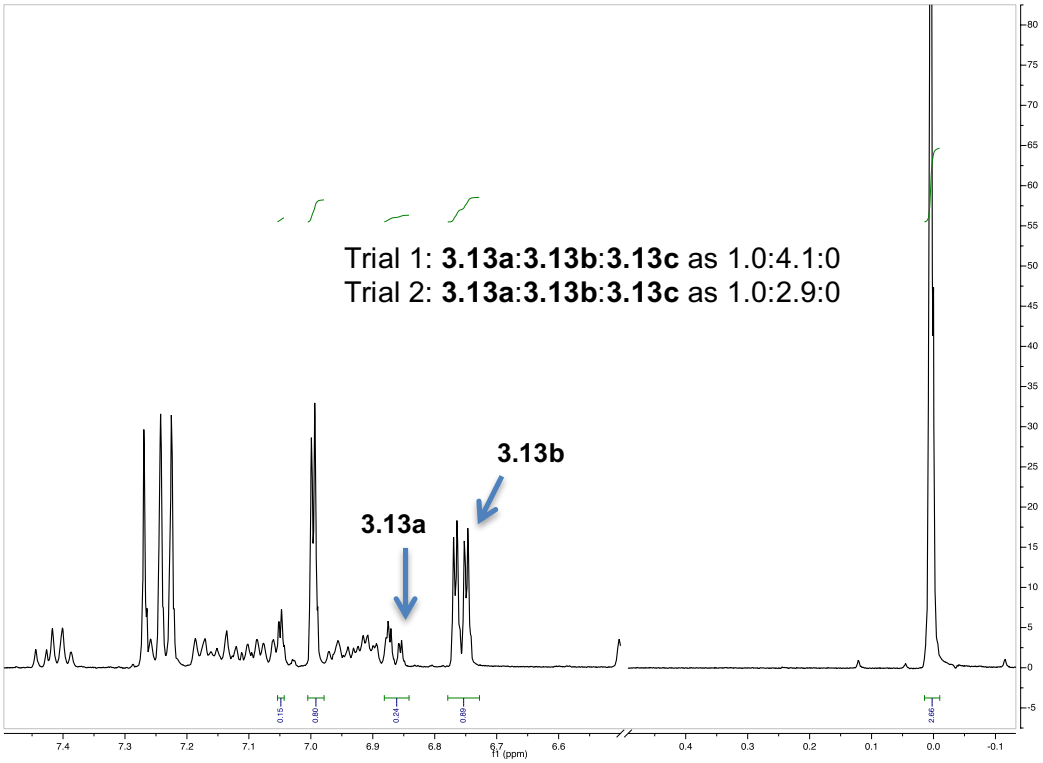

Figure 3.4.141. Example of ^{1}H NMR spectrum for 3.13a + 3.13b + 3.13c + 3.7 + succinimide; t = 2 h after addition of NCS (zoomed in for clear visualization of each isomer).

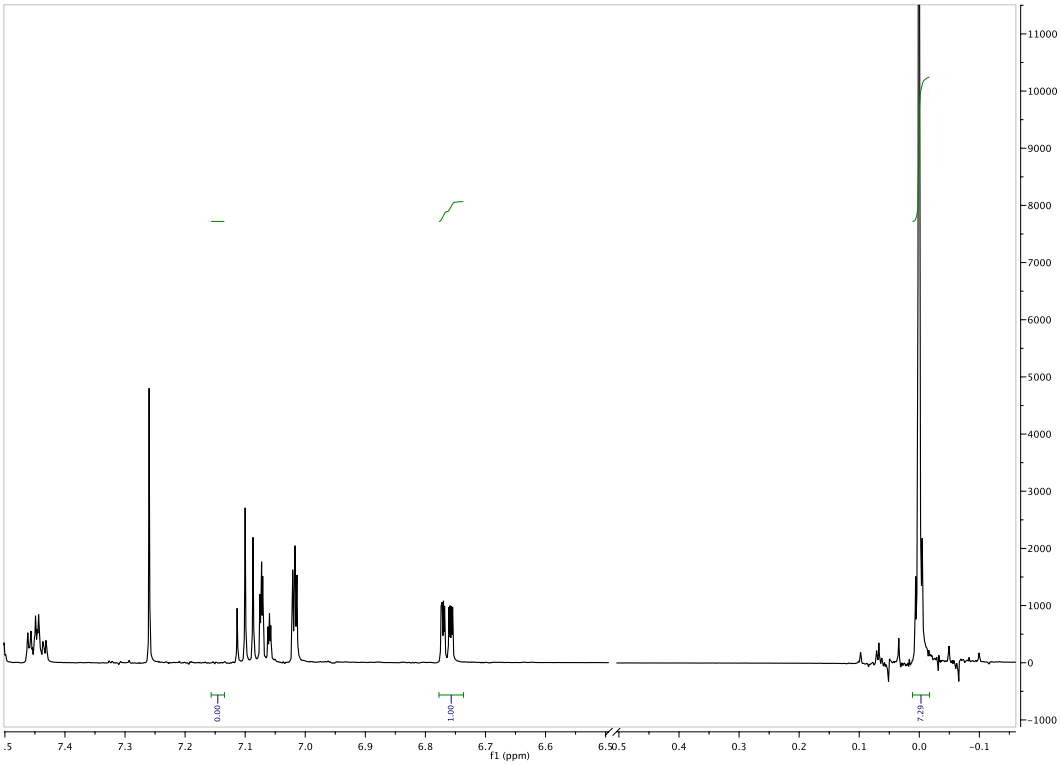

Figure 3.4.142. Example of ^{1}H NMR spectrum for 3.14 + 2.3; t = 0 h (zoomed in for clear visualization of each isomer).

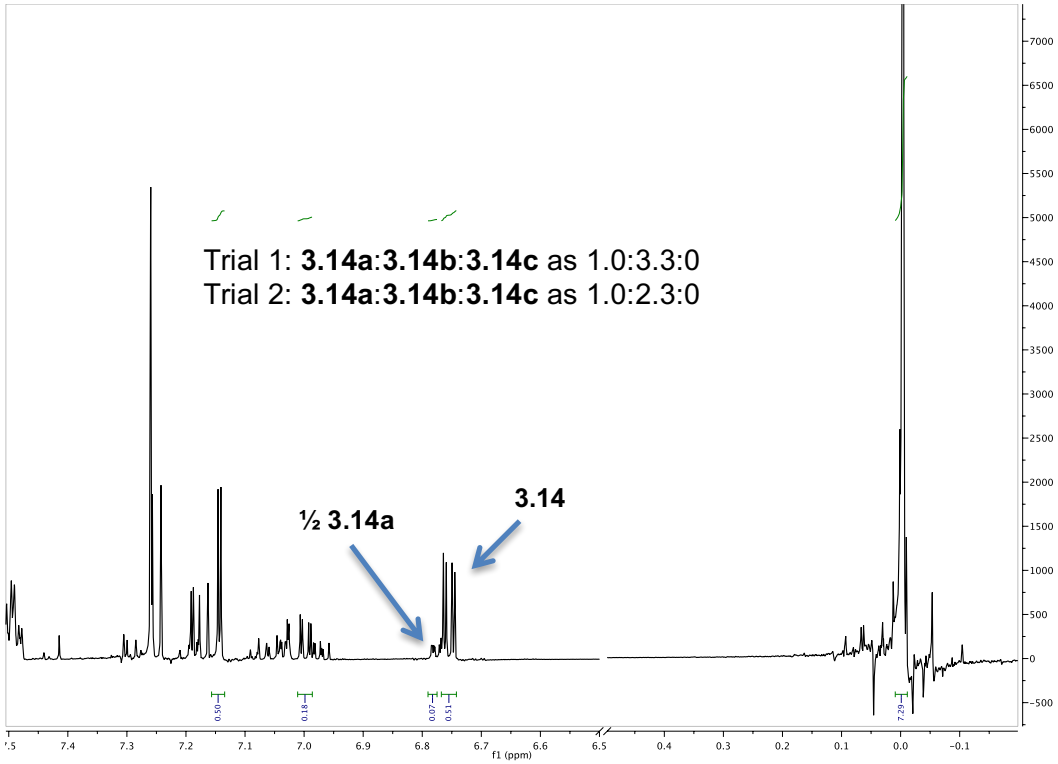

Figure 3.4.143. Example of ^{1}H NMR spectrum for 3.14a + 3.14b + 3.14c + 2.3 + succinimide; t = 3 h after addition of NCS (zoomed in for clear visualization of each isomer).

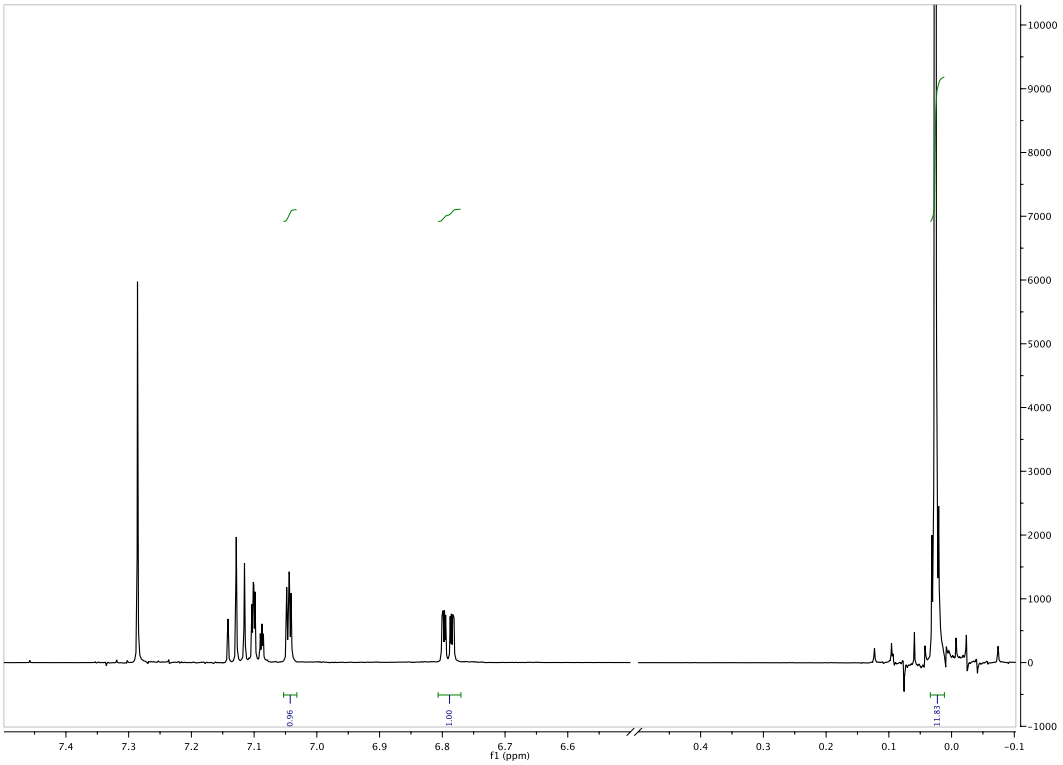

Figure 3.4.144. Example of ^{1}H NMR spectrum for 3.14 + 3.6; t = 0 h (zoomed in for clear visualization of each isomer).

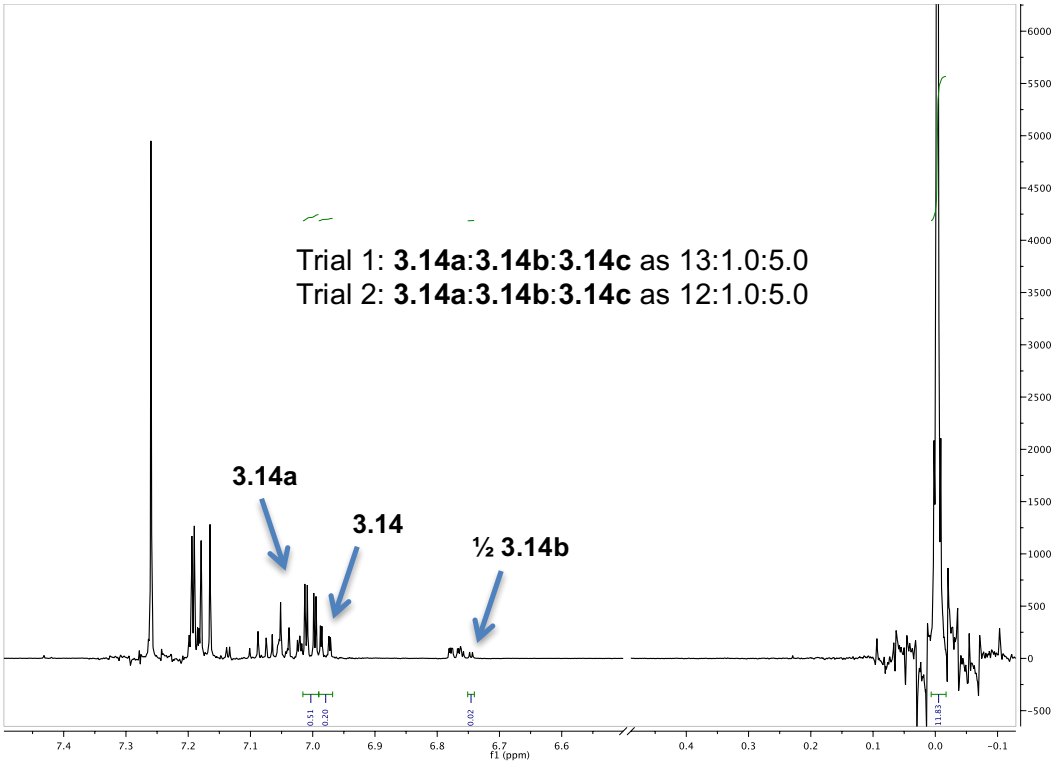

Figure 3.4.145. Example of ^{1}H NMR spectrum for 3.14a + 3.14b + 3.14c + 3.6 + succinimide; t = 3 h after addition of NCS (zoomed in for clear visualization of each isomer).

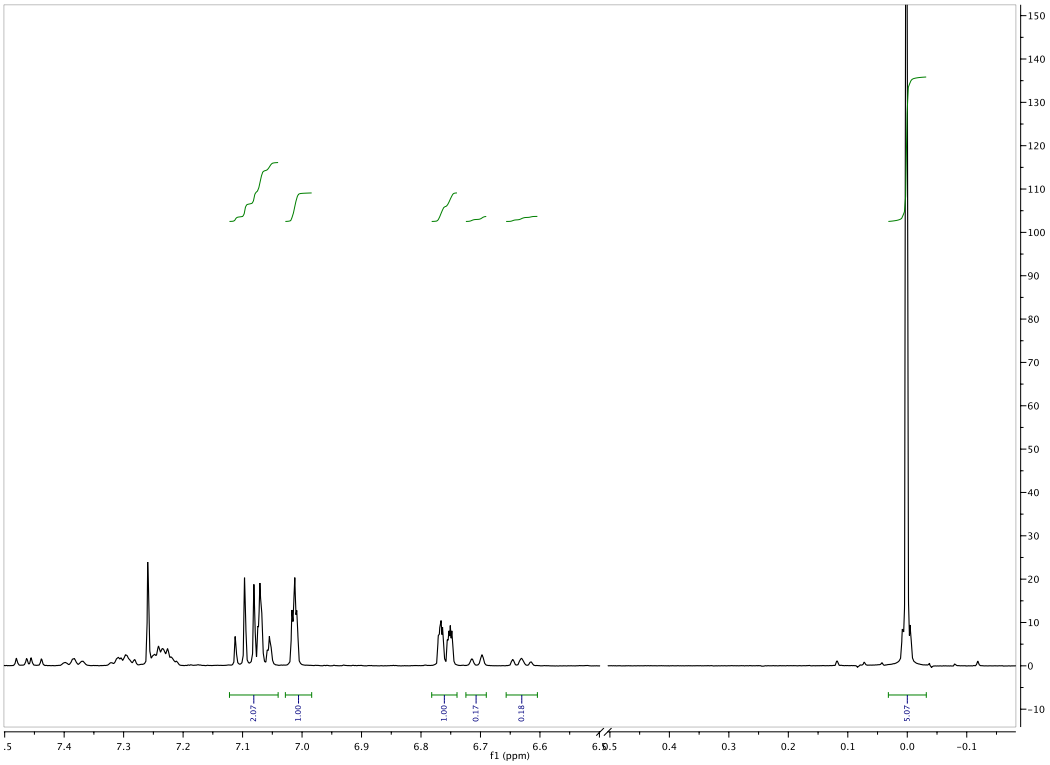

Figure 3.4.146. Example of ^{1}H NMR spectrum for 3.14 + 3.7; t = 0 h (zoomed in for clear visualization of each isomer).

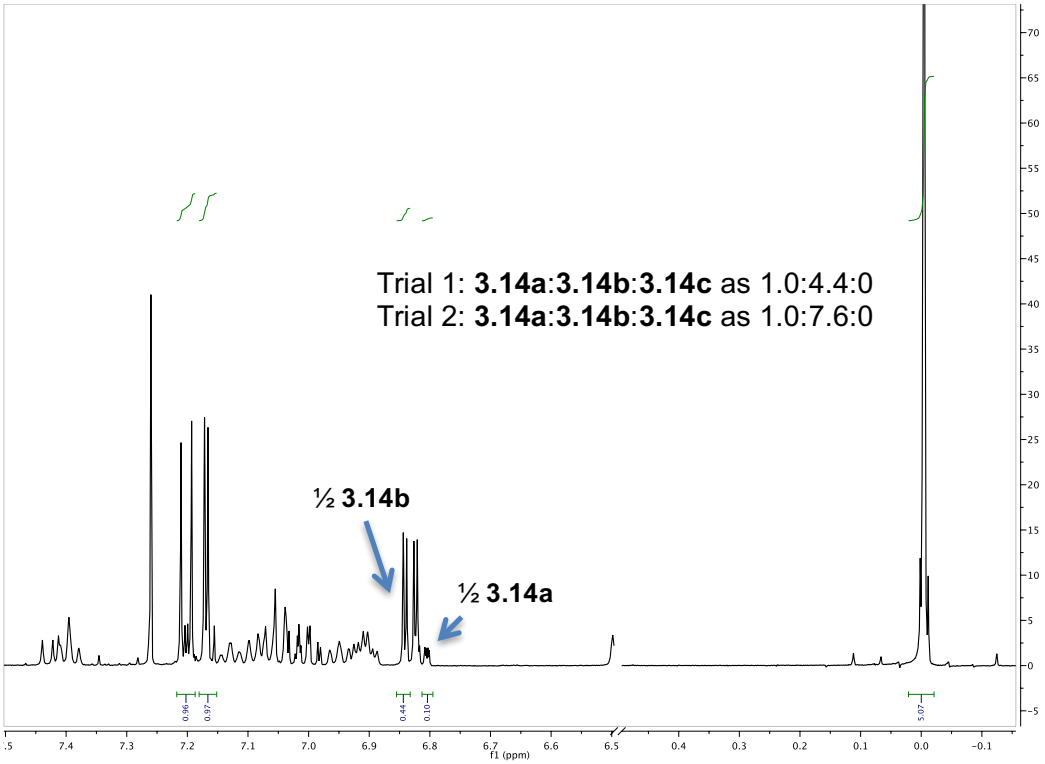

Figure 3.4.147. Example of ^{1}H NMR spectrum for 3.14a + 3.14b + 3.14c + 3.7 + succinimide; t = 2 h after addition of NCS (zoomed in for clear visualization of each isomer).

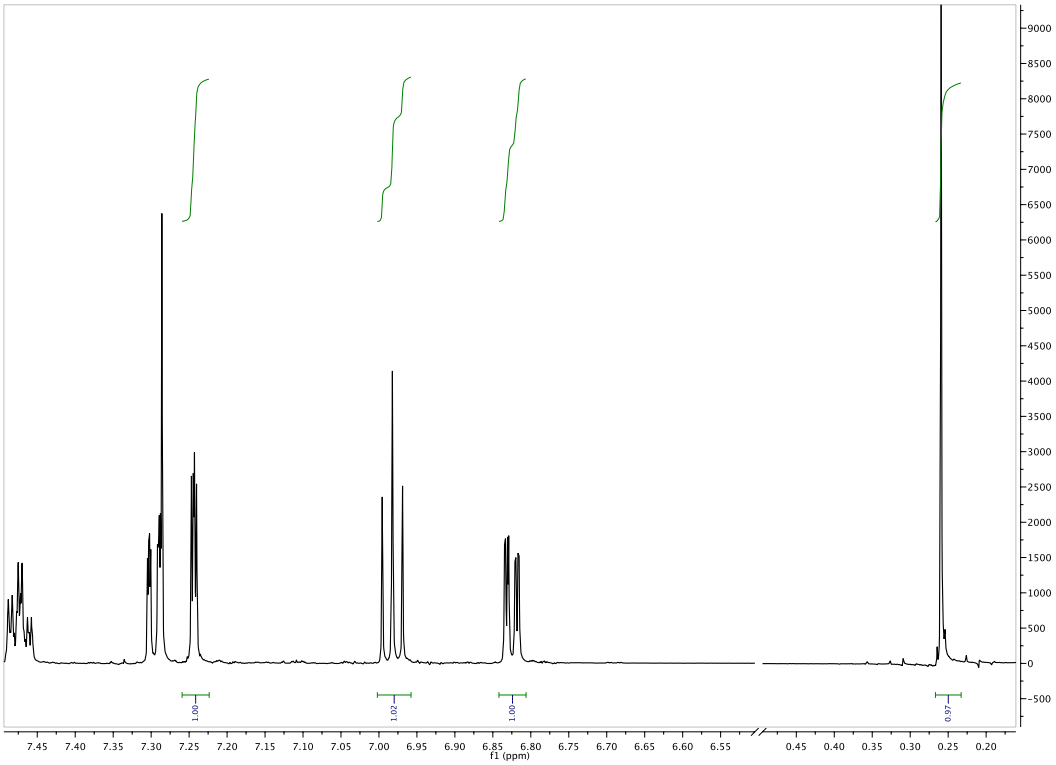

Figure 3.4.148. Example of ^{1}H NMR spectrum for 3.15 + 2.3; t = 0 h (zoomed in for clear visualization of each isomer).

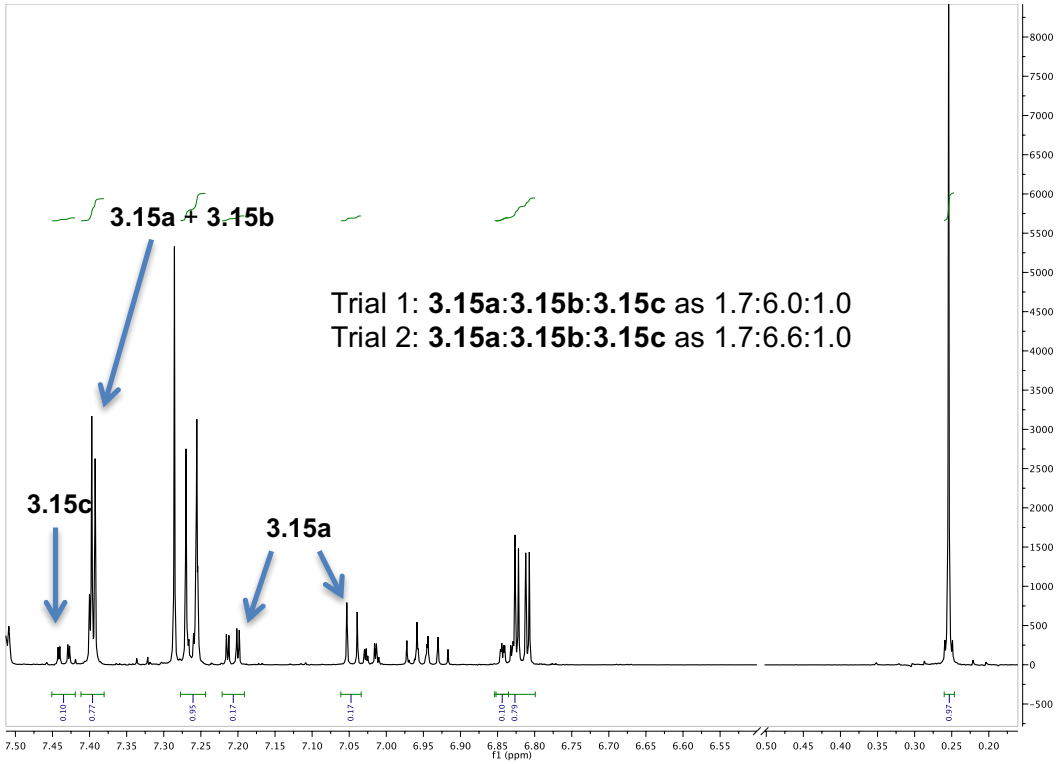

Figure 3.4.149. Example of ^{1}H NMR spectrum for 3.15a + 3.15b + 3.15c + 2.3 + succinimide; t = 5 h after addition of NCS (zoomed in for clear visualization of each isomer).

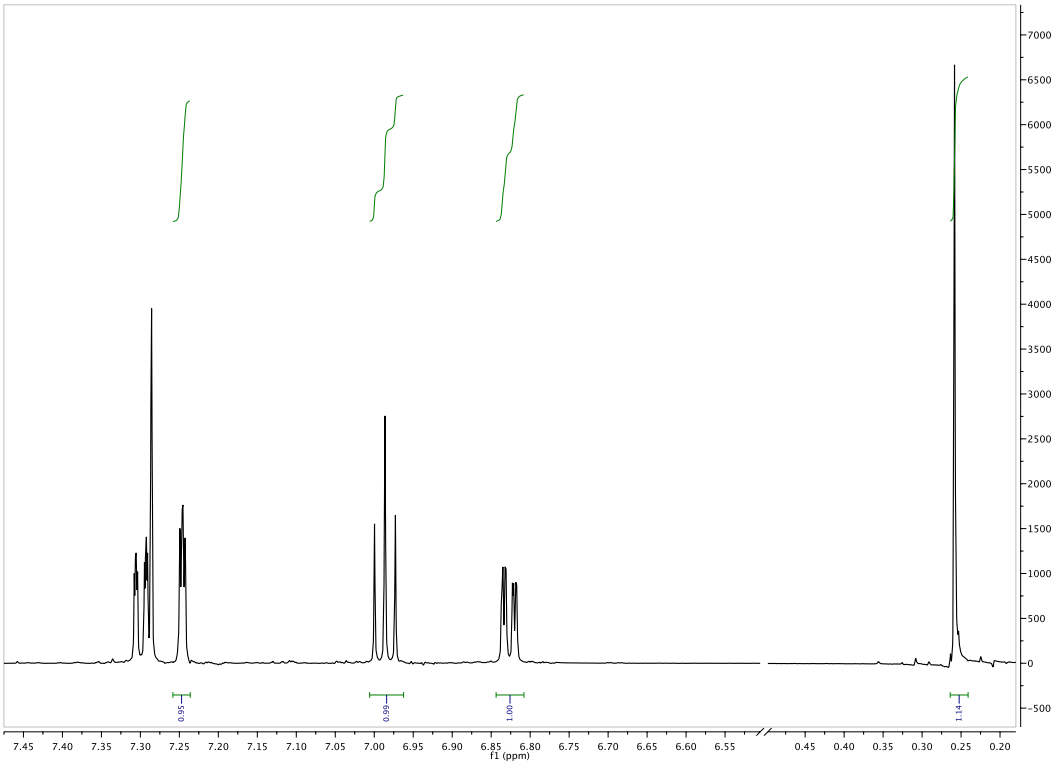

Figure 3.4.150. Example of ^{1}H NMR spectrum for 3.15 + 3.6; t = 0 h (zoomed in for clear visualization of each isomer).

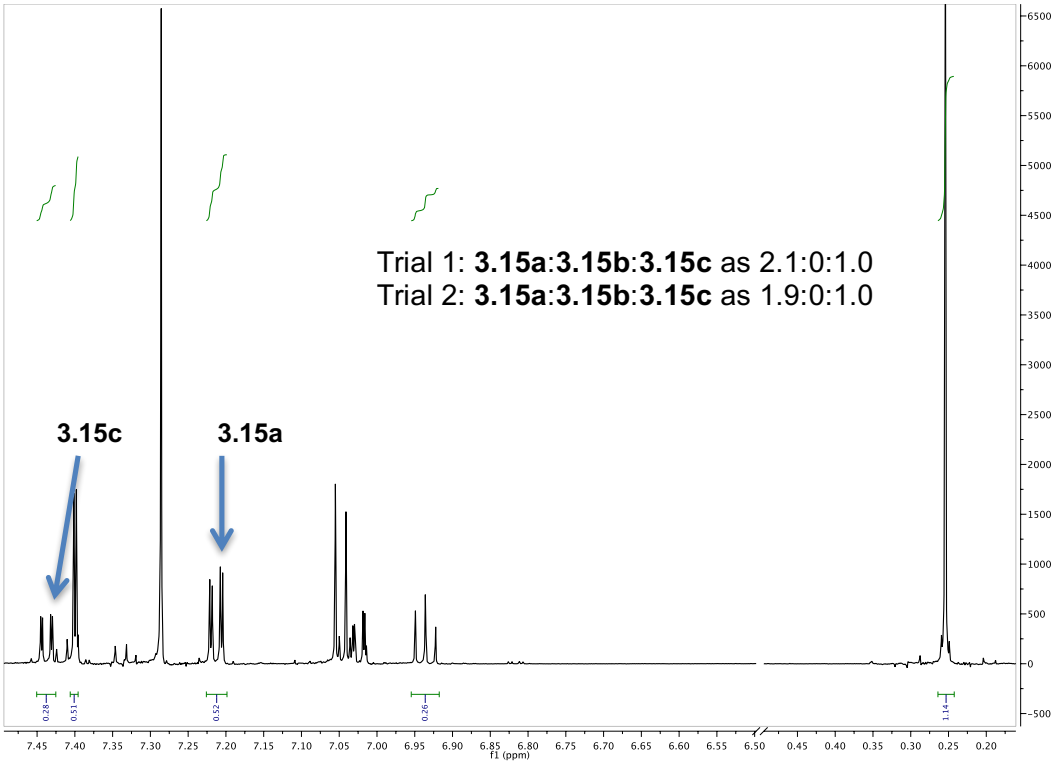

Figure 3.4.151. Example of ^{1}H NMR spectrum for 3.15a + 3.15b + 3.15c + 3.6 + succinimide; t = 5 h after addition of NCS (zoomed in for clear visualization of each isomer).

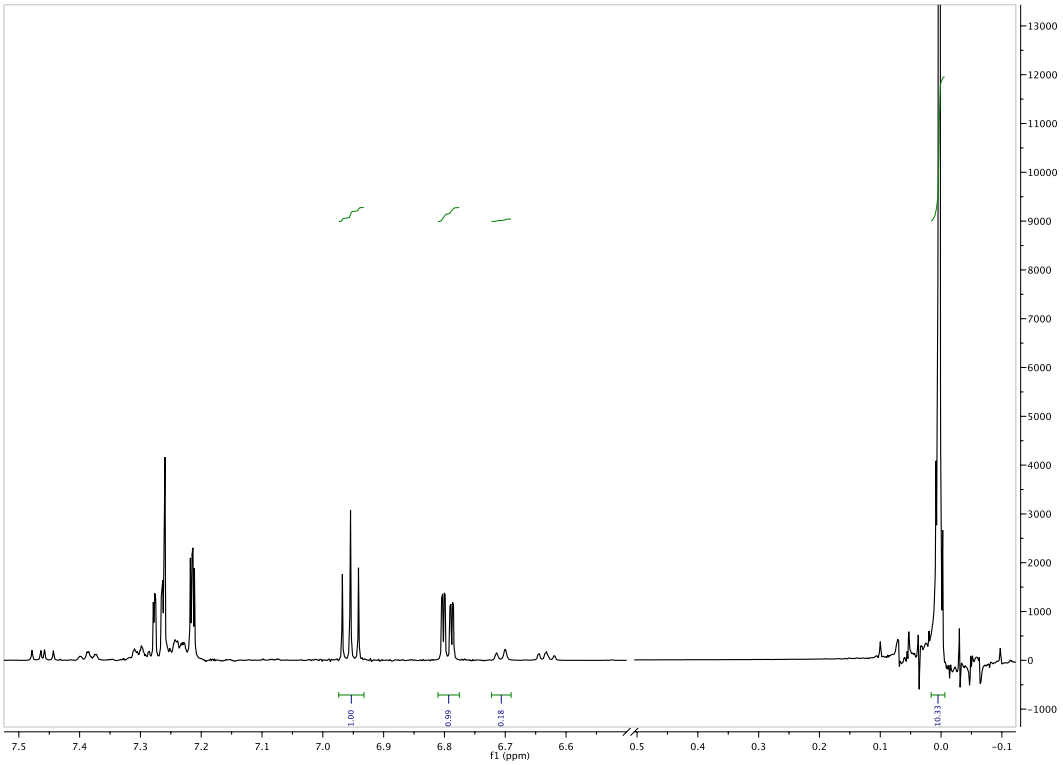

Figure 3.4.152. Example of ^{1}H NMR spectrum for 3.15 + 3.7; t = 0 h (zoomed in for clear visualization of each isomer).

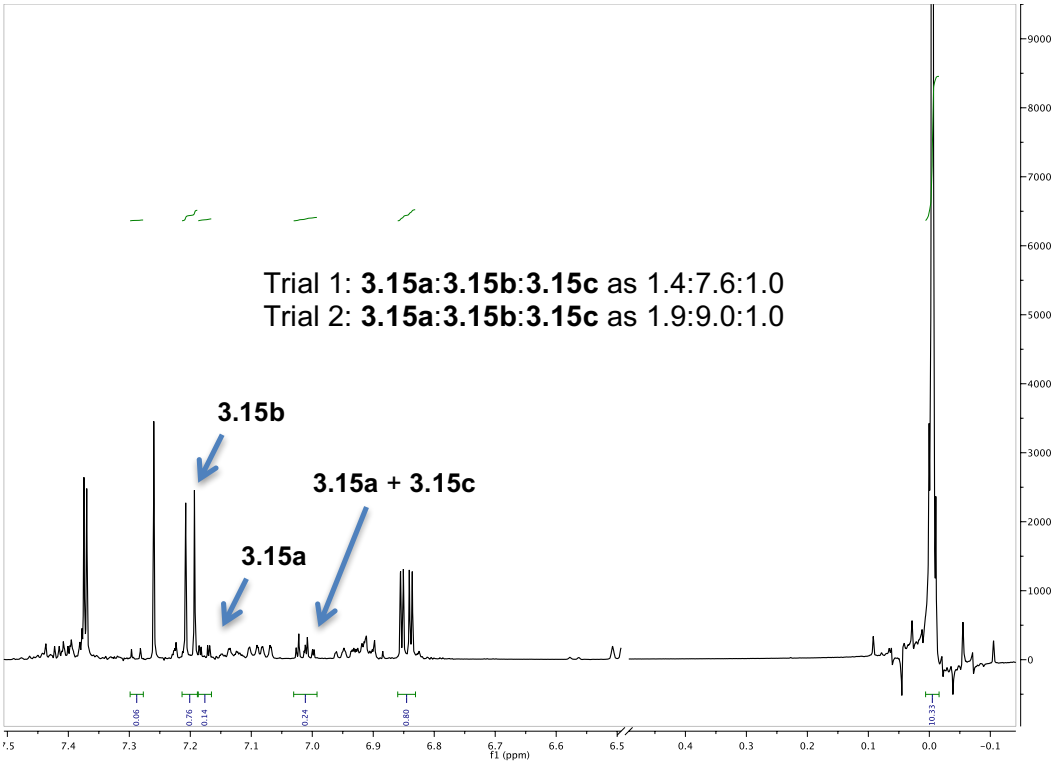

Figure 3.4.153. Example of ^{1}H NMR spectrum for 3.15a + 3.15b + 3.15c + 3.7 + succinimide; t = 1 h after addition of NCS (zoomed in for clear visualization of each isomer).

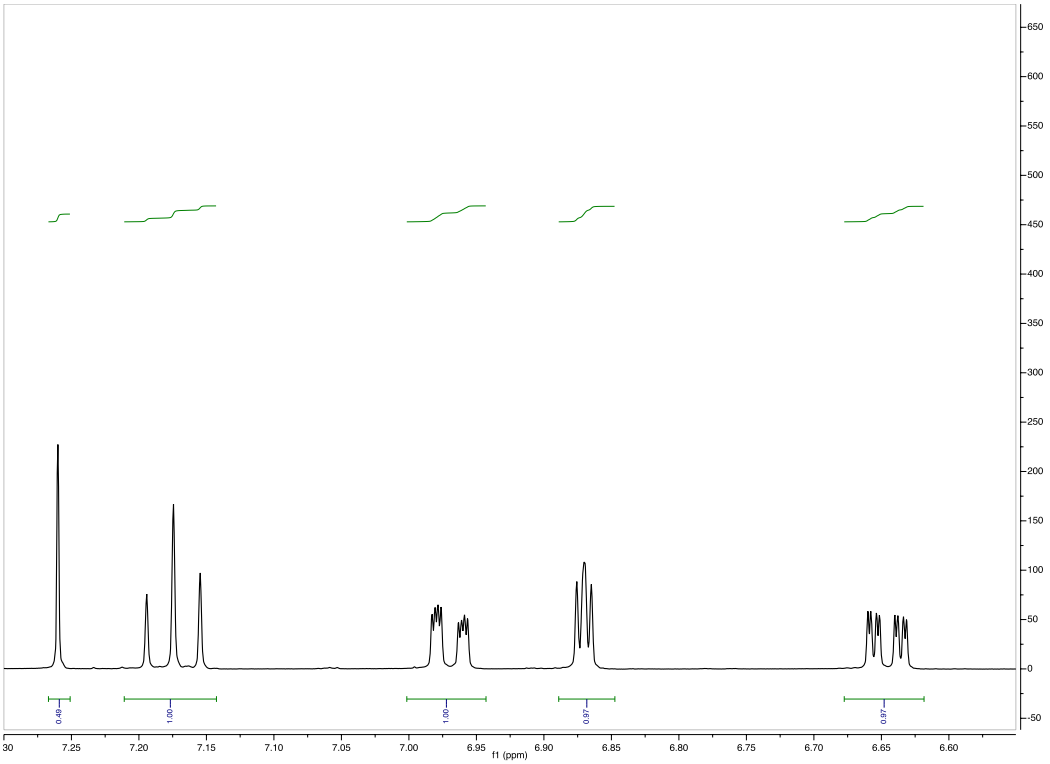

Figure 3.4.154. Example of ^{1}H NMR spectrum for 3.16 + 2.3; t = 0 h (zoomed in for clear visualization of each isomer).

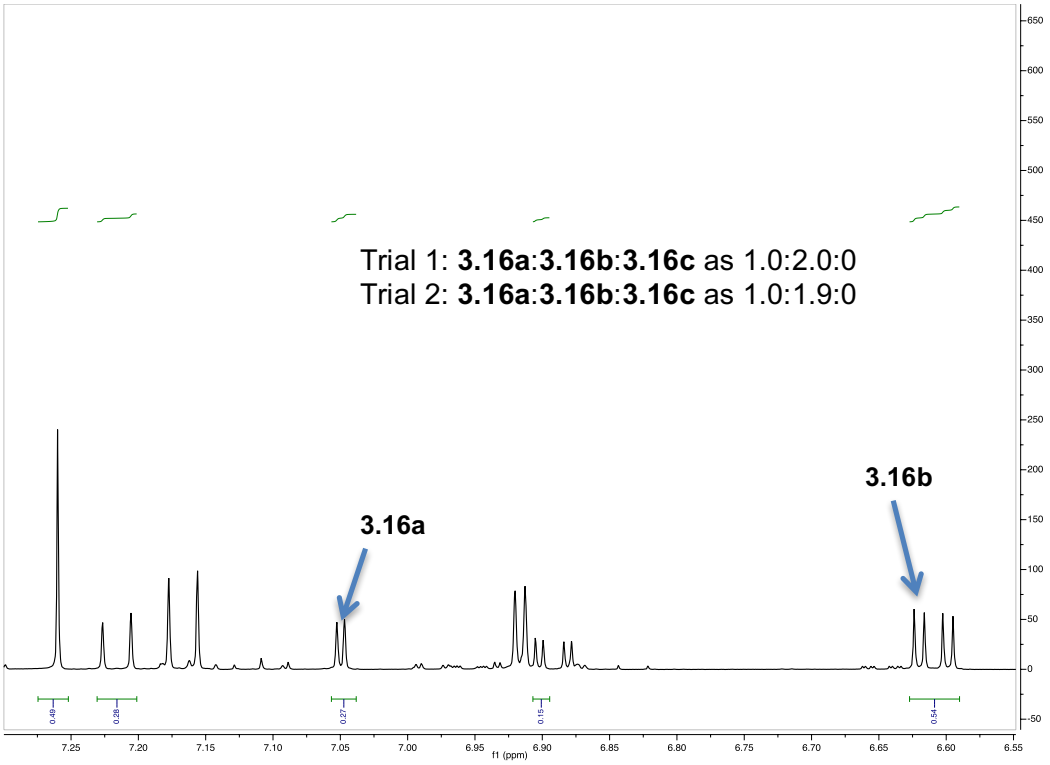

Figure 3.4.155. Example of ^{1}H NMR spectrum for 3.16a + 3.16b + 3.16c + 2.3 + succinimide; t = 12 h after addition of NCS (zoomed in for clear visualization of each isomer). Residual $CHCl_3$ was used as internal standard.

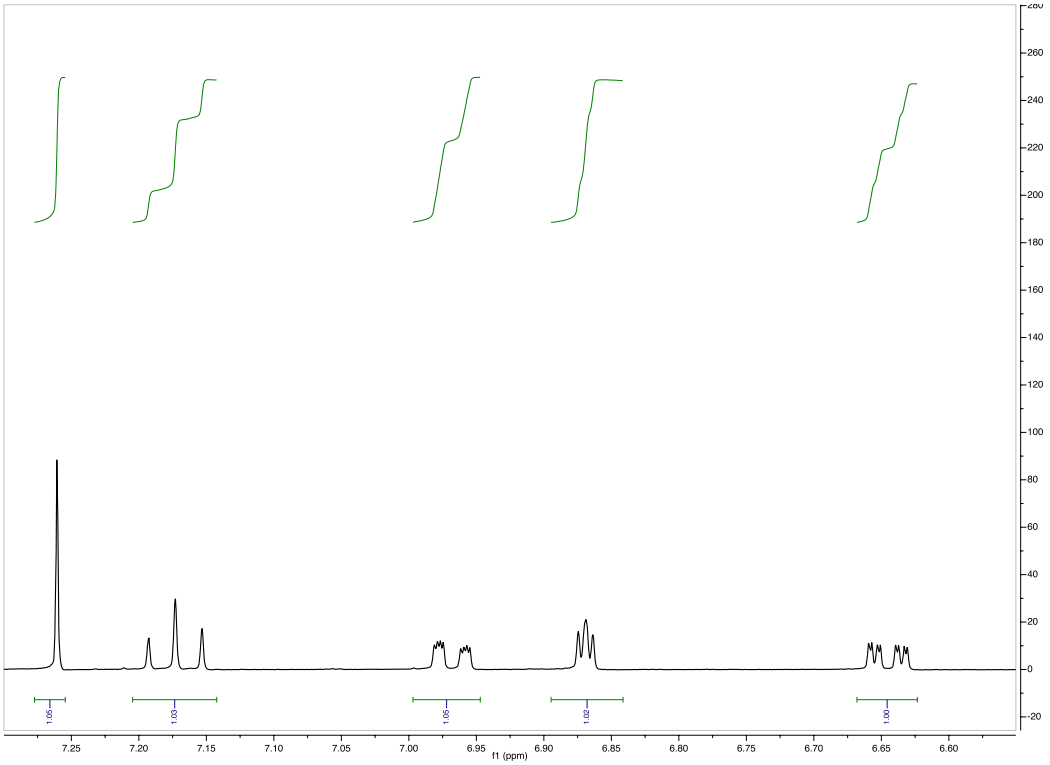

Figure 3.4.156. Example of ^{1}H NMR spectrum for 3.16 + 3.6; t = 0 h (zoomed in for clear visualization of each isomer).

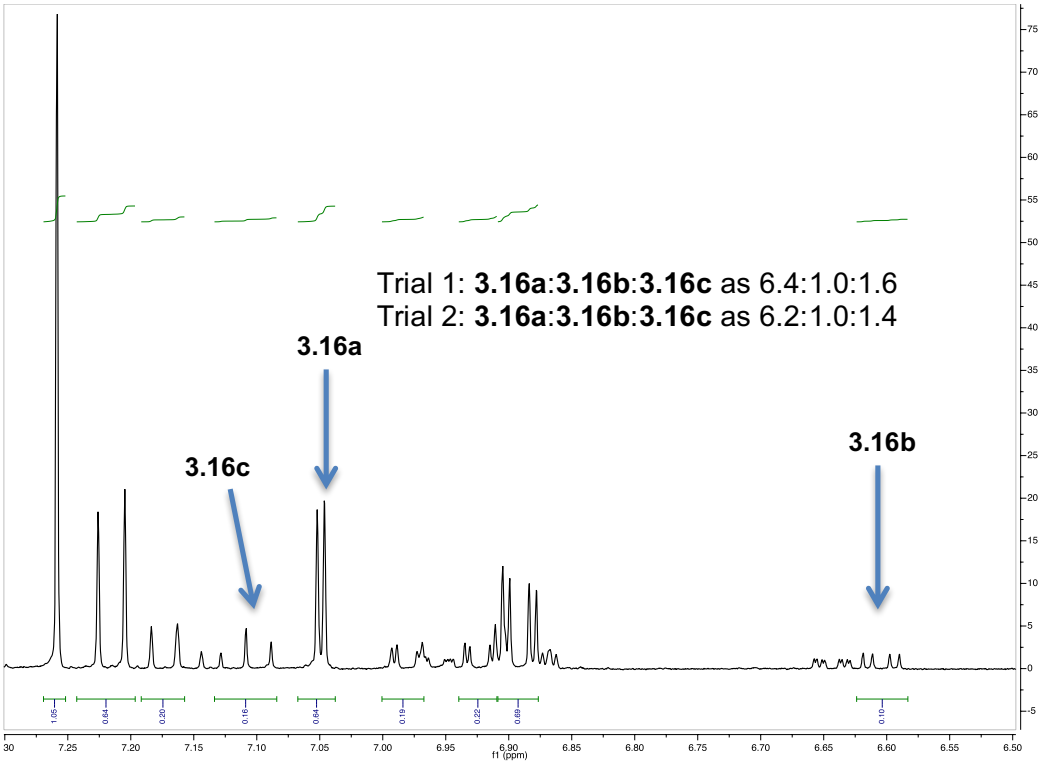

Figure 3.4.157. Example of ^{1}H NMR spectrum for 3.16a + 3.16b + 3.16c + 3.6 + succinimide; t = 12 h after addition of NCS (zoomed in for clear visualization of each isomer). Residual $CHCl_3$ was used as internal standard.

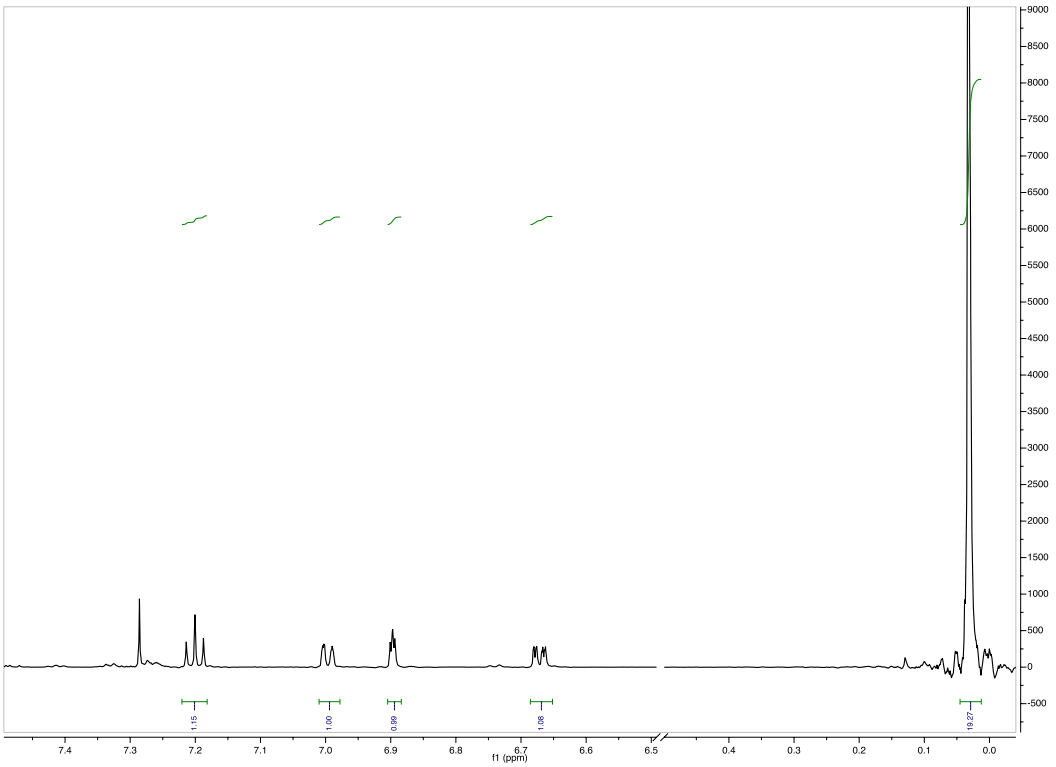

Figure 3.4.158. Example of ^{1}H NMR spectrum for 3.16 + 3.7; t = 0 h (zoomed in for clear visualization of each isomer).

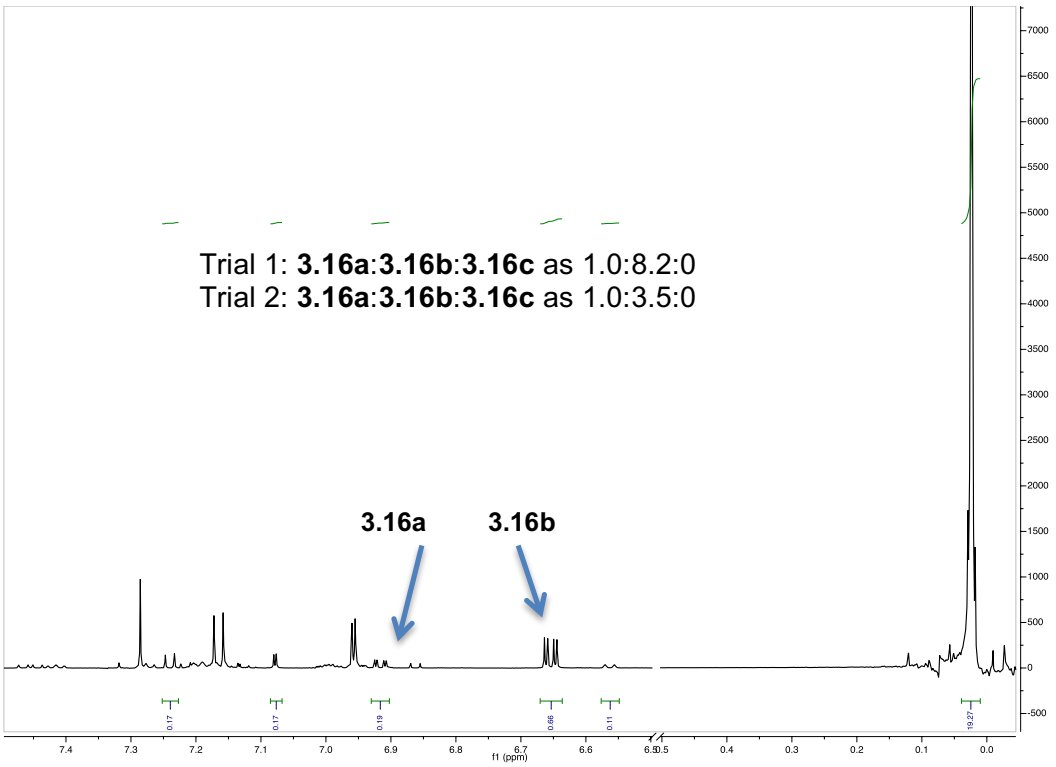

Figure 3.4.159. Example of ^{1}H NMR spectrum for 3.16a + 3.16b + 3.16c + 3.7 + succinimide; t = 1 h after addition of NCS (zoomed in for clear visualization of each isomer). Residual $CHCl_3$ was used as internal standard.

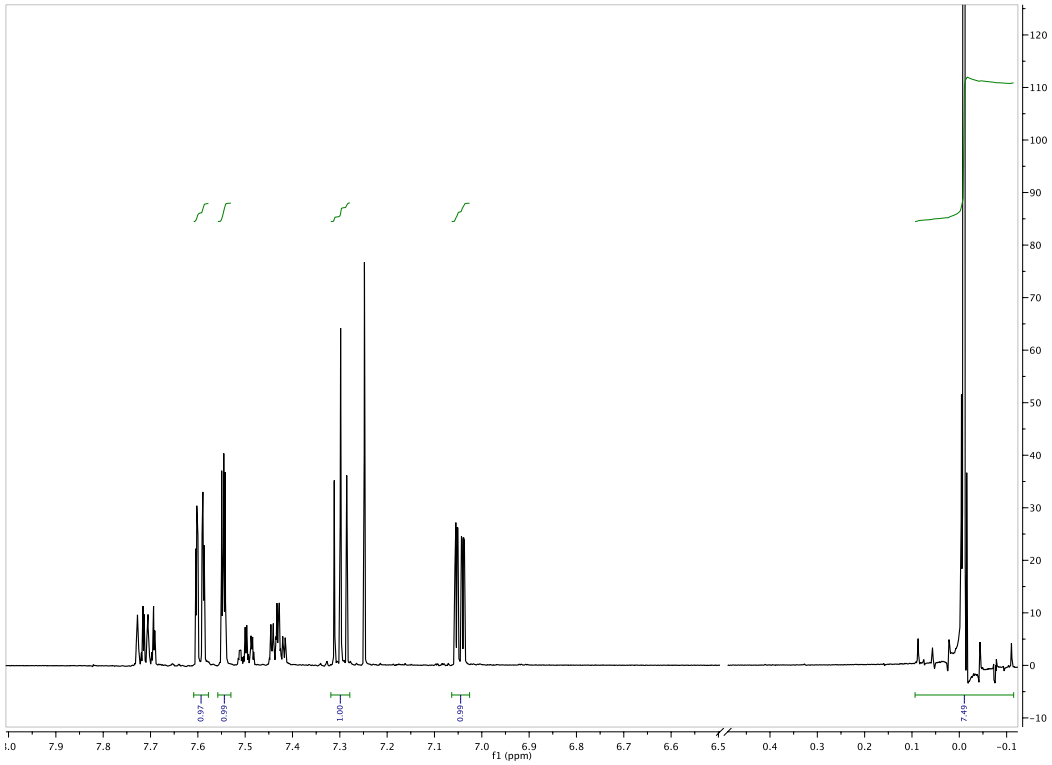

Figure 3.4.160. Example of ^{1}H NMR spectrum for 3.17 + 2.3; t = 0 h (zoomed in for clear visualization of each isomer).

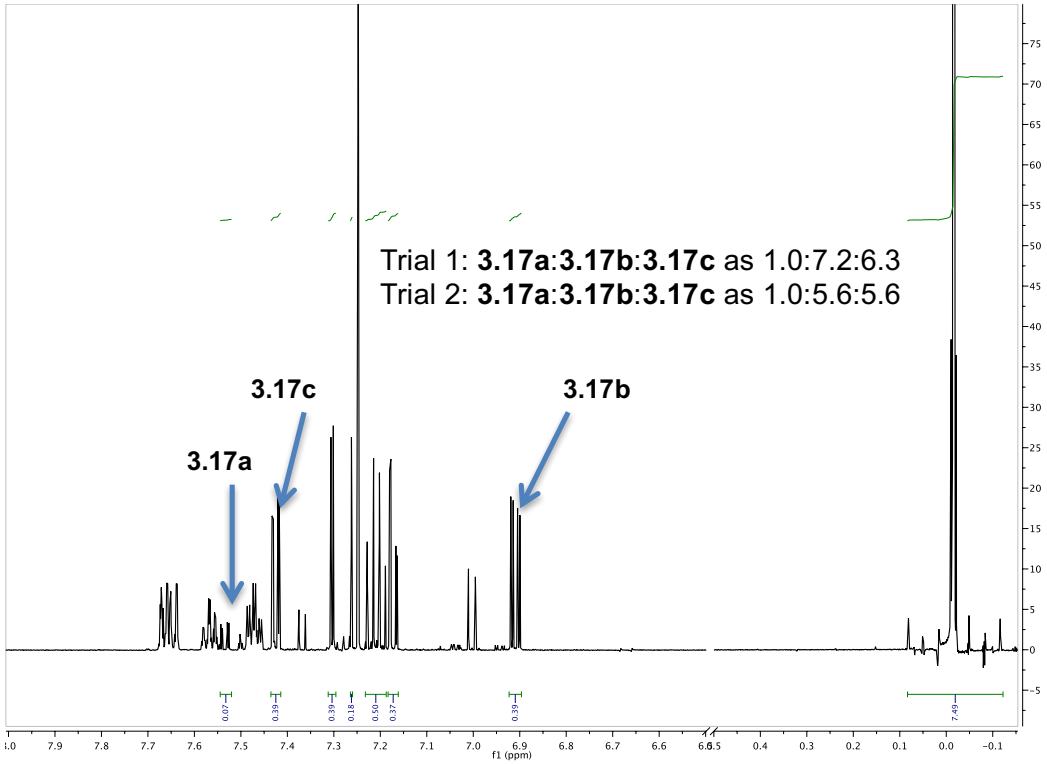

Figure 3.4.161. Example of ^{1}H NMR spectrum for 3.17a + 3.17b + 3.17c + 2.3 + succinimide; t = 20 h after addition of NCS (zoomed in for clear visualization of each isomer).

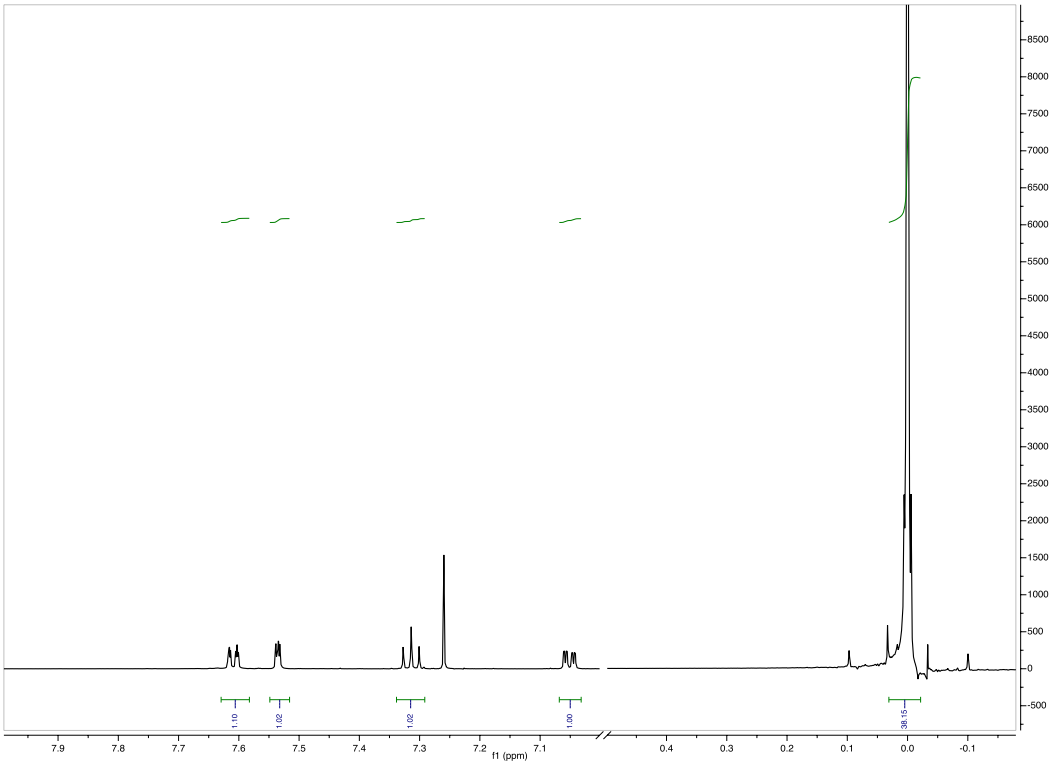

Figure 3.4.162. Example of ^{1}H NMR spectrum for 3.17 + 3.6; t = 0 h (zoomed in for clear visualization of each isomer).

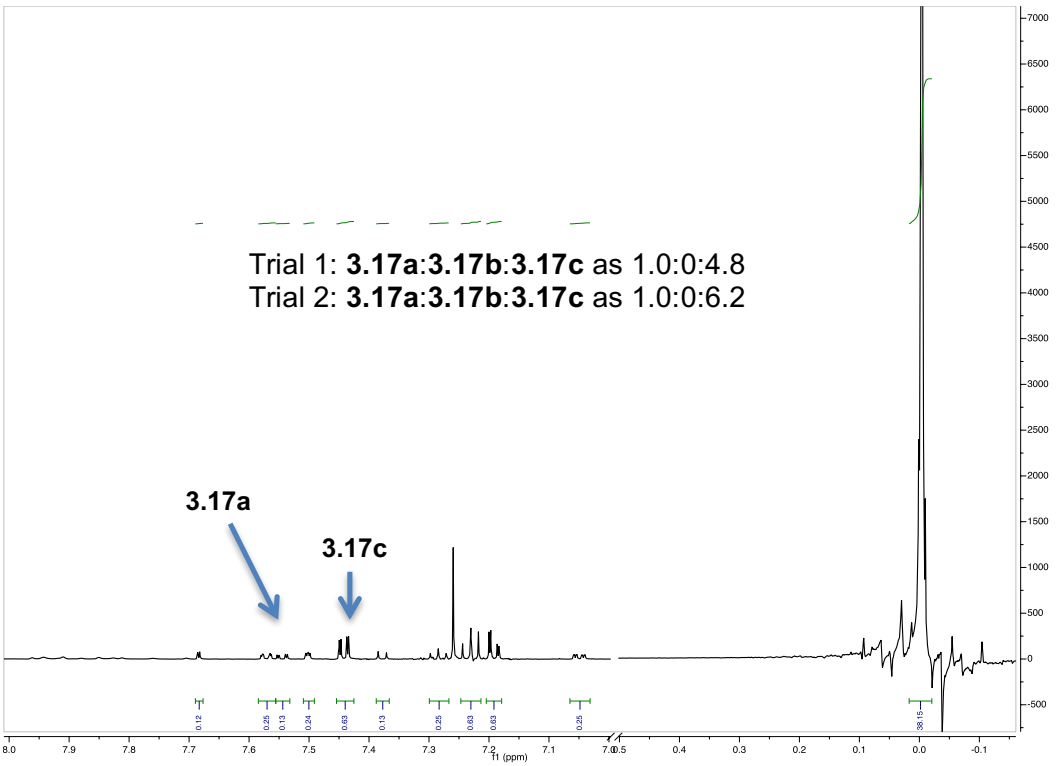

Figure 3.4.163. Example of ^{1}H NMR spectrum for 3.17a + 3.17b + 3.17c + 3.6 + succinimide; t = 20 h after addition of NCS (zoomed in for clear visualization of each isomer).

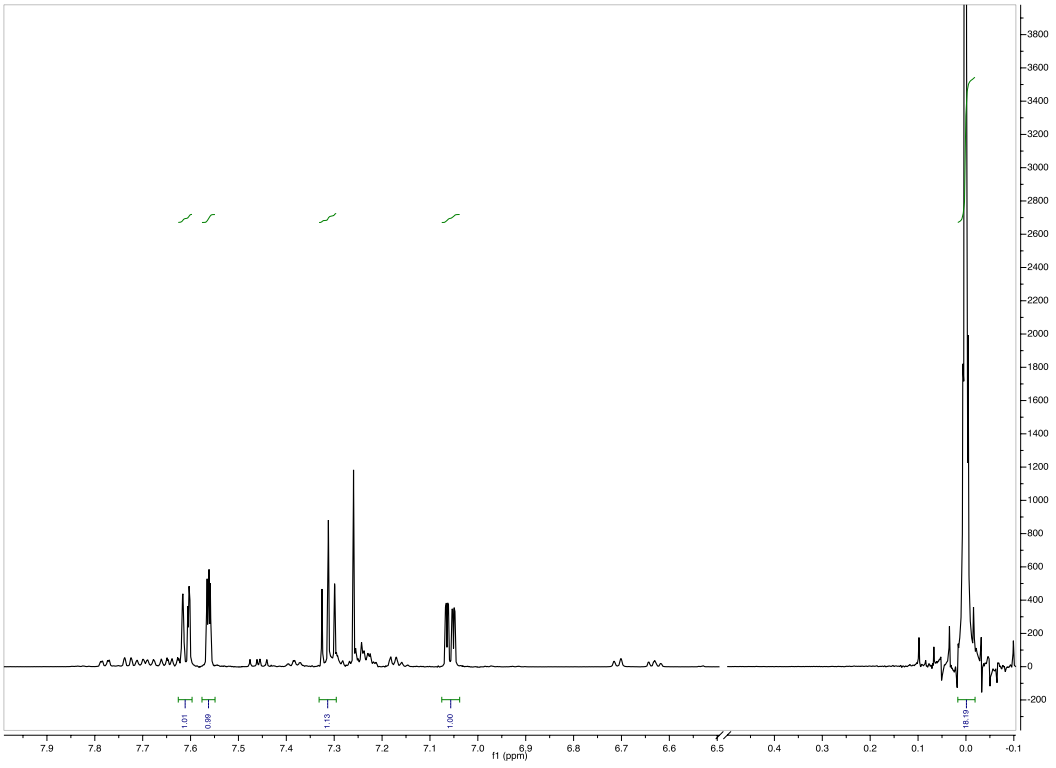

Figure 3.4.164. Example of ^{1}H NMR spectrum for 3.17 + 3.7; t = 0 h (zoomed in for clear visualization of each isomer).

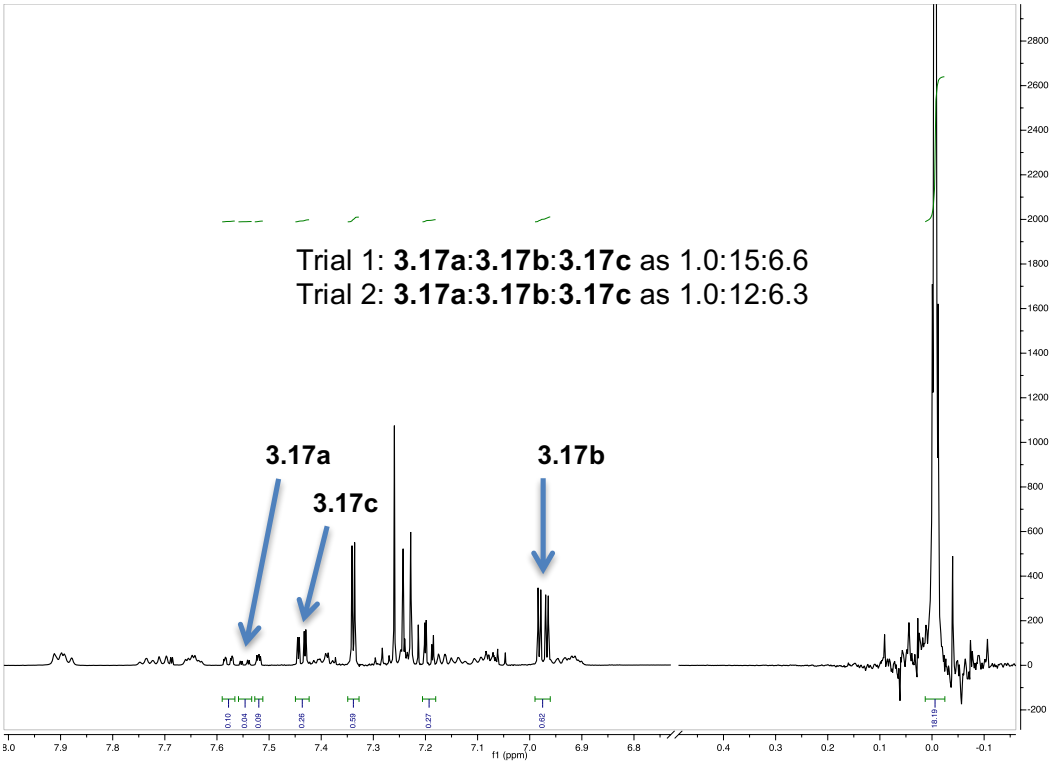

Figure 3.4.165. Example of ^{1}H NMR spectrum for 3.17a + 3.17b + 3.17c + 3.7 + succinimide; t = 2 h after addition of NCS (zoomed in for clear visualization of each isomer).

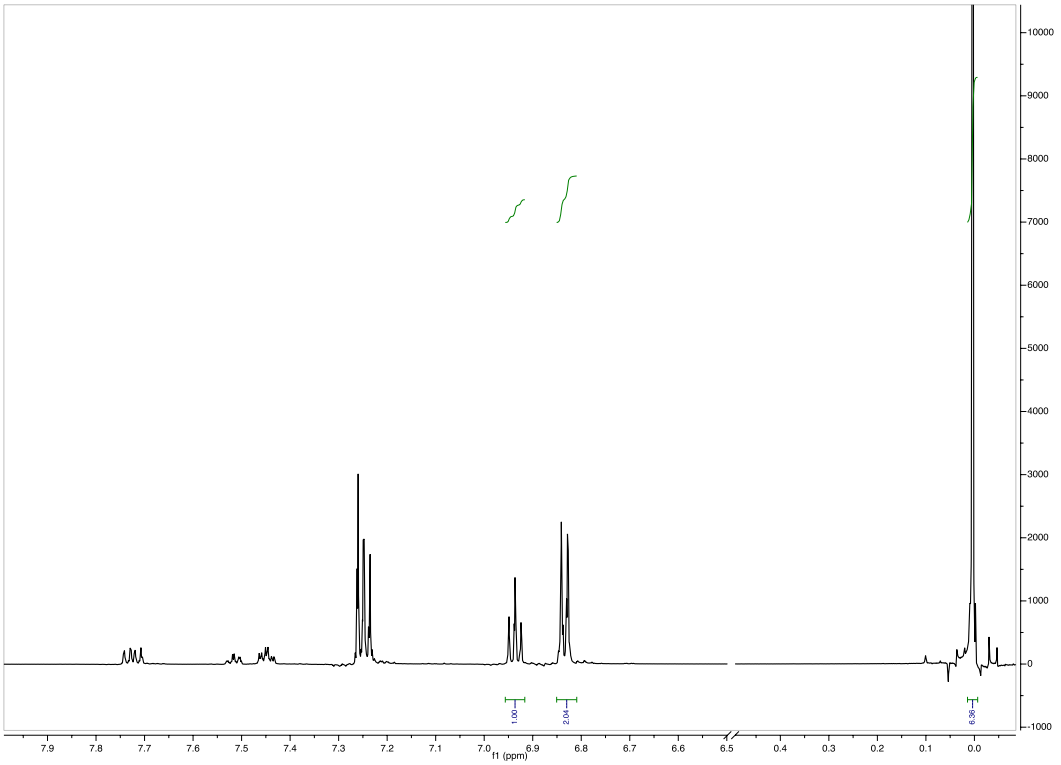

Figure 3.4.166. Example of ^{1}H NMR spectrum for 3.3 + 2.3; t = 0 h (zoomed in for clear visualization of each isomer).

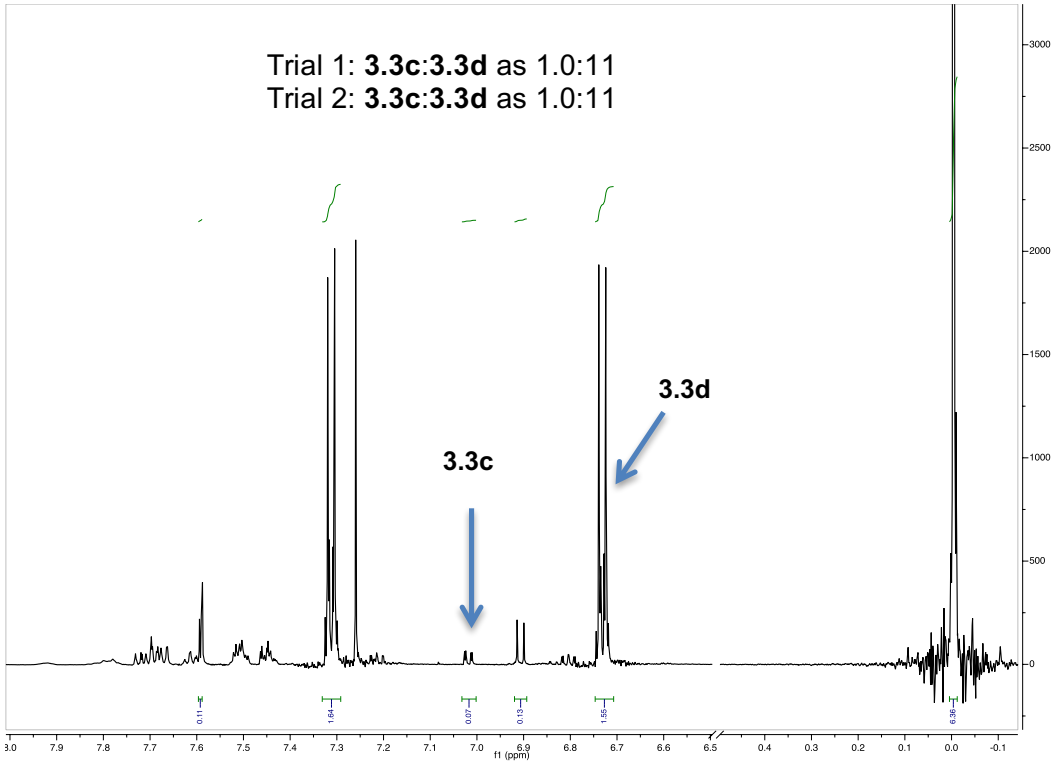

Figure 3.4.167. Example of ^{1}H NMR spectrum for 3.3c + 3.3d + 2.3 + succinimide; t = 30 min after addition of NBS (zoomed in for clear visualization of each isomer).

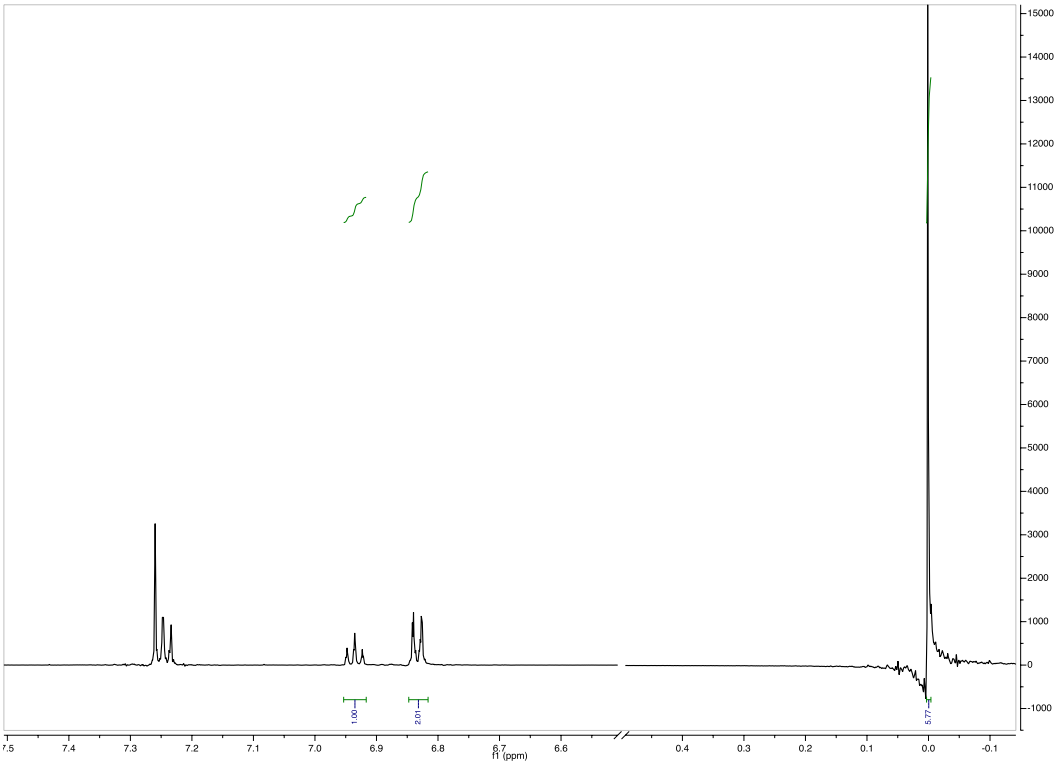

Figure 3.4.168. Example of ^{1}H NMR spectrum for 3.3 + 3.6; t = 0 h (zoomed in for clear visualization of each isomer).

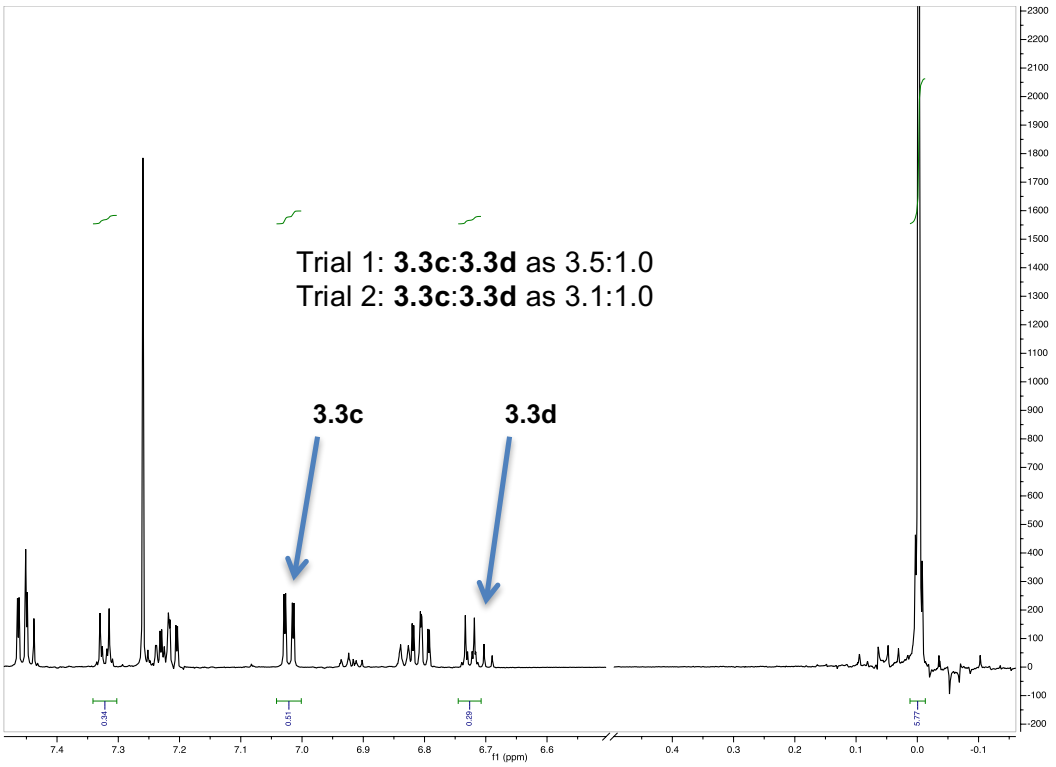

Figure 3.4.169. Example of ^{1}H NMR spectrum for 3.3c + 3.3d + 3.6 + succinimide; t = 30 min after addition of NBS (zoomed in for clear visualization of each isomer).

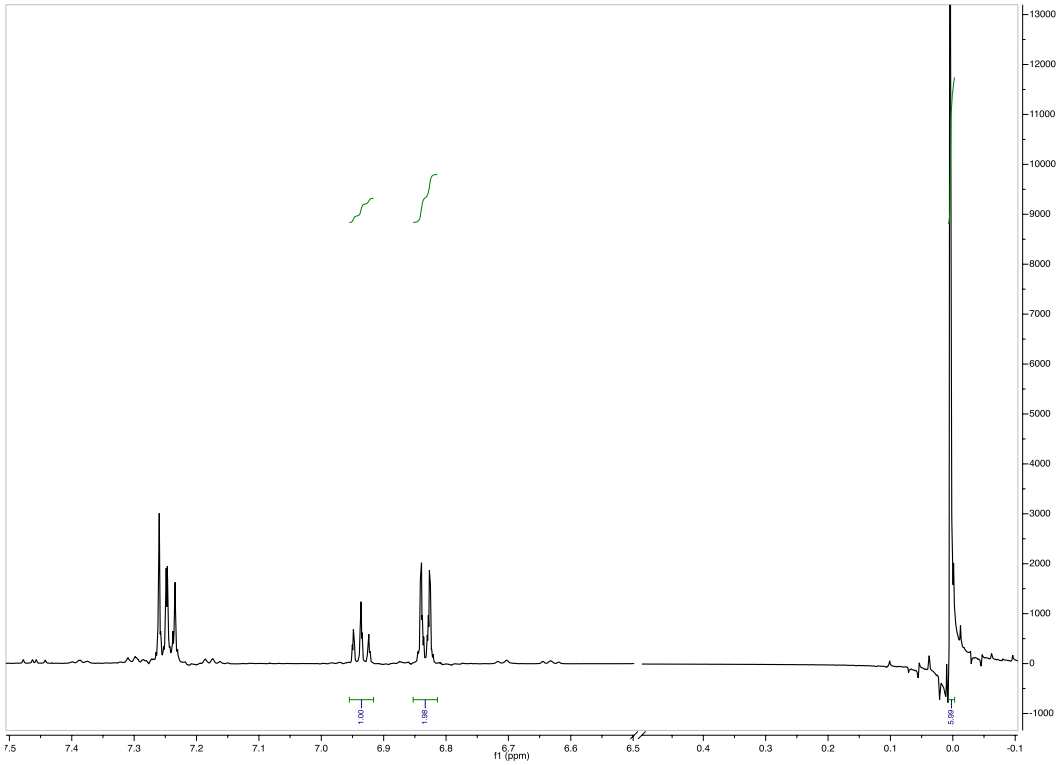

Figure 3.4.170. Example of ^{1}H NMR spectrum for 3.3 + 3.7; t = 0 h (zoomed in for clear visualization of each isomer).

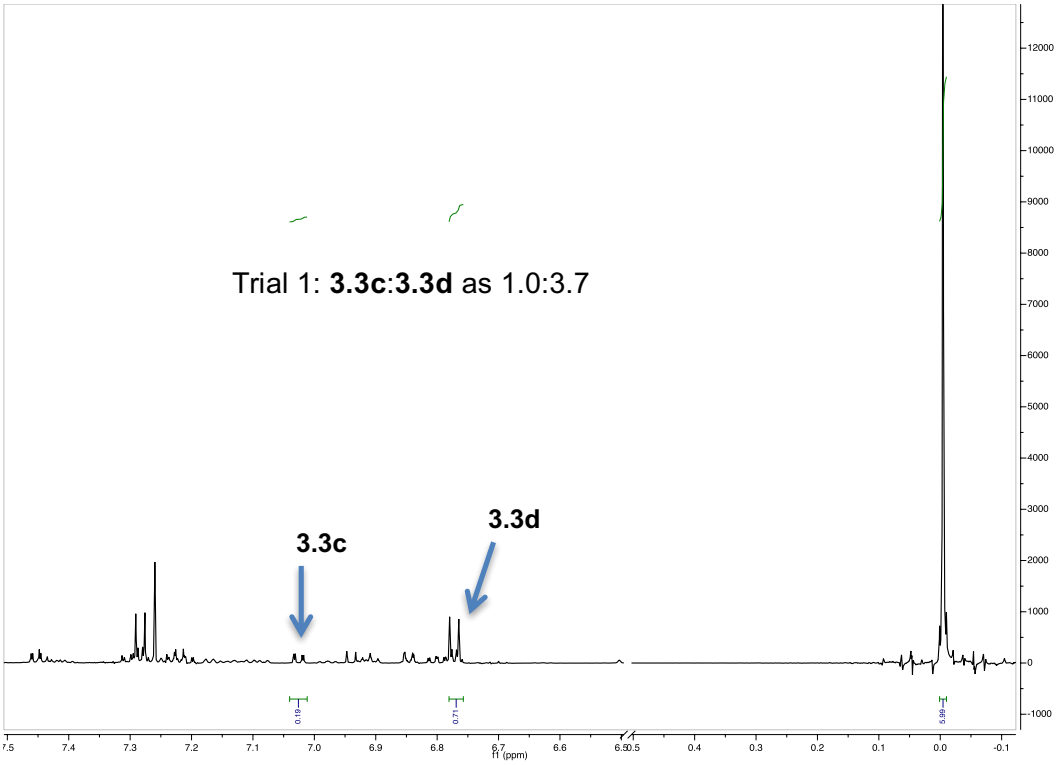

Figure 3.4.171. Example of ^{1}H NMR spectrum for 3.3c + 3.3d + 3.7 + succinimide; t = 30 min after addition of NBS (zoomed in for clear visualization of each isomer).

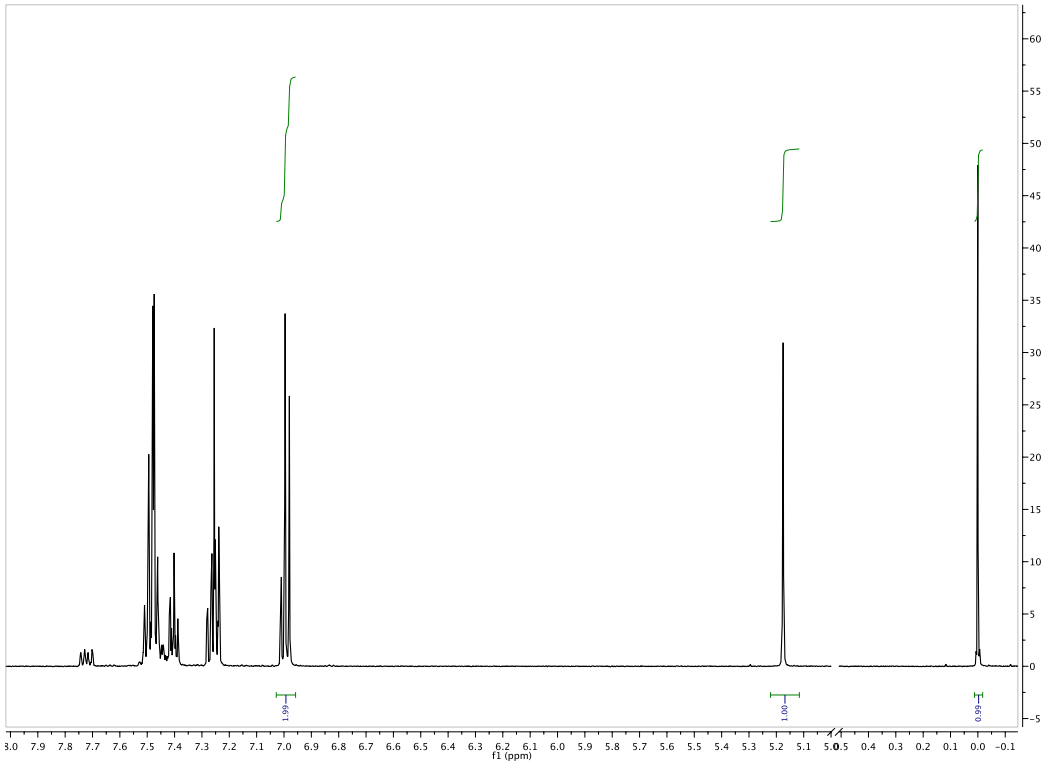

Figure 3.4.172. Example of ^{1}H NMR spectrum for 3.8 + 2.3; t = 0 h (zoomed in for clear visualization of each isomer).

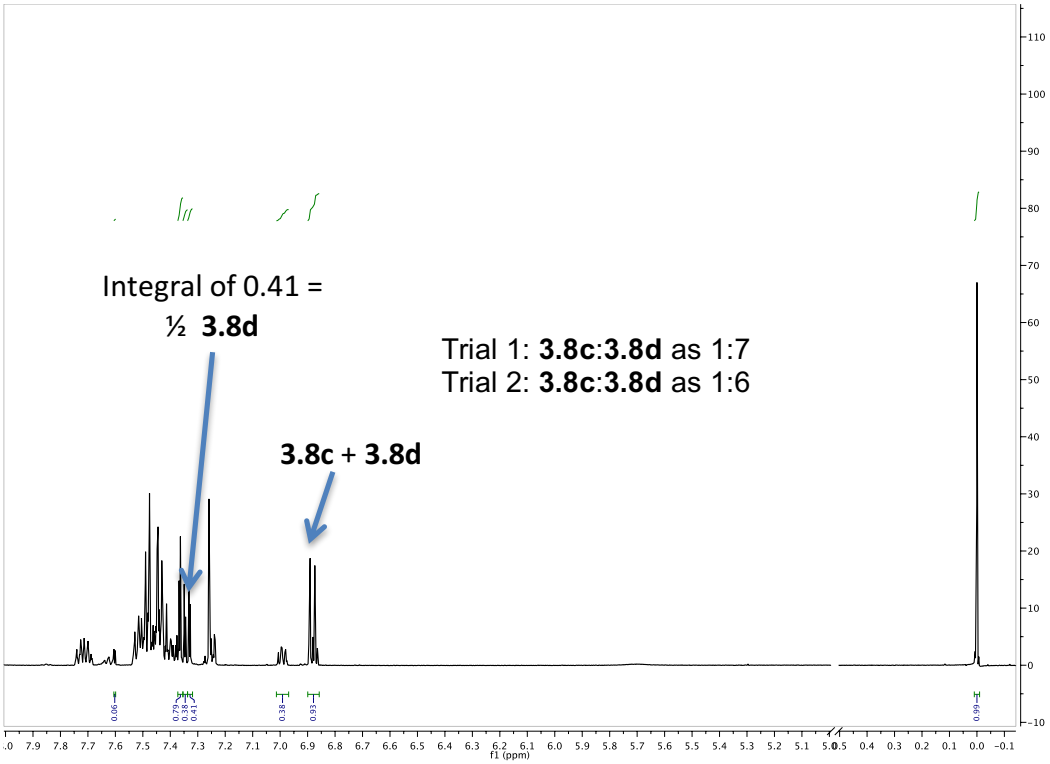

Figure 3.4.173. Example of ^{1}H NMR spectrum for 3.8c + 3.8d + 2.3 + succinimide; t = 12 h after addition of NBS (zoomed in for clear visualization of each isomer).

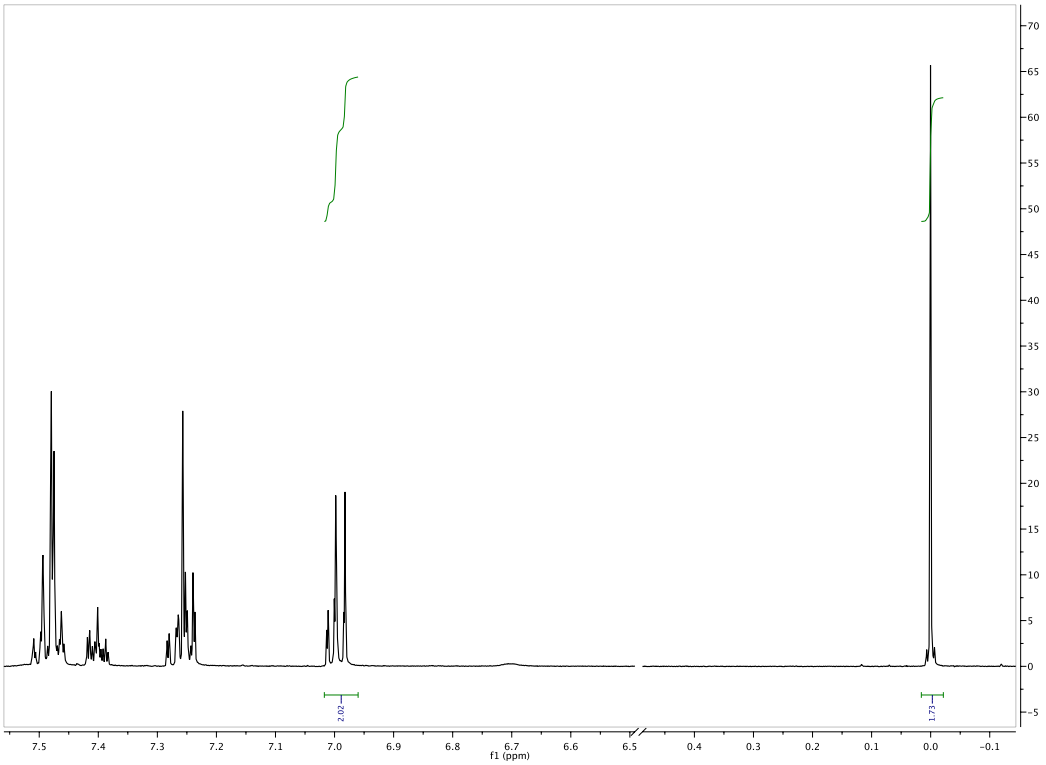

Figure 3.4.174. Example of ^{1}H NMR spectrum for 3.8 + 3.6; t = 0 h (zoomed in for clear visualization of each isomer).

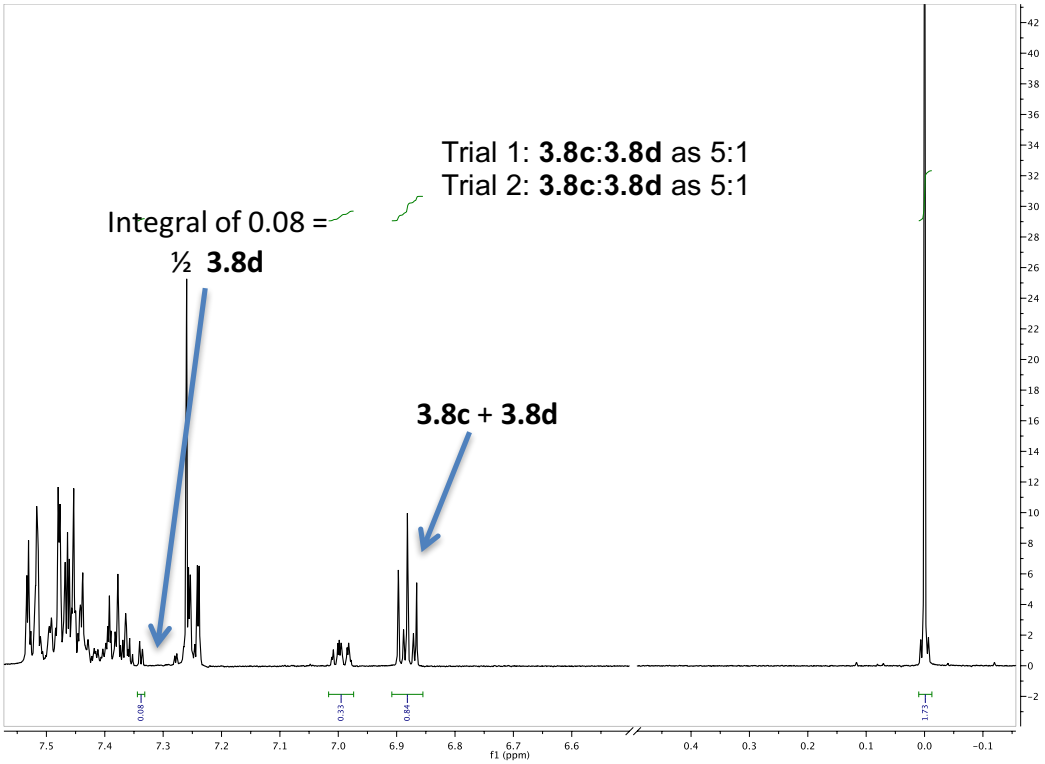

Figure 3.4.175. Example of ^{1}H NMR spectrum for 3.8c + 3.8d + 3.6 + succinimide; t = 12 h after addition of NBS (zoomed in for clear visualization of each isomer).

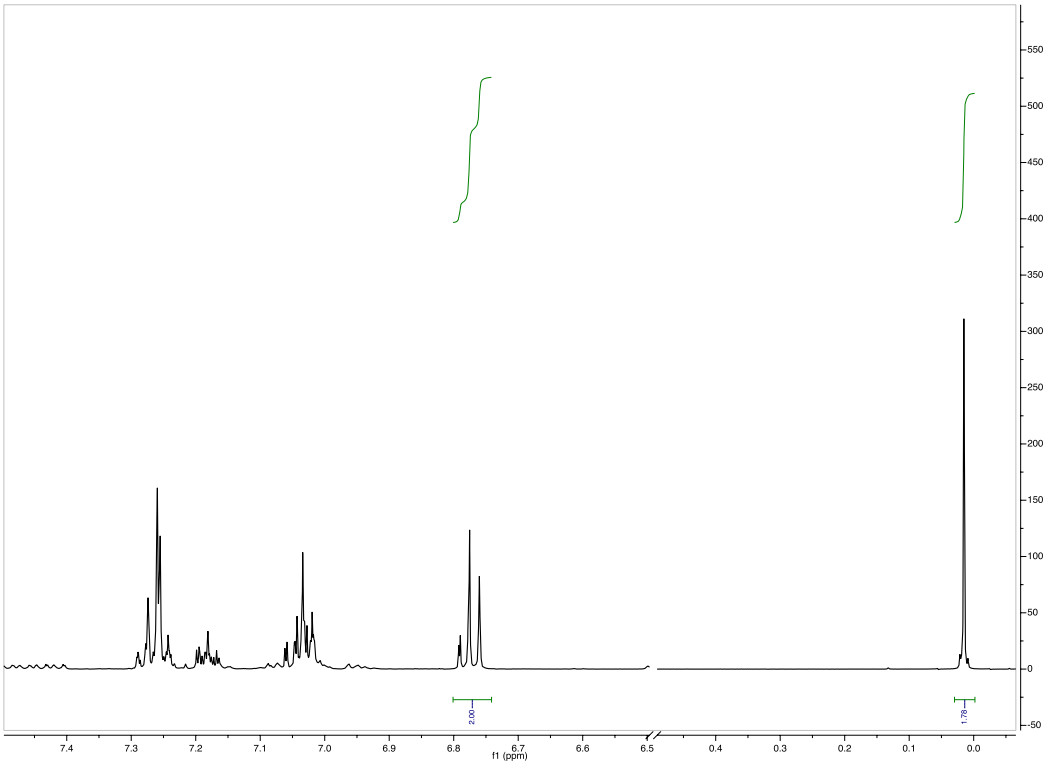

Figure 3.4.176. Example of ^{1}H NMR spectrum for 3.8 + 3.7; t = 0 h (zoomed in for clear visualization of each isomer).

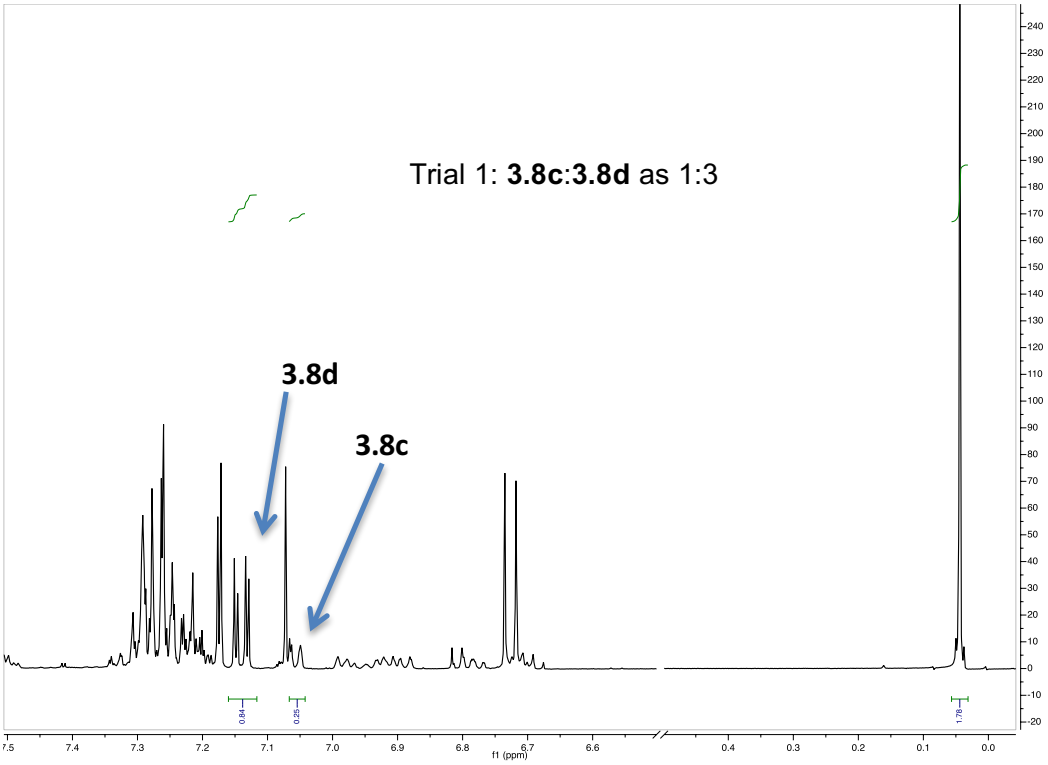

Figure 3.4.177. Example of ^{1}H NMR spectrum for 3.8c + 3.8d + 3.7 + succinimide; t = 12 h after addition of NBS (zoomed in for clear visualization of each isomer).

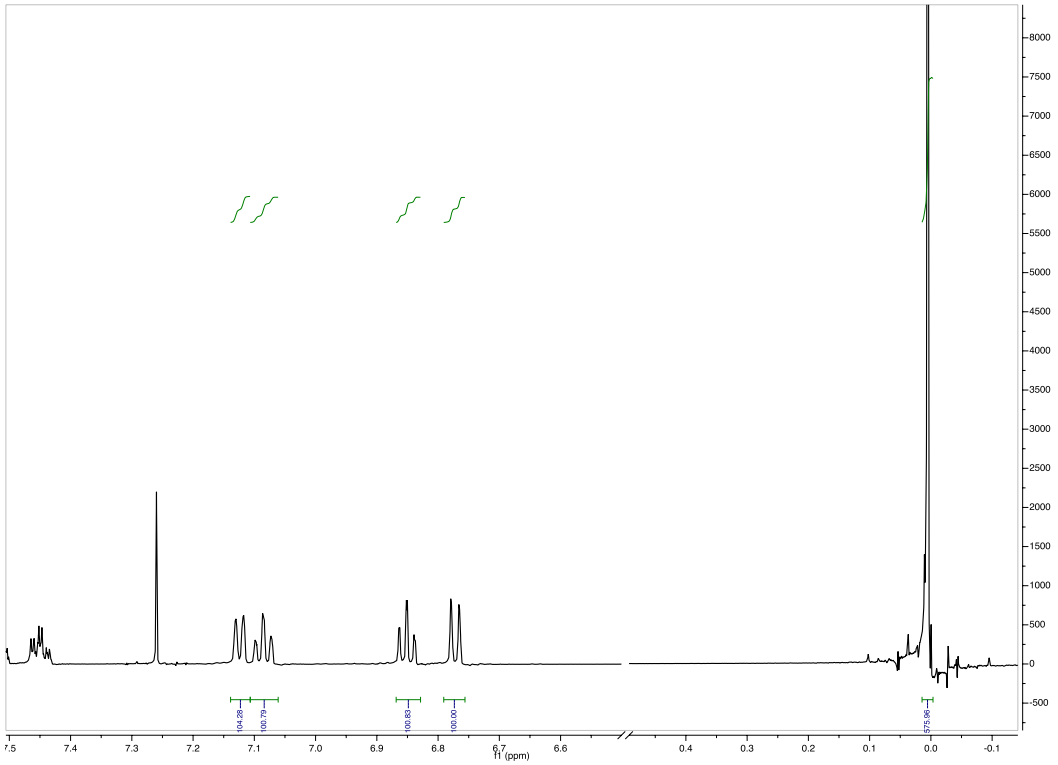

Figure 3.4.178. Example of ^{1}H NMR spectrum for 3.18 + 2.3; t = 0 h (zoomed in for clear visualization of each isomer).

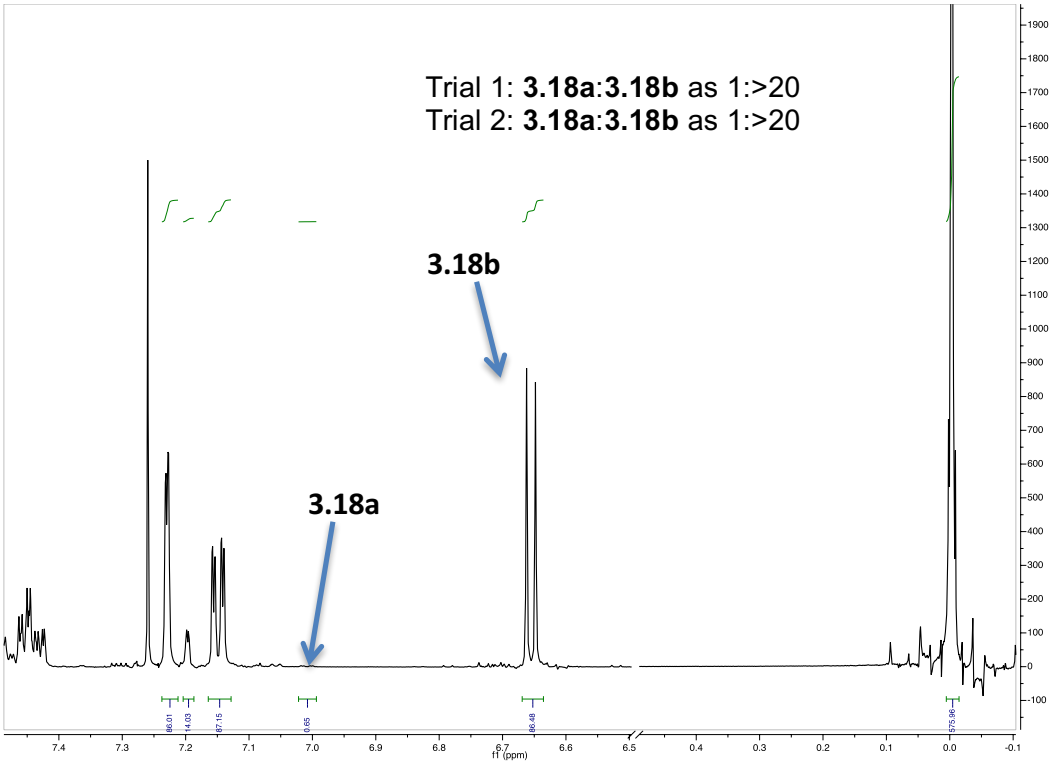

Figure 3.4.179. Example of ^{1}H NMR spectrum for 3.18a + 3.18b + 2.3 + succinimide; t = 30 min after addition of NBS (zoomed in for clear visualization of each isomer).

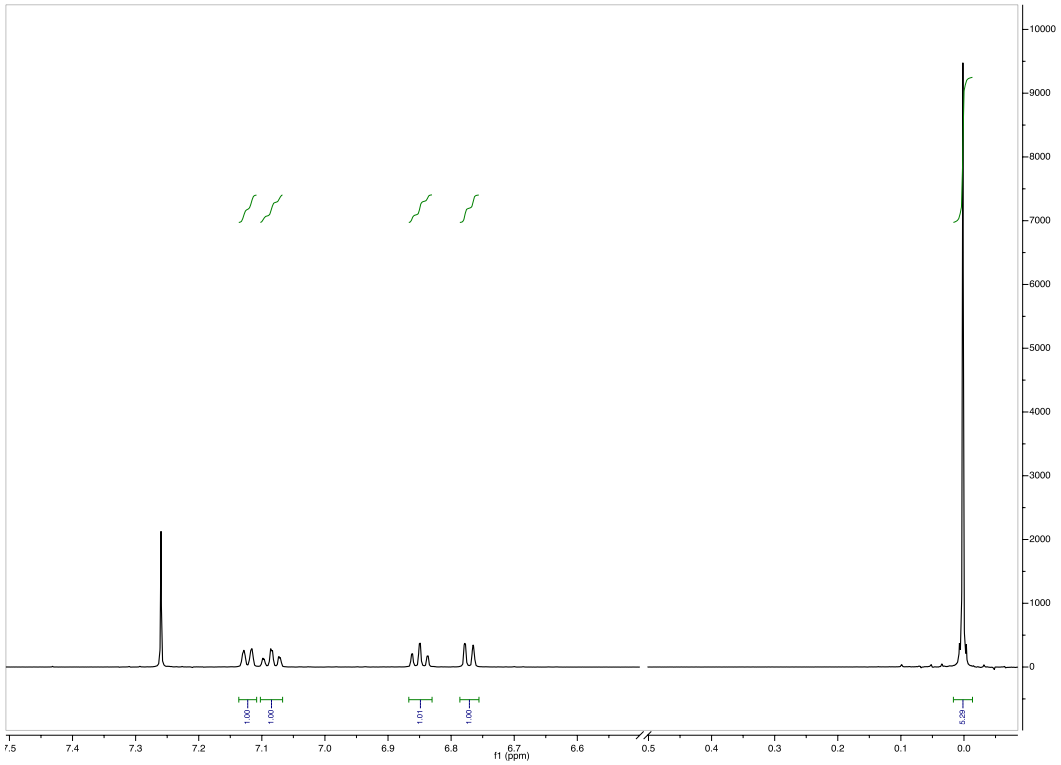

Figure 3.4.180. Example of ^{1}H NMR spectrum for 3.18 + 3.6; t = 0 h (zoomed in for clear visualization of each isomer).

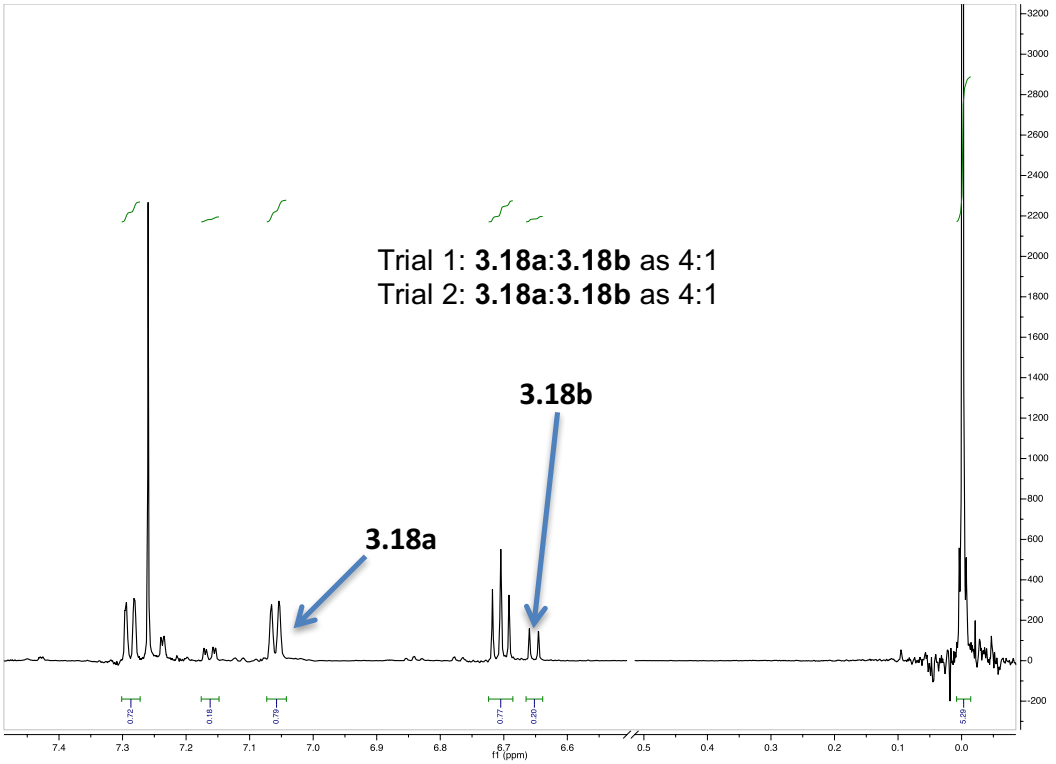

Figure 3.4.181. Example of ^{1}H NMR spectrum for 3.18a + 3.18b + 3.6 + succinimide; t = 30 min after addition of NBS (zoomed in for clear visualization of each isomer).

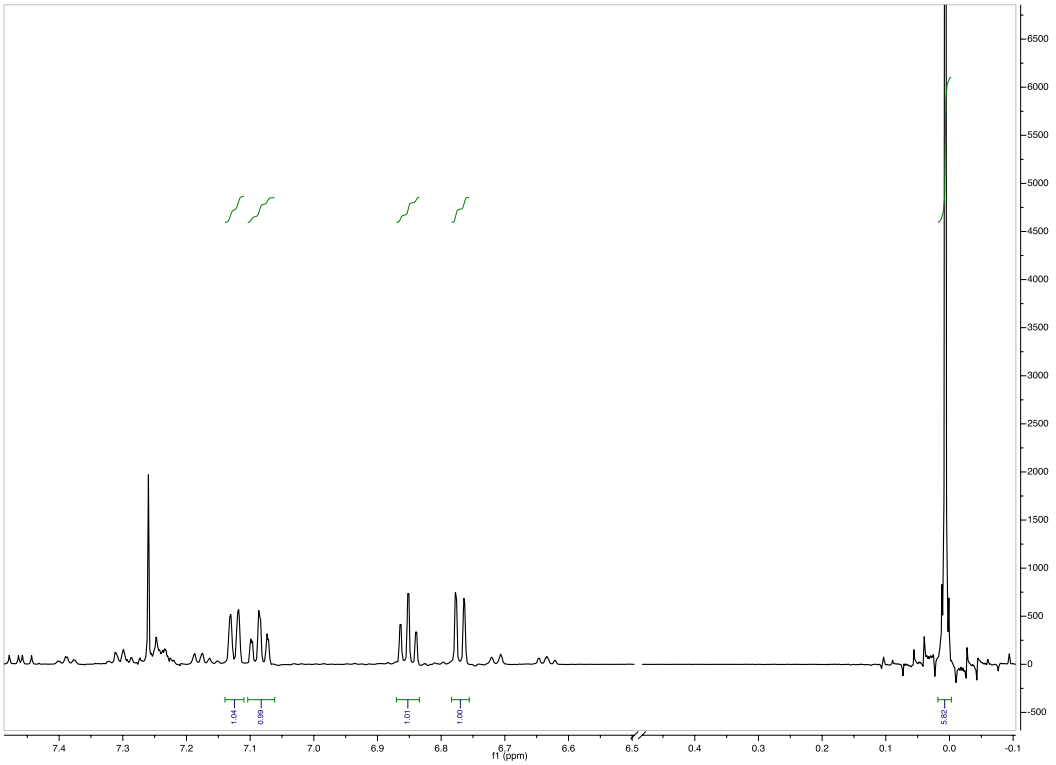

Figure 3.4.182. Example of ^{1}H NMR spectrum for 3.18 + 3.7; t = 0 h (zoomed in for clear visualization of each isomer).

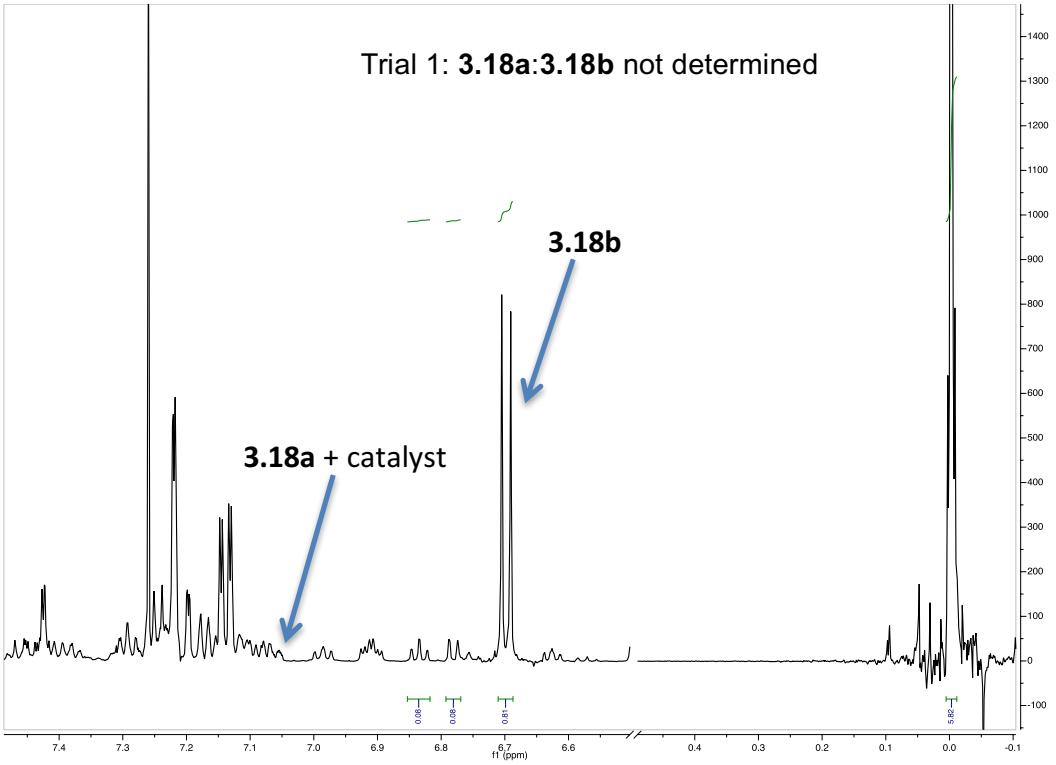

Figure 3.4.183. Example of ^{1}H NMR spectrum for 3.18a + 3.18b + 3.7 + succinimide; t = 30 min after addition of NBS (zoomed in for clear visualization of each isomer).

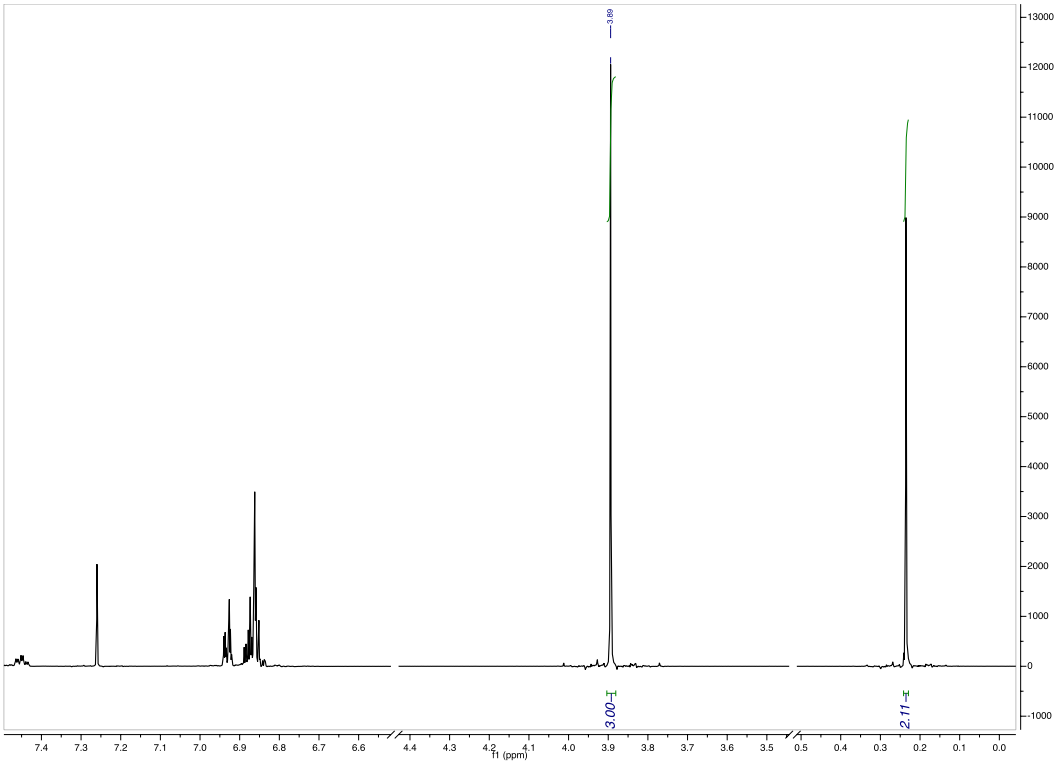

Figure 3.4.184. Example of ^{1}H NMR spectrum for 3.19 + 2.3; t = 0 h (zoomed in for clear visualization of each isomer).

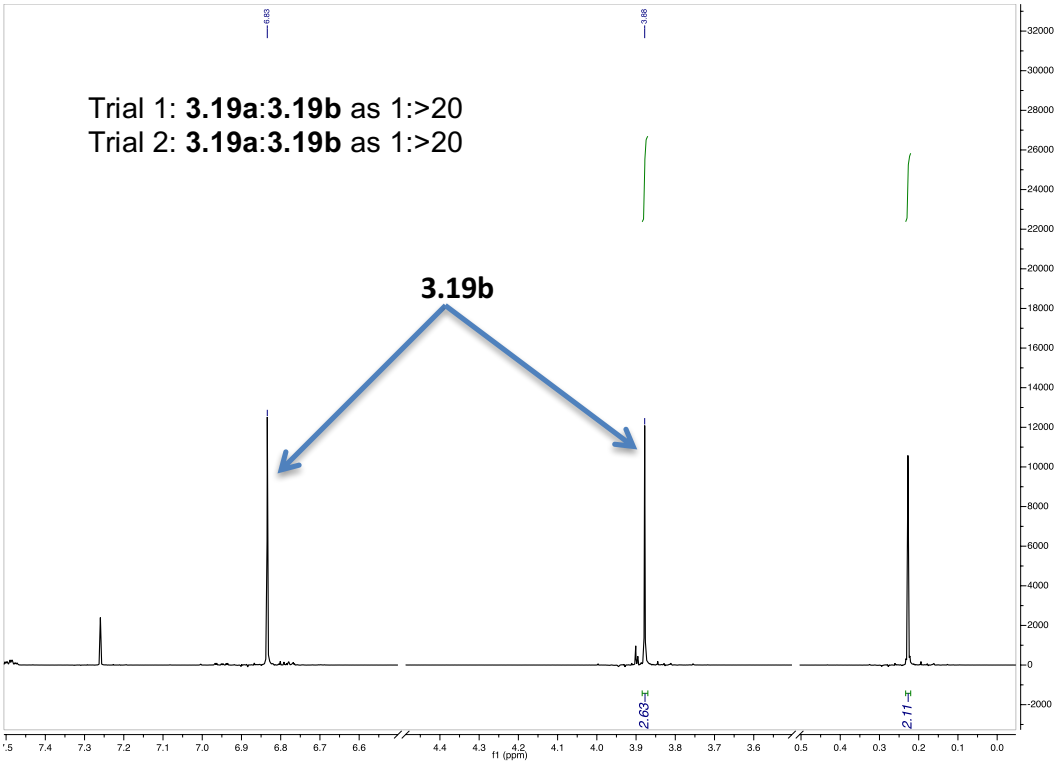

Figure 3.4.185. Example of ^{1}H NMR spectrum for 3.19a + 3.19b + 2.3 + succinimide; t = 1 h after addition of NCS (zoomed in for clear visualization of each isomer).

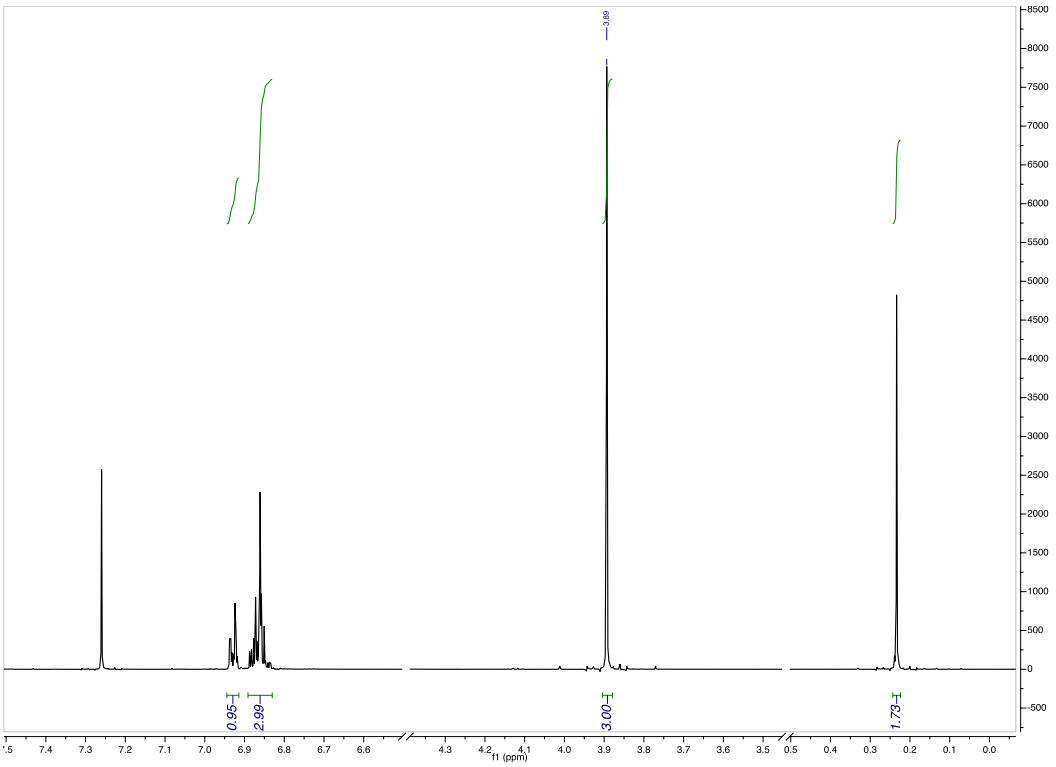

Figure 3.4.186. Example of ^{1}H NMR spectrum for 3.19 + 3.6; t = 0 h (zoomed in for clear visualization of each isomer).

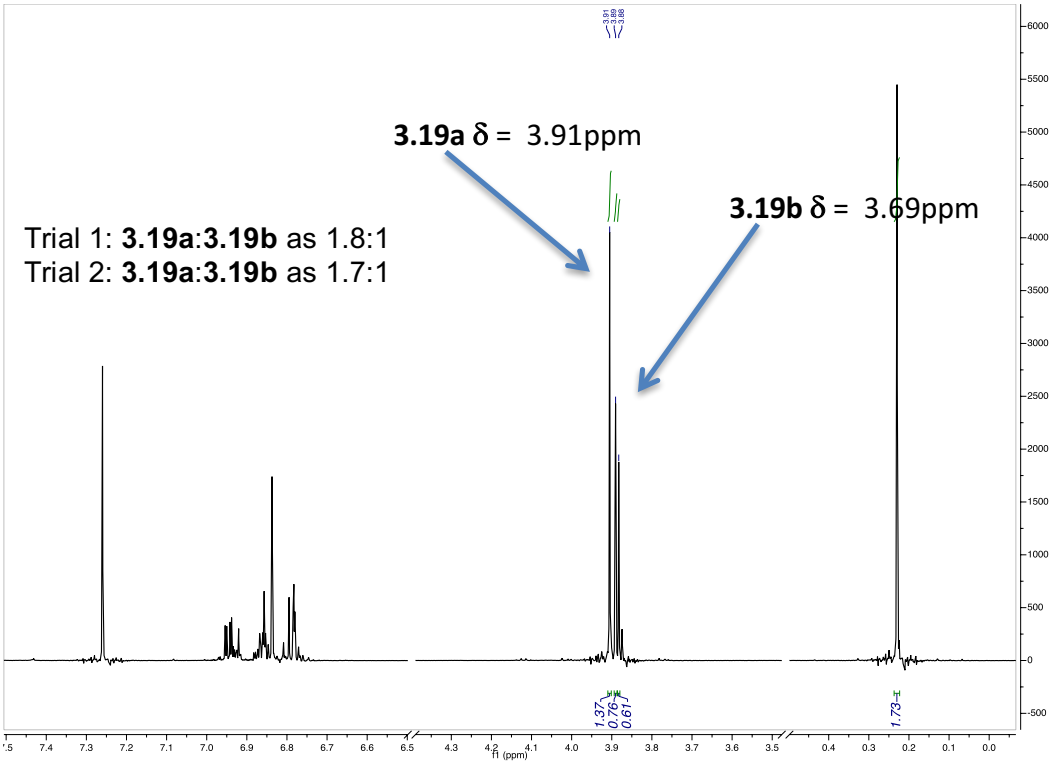

Figure 3.4.187. Example of ^{1}H NMR spectrum for 3.19a + 3.19b + 3.6 + succinimide; t = 2 h after addition of NCS (zoomed in for clear visualization of each isomer).

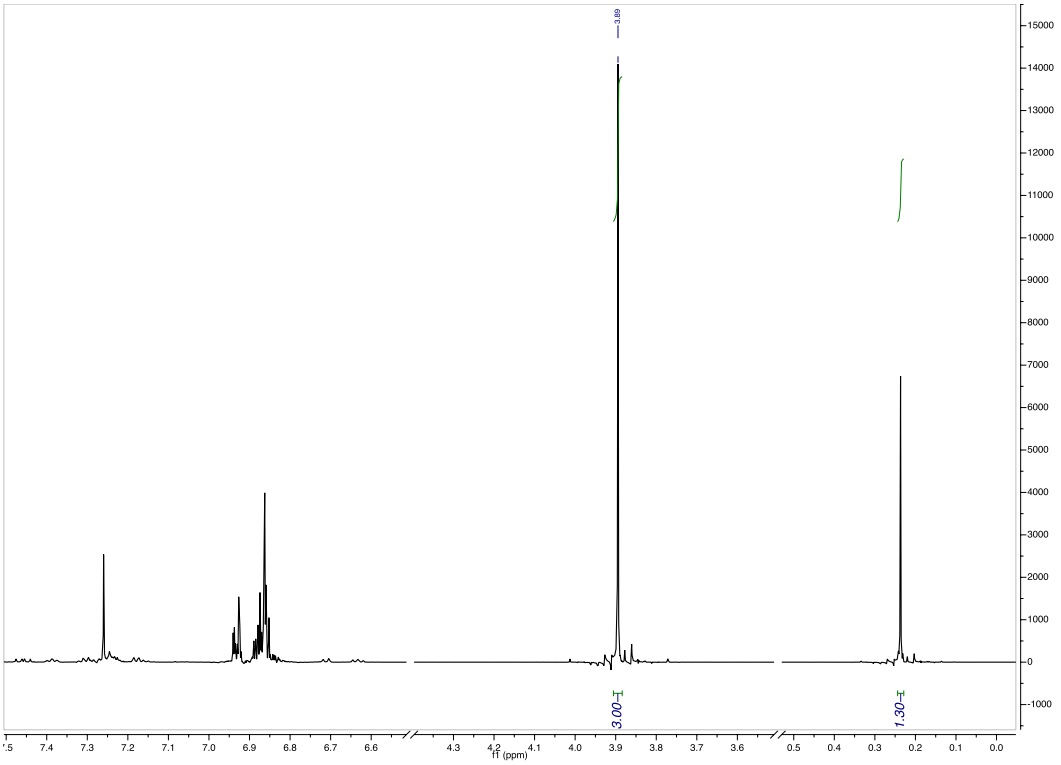

Figure 3.4.188. Example of ^{1}H NMR spectrum for 3.19 + 3.7; t = 0 h (zoomed in for clear visualization of each isomer).

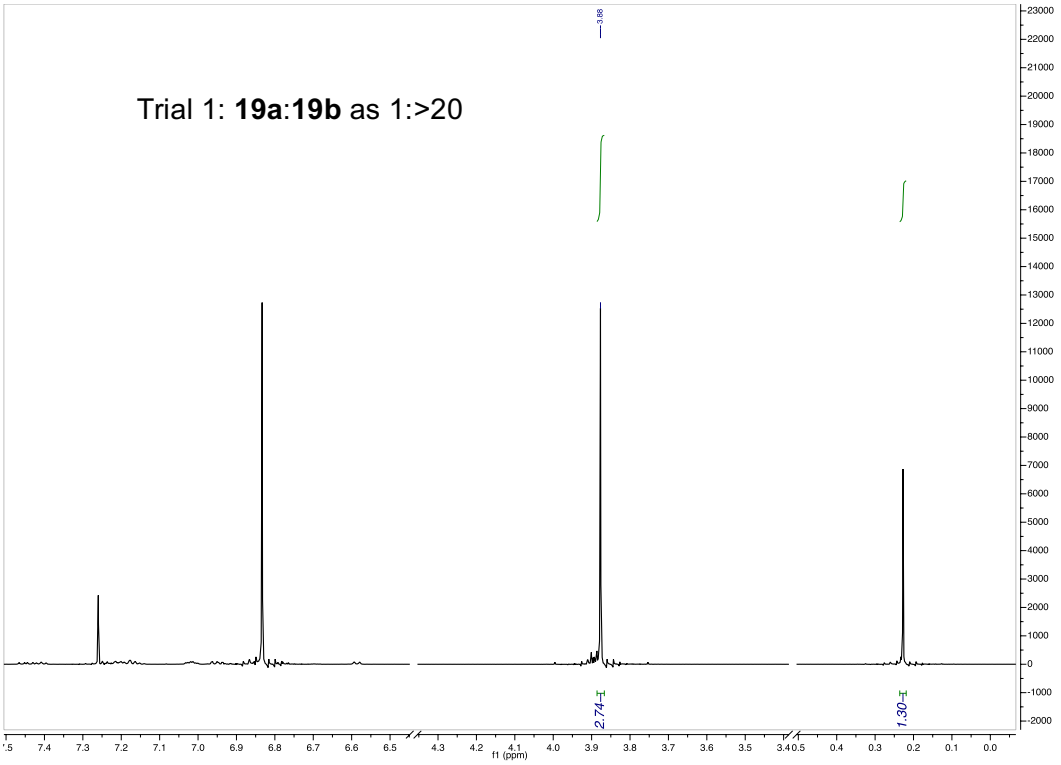

Figure 3.4.189. Example of ^{1}H NMR spectrum for 3.19a + 3.19b + 3.7 + succinimide; t = 1 h after addition of NCS (zoomed in for clear visualization of each isomer).

3.5 Acknowledgements

The contents in Chapter 3 are in part a reformatted reprint of the following manuscript, with permission from the American Chemical Society: Maddox, S. M.; Dinh, A. N.; Armenta, F.; Um, J.; Gustafson, J. L. "The Catalyst-Controlled Regiodivergent Chlorination of Phenols." *Org. Lett.* **2016**, *18*, 5476. The dissertation author was the primary researcher for the data presented. Support of this work by San Diego State University and the SDSU Presidential Leadership Fund is acknowledged.

Chapter 3 in part contains material that may be used in a future publication. The following are coauthors on the corresponding project: Maddox, S. M.; Dinh, A. N.; Janke, L.; Addison, J. B.; Cooksy, A. L.; Gustafson, J. L. "Experimental and Computational Probes into the Principles Driving Selectivity in the Catalyst-Controlled Regiodivergent Chlorination of Phenols." The dissertation author was the primary researcher for the data presented. Support of this work by the National Science Foundation is acknowledged (CHE-1664565).

Chapter 4: Enantioselective Synthesis of Biaryl Atropisomers via the Addition of Thiophenols into Aryl-Naphthoquinones

4.1 ACS Copyright

4.2 Introduction

As was noted in Chapter 1, atropisomerism is a hallmark of many bioactive small molecules[12,116] and privileged catalyst scaffolds.[7] As such, there has been significant effort towards developing atroposelective methodology[117–119] over the past decade. Seminal examples include strategies where the enantioselectivity is induced during formation of the chiral axis,[120–122] via cyclization[123,124] and via point-to-axial chirality transfer.[125] Recently, Miller[126–128] and others[129–131] have studied atropisomer selective dynamic kinetic resolutions (DKR), wherein a configurationally unstable atropisomer is rendered stereochemically stable through various means.

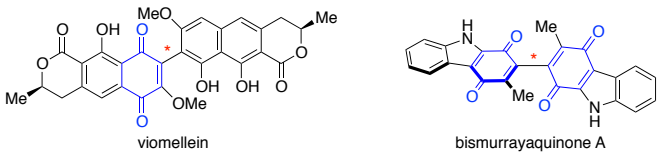

Figure 4.2.1. Examples of axial chirality in natural products

Quinones are common pharmacophores in small molecules and natural products, that can often covalently target nucleophilic protein residues.[16] As redox-active moieties, quinones and hydroquinones can also play distinct roles in redox cycling and cytotoxicity.[132,133] Many bioactive quinones and hydroquinones are atropisomeric (Figure 4.2.1). In 2015, Tan[134] reported the efficient synthesis of highly enantioenriched chiral biaryl diols from quinone and *β*-naphthol precursors using chiral phosphoric acid catalyst **CPA-4.1**. Other research programs[135–137] have successively reported the atroposelective addition of *β*-naphthol derivatives into quinone analogs using a chiral catalysts as well (Figure 4.2.2) to form BINOL and NOBIN derivatives in high yields and enantioselectivities.

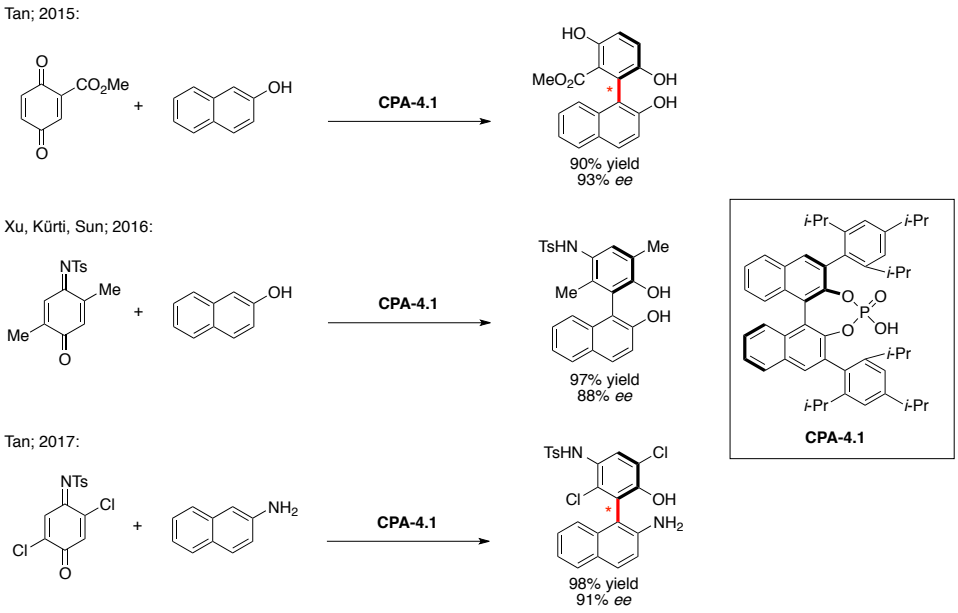

Figure 4.2.2. Previous work in the synthesis of atropisomers from quinones and naphthols

Inspired by these seminal reports, we posited that an enantioselective synthesis of atropisomers could be achieved by the addition of a nucleophile into a quinone, adjacent to a rapidly interconverting atropisomeric axis (Figure 4.2.3). We felt this strategy, which is analogous to a vicarious nucleophilic substitution, could potentially afford both biaryl and non-biaryl atropisomers with unparalleled diversity due to the plethora of nucleophiles that are amenable to catalytic activation coupled with the myriad atropisomeric scaffolds that quinones can be embedded in.

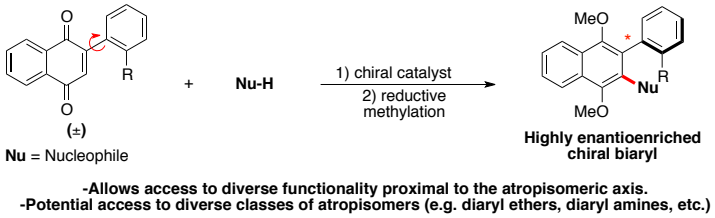

Figure 4.2.3. This work: Enantioselective synthesis of stable atropisomers from aryl-naphthoquinones

To test this approach, we chose to study the addition of thiophenols into naphthoquinones (as in Figure 4.2.3). The addition of thiophenols proximal to a rapidly interconverting, non-symmetrical aryl-naphthoquinone axis would be expected to yield stable biaryl atropisomers. Thus this approach would be amenable to a catalytic atroposelective variant. Such an approach could would be useful for diverse applications. For example, atropisomers with sulfur functionality are known to be effective chiral ligands.[138] Recent reports and perspectives have shed light on the ability for C-S bonds to be functionalized in a manner comparable to halogens, suggesting that the enantioenriched products from such a reaction could be further elaborated to diverse chiral scaffolds (Figure 4.2.4).[139,140] In support of the feasibility of an atroposelective addition, the nucleophilic addition of thiophenols is a well-studied topic in enantioselective catalysis,[141] exemplified by work by Wynberg.[142,143]. Furthermore, work from Smith[144] and a recent kinetic

resolution from our group[145] have shown that chiral quaternary ammonium salts can effect atroposelective thiophenol addition via S_NAr.

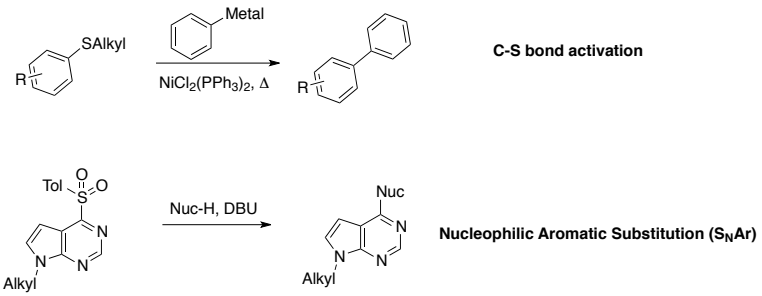

Figure 4.2.4. Two examples of C-S bond functionalizations

4.3 Discussion

To begin our studies, we evaluated different quinine derived catalysts for the addition of thiophenol into quinone biaryl **4.1a**. To remove any complexities caused by the quinone oxidation state (*vida infra*), we quenched each reaction by reductive methylation using $Na_2S_2O_4$ and dimethyl sulfate. The reaction of **4.1a** with thiophenol in the absence of catalyst proceeded with minimal conversion (Table 4.3.1, entry 1). Quinine (**4.C1**) did catalyze the addition of thiophenol, yielding 49% **4.2a** with preliminary levels of enantioselectivity (57:43 e.r.; Table 4.3.1, entry 2). Benzyl quinine (**4.C2**) and acetylated quinine (**4.C3**) proved ineffective catalysts (Table 4.3.1, entries 3 and 4), however 9-amino-epi-cinchona alkaloid analogs proved promising, with primary amine **4.C4** yielding 79% of **4.2a** in 75:25 e.r. and benzoylated analog **4.C5** yielding similar results (Table 4.3.1, entries 5 and 6).

Table 4.3.1. Optimization of Atropisomer Synthesis

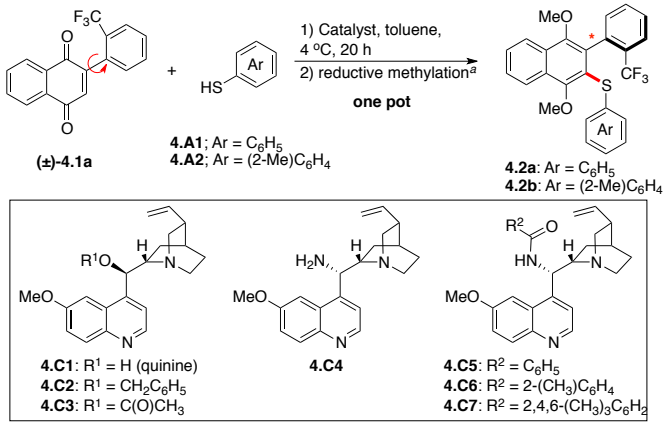

entry	catalyst (mol %)	nucleophile	substrate concentration (M)	temperature (°C)	yield (%)[b]	e.r.[b]
1	None	**4.A1**	0.025	4	<5	n/a
2	**4.C1** (10)	**4.A1**	0.025	4	49	57:43
3	**4.C2** (10)	**4.A1**	0.025	4	48	50:50
4	**4.C3** (10)	**4.A1**	0.025	4	17	46:54
5	**4.C4** (10)	**4.A1**	0.025	4	79	75:25
6	**4.C5** (10)	**4.A1**	0.025	4	70	78:22
7	**4.C6** (10)	**4.A1**	0.025	4	65	87:13
8	**4.C7** (10)	**4.A1**	0.025	4	69	93:7
9	**4.C7** (10)	**4.A1**	0.05	4	84	93:7
10[c]	**4.C7** (10)	**4.A1**	0.05	24	75	87:13
11	**4.C7** (10)	**4.A1**	0.05	-18	67	86:14
12	**4.C7** (2.5)	**4.A1**	0.1	4	80	88:12
13	**4.C7** (2.5)	**4.A1**	0.05	4	73	93:7
14	**4.C7** (5)	**4.A1**	0.05	4	89	93:7
15	**4.C7** (5)	**4.A2**	0.05	4	68	96:4
16[d]	**4.C7** (5)	**4.A2**	0.05	4	82	96:4

[a]See Section 4.2 for details. [b]Isolated yields and enantiomeric ratios (e.r.) are reported as an average of two trials. [c]Reaction was placed in -18 °C freezer for 20 hours without stirring. [d]Reaction was let stir for 44 hours before reductive quench.

Methodical elaboration of **4.C4** to diverse ureas, carbamates, and amides were met with little improvement in enantioselectivity. These results, however, proved informative and suggested a reliance on steric bulk distal to the "active site" of the catalyst (see Section 4.4). Based on these results, we hypothesized an *ortho*-substituted benzamide might improve selectivity due to catalyst conformational changes related to the "magic methyl effect."[146]

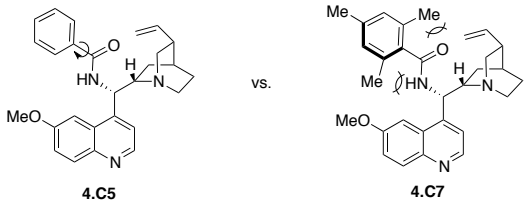

4.C5 4.C7

Figure 4.3.1. Effect of adding methyl substitution on the effective radius of the benzamide moiety

For example, adding a methyl group to the 2-position of the benzamide, as in **4.C6**, would be expected to bias the arene-carbonyl bond towards a pseudo-perpendicular conformation, thereby increasing the effective radius of the benzamide (Figure 4.3.1). This hypothesis proved fruitful, as **4.C6** yielded a notable increase in enantioselectivity (87:13 e.r., Table 4.3.1, entry 7). The addition of a second *ortho*- methyl group led to our best catalyst, **4.C7**, which yielded 69% of **4.2a** in 93:7 e.r. (Table 4.3.1, entry 8). Further modification of reaction conditions led to 89% yield of **4.2a** with retained 93:7 e.r. (Table 4.3.1, entries 9-14). Finally, using *o*-toluenethiol as the nucleophile afforded **4.2b** with an improved e.r. of 96:4 (Table 4.3.1, entries 15 and 16).

Scheme 4.3.1. Thiophenol and Atropisomer Substrate Scope

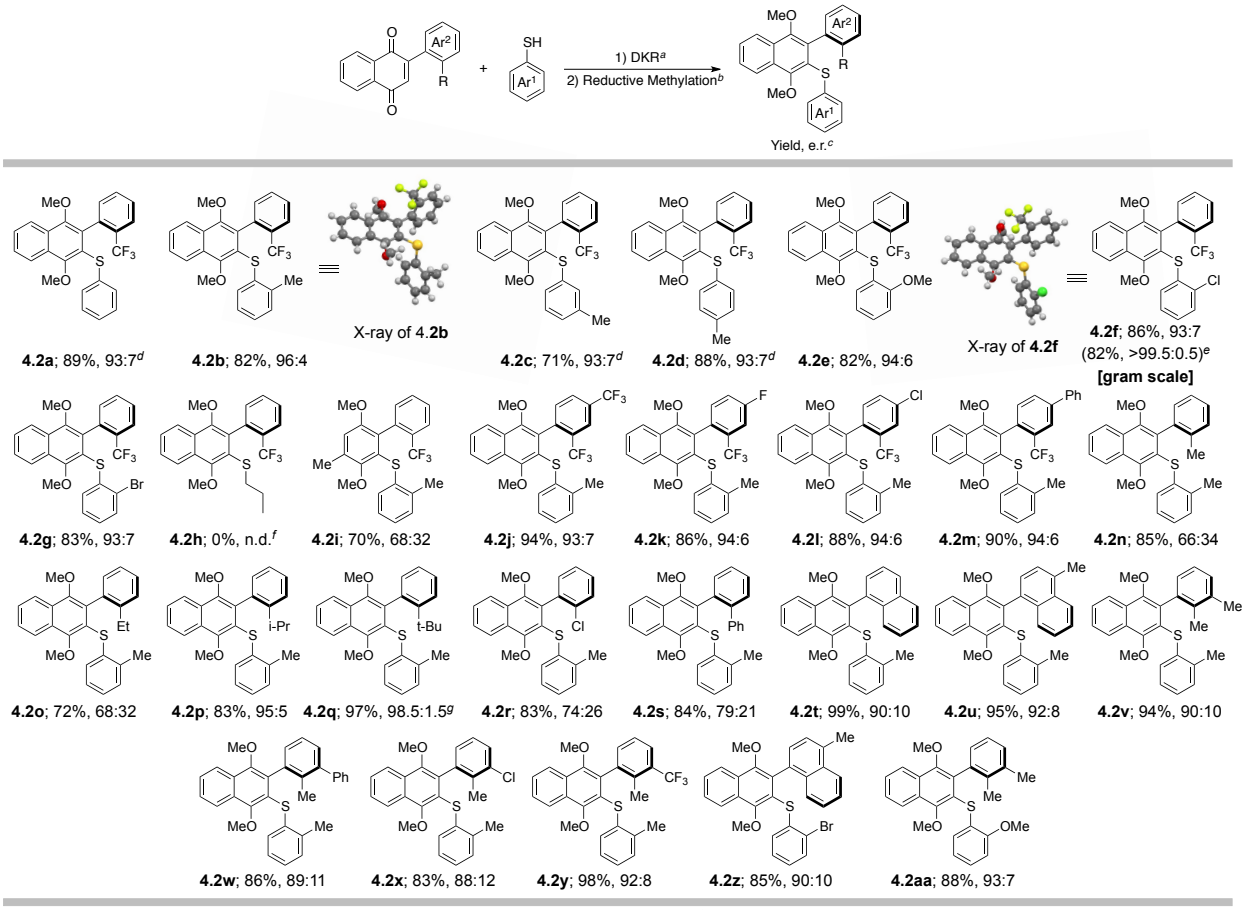

[a]Aryl-naphthoquinone (0.1mmol), toluene (2mL), 4.**C7** (0.005mmol), thiophenol (0.2mmol) was stirred at 4 °C for 44 hours. [b]$Na_2S_2O_{4(aq)}$, toluene, THF, MeOH, TBAB at 0 °C, then $KOH_{(aq)}$, Me_2SO_4. [c]Isolated yields are reported, and e.r. was determined by HPLC using a chiral stationary phase (average of three trials). [d]Enantioselective Thiophenol Addition ran for 20 hours. [e]After recrystallization. [f]No reaction was observed by TLC after 20 hours. [g]Enantioselective Thiophenol Addition ran for 68 hours.

With an optimized atroposelective synthesis in hand, we set out to gain a better understanding of the effect of the thiophenol structure (Scheme 4.3.1). Moving the methyl group on the thiophenol away from the *ortho*- position (**4.2c** and **4.2d**) resulted in decreased e.r.s. Replacing the *o*-methyl group with methoxy, chlorine, or bromine also led to slight decreases in e.r. (94:6, 93:7, 93:7; respectively), suggesting a mild reliance on the inductive capabilities of the *ortho*-substituent of the thiophenol. We were able to recrystallize **4.2f** on the gram scale in 82% overall yield as a near enantiopure atropisomer (>99.5:0.5 e.r.). We also obtained the crystal structures of **4.2b** and **4.2f**, revealing the major enantiomer arising from this reaction to be the (R_a)

atropisomer. Due to structural similarity, the stereochemistry of all other products were assigned by analogy. Reacting **4.1a** with 1-propane thiol, rather than thiophenol, resulted in no observable reaction. Lastly, performing this DKR on a quinone-based scaffold gave **4.2i** in 70% yield and 68:32 e.r., suggesting this chemistry could be applicable to quinone scaffolds upon further optimization.

Continuing with the naphthoquinone scaffold, we sought out to explore a range of substitutions on the non-quinone aryl ring (Scheme 4.3.1). In general, adding substitution at the *para*- position had little effect on enantioselectivity, giving **4.2j**-**4.2m** in high yields with 93:7 e.r. or better. However, replacing the $–CF_3$ group with methyl (**4.2n**) resulted in a drop in e.r. to 66:34. Enantioselectivity was improved as we increased the steric bulk of the alkyl substituent, with *–i*-Pr (**4.2p**) resulting in 95:5 e.r. and *–t*-Bu (**4.2q**) resulting in 98.5:1.5 e.r. Moreover, replacing $–CF_3$ with –Cl (**4.2r**) resulted in a drop in e.r. to 74:26, and a similar result was observed with a phenyl group *ortho*- to the atropisomeric axis (**4.2s**, 79:21 e.r.). The [1,2'-binaphthalene] atropisomer (**4.2t**) was isolated in 99% yield and 90:10 e.r., and the structurally analogous 4-methyl-[1,2'-binaphthalene], **4.2u**, was isolated in 95% yield and 92:8 e.r. These results encouraged us to probe the effect of *meta*- substitution on the non-quinone aryl, finding that adding adjacent *meta*-substituents to poor substrates such as **4.2n**, (**4.2v-4.2y**), afforded significantly improved enantioselectivities ranging from 88:12 to 92:8 e.r., all in high yields. Notably, these selectivities were conserved when different thiophenols were used, as exemplified by **4.2z** and **4.2aa**. Overall, this methodology proved amenable to a diversity of substitution patterns within the confines of atropisomer stability.

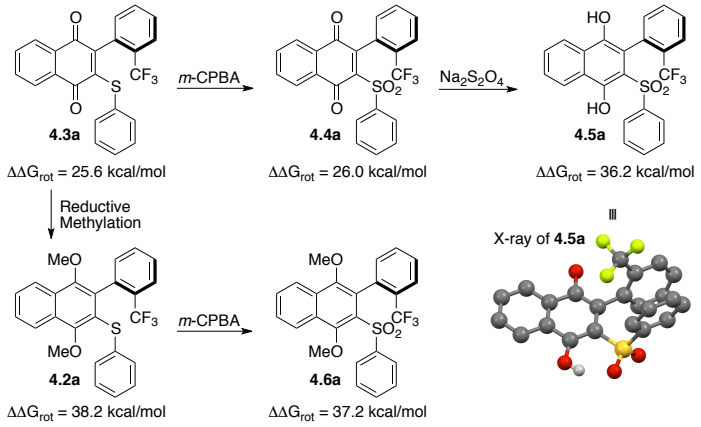

Figure 4.3.2. The effect of quinone oxidation state on the conformational stability

When we did not quench the reaction via reductive methylation, we observed spontaneous oxidation of the dihydroquinone to the naphthoquinone product (i.e. **4.3a**), resulting in lower yields and enantioselectivities. The lower selectivity in the absence of reductant is likely due to racemization of the quinone as the reaction warms to room temperature. We experimentally determined the barrier to rotation of **4.3a** to be 25.6 kcal/mol in toluene at 50 ^{o}C, which translates to an undesirable stereochemical stability at room temperature (Figure 4.3.2). Upon oxidizing **4.3a** to sulfone **4.4a**, we observed a small increase in stereochemical stability to 26.0 kcal/mol, also in toluene at 50 ^{o}C. Moreover, this quinone could now be reduced to **4.5a**, which does not spontaneously oxidize due to the electron withdrawing sulfone. This allowed us to obtain a crystal structure (enantiomer was R_a) and to determine its stereochemical stability, observing a barrier to rotation of 36.2 kcal/mol for **4.5a** in diphenyl ether at 169 ^{o}C. Thus, the observed barrier to rotation should preclude any observable racemization at room temperature. This drastic increase in stereochemical stability compared to **4.4a** is likely due to the longer C-O bond length in hydroquinones. Furthermore, analysis of aryl-quinone crystal structures reveal an out-of-plane distortion across the atropisomeric axis, which could also account for the lower observed barriers

to rotation in aryl-quinones.[147] The methylated dihydroquinones proved even more stable, as **4.2a** exhibits an experimentally determined barrier to rotation of 38.2 kcal/mol in diphenyl ether at 207 ^{o}C.

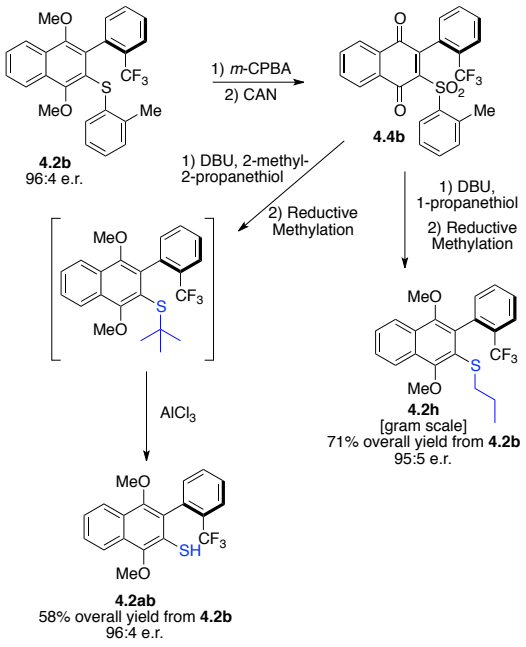

Figure 4.3.3. Enantioretentive Nucleophilic Aromatic Substitutions

Next, we performed an S_NAr-like reaction sequence on **4.2b** to arrive at **4.2h** in 71% overall yield on the gram scale with nearly complete enantioretention (Figure 4.3.3), despite proceeding thru the low-barrier quinone oxidation state. Moreover, when 2-methyl-2-propanethiol is used instead of 1-propanethiol, the *tert*-butyl group could be removed from the resulting *tert*-butyl thioether with $AlCl_3$ to furnish the corresponding atropisomeric biaryl thiol with complete enantioretention. This result suggests that enantioretentive substitutions with other nucleophiles are possible, however that is perhaps beyond the scope of this work. Furthermore, having alkyl-sulfide substitution also provides a starting point for atropisomer diversification as there are several recent methodologies concerning C-S bond activation.[148–151]

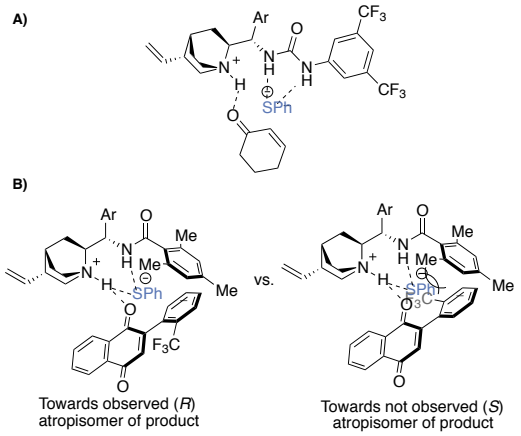

Figure 4.3.4. Mechanistic model. A) Houk's Bronsted Acid-Hydrogen Bonding Model. B) Plausible model for stereochemical induction.

Houk has recently reported a Brønsted acid-hydrogen bonding model (Figure 4.3.4A)[152,153] for cinchona alkaloid-catalyzed sulfa-michael reactions, based on Wynberg's work.[142,143] We postulate this transformation likely parallels Houk's model, as we found that **4.C7** can affect the addition of thiophenol into cyclohexanone with moderate levels of enantioselectivity (see Section 4.4).

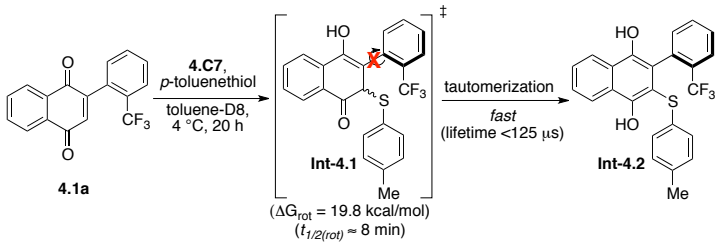

Figure 4.3.5. Tautomerism is likely much faster than atropisomer bond rotation

This result opens the possibility that the stereoselectivity of this transformation is induced via a 'point-to-axial' chirality transfer mechanism in which the thiophenol adds enantioselectively into the quinone to give diastereomeric **Int-4.1**, followed by the equilibration of the atropisomeric axis to the more stable diastereomer and tautomerization of **Int-4.1** to the corresponding hydroquinone **Int-4.2.** To probe this, we monitored the reaction of **4.1a** with *p*-toluenethiol in the

presence of **4.C7** by ^{1}H NMR, observing no evidence of the point chiral addition adduct **Int-4.1**, meaning tautomerization of **Int-4.1** to the corresponding hydroquinone (**Int-4.2**) likely occurs on the hundred-millisecond time scale or faster (Figure 4.3.5, refer to discussion of NMR kinetics study in Section 4.4.9). We next computationally determined the barrier to rotation of **Int-4.1** to be approximately 19.8 kcal/mol in the gas phase, which roughly translates to a $t_{1/2}$ to atropisomer bond rotation of about 8 minutes at 4 ^{o}C. While the error to the calculated barriers to rotation may not be accurate enough to draw an absolute conclusion, these experiments do suggest that tautomerization of **Int-4.1** to **Int-4.2** likely occurs faster than rotation of the atropisomeric bond, offering evidence against point-to-axial chirality, and perhaps in favor of a mechanism in which the axis is set prior to thiophenol addition.

One possible model for stereochemical induction, largely inspired by Houk's model, is proposed in Figure 4.3.4B in which the thiophenol is deprotonated by the quinuclidine base and oriented via H-bonding with the *C*-9 benzamide. In this model, quinone is activated by an H-bond with the quinuclidinium ion, orienting the atropisomer axis in a way such that the *ortho*-substitution of the aryl group avoids steric interaction with the catalyst. More detailed studies are underway, including those aimed to better understand the atropisomer differentiation by **4.C7** to further probe the likelihood of potential modes of stereoinduction.

In conclusion, we have developed a novel atroposelective addition of thiophenol into rapidly interconverting aryl-naphthoquinones to afford stereochemically stable enantioenriched biaryl sulfides. This report lends itself as a proof-of-concept towards a general strategy towards the enantioselective synthesis of diverse biaryl and non-biaryl atropisomers. With proper control of the redox properties of the quinone moiety, we showed that we can modulate the atropisomer's stereochemical stability, as well as its reactivity. Furthermore, the resulting biaryl sulfide was

moved on in an S_NAr-like reaction sequence with near complete enantioretention. Finally, an argument was made for the mode of asymmetric induction, as point-to-axial chirality transfer may not be the likely driving force for stereoinduction.

As this work serves as a proof of concept, our group has since reported on the atroposelective synthesis of diaryl ethers using similar methodology. The idea for the synthesis of diaryl ethers via this strategy was conceived by the author of this thesis and Professor Jeffrey L. Gustafson. However, the majority of reaction optimization and substrate scope validation was carried out by my colleagues Andrew Dinh and Ryan Noorbehesht.

4.4 Experimental Section

4.4.1 General Information

^{1}H and ^{13}C NMR spectra were recorded on Varian VNMRS 400 MHz, Varian Inova 500 MHz, Varian VNMRS 600 MHz, and Bruker Avance III 600 MHz spectrometers at 25 ^{o}C, unless otherwise noted. ^{19}F NMR spectra were referenced to an external TFA standard. For quantifiable data, the Bruker Avance III 600 MHz spectrometer was used with a 5mm TXI H-C-N liquids NMR probe with Z-axis gradient. All chemical shifts were reported in parts per million (ppm) and were internally referenced to residual protio solvents, unless otherwise noted. Fluorine spectra were reference to an external TFA standard. Spectral data were reported as follows: chemical shift (multiplicity [singlet (s), doublet (d), triplet (t), quartet (q), pentet (p), and multiplet (m)], coupling constants [Hz], integration). Carbon spectra were recorded with complete proton decoupling. Conventional mass spectra were obtained using Advion Expression^{s} CMS (APCI, ASAP). All chemicals used were purchased from Sigma Aldrich, TCI, Frontier Scientific, Acros Organics, Strem, Oakwood, Matrix Scientific, Cambridge Isotope Laboratories, or Fisher and were used as received without further purification, unless otherwise noted. All normal phase flash column chromatography (FCC) was performed using Grade 60 Silica Gel (230-400 mesh) purchased from Fisher Scientific. Normal phase flash chromatography was performed on a Biotage Isolera One with Biotage SNAP cartridges (KP Sil 10g-50g) or via manual FCC. All enantioselective dynamic kinetic resolutions were performed in the absence of light by covering the flask/vial in aluminum foil (Reynolds Wrap), and were stirred in a temperature controlled facility at 4 ^{o}C. Unless otherwise noted, reactions were run open to air and solvent were used straight out of the bottle without drying or degassing. Enantioselectivities were recorded using an Agilent 1100 series

HPLC using a chiral stationary phase. CHIRALPAK IA, IB, and IC columns were purchased from Diacel Technologies Corporation.

Abbreviations:

CAN = ammonium cerium(IV) nitrate

DCM = dichloromethane

DMF = dimethylformamide

EtOAc = ethyl acetate

FCC = flash column chromatography

MeCN = acetonitrile

r.b. = round bottom

TBAB = *N*,*N*,*N*,*N*-tetrabutylammonium bromide

TEA = triethylamine

TFA = trifluoroacetic acid

THF = tetrahydrofuran

4.4.2 Synthesis of Catalysts

Quinine, 99% (**4.C1**) was purchased from Alfa Aesar and used as is. **4.C4** was synthesized following procedure 1A from Nature Protocols, **2013**, vol. 8, no. 2, 325-344, to arrive at the HCl salt of **4.C4**, which was free based in saturated sodium bicarbonate. The aqueous mixture was extracted 3 times with DCM. The organic layers were washed with brine, dried over sodium sulfate, concentrated on a rotovap, and placed under hivac overnight to give **4.C4** as a clear oil. The ^{1}H NMR matched those reported in literature.[154] **4.C3**[155] and **4.C5**[156] were also synthesized from known procedures and the spectral data matched those reported within.

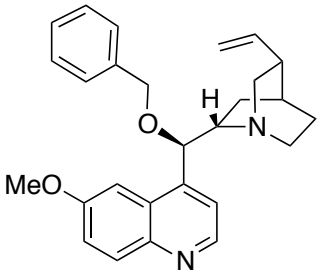

Figure 4.4.1. Catalyst 4.C2

(1*S*,2*S*,4*S*,5*R*)-2-((*R*)-(benzyloxy)(6-methoxyquinolin-4-yl)methyl)-5-vinylquinuclidine (**4.C2**): Quinine (3.0g, 9.2mmol, 1.0 equiv) was dissolved in anhydrous DMF (30mL) in a flame-dried 100mL r.b. flask equipped with a stir bar. The flask was lowered into a water/ice bath and let cool to 0 ^{o}C with stirring, under argon. NaH (410mg, 10mmol, 1.1 equiv, 60% in oil) was added in batches of approximately 150mg. Once the evolution of gas was complete, benzyl bromide (1.2mL, 10mmol, 1.1 equiv) was added to the stirring solution at 0 ^{o}C, then the reaction was brought to room temperature and let stir overnight. The reaction was brought back to 0 ^{o}C and slowly diluted with 50mL of deionized water. The reaction mixture was extracted with EtOAc 3 times, and the organic layers were washed with water, brine, dried over sodium sulfate, and concentrated on the rotovap to afford a viscous dark brown oil. The oil was taken up in minimal

DCM and purified by FCC eluting with DCM/methanol(1% NH_4OH) (98/2 → 95/5 → 93:7) to afford 1.8g (47% yield) of **4.C2** as a clear viscous oil, which settled to a cloudy amorphous solid over several weeks.

^{1}H NMR (500 MHz, $CDCl_3$) δ 8.76 (d, *J* = 4.5 Hz, 1H), 8.05 (d, *J* = 9.5 Hz, 1H), 7.48 (d, *J* = 3.4 Hz, 1H), 7.40 – 7.28 (m, 7H), 5.77 – 5.70 (m, 1H), 5.24 (bs, 1H), 4.96 – 4.89 (m, 2H), 4.46 (d, *J* = 11.6 Hz, 1H), 4.40 (d, *J* = 11.6 Hz, 1H), 3.91 (s, 3H), 3.41 (bs, 1H), 3.17– 3.15 (m, 1H), 3.08 (dd, *J* = 13.7, 10.1 Hz, 1H), 2.72 – 2.66 (m, 1H), 2.64 – 2.60 (m, 1H), 2.28 – 2.24 (m, 1H), 1.85 – 1.79 (m, 2H), 1.76 – 1.70 (m, 1H), 1.65 (bs, 1H), 1.54 – 1.47 (m, 1H).

^{13}C NMR (126 MHz, $CDCl_3$) δ 157.88, 147.70, 144.84, 144.68, 141.92, 137.96, 131.96, 128.49, 127.80, 127.73, 127.51, 121.84, 119.08, 114.37, 101.35, 81.06, 71.24, 60.42, 57.13, 55.80, 43.26, 40.06, 27.96, 27.84, 22.80.

MS (APCI) Calculated for $C_{27}H_{31}N_2O$ $[M+H]^+$: 415.2; Found: 415.1 m/z

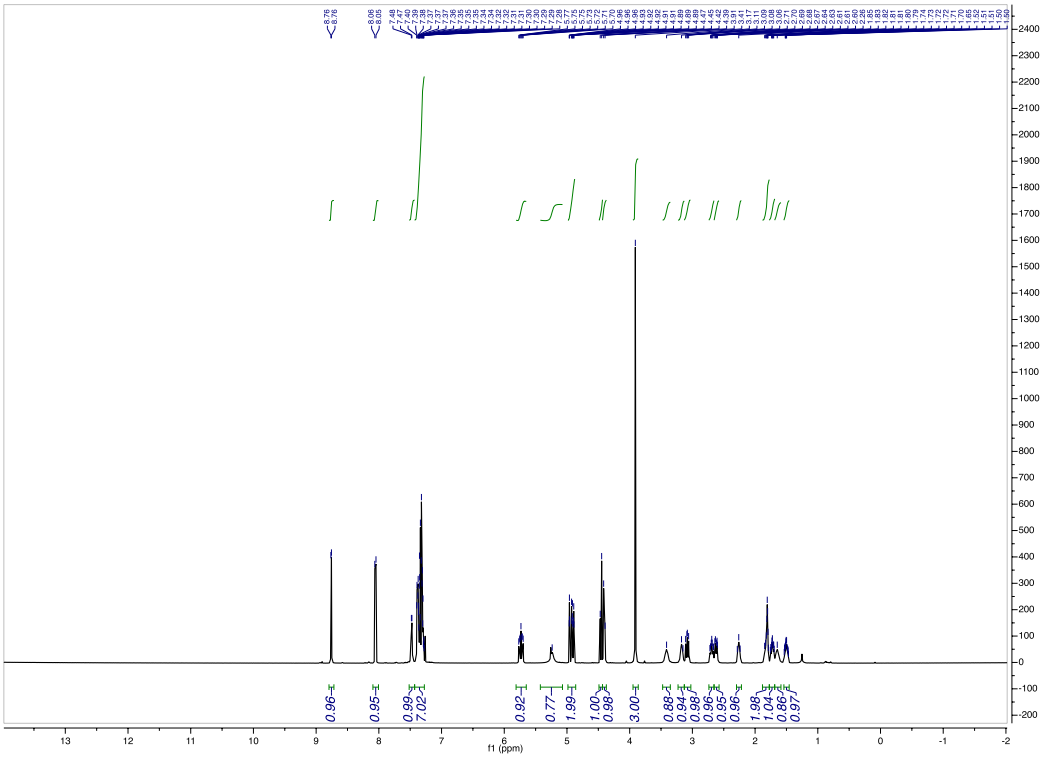

Figure 4.4.2. ^{1}H of 4.C2

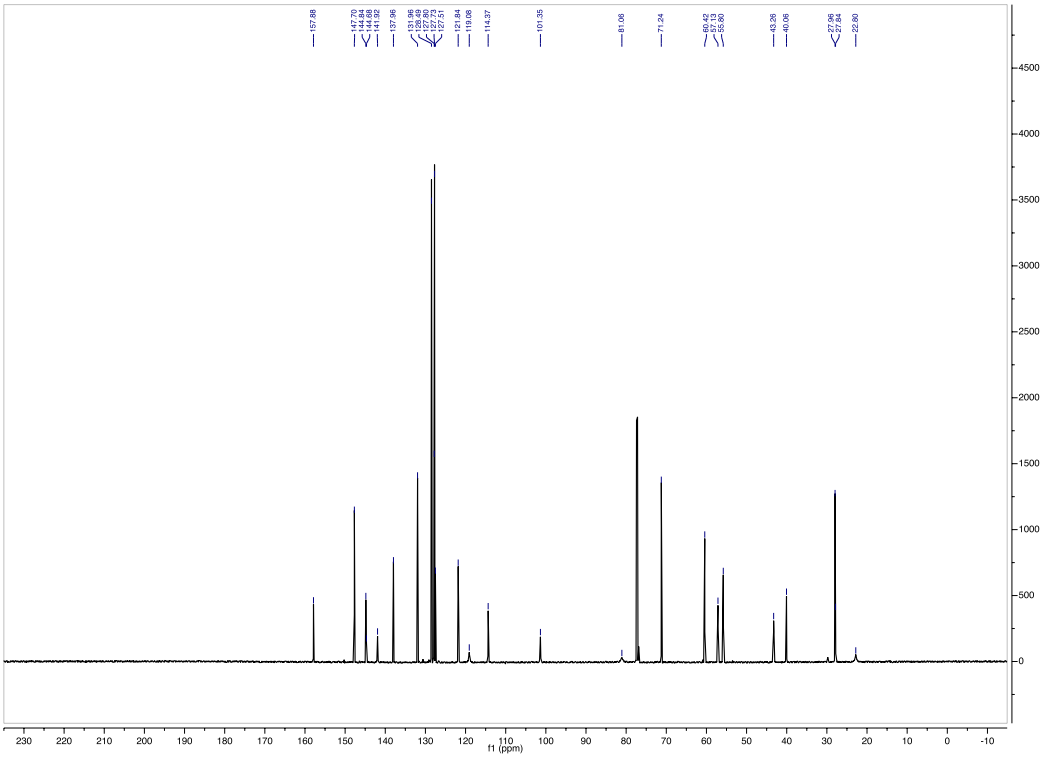

Figure 4.4.3. ^{13}C of 4.C2

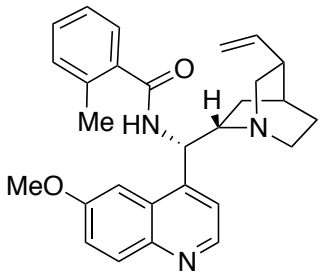

Figure 4.4.4. Catalyst 4.C6

N-((*S*)-(6-methoxyquinolin-4-yl)((1*S*,2*S*,4*S*,5*R*)-5-vinylquinuclidin-2-yl)methyl)-2-methylbenzamide (**4.C6**): **4.C4** (60mg, 0.19mmol, 1 equiv) was placed in a 2-dram vial equipped with a stir bar. DCM (2mL) was then added to the vial followed by TEA (52μL, 0.38mmol, 2 equiv) and then *o*-toluoyl chloride (27μL, 0.21mmol, 1.1 equiv). The reaction was stirred for 10 minutes at room temperature. The reaction was then diluted with DCM and washed with water, brine, dried over sodium sulfate, and concentrated on rotovap. The resulting crude oil was purified by FCC eluting with DCM/methanol(1% NH_4OH) (95/5 → 97/3) to afford 62mg (75% yield) **4.C6** as a white foam.

^{1}H NMR (500 MHz, $CDCl_3$) δ 8.76 (d, *J* = 4.6 Hz, 1H), 8.04 (d, *J* = 9.3 Hz, 1H), 7.77 (s, 1H), 7.46 (d, *J* = 4.1 Hz, 1H), 7.41 – 7.37 (m, 2H), 7.29 – 7.23 (m, 1H), 7.18 – 7.15 (m, 2H), 5.77 – 5.70 (m, 1H), 5.62 (bs, 1H), 5.03 – 4.99 (m, 2H), 3.35 – 3.20 (m, 3H), 2.85 – 2.73 (m, 2H), 2.40 – 2.33 (m, 4H), 1.75 – 1.55 (m, 4H), 1.25 (bs, 1H), 1.07 – 1.04 (m, 1H).

^{13}C NMR (126 MHz, $CDCl_3$) δ 170.01, 158.11, 147.75, 145.11, 140.78, 136.63, 135.97, 132.05, 131.13, 130.13, 128.36, 127.30, 125.81, 121.92, 119.11, 115.22, 102.14, 59.95, 55.96, 55.80, 41.25, 39.29, 29.84, 27.60, 27.54, 26.33, 20.11.

MS (APCI) Calculated for $C_{28}H_{32}N_3O$ $[M+H]^+$: 442.3; Found: 442.1 m/z

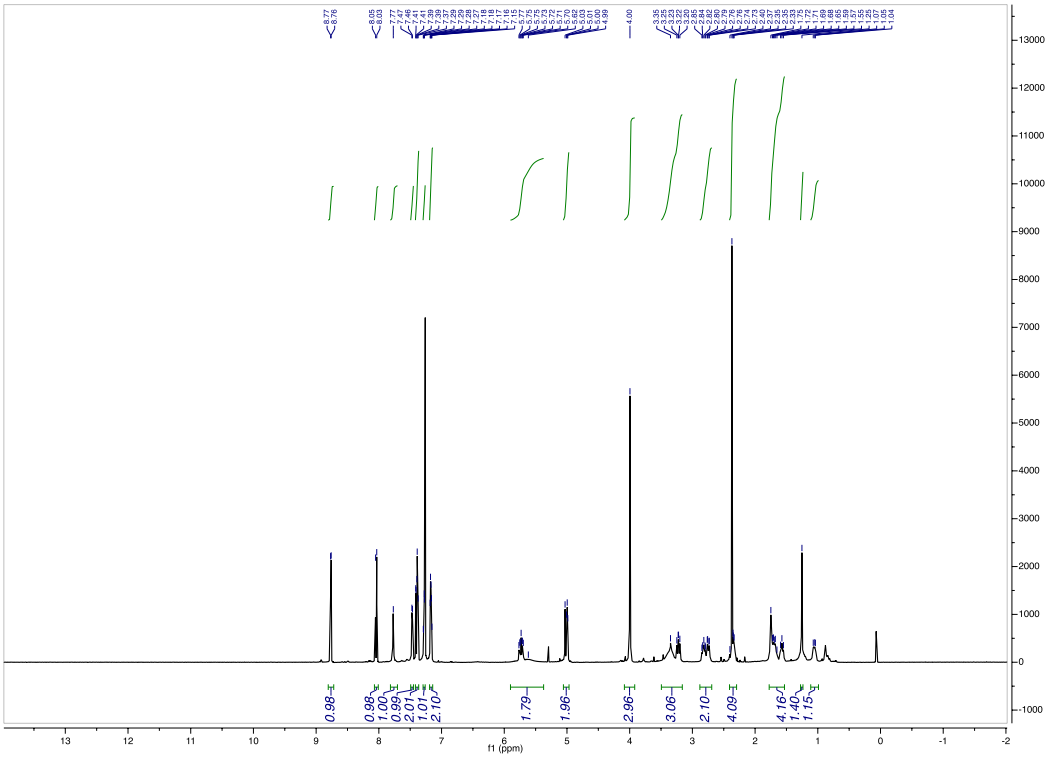

Figure 4.4.5. ^{1}H of 4.C6

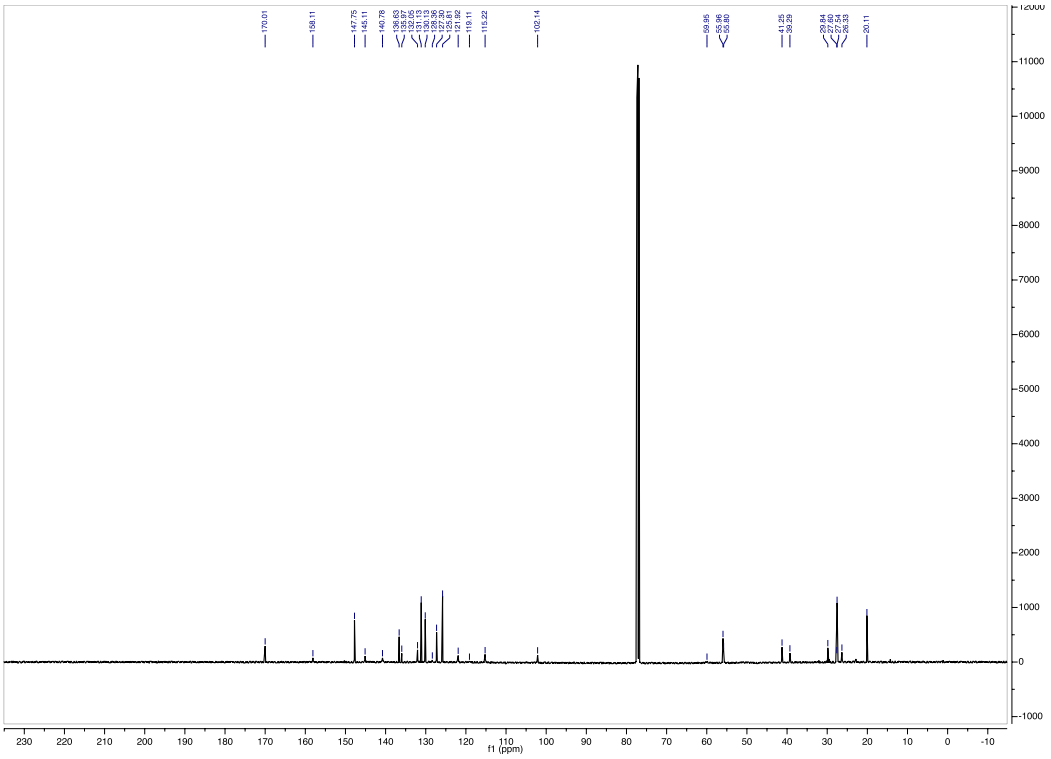

Figure 4.4.6. ^{13}C of 4.C6

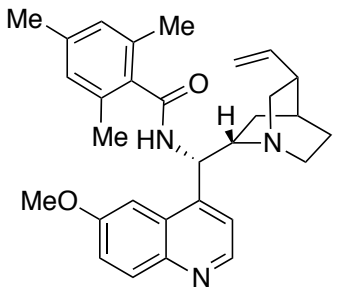

Figure 4.4.7. Catalyst 4.C7

N-((*S*)-(6-methoxyquinolin-4-yl)((1*S*,2*S*,4*S*,5*R*)-5-vinylquinuclidin-2-yl)methyl)-2,4,6-trimethylbenzamide (**4.C7**): The HCl salt of **4.C4** [see above] (1.0g, 2.3mmol, 1.0 equiv) was added to a 100mL r.b. flask equipped with a stir bar, followed by the addition of DCM (23mL). TEA (3.9mL, 28mmol, 12 equiv) was then added to the reaction flask with stirring at room temperature. 2,4,6-Trimethylbenzoyl chloride (462μL, 2.8mmol, 1.2 equiv) was added to the mixture and let stir for 30 minutes. The reaction was diluted with DCM (200mL), and the organic phase was washed with water and brine, dried over sodium sulfate, and concentrated on the rotovap to afford a brown oil. The crude brown oil was purified by FCC, eluting with DCM/methanol(1%NH_4OH) (97/3 → 95/5 → 93/7) to afford 801mg (74% yield) of **4.C7** as a white foam. The ^{1}H NMR of **4.C7** showed the presence of approximately a 4:1 mixture of rotamers (ratio varies with concentration). 1D NOE experiments (shown below) further supported that the minor peaks were in fact rotamers by the signals that arise from chemical exchange (same phase as excited frequency). The rotamers could not be resolved on the ^{1}H NMR spectrum, therefore only the peaks are tabulated. Normalizing one proton signal that represents two protons, one from each rotamer, to a value of 1 results in the sum of all integrals to be equal to 35 (the total number of protons on **4.C7**).

^{1}H NMR (500 MHz, $CDCl_3$) δ 8.74 (d), 8.10 – 7.99 (m), 7.86 (d, J = 2.7 Hz, $1H_{\text{major rotamer}}$), 7.57 (s), 7.52 (d, J = 4.2 Hz, $1H_{\text{minor rotamer}}$), 7.44 – 7.31 (m, 2H), 6.87 – 6.70 (m, 3H), 5.83 – 5.56 (m,

2H), 5.07 – 4.82 (m, 3H), 4.03 (s, $3H_{major\ rotamer}$), 3.84 (s, $3H_{minor\ rotamer}$), 3.58 – 3.30 (m), 3.29 – 3.02 (m), 2.85 – 2.59 (m), 2.35 – 2.00 (m), 1.82 – 1.36 (m), 1.17 – 0.92 (m).

^{13}C NMR (126 MHz, $CDCl_3$) δ 170.41, 158.21, 147.56, 145.38, 144.96, 141.27, 138.45, 134.61, 131.77, 128.86, 128.25, 122.14, 118.69, 114.79, 102.11, 60.39, 55.99, 55.93, 50.25, 41.36, 39.51, 27.95, 27.56, 26.39, 21.16, 19.15.

MS (APCI) Calculated for $C_{30}H_{36}N_3O_2$ $[M+H]^+$: 470.3; Found: 470.2 m/z

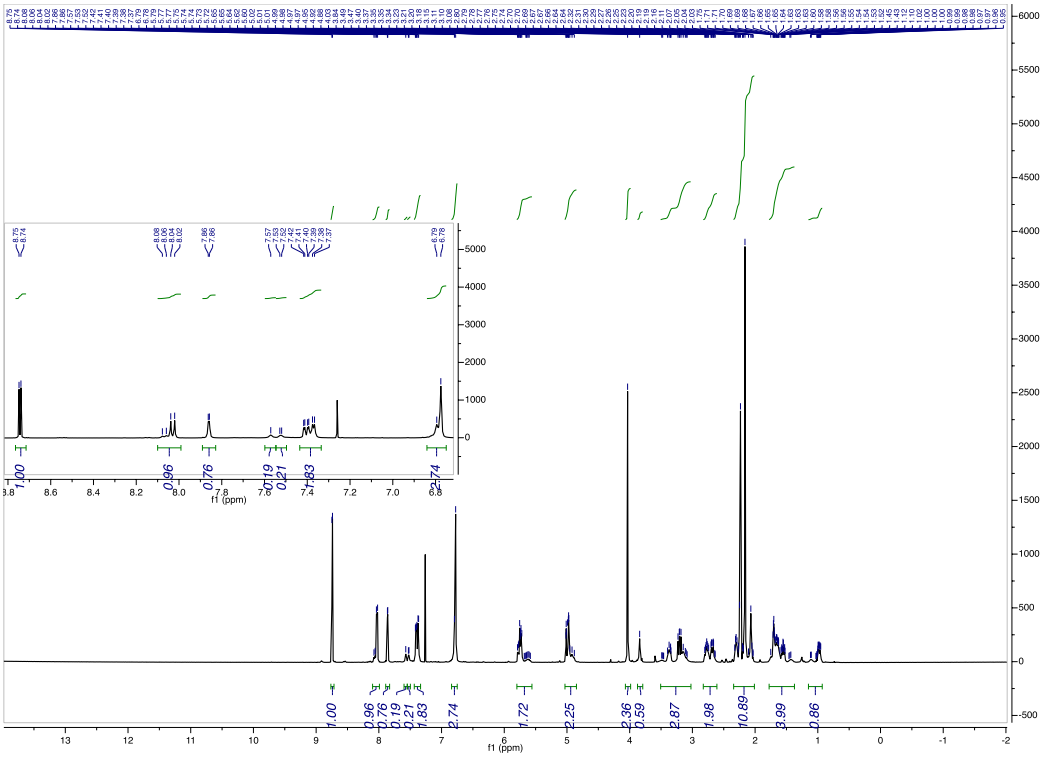

Figure 4.4.8. ^{1}H of 4.C7

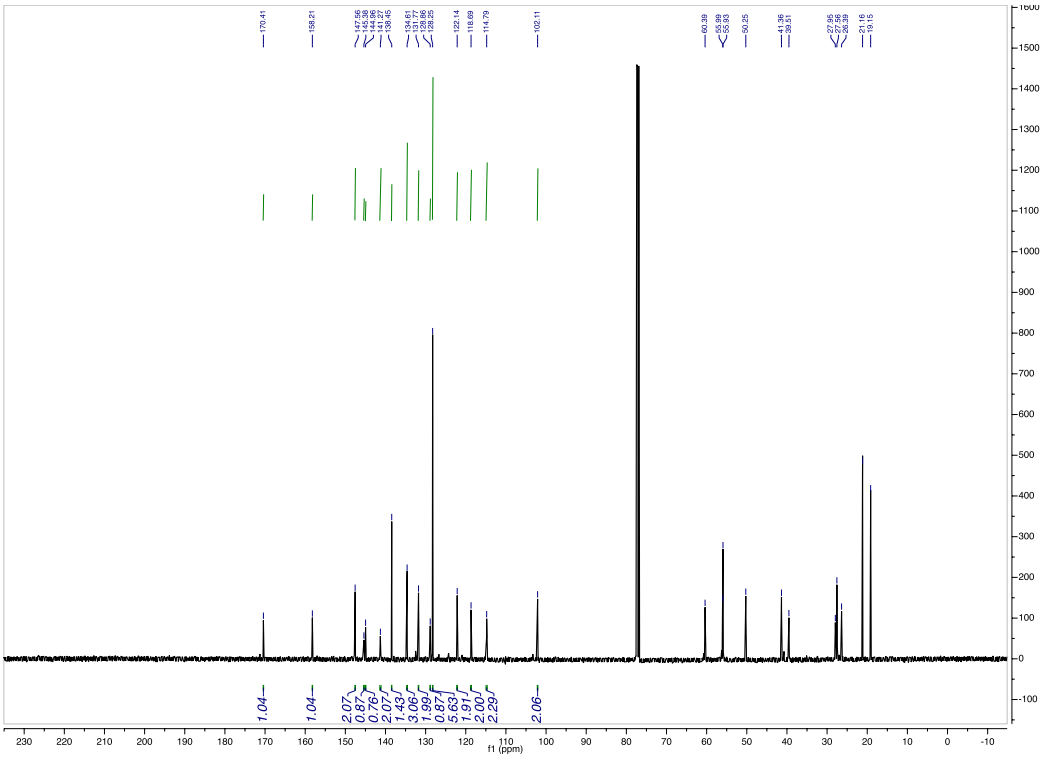

Figure 4.4.9. ^{13}C of 4.C7

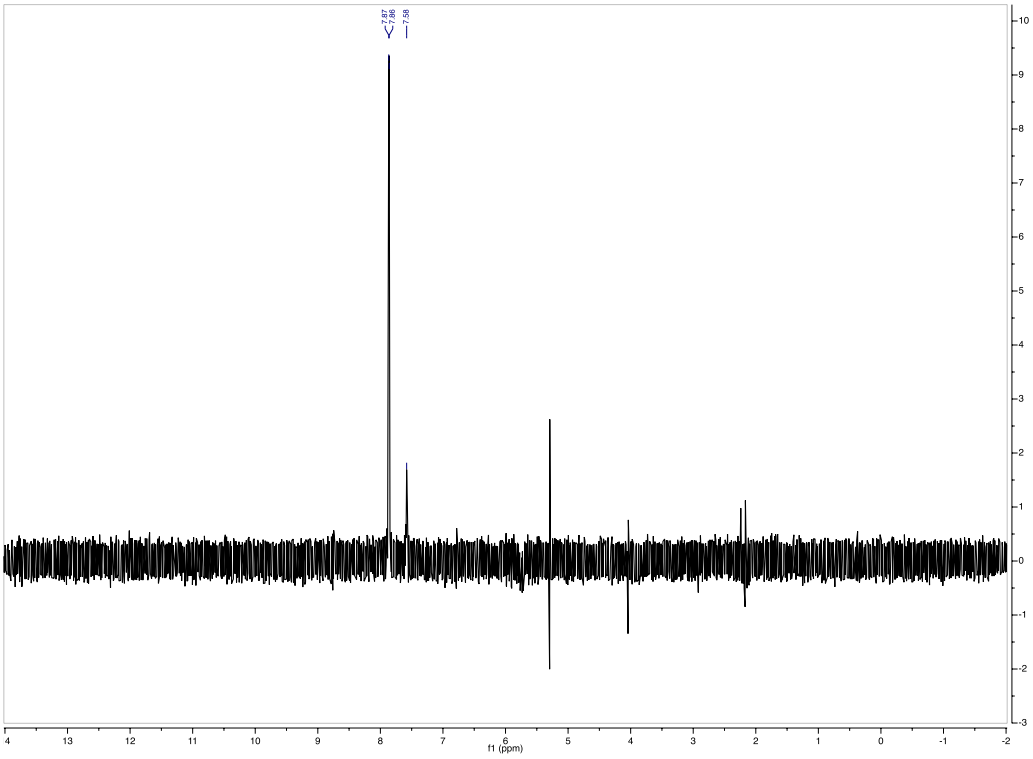

Figure 4.4.10. 1D NOESY (^{1}H/^{1}H) of 4.C7 irradiating at 7.87ppm

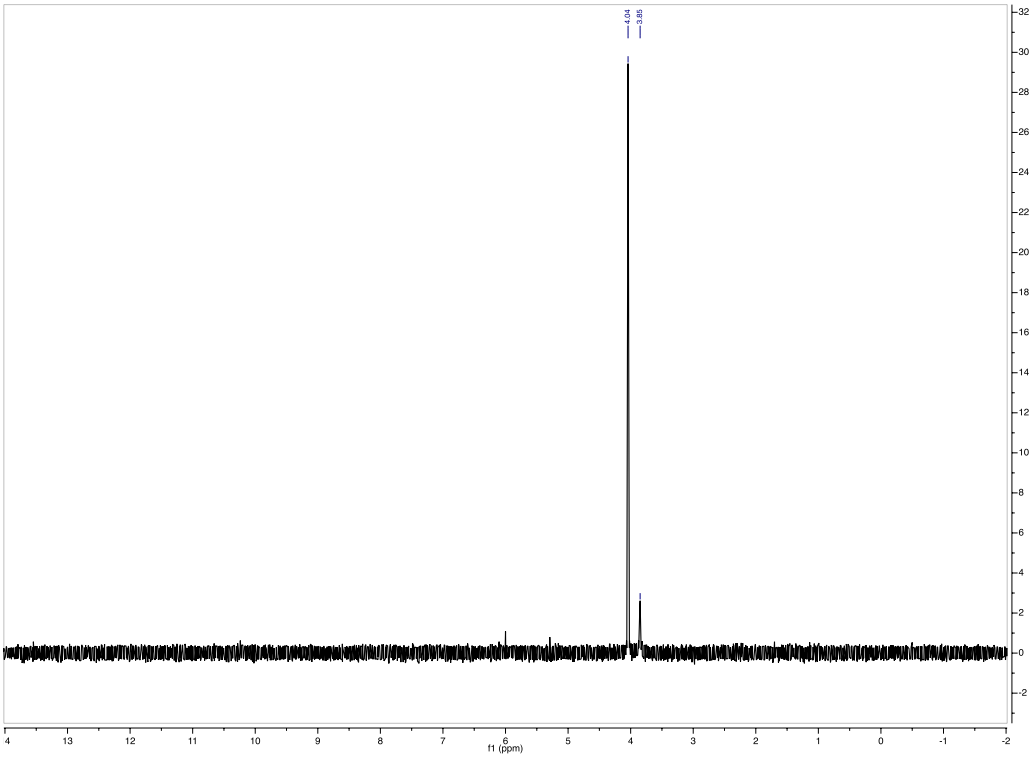

Figure 4.4.11. 1D NOESY (^{1}H/^{1}H) of 4.C7 irradiating at 4.04ppm

4.4.3 Effect of Catalyst Modifications

Catalyst modification reactions were run on a 0.05mmol scale, exposed to light, at room temperature. After 12 hours, 2.0 equiv of PIDA was added to the reaction and let stir at room temperature. After 30 minutes, an aliquot was removed from the crude reaction, diluted in hexanes, and analyzed by HPLC on a chiral stationary phase. The crude e.r.s were recorded. To maximize efficiency, the yields were not determined across this reaction scope.

Scheme 4.4.1. Hypothesis-Driven Catalyst Exploration

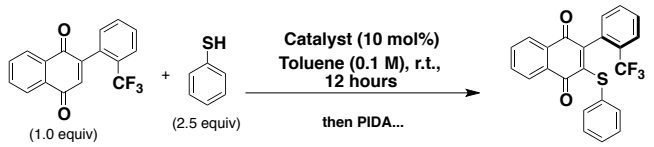

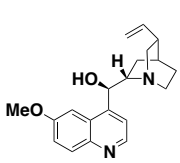
60 : 40 e.r.
ΔΔG = 0.239 kcal/mol
1.00 kJ/mol

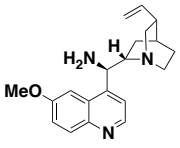
73 : 27 e.r.
ΔΔG = 0.583 kcal/mol
2.44 kJ/mol

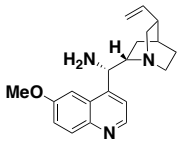
73 : 27 e.r.
ΔΔG = 0.583 kcal/mol
2.44 kJ/mol

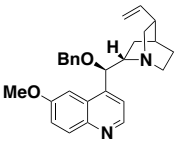
52 : 48 e.r.
ΔΔG = 0.057 kcal/mol
0.196 kJ/mol

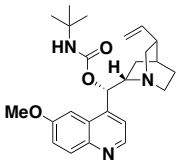
50 : 50 e.r.
ΔΔG = 0 kcal/mol
0 kJ/mol

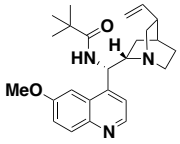
65 : 35 e.r.
ΔΔG = 0.363 kcal/mol
1.52 kJ/mol

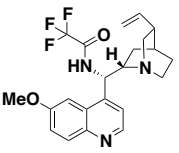
75 : 25 e.r.
ΔΔG = 0.644 kcal/mol
2.69 kJ/mol

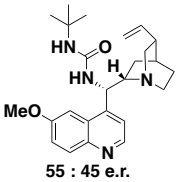
55 : 45 e.r.
ΔΔG = 0.118 kcal/mol
0.118 kJ/mol

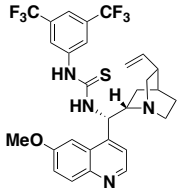
52 : 48 e.r.
ΔΔG = 0.057 kcal/mol
0.196 kJ/mol

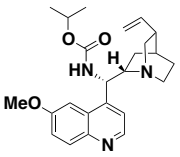
79 : 21 e.r.
ΔΔG = 0.777 kcal/mol
3.25 kJ/mol

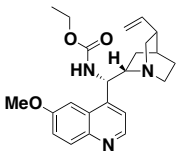
75 : 25 e.r.
ΔΔG = 0.644 kcal/mol
2.69 kJ/mol

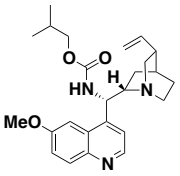
74 : 26 e.r.
ΔΔG = 0.613 kcal/mol
2.57 kJ/mol

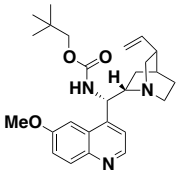
82 : 18 e.r.
ΔΔG = 0.889 kcal/mol
3.72 kJ/mol

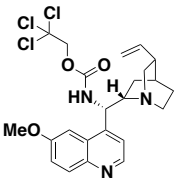
84 : 16 e.r.
ΔΔG = 0.972 kcal/mol
4.07 kJ/mol

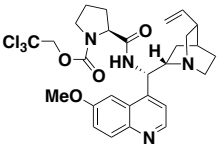
69 : 31 e.r.
ΔΔG = 0.469 kcal/mol
1.96 kJ/mol

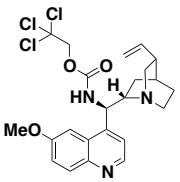
79 : 21 e.r.
ΔΔG = 0.777 kcal/mol
3.25 kJ/mol

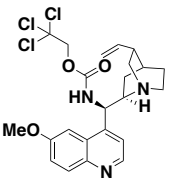
22 : 78 e.r.
ΔΔG = 0.741 kcal/mol
3.10 kJ/mol

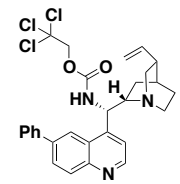
75 : 25 e.r.
ΔΔG = 0.644 kcal/mol
2.69 kJ/mol

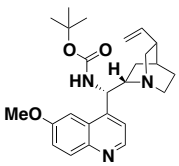
64 : 36 e.r.
ΔΔG = 0.337 kcal/mol
1.41 kJ/mol

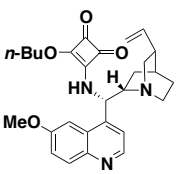
50 : 50 e.r.
ΔΔG = 0 kcal/mol
0 kJ/mol

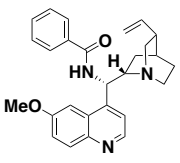
61 : 39 e.r.
ΔΔG = 0.259 kcal/mol
1.08 kJ/mol

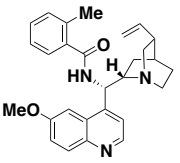
85 : 15 e.r.
ΔΔG = 1.01 kcal/mol
4.21 kJ/mol

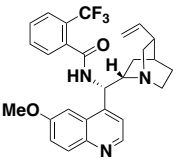
79 : 21 e.r.
ΔΔG = 0.775 kcal/mol
3.24 kJ/mol

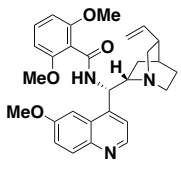
62 : 38 e.r.
ΔΔG = 0.276 kcal/mol
1.16 kJ/mol

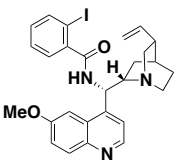
81 : 19 e.r.
ΔΔG = 0.856 kcal/mol
3.58 kJ/mol

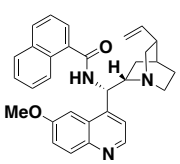
79 : 21 e.r.
ΔΔG = 0.764 kcal/mol
3.20 kJ/mol

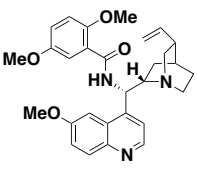
58 : 42 e.r.
ΔΔG = 0.188 kcal/mol
0.787 kJ/mol

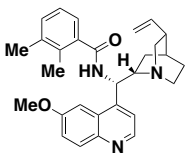
80 : 20 e.r.
ΔΔG = 0.829 kcal/mol
3.47 kJ/mol

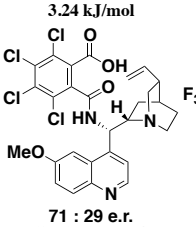
71 : 29 e.r.
ΔΔG = 0.523 kcal/mol
2.19 kJ/mol

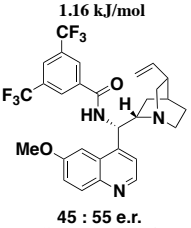
45 : 55 e.r.
ΔΔG = -0.126 kcal/mol
-0.525 kJ/mol

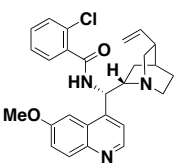
80 : 20 e.r.
ΔΔG = 0.804 kcal/mol
3.61 kJ/mol

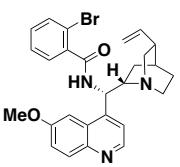
81 : 19 e.r.
ΔΔG = 0.863 kcal/mol
3.61 kJ/mol

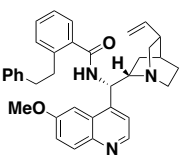
84 : 16 e.r.
ΔΔG = 0.983 kcal/mol
4.11 kJ/mol

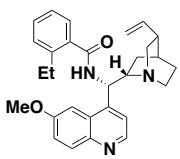
84 : 16 e.r.
ΔΔG = 0.974 kcal/mol
4.08 kJ/mol

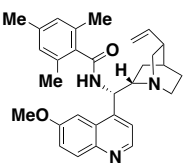
88 : 12 e.r.
ΔΔG = 1.19 kcal/mol
4.99 kJ/mol

4.4.4 Synthesis of Aryl-Naphthoquinone Atropisomers

General Procedure 1:

2-Bromo-1,4-dimethoxynaphthalene (500mg, 1.87 mmol, 1 equiv) was placed in a 20 mL scintillation vial with a Teflon screw cap and a stir bar followed by the addition of potassium carbonate (2.3 equiv), palladium(tetrakis)triphenylphosphine (0.05 equiv), and aryl-boronic acid (1.3 equiv). Dioxane (8 mL, degassed by bubbling with argon for 20 minutes) and deionized water (2 mL, degassed by bubbling with argon for 20 minutes) were added to the scintillation vial, and the vial was quickly purged with argon and capped tightly. The reaction was placed on a reaction block at 80 ^{o}C and stirred vigorously for 12 hours. The reaction was then cooled to room temperature and filtered thru a thick silica plug, eluting with DCM. The solvents were evaporated on a rotovap to afford a crude oil. The crude oil was then dissolved in MeCN (4 mL) and cooled to 0 ^{o}C with vigorous stirring. A solution of CAN (2.5 equiv) in deionized water (4 mL) was slowly added to the stirring solution via glass pipette. The added solution usually creates a dark cloud, which quickly changes the color of the solution to orange/yellow. After stirring for 2 hours, the reaction was diluted with EtOAc (4 mL), and let warm to r.t. over an hour. Once the reaction was complete by TLC, the mixture was further diluted with additional EtOAc and washed with water, brine, dried over sodium sulfate, and concentrated on a rotovap. The resulting crude oil was purified by FCC eluting with either a mixture of hexanes/EtOAc (95/5 → 90/10) or hexanes/DCM (90/10 → 80/20 → 70/30). When noted, naphthoquinones were also purified by recrystallization from DCM/hexanes.

Aryl-Naphthoquinone Substrates:

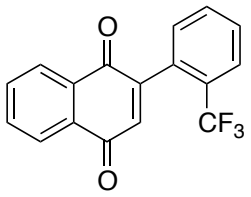

Figure 4.4.12. Substrate 4.1a

2-(2-(trifluoromethyl)phenyl)naphthalene-1,4-dione (**4.1a**): Followed General Procedure 1 with 2-trifluoromethylphenylboronic acid, purifying with hexanes/EtOAc (95/5 → 90/10) to afford 536mg (95%) **4.1a** as a yellow solid.

^{1}H NMR (400 MHz, $CDCl_3$) δ 8.18 – 8.12 (m, 2H), 7.84 – 7.75 (m, 3H), 7.67 – 7.55 (m, 2H), 7.34 – 7.28 (m, 1H), 6.94 (s, 1H).

^{13}C NMR (101 MHz, $CDCl_3$) δ 184.73, 183.95, 148.56, 136.85 (q, J = 1.6 Hz), 134.24, 134.20, 132.24, 132.19 (q, J = 2.2 Hz), 132.00, 131.70 (q, J = 1.0 Hz), 130.73, 129.43, 129.10 (q, J = 30 Hz), 127.19, 126.65 (q, J = 4.8 Hz), 126.45, 124.12 (q, J = 274 Hz).

^{19}F NMR (376 MHz, $CDCl_3$) δ -56.83.

MS (APCI) Calculated for $C_{17}H_{10}F_3O_2$ $[M+H]^+$: 303.1; Found: 303.1 m/z

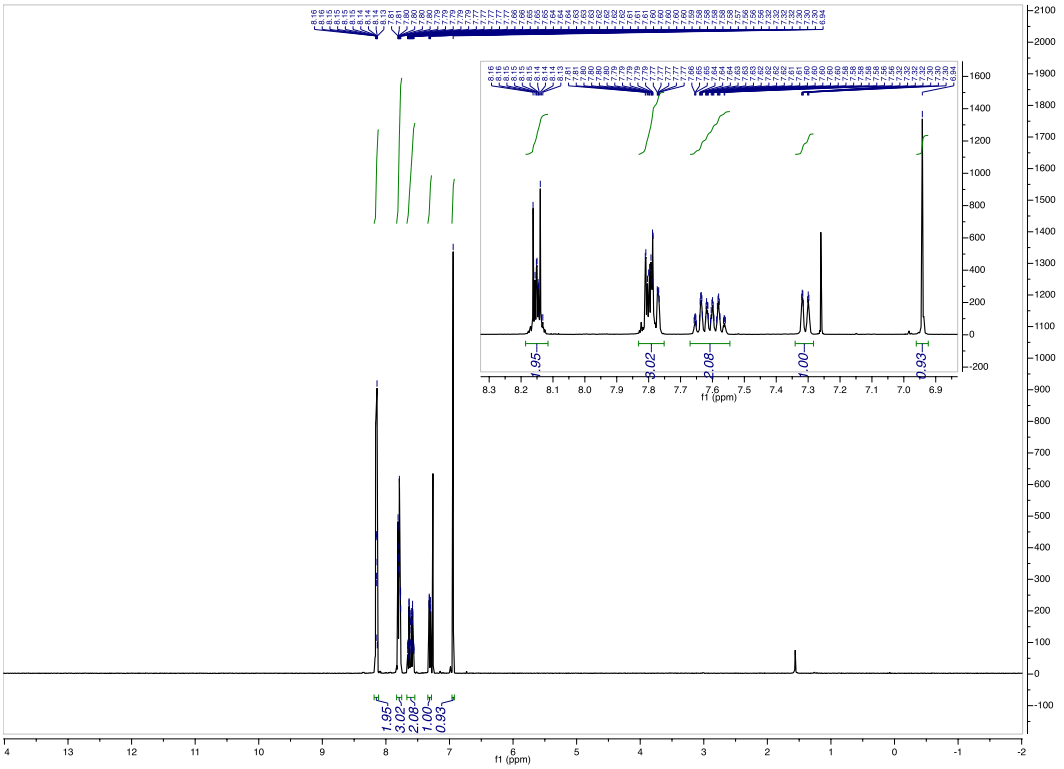

Figure 4.4.13. ^{1}H of 4.1a

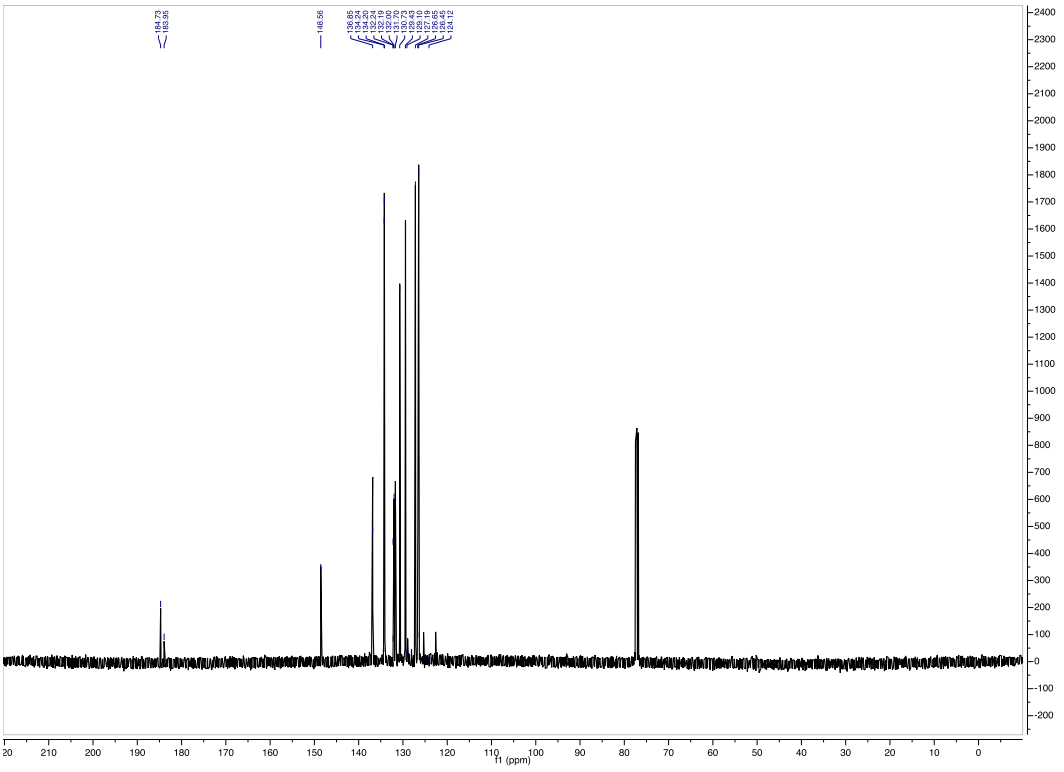

Figure 4.4.14. ^{13}C of 4.1a

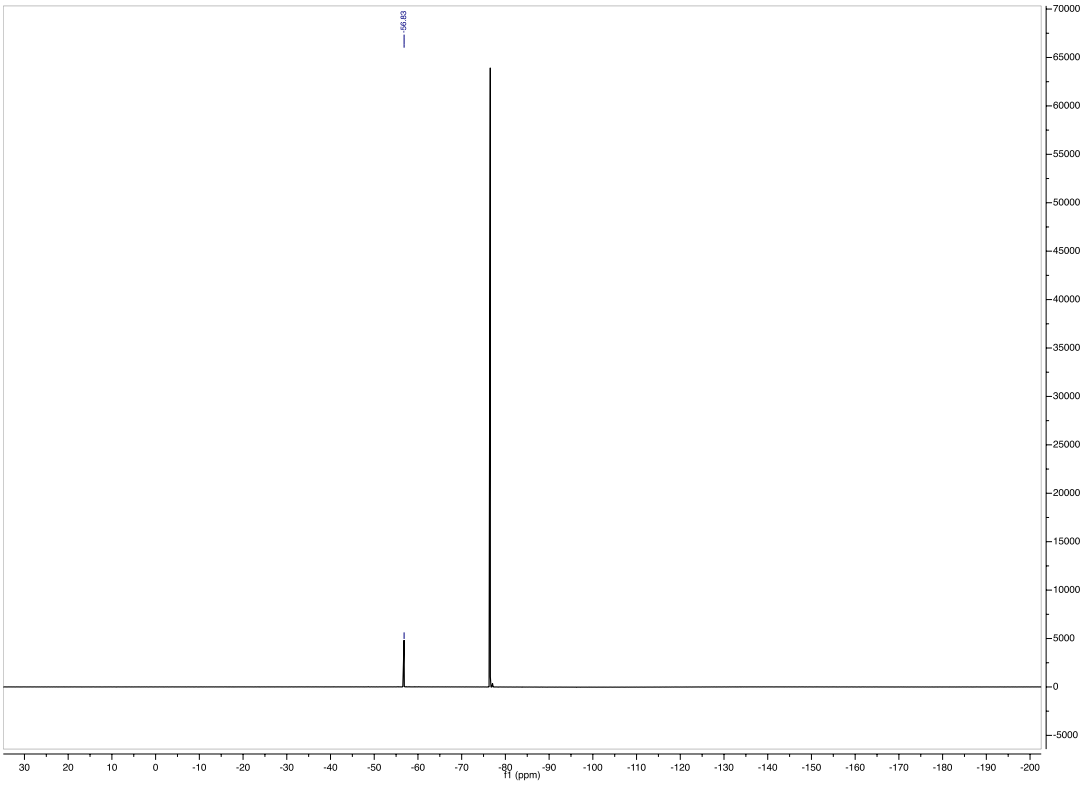

Figure 4.4.15. ^{19}F of 4.1a

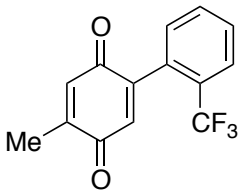

Figure 4.4.16. Substrate 4-methyl-2'-(trifluoromethyl)-[1,1'-biphenyl]-2,5-dione

4-methyl-2'-(trifluoromethyl)-[1,1'-biphenyl]-2,5-dione: Followed General Procedure 1 with 2-trifluoromethylphenylboronic acid using the following modifications: 1-bromo-2,5-dimethoxy-4-methylbenzene was used instead of 2-bromo-1,4-dimethoxynaphthalene. The resulting crude oil was purified from hexanes/EtOAc (95/5 →90/10) to afford 430mg (86% yield) 4-methyl-2'-(trifluoromethyl)-[1,1'-biphenyl]-2,5-dione as a yellow solid.

^{1}H NMR (500 MHz, $CDCl_3$) δ 7.74 (d, *J* = 7.5 Hz, 1H), 7.61 (t, *J* = 7.1 Hz, 1H), 7.55 (t, *J* = 7.1 Hz, 1H), 7.22 (d, *J* = 7.5 Hz, 1H), 6.73 – 6.71 (m, 2H), 2.13 (d, *J* = 1.5 Hz, 3H).

^{13}C NMR (101 MHz, $CDCl_3$) δ 187.51, 185.98, 146.17, 146.10, 134.44 (q, *J* = 1.5 Hz), 133.33, 131.50, 131.32, 130.63, 129.26, 128.95 (q, *J* = 30 Hz), 126.46 (q, *J* = 4.8 Hz), 123.76 (q, *J* = 274 Hz), 15.66.

^{19}F NMR (376 MHz, $CDCl_3$) δ -56.82.

MS (APCI) Calculated for $C_{14}H_{10}F_3O_2$ $[M+H]^+$: 267.1; Found: 267.1 m/z

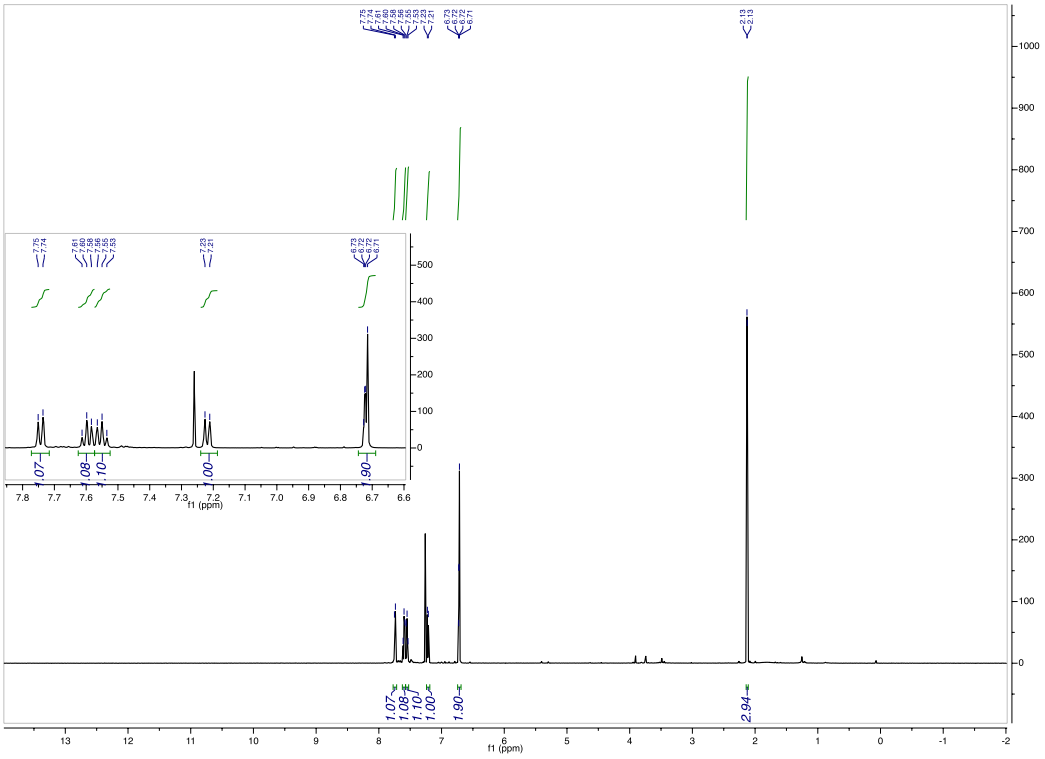

Figure 4.4.17. ^{1}H of 4-methyl-2'-(trifluoromethyl)-[1,1'-biphenyl]-2,5-dione

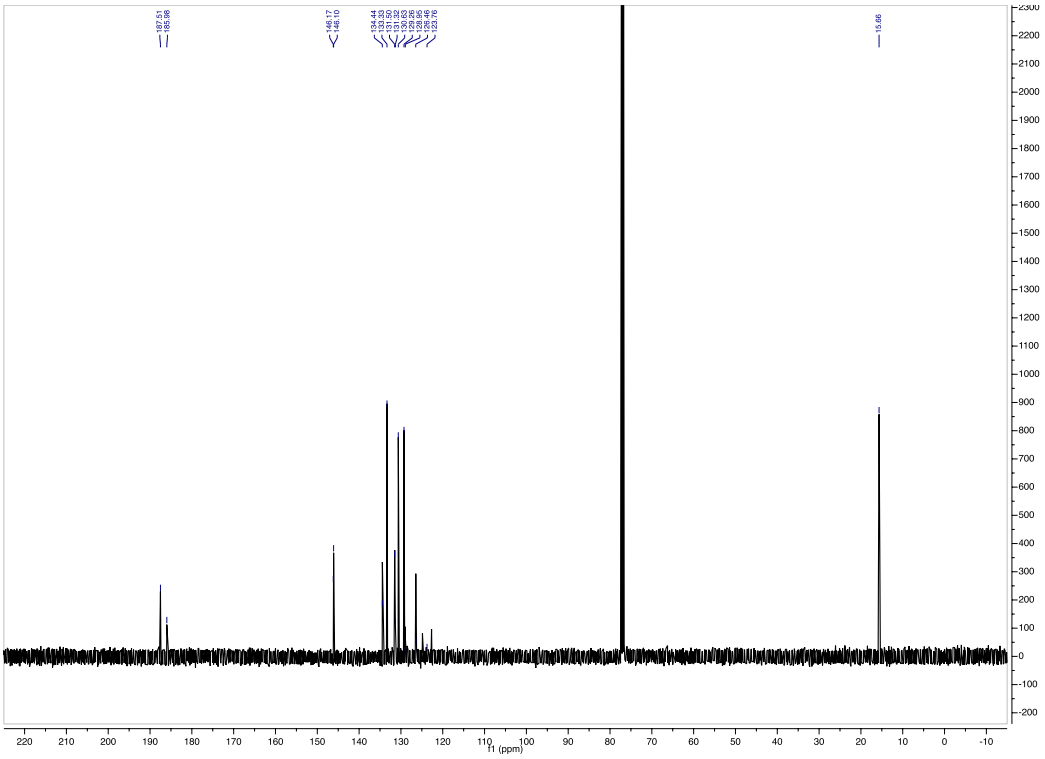

Figure 4.4.18. ^{13}C of 4-methyl-2'-(trifluoromethyl)-[1,1'-biphenyl]-2,5-dione

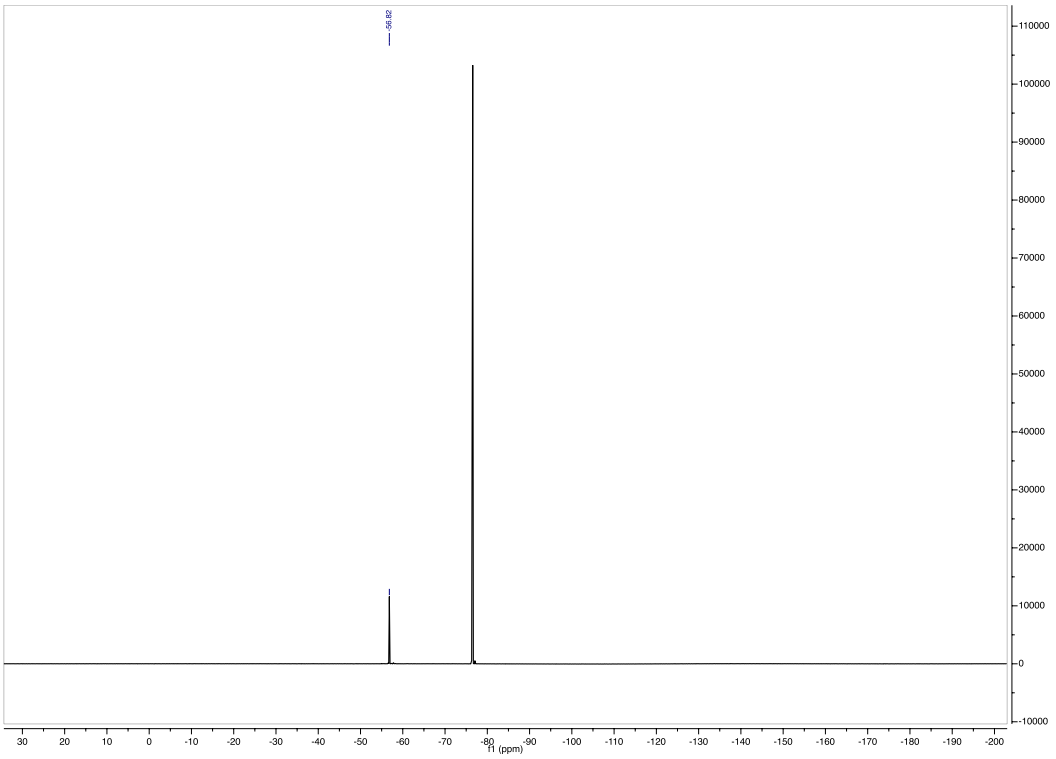

Figure 4.4.19. ^{19}F of 4-methyl-2'-(trifluoromethyl)-[1,1'-biphenyl]-2,5-dione

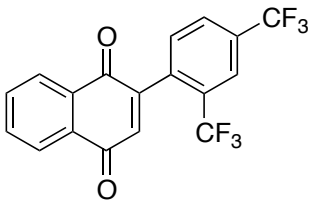

Figure 4.4.20. Substrate 2-(2,4-bis(trifluoromethyl)phenyl)naphthalene-1,4-dione

2-(2,4-bis(trifluoromethyl)phenyl)naphthalene-1,4-dione: Followed General Procedure 1 using (2,4-bis(trifluoromethyl)phenyl)boronic acid. Purified by FCC (hexanes/EtOAc = 98/2 → 85/15) to obtain 578mg (84% yield) 2-(2,4-bis(trifluoromethyl)phenyl)naphthalene-1,4-dione as a yellow solid.

^{1}H NMR (500 MHz, $CDCl_3$) δ 8.20 – 8.13 (m, 2H), 8.04 (s, 1H), 7.91 (d, *J* = 7.8 Hz, 1H), 7.86 – 7.79 (m, 2H), 7.48 (d, *J* = 8.0 Hz, 1H), 6.95 (s, 1H).

^{13}C NMR (126 MHz, $CDCl_3$) δ 184.23, 183.49, 147.12, 137.15 (q, *J* = 1.4 Hz), 135.93, 134.51, 134.46, 132.15, 132.02 (q, *J* = 33.7 Hz), 131.76, 131.75, 130.15 (q, *J* = 31.7 Hz), 128.63 (q, *J* = 3.4 Hz), 127.27, 126.64, 123.93 (m), 123.23 (q, *J* = 273 Hz), 123.17 (q, *J* = 274 Hz).

^{19}F NMR (470 MHz, $CDCl_3$) δ -57.26, -61.29.

MS (APCI) Calculated for $C_{18}H_9F_6O_2$ $[M+H]^+$: 371.1; Found: 370.9 m/z

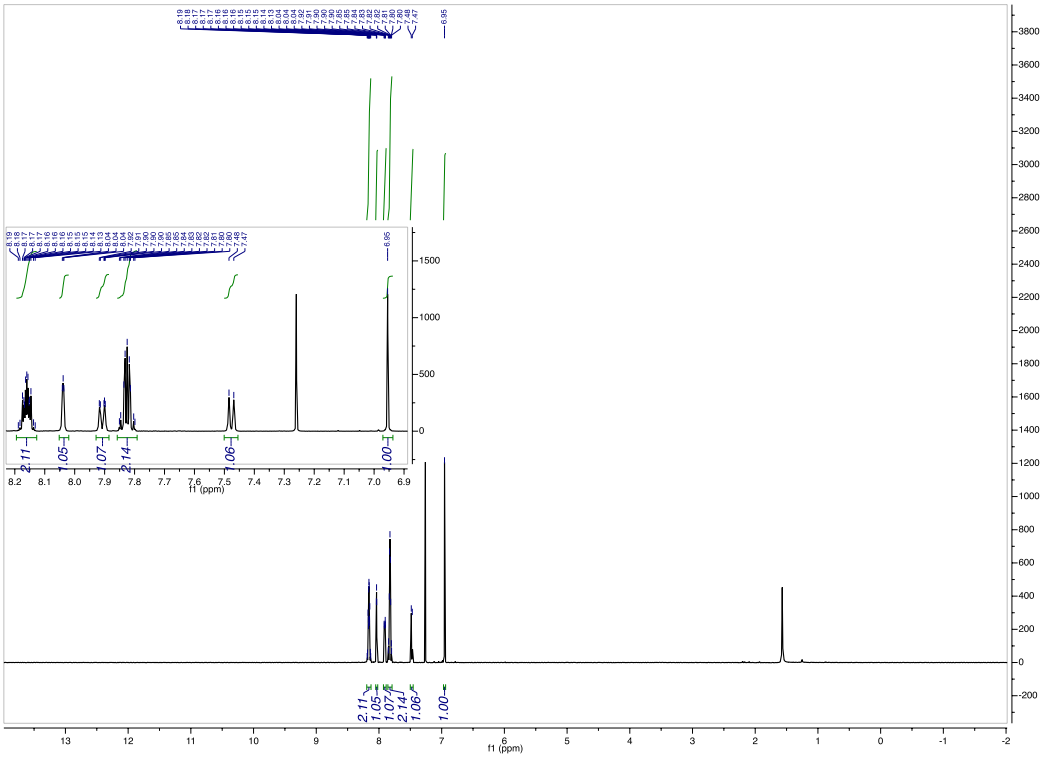

Figure 4.4.21. ^{1}H of 2-(2,4-bis(trifluoromethyl)phenyl)naphthalene-1,4-dione

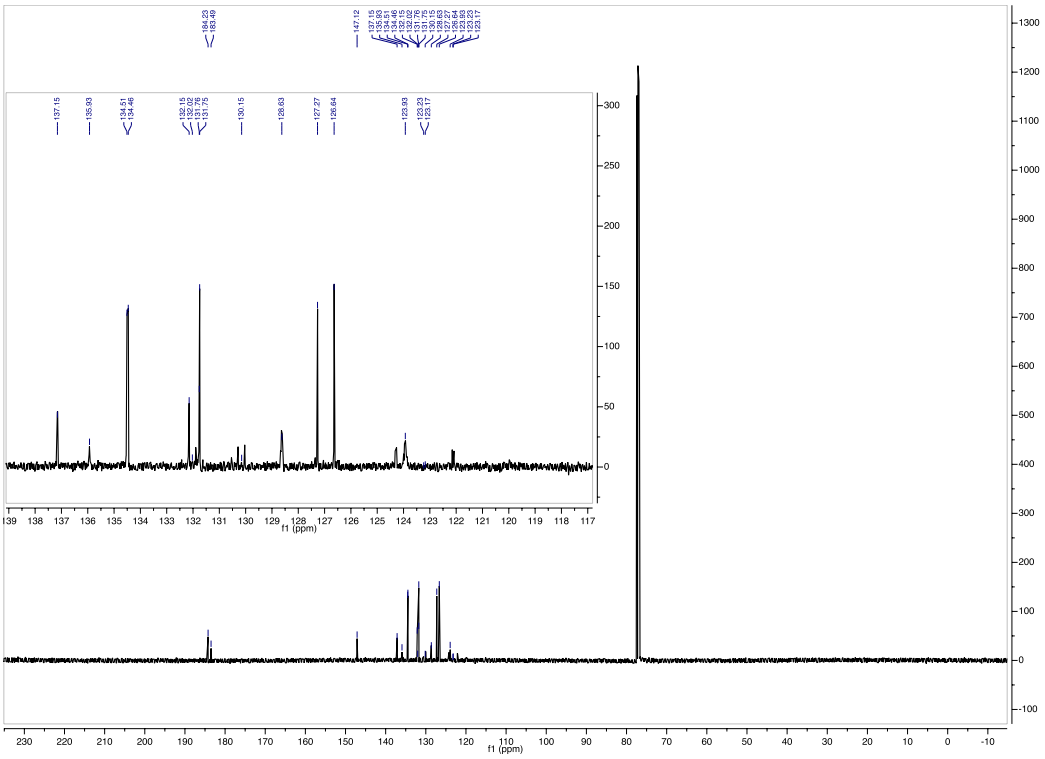

Figure 4.4.22. ^{13}C of 2-(2,4-bis(trifluoromethyl)phenyl)naphthalene-1,4-dione

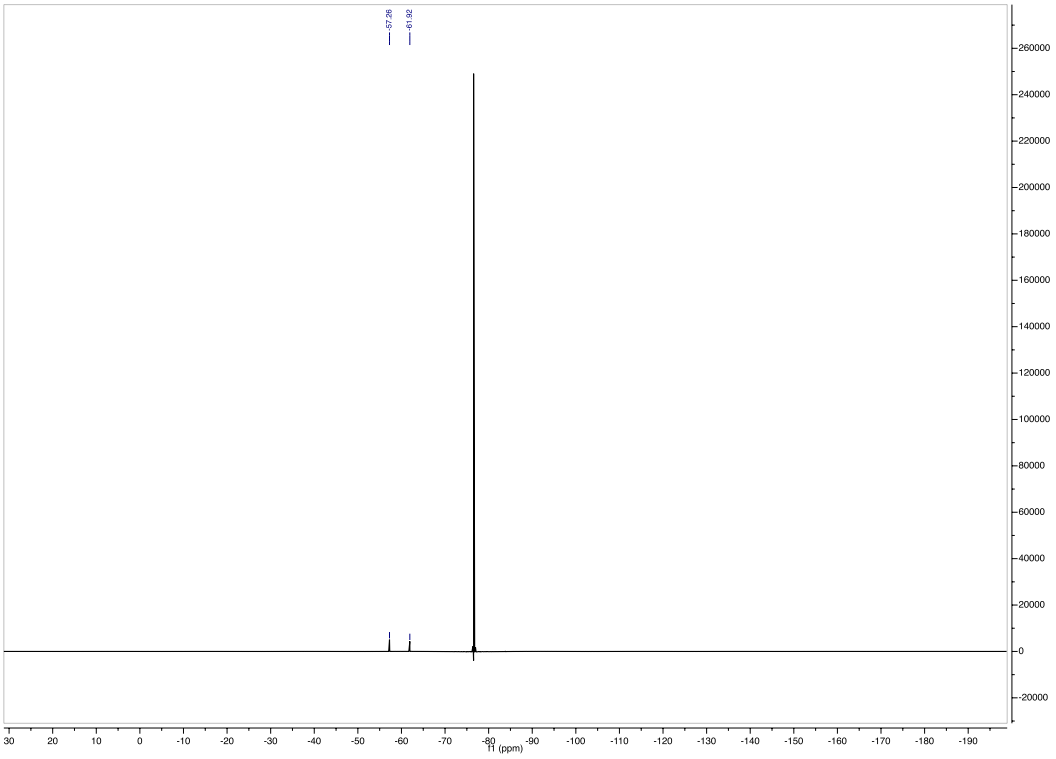

Figure 4.4.23. ^{19}F of 2-(2,4-bis(trifluoromethyl)phenyl)naphthalene-1,4-dione

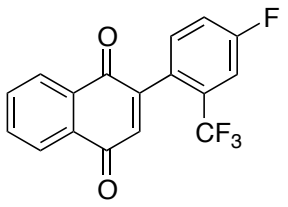

Figure 4.4.24. Substrate 2-(4-fluoro-2-(trifluoromethyl)phenyl)naphthalene-1,4-dione

2-(4-fluoro-2-(trifluoromethyl)phenyl)naphthalene-1,4-dione: Followed General Procedure 1 using (4-fluoro-2-(trifluoromethyl)phenyl)boronic acid. Recrystallized from DCM/hexanes to obtain 308mg (51% yield) 2-(4-fluoro-2-(trifluoromethyl)phenyl)naphthalene-1,4-dione as fine yellow crystals.

^{1}H NMR (500 MHz, $CDCl_3$) δ 8.19 – 8.12 (m, 2H), 7.84 – 7.77 (m, 2H), 7.49 (dd, *J* = 8.8, 2.5 Hz, 1H), 7.37 – 7.28 (m, 2H), 6.94 (s, 1H).

^{13}C NMR (126 MHz, $CDCl_3$) δ 184.53, 183.83, 162.63 (d, *J* = 251 Hz), 147.51, 137.27, 134.31, 133.00 (d, *J* = 8.1 Hz), 132.20, 131.89, 131.18 (qd, *J* = 32, 7.6 Hz), 128.19 (m), 127.21, 126.50, 123.06 (qd, *J* = 274, 2.5 Hz), 118.91 (d, *J* = 21 Hz), 114.47 (dq, *J* = 25, 4.8 Hz).

^{19}F NMR (470 MHz, $CDCl_3$) δ -57.35, -108.74 (td, *J* = 7.9, 5.6 Hz).

MS (APCI) Calculated for $C_{17}H_9F_4O_2$ $[M+H]^+$: 321.1; Found: 321.1 m/z

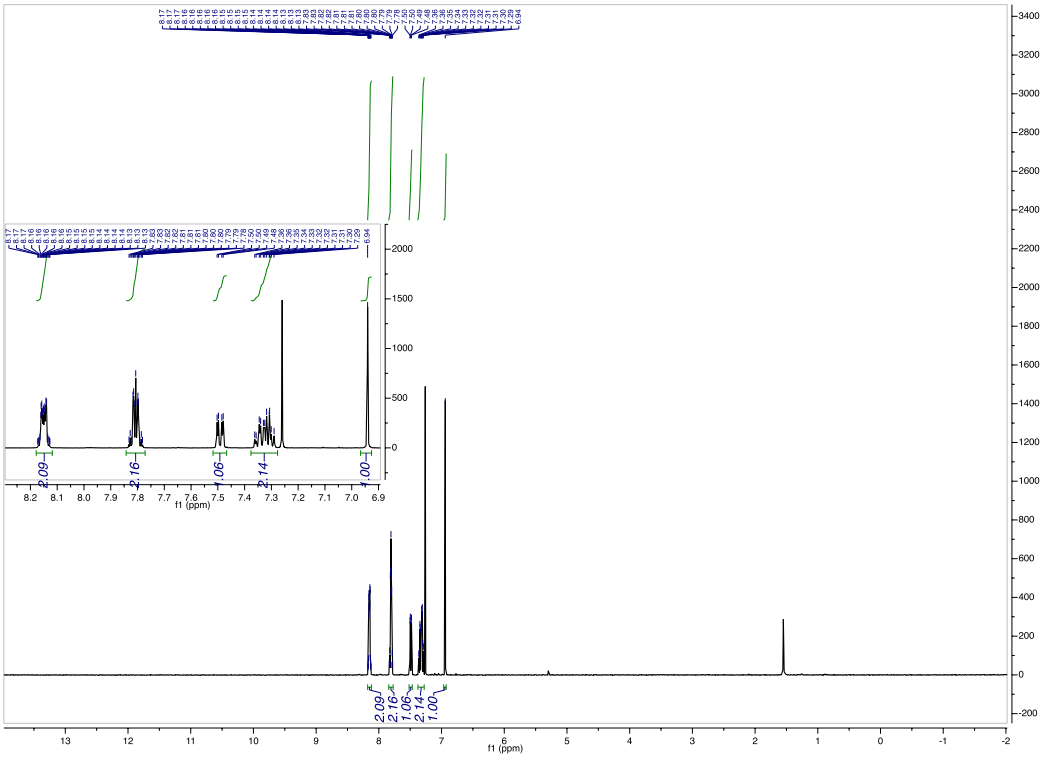

Figure 4.4.25. ^{1}H of 2-(4-fluoro-2-(trifluoromethyl)phenyl)naphthalene-1,4-dione

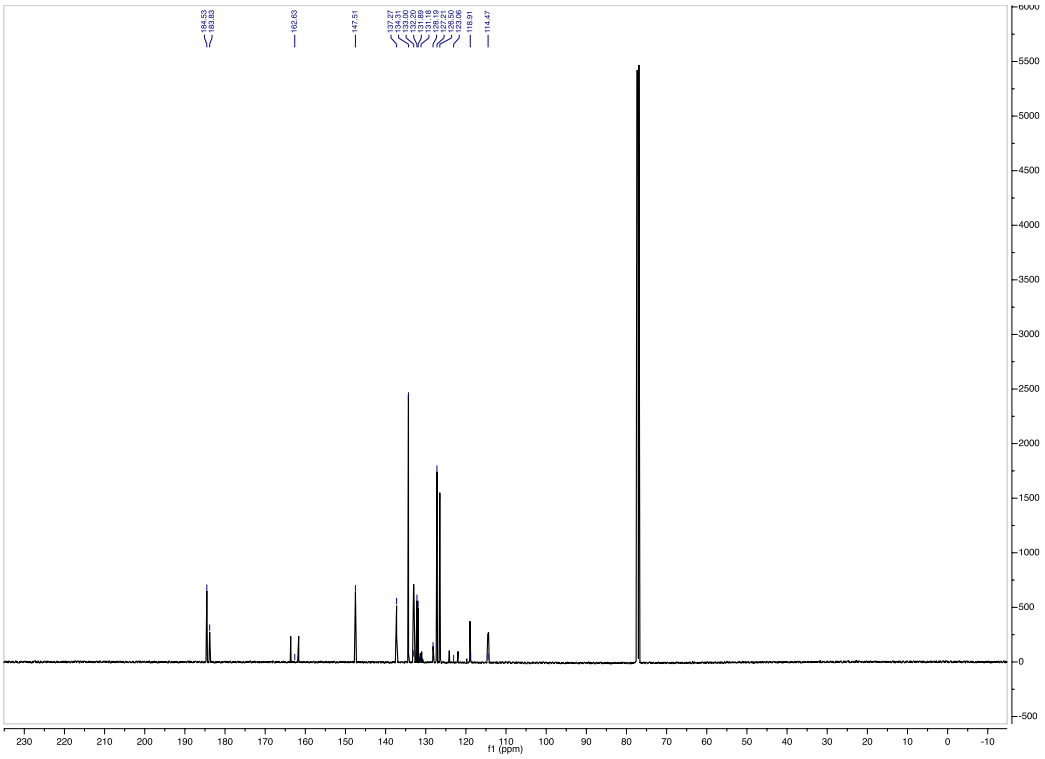

Figure 4.4.26. ^{13}C of 2-(4-fluoro-2-(trifluoromethyl)phenyl)naphthalene-1,4-dione

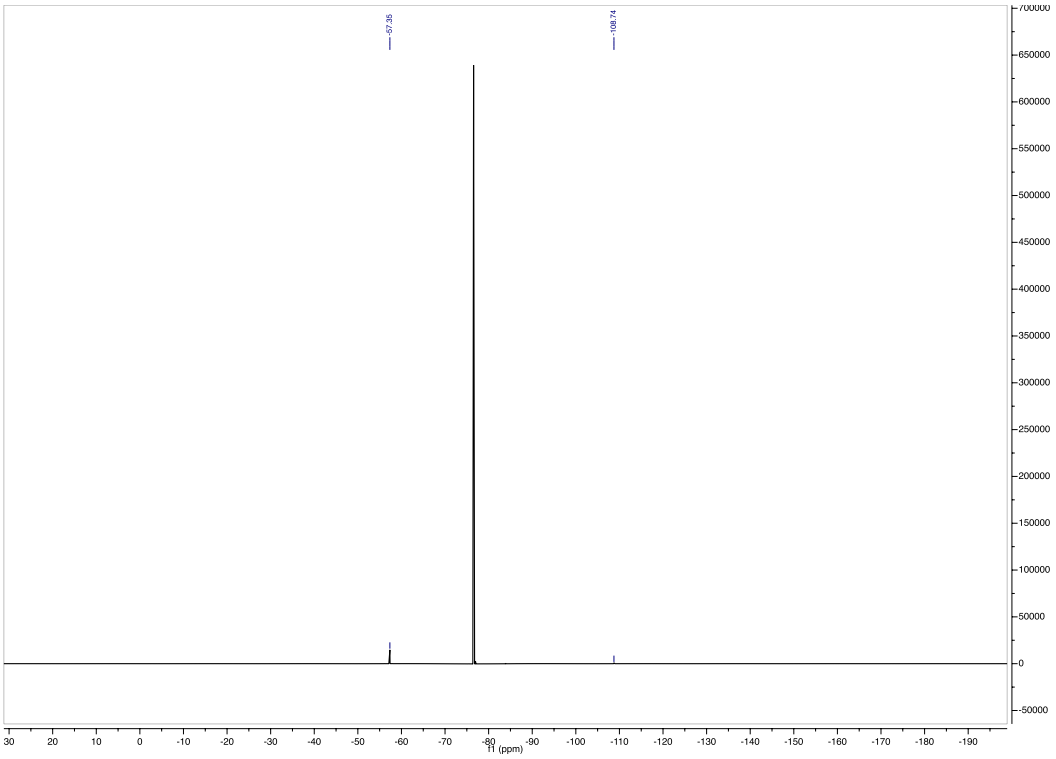

Figure 4.4.27. ^{19}F of 2-(4-fluoro-2-(trifluoromethyl)phenyl)naphthalene-1,4-dione

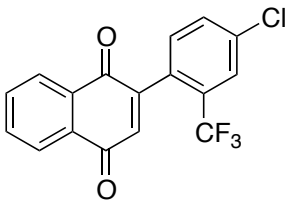

Figure 4.4.28. Substrate 2-(4-chloro-2-(trifluoromethyl)phenyl)naphthalene-1,4-dione

2-(4-chloro-2-(trifluoromethyl)phenyl)naphthalene-1,4-dione: Followed General Procedure 1 using (4-chloro-2-(trifluoromethyl)phenyl)boronic acid. Purified by FCC (hexanes/EtOAc = 98/2 → 85/15) to obtain 376mg (60% yield) 2-(4-chloro-2-(trifluoromethyl)phenyl)naphthalene-1,4-dione as a yellow solid.

^{1}H NMR (500 MHz, $CDCl_3$) δ 8.18 – 8.12 (m, 2H), 7.84 – 7.78 (m, 2H), 7.77 (d, *J* = 2.1 Hz, 1H), 7.61 (ddd, *J* = 8.3, 2.1, 0.6 Hz, 1H), 7.26 (d, *J* = 8.5 Hz, 1H), 6.93 (s, 1H).

^{13}C NMR (126 MHz, $CDCl_3$) δ 184.46, 183.69, 147.44, 137.12, 135.80, 134.36, 134.35, 132.24, 132.18, 131.91, 131.86, 130.69 (q, *J* = 31.3 Hz), 130.61 (q, *J* = 1.9 Hz), 127.23, 127.09 (q, *J* = 4.8 Hz), 126.54, 123.13 (q, *J* = 274 Hz).

^{19}F NMR (470 MHz, $CDCl_3$) δ -57.24.

MS (APCI) Calculated for $C_{17}H_9ClF_3O_2$ $[M+H]^+$: 337.0; Found: 337.1 m/z

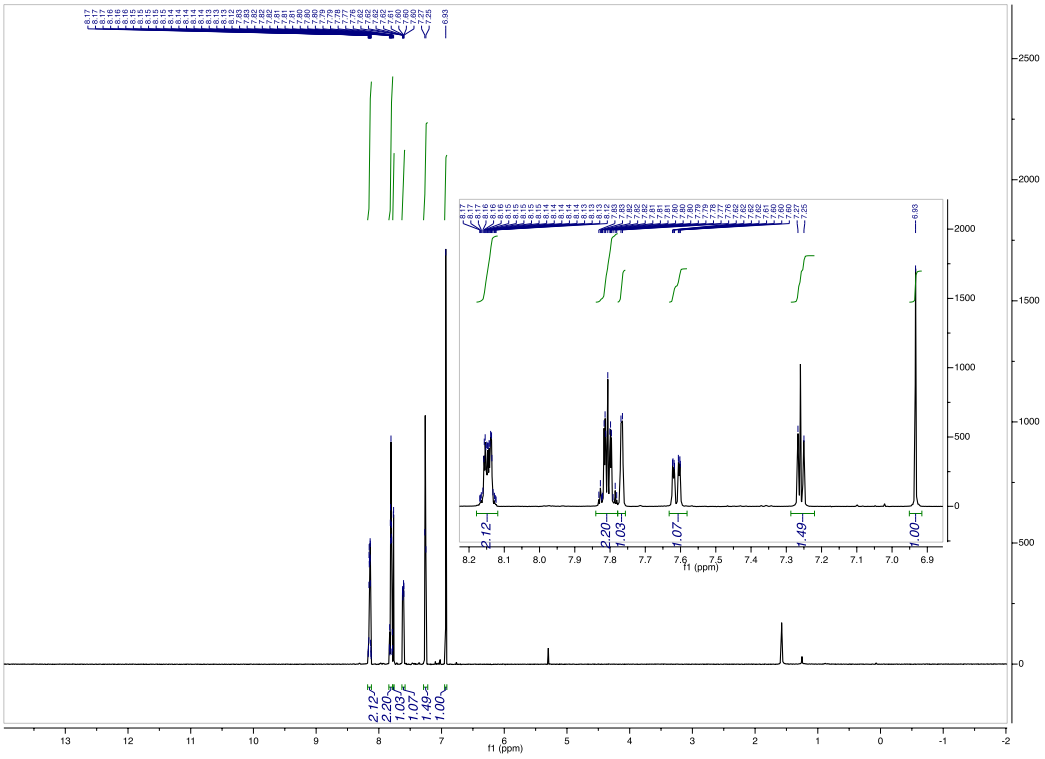

Figure 4.4.29. ^{1}H of 2-(4-chloro-2-(trifluoromethyl)phenyl)naphthalene-1,4-dione

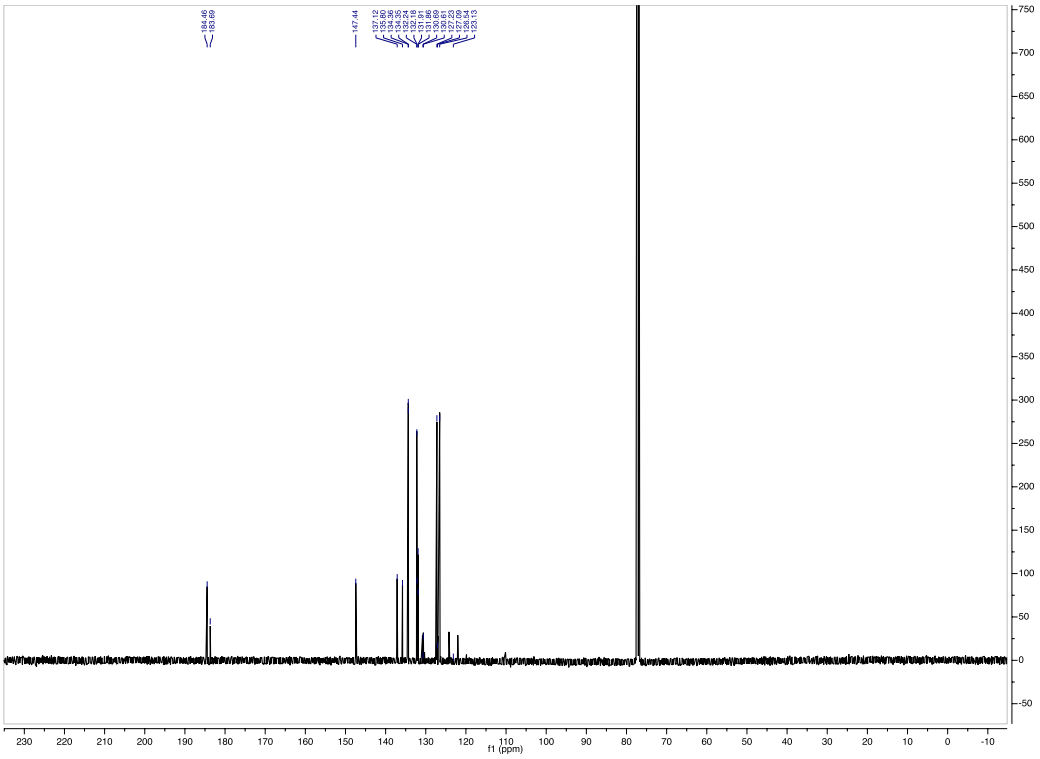

Figure 4.4.30. ^{13}C of 2-(4-chloro-2-(trifluoromethyl)phenyl)naphthalene-1,4-dione

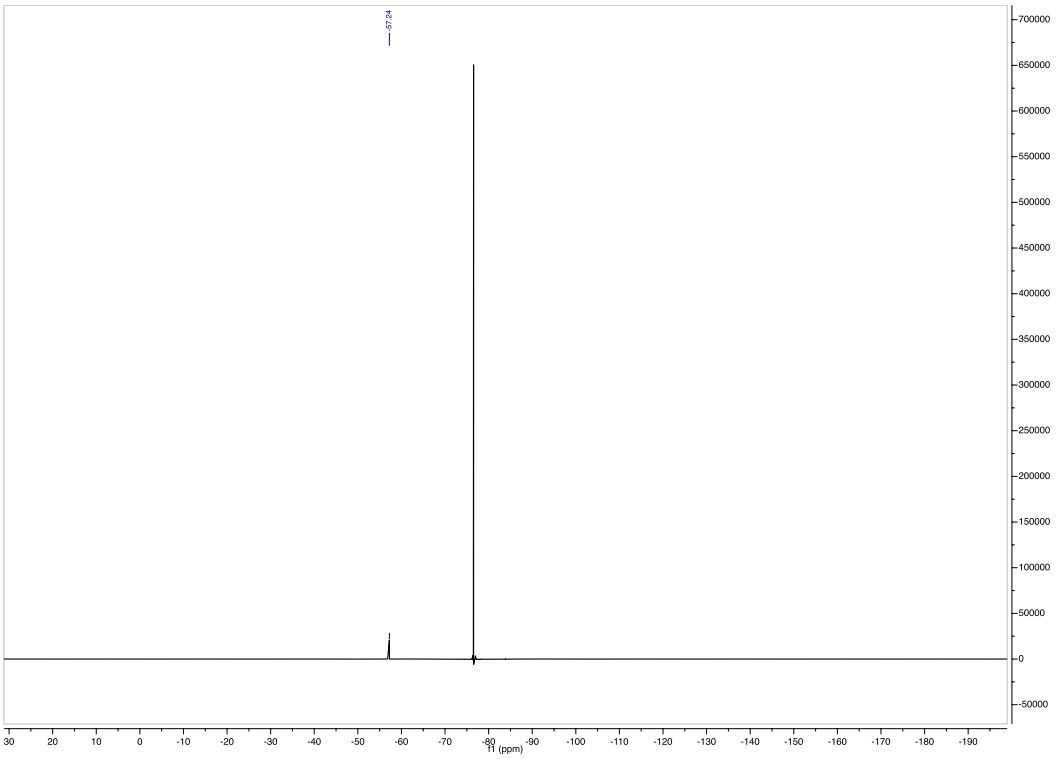

Figure 4.4.31. ^{19}F of 2-(4-chloro-2-(trifluoromethyl)phenyl)naphthalene-1,4-dione

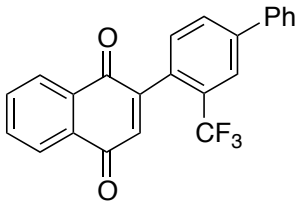

Figure 4.4.32. Substrate 2-(3-(trifluoromethyl)-[1,1'-biphenyl]-4-yl)naphthalene-1,4-dione

2-(3-(trifluoromethyl)-[1,1'-biphenyl]-4-yl)naphthalene-1,4-dione: Followed General Procedure 1 using (3-(trifluoromethyl)-[1,1'-biphenyl]-4-yl)boronic acid. Purified by FCC eluting with hexanes/EtOAc (90/10) to afford 283mg (40% yield) of 2-(3-(trifluoromethyl)-[1,1'-biphenyl]-4-yl)naphthalene-1,4-dione as a yellow solid.

^{1}H NMR (500 MHz, $CDCl_3$) δ 8.21 – 8.13 (m, 2H), 7.98 (d, *J* = 1.8 Hz, 1H), 7.86 – 7.78 (m, 3H), 7.67 – 7.61 (m, 2H), 7.53 – 7.47 (m, 2H), 7.46 – 7.41 (m, 1H), 7.38 (dt, *J* = 7.9, 0.6 Hz, 1H), 6.99 (s, 1H).

^{13}C NMR (126 MHz, $CDCl_3$) δ 184.73, 184.03, 148.44, 142.77, 139.17, 136.93, 134.25, 134.23, 132.26, 132.03, 131.35, 130.80, 130.19, 129.62, 129.26, 128.57, 127.37, 127.23, 126.47, 125.42, 124.00.

^{19}F NMR (376 MHz, $CDCl_3$) δ -56.81.

MS (APCI) Calculated for $C_{23}H_{14}F_3O_2$ $[M+H]^+$: 379.1; Found: 379.2 m/z

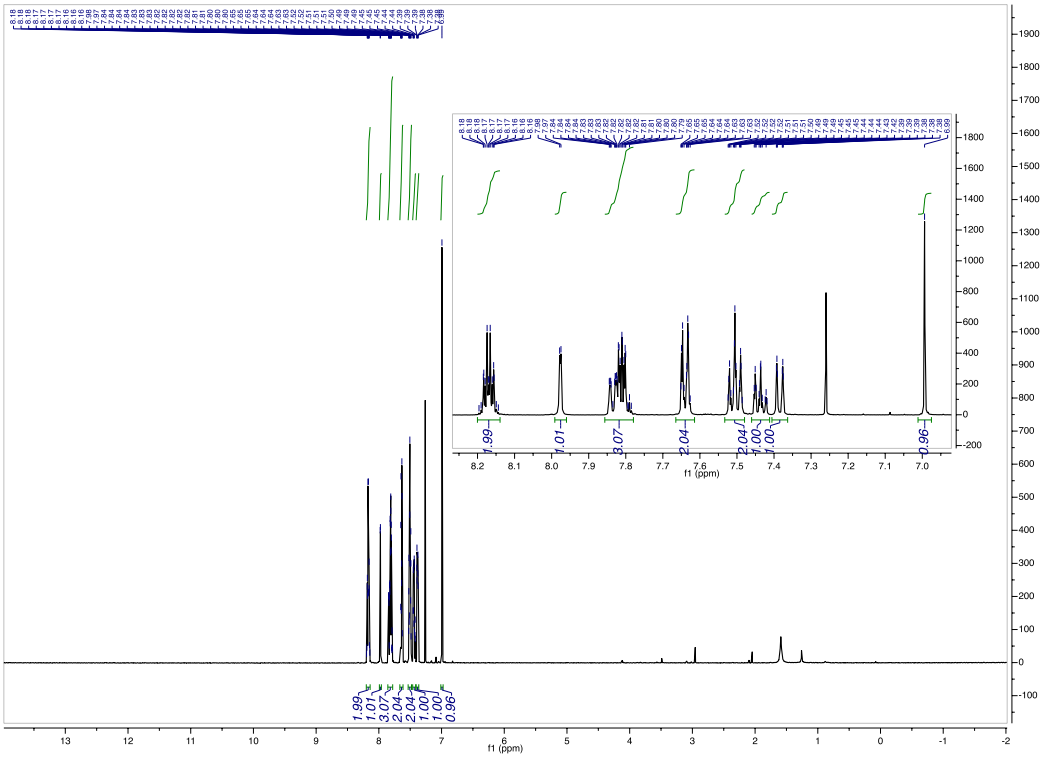

Figure 4.4.33. ^{1}H of 2-(3-(trifluoromethyl)-[1,1'-biphenyl]-4-yl)naphthalene-1,4-dione

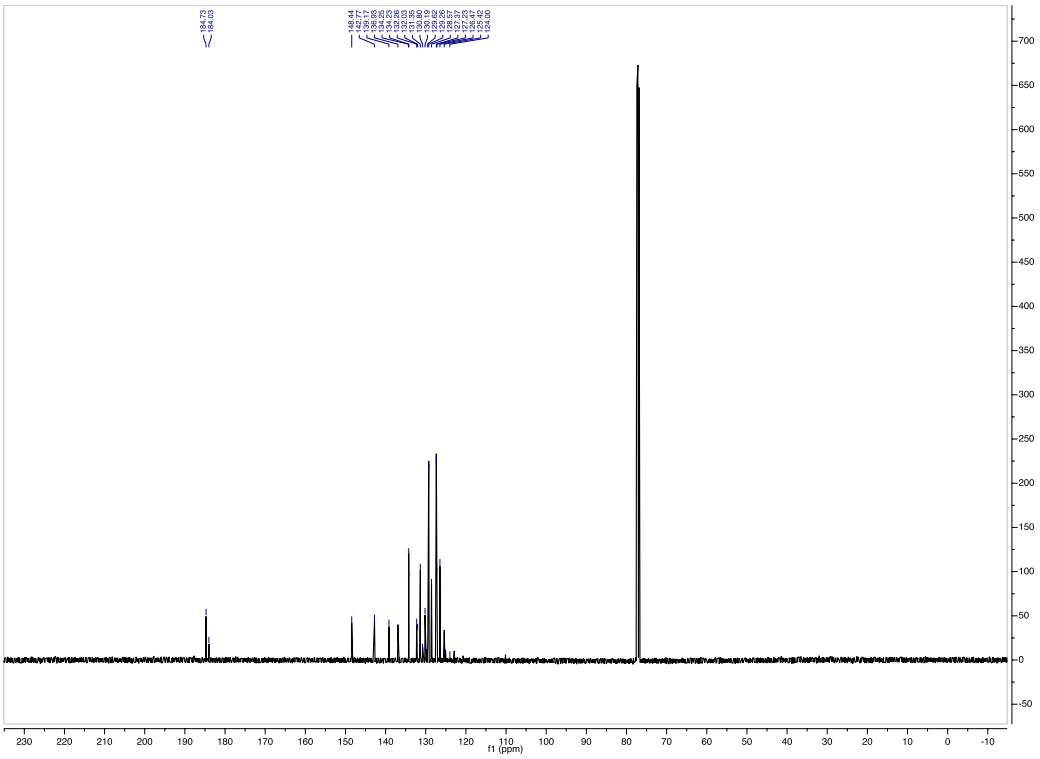

Figure 4.4.34. ^{13}C of 2-(3-(trifluoromethyl)-[1,1'-biphenyl]-4-yl)naphthalene-1,4-dione

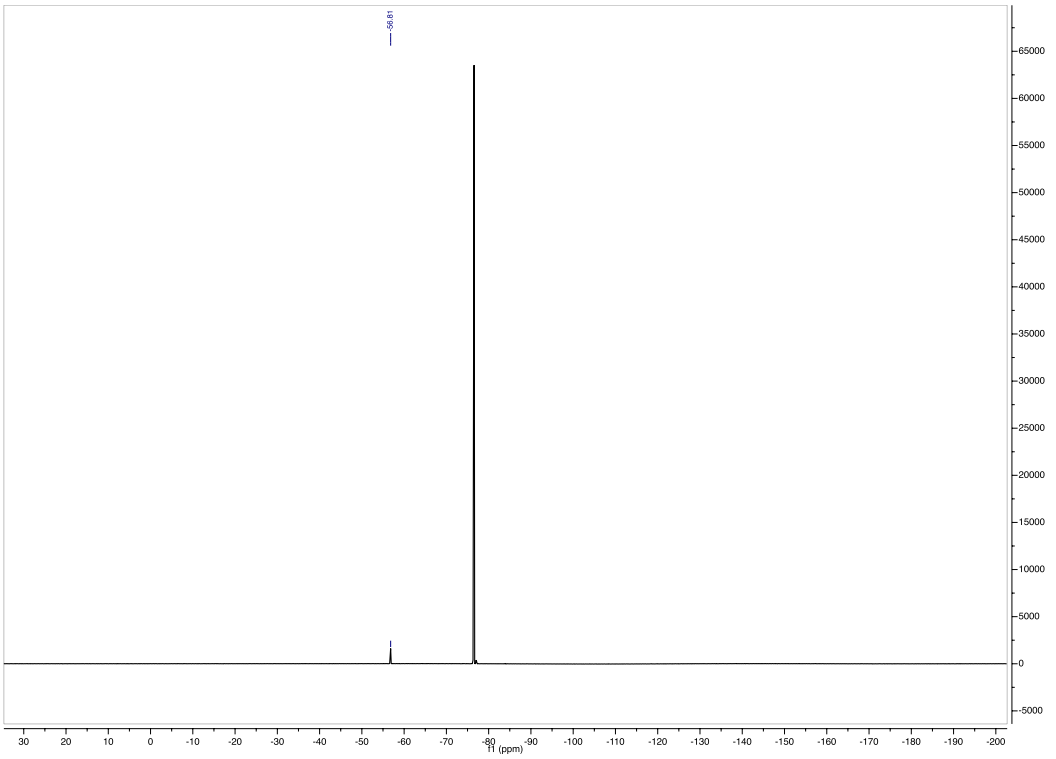

Figure 4.4.35. ^{19}F of 2-(3-(trifluoromethyl)-[1,1'-biphenyl]-4-yl)naphthalene-1,4-dione

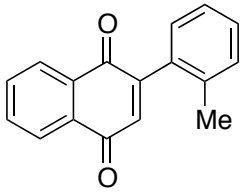

Figure 4.4.36. Substrate 2-(*o*-tolyl)naphthalene-1,4-dione

2-(*o*-tolyl)naphthalene-1,4-dione: Followed General Procedure 1 using 2-tolylboronic acid, and purified by FCC (hexanes/EtOAc = 96:4 → 90:10) to afford 322mg (69% yield) of 2-(*o*-tolyl)naphthalene-1,4-dione as a yellow solid.

^{1}H NMR (500 MHz, $CDCl_3$) δ 8.21 – 8.12 (m, 2H), 7.84 – 7.77 (m, 2H), 7.37 (td, *J* = 7.5, 1.4 Hz, 1H), 7.33 – 7.25 (m, 2H), 7.19 (d, *J* = 7.6 Hz, 1H), 6.95 (s, 1H), 2.24 (s, 3H).

^{13}C NMR (126 MHz, $CDCl_3$) δ 185.34, 184.13, 150.74, 137.03, 136.33, 134.07, 133.99, 133.93, 132.38, 132.25, 130.50, 129.50, 129.32, 127.18, 126.27, 125.92, 20.57.

MS (APCI) Calculated for $C_{17}H_{13}O_2$ $[M+H]^+$: 249.1; Found: 249.3 m/z

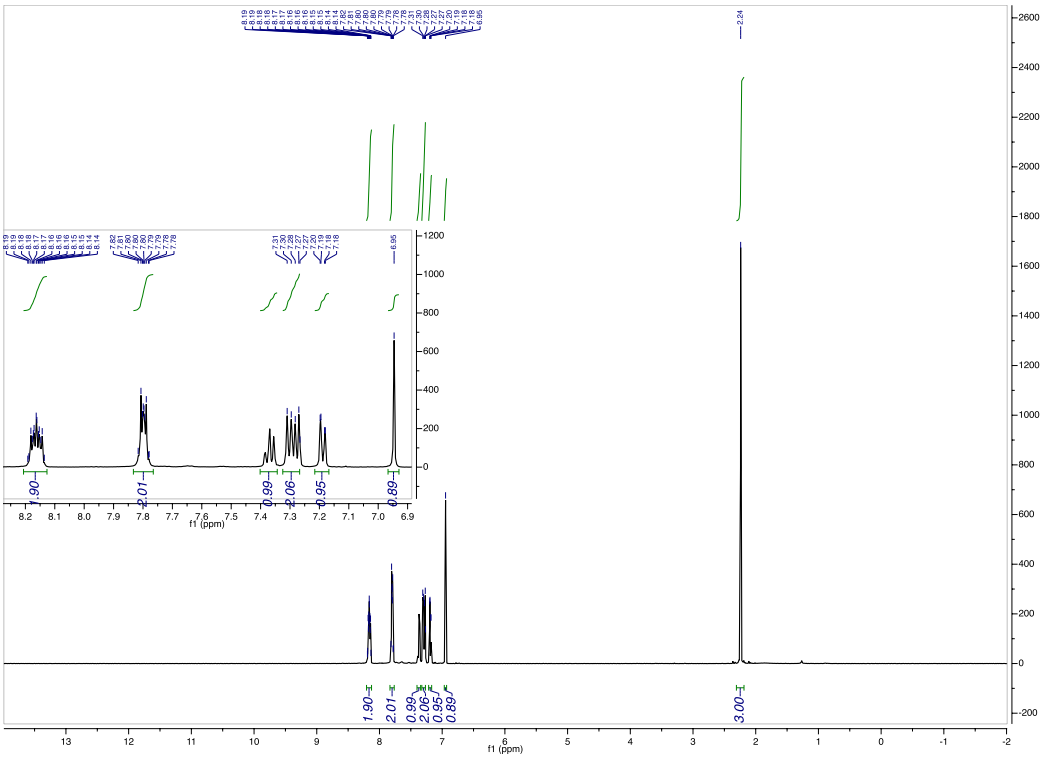

Figure 4.4.37. ^{1}H of 2-(*o*-tolyl)naphthalene-1,4-dione

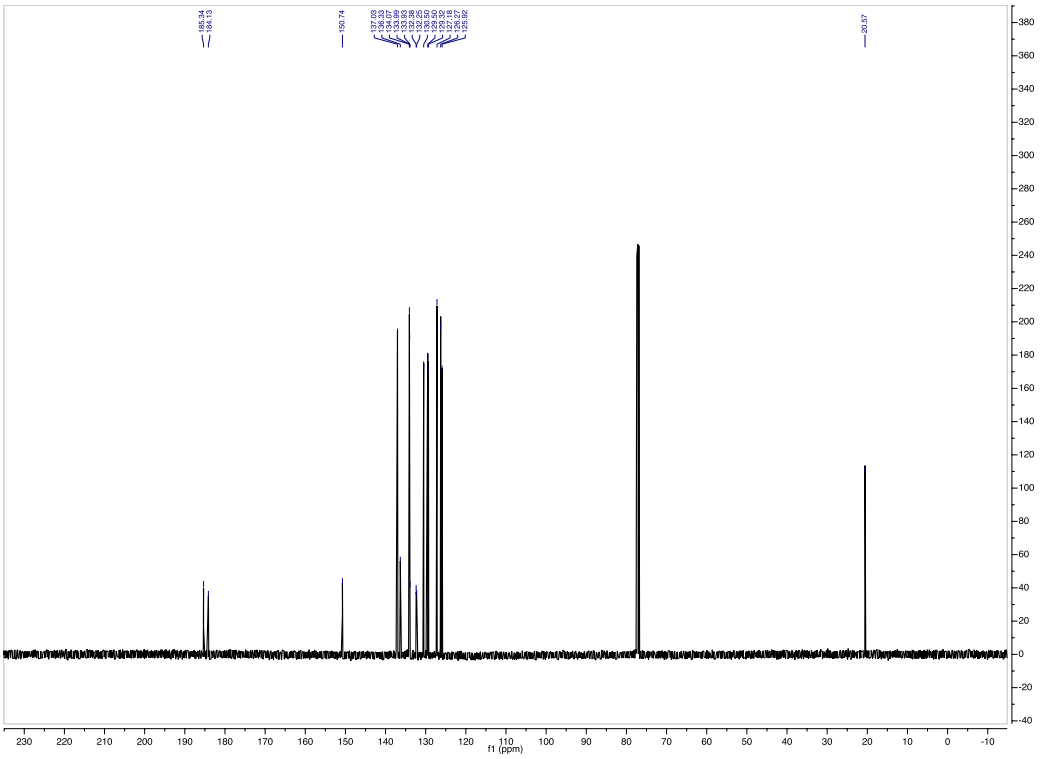

Figure 4.4.38. ^{13}C of 2-(*o*-tolyl)naphthalene-1,4-dione

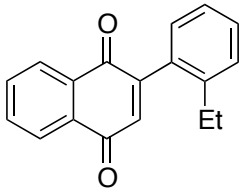

Figure 4.4.39. Substrate 2-(2-ethylphenyl)naphthalene-1,4-dione

2-(2-ethylphenyl)naphthalene-1,4-dione: Followed General Procedure 1 using 2-ethylbenzeneboronic acid, and purified by FCC (hexanes/EtOAc = 96:4 → 90:10) to obtain 356mg (73% yield) of 2-(2-ethylphenyl)naphthalene-1,4-dione as a yellow solid.

^{1}H NMR (500 MHz, $CDCl_3$) δ 8.18 – 8.12 (m, 2H), 7.82 – 7.76 (m, 2H), 7.41 (td, *J* = 7.5, 1.4 Hz, 1H), 7.35 (ddd, *J* = 7.8, 1.4, 0.7 Hz, 1H), 7.27 (td, *J* = 7.4, 1.3 Hz, 1H), 7.15 (dd, *J* = 7.6, 1.4 Hz, 1H), 6.95 (s, 1H), 2.53 (q, *J* = 7.5 Hz, 2H), 1.16 (t, *J* = 7.5 Hz, 3H).

^{13}C NMR (126 MHz, $CDCl_3$) δ 185.26, 184.48, 150.84, 142.31, 137.04, 134.06, 133.99, 133.29, 132.35, 132.29, 129.62, 129.29, 128.59, 127.19, 126.28, 125.86, 26.87, 15.35.

MS (APCI) Calculated for $C_{18}H_{15}O_2$ $[M+H]^+$: 263.1; Found: 263.0 m/z

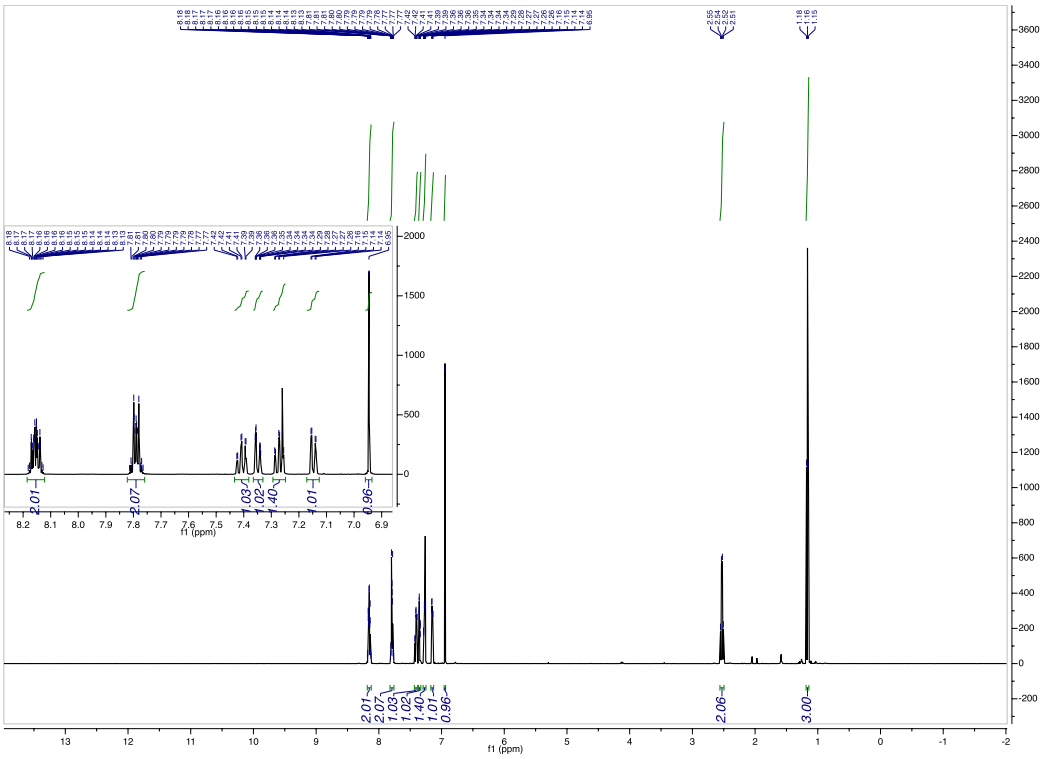

Figure 4.4.40. ^{1}H of 2-(2-ethylphenyl)naphthalene-1,4-dione

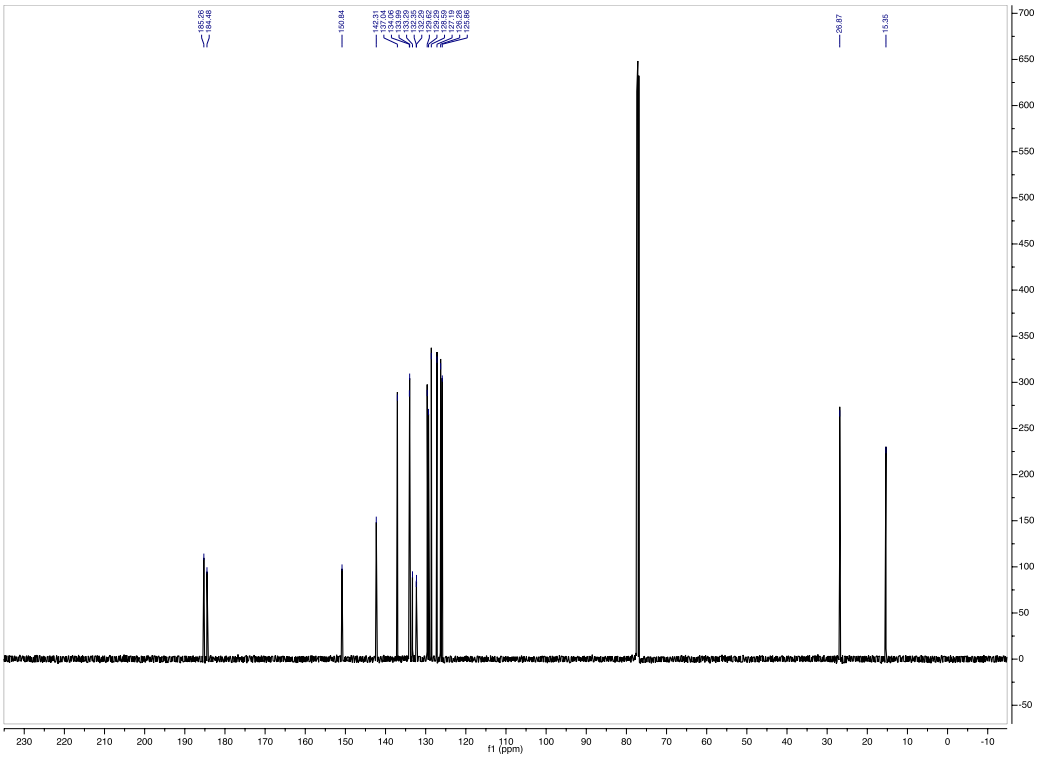

Figure 4.4.41. ^{13}C of 2-(2-ethylphenyl)naphthalene-1,4-dione

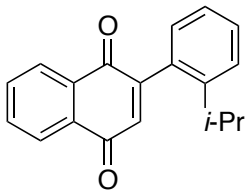

Figure 4.4.42. Substrate 2-(2-isopropylphenyl)naphthalene-1,4-dione

2-(2-isopropylphenyl)naphthalene-1,4-dione: Followed General Procedure 1 modified with the proper equivalents (starting from 180mg of 2-bromo-1,4-dimethoxynaphthalene) using (2-isopropylphenyl)boronic acid, and purified by FCC (hexanes/EtOAc = 96:4 → 92:8) to obtain 176mg (95% yield) 2-(2-isopropylphenyl)naphthalene-1,4-dione as a yellow solid.

^{1}H NMR (500 MHz, $CDCl_3$) δ 8.19 – 8.13 (m, 2H), 7.83 – 7.76 (m, 2H), 7.46 – 7.39 (m, 2H), 7.28 – 7.23 (m, 1H), 7.11 (dd, *J* = 7.6, 1.3 Hz, 1H), 6.94 (s, 1H), 2.72 (hept, *J* = 6.8 Hz, 1H), 1.20 (d, *J* = 9.1 Hz, 6H).

^{13}C NMR (126 MHz, $CDCl_3$) δ 185.25, 184.62, 151.23, 147.27, 137.03, 134.06, 133.99, 132.64, 132.37, 132.35, 129.81, 129.09, 127.23, 126.31, 125.87, 125.76, 31.65, 24.29 (bs).

MS (APCI) Calculated for $C_{19}H_{16}O_2$ $[M+H]^+$: 276.1; Found: 276.2 m/z

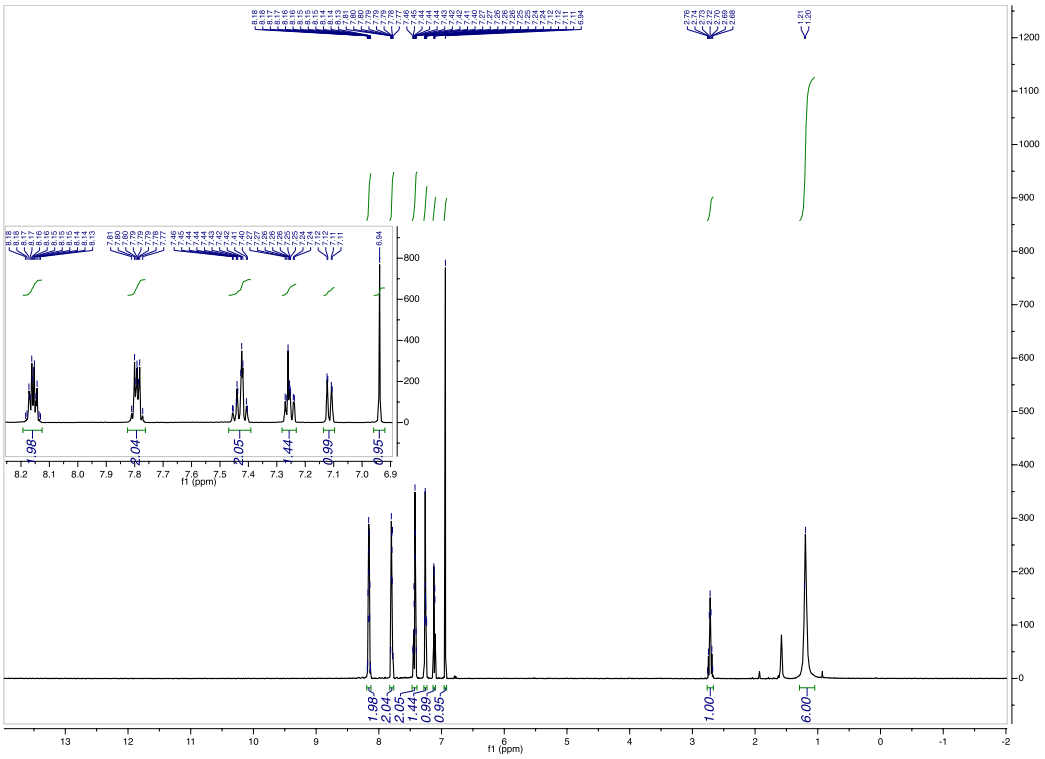

Figure 4.4.43. ^{1}H of 2-(2-isopropylphenyl)naphthalene-1,4-dione

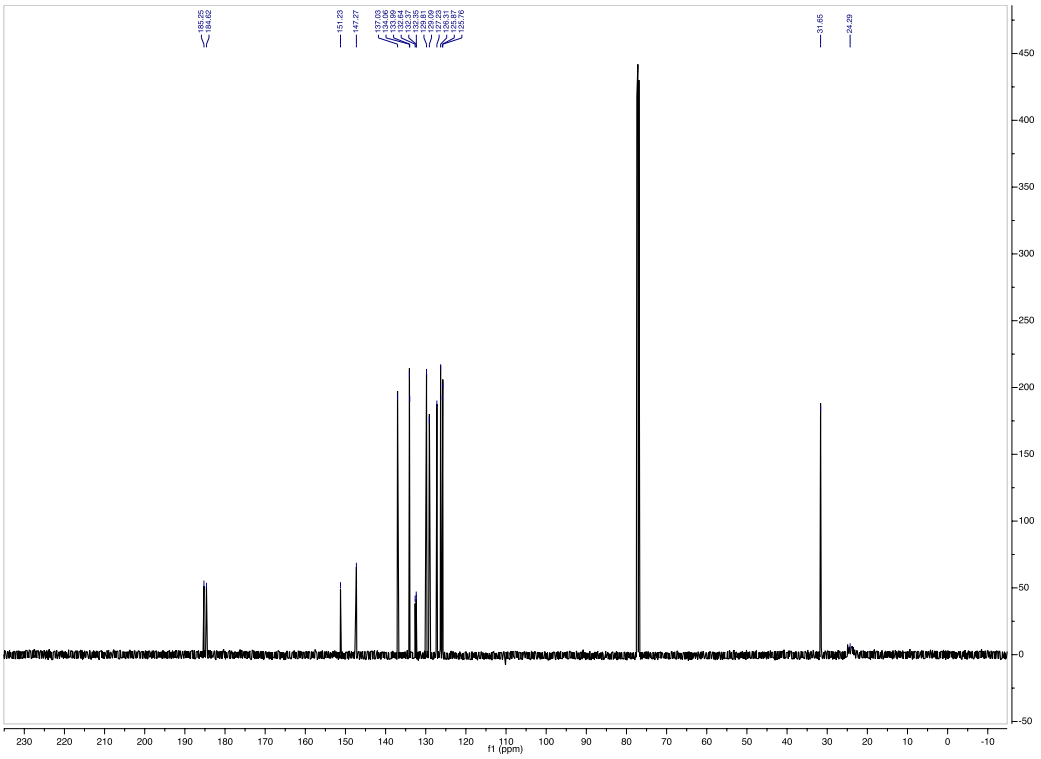

Figure 4.4.44. ^{13}C of 2-(2-isopropylphenyl)naphthalene-1,4-dione

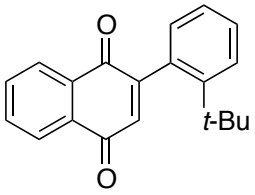

Figure 4.4.45. Substrate 2-(2-(*tert*-butyl)phenyl)naphthalene-1,4-dione

2-(2-(*tert*-butyl)phenyl)naphthalene-1,4-dione: Followed General Procedure 1 with the following modifications: 1,4-dimethoxynaphthalen-2-yl)boronic acid (441mg, 1.9mmol) as the boronic acid, 1-bromo-2-(*tert*-butyl)benzene (341mg, 1.9mmol) as the aryl bromide, XPhos Pd G3 (13mg, .0162mmol) as Pd catalyst, and K_3PO_4 as base (using appropriate equivalents, the oxidation using CAN was not modified). Purified by FCC (hexanes/EtOAc = 100/0 → 98/2) to obtain 221mg (40% yield) 2-(2-(*tert*-butyl)phenyl)naphthalene-1,4-dione as a yellow oil.

^{1}H NMR (400 MHz, $CDCl_3$) δ 8.19 – 8.12 (m, 2H), 7.83 – 7.75 (m, 2H), 7.57 (dd, *J* = 8.1, 1.2 Hz, 1H), 7.41 – 7.36 (m, 1H), 7.23 (dd, *J* = 7.4, 1.3 Hz, 1H), 6.97 (dd, *J* = 7.6, 1.5 Hz, 1H), 6.91 (s, 1H), 1.30 (s, 9H).

^{13}C NMR (101 MHz, $CDCl_3$) δ 185.56, 185.22, 154.53, 148.12, 136.32, 134.10, 134.05, 132.44, 132.32, 132.31, 130.73, 128.97, 127.57, 127.25, 126.32, 125.49, 36.72, 32.55.

MS (APCI) Calculated for $C_{20}H_{19}O_2$ $[M+H]^+$: 291.1; Found: 290.9 m/z

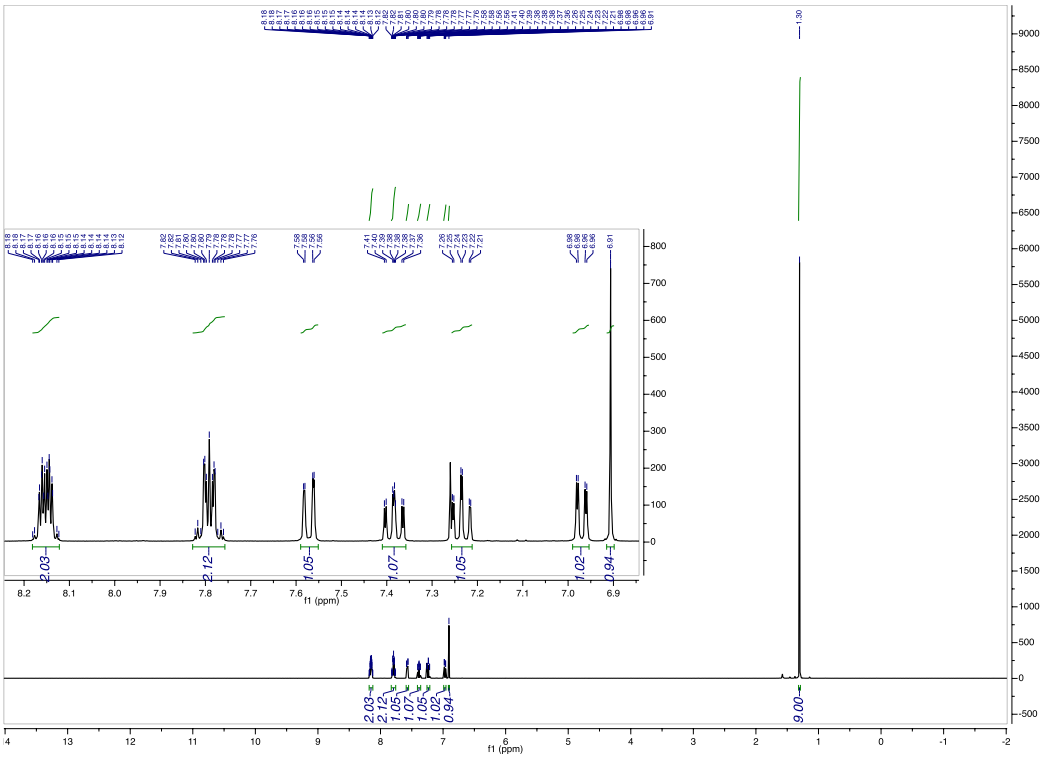

Figure 4.4.46. ^{1}H of 2-(2-(*tert*-butyl)phenyl)naphthalene-1,4-dione

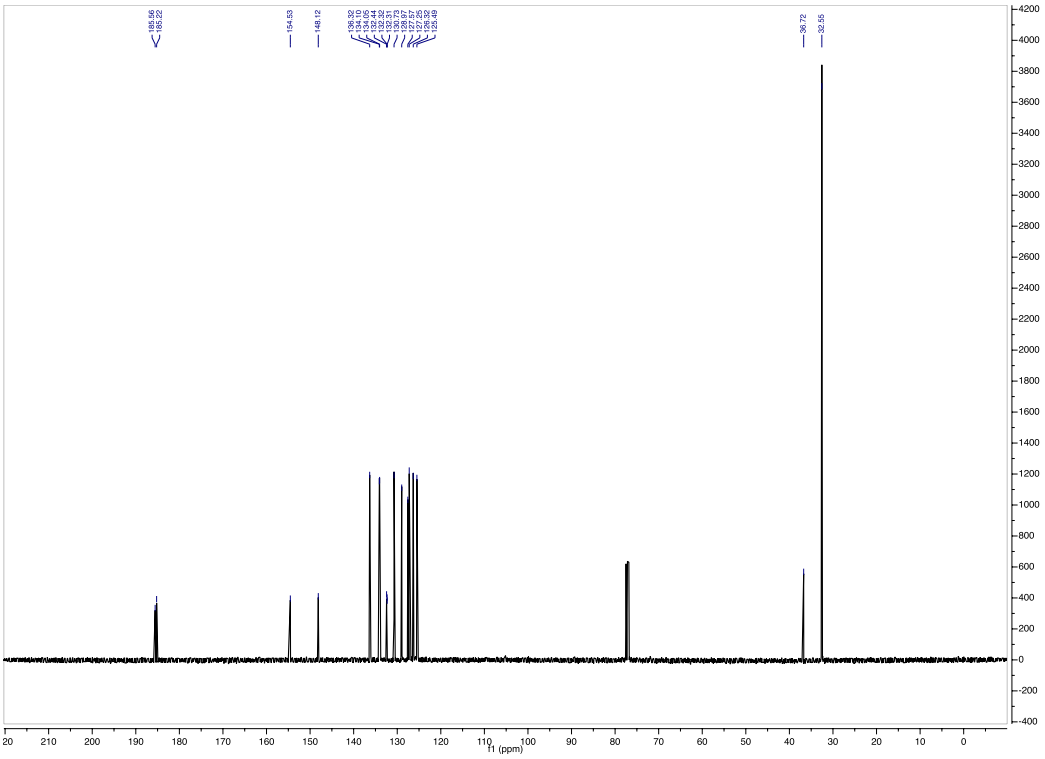

Figure 4.4.47. ^{13}C of 2-(2-(*tert*-butyl)phenyl)naphthalene-1,4-dione

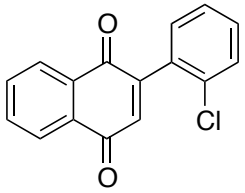

Figure 4.4.48. Substrate 2-(2-chlorophenyl)naphthalene-1,4-dione

2-(2-chlorophenyl)naphthalene-1,4-dione: Followed General Procedure 1 with the following modifications: 2-bromo-1,4-dimethoxynaphthalene was used (600mg, 2.24mmol) as aryl halide with (2-chlorophenyl)boronic acid (the appropriate equivalents were used during the CAN oxidation). Purified by FCC (hexanes/EtOAc = 97/3 → 90/10) to obtain 399mg (66% yield) 2-(2-chlorophenyl)naphthalene-1,4-dione as a yellow oil.

^{1}H NMR (500 MHz, $CDCl_3$) δ 8.20 – 8.11 (m, 2H), 7.82 – 7.77 (m, 2H), 7.51 – 7.47 (m, 1H), 7.40 (td, *J* = 7.7, 1.9 Hz, 1H), 7.36 (td, *J* = 7.5, 1.4 Hz, 1H), 7.29 (dd, *J* = 7.6, 1.8 Hz, 1H), 7.00 (s, 1H).

^{13}C NMR (126 MHz, $CDCl_3$) δ 185.01, 183.22, 148.34, 137.50, 134.17, 134.06, 133.30, 133.27, 132.26, 132.20, 130.76, 130.74, 129.95, 127.24, 126.92, 126.34.

MS (APCI) Calculated for $C_{16}H_{10}ClO_2$ $[M+H]^+$: 269.0; Found: 268.8 m/z

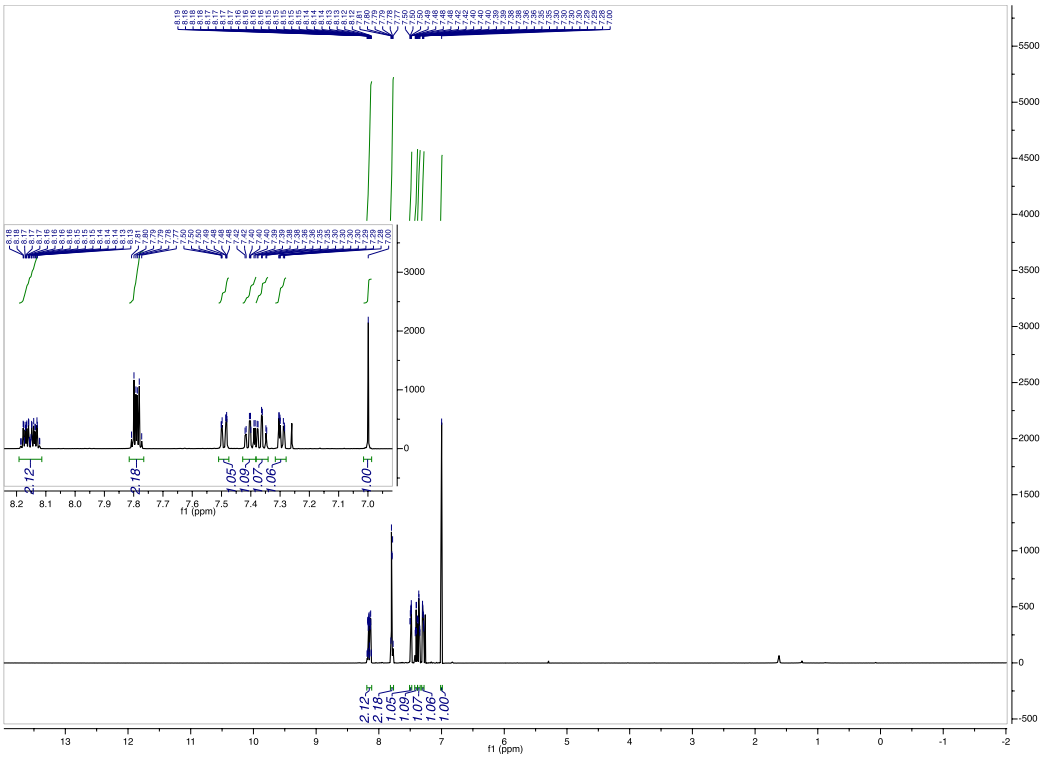

Figure 4.4.49. ^{1}H of 2-(2-chlorophenyl)naphthalene-1,4-dione

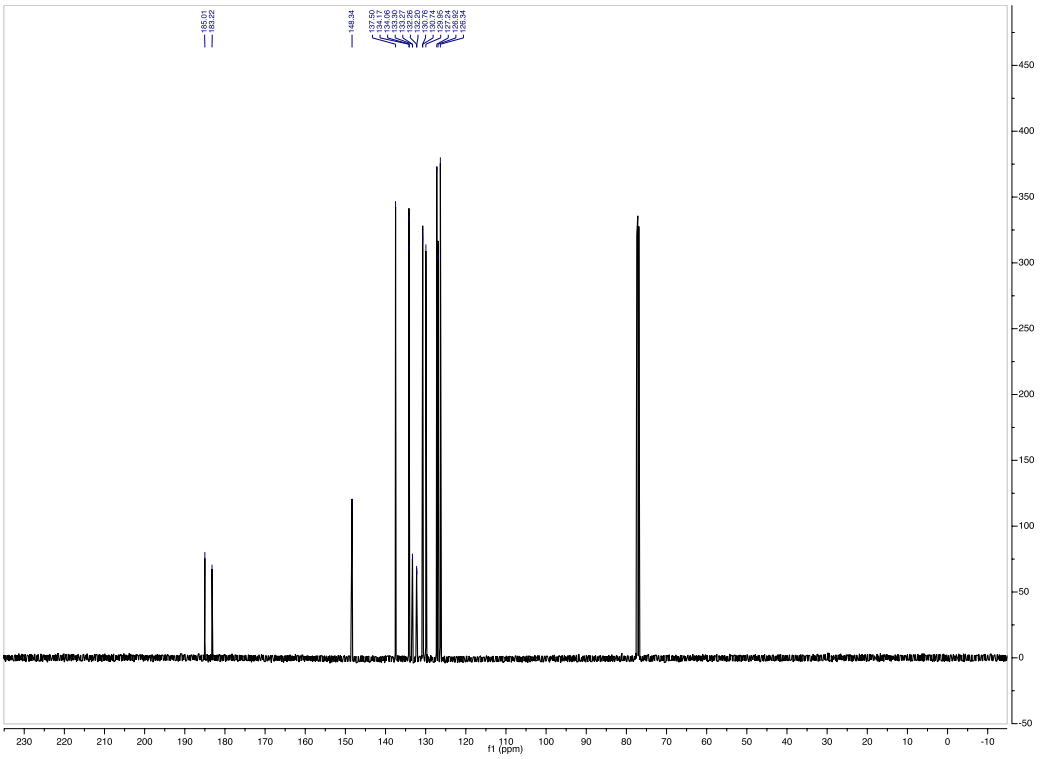

Figure 4.4.50. ^{13}C of 2-(2-chlorophenyl)naphthalene-1,4-dione

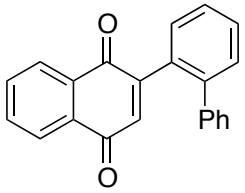

Figure 4.4.51. Substrate 2-([1,1'-biphenyl]-2-yl)naphthalene-1,4-dione

2-([1,1'-biphenyl]-2-yl)naphthalene-1,4-dione: Followed General Procedure 1 with (2-biphenylboronic acid. Recrystallized from toluene to obtain 182mg (31% yield) 2-([1,1'-biphenyl]-2-yl)naphthalene-1,4-dione as yellow prisms.

^{1}H NMR (500 MHz, $CDCl_3$) δ 8.08 – 8.03 (m, 1H), 7.89 – 7.84 (m, 1H), 7.71 (td, *J* = 7.5, 1.5 Hz, 1H), 7.67 (td, *J* = 7.5, 1.5 Hz, 1H), 7.57 – 7.51 (m, 1H), 7.51 – 7.43 (m, 2H), 7.38 (ddd, *J* = 7.6, 1.4, 0.6 Hz, 1H), 7.30 – 7.22 (m, 4H), 7.22 – 7.16 (m, 1H), 6.92 (s, 1H).

^{13}C NMR (126 MHz, $CDCl_3$) δ 185.03, 183.83, 151.19, 141.94, 141.39, 137.31, 133.87, 133.72, 132.97, 132.40, 132.05, 130.33, 130.15, 129.85, 129.08, 128.53, 127.44, 127.26, 126.86, 126.09.

MS (APCI) Calculated for $C_{22}H_{15}ClO_2$ $[M+H]^+$: 311.1; Found: 311.1 m/z

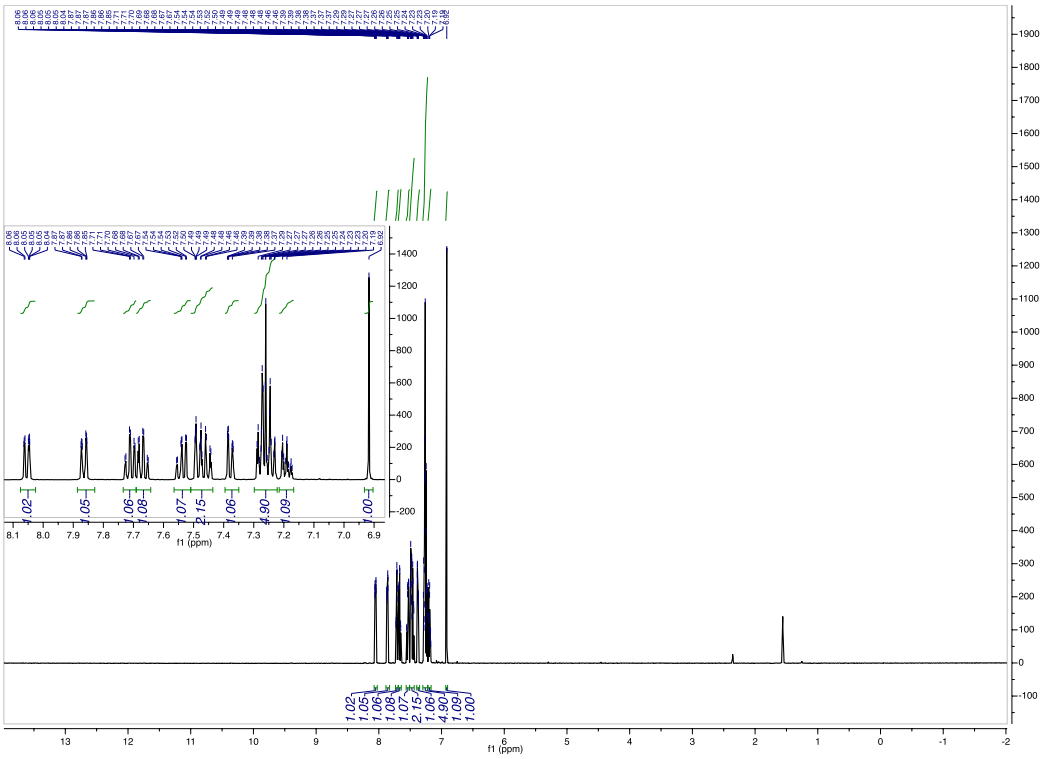

Figure 4.4.52. ^{1}H of 2-([1,1'-biphenyl]-2-yl)naphthalene-1,4-dione

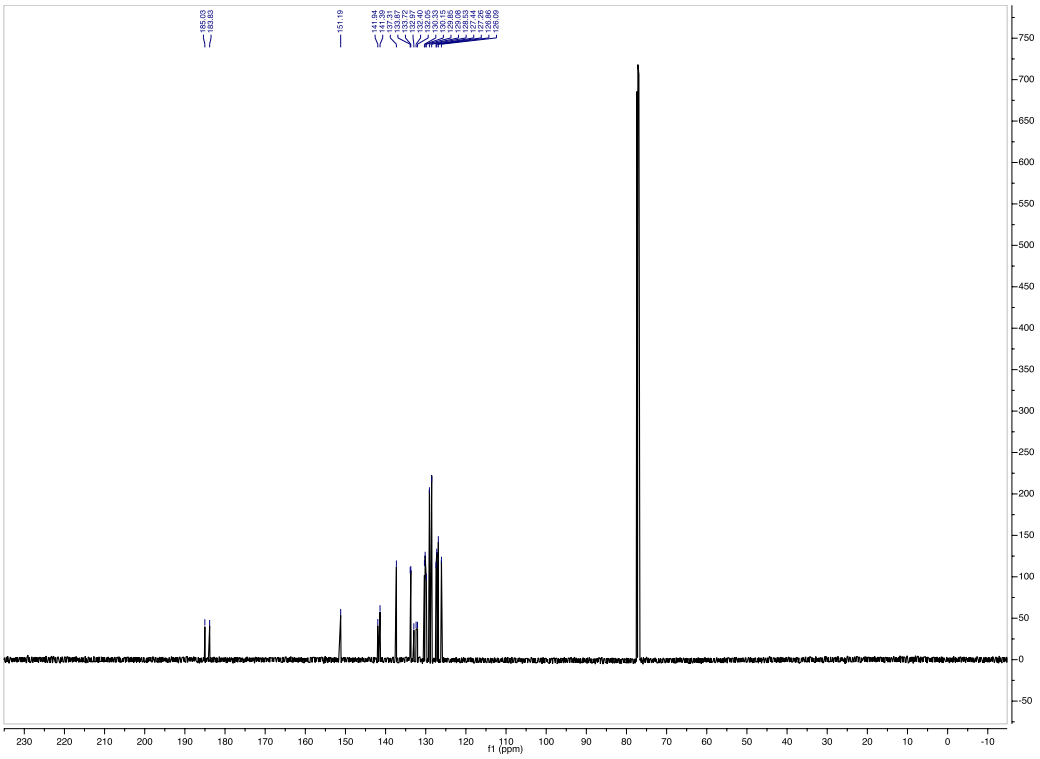

Figure 4.4.53. ^{13}C of 2-([1,1'-biphenyl]-2-yl)naphthalene-1,4-dione

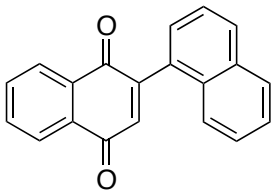

Figure 4.4.54. Substrate [1,2'-binaphthalene]-1',4'-dione

[1,2'-binaphthalene]-1',4'-dione: Followed General Procedure 1 with 1-naphthaleneboronic acid. Purified by FCC (hexanes/EtOAc = 96:4) to obtain 438mg (82% yield) [1,2'-binaphthalene]-1',4'-dione as a yellow solid.

^{1}H NMR (500 MHz, $CDCl_3$) δ 8.23 – 8.17 (m, 2H), 7.96 (dd, *J* = 8.3, 1.1 Hz, 1H), 7.94 – 7.89 (m, 1H), 7.85 – 7.78 (m, 2H), 7.68 (dq, *J* = 8.3, 0.9 Hz, 1H), 7.59 – 7.41 (m, 4H), 7.14 (s, 1H).

^{13}C NMR (126 MHz, $CDCl_3$) δ 185.18, 184.44, 149.62, 138.01, 134.13, 134.09, 133.60, 132.42, 132.32, 131.85, 131.49, 130.04, 128.66, 127.45, 127.30, 126.71, 126.32, 126.29, 125.47, 125.19.

MS (APCI) Calculated for $C_{20}H_{13}O_2$ $[M+H]^+$: 284.1; Found: 284.3 m/z

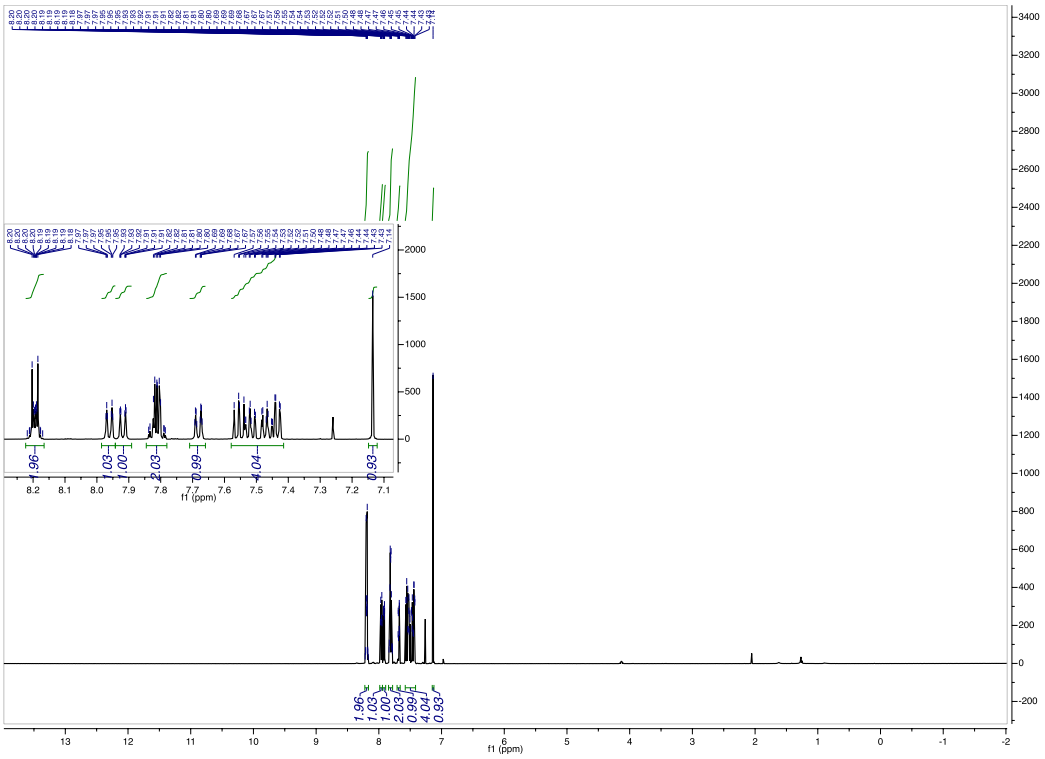

Figure 4.4.55. ^{1}H of [1,2'-binaphthalene]-1',4'-dione

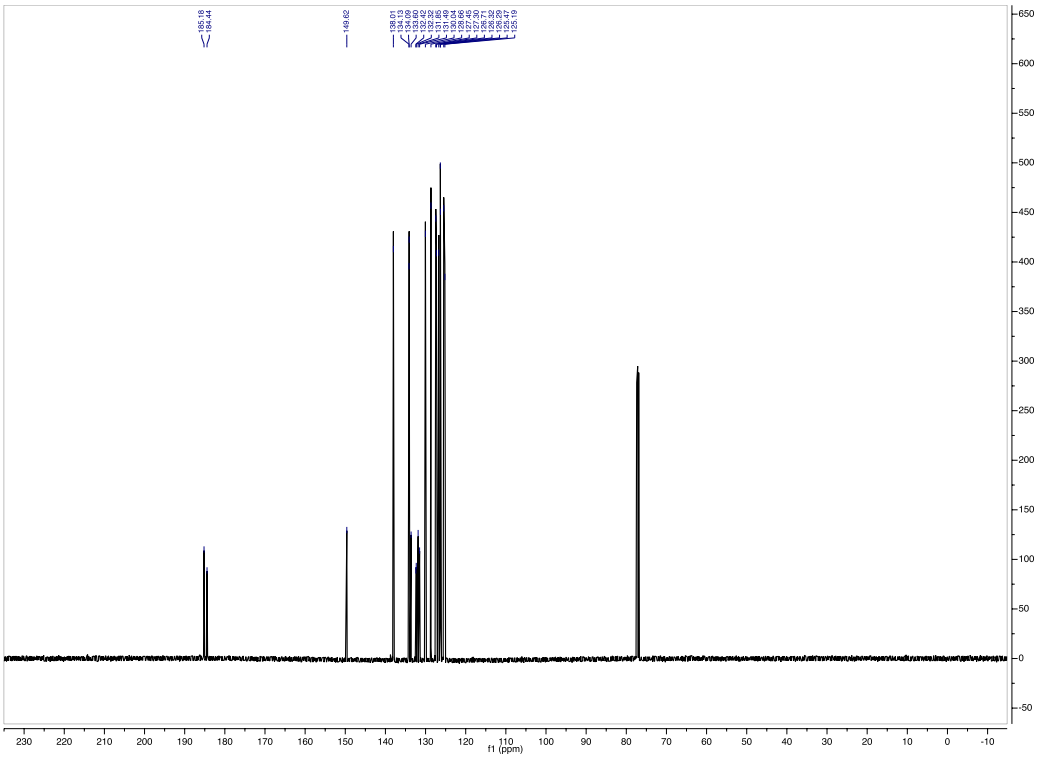

Figure 4.4.56. ^{13}C of [1,2'-binaphthalene]-1',4'-dione

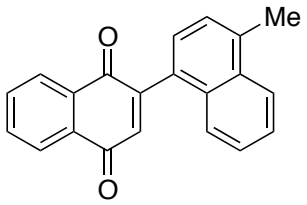

Figure 4.4.57. Substrate 4-methyl-[1,2'-binaphthalene]-1',4'-dione

4-methyl-[1,2'-binaphthalene]-1',4'-dione: Followed General Procedure 1 with (4-methylnaphthalen-1-yl)boronic acid. Purified by FCC (hexanes/EtOAc = 96:4) to afford 438mg (82% yield) of 4-methyl-[1,2'-binaphthalene]-1',4'-dione as a yellow solid.

^{1}H NMR (500 MHz, $CDCl_3$) δ 8.22 – 8.16 (m, 2H), 8.08 (dt, *J* = 8.5, 1.0 Hz, 1H), 7.84 – 7.78 (m, 2H), 7.68 (ddd, *J* = 8.5, 1.3, 0.7 Hz, 1H), 7.56 (ddd, *J* = 8.4, 6.8, 1.3 Hz, 1H), 7.47 (ddd, *J* = 8.2, 6.8, 1.3 Hz, 1H), 7.40 (dd, *J* = 7.2, 1.1 Hz, 1H), 7.33 (d, *J* = 7.1 Hz, 1H), 7.12 (s, 1H), 2.76 (d, *J* = 0.9 Hz, 3H).

^{13}C NMR (126 MHz, $CDCl_3$) δ 185.30, 184.60, 150.00, 137.92, 136.73, 134.09, 134.06, 132.78, 132.52, 132.39, 131.55, 130.30, 127.33, 127.20, 126.34, 126.32, 126.17, 126.06, 124.78, 19.84.

MS (APCI) Calculated for $C_{21}H_{15}O_2$ $[M+H]^+$: 299.1; Found: 299.0 m/z.

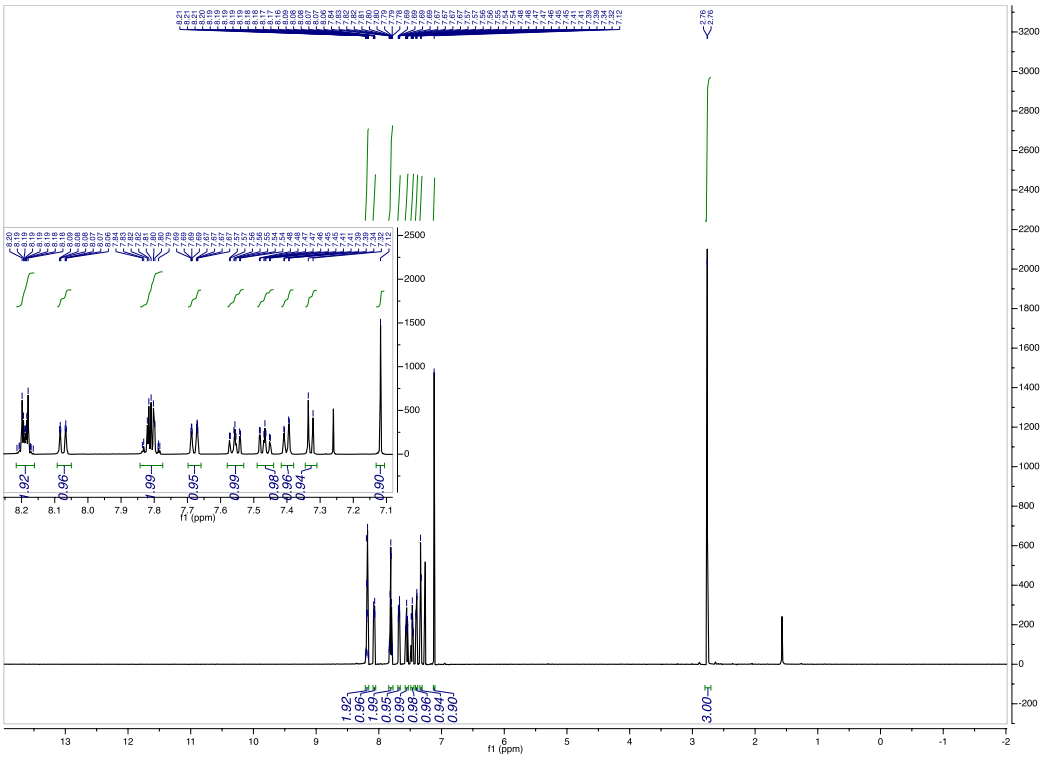

Figure 4.4.58. ^{1}H of 4-methyl-[1,2'-binaphthalene]-1',4'-dione

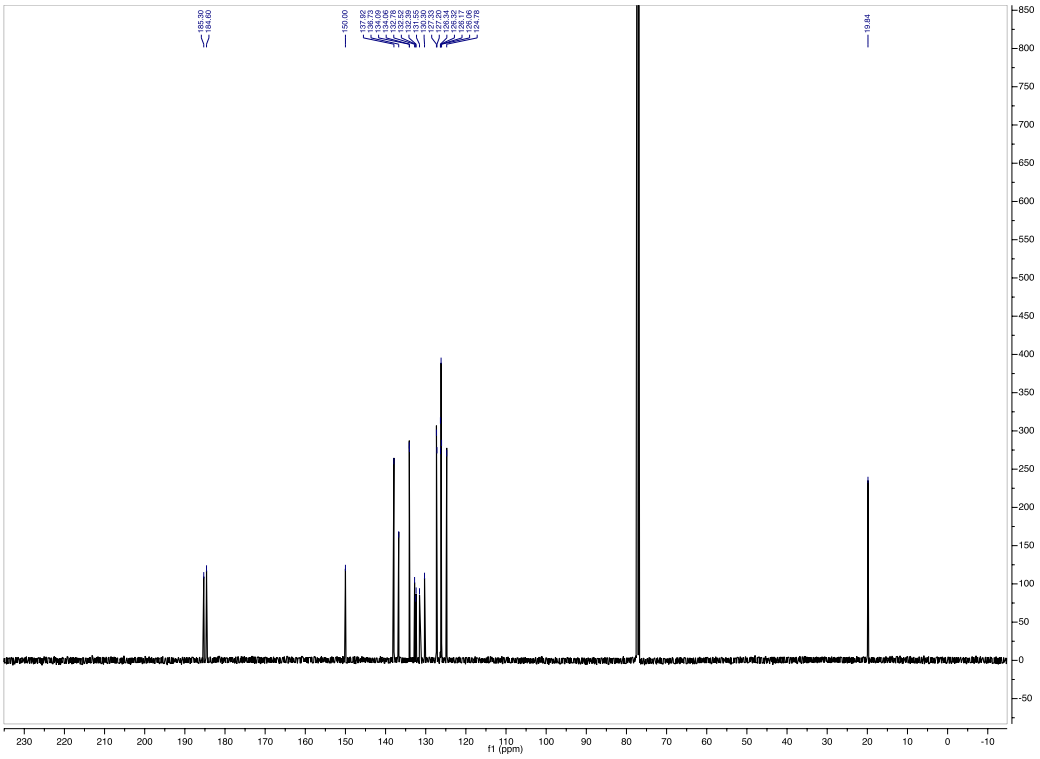

Figure 4.4.59. ^{13}C of 4-methyl-[1,2'-binaphthalene]-1',4'-dione

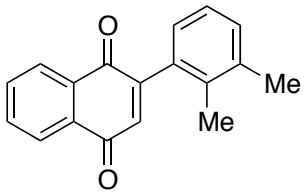

Figure 4.4.60. Substrate 2-(2,3-dimethylphenyl)naphthalene-1,4-dione

2-(2,3-dimethylphenyl)naphthalene-1,4-dione: Followed General Procedure 1 with (2,3-dimethylphenyl)boronic acid. Purified by FCC (hexanes/EtOAc = 96:4 → 90:10) to obtain 346mg (71% yield) 2-(2,3-dimethylphenyl)naphthalene-1,4-dione as a yellow solid.

^{1}H NMR (400 MHz, $CDCl_3$) δ 8.19 – 8.12 (m, 2H), 7.82 – 7.75 (m, 2H), 7.25 (d, *J* = 7.6 Hz, 1H), 7.18 (t, *J* = 7.6 Hz, 1H), 7.02 (dd, *J* = 7.6, 1.4 Hz, 1H), 6.93 (s, 1H), 2.34 (s, 3H), 2.11 (s, 3H).

^{13}C NMR (101 MHz, $CDCl_3$) δ 185.41, 184.30, 151.53, 137.44, 136.88, 134.86, 134.12, 134.03, 133.97, 132.39, 132.31, 131.11, 127.20, 127.01, 126.26, 125.73, 20.47, 17.87.

MS (APCI) Calculated for $C_{18}H_{15}O_2$ $[M+H]^+$: 263.1; Found: 263.1 m/z

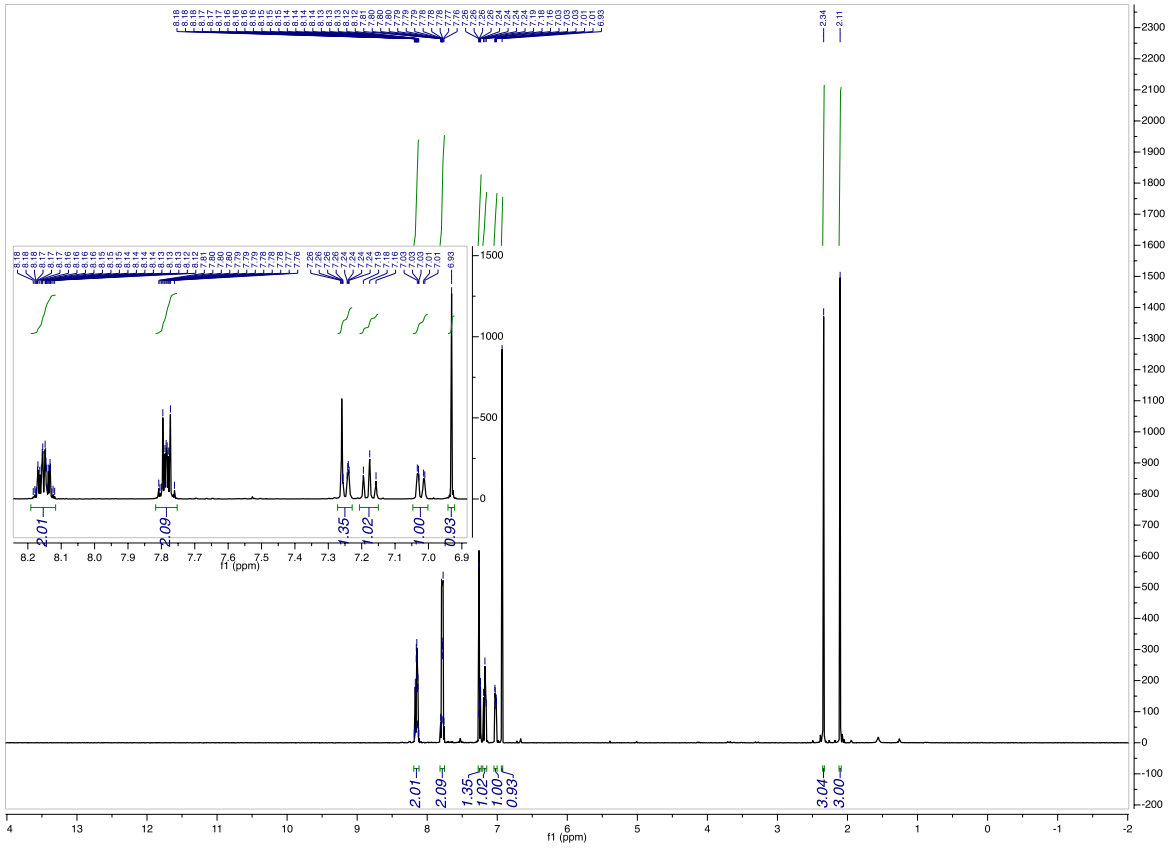

Figure 4.4.61. ^{1}H of 2-(2,3-dimethylphenyl)naphthalene-1,4-dione

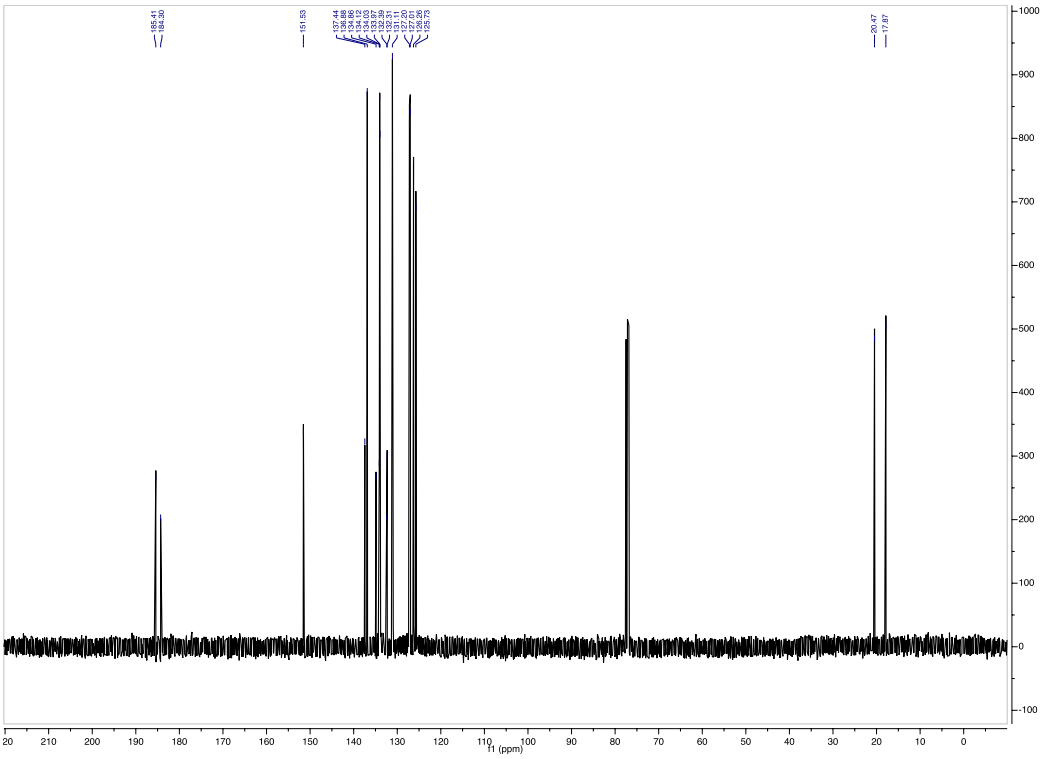

Figure 4.4.62. ^{13}C of 2-(2,3-dimethylphenyl)naphthalene-1,4-dione

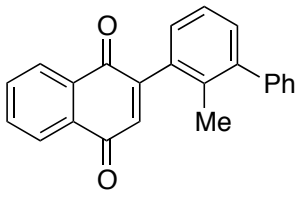

Figure 4.4.63. Substrate 2-(2-methyl-[1,1'-biphenyl]-3-yl)naphthalene-1,4-dione

2-(2-methyl-[1,1'-biphenyl]-3-yl)naphthalene-1,4-dione: Followed General Procedure 1 with the following modifications: crude Intermediate 1 (vida infra) was used as aryl halide, SPhos Pd G3 was used as palladium catalyst, K_3PO_4 was used as base, and phenylboronic acid (the CAN oxidation was unmodified). Recrystallized from DCM/hexane to obtain 203mg (33% overall yield from 2-bromo-1,4-dimethoxynaphthalene) 2-(2-methyl-[1,1'-biphenyl]-3-yl)naphthalene-1,4-dione as fine yellow crystals.

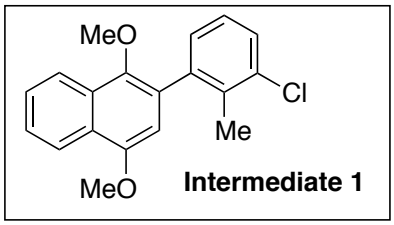

Figure 4.4.64. Structure of Intermediate 1

^{1}H NMR (500 MHz, $CDCl_3$) δ 8.20 – 8.13 (m, 2H), 7.82 – 7.77 (m, 2H), 7.46 – 7.40 (m, 2H), 7.39 – 7.30 (m, 5H), 7.21 – 7.16 (m, 1H), 7.00 (s, 1H), 2.08 (s, 3H).

^{13}C NMR (126 MHz, $CDCl_3$) δ 185.38, 184.19, 151.35, 143.02, 141.69, 137.08, 134.85, 134.10, 134.04, 133.81, 132.38, 132.30, 131.15, 129.51, 128.38, 128.29, 127.22, 127.18, 126.31, 125.77, 18.95.

MS (APCI) Calculated for $C_{23}H_{17}O_2$ $[M+H]^+$: 325.1; Found: 324.9 m/z

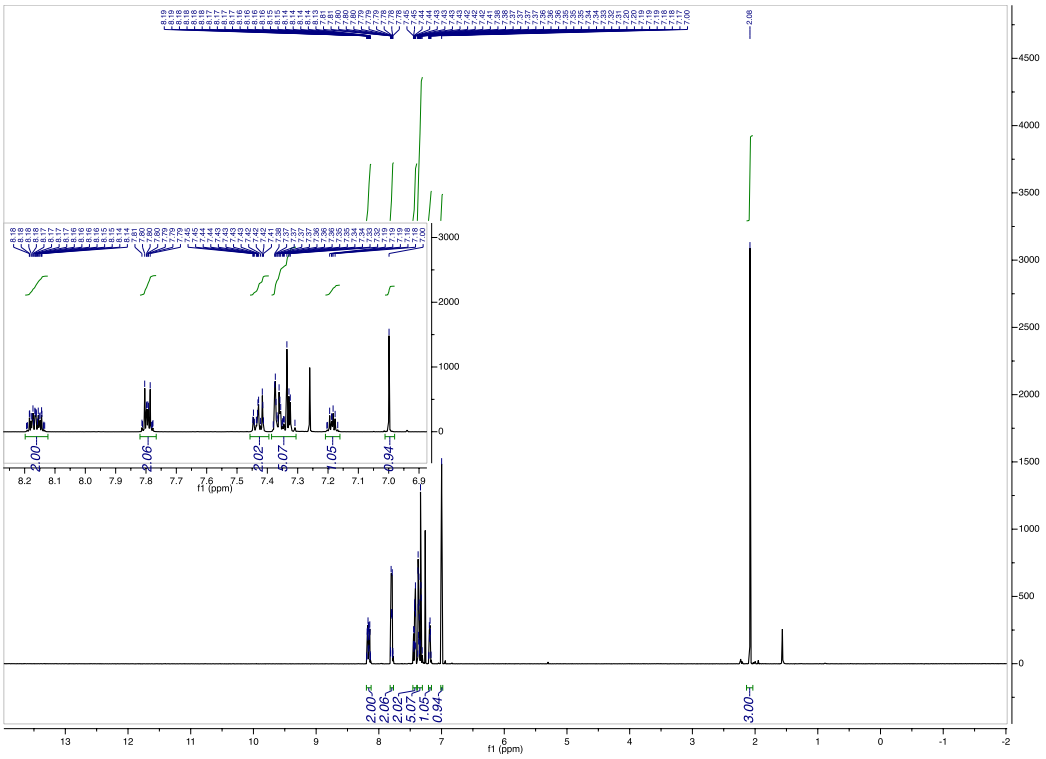

Figure 4.4.65. ^{1}H of 2-(2-methyl-[1,1'-biphenyl]-3-yl)naphthalene-1,4-dione

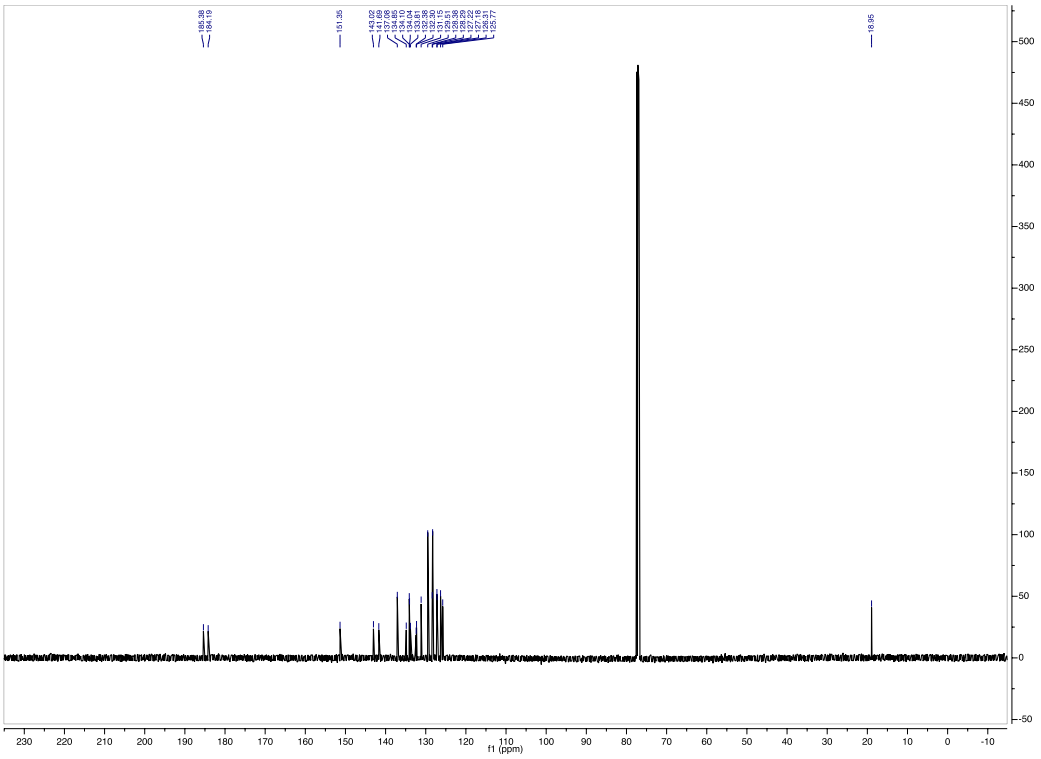

Figure 4.4.66. ^{13}C of 2-(2-methyl-[1,1'-biphenyl]-3-yl)naphthalene-1,4-dione

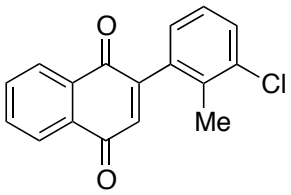

Figure 4.4.67. Substrate 2-(3-chloro-2-methylphenyl)naphthalene-1,4-dione

2-(3-chloro-2-methylphenyl)naphthalene-1,4-dione: Followed the General Cross Coupling Procedure with (3-chloro-2-methylphenyl)boronic acid (1.0g, 3.74mmol). Before CAN oxidation, the crude Intermediate 1 was divided equally into 2 separate flasks. One flask was set aside for a future experiment, and the other flask was moved on to CAN oxidation for this experiment. Purified by FCC (hexanes/EtOAc = 98/2 → 85/15) to obtain 257mg (49% overall yield from 2-bromo-1,4-dimethoxynaphthalene) 2-(3-chloro-2-methylphenyl)naphthalene-1,4-dione as a yellow solid.

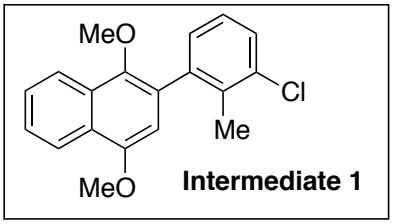

Figure 4.4.68. Structure of Intermediate 1

^{1}H NMR (500 MHz, $CDCl_3$) δ 8.19 – 8.12 (m, 2H), 7.83 – 7.77 (m, 2H), 7.46 (dd, J = 8.1, 1.3 Hz, 1H), 7.24 – 7.19 (m, 1H), 7.08 (dd, J = 7.6, 1.3 Hz, 1H), 6.93 (s, 1H), 2.23 (s, 3H).

^{13}C NMR (126 MHz, $CDCl_3$) δ 184.98, 183.74, 150.01, 136.99, 135.64, 135.36, 134.51, 134.07, 134.04, 132.08, 132.04, 130.22, 127.58, 127.11, 126.79, 126.24, 18.41.

MS (APCI) Calculated for $C_{17}H_{12}ClO_2$ $[M+H]^+$: 283.1; Found: 282.7 m/z.

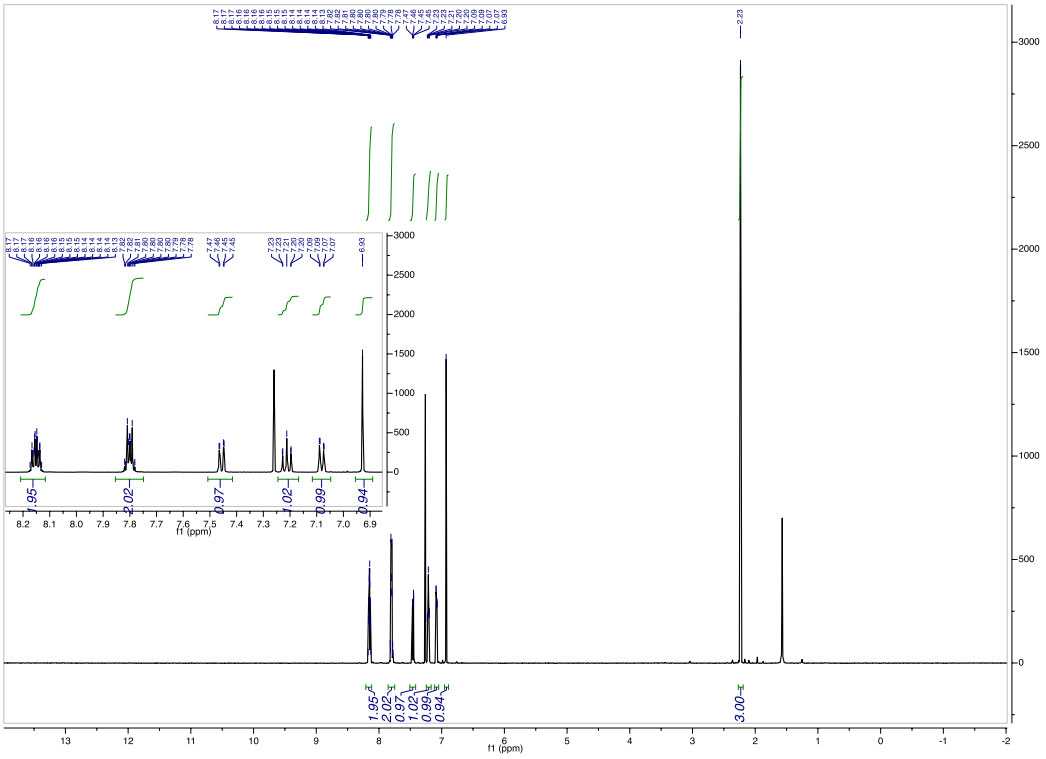

Figure 4.4.69. ^{1}H of 2-(3-chloro-2-methylphenyl)naphthalene-1,4-dione

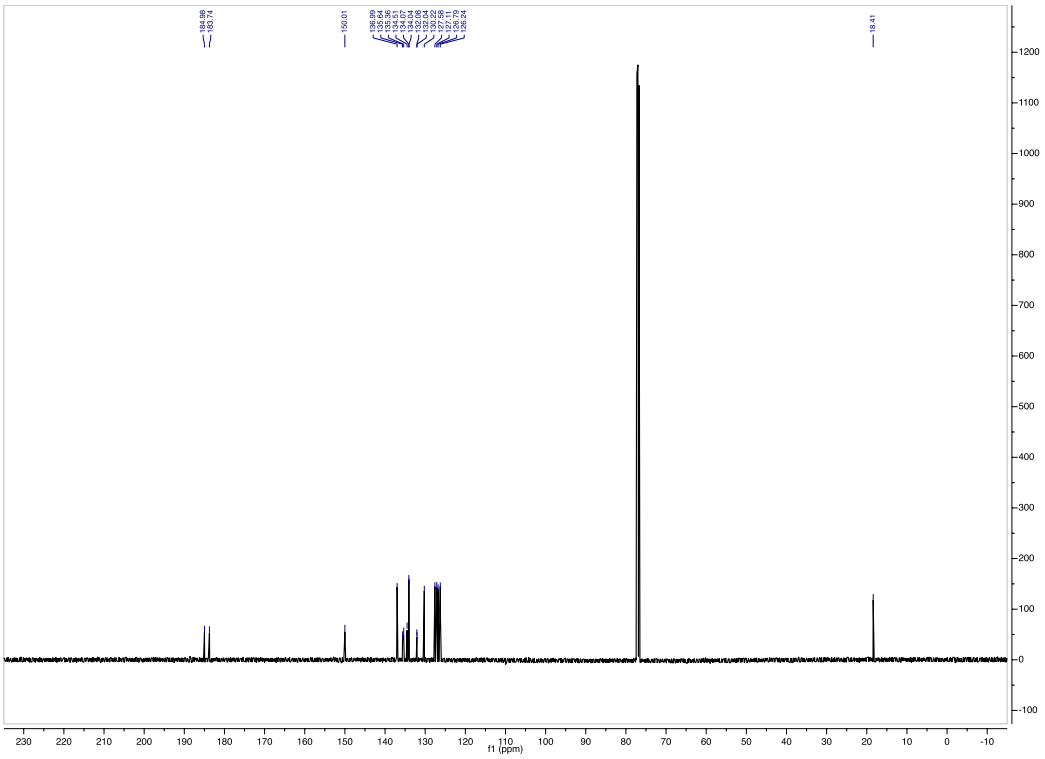

Figure 4.4.70. ^{13}C of 2-(3-chloro-2-methylphenyl)naphthalene-1,4-dione

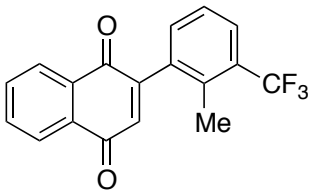

Figure 4.4.71. Substrate 2-(2-methyl-3-(trifluoromethyl)phenyl)naphthalene-1,4-dione

2-(2-methyl-3-(trifluoromethyl)phenyl)naphthalene-1,4-dione: Followed General Procedure 1 using (2-methyl-3-(trifluoromethyl)phenyl)boronic acid. Purified by FCC (hexanes/EtOAc = 96/4 → 90/10) to obtain 460mg (78% yield) 2-(4-fluoro-2-(trifluoromethyl)phenyl)naphthalene-1,4-dione as a yellow solid.

^{1}H NMR (500 MHz, $CDCl_3$) δ 8.18 – 8.13 (m, 2H), 7.84 – 7.78 (m, 2H), 7.73 (dd, *J* = 7.7, 1.7 Hz, 1H), 7.40 – 7.32 (m, 2H), 6.95 (s, 1H), 2.32 (q, *J* = 1.7 Hz, 3H).

^{13}C NMR (126 MHz, $CDCl_3$) δ 184.79, 183.66, 149.85, 137.38, 136.14, 135.28 (q, *J* = 1.4 Hz), 134.14, 134.13, 132.52, 132.08, 131.99, 129.77 (q, *J* = 29.7 Hz), 127.12, 126.91 (q, *J* = 5.7 Hz), 126.30, 125.82, 124.33 (q, *J* = 274 Hz), 17.11 (q, *J* = 2.4 Hz).

^{19}F NMR (470 MHz, $CDCl_3$) δ -59.89.

MS (APCI) Calculated for $C_{18}H_{12}F_3O_2$ $[M+H]^+$: 317.1; Found: 317.0 m/z

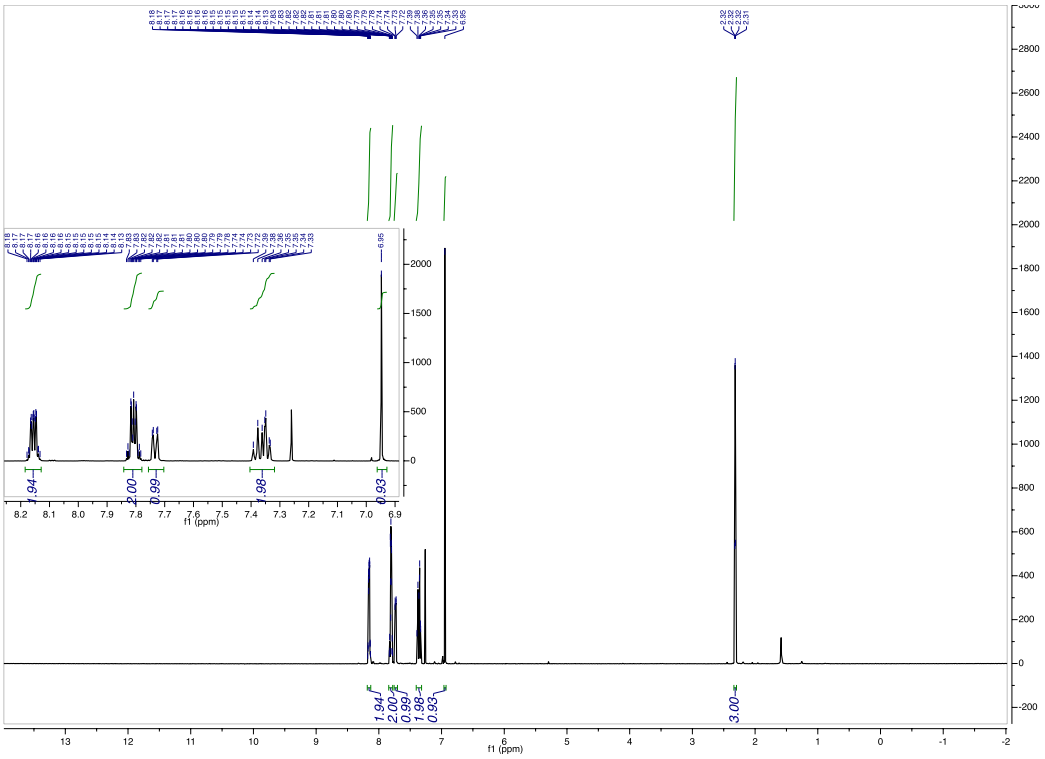

Figure 4.4.72. ^{1}H of 2-(2-methyl-3-(trifluoromethyl)phenyl)naphthalene-1,4-dione

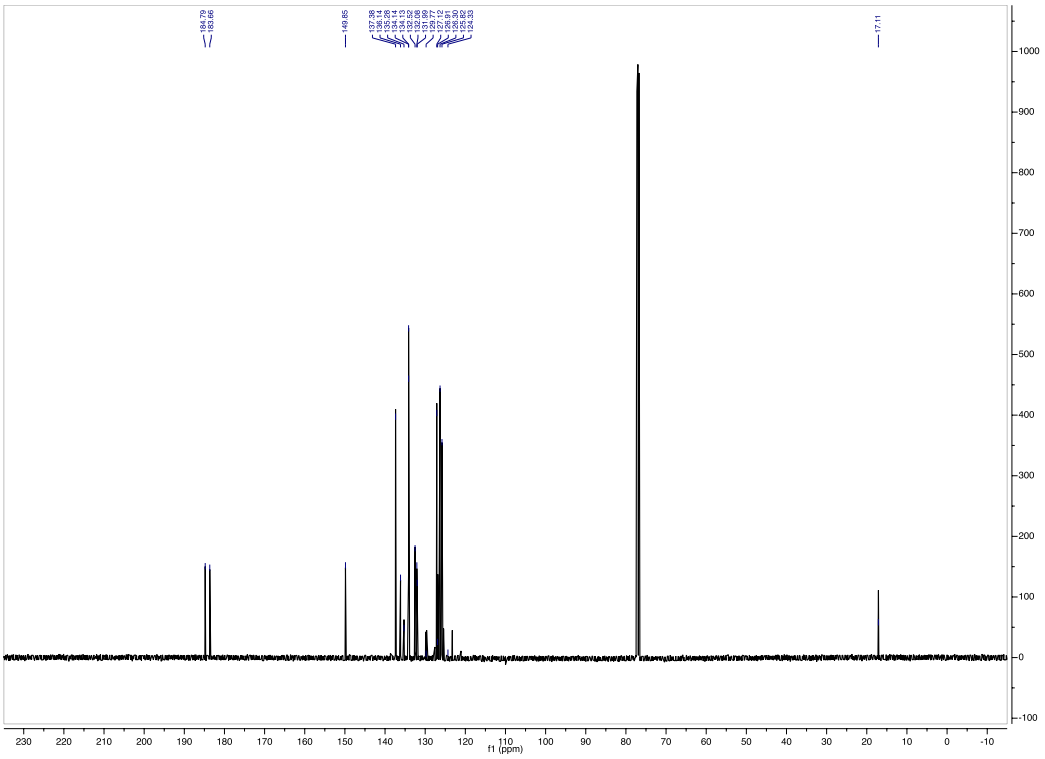

Figure 4.4.73. ^{13}C of 2-(2-methyl-3-(trifluoromethyl)phenyl)naphthalene-1,4-dione

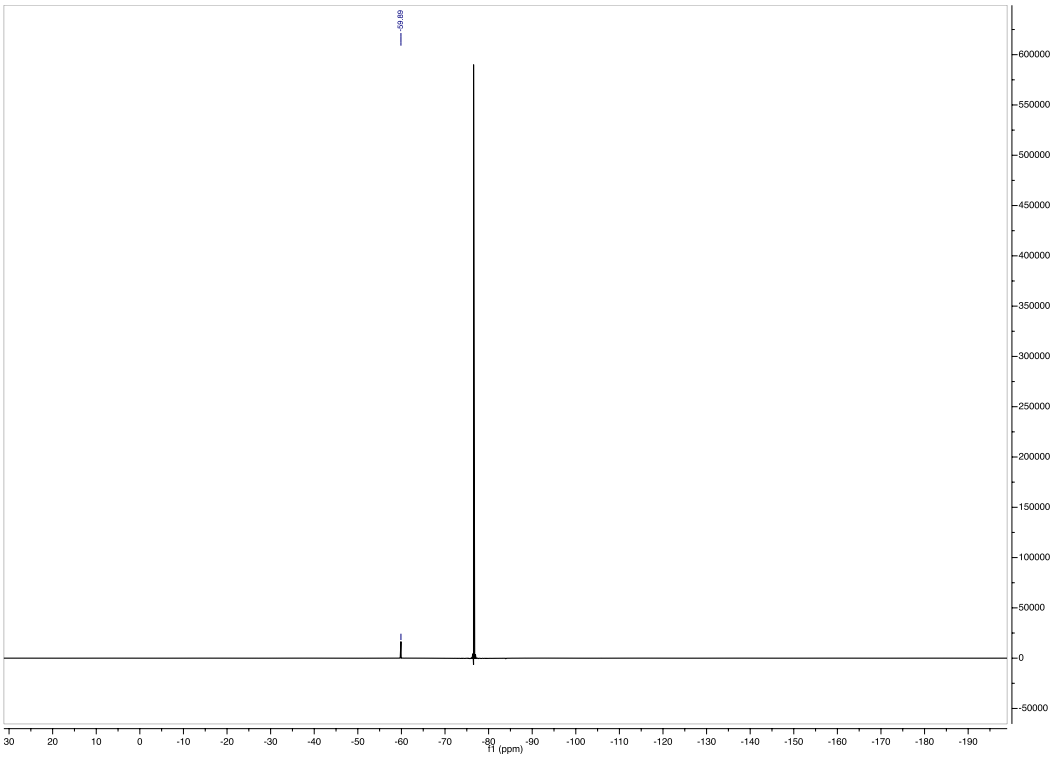

Figure 4.4.74. ^{19}F of 2-(2-methyl-3-(trifluoromethyl)phenyl)naphthalene-1,4-dione

4.4.5 Enantioselective Synthesis of Biaryl Atropisomers from Aryl-Naphthoquinones

Dynamic Kinetic Resolution Procedure:

Aryl-naphthoquinone (0.1mmol, 1.0 equiv) was added to a 20mL scintillation vial equipped with a stir bar. Toluene (2mL) was added to the vial followed by the addition of catalyst **4.C9** (0.005mmol, 0.05 equiv). The vial was wrapped with aluminum foil and placed in an ice/water bath with stirring. Once the solution reached 0 ^{o}C, aryl-thiol (0.2mmol, 2.0 equiv.) was added, and the vial was quickly transferred on ice to a temperature controlled facility and let stir at 4 ^{o}C for 44 hours. The reaction was then moved to a freshly prepared water/ice bath, followed by the addition of a solution of $Na_2S_2O_4$ (140mg) dissolved in 1mL of water. 1mL of tetrahydrofuran, 1mL of MeOH and TBAB (6.4mg) were quickly added, and the biphasic mixture was rigorously stirred for 5 minutes in the ice bath. At this point, the reaction becomes clear/milky white. A solution of KOH (168mg) in 1mL of water was then added to the stirring solution at 0 ^{o}C, resulting in a darkening of the stirring mixture. Me_2SO_4 (275μL) was then quickly added to the stirring mixture, and the vial was removed from the ice bath and let warm to room temperature. The reaction generally goes clear/milky white again upon complete methylation, as observed by TLC. The biphasic mixture was then diluted with water (2mL) and extracted with ethyl acetate (4mL). The organic layer was washed with 2mL brine (2x) and set aside. The combined aqueous layers were back-extracted with ethyl acetate (3mL). The back-extracted organic layer was washed with 2mL brine (2x). Both organic layers were then combined, dried over sodium sulfate, and concentrated in vacuo. The crude oil was then purified by FCC, generally eluting with either hexanes/DCM, or hexanes/EtOAc to afford the corresponding 1,4-dimethoxynaphthalene atropisomer.

1,4-Dimethoxynaphthalene Atropisomers:

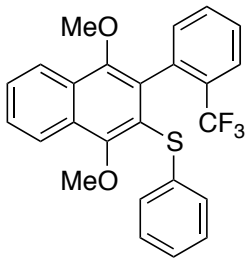

Figure 4.4.75. Product 4.2a

(1,4-dimethoxy-3-(2-(trifluoromethyl)phenyl)naphthalen-2-yl)(phenyl)sulfane (**4.2a**):

DKR was let stir for 20 hours at 0 ^{o}C, rather than 44 hours. 89% yield, purified by FCC, hexanes/DCM = 96/4. 93:7 e.r.

^{1}H NMR (400 MHz, $CDCl_3$) δ 8.27 – 8.21 (m, 1H), 8.18 – 8.13 (m, 1H), 7.79 – 7.73 (m, 1H), 7.67 – 7.58 (m, 2H), 7.47 (tt, *J* = 7.8, 1.1 Hz, 1H), 7.38 (tdd, *J* = 7.5, 1.4, 0.7 Hz, 1H), 7.14 – 7.01 (m, 4H), 6.96 – 6.90 (m, 2H), 4.01 (s, 3H), 3.61 (s, 3H).

^{13}C NMR (101 MHz, $CDCl_3$) δ 155.47, 150.45, 137.62, 135.32 (q, *J* = 2.1 Hz), 132.94, 132.00, 130.72 (q, *J* = 0.9 Hz), 129.50 (q, *J* = 30 Hz), 129.49, 129.38, 128.65, 127.92, 127.69, 127.60, 127.12, 126.43 (q, *J* = 4.9 Hz), 125.54, 124.23 (q, *J* = 274 Hz), 123.47, 123.17, 122.73, 62.32, 61.85.

^{19}F NMR (376 MHz, $CDCl_3$) δ -58.15.

MS (APCI) Calculated for $C_{25}H_{20}F_3O_2S$ $[M+H]^+$: 441.1; Found: 441.2 m/z

HPLC trace: Chiralpak IA (hexanes/2-propanol = 80/20, 1.0 mL/min, t_{ent1} = 4.2 min, t_{ent2} = 5.1 min)

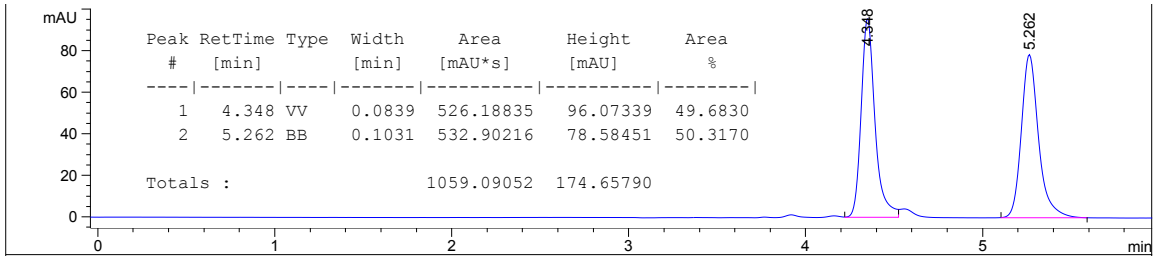

Figure 4.4.76. Racemic HPLC Trace of 4.2a

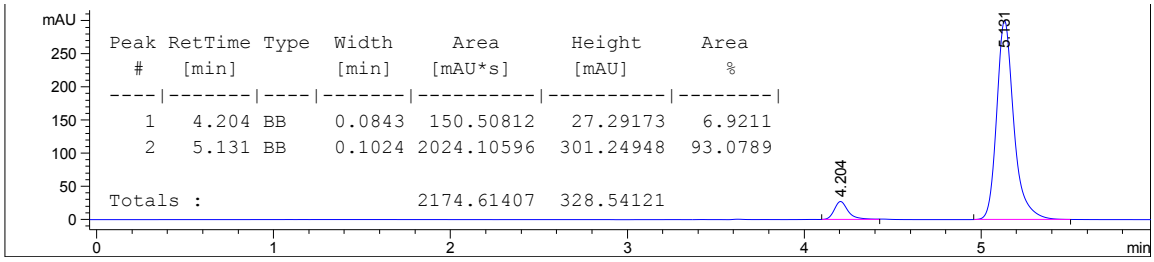

Figure 4.4.77. Asymmetric HPLC Trace of 4.2a

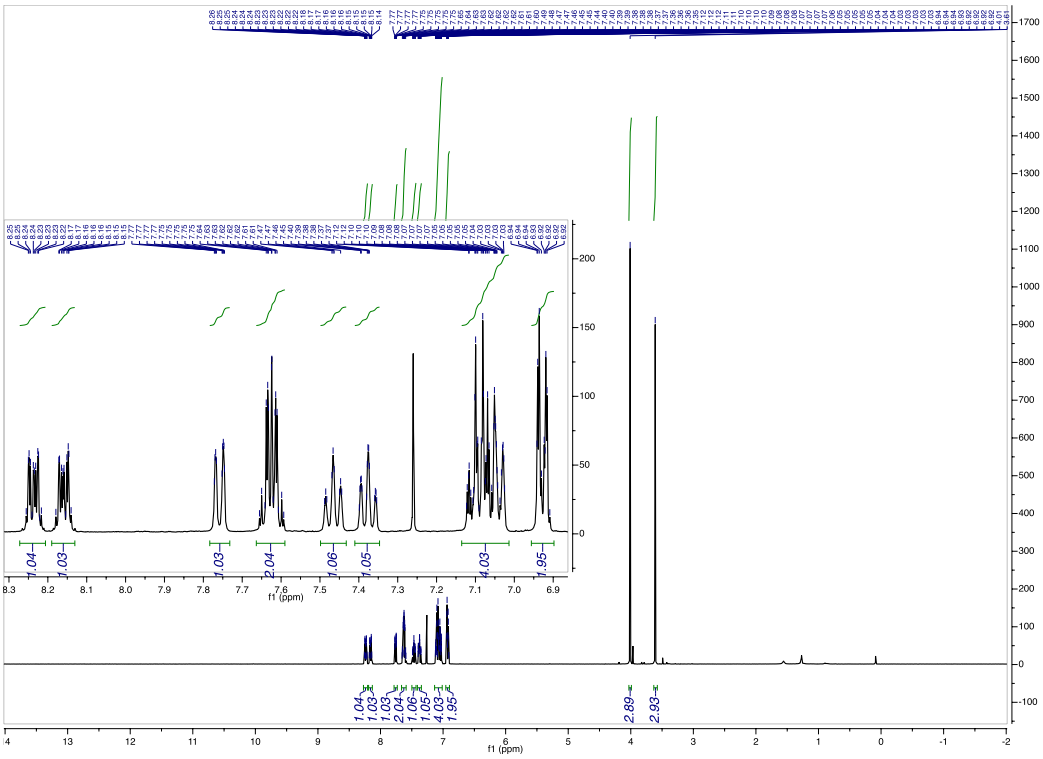

Figure 4.4.78. ^{1}H of 4.2a

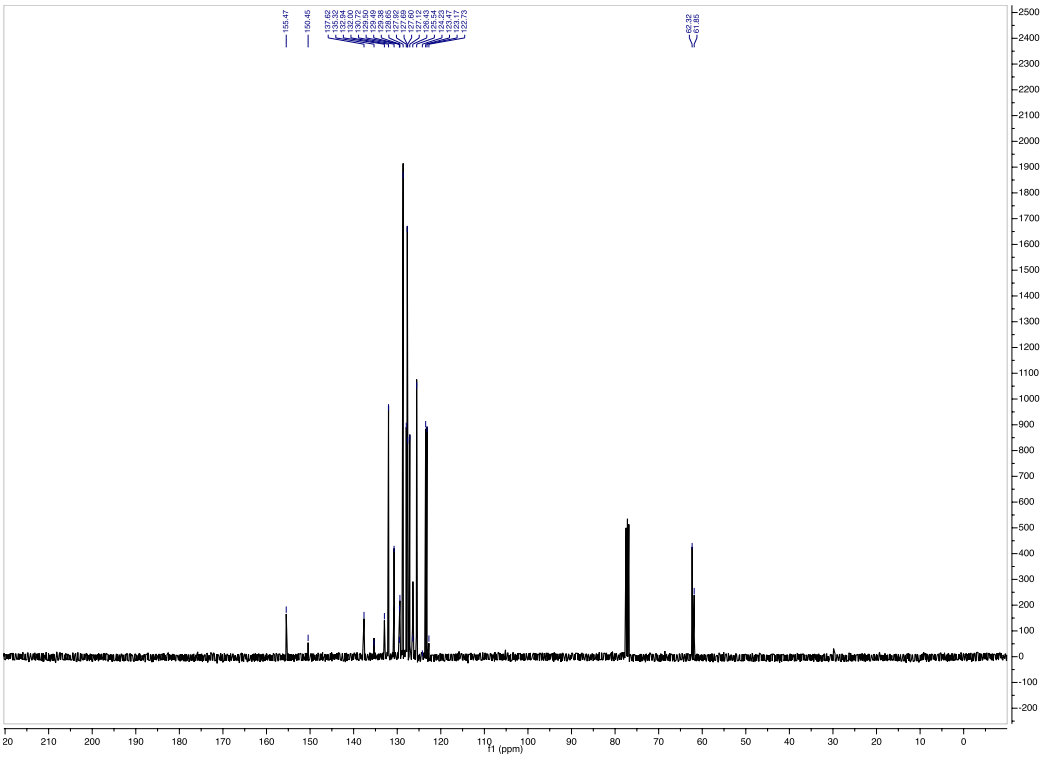

Figure 4.4.79. ^{13}C of 4.2a

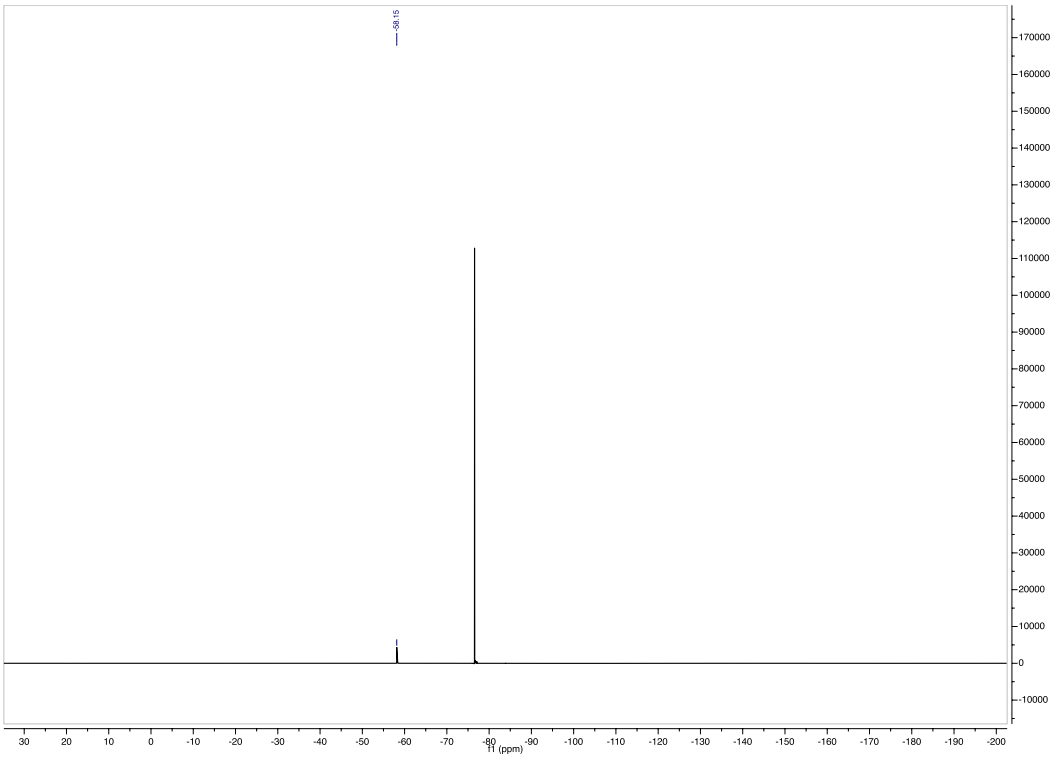

Figure 4.4.80. ^{19}F of 4.2a

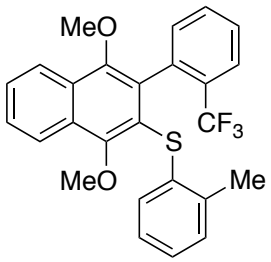

Figure 4.4.81. Product 4.2b

(1,4-dimethoxy-3-(2-(trifluoromethyl)phenyl)naphthalen-2-yl)(*o*-tolyl)sulfane (**4.2b**):

82% yield, purified by FCC, hexanes/DCM = 98/2 → 95/5. 96:4 e.r.

^{1}H NMR (500 MHz, $CDCl_3$) δ 8.30 – 8.22 (m, 1H), 8.19 – 8.14 (m, 1H), 7.74 (d, *J* = 8.0 Hz, 1H), 7.67 – 7.60 (m, 2H), 7.43 (d, *J* = 7.7 Hz, 1H), 7.28 (d, *J* = 7.7 Hz, 1H), 6.99 – 6.90 (m, 3H), 6.88 (d, *J* = 7.7 Hz, 1H), 6.73 (d, *J* = 7.8 Hz, 1H), 4.03 (s, 3H), 3.60 (s, 3H), 2.04 (s, 3H).

^{13}C NMR (126 MHz, $CDCl_3$) δ 155.85, 150.61, 137.03, 136.00, 135.11 (q, *J* = 1.9 Hz), 133.04, 131.77, 130.52, 129.76, 129.53, 129.46 (q, *J* = 30 Hz), 129.29, 127.84, 127.77, 127.57, 127.12, 126.33 (q, *J* = 4.8 Hz), 126.25, 125.30, 124.61 (q, *J* = 274 Hz), 123.45, 123.19, 122.98, 62.73, 61.85, 20.10.

^{19}F NMR (470 MHz, $CDCl_3$) δ -58.10.

MS (APCI) Calculated for $C_{26}H_{22}F_3O_2S$ $[M+H]^+$: 455.1; Found: 455.0 m/z

HPLC trace: Chiralpak IA (hexanes/2-propanol = 90/10, 1.0 mL/min, t_{ent1} = 4.1 min, t_{ent2} = 4.6 min)

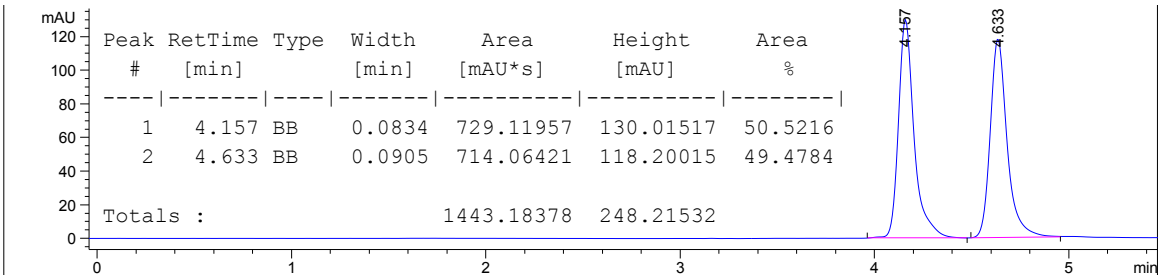

Figure 4.4.82. Racemic HPLC Trace of 4.2b

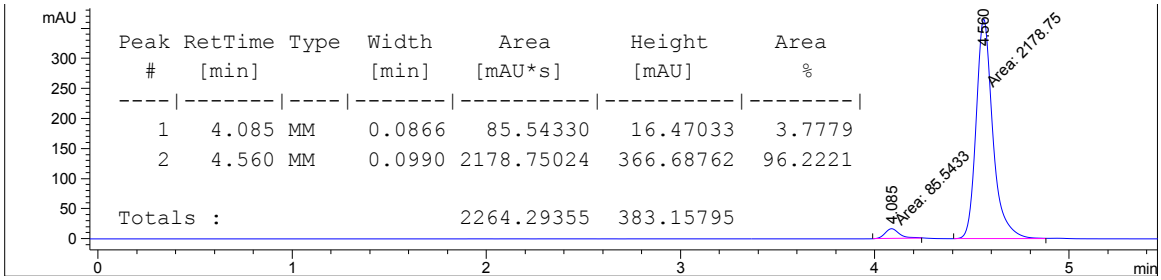

Figure 4.4.83. Asymmetric HPLC Trace of 4.2b

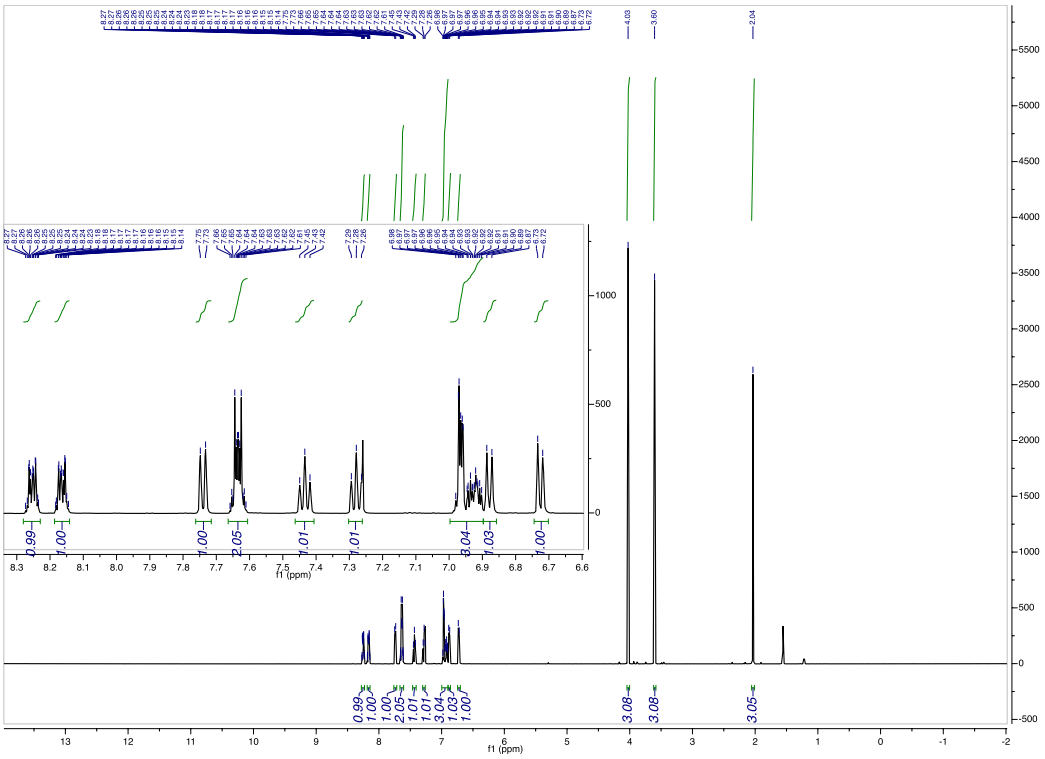

Figure 4.4.84. ^{1}H of 4.2b

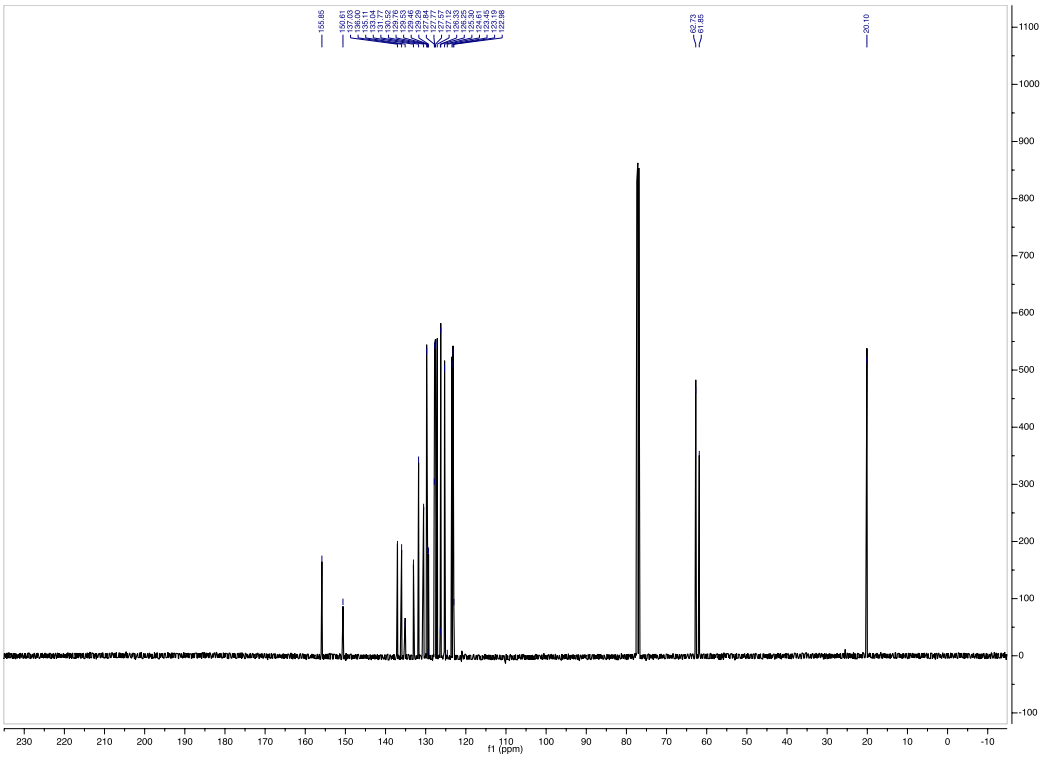

Figure 4.4.85. ^{13}C of 4.2b

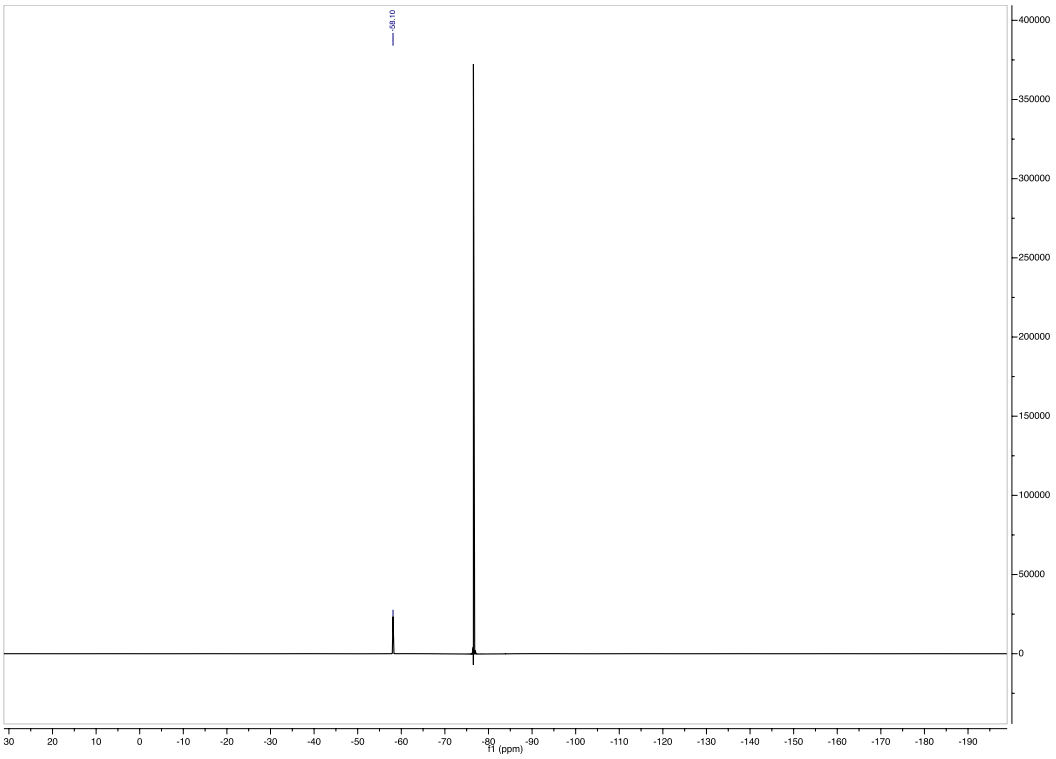

Figure 4.4.86. ^{19}F of 4.2b

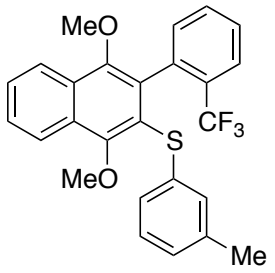

Figure 4.4.87. Product 4.2c

(1,4-dimethoxy-3-(2-(trifluoromethyl)phenyl)naphthalen-2-yl)(*m*-tolyl)sulfane (**4.2c**):

DKR was let stir for 20 hours at 0 ^{o}C, rather than 44 hours. 71% yield, purified by FCC, hexanes/EtOAc = 98/2. 93:7 e.r.

^{1}H NMR (500 MHz, $CDCl_3$) δ 8.26 – 8.20 (m, 1H), 8.18 – 8.12 (m, 1H), 7.74 (d, *J* = 7.9 Hz, 1H), 7.66 – 7.59 (m, 2H), 7.46 (t, *J* = 7.9 Hz, 1H), 7.38 (t, *J* = 7.6 Hz, 1H), 7.04 (d, *J* = 7.6 Hz, 1H), 6.97 (t, *J* = 7.7 Hz, 1H), 6.86 (d, *J* = 7.8 Hz, 1H), 6.74 (s, 1H), 6.70 (d, *J* = 7.8 Hz, 1H), 4.01 (s, 3H), 3.60 (s, 3H), 2.18 (s, 3H).z

^{13}C NMR (126 MHz, $CDCl_3$) δ 155.37, 150.38, 138.32, 137.24, 135.26 (q, *J* = 2.1 Hz), 132.96, 132.11, 130.64, 129.48 (q, *J* = 30 Hz), 129.42, 129.36, 128.53, 128.49, 127.84, 127.52, 127.08, 126.56, 126.43 (q, *J* = 4.7 Hz), 124.98, 124.26 (q, *J* = 274 Hz), 123.48, 123.15, 123.00, 62.33, 61.81, 21.44.

^{19}F NMR (470 MHz, $CDCl_3$) δ -58.12.

MS (APCI) Calculated for $C_{26}H_{22}F_3O_2S$ $[M+H]^+$: 455.1; Found: 455.2 m/z

HPLC trace: Chiralpak IA (hexanes/2-propanol = 90/10, 1.0 mL/min, t_{ent1} = 4.1 min, t_{ent2} = 4.9 min)

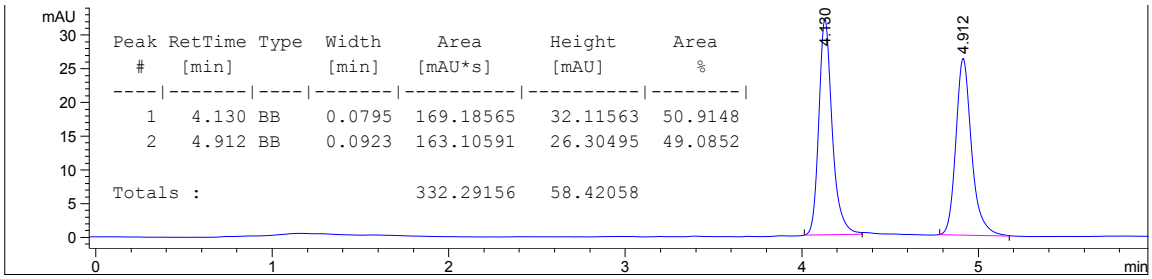

Figure 4.4.88. Racemic HPLC trace of 4.2c

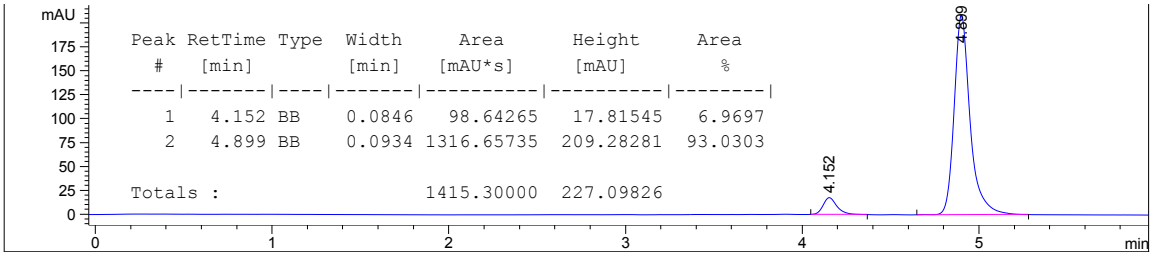

Figure 4.4.89. Asymmetric HPLC trace of 4.2c

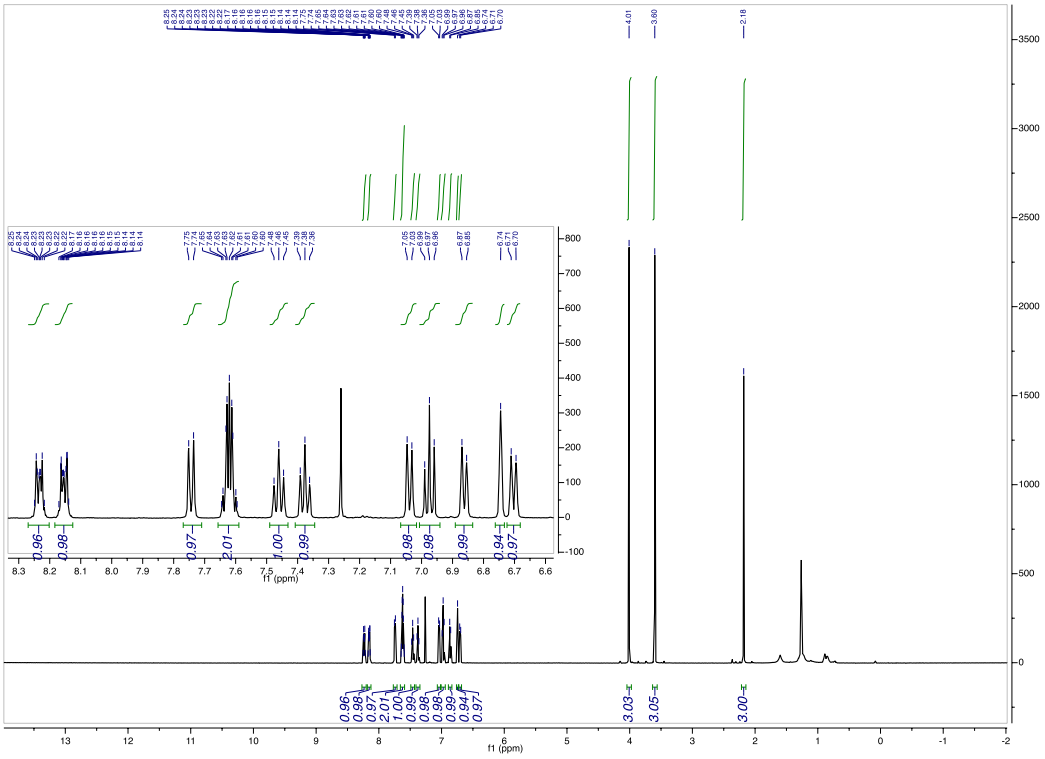

Figure 4.4.90. ^{1}H of 4.2c

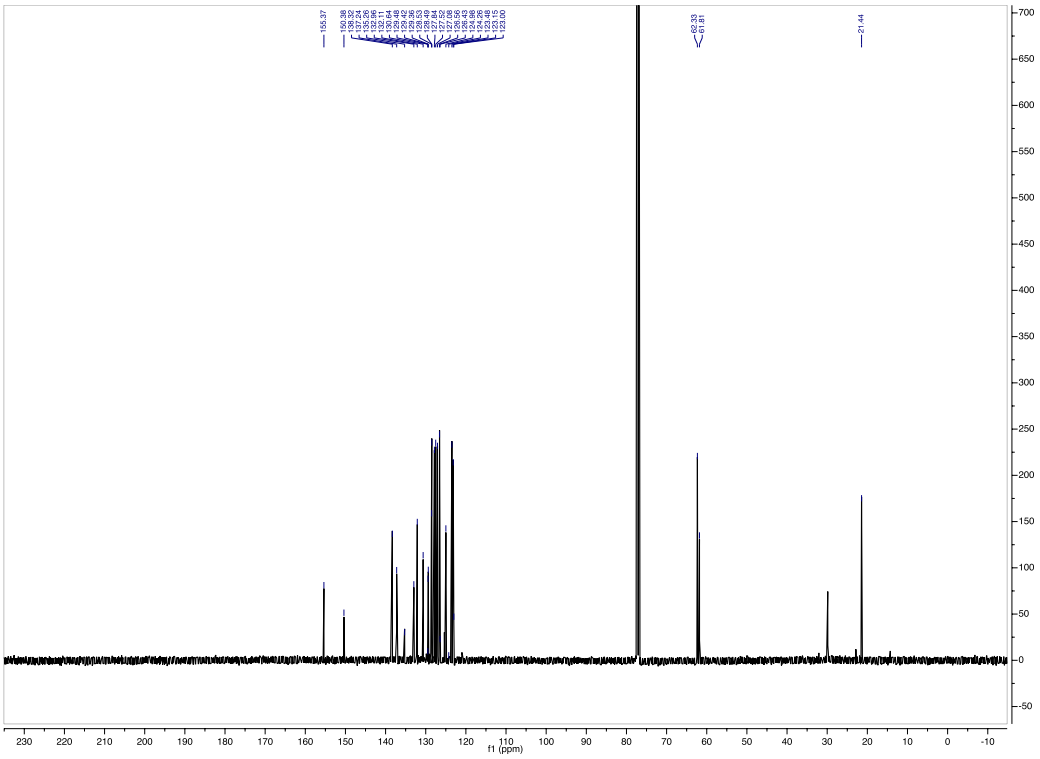

Figure 4.4.91. ^{13}C of 4.2c

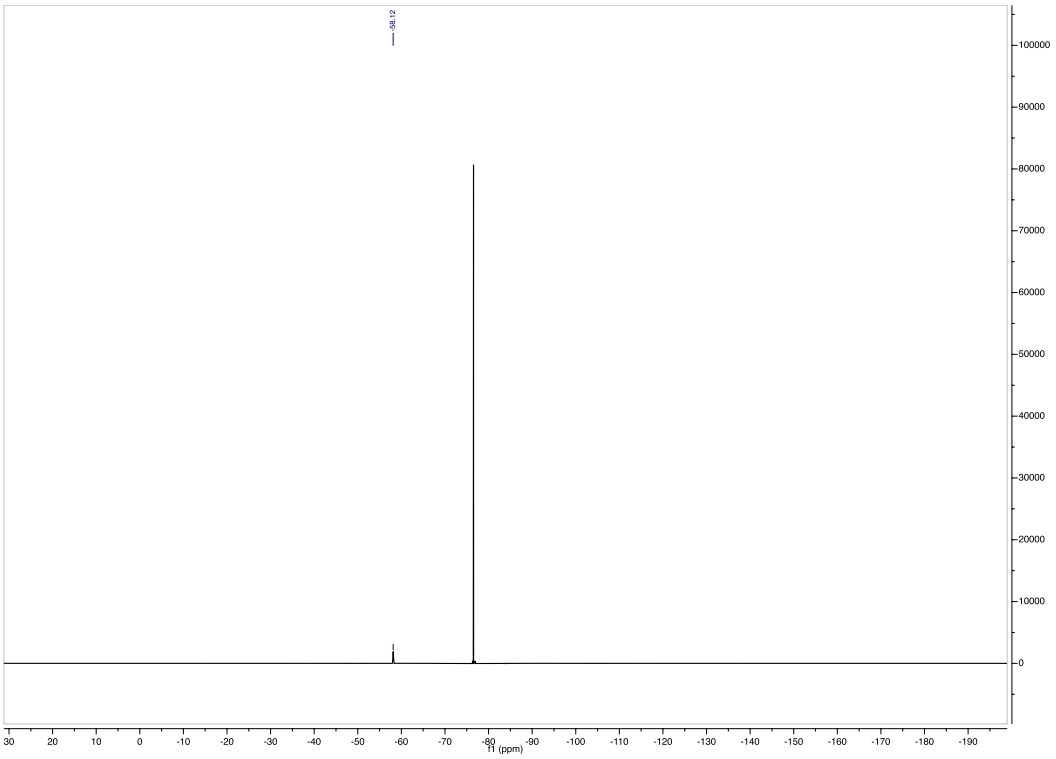

Figure 4.4.92. ^{19}F of 4.2c

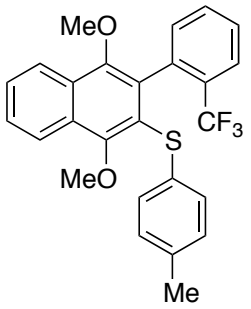

Figure 4.4.93. Product 4.2d

(1,4-dimethoxy-3-(2-(trifluoromethyl)phenyl)naphthalen-2-yl)(*p*-tolyl)sulfane (**4.2d**):

DKR was let stir for 20 hours at 0 ^{o}C, rather than 44 hours. 88% yield, purified by FCC, hexanes/EtOAc = 98/2. 93:7 e.r.

^{1}H NMR (500 MHz, $CDCl_3$) δ 8.25 – 8.20 (m, 1H), 8.17 – 8.13 (m, 1H), 7.76 (d, *J* = 7.3 Hz, 1H), 7.64 – 7.58 (m, 2H), 7.48 (d, *J* = 7.7 Hz, 1H), 7.41 (d, *J* = 7.6 Hz, 1H), 7.07 (d, *J* = 7.6 Hz, 1H), 6.94 – 6.89 (m, 2H), 6.87 – 6.83 (m, 2H), 4.00 (s, 3H), 3.60 (s, 3H), 2.24 (s, 3H).

^{13}C NMR (126 MHz, $CDCl_3$) δ 155.18, 150.32, 135.47, 135.46 (q, *J* = 2.0 Hz), 133.91, 132.91, 132.07, 130.77, 129.50 (q, *J* = 30 Hz), 129.45, 129.41, 129.31, 128.02, 127.89, 127.46, 127.05, 126.42 (q, *J* = 4.8 Hz), 124.25 (q, *J* = 274 Hz), 123.42, 123.35, 123.13, 62.13, 61.84, 21.11.

^{19}F NMR (470 MHz, $CDCl_3$) δ -58.16.

MS (APCI) Calculated for $C_{26}H_{22}F_3O_2S$ $[M+H]^+$: 455.1; Found: 455.1 m/z

HPLC trace: Chiralpak IA (hexanes/2-propanol = 90/10, 1.0 mL/min, t_{ent1} = 4.9 min, t_{ent2} = 5.7 min)

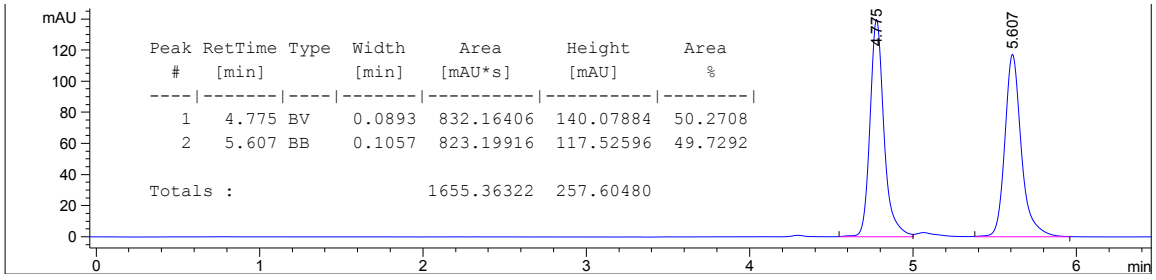

Figure 4.4.94. Racemic HPLC trace of 4.2d

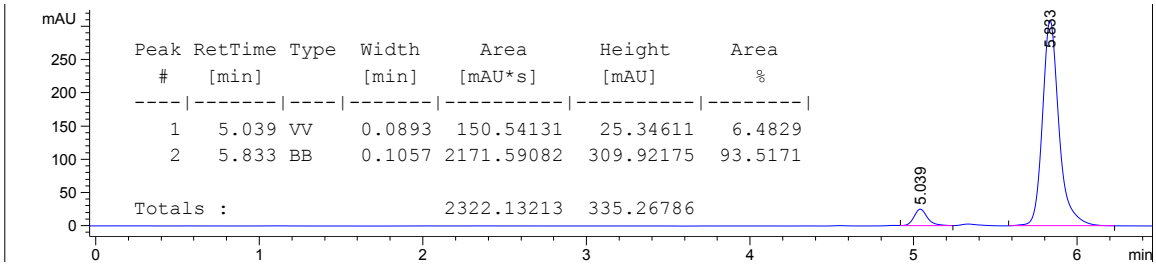

Figure 4.4.95. Asymmetric HPLC trace of 4.2d

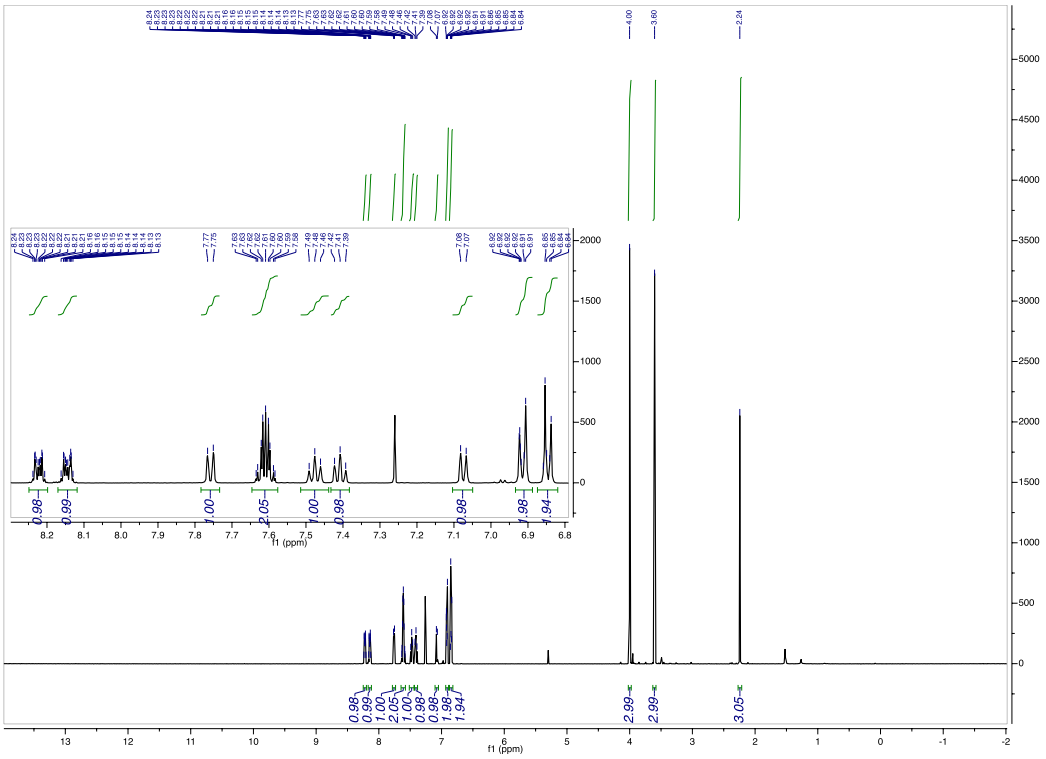

Figure 4.4.96. ^{1}H of 4.2d

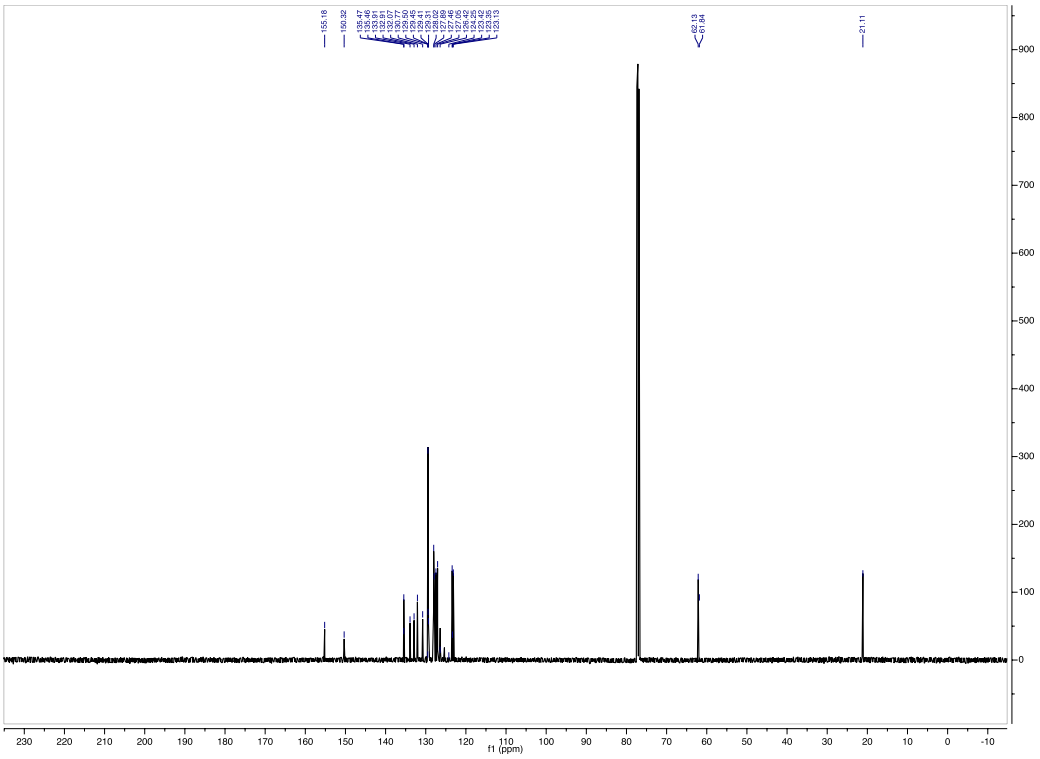

Figure 4.4.97. ^{13}C of 4.2d

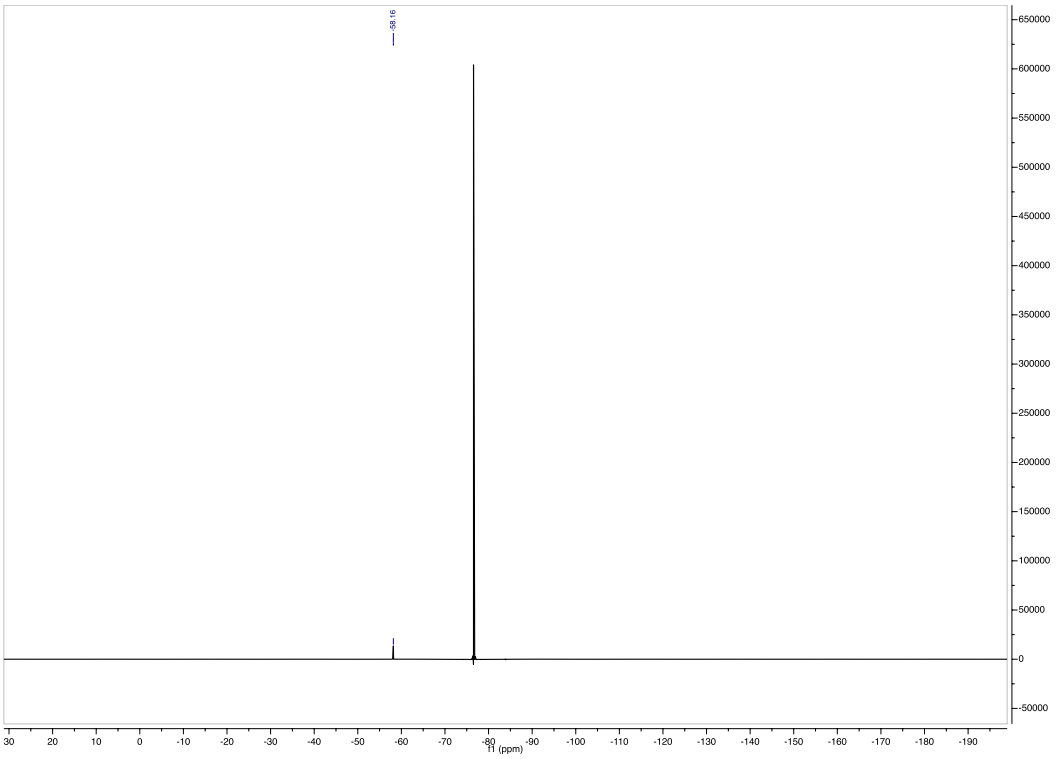

Figure 4.4.98. ^{19}F of 4.2d

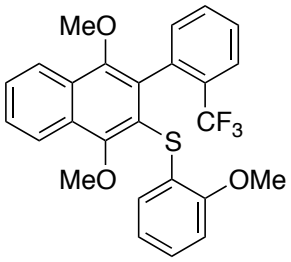

Figure 4.4.99. Product 4.2e

(1,4-dimethoxy-3-(2-(trifluoromethyl)phenyl)naphthalen-2-yl)(2-methoxyphenyl)sulfane (**4.2e**): 82% yield, purified by FCC, hexanes/DCM = 94/6. 94:6 e.r.

^{1}H NMR (500 MHz, $CDCl_3$) δ 8.24 – 8.19 (m, 1H), 8.18 – 8.13 (m, 1H), 7.72 (d, *J* = 7.9 Hz, 1H), 7.65 – 7.58 (m, 2H), 7.43 (t, *J* = 7.7 Hz, 1H), 7.35 (t, *J* = 7.4 Hz, 1H), 7.08 (d, *J* = 7.0 Hz, 1H), 7.03 (ddd, *J* = 8.2, 7.3, 1.7 Hz, 1H), 6.72 – 6.67 (m, 2H), 6.61 (dd, *J* = 7.7, 1.7 Hz, 1H), 3.99 (s, 3H), 3.70 (s, 3H), 3.60 (s, 3H).

^{13}C NMR (126 MHz, $CDCl_3$) δ 155.96, 155.65, 150.51, 135.32 (q, *J* = 1.9 Hz), 133.13, 131.72, 130.65, 129.52 (q, *J* = 30 Hz), 129.43, 129.37, 127.79, 127.48, 127.02, 126.39 (q, *J* = 4.8 Hz), 126.31, 126.20, 124.25 (q, *J* = 274 Hz), 123.45, 123.17, 122.05, 121.10, 110.70, 62.45, 61.85, 55.95.

^{19}F NMR (470 MHz, $CDCl_3$) δ -58.14

MS (APCI) Calculated for $C_{26}H_{22}F_3O_3S$ $[M+H]^+$: 471.1; Found: 471.2 m/z

HPLC trace: Chiralpak IA (hexanes/2-propanol = 90/10, 1.0 mL/min, t_{ent1} = 5.7 min, t_{ent2} = 7.0 min)

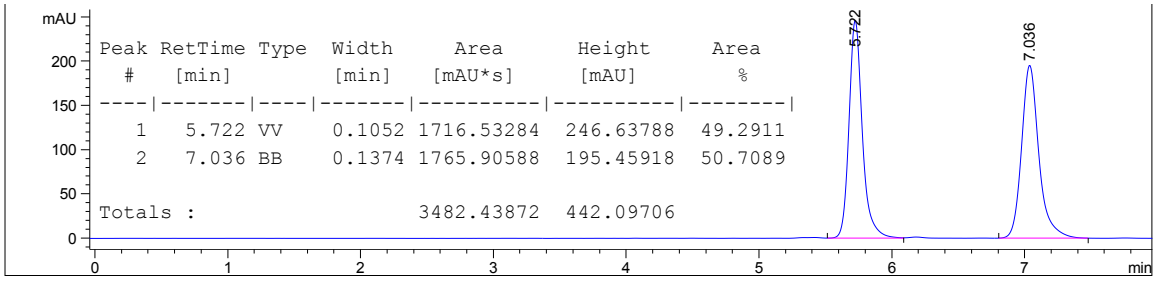

Figure 4.4.100. Racemic HPLC trace of 4.2e

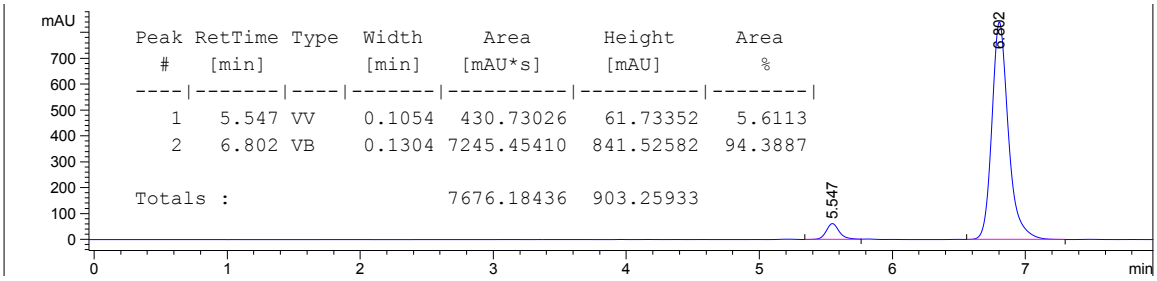

Figure 4.4.101. Asymmetric HPLC trace of 4.2e

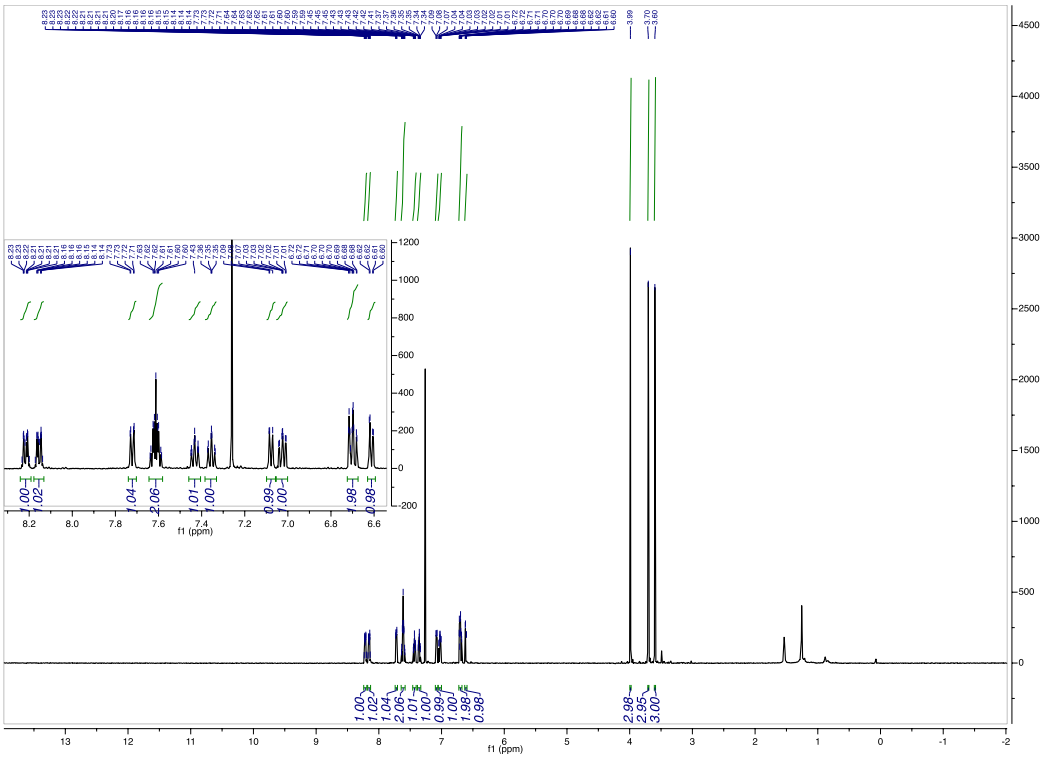

Figure 4.4.102. ^{1}H of 4.2e

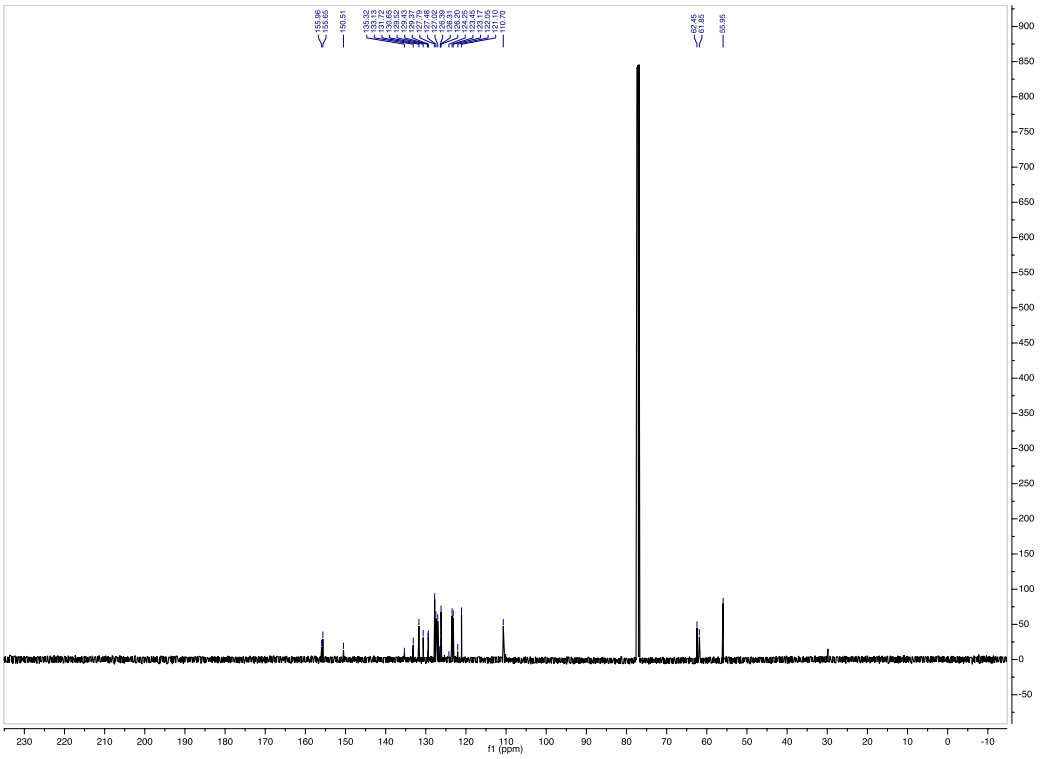

Figure 4.4.103. ^{13}C of 4.2e

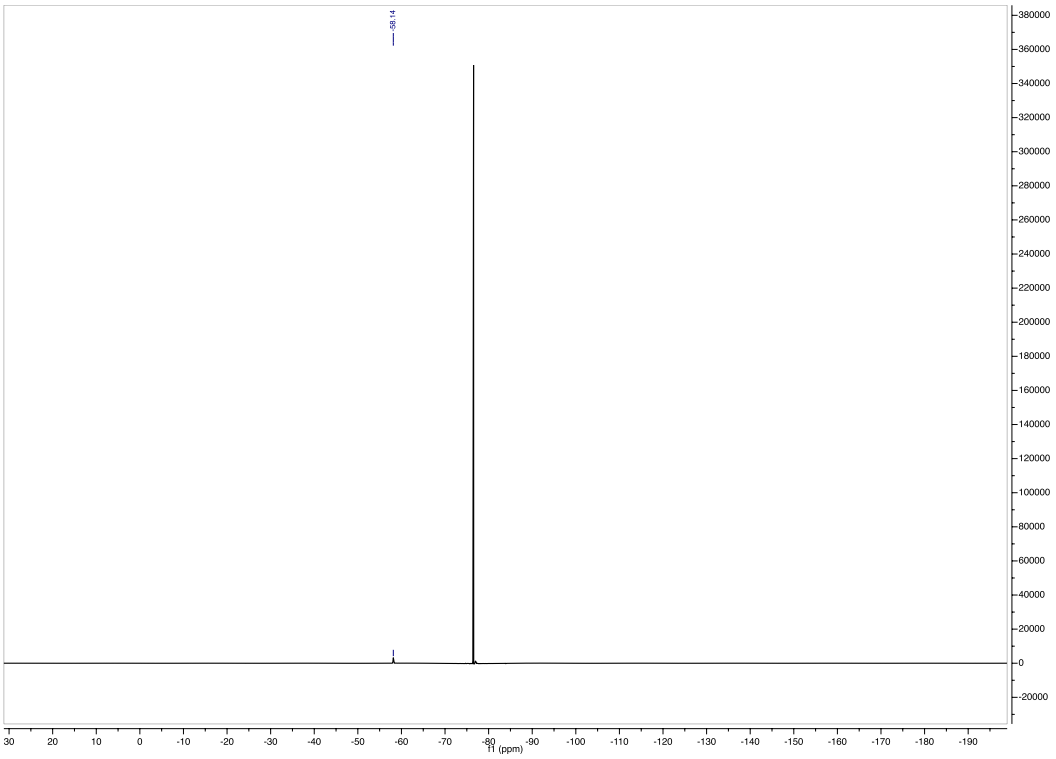

Figure 4.4.104. ^{19}F of 4.2e

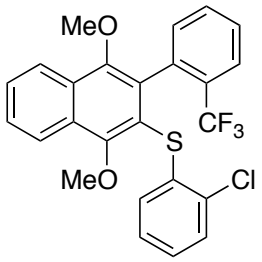

Figure 4.4.105. Product 4.2f

(2-chlorophenyl)(1,4-dimethoxy-3-(2-(trifluoromethyl)phenyl)naphthalen-2-yl)sulfane (**4.2f**): 86% yield, purified by FCC, hexanes/EtOAc = 98/2. 96:4 e.r.

^{1}H NMR (599 MHz, $CDCl_3$) δ 8.26 – 8.20 (m, 1H), 8.20 – 8.15 (m, 1H), 7.76 (d, *J* = 7.9 Hz, 1H), 7.68 – 7.61 (m, 2H), 7.47 (d, *J* = 7.7 Hz, 1H), 7.37 (d, *J* = 7.5 Hz, 1H), 7.22 – 7.17 (m, 1H), 7.03 (d, *J* = 7.5 Hz, 1H), 7.00 – 6.95 (m, 2H), 6.71 – 6.65 (m, 1H), 4.01 (s, 3H), 3.62 (s, 3H).

^{13}C NMR (151 MHz, $CDCl_3$) δ 155.82, 150.71, 136.98, 135.00 (q, *J* = 2.0 Hz), 132.87, 131.56, 131.42, 130.79, 129.77, 129.47 (q, *J* = 30 Hz), 129.37, 129.31, 128.12, 128.02, 127.87, 127.25, 126.90, 126.57 (q, *J* = 4.5 Hz), 126.06, 124.25 (q, *J* = 274 Hz), 123.50, 123.25, 121.57, 62.65, 61.91.

^{19}F NMR (376 MHz, $CDCl_3$) δ -58.08.

MS (APCI) Calculated for $C_{25}H_{19}ClF_3O_2S$ $[M+H]^+$: 475.1; Found: 475.2 m/z

HPLC trace: Chiralpak IA (hexanes/2-propanol = 90/10, 1.0 mL/min, t_{ent1} = 4.4 min, t_{ent2} = 5.0 min)

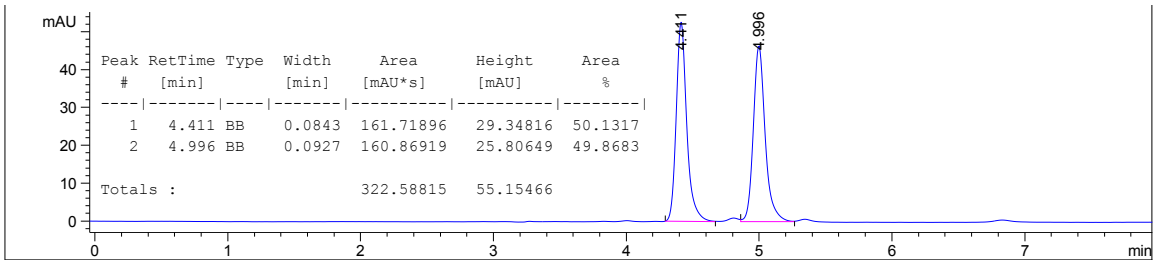

Figure 4.4.106. Racemic HPLC trace of 4.2f

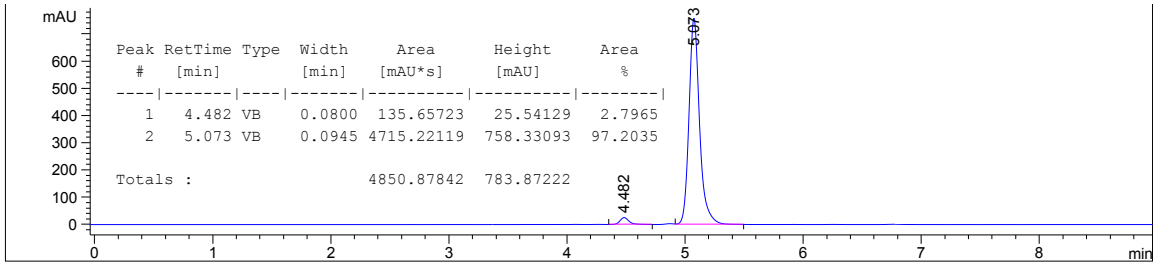

Figure 4.4.107. Asymmetric HPLC trace of 4.2f

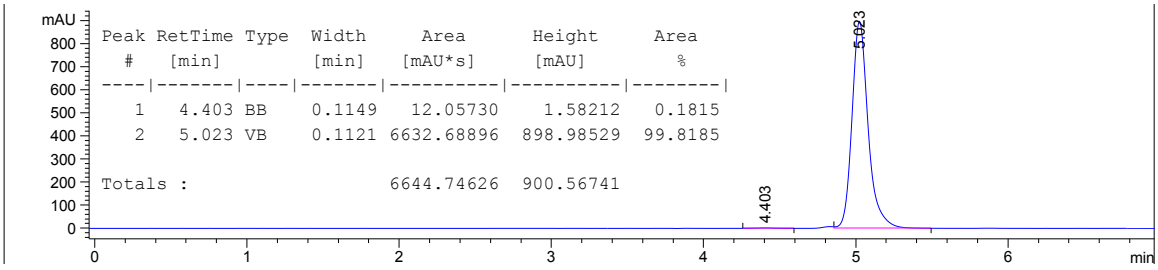

Figure 4.4.108. HPLC trace of recrystallized 4.2f

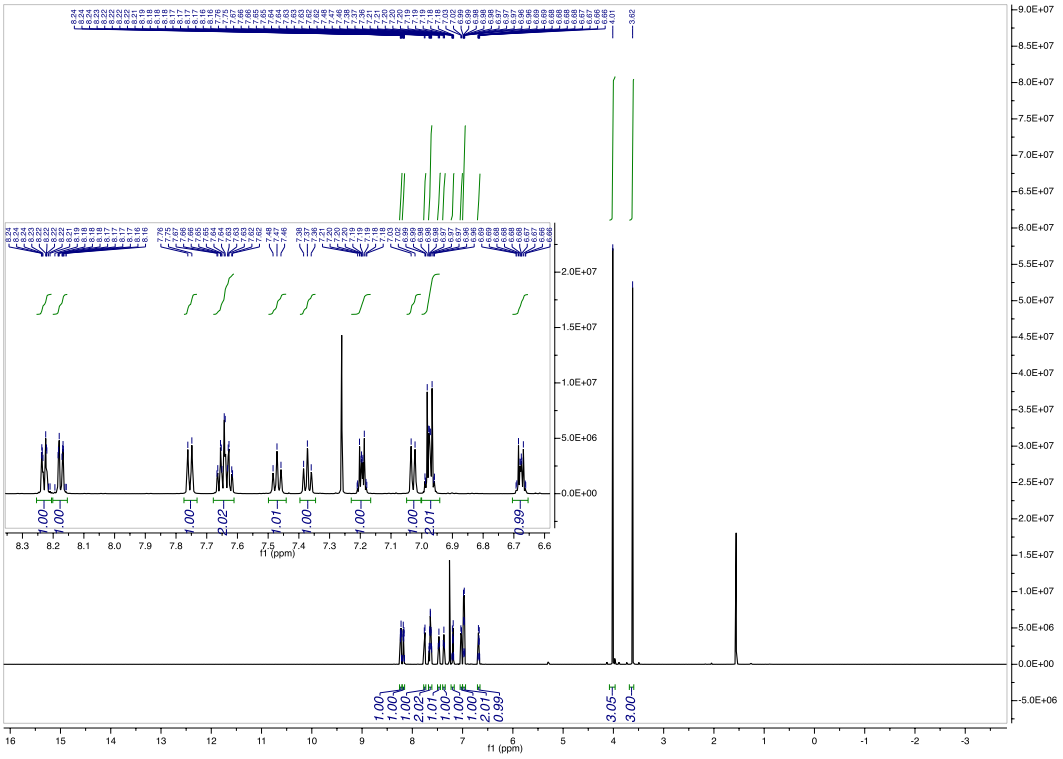

Figure 4.4.109. ^{1}H of 4.2f

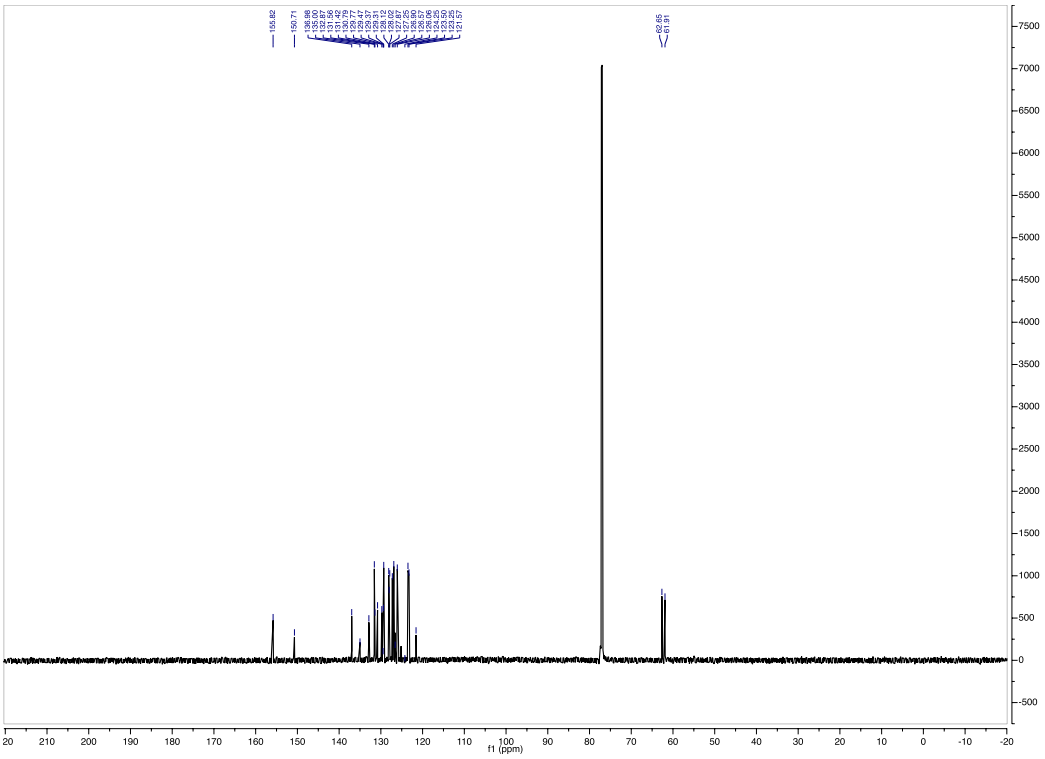

Figure 4.4.110. ^{13}C of 4.2f

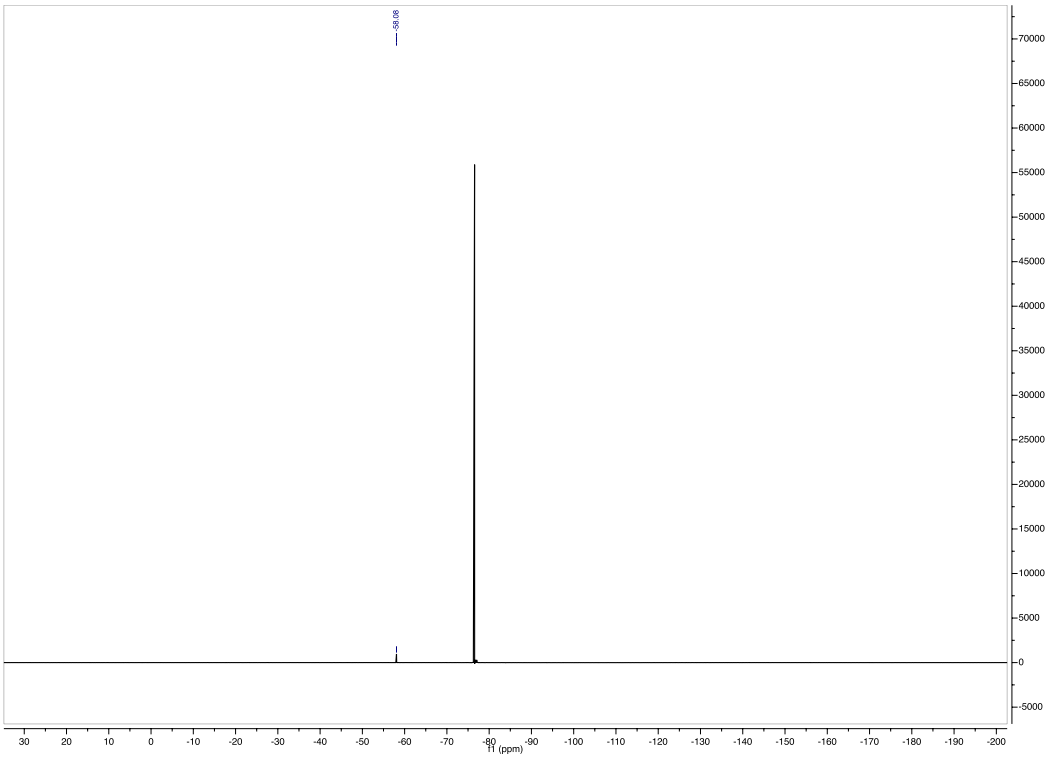

Figure 4.4.111. ^{19}F of 4.2f

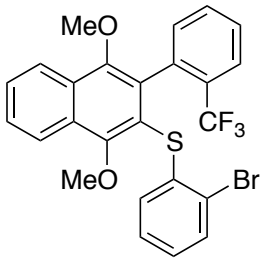

Figure 4.4.112. Product 4.2g

(2-bromophenyl)(1,4-dimethoxy-3-(2-(trifluoromethyl)phenyl)naphthalen-2-yl)sulfane (**4.2g**): 83% yield, purified by FCC, hexanes/EtOAc = 99/1. 97:3 e.r.

^{1}H NMR (500 MHz, $CDCl_3$) δ 8.27 – 8.21 (m, 1H), 8.20 – 8.15 (m, 1H), 7.76 (d, *J* = 7.9 Hz, 1H), 7.68 – 7.61 (m, 2H), 7.47 (t, *J* = 7.7 Hz, 1H), 7.39 – 7.34 (m, 2H), 7.04 – 6.98 (m, 2H), 6.89 (ddd, *J* = 7.9, 7.3, 1.6 Hz, 1H), 6.66 (dd, *J* = 8.0, 1.6 Hz, 1H), 4.02 (s, 3H), 3.62 (s, 3H).

^{13}C NMR (126 MHz, $CDCl_3$) δ 155.82, 150.73, 139.07, 134.98 (q, *J* = 2.2 Hz), 132.85, 132.56, 131.57, 130.78, 129.81, 129.48 (q, *J* = 30 Hz), 129.40, 128.12, 128.04, 127.88, 127.49, 127.25, 126.59 (q, *J* = 4.9 Hz), 126.24, 124.26 (q, *J* = 274 Hz), 123.53, 123.26, 122.07, 121.18, 62.71, 61.90.

MS (APCI) Calculated for $C_{25}H_{19}BrF_3O_2S$ $[M+H]^+$: 519.0; Found: 518.9 m/z

HPLC trace: Chiralpak IA (hexanes/2-propanol = 90/10, 1.0 mL/min, t_{ent1} = 4.6 min, t_{ent2} = 5.0 min)

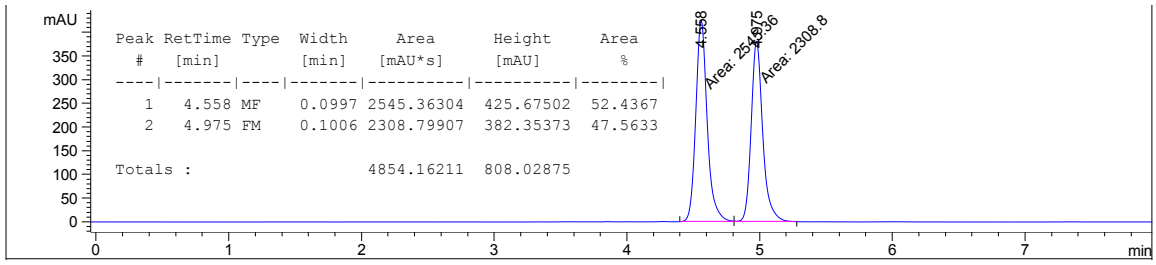

Figure 4.4.113. Racemic HPLC trace of 4.2g

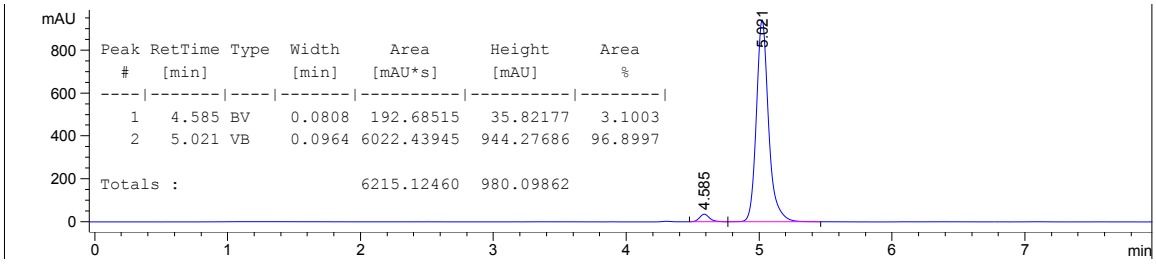

Figure 4.4.114. Asymmetric HPLC trace of 4.2g

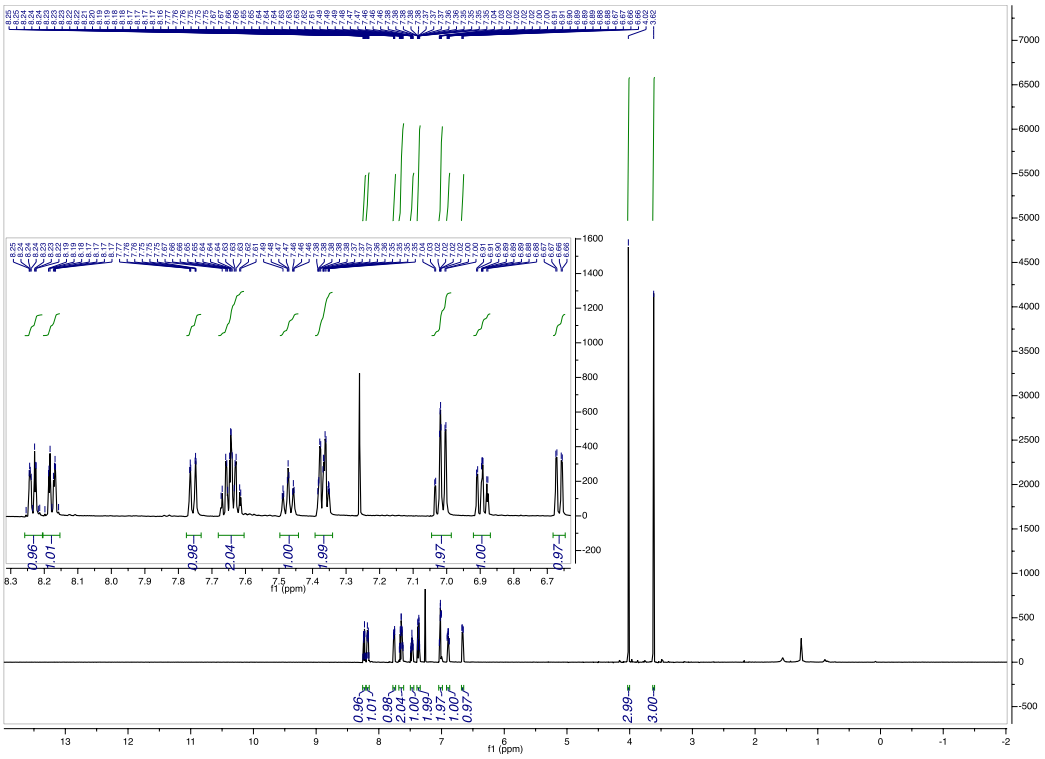

Figure 4.4.115. ^{1}H of 4.2g

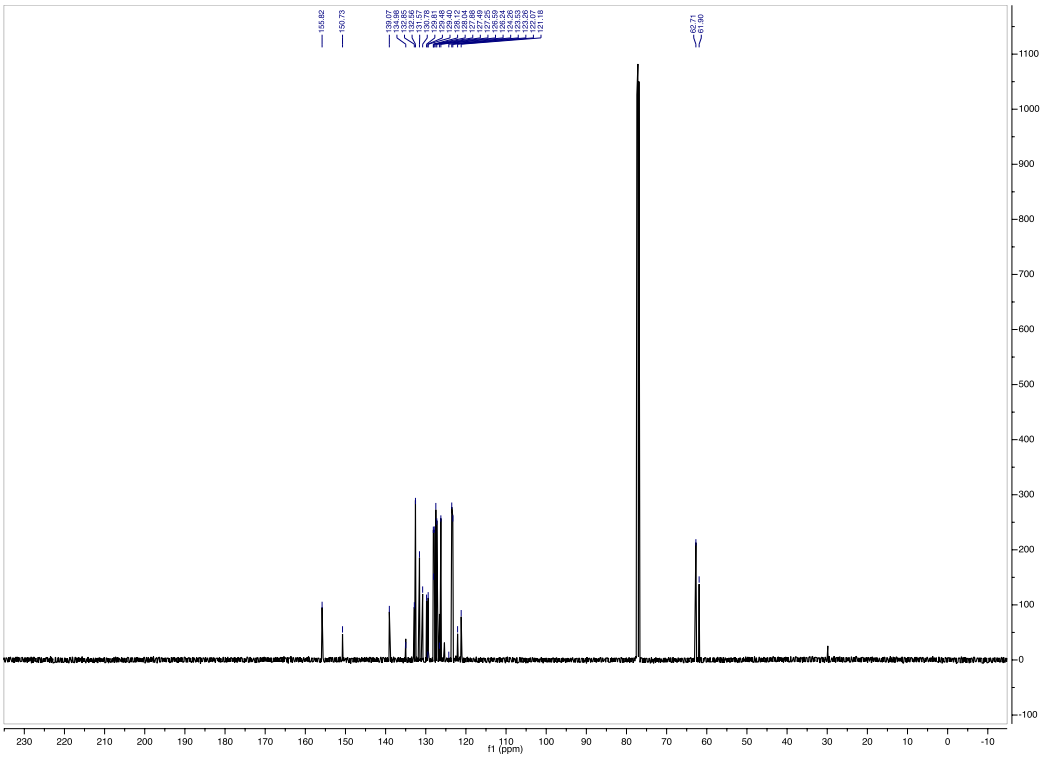

Figure 4.4.116. ^{13}C of 4.2g

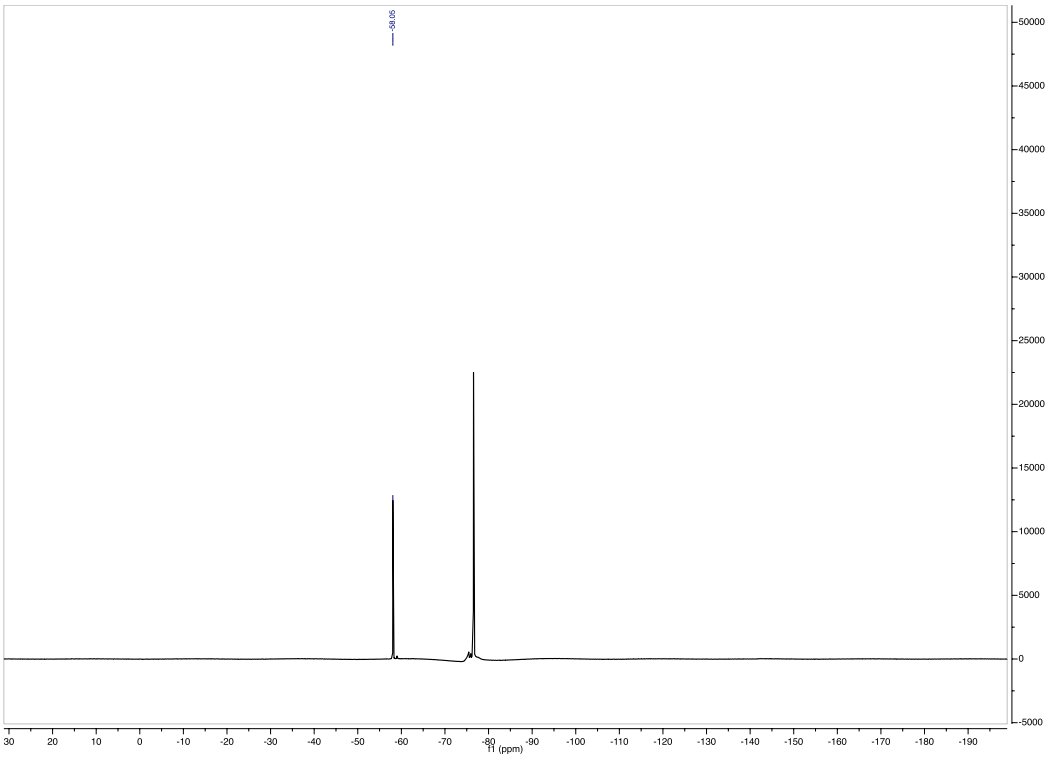

Figure 4.4.117. ^{19}F of 4.2g

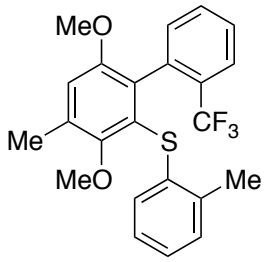

Figure 4.4.118. Product 4.2i

(3,6-dimethoxy-4-methyl-2'-(trifluoromethyl)-[1,1'-biphenyl]-2-yl)(*o*-tolyl)sulfane (**4.2i**):

70% yield, purified by FCC, hexanes/DCM = 99.5:0.5 → 99:1. 68:32 e.r.

^{1}H NMR (500 MHz, $CDCl_3$) δ 7.67 (d, *J* = 7.9 Hz, 1H), 7.38 (tt, *J* = 7.8, 1.1 Hz, 1H), 7.32 (t, *J* = 7.6 Hz, 1H), 7.01 – 6.93 (m, 3H), 6.89 (d, *J* = 7.6 Hz, 1H), 6.85 (s, 1H), 6.78 – 6.72 (m, 1H), 3.73 (s, 3H), 3.67 (s, 3H), 2.40 (d, *J* = 0.6 Hz, 3H), 2.07 (s, 3H).

^{13}C NMR (126 MHz, $CDCl_3$) δ 153.73, 137.60, 135.96 (q, *J* = 2.2 Hz), 135.56, 132.57, 131.82, 131.43, 131.04, 129.70, 129.18 (q, *J* = 30 Hz), 127.76, 127.46, 127.41, 126.24, 125.97 (q, *J* = 5.0 Hz), 125.08, 124.24 (q, *J* = 274 Hz), 114.59, 61.02, 56.09, 20.18, 17.21.

^{19}F NMR (470 MHz, $CDCl_3$) δ -59.39.

MS (APCI) Calculated for $C_{23}H_{22}F_3O_2S$ $[M+H]^+$: 419.1; Found: 418.9 m/z

HPLC trace: Chiralpak IA (hexanes/2-propanol = 99/1, 1.0 mL/min, t_{ent1} = 5.7 min, t_{ent2} = 6.1 min)

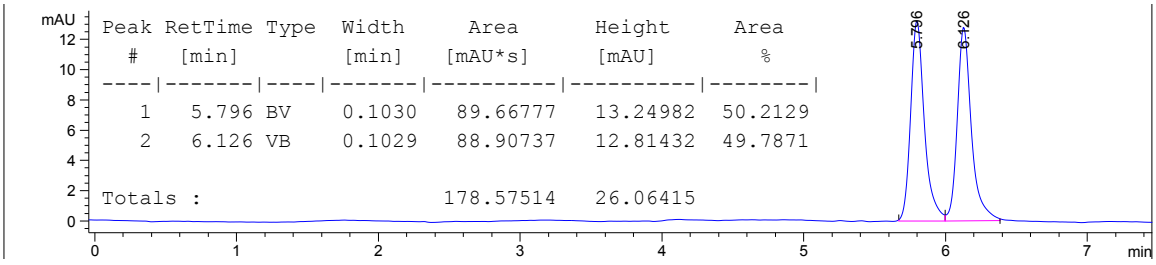

Figure 4.4.119. Racemic HPLC trace of 4.2i

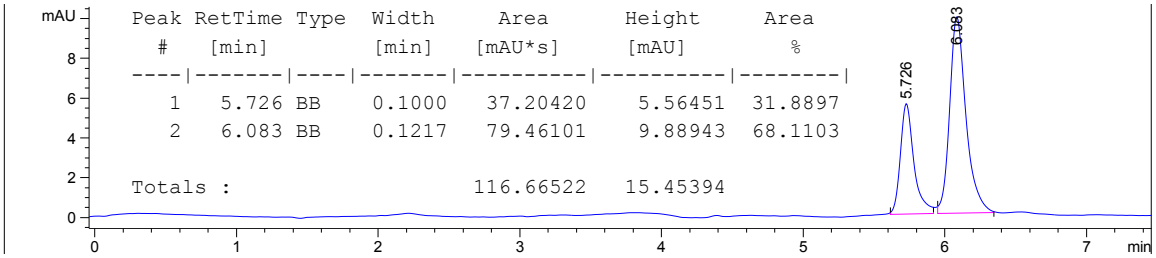

Figure 4.4.120. Asymmetric HPLC trace of 4.2i

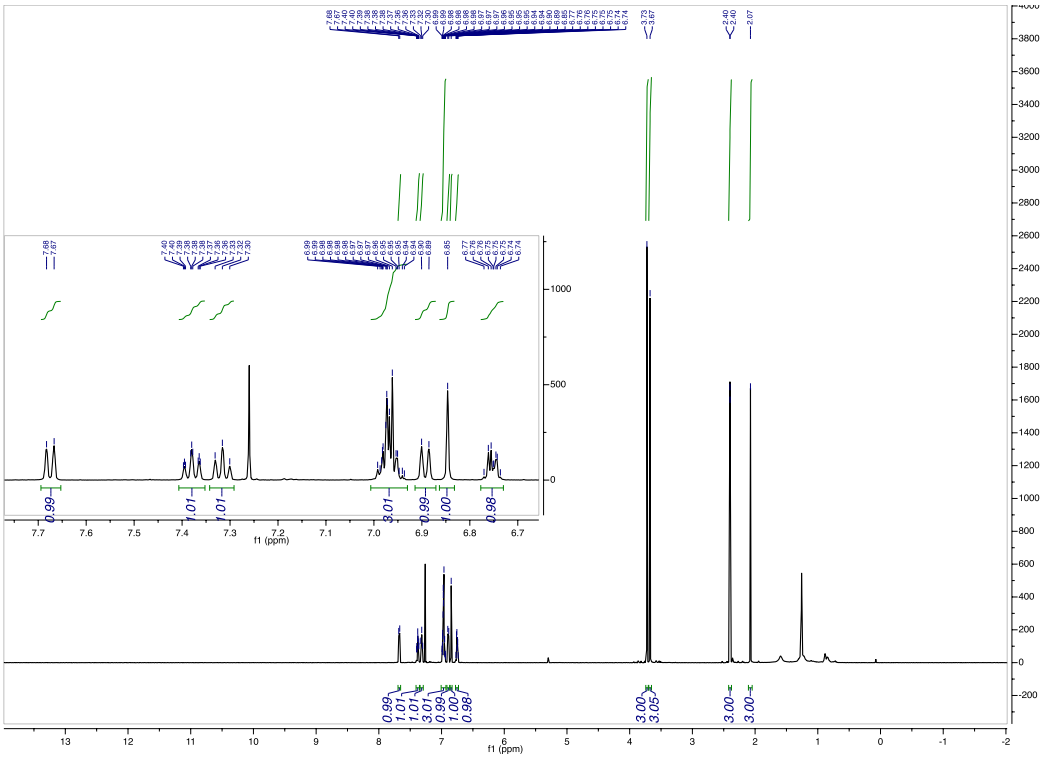

Figure 4.4.121. ^{1}H of 4.2i

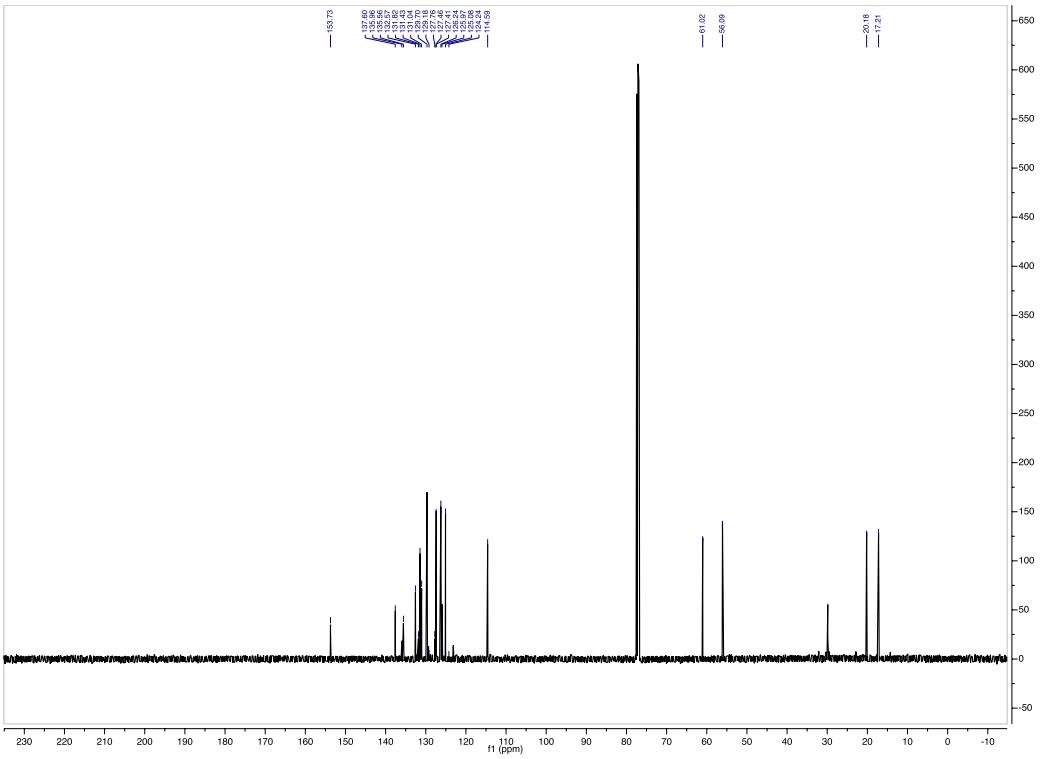

Figure 4.4.122. ^{13}C of 4.2i

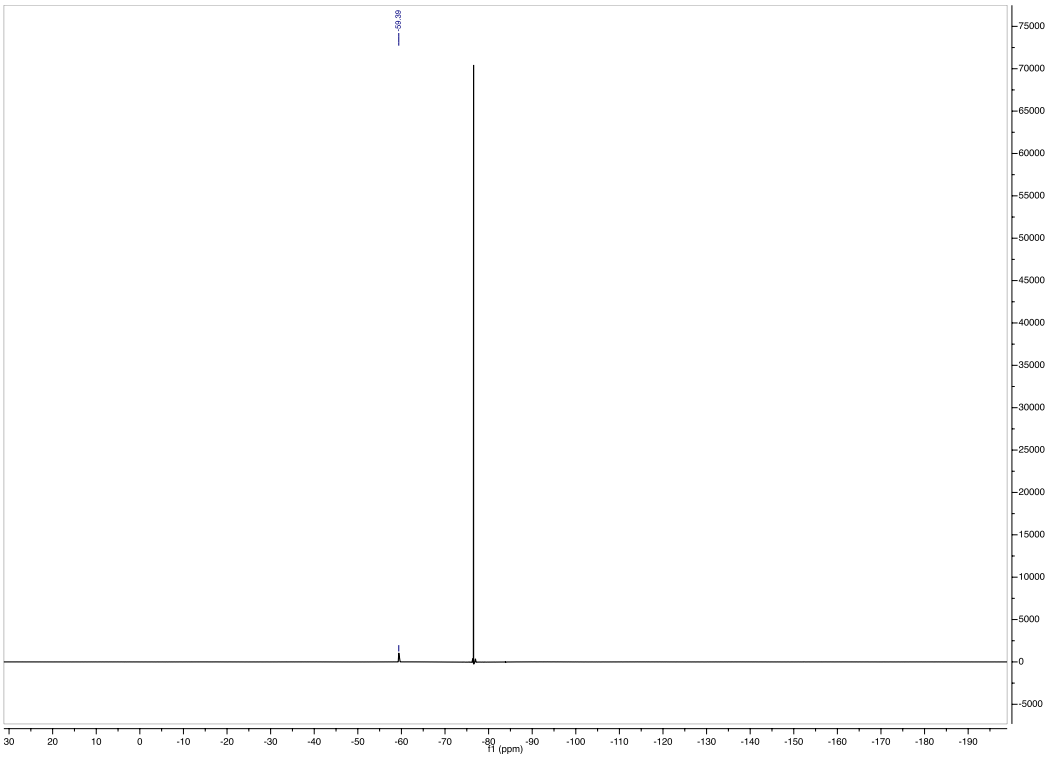

Figure 4.4.123. ^{19}F of 4.2i

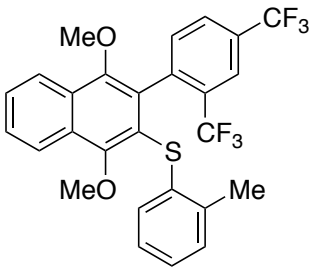

Figure 4.4.124. Product 4.2j

(3-(2,4-bis(trifluoromethyl)phenyl)-1,4-dimethoxynaphthalen-2-yl)(*o*-tolyl)sulfane (**4.2j**):

94% yield, purified by FCC, hexanes/EtOAc = 98/2. 93:7 e.r.

^{1}H NMR (500 MHz, $CDCl_3$) δ 8.30 – 8.24 (m, 1H), 8.17 – 8.12 (m, 1H), 7.98 (s, 1H), 7.68 – 7.63 (m, 2H), 7.47 (d, J = 8.0 Hz, 1H), 7.02 – 6.89 (m, 4H), 6.69 (d, J = 7.7 Hz, 1H), 4.05 (s, 3H), 3.61 (s, 3H), 1.98 (s, 3H).

^{13}C NMR (126 MHz, $CDCl_3$) δ 156.18, 150.62, 139.00, 136.55, 136.32, 132.63, 131.57, 130.42 (q, J = 31 Hz), 130.27 (q, J = 34 Hz), 129.96, 129.56, 129.44, 128.17, 127.83, 127.52, 127.06 (q, J = 3.1 Hz), 126.40, 125.69, 123.61 (q, J = 273 Hz), 123.57 (p, J = 4.2 Hz), 123.47 (J = 274 Hz), 123.20, 122.43, 62.98, 62.02, 19.91.

^{19}F NMR (470 MHz, $CDCl_3$) δ -58.49, -61.75.

MS (APCI) Calculated for $C_{27}H_{21}F_6O_2S$ $[M+H]^+$: 523.1; Found: 523.1 m/z

HPLC trace: Chiralpak IA (hexanes/2-propanol = 90/10, 1.0 mL/min, t_{ent1} = 3.7 min, t_{ent2} = 4.5 min)

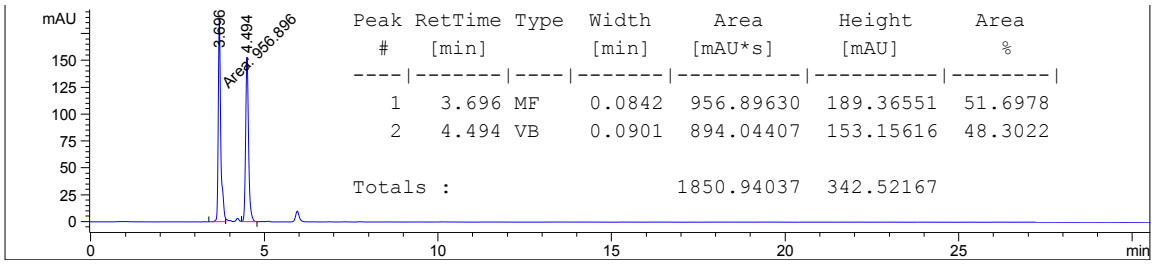

Figure 4.4.125. Racemic HPLC trace of 4.2j

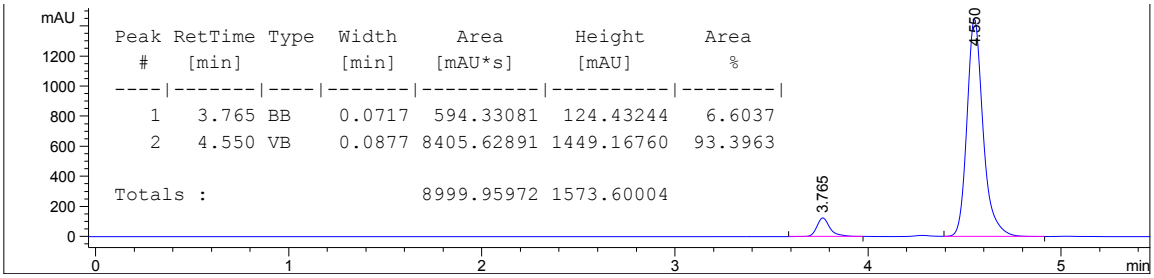

Figure 4.4.126. Asymmetric HPLC trace of 4.2j

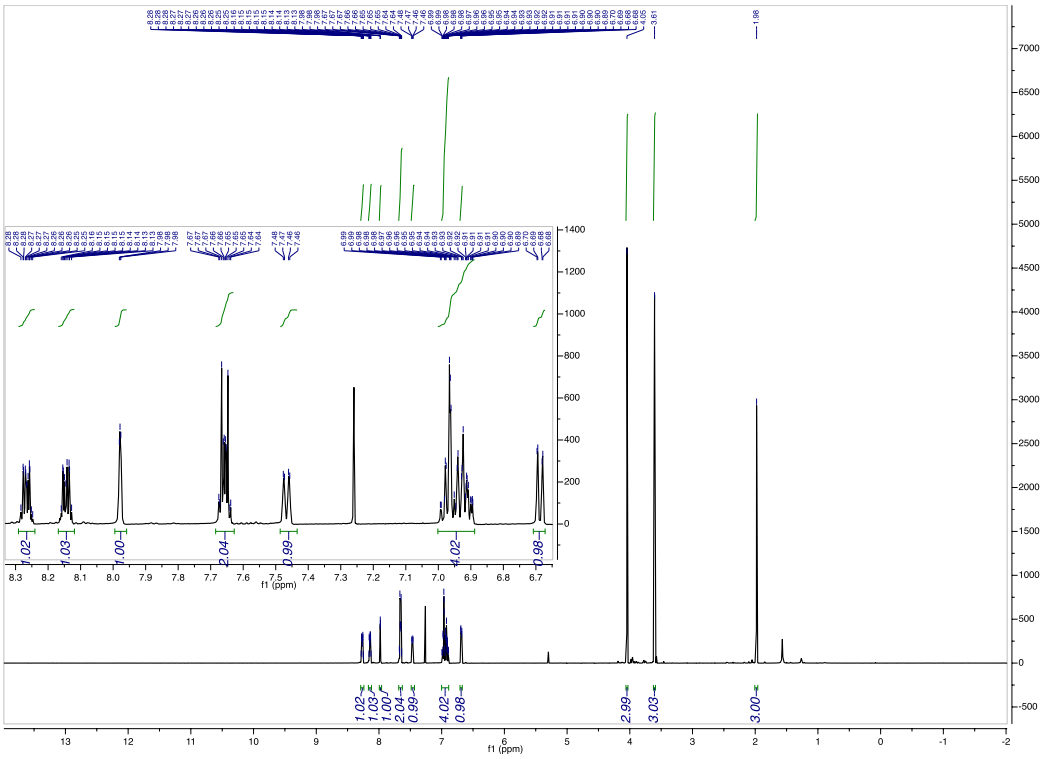

Figure 4.4.127. ^{1}H of 4.2j

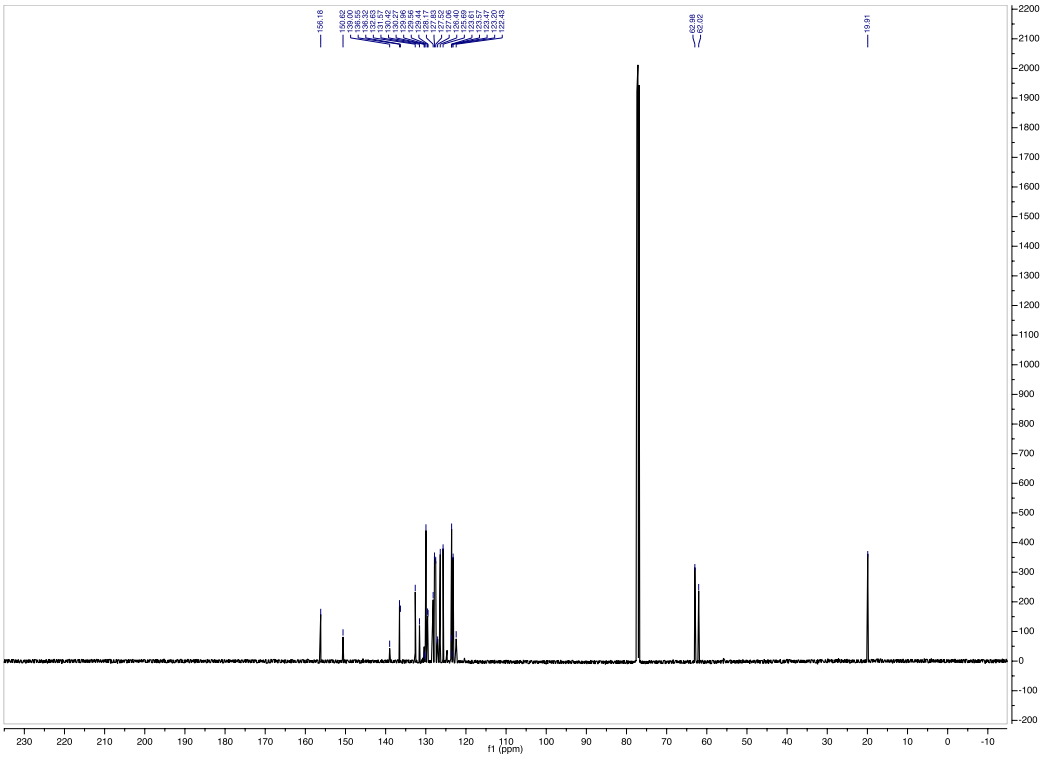

Figure 4.4.128. ^{13}C of 4.2j

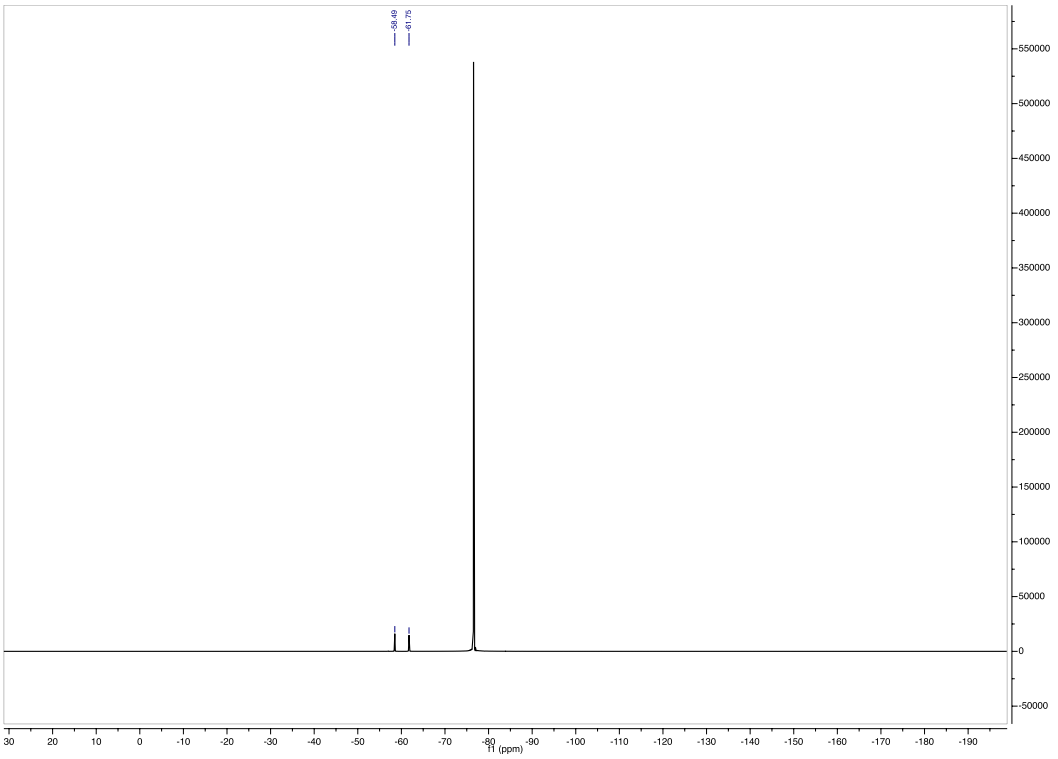

Figure 4.4.129. ^{19}F of 4.2j

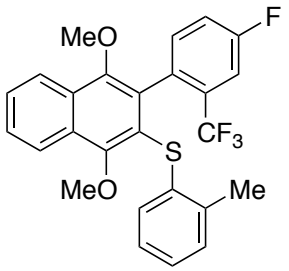

Figure 4.4.130. Product 4.2k

(3-(4-fluoro-2-(trifluoromethyl)phenyl)-1,4-dimethoxynaphthalen-2-yl)(*o*-tolyl)sulfane (**4.2k**): 86% yield, purified by FCC, hexanes/EtOAc = 97/3. 94:6 e.r.

^{1}H NMR (500 MHz, $CDCl_3$) δ 8.28 – 8.23 (m, 1H), 8.18 – 8.13 (m, 1H), 7.67 – 7.62 (m, 2H), 7.44 (dd, *J* = 9.1, 2.7 Hz, 1H), 7.01 – 6.94 (m, 3H), 6.91 (td, *J* = 7.4, 2.1 Hz, 1H), 6.82 (dd, *J* = 8.5, 5.5 Hz, 1H), 6.68 (dd, *J* = 7.8, 1.2 Hz, 1H), 4.03 (s, 3H), 3.60 (s, 3H), 2.07 (s, 3H).

^{13}C NMR (126 MHz, $CDCl_3$) δ 161.74 (d, *J* = 246 Hz), 156.02, 150.93, 136.85, 136.01, 133.72 (d, *J* = 7.7 Hz), 131.88, 131.24 (qd, *J* = 31, 7.6 Hz), 131.09, 129.87, 129.45 (d, *J* = 8.7 Hz), 127.76, 127.70, 127.31, 126.31, 125.43, 123.50, 123.33 (qd, *J* = 274, 2.3 Hz), 123.18, 122.92, 117.63, 117.46, 113.84 (dq, *J* = 25, 4.9 Hz), 62.83, 61.86, 20.06.

^{19}F NMR (470 MHz, $CDCl_3$) δ -58.67, -111.94 (dt, *J* = 8.5, 5.6 Hz).

MS (APCI) Calculated for $C_{26}H_{21}F_4O_2S$ $[M+H]^+$: 473.1; Found: 472.9 m/z

HPLC trace: Chiralpak IA (hexanes/2-propanol = 90/10, 1.0 mL/min, t_{ent1} = 4.2 min, t_{ent2} = 5.3 min)

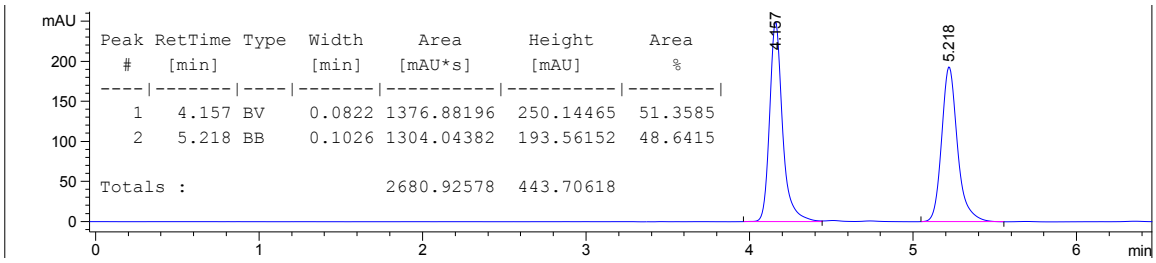

Peak #	RetTime [min]	Type	Width [min]	Area [mAU*s]	Height [mAU]	Area %
1	4.157	BV	0.0822	1376.88196	250.14465	51.3585
2	5.218	BB	0.1026	1304.04382	193.56152	48.6415
Totals :				2680.92578	443.70618	

Figure 4.4.131. Racemic HPLC trace of 4.2k

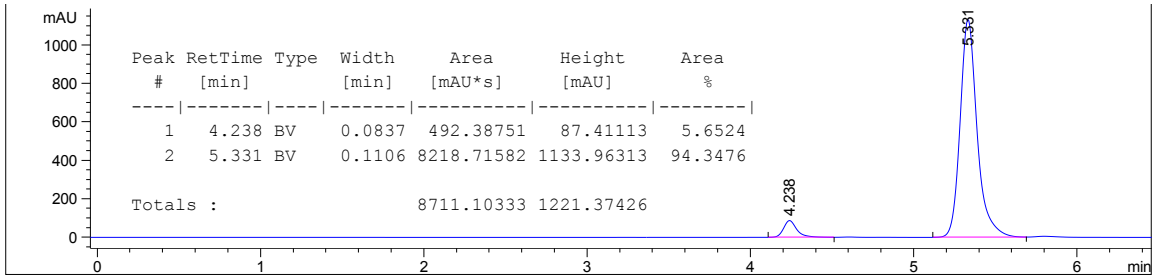

Peak #	RetTime [min]	Type	Width [min]	Area [mAU*s]	Height [mAU]	Area %
1	4.238	BV	0.0837	492.38751	87.41113	5.6524
2	5.331	BV	0.1106	8218.71582	1133.96313	94.3476
Totals :				8711.10333	1221.37426	

Figure 4.4.132. Asymmetric HPLC trace of 4.2k

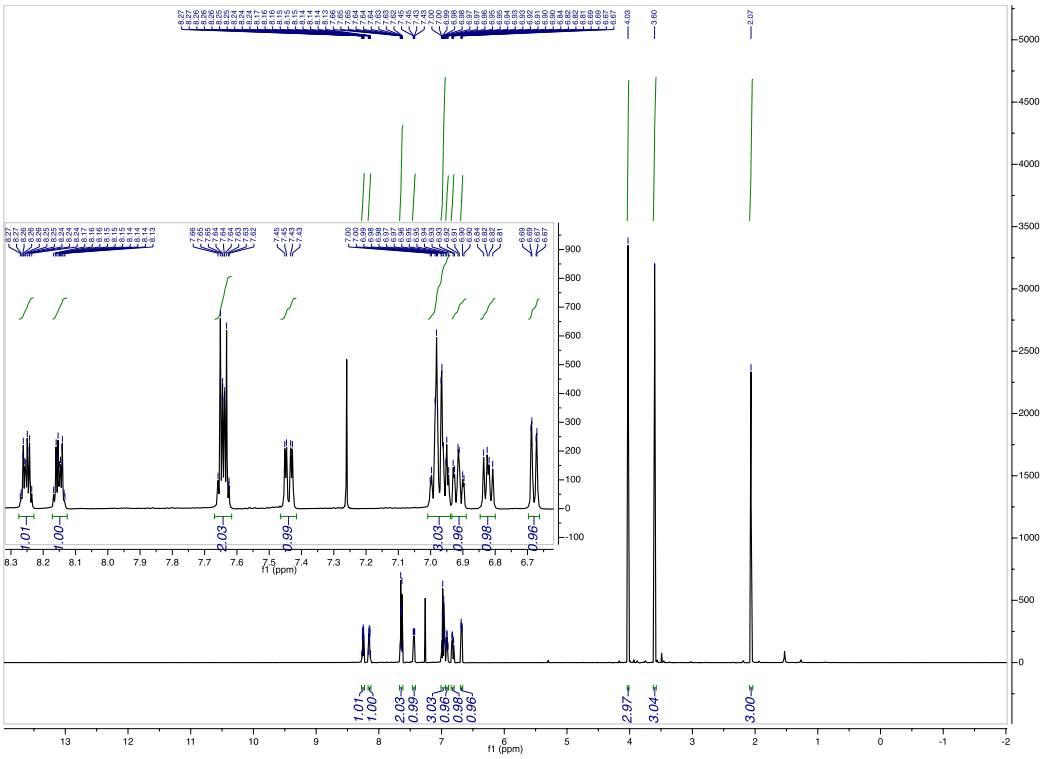

Figure 4.4.133. ^{1}H of 4.2k

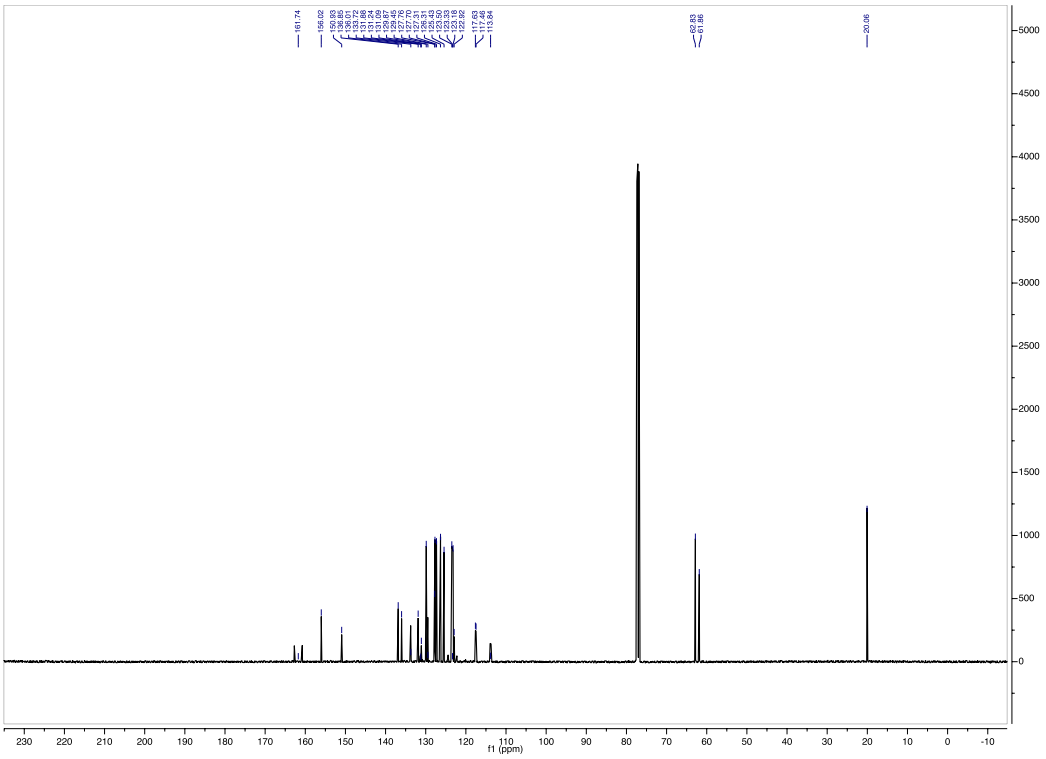

Figure 4.4.134. ^{13}C of 4.2k

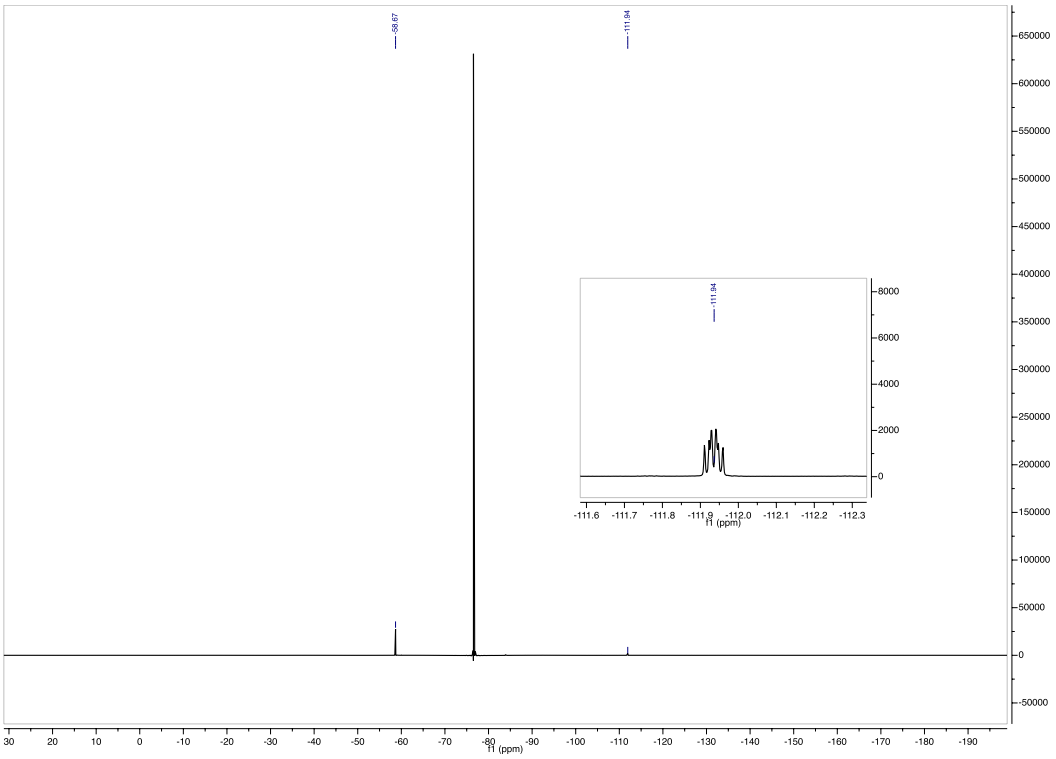

Figure 4.4.135. ^{19}F of 4.2k

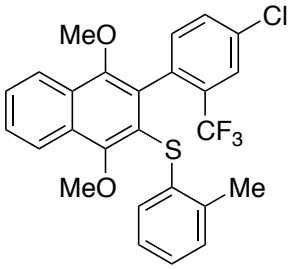

Figure 4.4.136. Product 4.2l

(3-(4-chloro-2-(trifluoromethyl)phenyl)-1,4-dimethoxynaphthalen-2-yl)(*o*-tolyl)sulfane (**4.2l**): 88% yield, purified by FCC, hexanes/DCM = 96/4. 94:6 e.r.

^{1}H NMR (500 MHz, $CDCl_3$) δ 8.27 – 8.22 (m, 1H), 8.17 – 8.12 (m, 1H), 7.72 (d, *J* = 2.2 Hz, 1H), 7.66 – 7.62 (m, 2H), 7.23 (dd, *J* = 8.2, 2.2 Hz, 1H), 7.02 – 6.94 (m, 2H), 6.91 (td, *J* = 7.4, 1.8 Hz, 1H), 6.79 (d, *J* = 8.3 Hz, 1H), 6.67 (dd, *J* = 7.8, 1.2 Hz, 1H), 4.02 (s, 3H), 3.61 (s, 3H), 2.07 (s, 3H).

^{13}C NMR (126 MHz, $CDCl_3$) δ 156.01, 150.76, 136.77, 136.11, 133.83, 133.66, 133.18, 131.79, 131.01 (q, *J* = 31 Hz), 130.58, 129.91, 129.46, 127.84, 127.71, 127.35, 126.68 (q, *J* = 4.9 Hz), 126.32, 125.51, 123.51, 123.40 (q, *J* = 274 Hz), 123.18, 122.70, 62.82, 61.92, 20.04.

^{19}F NMR (470 MHz, $CDCl_3$) δ -58.54.

MS (APCI) Calculated for $C_{26}H_{21}ClF_3O_2S$ $[M+H]^+$: 489.1; Found: 489.2 m/z

HPLC trace: Chiralpak IA (hexanes/2-propanol = 90/10, 1.0 mL/min, t_{ent1} = 4.2 min, t_{ent2} = 5.5 min)

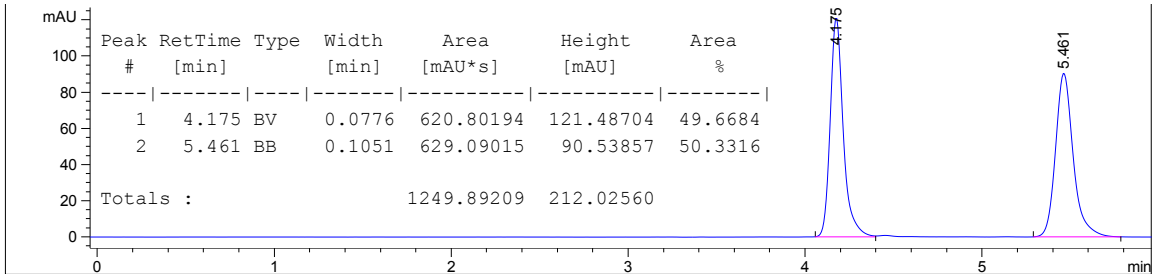

Figure 4.4.137. Racemic HPLC trace of 4.2l

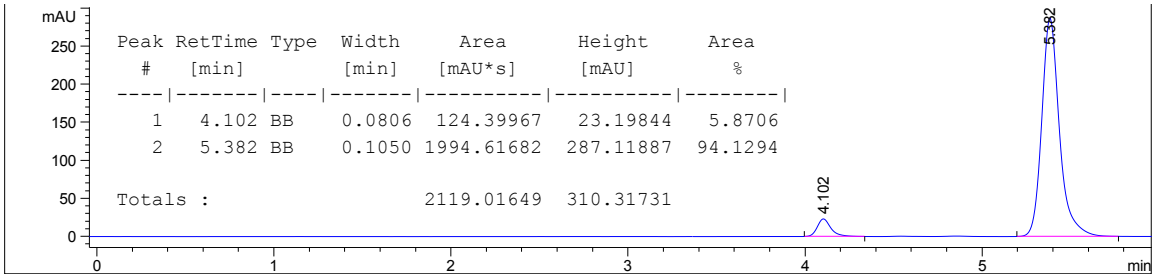

Figure 4.4.138. Asymmetric HPLC trace of 4.2l

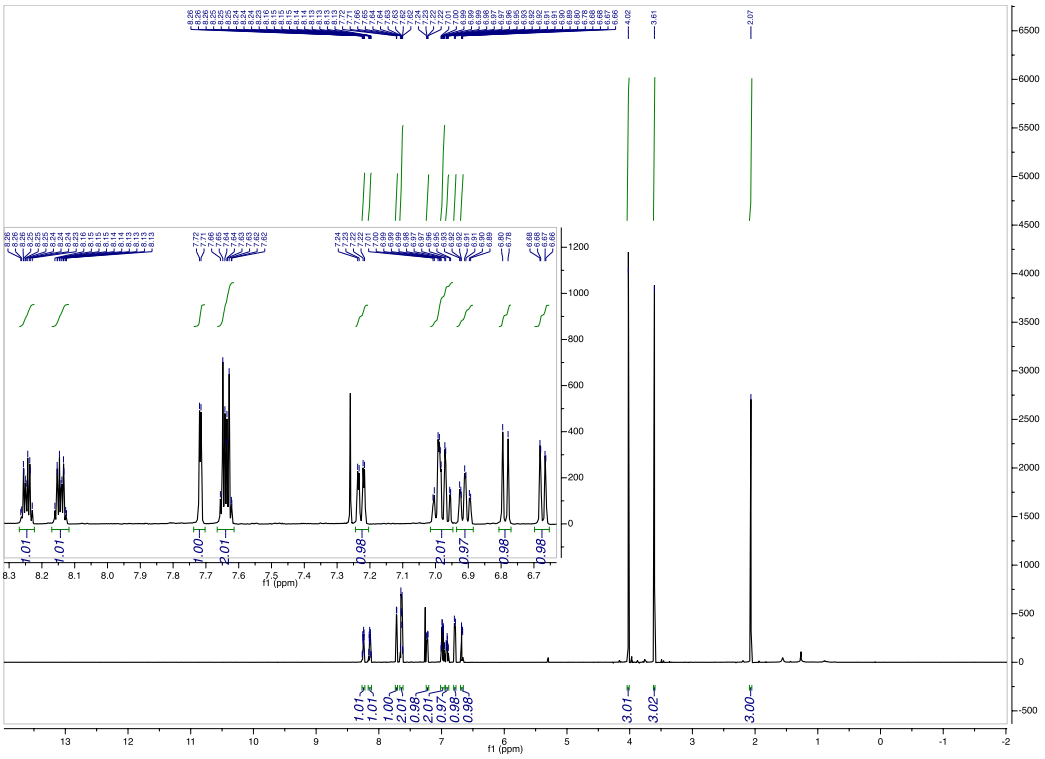

Figure 4.4.139. ^{1}H of 4.2l

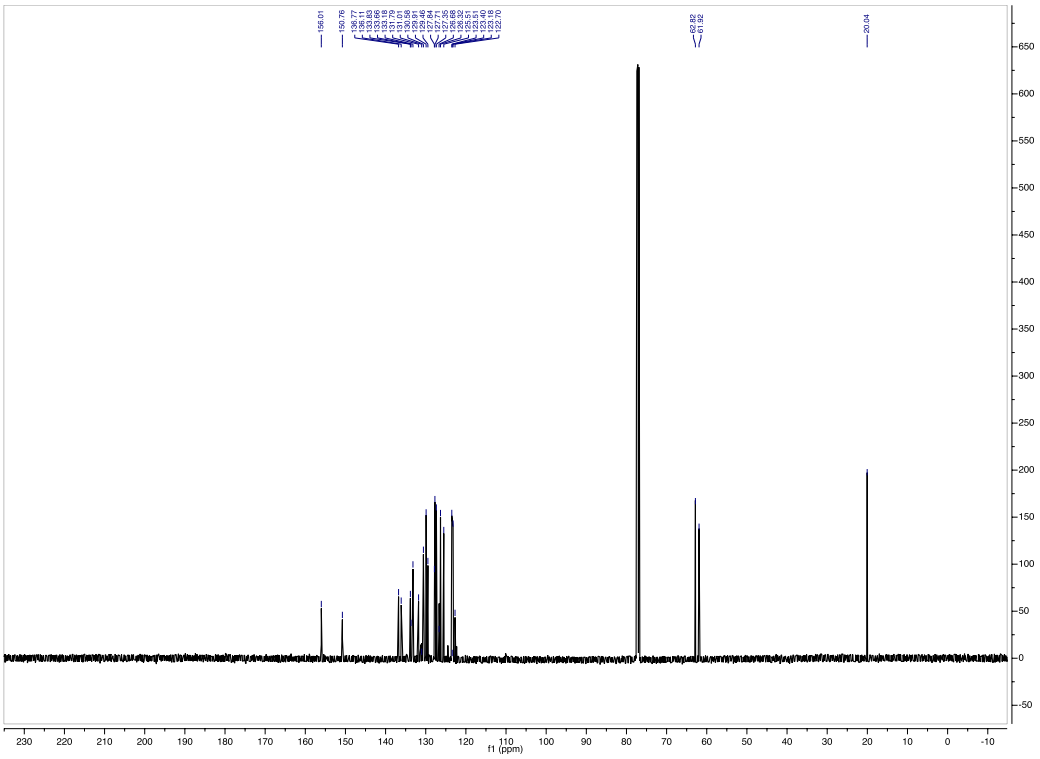

Figure 4.4.140. ^{13}C of 4.2l

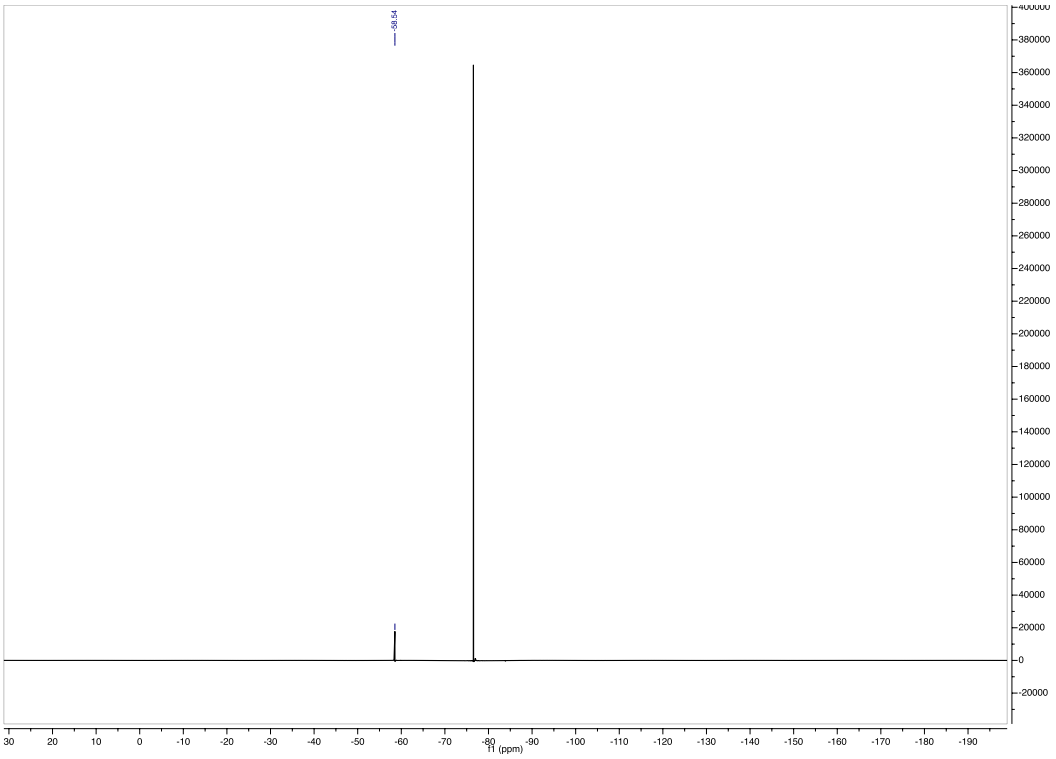

Figure 4.4.141. ^{19}F of 4.2l

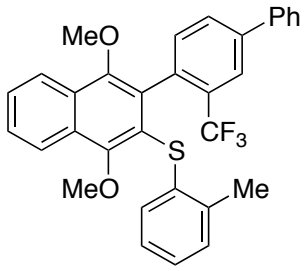

Figure 4.4.142. Product 4.2m

(1,4-dimethoxy-3-(3-(trifluoromethyl)-[1,1'-biphenyl]-4-yl)naphthalen-2-yl)(*o*-tolyl)sulfane (**4.2m**):

90% yield, purified by FCC, hexanes/DCM = 97/3. 94:6 e.r.

^{1}H NMR (500 MHz, $CDCl_3$) δ 8.29 – 8.23 (m, 1H), 8.20 – 8.14 (m, 1H), 7.94 (d, *J* = 1.9 Hz, 1H), 7.67 – 7.61 (m, 4H), 7.53 – 7.39 (m, 4H), 7.00 – 6.87 (m, 4H), 6.75 (d, *J* = 7.4 Hz, 1H), 4.04 (s, 3H), 3.65 (s, 3H), 2.03 (s, 3H).

^{13}C NMR (126 MHz, $CDCl_3$) δ 155.84, 150.72, 140.79, 139.75, 137.00, 136.31, 133.88 (q, *J* = 1.8 Hz), 132.78, 132.36, 129.90 (q, *J* = 30 Hz), 129.78, 129.52, 129.32, 129.13, 128.90, 128.22, 128.11, 127.57, 127.22, 127.17, 126.28, 125.44, 125.03 (q, *J* = 4.8 Hz), 124.32 (q, *J* = 274 Hz), 123.46, 123.21, 62.80, 61.96, 20.08.

^{19}F NMR (376 MHz, $CDCl_3$) δ -58.08.

MS (APCI) Calculated for $C_{32}H_{25}F_3O_2S$ $[M+H]^+$: 531.2; Found: 531.3 m/z

HPLC trace: Chiralpak IA (hexanes/2-propanol = 90/10, 1.0 mL/min, t_{ent1} = 4.6 min, t_{ent2} = 6.3 min)

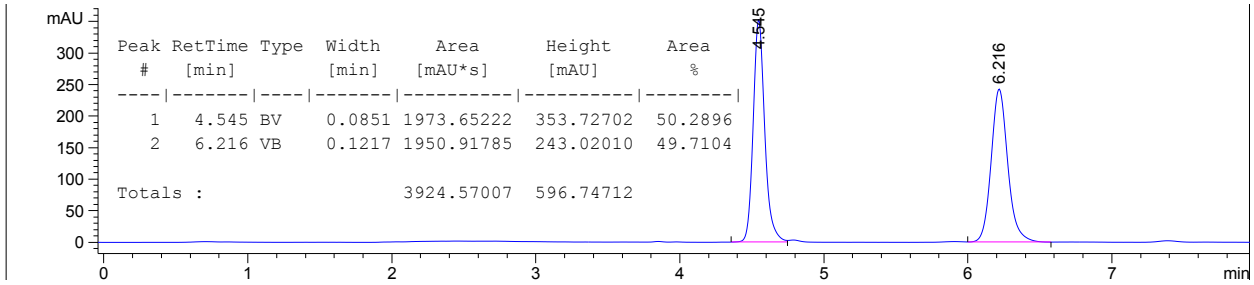

Figure 4.4.143. Racemic HPLC trace of 4.2m

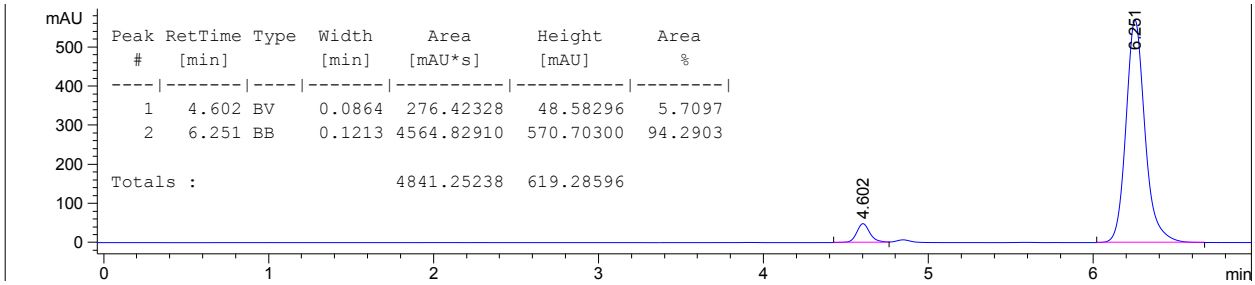

Figure 4.4.144. Asymmetric HPLC trace of 4.2m

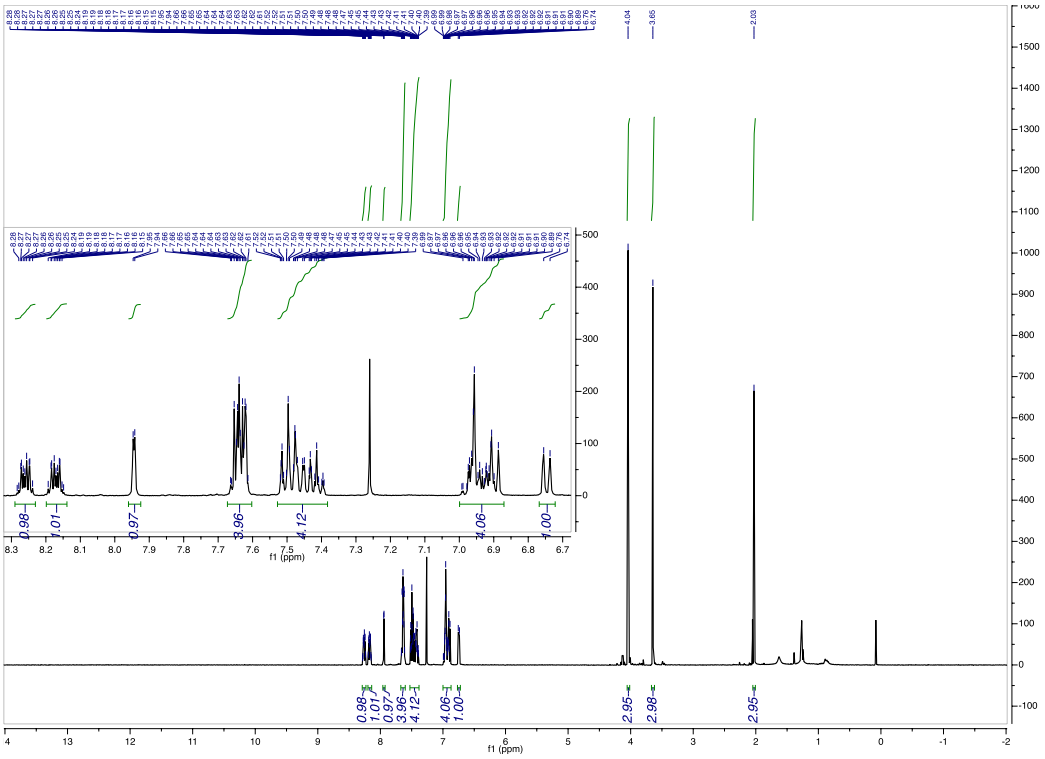

Figure 4.4.145. ^{1}H of 4.2m

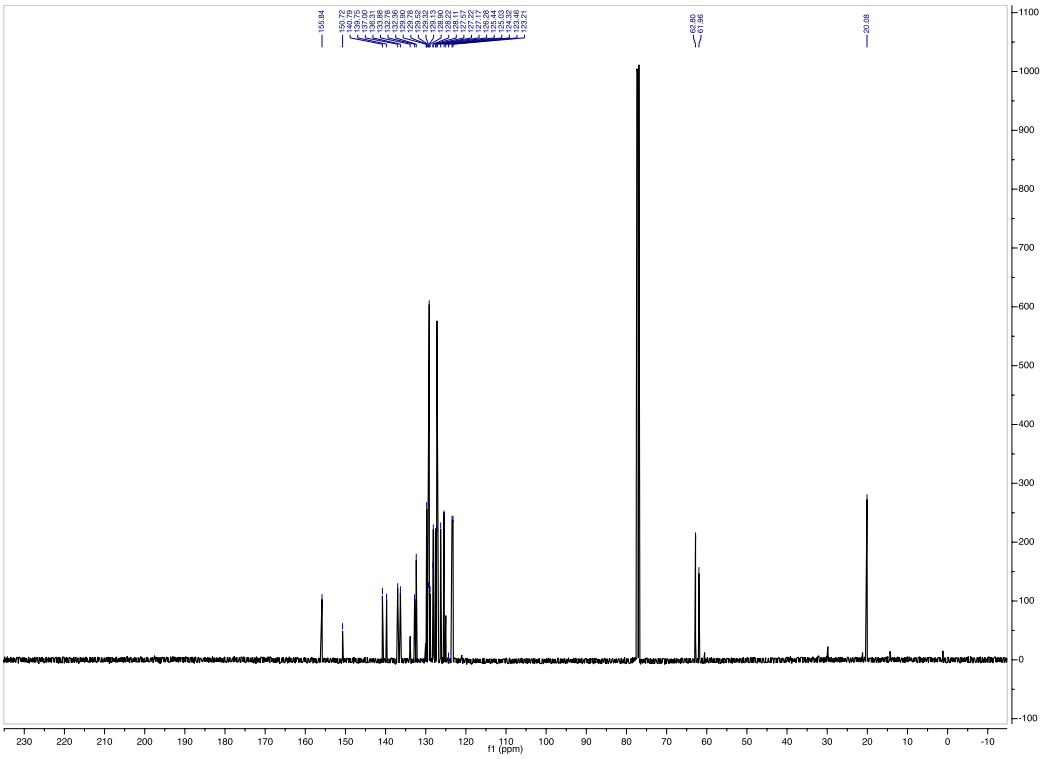

Figure 4.4.146. ^{13}C of 4.2m

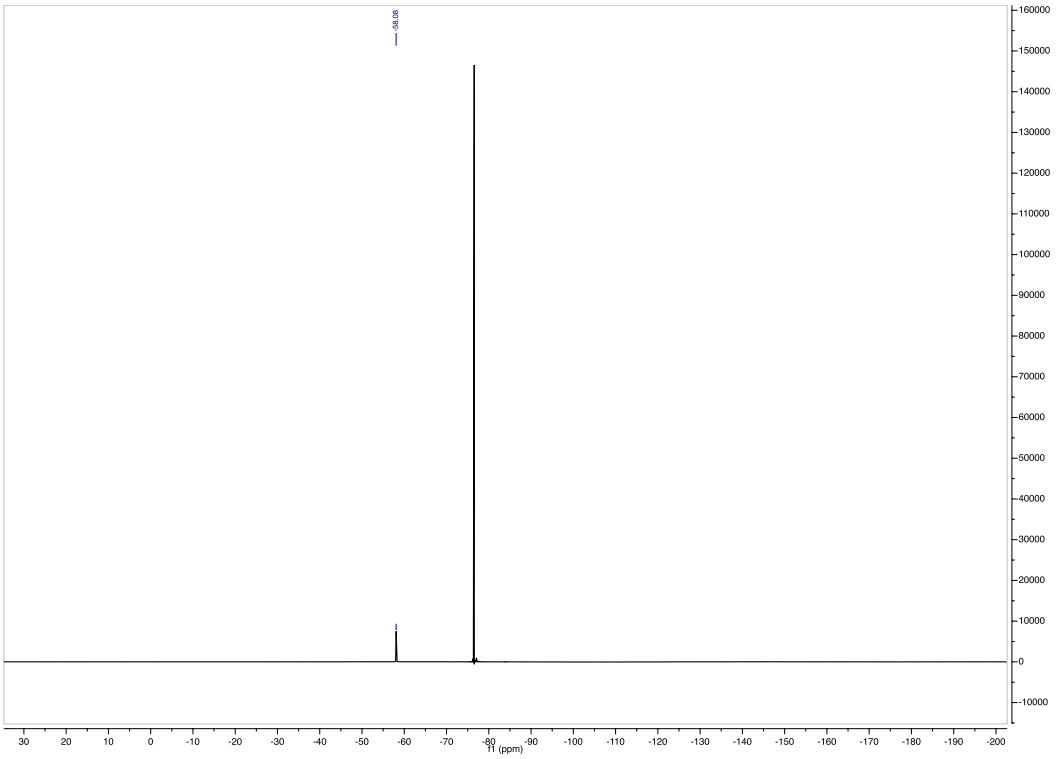

Figure 4.4.147. ^{19}F of 4.2m

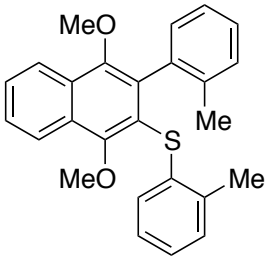

Figure 4.4.148. Product 4.2n

(1,4-dimethoxy-3-(*o*-tolyl)naphthalen-2-yl)(*o*-tolyl)sulfane (**4.2n**):

85% yield, purified by FCC, hexanes/EtOAc = 99/1. 66:34 e.r.

^{1}H NMR (500 MHz, $CDCl_3$) δ 8.26 – 8.21 (m, 1H), 8.20 – 8.15 (m, 1H), 7.64 – 7.58 (m, 2H), 7.22 – 7.15 (m, 2H), 7.01 (td, *J* = 7.3, 1.7 Hz, 1H), 6.97 – 6.91 (m, 2H), 6.91 – 6.85 (m, 2H), 6.77 (d, *J* = 7.4 Hz, 1H), 4.03 (s, 3H), 3.49 (s, 3H), 2.02 (s, 3H), 1.99 (s, 3H).

^{13}C NMR (126 MHz, $CDCl_3$) δ 155.63, 150.45, 137.04, 136.90, 136.75, 136.32, 134.74, 130.47, 129.78, 129.68, 129.54, 128.82, 128.72, 127.48, 127.33, 126.81, 126.12, 125.46, 124.81, 123.81, 123.24, 123.09, 62.57, 61.30, 20.21, 20.17.

MS (APCI) Calculated for $C_{26}H_{25}O_2S$ $[M+H]^+$: 401.2; Found: 401.3 m/z

HPLC trace: Chiralpak IA (hexanes/2-propanol = 95/5, 0.5 mL/min, t_{ent1} = 8.6 min, t_{ent2} = 9.0 min)

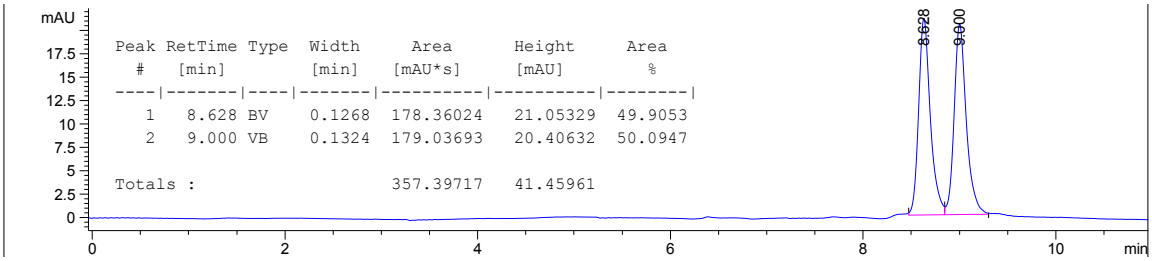

Peak #	RetTime [min]	Type	Width [min]	Area [mAU*s]	Height [mAU]	Area %
1	8.628	BV	0.1268	178.36024	21.05329	49.9053
2	9.000	VB	0.1324	179.03693	20.40632	50.0947
Totals :				357.39717	41.45961	

Figure 4.4.149. Racemic HPLC trace of 4.2n

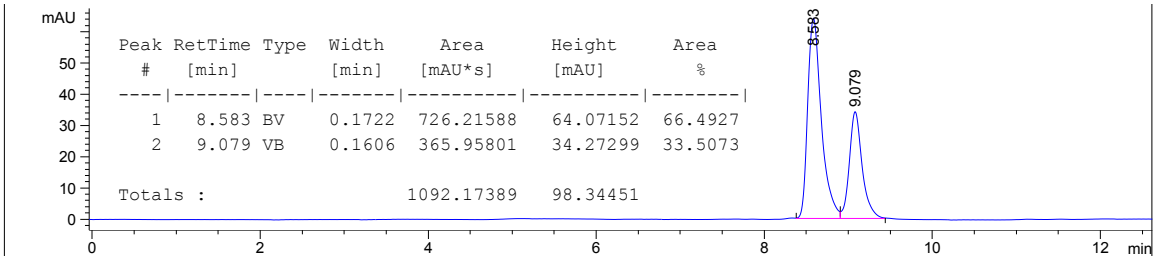

Peak #	RetTime [min]	Type	Width [min]	Area [mAU*s]	Height [mAU]	Area %
1	8.583	BV	0.1722	726.21588	64.07152	66.4927
2	9.079	VB	0.1606	365.95801	34.27299	33.5073
Totals :				1092.17389	98.34451	

Figure 4.4.150. Asymmetric HPLC trace of 4.2n

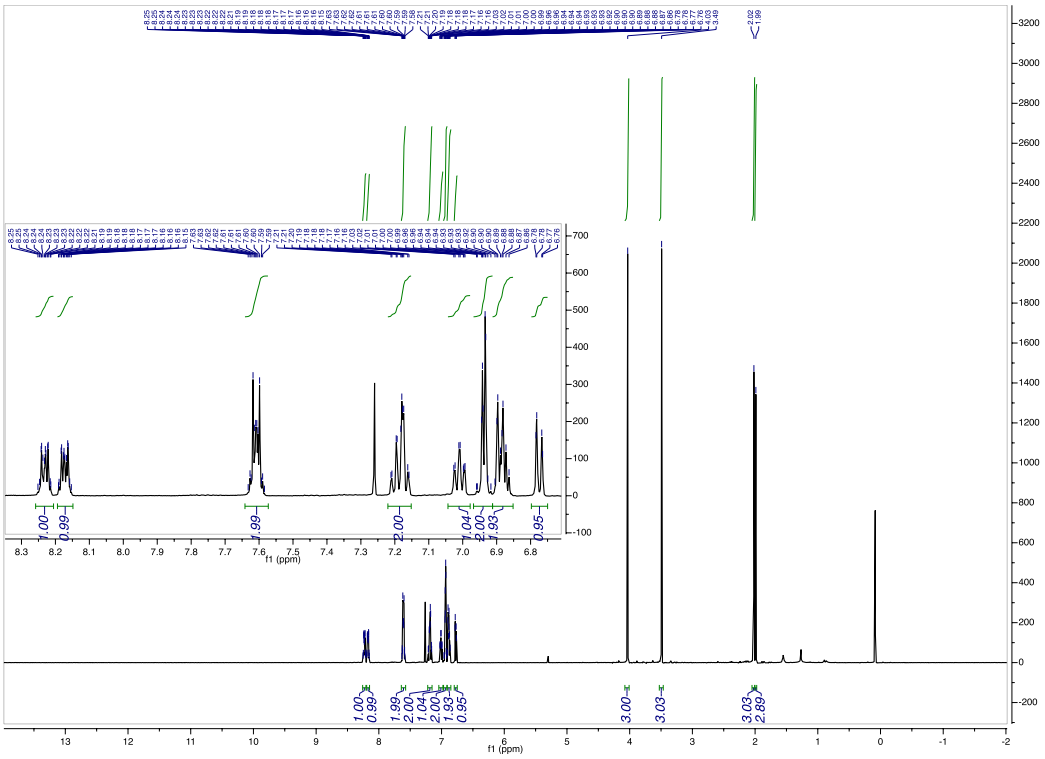

Figure 4.4.151. ^{1}H of 4.2n

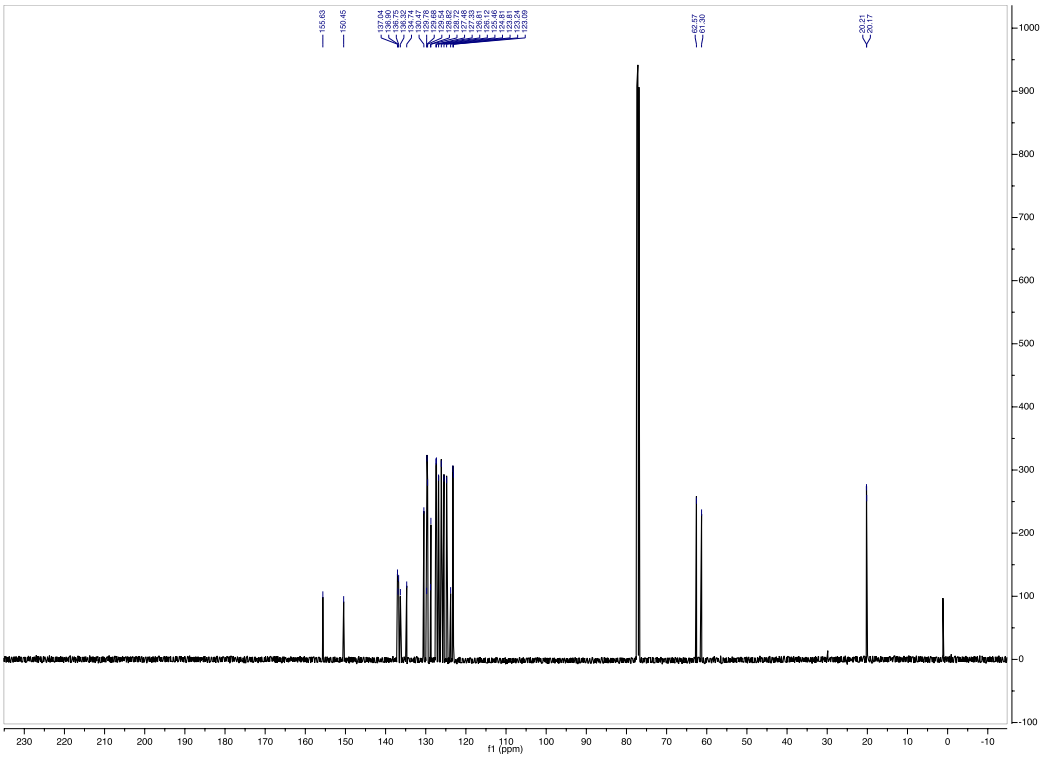

Figure 4.4.152. ^{13}C of 4.2n

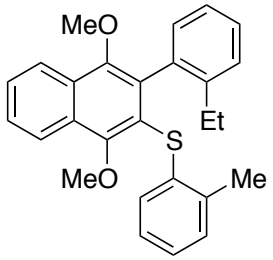

Figure 4.4.153. Product 4.2o

(3-(2-ethylphenyl)-1,4-dimethoxynaphthalen-2-yl)(*o*-tolyl)sulfane (**4.2o**):

72% yield, purified by FCC, hexanes/EtOAc = 99/1. 68:32 e.r.

^{1}H NMR (500 MHz, $CDCl_3$) δ 8.27 – 8.20 (m, 1H), 8.20 – 8.14 (m, 1H), 7.65 – 7.57 (m, 2H), 7.30 – 7.26 (m, 2H), 7.04 – 6.98 (m, 1H), 6.97 – 6.87 (m, 3H), 6.86 (d, *J* = 7.5 Hz, 1H), 6.79 (d, *J* = 7.3 Hz, 1H), 4.02 (s, 3H), 3.52 (s, 3H), 2.41 – 2.24 (m, 2H), 2.03 (s, 3H), 1.06 (t, *J* = 7.6 Hz, 3H).

^{13}C NMR (126 MHz, $CDCl_3$) δ 155.62, 150.54, 142.55, 137.02, 136.56, 135.80, 134.77, 130.40, 129.76, 129.70, 128.84, 128.43, 127.69, 127.33, 127.27, 126.78, 126.13, 125.38, 124.66, 123.87, 123.26, 123.12, 62.48, 61.49, 26.04, 20.22, 14.14.

MS (APCI) Calculated for $C_{27}H_{27}O_2S$ $[M+H]^+$: 415.2; Found: 415.2 m/z

HPLC trace: Chiralpak IA (hexanes/2-propanol = 95/5, 0.5 mL/min, t_{ent1} = 8.1 min, t_{ent2} = 8.4 min)

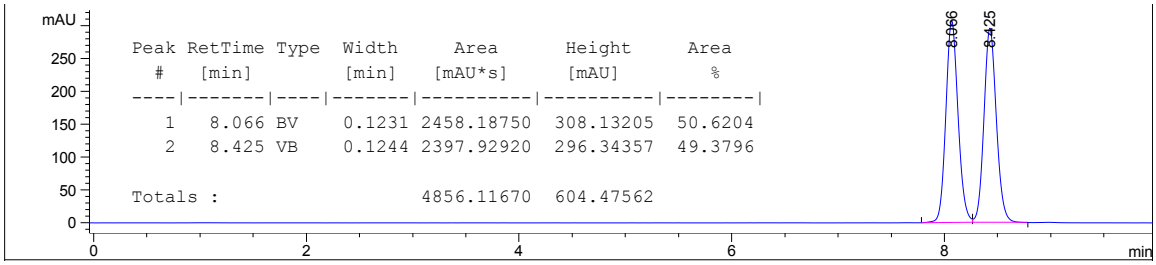

Peak #	RetTime [min]	Type	Width [min]	Area [mAU*s]	Height [mAU]	Area %
1	8.066	BV	0.1231	2458.18750	308.13205	50.6204
2	8.425	VB	0.1244	2397.92920	296.34357	49.3796
Totals :				4856.11670	604.47562	

Figure 4.4.154. Racemic HPLC trace of 4.2o

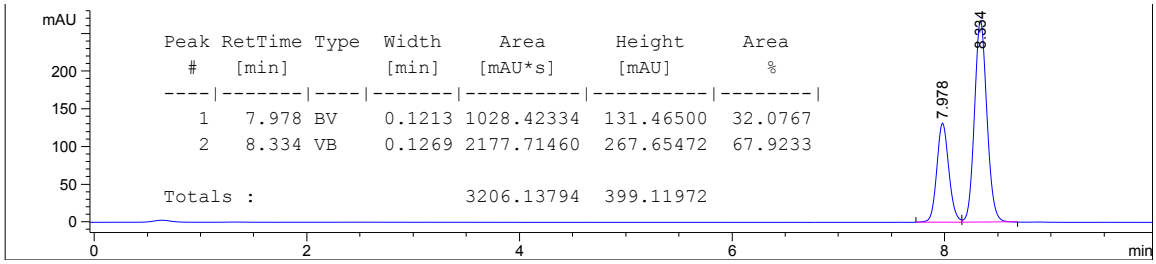

Peak #	RetTime [min]	Type	Width [min]	Area [mAU*s]	Height [mAU]	Area %
1	7.978	BV	0.1213	1028.42334	131.46500	32.0767
2	8.334	VB	0.1269	2177.71460	267.65472	67.9233
Totals :				3206.13794	399.11972	

Figure 4.4.155. Asymmetric HPLC trace of 4.2o

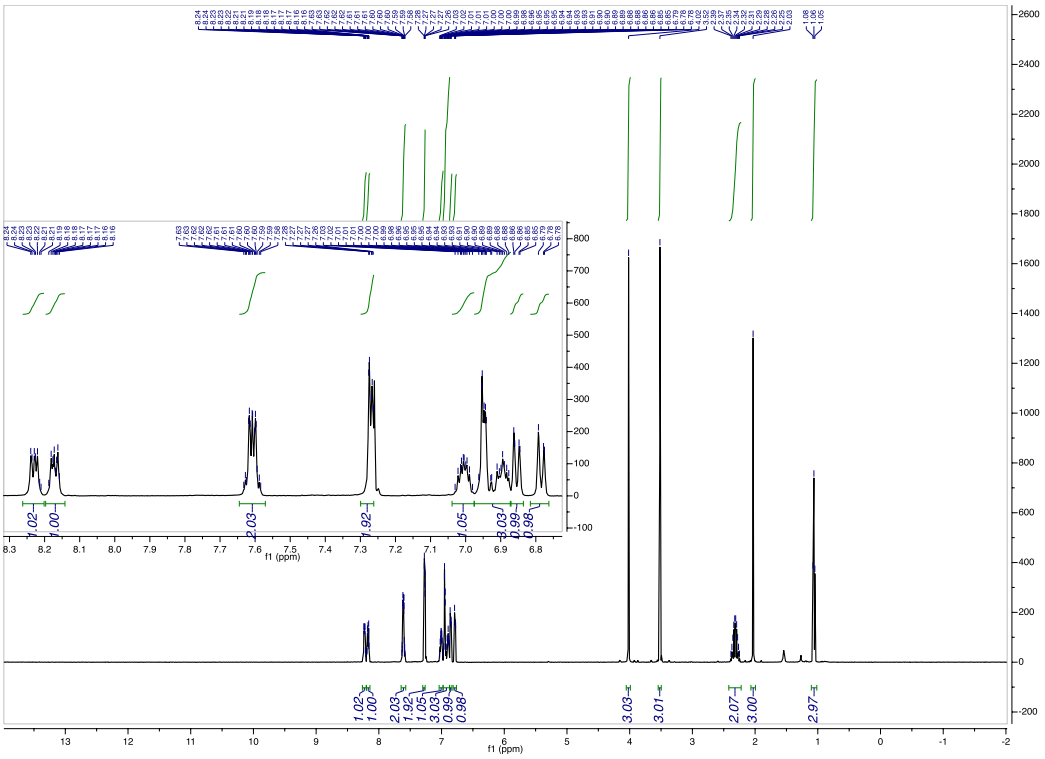

Figure 4.4.156. ^{1}H of 4.2o

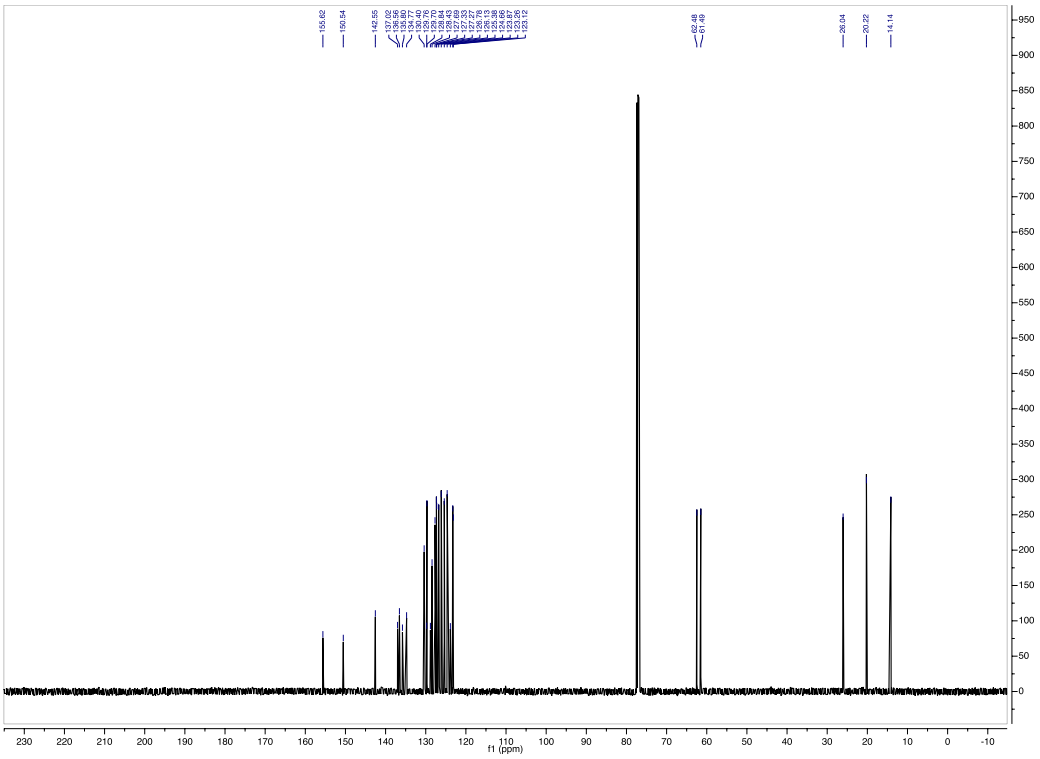

Figure 4.4.157. ^{13}C of 4.2o

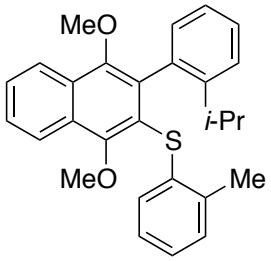

Figure 4.4.158. Product 4.2p

(3-(2-isopropylphenyl)-1,4-dimethoxynaphthalen-2-yl)(*o*-tolyl)sulfane (**4.2p**):

83% yield, purified by FCC, hexanes/EtOAc = 99.5/0.5 → 99/1. 95:5 e.r.

^{1}H NMR (500 MHz, $CDCl_3$) δ 8.25 – 8.15 (m, 2H), 7.64 – 7.58 (m, 2H), 7.37 (dd, *J* = 7.9, 1.4 Hz, 1H), 7.34 – 7.29 (m, 1H), 7.01 – 6.89 (m, 4H), 6.79 (dt, *J* = 7.6, 1.7 Hz, 2H), 3.99 (s, 3H), 3.56 (s, 3H), 2.61 (hept, *J* = 6.8 Hz, 1H), 2.07 (s, 3H), 1.14 (d, *J* = 6.8 Hz, 3H), 1.04 (d, *J* = 6.9 Hz, 3H).

^{13}C NMR (126 MHz, $CDCl_3$) δ 155.59, 150.71, 147.54, 137.28, 136.08, 135.09, 135.00, 130.32, 129.75, 128.86, 127.96, 127.71, 127.34, 126.73, 126.18, 125.25, 125.22, 124.45, 123.70, 123.29, 123.21, 62.31, 61.75, 30.77, 24.30, 23.93, 20.23.

MS (APCI) Calculated for $C_{28}H_{29}O_2S$ $[M+H]^+$: 429.2; Found: 429.2 m/z

HPLC trace: Chiralpak IC (hexanes/2-propanol = 99.5/0.5, 0.5 mL/min, t_{ent1} = 8.4 min, t_{ent2} = 9.2 min)

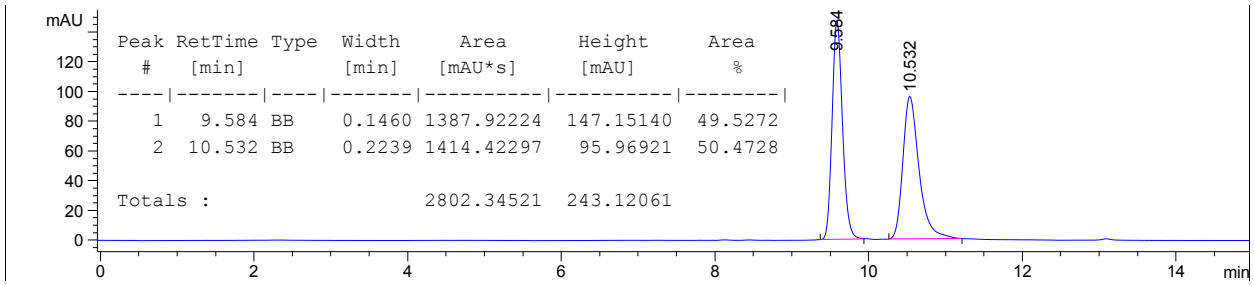

Figure 4.4.159. Racemic HPLC trace of 4.2p

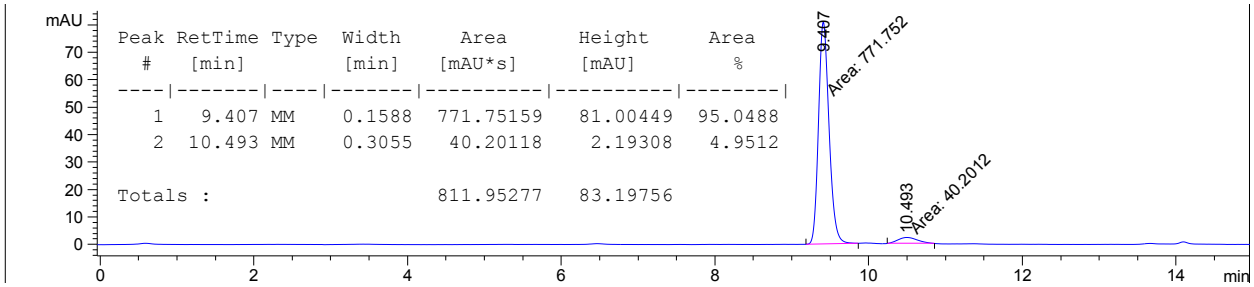

Figure 4.4.160. Asymmetric HPLC trace of 4.2p

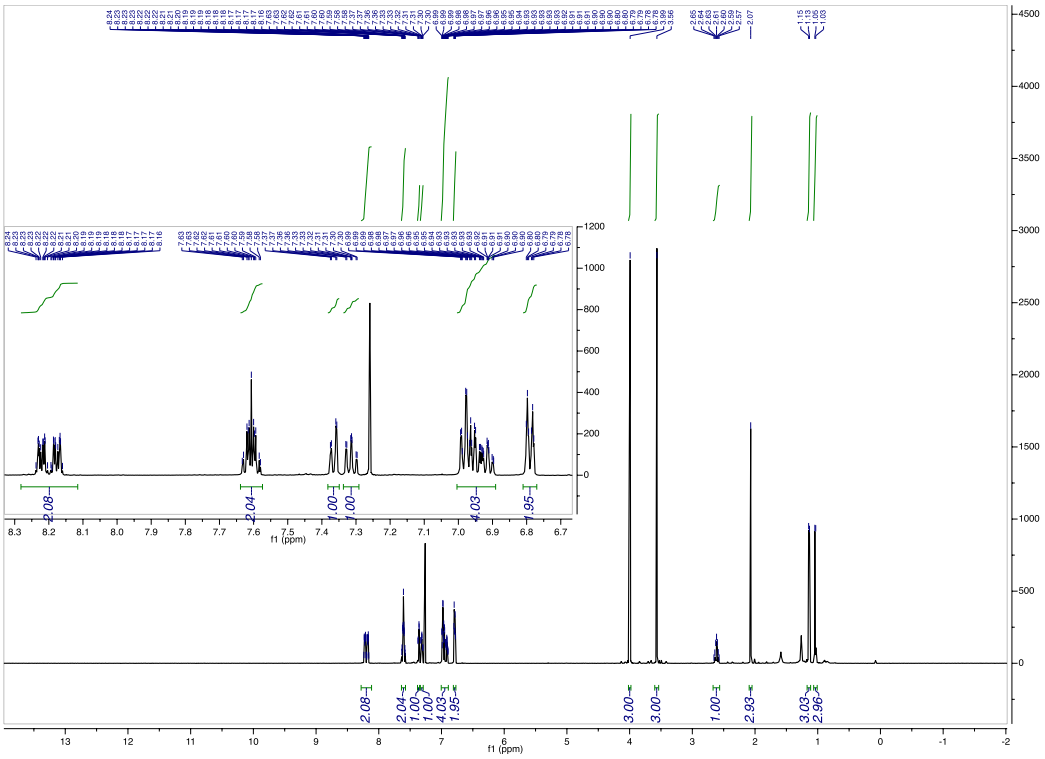

Figure 4.4.161. ^{1}H of 4.2p

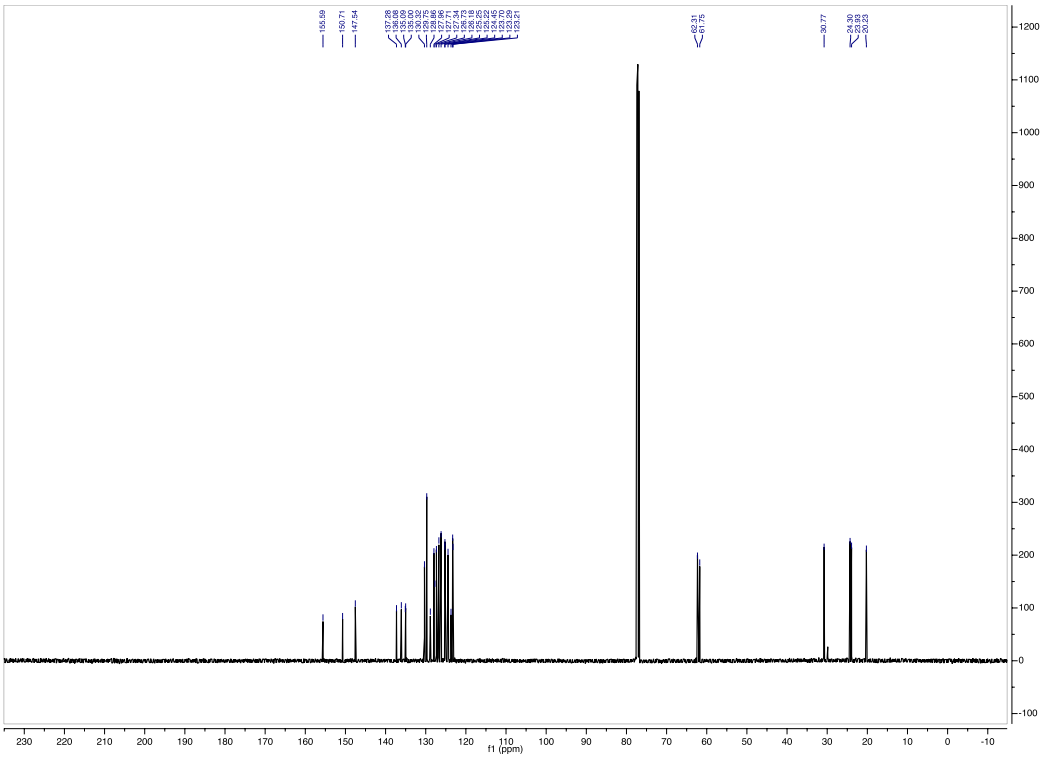

Figure 4.4.162. ^{13}C of 4.2p

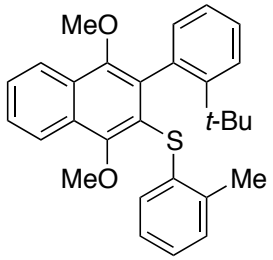

Figure 4.4.163. Product 4.2q

(3-(2-(*tert*-butyl)phenyl)-1,4-dimethoxynaphthalen-2-yl)(*o*-tolyl)sulfane (**4.2q**):

Reaction was stirred for 68 hours instead of 44 hours. 97% yield, purified by FCC, hexanes/EtOAc = 99/1. 98.5:1.5 e.r.

^{1}H NMR (500 MHz, $CDCl_3$) δ 8.26 – 8.20 (m, 1H), 8.19 – 8.13 (m, 1H), 7.65 – 7.56 (m, 3H), 7.27 (td, *J* = 7.3, 1.5 Hz, 1H), 7.05 – 6.86 (m, 5H), 6.63 (dd, *J* = 7.6, 1.5 Hz, 1H), 3.98 (s, 3H), 3.60 (s, 3H), 2.08 (s, 3H), 1.19 (s, 9H).

^{13}C NMR (126 MHz, $CDCl_3$) δ 155.49, 149.90, 148.28, 138.52, 137.07, 136.21, 134.55, 132.09, 129.79, 129.63, 128.78, 128.10, 127.99, 127.42, 127.34, 126.61, 126.08, 125.26, 124.32, 124.23, 123.32, 123.22, 62.25, 61.41, 36.99, 32.38, 20.30.

MS (APCI) Calculated for $C_{29}H_{31}O_2S$ $[M+H]^+$: 443.2; Found: 443.2 m/z

HPLC trace: Chiralpak IA (hexanes/2-propanol = 98/2, 1.0 mL/min, t_{ent1} = 3.9 min, t_{ent2} = 4.6 min)

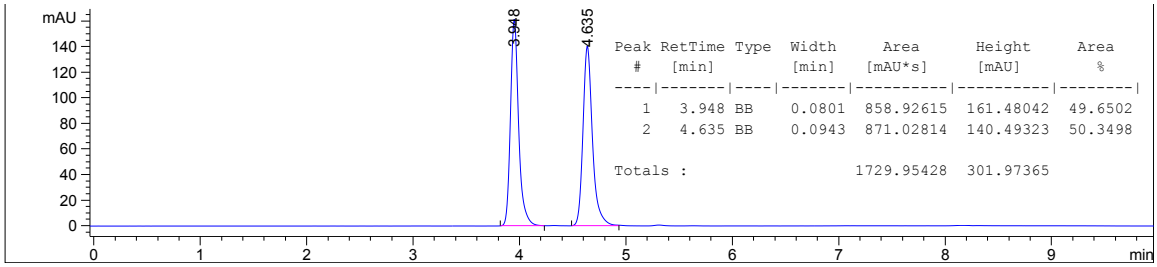

Figure 4.4.164. Racemic HPLC trace of 4.2q

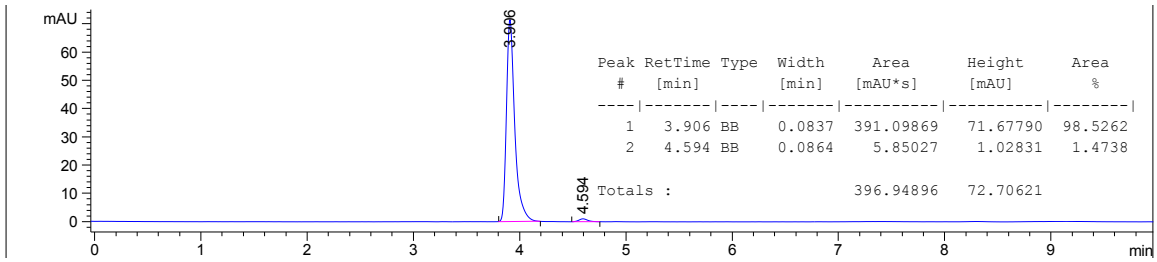

Figure 4.4.165. Asymmetric HPLC trace of 4.2q

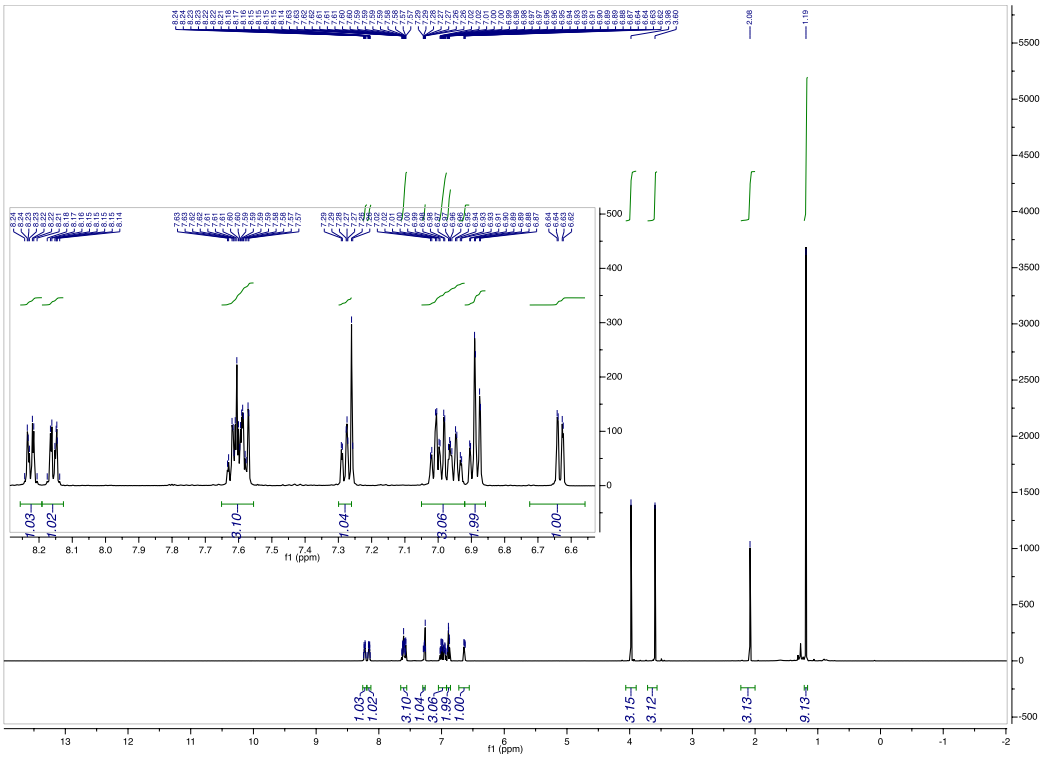

Figure 4.4.166. ^{1}H of 4.2q

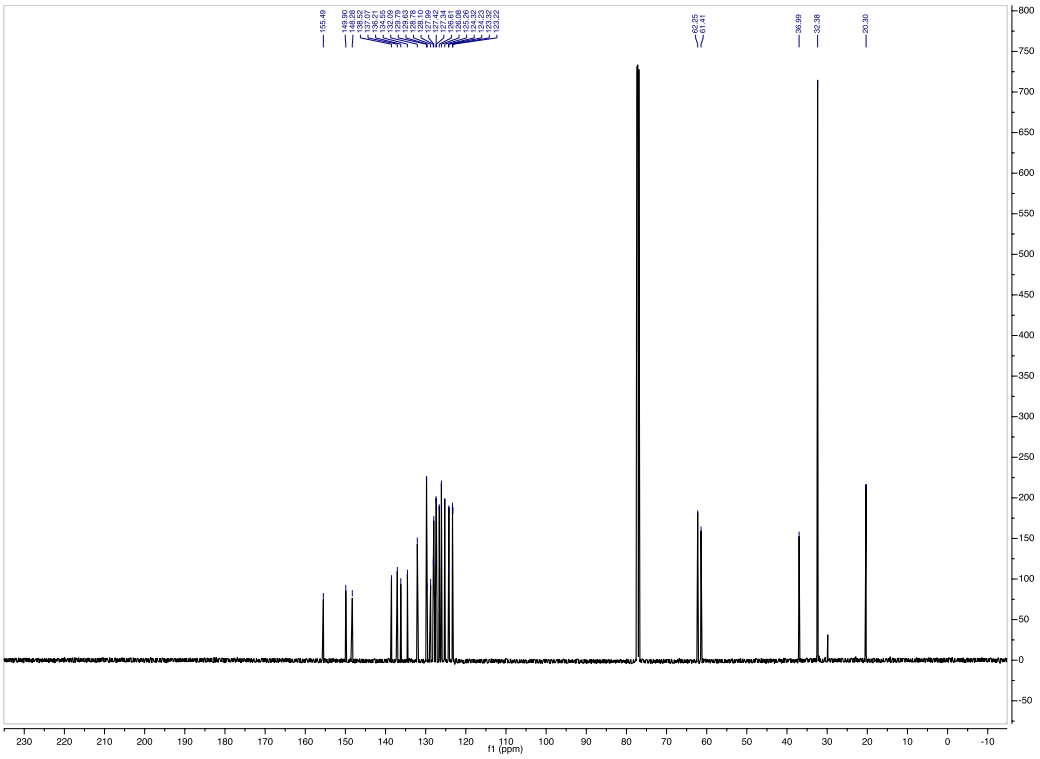

Figure 4.4.167. ^{13}C of 4.2q

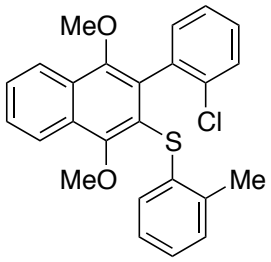

Figure 4.4.168. Product 4.2r

(3-(2-chlorophenyl)-1,4-dimethoxynaphthalen-2-yl)(*o*-tolyl)sulfane (**4.2r**):

83% yield, purified by FCC, hexanes/EtOAc = 98/2. 74:26 e.r.

^{1}H NMR (500 MHz, $CDCl_3$) δ 8.26 – 8.21 (m, 1H), 8.21 – 8.17 (m, 1H), 7.65 – 7.60 (m, 2H), 7.42 (dd, *J* = 8.1, 1.2 Hz, 1H), 7.24 (ddd, *J* = 8.1, 7.5, 1.7 Hz, 1H), 7.07 (td, *J* = 7.5, 1.2 Hz, 1H), 6.97 – 6.85 (m, 5H), 6.75 (d, *J* = 7.4 Hz, 1H), 4.03 (s, 3H), 3.57 (s, 3H), 2.08 (s, 3H).

^{13}C NMR (126 MHz, $CDCl_3$) δ 155.76, 150.81, 137.00, 136.31, 135.87, 134.57, 132.85, 131.89, 129.75, 129.68, 129.26, 129.06, 128.85, 128.28, 127.45, 127.14, 126.23, 125.95, 125.37, 123.33, 123.32, 123.16, 62.63, 61.56, 20.23.

MS (APCI) Calculated for $C_{25}H_{22}ClO_2S$ $[M+H]^+$: 421.1; Found: 421.3 m/z

HPLC trace: Chiralpak IA (hexanes/2-propanol = 90/10, 1.0 mL/min, t_{ent1} = 4.4 min, t_{ent2} = 5.3 min)

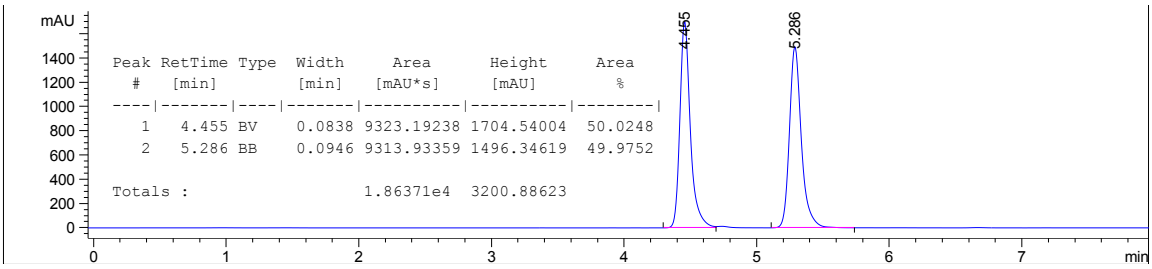

Figure 4.4.169. Racemic HPLC trace of 4.2r

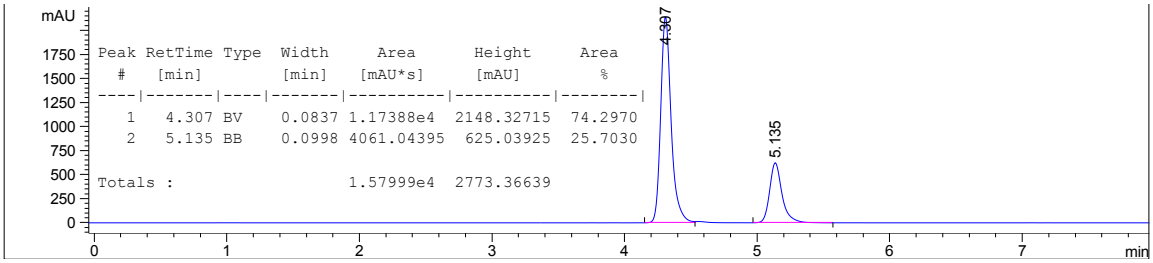

Figure 4.4.170. Asymmetric HPLC trace of 4.2r

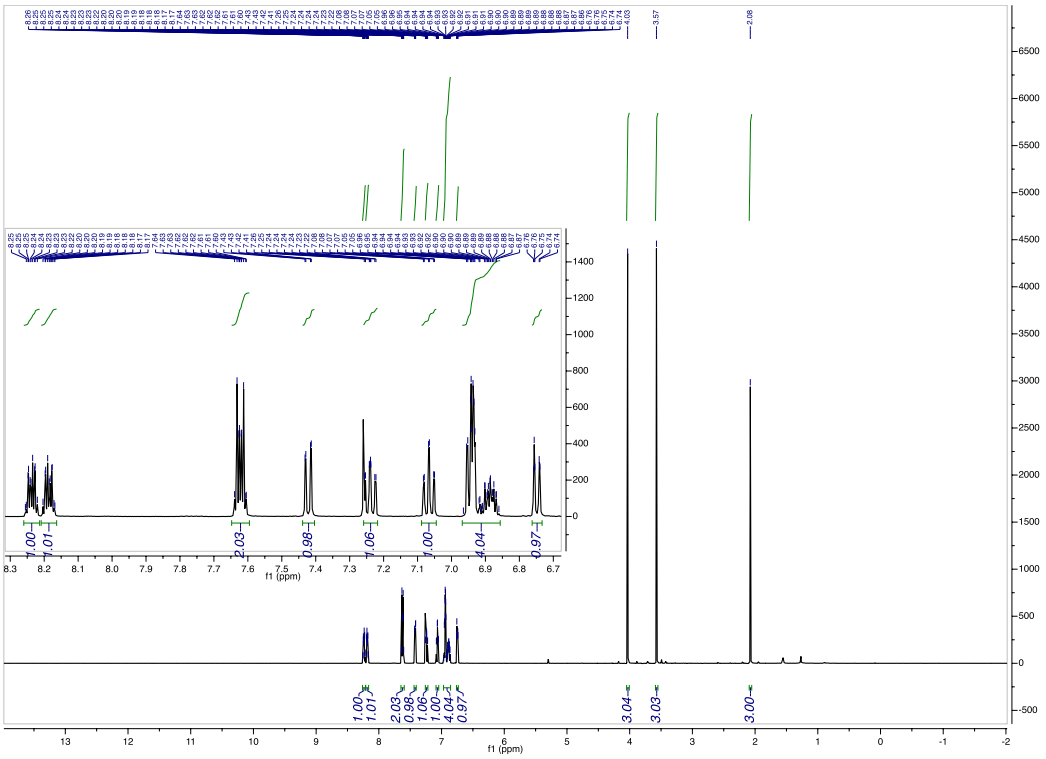

Figure 4.4.171. ^{1}H of 4.2r

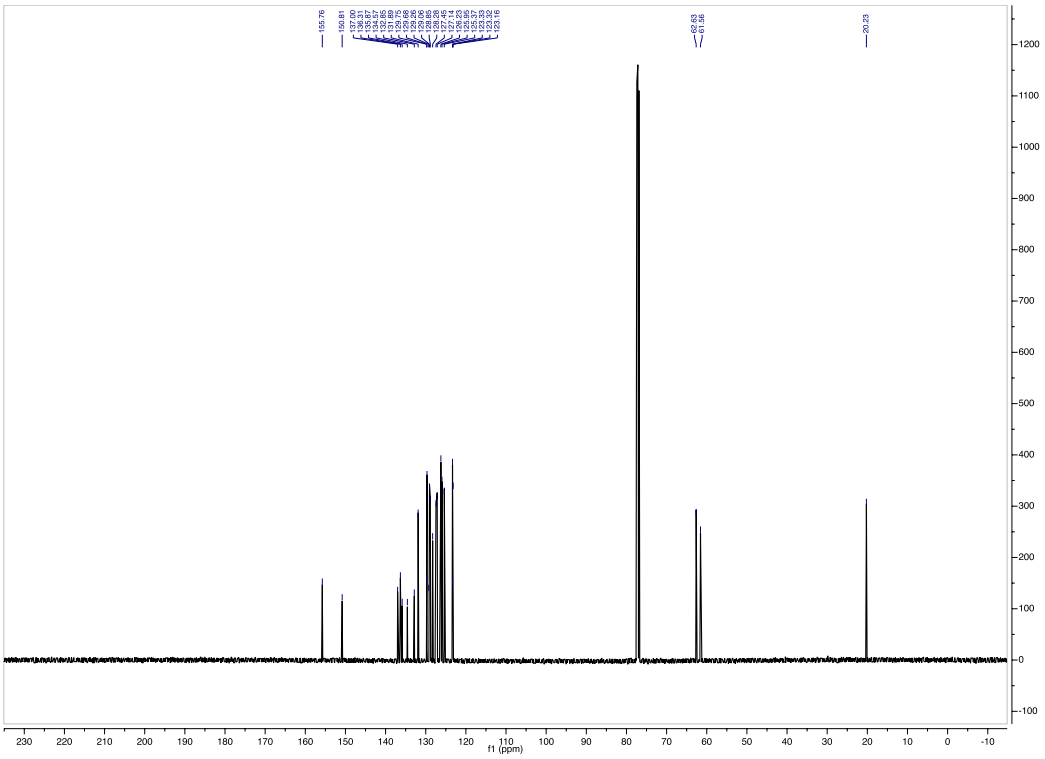

Figure 4.4.172. ^{13}C of 4.2r

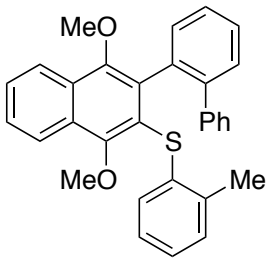

Figure 4.4.173. Product 4.2s

(3-([1,*1'-b*iphenyl]-2-yl)-1,4-dimethoxynaphthalen-2-yl)(*o*-tolyl)sulfane (**4.2s**):

84 % yield, purified by FCC, hexanes/EtOAc = 99:1 → 95:5. 79:21 e.r.

^{1}H NMR (599 MHz, $CDCl_3$) δ 8.12 (d, *J* = 9.3 Hz, 2H), 7.60 – 7.52 (m, 2H), 7.47 – 7.43 (m, 1H), 7.40 (t, *J* = 7.5 Hz, 1H), 7.24 – 7.19 (m, 2H), 7.17 (t, *J* = 7.5 Hz, 1H), 7.10 – 7.04 (m, 3H), 7.02 – 6.95 (m, 2H), 6.94 (t, *J* = 7.4 Hz, 1H), 6.84 (t, *J* = 7.6 Hz, 1H), 6.55 (d, *J* = 8.0 Hz, 1H), 3.78 (d, *J* = 1.6 Hz, 3H), 3.67 (d, *J* = 1.5 Hz, 3H), 2.09 (s, 3H).

^{13}C NMR (151 MHz, $CDCl_3$) δ 155.55, 150.65, 141.96, 141.65, 137.20, 136.07, 135.23, 135.10, 130.88, 129.83, 129.66, 129.49, 129.29, 128.86, 127.96, 127.86, 127.60, 127.17, 126.60, 126.46, 126.23, 126.11, 125.20, 123.47, 123.22, 123.11, 62.21, 61.72, 20.24.

MS (APCI) Calculated for $C_{31}H_{27}O_2S$ $[M+H]^+$: 463.2; Found: 463.3 m/z

HPLC trace: Chiralpak IA (hexanes/2-propanol = 95/5, 1.0 mL/min, t_{ent1} = 4.3 min, t_{ent2} = 4.8 min)

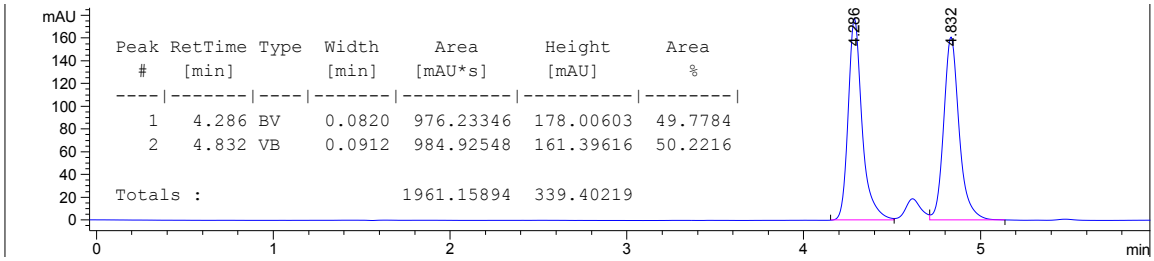

Figure 4.4.174. Racemic HPLC trace of 4.2s

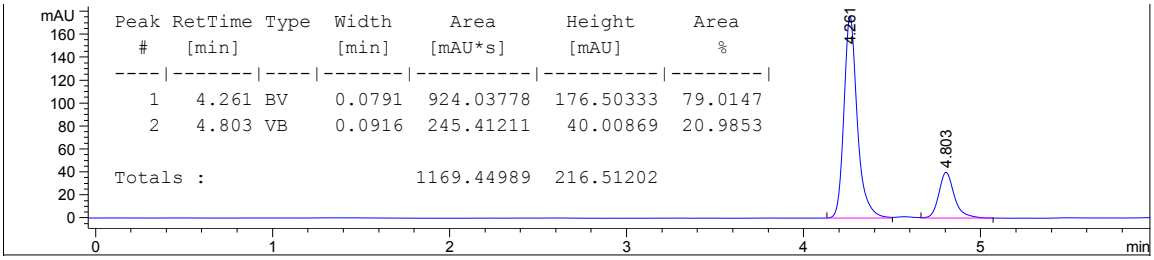

Figure 4.4.175. Asymmetric HPLC trace of 4.2s

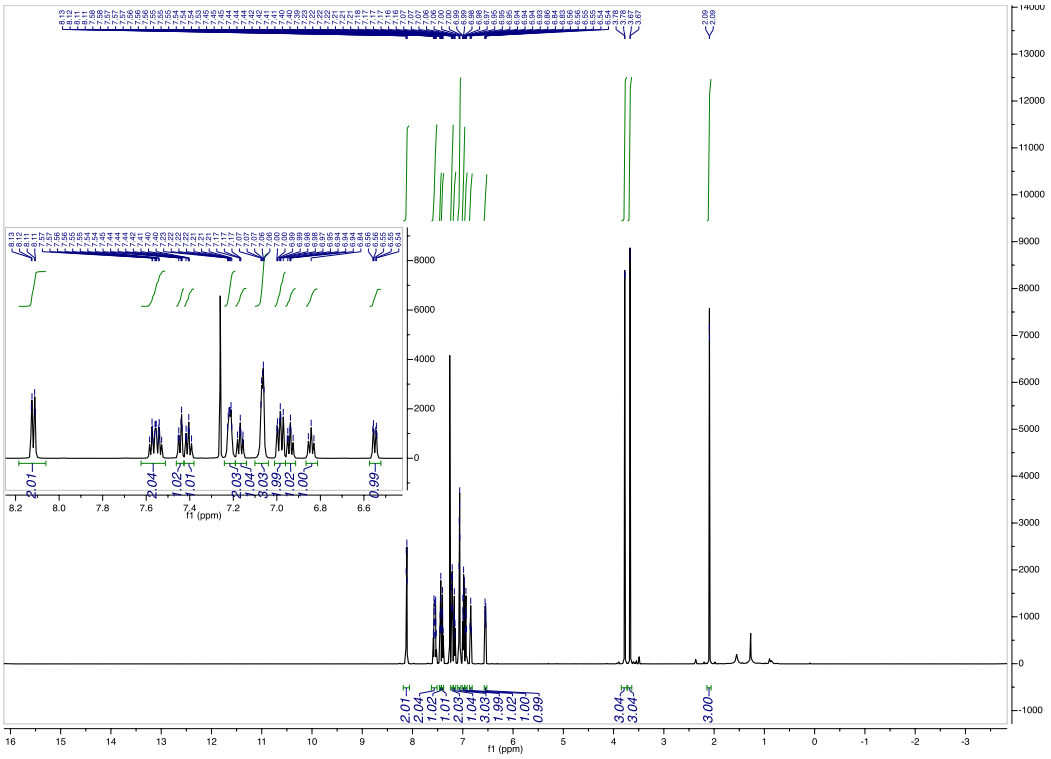

Figure 4.4.176. ^{1}H of 4.2s

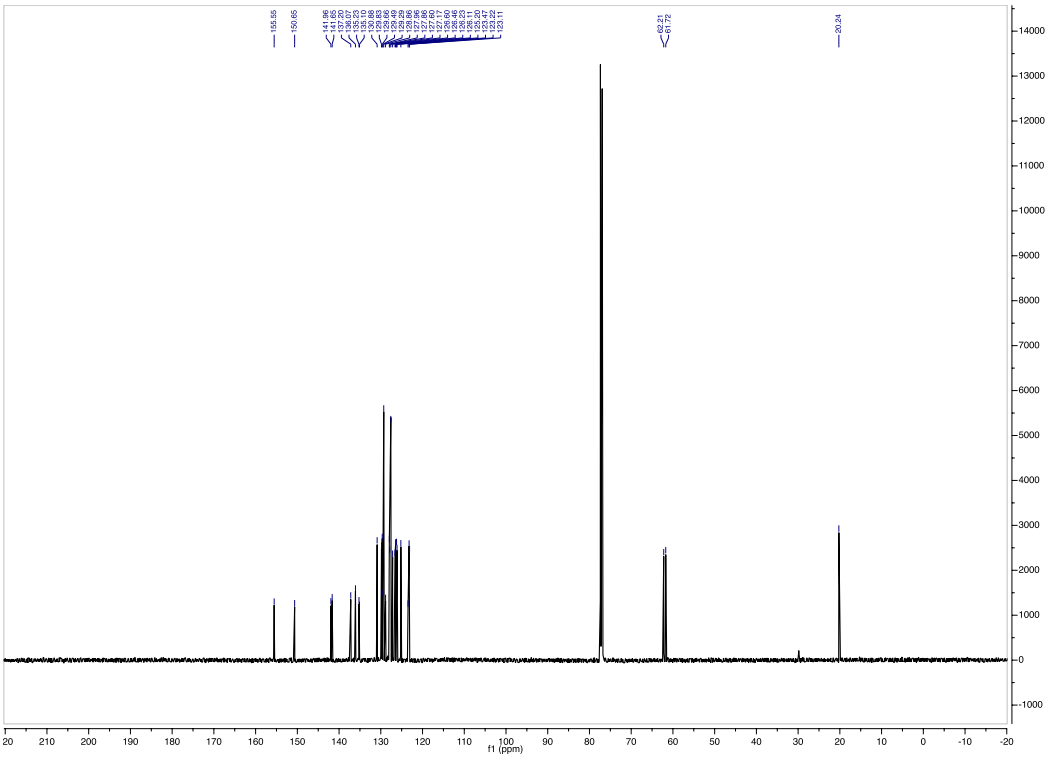

Figure 4.4.177. ^{13}C of 4.2s

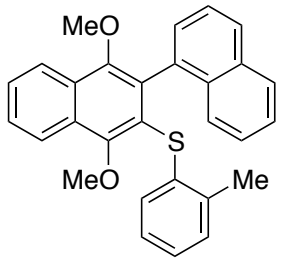

Figure 4.4.178. Product 4.2t

(1',4'-dimethoxy-[1,2'-binaphthalen]-3'-yl)(*o*-tolyl)sulfane (**4.2t**):

99% yield, purified by FCC, hexanes/EtOAc = 97/3. 90:10 e.r.

^{1}H NMR (500 MHz, $CDCl_3$) δ 8.31 – 8.26 (m, 1H), 8.23 – 8.18 (m, 1H), 7.84 (dt, *J* = 8.2, 0.9 Hz, 1H), 7.80 (dt, *J* = 8.3, 1.0 Hz, 1H), 7.68 – 7.61 (m, 2H), 7.44 – 7.37 (m, 2H), 7.31 (dd, *J* = 8.3, 7.0 Hz, 1H), 7.27 (ddd, *J* = 8.3, 6.7, 1.3 Hz, 1H), 7.09 (dd, *J* = 7.0, 1.2 Hz, 1H), 6.88 – 6.79 (m, 4H), 4.06 (s, 3H), 3.39 (s, 3H), 1.76 (s, 3H).

^{13}C NMR (126 MHz, $CDCl_3$) δ 155.57, 151.38, 137.13, 136.54, 134.44, 133.41, 133.37, 132.55, 129.74, 129.60, 129.12, 128.55, 128.13, 128.10, 127.80, 127.42, 127.03, 126.16, 126.01, 125.87, 125.56, 125.41, 124.93, 124.64, 123.29, 123.21, 62.52, 61.94, 20.02.

MS (APCI) Calculated for $C_{29}H_{25}O_2S$ $[M+H]^+$: 437.2; Found: 437.1 m/z

HPLC trace: Chiralpak IA (hexanes/2-propanol = 90/10, 1.0 mL/min, t_{ent1} = 4.4 min, t_{ent2} = 5.0 min)

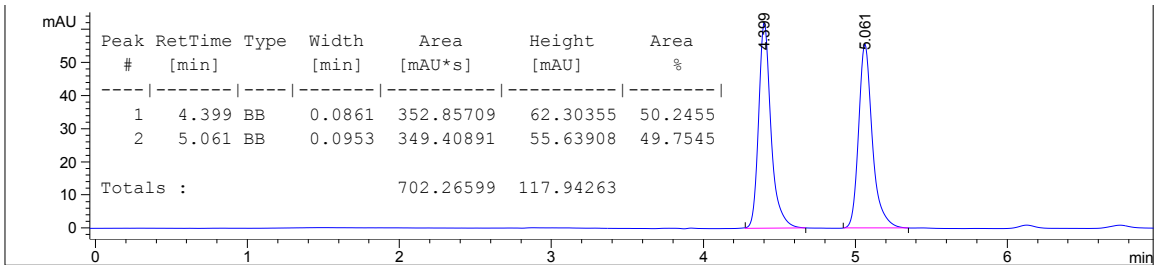

Figure 4.4.179. Racemic HPLC trace of 4.2t

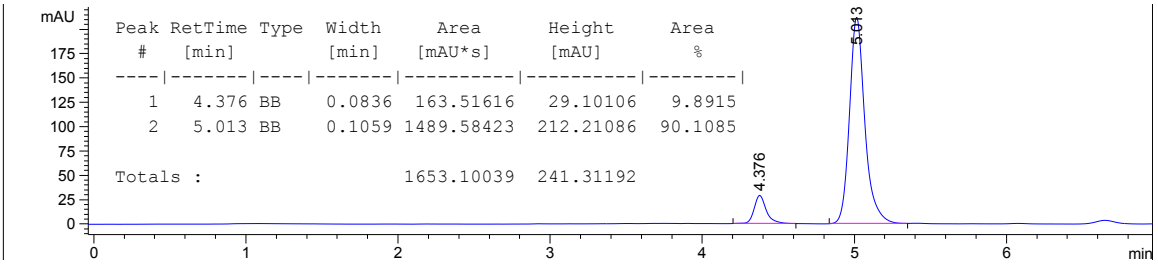

Figure 4.4.180. Asymmetric HPLC trace of 4.2t

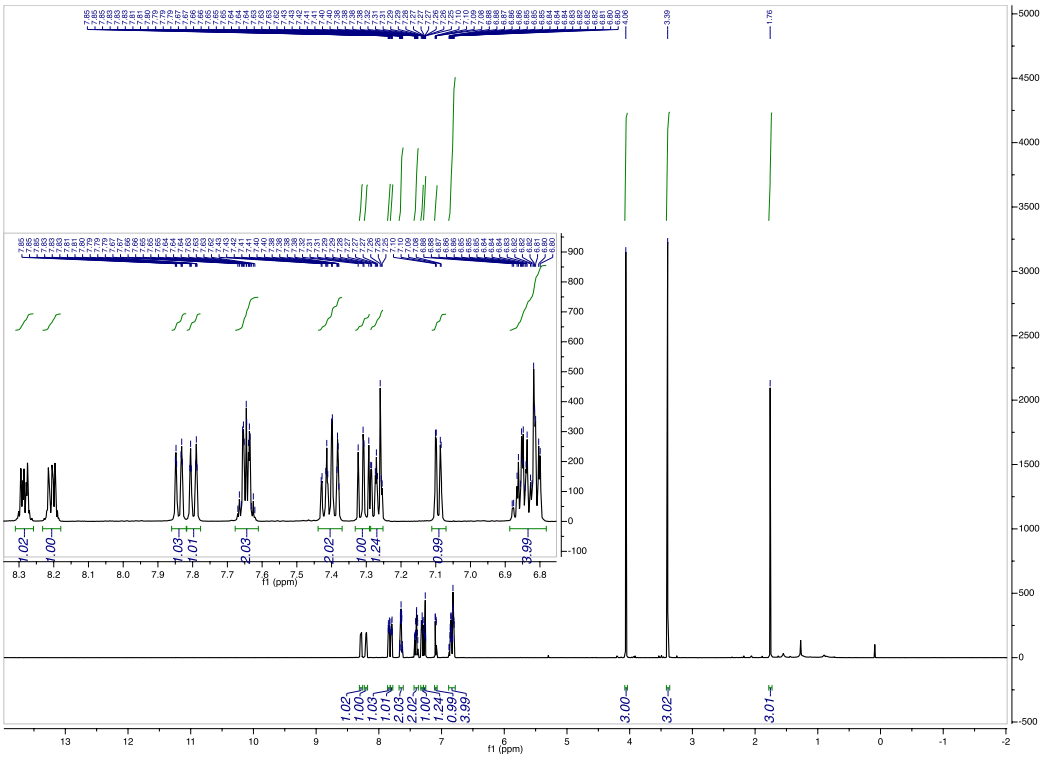

Figure 4.4.181. ^{1}H of 4.2t

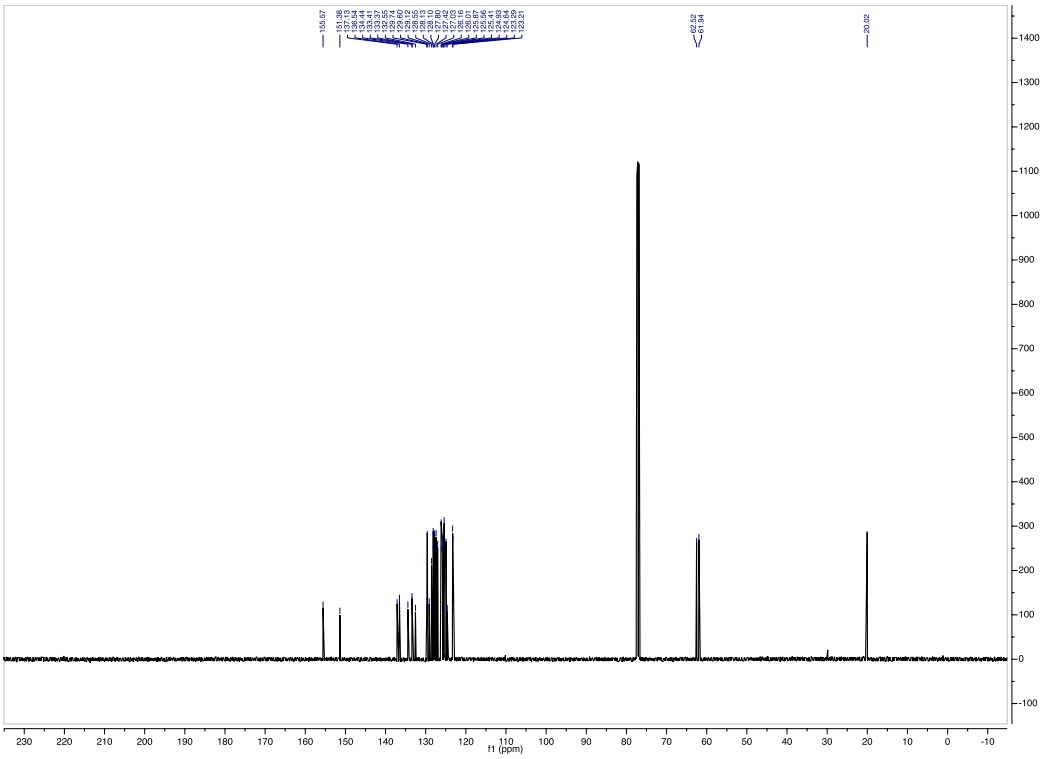

Figure 4.4.182. ^{13}C of 4.2t

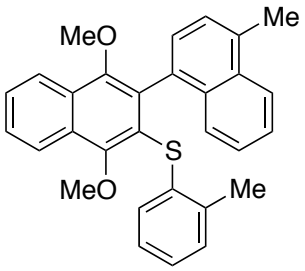

Figure 4.4.183. Product 4.2u

(1',4'-dimethoxy-4-methyl-[1,2'-binaphthalen]-3'-yl)(*o*-tolyl)sulfane (**4.2u**):

95% yield, purified by FCC, hexanes/DCM = 97/3 → 95/5. 92:8 e.r.

^{1}H NMR (500 MHz, $CDCl_3$) δ 8.29 – 8.24 (m, 1H), 8.23 – 8.18 (m, 1H), 8.01 (dt, *J* = 8.5, 0.9 Hz, 1H), 7.66 – 7.60 (m, 2H), 7.46 (ddd, *J* = 8.4, 6.7, 1.3 Hz, 1H), 7.41 (ddd, *J* = 8.4, 1.4, 0.7 Hz, 1H), 7.28 (ddd, *J* = 8.3, 6.8, 1.3 Hz, 1H), 7.17 (dd, *J* = 7.1, 1.0 Hz, 1H), 7.02 (d, *J* = 7.1 Hz, 1H), 6.90 – 6.80 (m, 4H), 4.04 (s, 3H), 3.41 (s, 3H), 2.73 (d, *J* = 0.9 Hz, 3H), 1.80 (s, 3H).

^{13}C NMR (126 MHz, $CDCl_3$) δ 155.32, 151.37, 137.15, 136.59, 134.00, 133.58, 132.80, 132.60, 132.54, 129.68, 129.56, 129.08, 128.62, 127.73, 127.32, 126.92, 126.59, 126.10, 125.82, 125.50, 125.43, 125.39, 124.95, 124.27, 123.25, 123.20, 62.37, 61.95, 20.06, 19.68.

MS (APCI) Calculated for $C_{30}H_{27}O_2S$ $[M+H]^+$: 451.2; Found: 451.2 m/z

HPLC trace: Chiralpak IA (hexanes/2-propanol = 90/10, 1.0 mL/min, t_{ent1} = 4.9 min, t_{ent2} = 5.9 min)

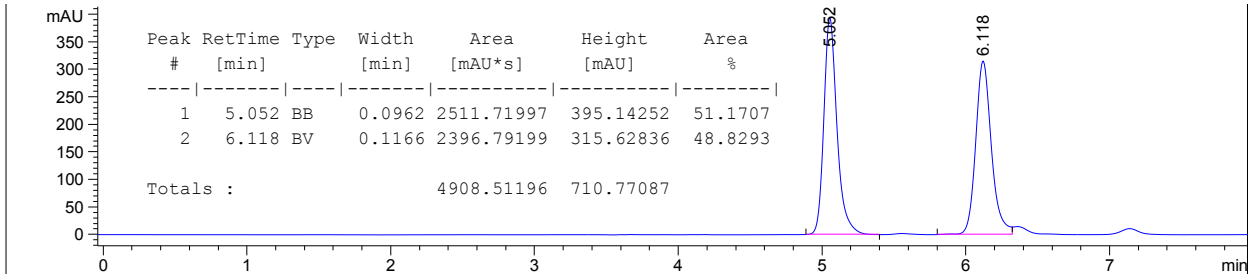

Figure 4.4.184. Racemic HPLC trace of 4.2u

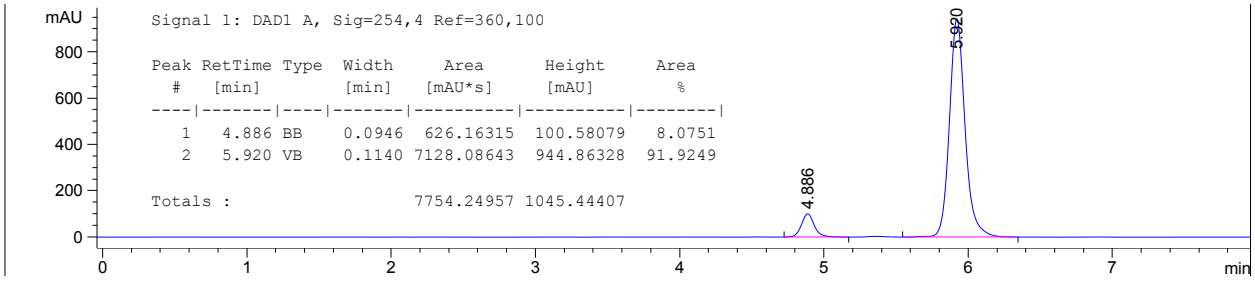

Figure 4.4.185. Asymmetric HPLC trace of 4.2u

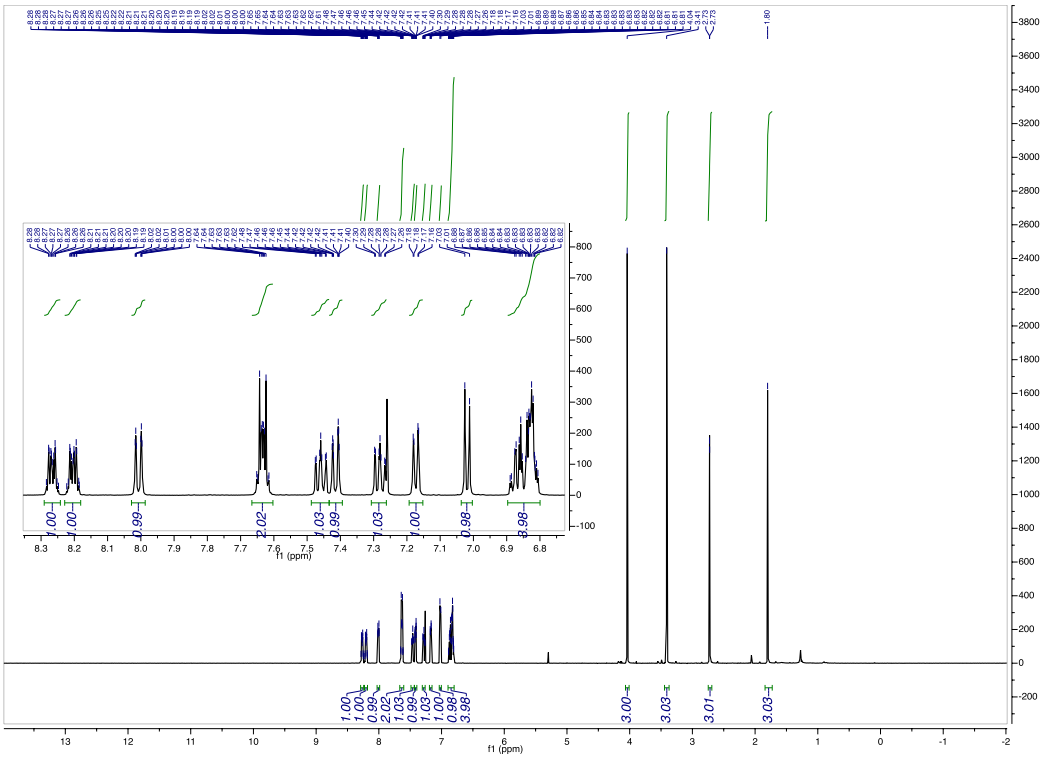

Figure 4.4.186. ^{1}H of 4.2u

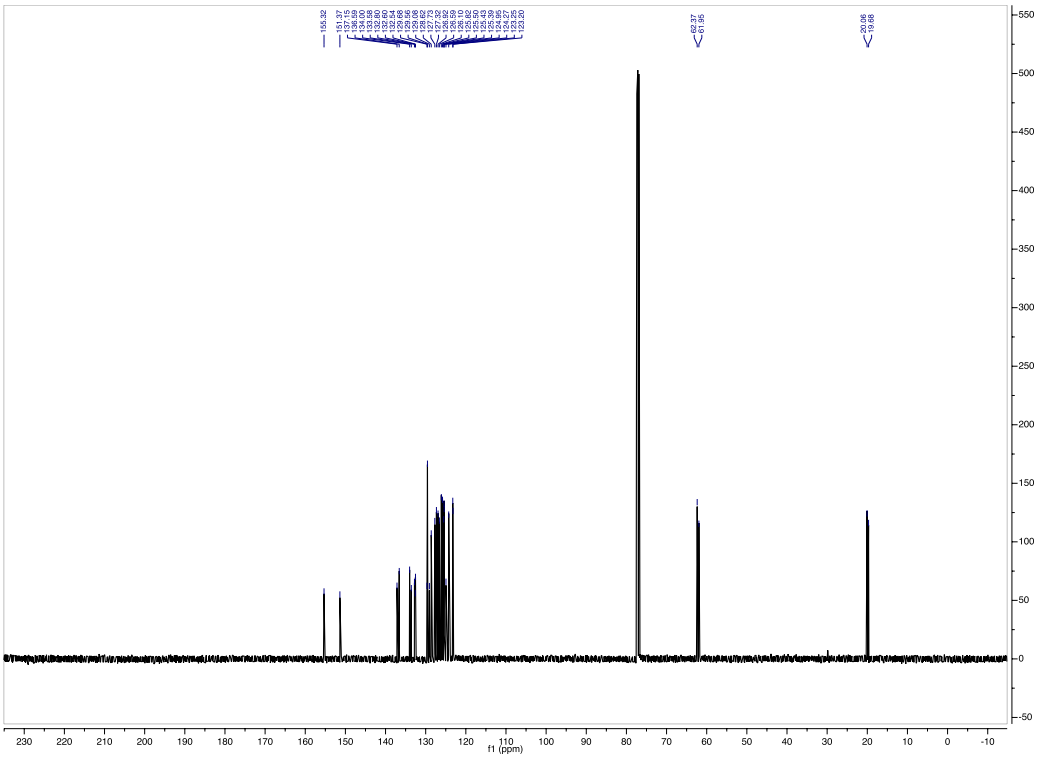

Figure 4.4.187. ^{13}C of 4.2u

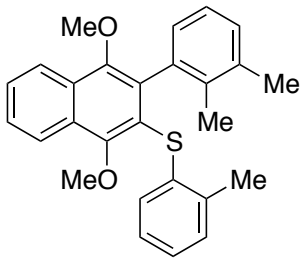

Figure 4.4.188. Product 4.2v

(3-(2,3-dimethylphenyl)-1,4-dimethoxynaphthalen-2-yl)(*o*-tolyl)sulfane (**4.2v**):

94% yield, purified by FCC, hexanes/EtOAc = 98/2. 90:10 e.r.

^{1}H NMR (500 MHz, $CDCl_3$) δ 8.24 – 8.20 (m, 1H), 8.18 – 8.14 (m, 1H), 7.63 – 7.57 (m, 2H), 7.07 (d, *J* = 7.4 Hz, 1H), 6.96 – 6.92 (m, 3H), 6.89 – 6.84 (m, 1H), 6.79 (d, *J* = 7.7 Hz, 2H), 4.02 (s, 3H), 3.49 (s, 3H), 2.24 (s, 3H), 2.01 (s, 3H), 1.81 (s, 3H).

^{13}C NMR (126 MHz, $CDCl_3$) δ 155.37, 150.36, 137.00, 136.70, 136.33, 136.29, 135.56, 135.31, 129.63, 129.16, 128.89, 128.73, 128.36, 127.27, 126.73, 126.06, 125.55, 124.51, 124.32, 123.20, 123.07, 62.51, 61.33, 20.63, 20.24, 16.91.

MS (APCI) Calculated for $C_{27}H_{27}O_2S$ $[M+H]^+$: 415.2; Found: 415.3 m/z

HPLC trace: Chiralpak IA (hexanes/2-propanol = 90/10, 1.0 mL/min, t_{ent1} = 4.1 min, t_{ent2} = 4.4 min)

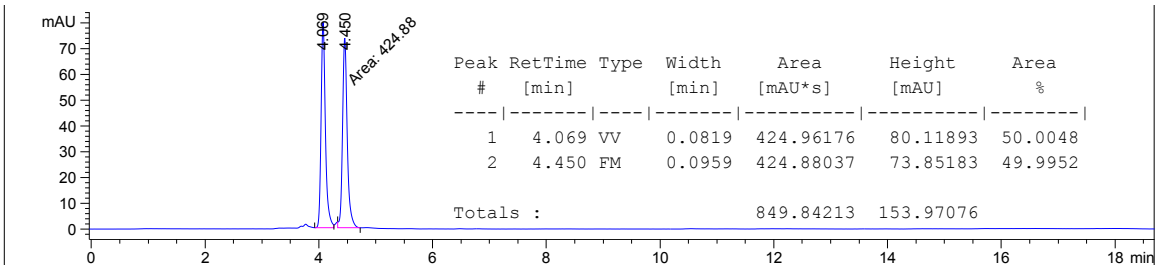

Figure 4.4.189. Racemic HPLC trace of 4.2v

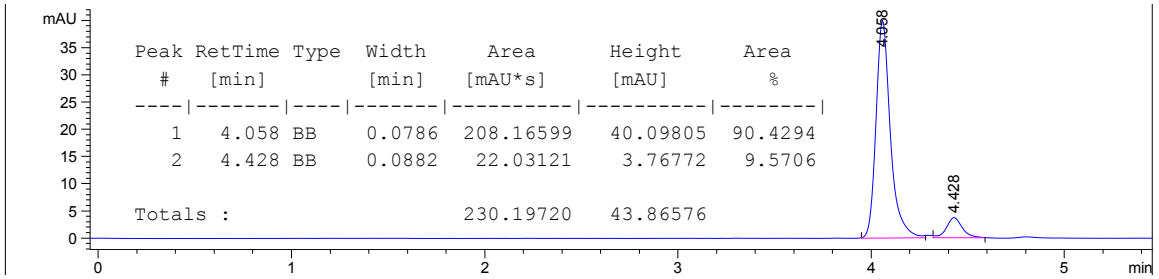

Figure 4.4.190. Asymmetric HPLC trace of 4.2v

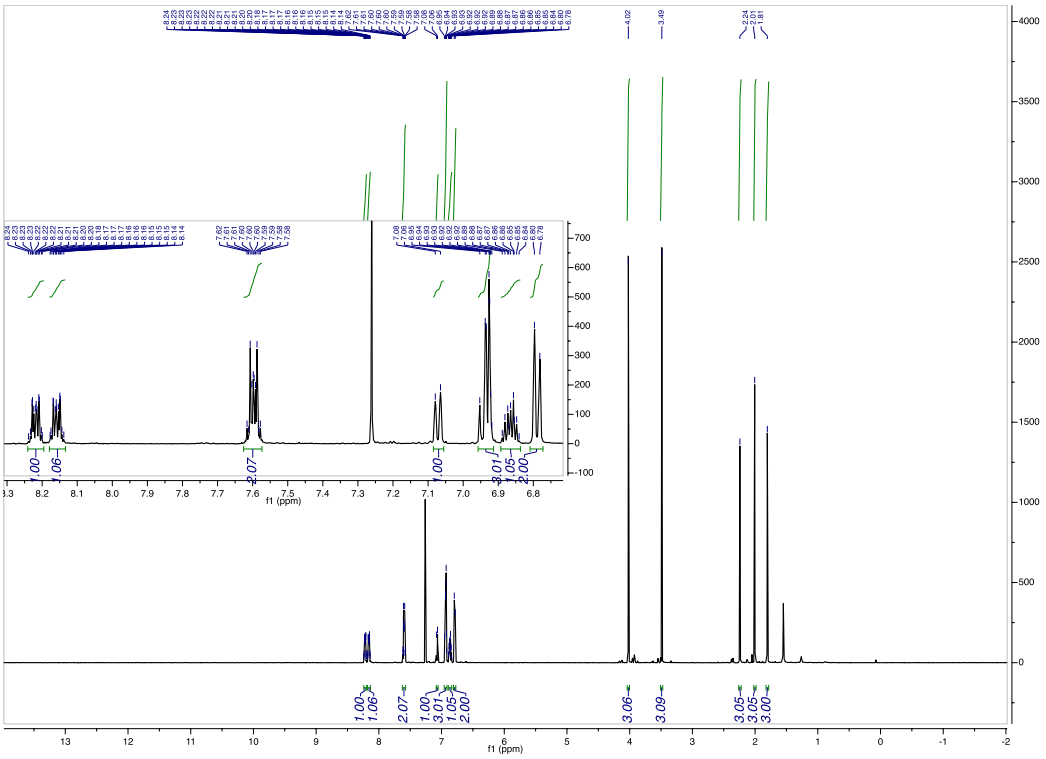

Figure 4.4.191. ^{1}H of 4.2v

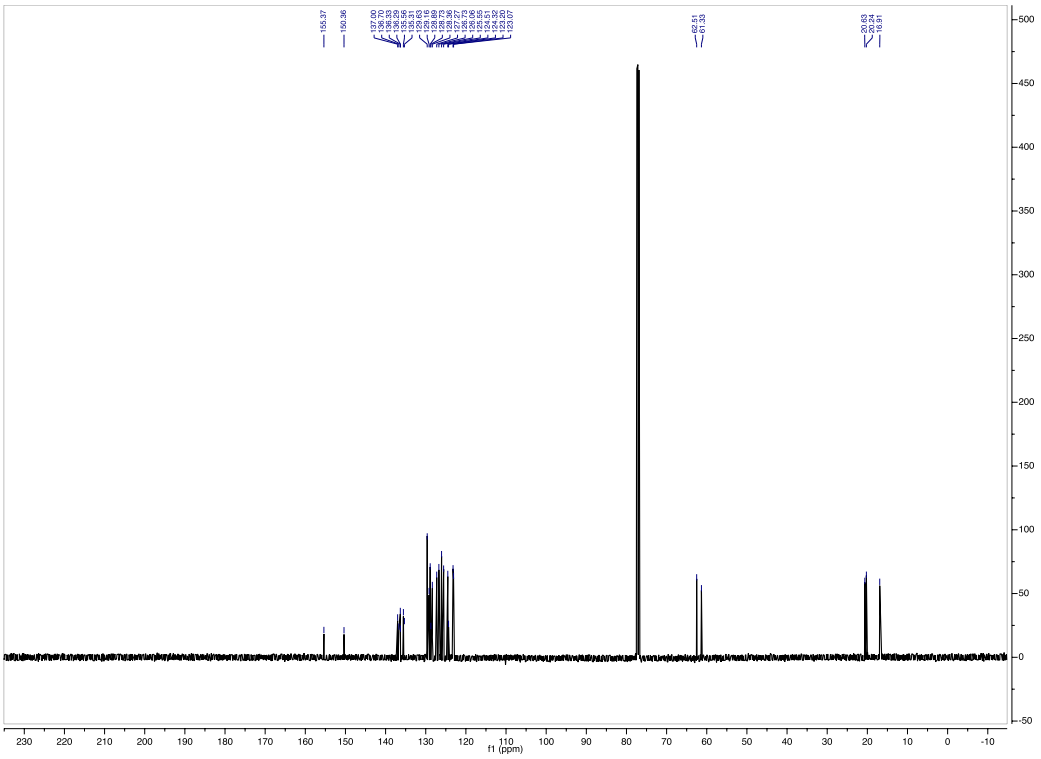

Figure 4.4.192. ^{13}C of 4.2v

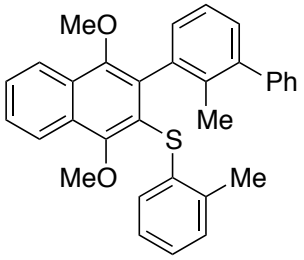

Figure 4.4.193. Product 4.2w

(1,4-dimethoxy-3-(2-methyl-[1,1'-biphenyl]-3-yl)naphthalen-2-yl)(*o*-tolyl)sulfane (**4.2w**):

86% yield, purified by FCC, hexanes/EtOAc = 95/5. 89:11 e.r.

^{1}H NMR (500 MHz, $CDCl_3$) δ 8.27 – 8.22 (m, 1H), 8.20 – 8.15 (m, 1H), 7.64 – 7.59 (m, 2H), 7.42 – 7.37 (m, 2H), 7.35 – 7.27 (m, 3H), 7.14 (dd, *J* = 7.6, 1.4 Hz, 1H), 7.05 (t, *J* = 7.6 Hz, 1H), 6.97 – 6.92 (m, 2H), 6.92 – 6.85 (m, 2H), 6.82 (d, *J* = 7.5 Hz, 1H), 4.06 (s, 3H), 3.55 (s, 3H), 2.05 (s, 3H), 1.81 (s, 3H).

^{13}C NMR (126 MHz, $CDCl_3$) δ 155.78, 150.45, 142.73, 142.11, 136.99, 136.92, 136.75, 135.13, 134.53, 129.79, 129.69, 129.49, 129.21, 129.03, 128.80, 128.04, 127.38, 126.86, 126.70, 126.17, 125.62, 124.51, 124.05, 123.26, 123.10, 62.75, 61.34, 20.30, 18.20.

MS (APCI) Calculated for $C_{32}H_{29}O_2S$ $[M+H]^+$: 477.2; Found: 477.2 m/z

HPLC trace: Chiralpak IB (hexanes/2-propanol = 98/2, 0.5 mL/min, t_{ent1} = 9.7 min, t_{ent2} = 10.2 min)

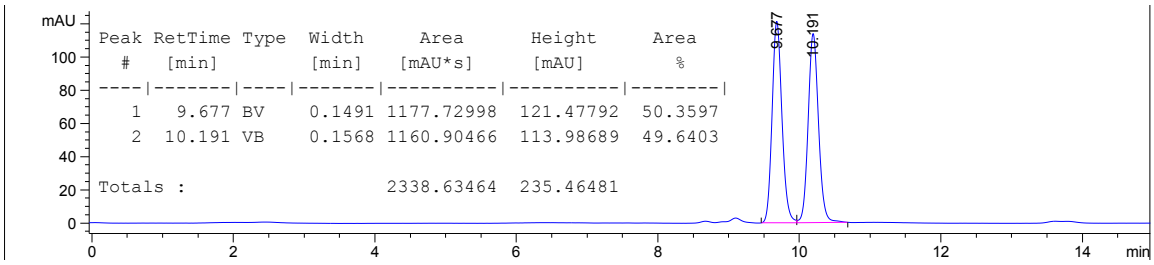

Figure 4.4.194. Racemic HPLC trace of 4.2w

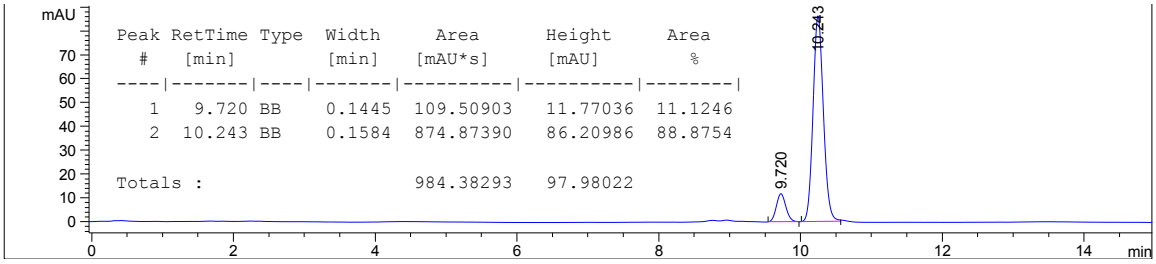

Figure 4.4.195. Asymmetric HPLC trace of 4.2w

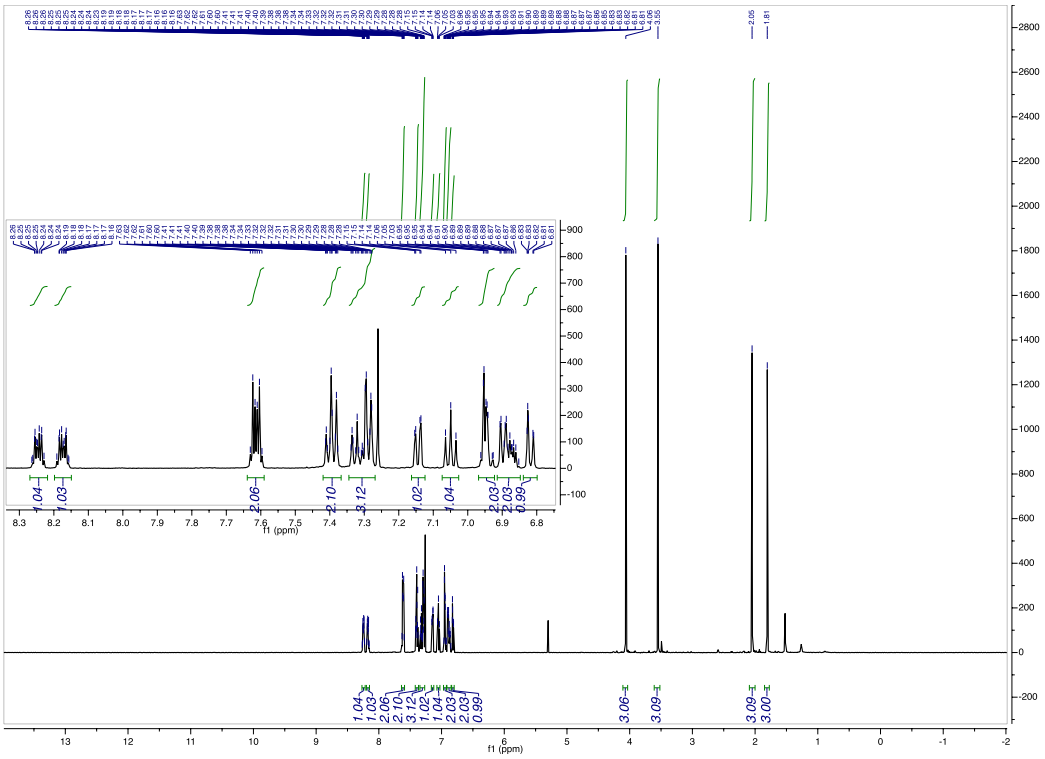

Figure 4.4.196. ^{1}H of 4.2w

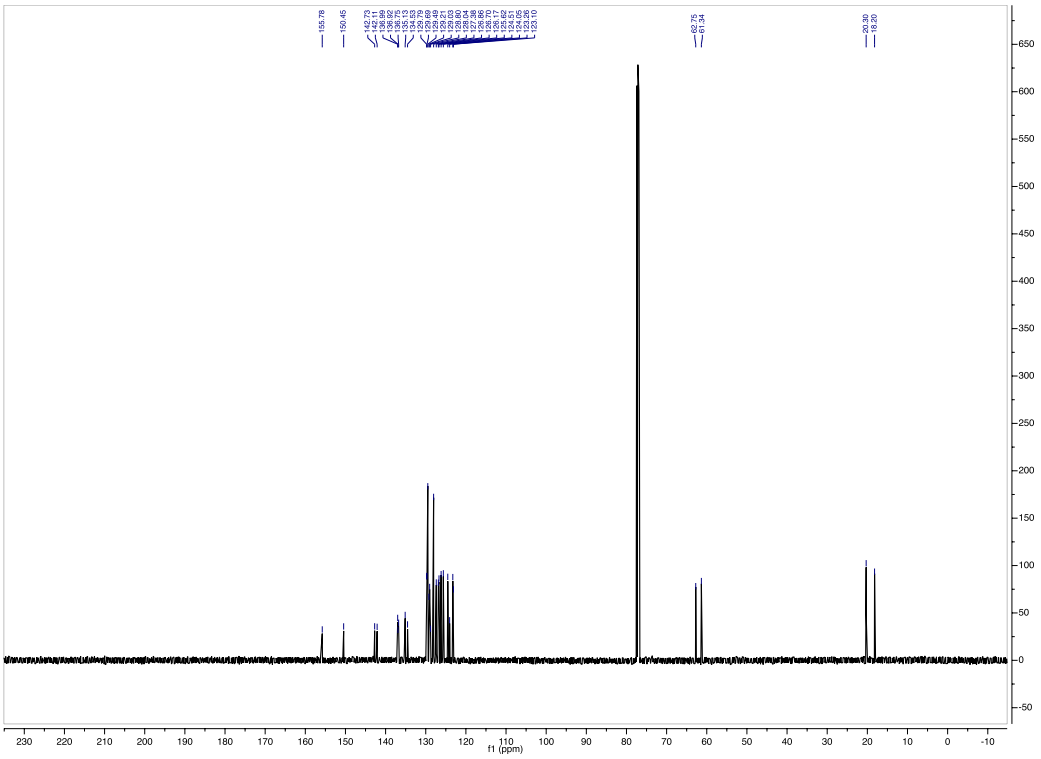

Figure 4.4.197. ^{13}C of 4.2w

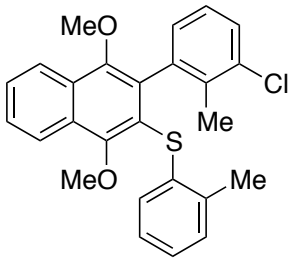

Figure 4.4.198. Product 4.2x

(3-(3-chloro-2-methylphenyl)-1,4-dimethoxynaphthalen-2-yl)(*o*-tolyl)sulfane (**4.2x**):

83% yield, purified by FCC, hexanes/EtOAc = 99/1. 88:12 e.r.

^{1}H NMR (500 MHz, CD_2Cl_2) δ 8.25 – 8.20 (m, 1H), 8.18 – 8.13 (m, 1H), 7.66 – 7.61 (m, 2H), 7.30 (dd, *J* = 7.9, 1.2 Hz, 1H), 7.00 – 6.93 (m, 3H), 6.90 – 6.83 (m, 2H), 6.71 (d, *J* = 7.6 Hz, 1H), 4.02 (s, 3H), 3.48 (s, 3H), 2.04 (s, 3H), 1.98 (s, 3H).

^{13}C NMR (126 MHz, CD_2Cl_2) δ 156.02, 150.84, 138.68, 136.99, 136.91, 135.67, 134.67, 134.28, 130.06, 130.00, 129.57, 129.33, 128.93, 128.46, 127.79, 127.36, 126.44, 126.01, 125.87, 123.67, 123.44, 123.33, 62.81, 61.60, 20.16, 17.90.

MS (APCI) Calculated for $C_{26}H_{24}ClO_2S$ $[M+H]^+$: 435.1; Found: 435.1 m/z

HPLC trace: Chiralpak IB (hexanes/2-propanol = 98/2, 0.5 mL/min, t_{ent1} = 8.7 min, t_{ent2} = 9.2 min)

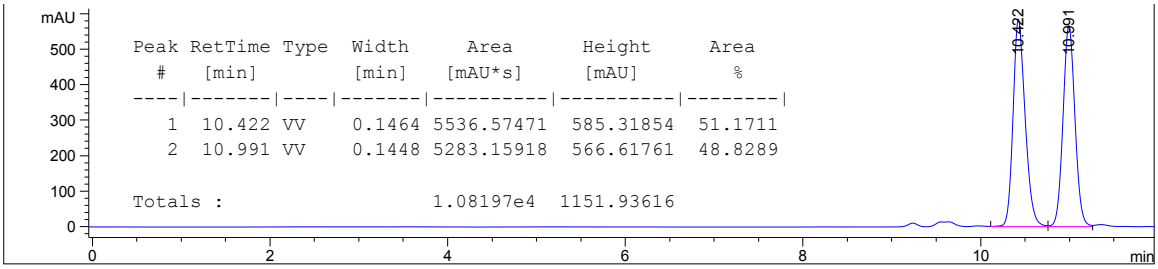

Figure 4.4.199. Racemic HPLC trace of 4.2x

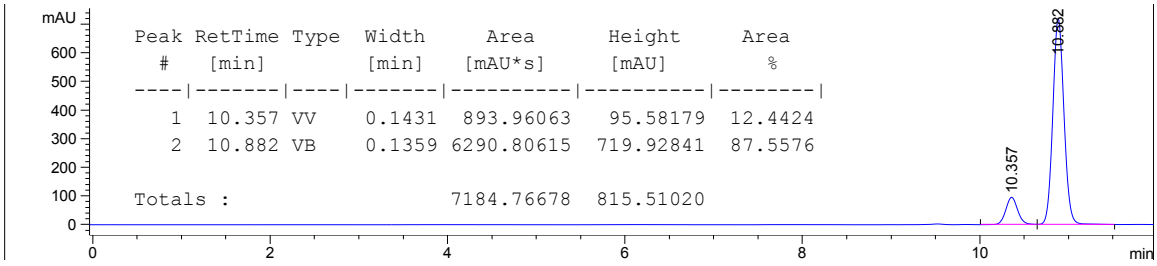

Figure 4.4.200. Asymmetric HPLC trace of 4.2x

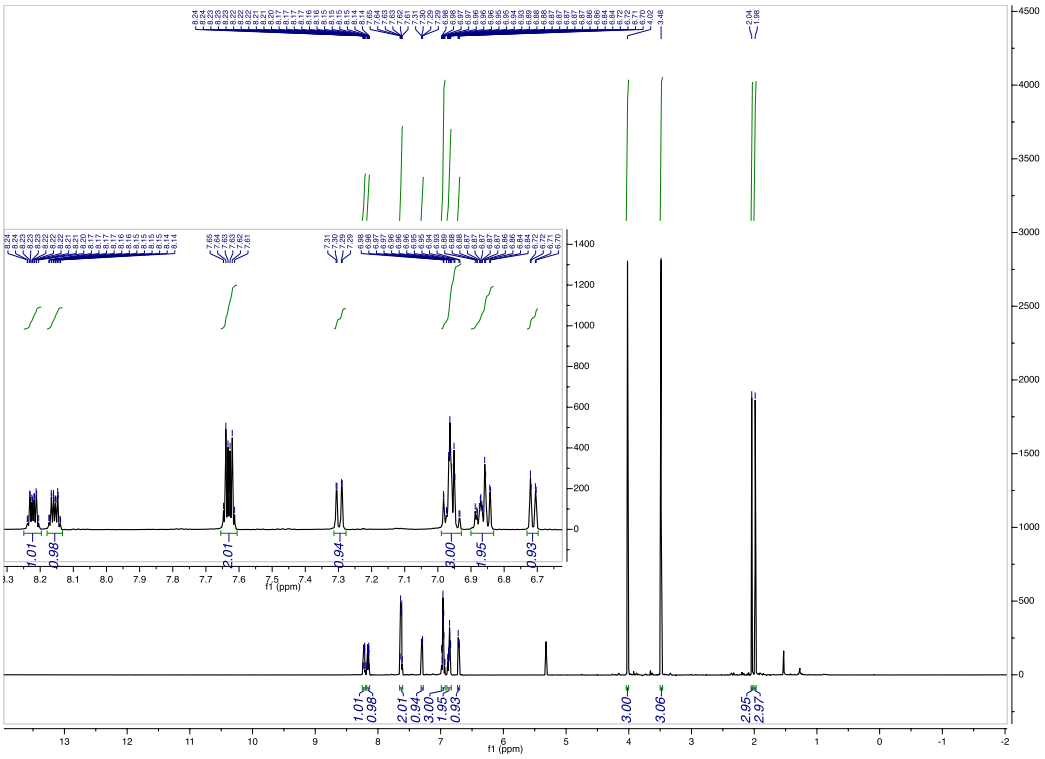

Figure 4.4.201. ^{1}H of 4.2x

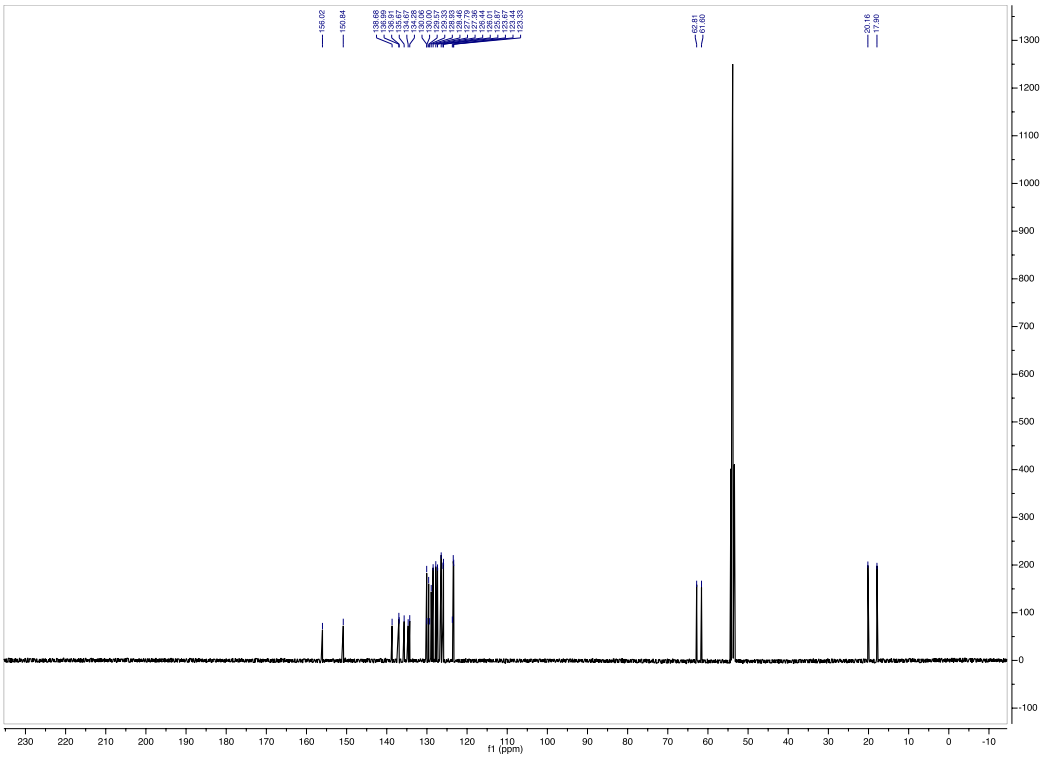

Figure 4.4.202. ^{13}C of 4.2x

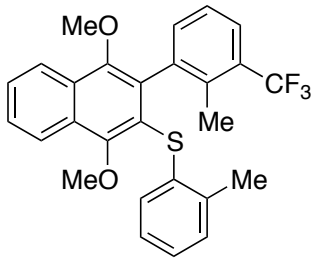

Figure 4.4.203. Product 4.2y

(1,4-dimethoxy-3-(2-methyl-3-(trifluoromethyl)phenyl)naphthalen-2-yl)(*o*-tolyl)sulfane (**4.2y**): 98% yield, purified by FCC, hexanes/DCM = 96/4. 92:8 e.r.

^{1}H NMR (400 MHz, $CDCl_3$) δ 8.30 – 8.23 (m, 1H), 8.19 – 8.13 (m, 1H), 7.68 – 7.60 (m, 2H), 7.58 – 7.51 (m, 1H), 7.09 – 7.02 (m, 2H), 6.97 – 6.84 (m, 3H), 6.74 (dd, *J* = 7.8, 1.3 Hz, 1H), 4.08 (s, 3H), 3.47 (s, 3H), 2.05 (q, *J* = 1.8 Hz, 3H), 1.94 (s, 3H).

^{13}C NMR (126 MHz, $CDCl_3$) δ 156.03, 150.68, 138.45, 137.02, 136.26, 136.11, 134.21, 133.56, 129.81, 129.71, 129.11, 129.06, 128.95 (q, *J* = 30 Hz), 127.62, 127.22, 126.23, 125.81, 125.06 (q, *J* = 5.8 Hz), 124.85 (q, *J* = 274 Hz), 124.53, 123.63, 123.34, 123.10, 62.91, 61.31, 20.00, 16.40.

^{19}F NMR (470 MHz, $CDCl_3$) δ -59.92.

MS (APCI) Calculated for $C_{27}H_{24}F_3O_2S$ $[M+H]^+$: 469.1; Found: 468.9 m/z

HPLC trace: Chiralpak IA (hexanes/2-propanol = 98/2, 0.7 mL/min, t_{ent1} = 6.6 min, t_{ent2} = 7.0 min)

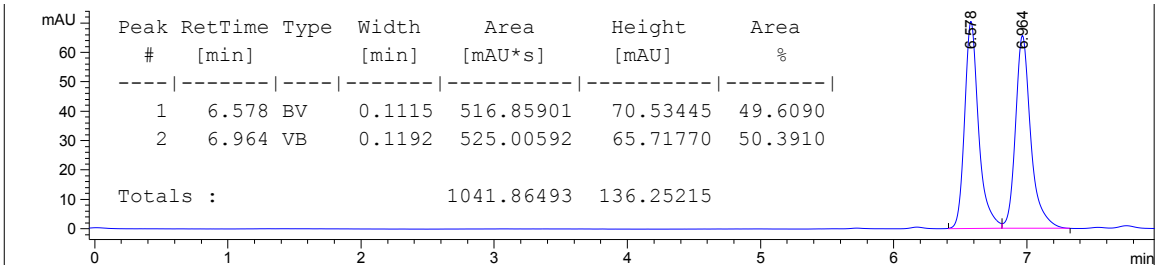

Figure 4.4.204. Racemic HPLC trace of 4.2y

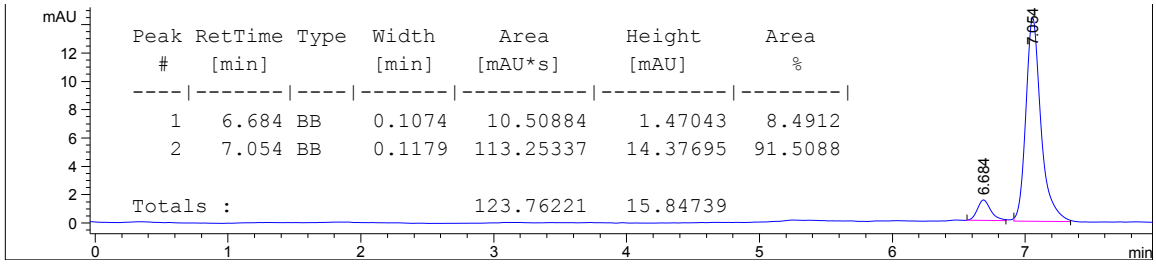

Figure 4.4.205. Asymmetric HPLC trace of 4.2y

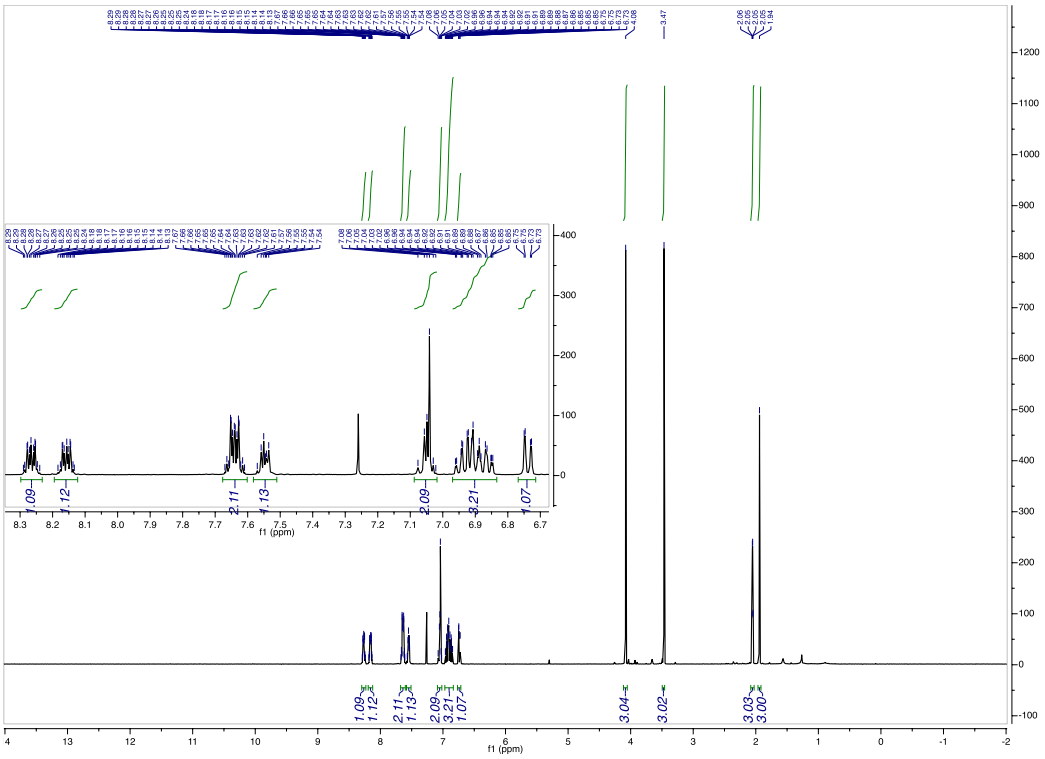

Figure 4.4.206. ^{1}H of 4.2y

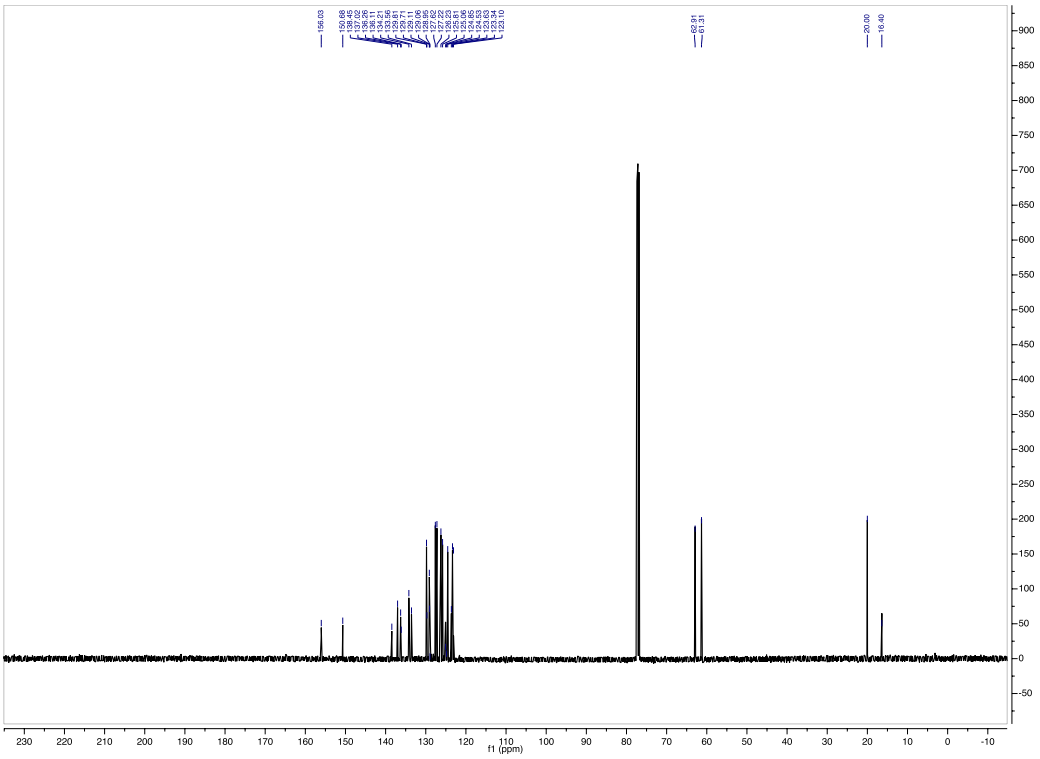

Figure 4.4.207. ^{13}C of 4.2y

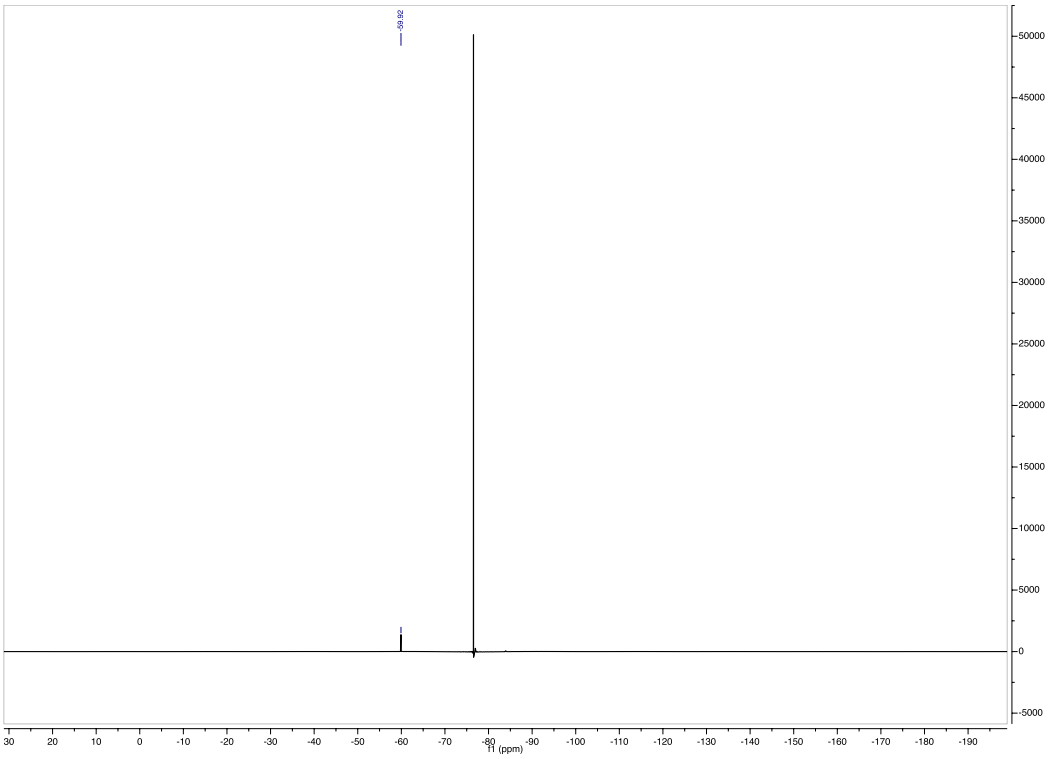

Figure 4.4.208. ^{19}F of 4.2y

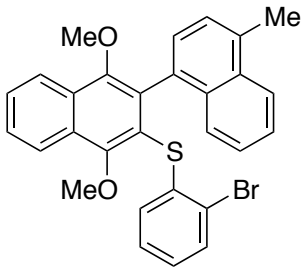

Figure 4.4.209. Product 4.2z

(2-bromophenyl)(1',4'-dimethoxy-4-methyl-[1,2'-binaphthalen]-3'-yl)sulfane (**4.2z**):

85% yield, purified by FCC, hexanes/DCM = 96/4. 90:10 e.r.

^{1}H NMR (500 MHz, $CDCl_3$) δ 8.27 – 8.20 (m, 2H), 8.01 (dd, *J* = 8.4, 1.1 Hz, 1H), 7.68 – 7.61 (m, 2H), 7.48 – 7.40 (m, 2H), 7.29 (ddd, *J* = 8.2, 6.7, 1.2 Hz, 1H), 7.23 (dt, *J* = 7.5, 1.4 Hz, 2H), 7.13 (d, *J* = 7.1 Hz, 1H), 6.92 (td, *J* = 7.6, 1.4 Hz, 1H), 6.79 (td, *J* = 7.6, 1.6 Hz, 1H), 6.75 (dd, *J* = 7.9, 1.6 Hz, 1H), 4.04 (s, 3H), 3.42 (s, 3H), 2.73 (s, 3H).

^{13}C NMR (126 MHz, $CDCl_3$) δ 155.45, 151.43, 139.36, 134.41, 133.45, 132.68, 132.60, 132.59, 132.35, 129.99, 129.18, 128.74, 127.67, 127.65, 127.37, 127.05, 126.46, 126.25, 125.91, 125.62, 125.47, 124.46, 123.97, 123.36, 123.26, 121.82, 62.47, 62.00, 19.75.

MS (APCI) Calculated for $C_{29}H_{24}BrO_2S$ $[M+H]^+$: 515.1; Found: 514.6 m/z

HPLC trace: Chiralpak IA (hexanes/2-propanol = 95/5, 0.7 mL/min, t_{ent1} = 5.8 min, t_{ent2} = 7.3 min)

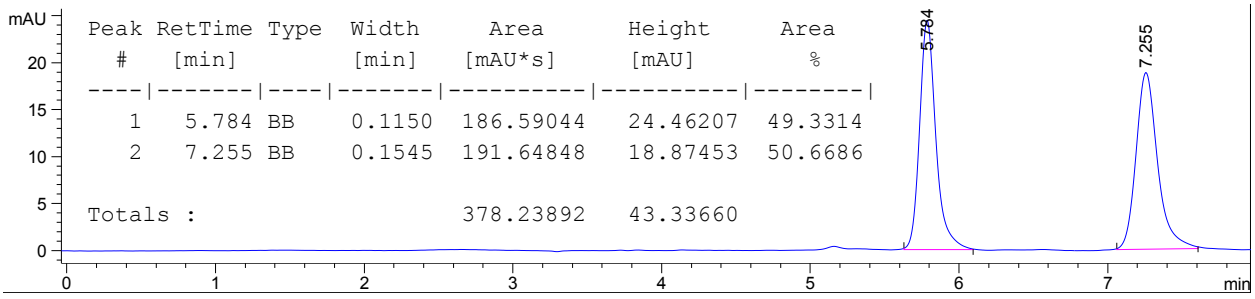

Figure 4.4.210. Racemic HPLC trace of 4.2z

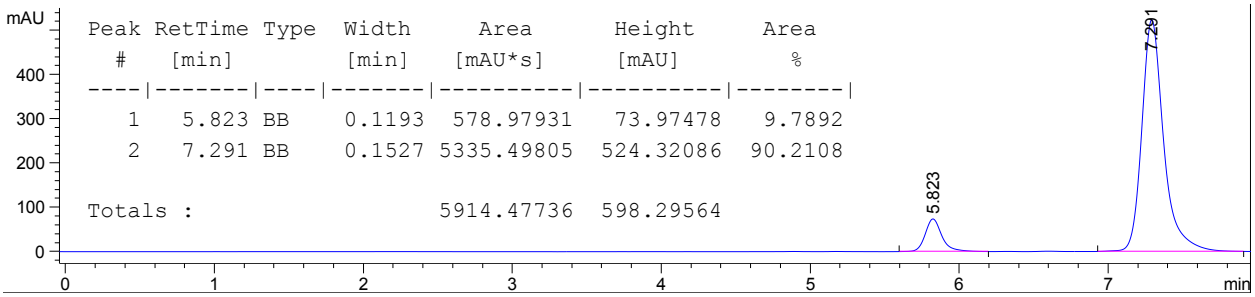

Figure 4.4.211. Asymmetric HPLC trace of 4.2z

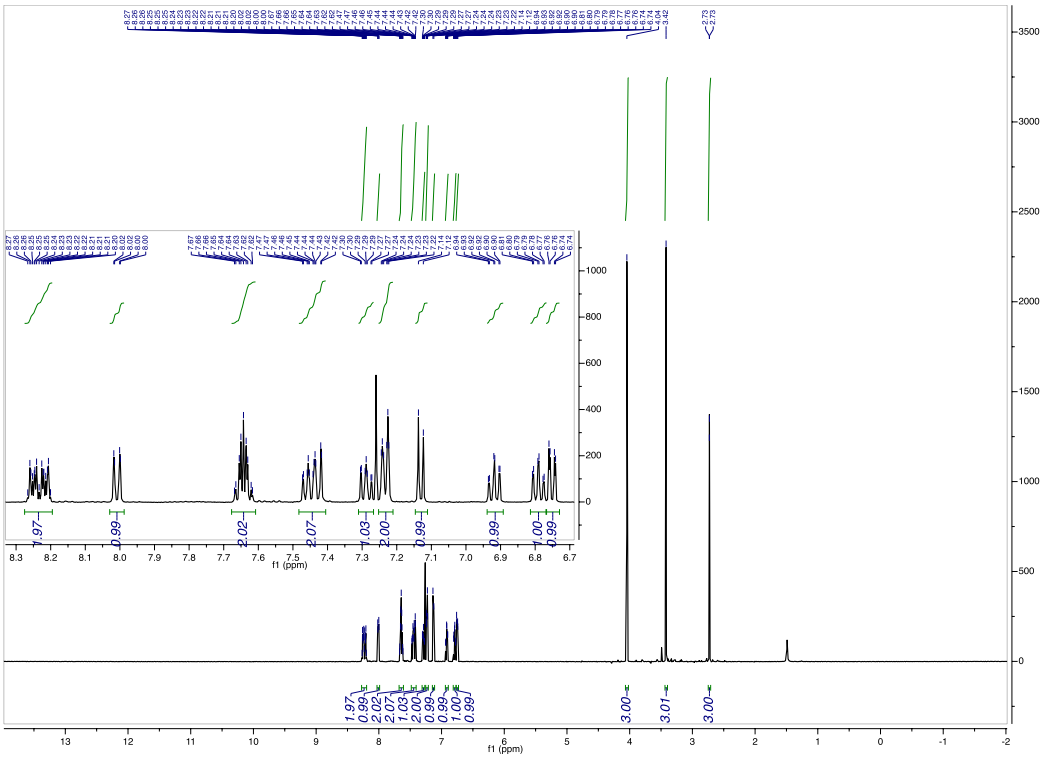

Figure 4.4.212. ^{1}H of 4.2z

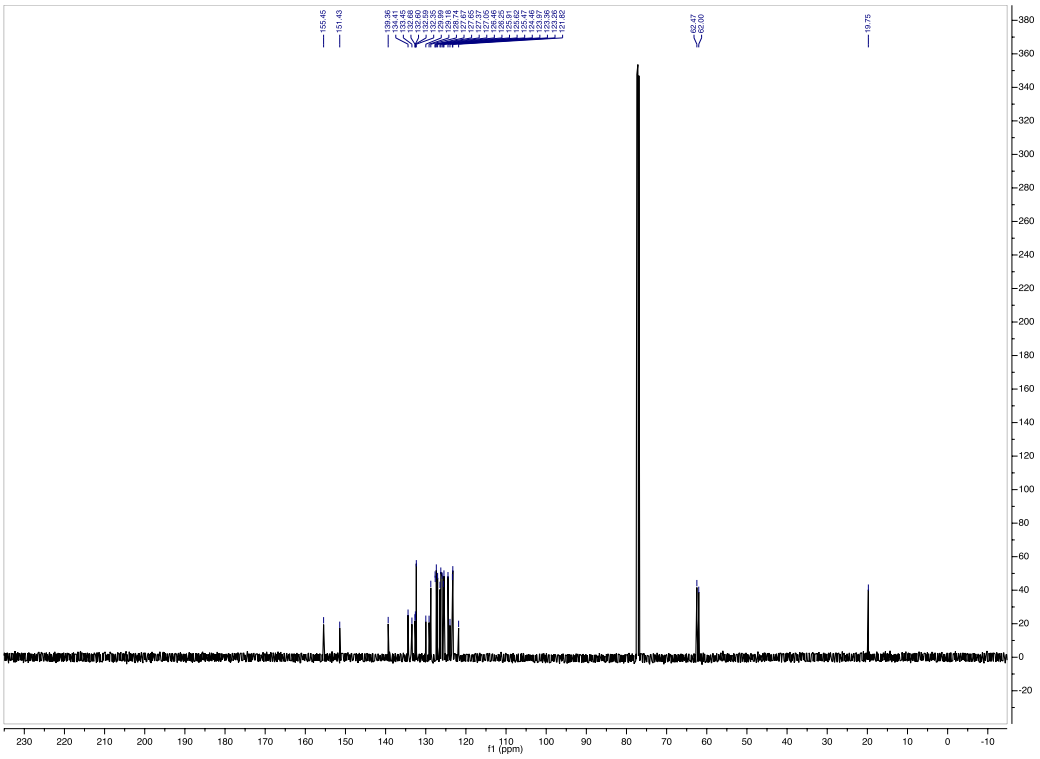

Figure 4.4.213. ^{13}C of 4.2z

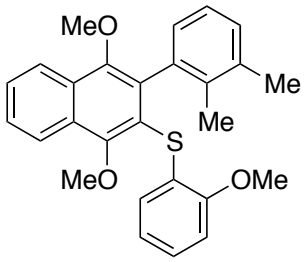

Figure 4.4.214. Product 4.2aa

(3-(2,3-dimethylphenyl)-1,4-dimethoxynaphthalen-2-yl)(2-methoxyphenyl)sulfane (**4.2aa**):

88% yield, purified by FCC, hexanes/DCM = 98/2. 97:7 e.r.

^{1}H NMR (500 MHz, $CDCl_3$) δ 8.23 – 8.14 (m, 2H), 7.62 – 7.56 (m, 2H), 7.09 – 7.05 (m, 1H), 7.03 – 6.95 (m, 2H), 6.89 (dd, *J* = 7.6, 1.4 Hz, 1H), 6.73 – 6.62 (m, 3H), 4.00 (s, 3H), 3.66 (s, 3H), 3.49 (s, 3H), 2.25 (s, 3H), 1.88 (s, 3H).

^{13}C NMR (126 MHz, $CDCl_3$) δ 156.52, 155.16, 150.21, 136.28, 136.24, 135.58, 135.33, 129.54, 129.15, 128.90, 128.77, 128.29, 127.16, 126.62, 126.46, 125.90, 124.49, 123.41, 123.19, 123.03, 120.93, 110.60, 62.22, 61.31, 55.83, 20.67, 17.01.

MS (APCI) Calculated for $C_{27}H_{27}O_3S$ $[M+H]^+$: 431.2; Found: 430.8 m/z

HPLC trace: Chiralpak IA (hexanes/2-propanol = 95/5, 1.0 mL/min, t_{ent1} = 5.9 min, t_{ent2} = 7.0 min)

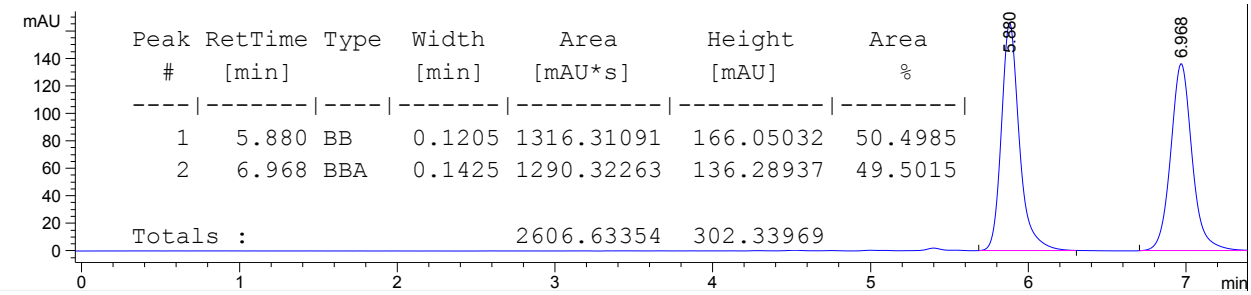

Figure 4.4.215. Racemic HPLC trace of 4.2aa

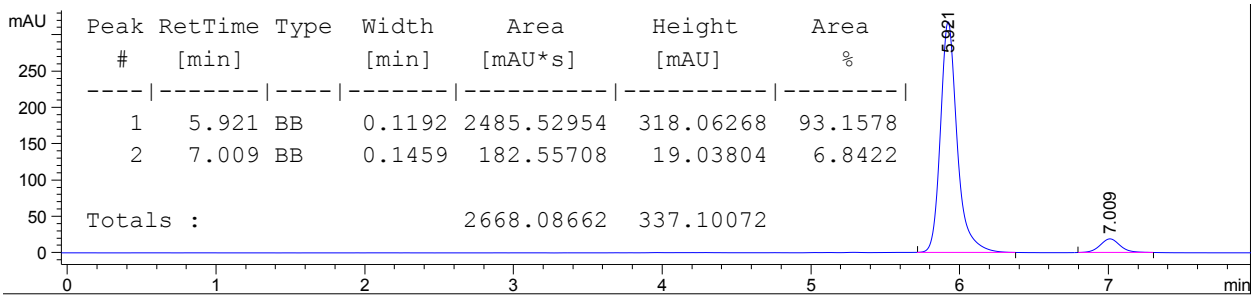

Figure 4.4.216. Asymmetric HPLC trace of 4.2aa

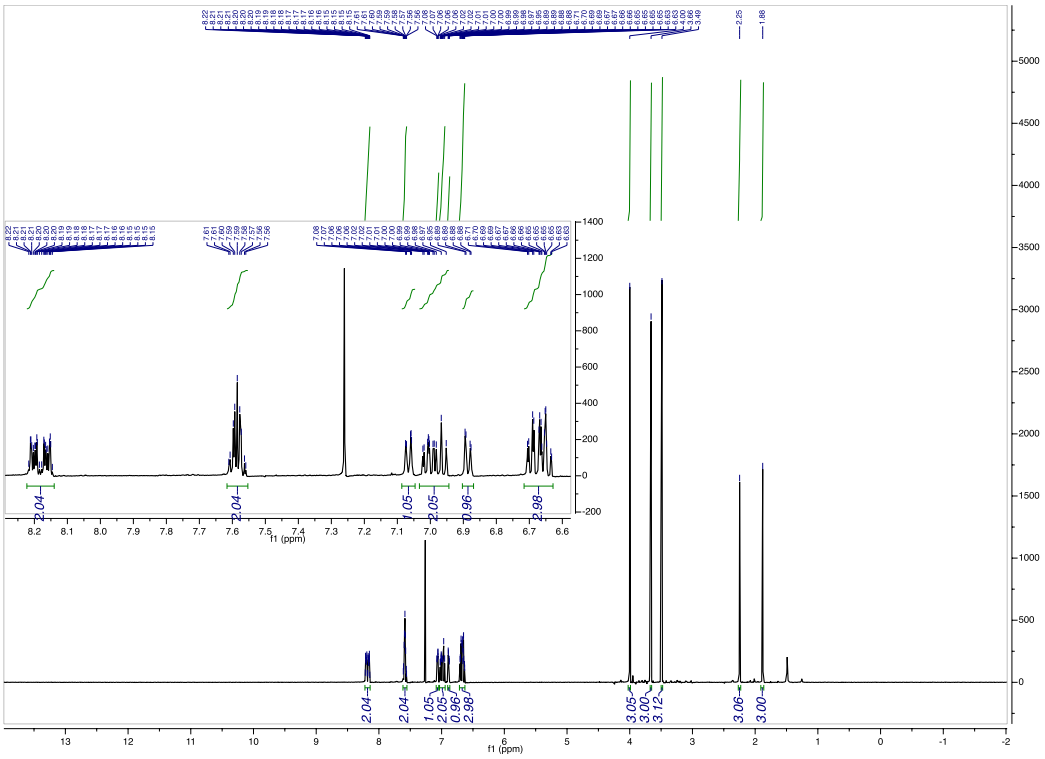

Figure 4.4.217. ^{1}H of 4.2aa

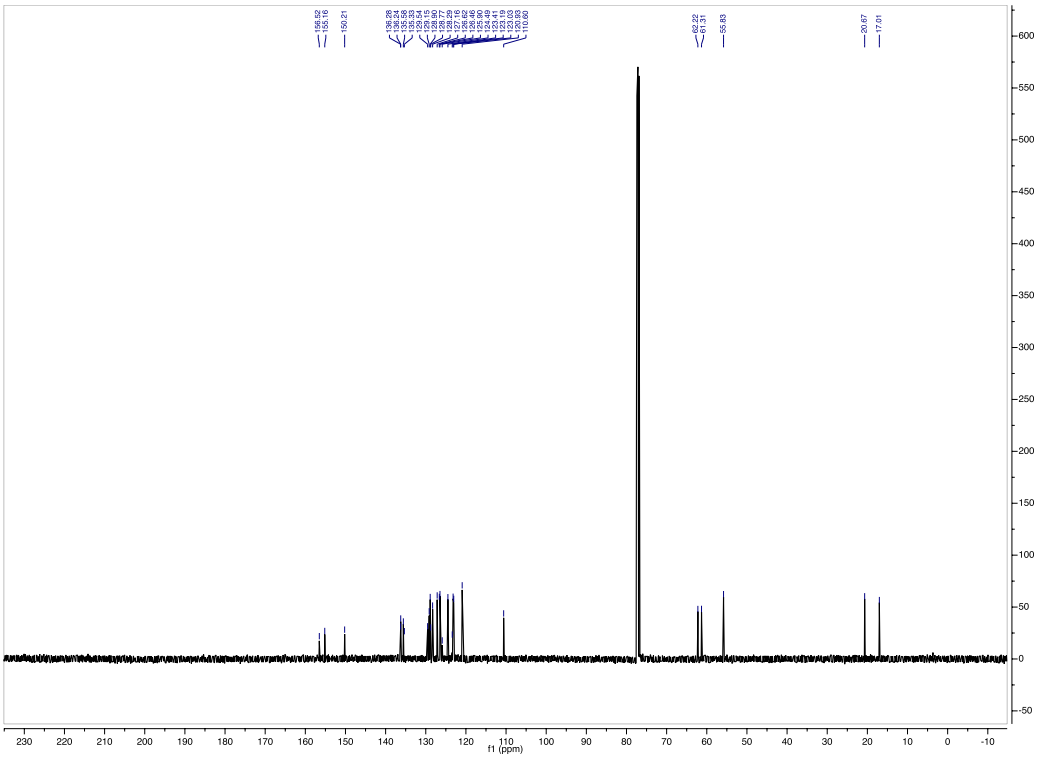

Figure 4.4.218. ^{13}C of 4.2aa

4.4.6 Barrier to Rotation Studies

Barrier to rotations were experimentally determined by first dissolving the enantiomerically enriched samples in toluene or diphenyl ether and placing them in a vial equipped with a stir bar open to air. The vials were then placed in an oil bath equilibrated to the specified temperature noted for each compound. At each time-point, an aliquot of the mixture was removed and quenched in an HPLC vial containing hexanes. The first time-point represents the first point at which an aliquot of the sample was removed once the stirring sample reached the same temperature as the oil bath. Each sample was then injected into the HPLC, and the observed enantiomeric excess (*ee*) was recorded. The time point and *ee* data were then plotted to determine an observed rate constant, k_{obs}, for the corresponding temperature. The barrier to rotation was then derived from the Gibbs Free Energy Equation:

$$\Delta G = -RT \ln \frac{hk_{rac}}{k_B T}$$

where:

R = gas constant

T = absolute temperature (K)

k_B = Boltzmann's constant

h = Planck's constant

$k_{rac} = 2 * k_{obs}$

Substrate Barriers:

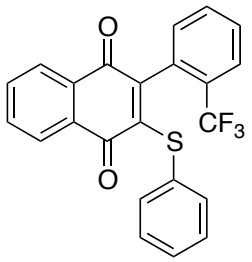

Figure 4.4.219. Structure of 4.3a

2-(phenylthio)-3-(2-(trifluoromethyl)phenyl)naphthalene-1,4-dione (**4.3a**):

Barrier to rotation (ΔG) = 25.6 kcal/mol

Enantioenriched material was stirred in toluene @ 50 ^{o}C and monitored by chiral HPLC

Experiment was run in triplicate.

Timepoint	Trial 1 (e.r.)	Trial 2 (e.r.)	Trial 3 (e.r.)
0 minutes	90.3:9.7	90.0:10.0	89.9:10.1
30 minutes	85.1:14.9	85.7:14.3	84.9:15.1
60 minutes	80.5:19.5	81.5:18.5	81.3:18.7
90 minutes	77.2:22.8	77.6:22.4	77.8:22.2
120 minutes	73.2:26.8	75.2:24.8	73.6:26.4

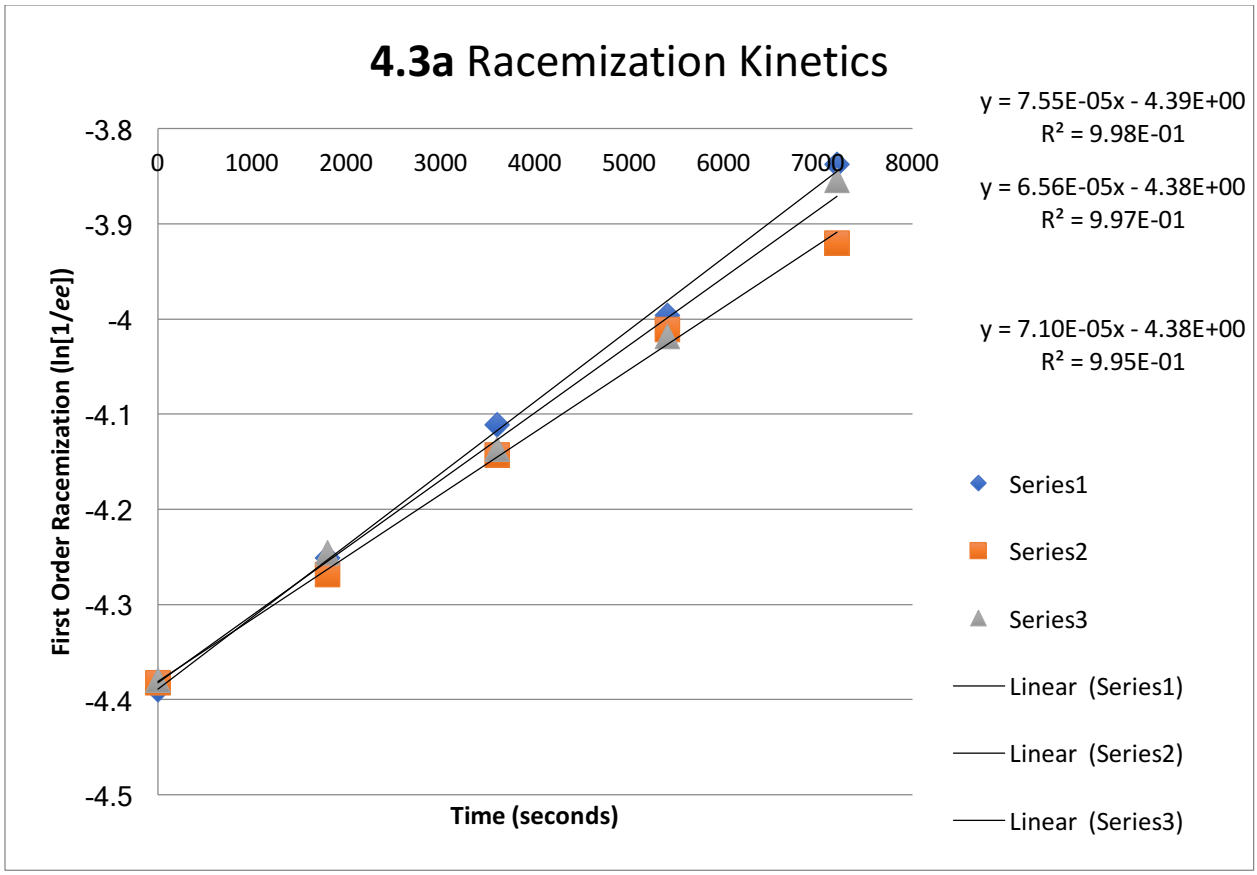

Figure 4.4.220. 4.3a Racemization Kinetics

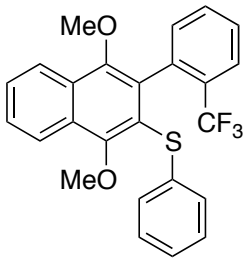

Figure 4.4.221. Structure of 4.2a

(1,4-dimethoxy-3-(2-(trifluoromethyl)phenyl)naphthalen-2-yl)(phenyl)sulfane (**4.2a**):

Barrier to rotation (ΔG) = 38.2 kcal/mol

Enantioenriched material was stirred in diphenyl ether @ 207 ^{o}C and monitored by chiral HPLC

Experiment was run in triplicate.

Timepoint	Trial 1 (e.r.)	Trial 2 (e.r.)	Trial 3 (e.r.)
0 minutes	91.2:8.8	92.1:7.9	91.6:8.4
30 minutes	85.4:14.6	88.0:12.0	87.0:13.0
60 minutes	78.7:21.3	83.1:16.9	82.8:17.2
90 minutes	73.9:26.1	79.1:20.9	79.0:21.0
120 minutes	69.2:30.8	74.5:25.5	74.7:25.3

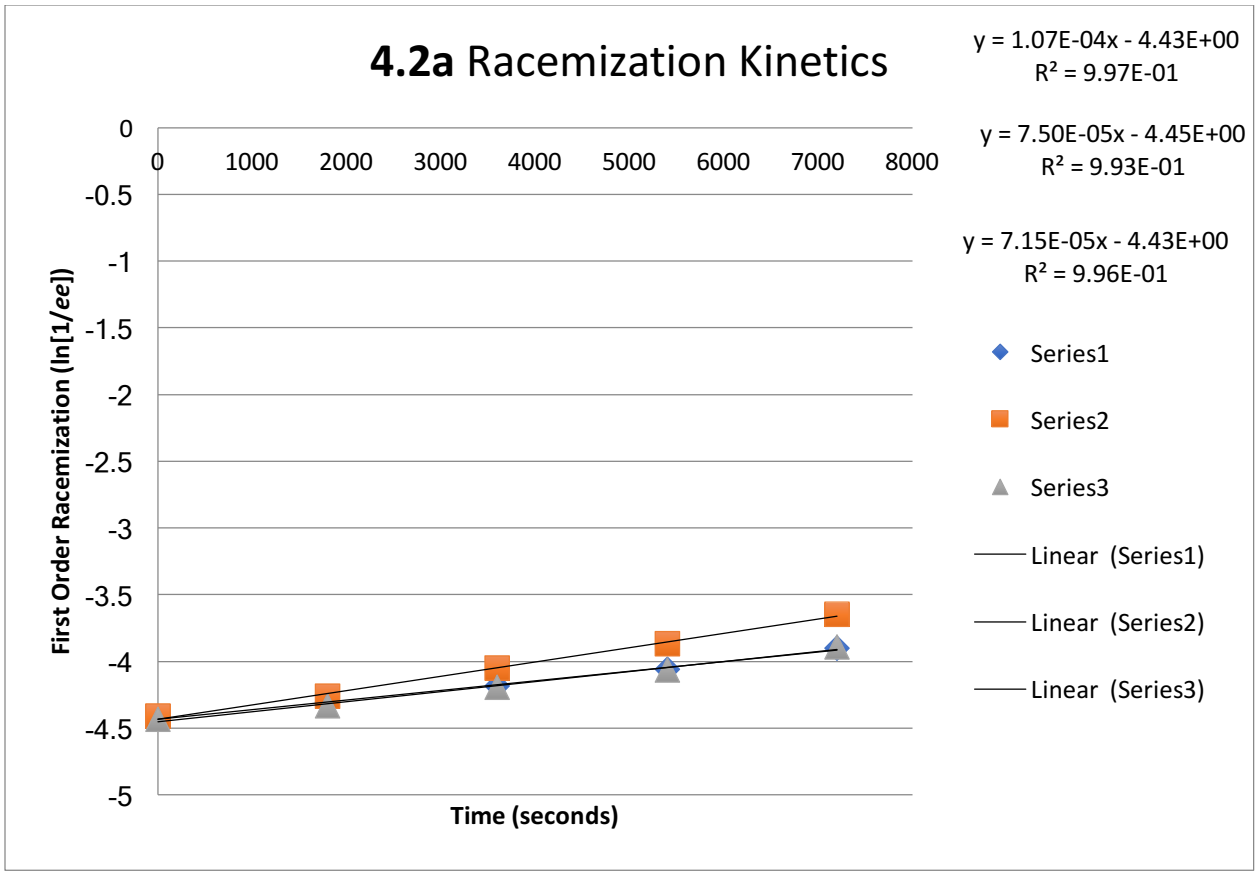

Figure 4.4.222. 4.2a Racemization Kinetics

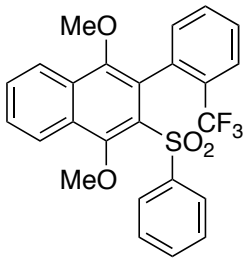

Figure 4.4.223. Structure of 4.6a

1,4-dimethoxy-2-(phenylsulfonyl)-3-(2-(trifluoromethyl)phenyl)naphthalene (**4.6a**):

Barrier to rotation (ΔG) = 37.2 kcal/mol

Enantioenriched material was stirred in diphenyl ether @ 206 ^{o}C and monitored by chiral HPLC

Experiment was run in triplicate.

Timepoint	Trial 1 (e.r.)	Trial 2 (e.r.)	Trial 3 (e.r.)
0 minutes	90.0:10.0	90.7:9.3	88.3:11.7
30 minutes	79.1:20.9	80.3:19.7	73.7:26.3
60 minutes	71.2:28.8	71.3:28.7	65.9:34.1
90 minutes	63.8:36.2	64.7:35.3	60.8:39.2
120 minutes	61.2:38.8	61.1:38.9	54.4:45.6

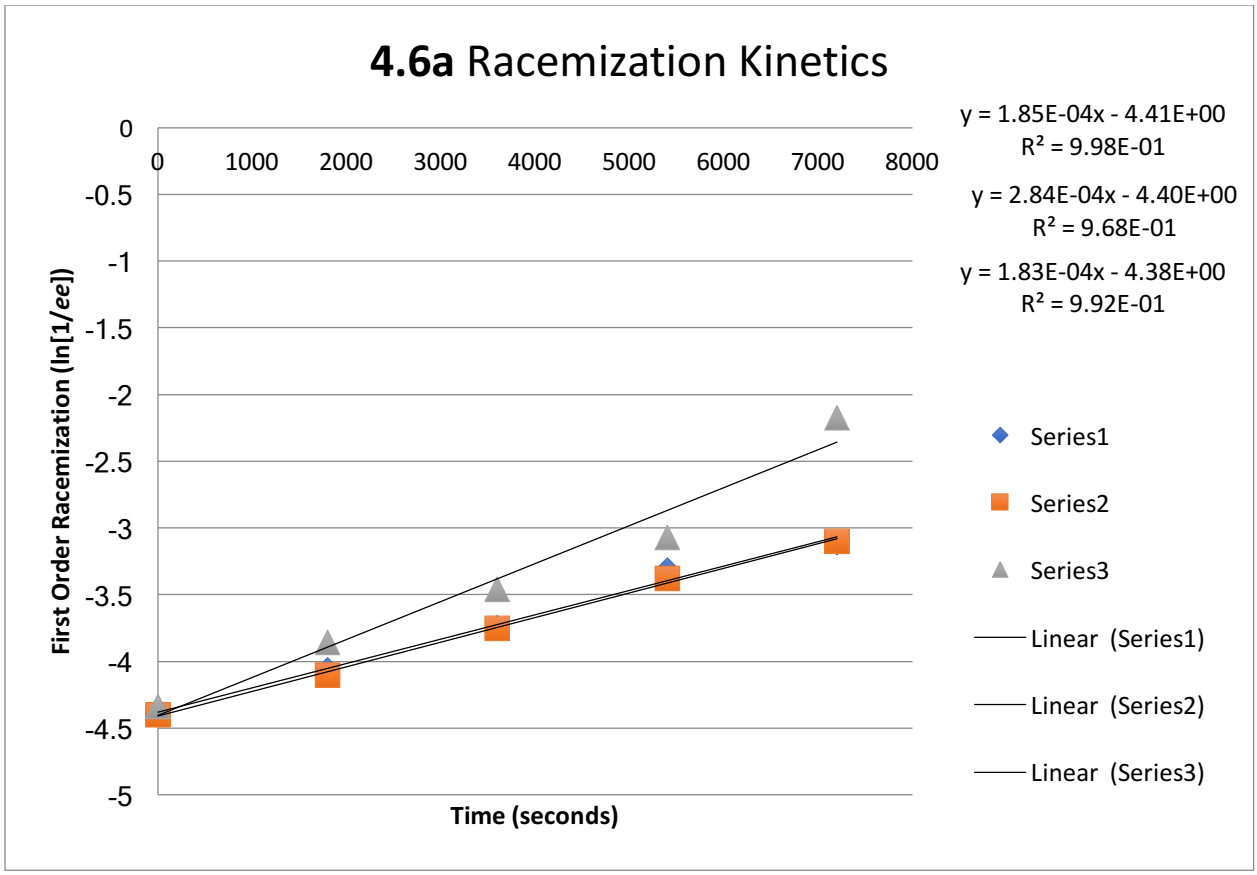

Figure 4.4.224. 4.6a Racemization Kinetics

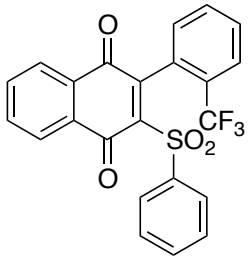

Figure 4.4.225. Structure of 4.4a

2-(phenylsulfonyl)-3-(2-(trifluoromethyl)phenyl)naphthalene-1,4-dione (**4.4a**):

Barrier to rotation (ΔG) = 26.0 kcal/mol

Enantioenriched material was stirred in toluene @ 50 ^{o}C and monitored by chiral HPLC

Experiment was run in triplicate.

Timepoint	Trial 1 (e.r.)	Trial 2 (e.r.)	Trial 3 (e.r.)
0 minutes	92.9:7.1	92.5:7.5	92.7:7.3
30 minutes	89.6:10.4	89.5:10.9	90.6:9.4
60 minutes	86.2:13.8	87.0:13.0	87.2:12.8
90 minutes	85.9:14.1	85.2:14.8	85.5:14.5
120 minutes	83.6:16.4	82.8:17.2	84.0:16.0

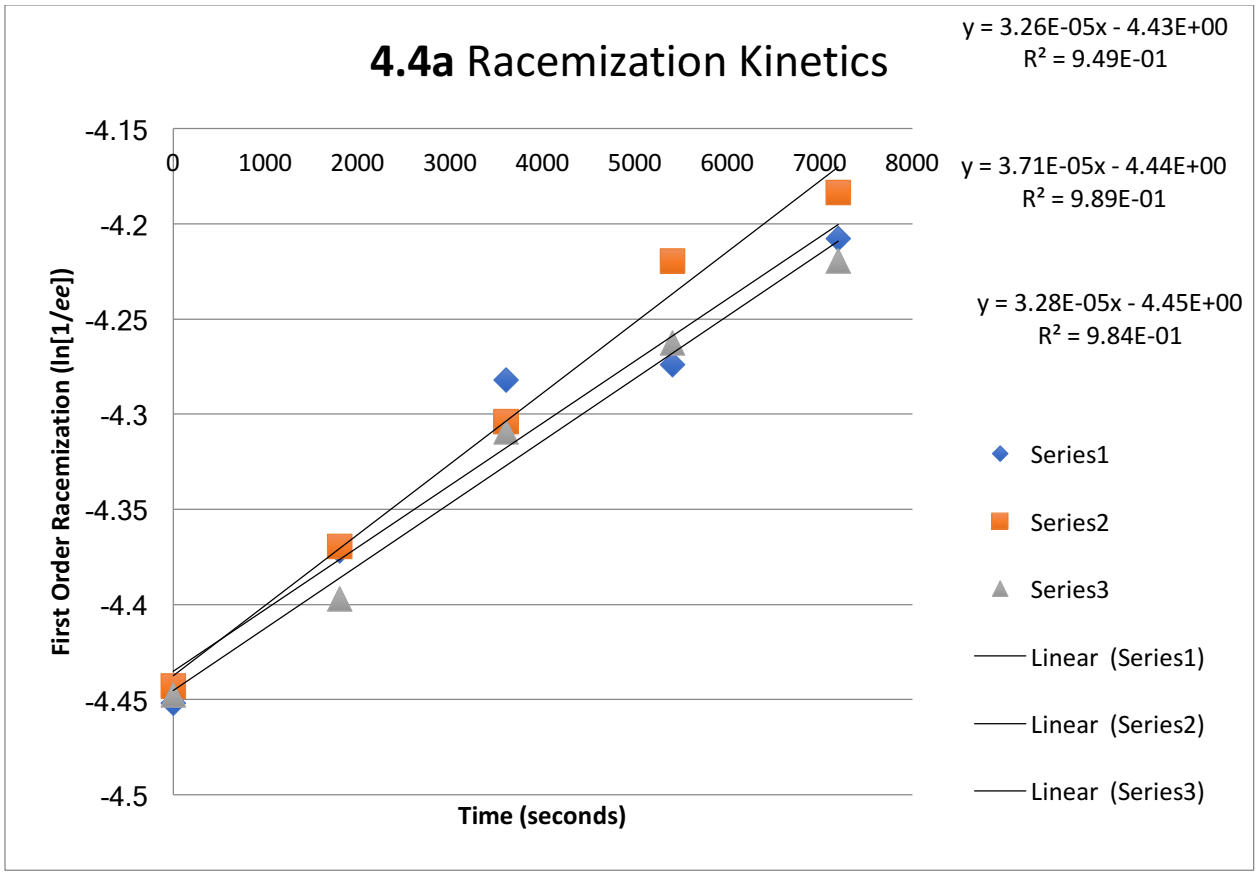

Figure 4.4.226. 4.4a Racemization Kinetics

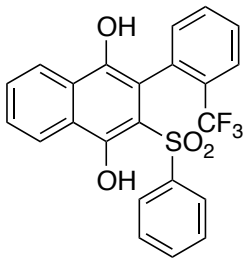

Figure 4.4.227. Structure of 4.5a

2-(phenylsulfonyl)-3-(2-(trifluoromethyl)phenyl)naphthalene-1,4-diol (**4.5a**):

Barrier to rotation (ΔG) = 36.2 kcal/mol

Enantioenriched material was stirred in diphenyl ether @ 169 ^{o}C and monitored by chiral HPLC

Experiment was run in triplicate.

Timepoint	Trial 1 (e.r.)	Trial 2 (e.r.)	Trial 3 (e.r.)
0 minutes	99.5:0.5	98.7:2.3	98.9:1.1
30 minutes	98.3:1.7	97.2:2.8	97.0:3.0
60 minutes	96.9:3.1	94.7:5.3	94.5:5.5
90 minutes	95.3:4.7	93.0:7.0	92.3:7.7
120 minutes	92.7:7.3	89.8:10.2	89.4:10.6

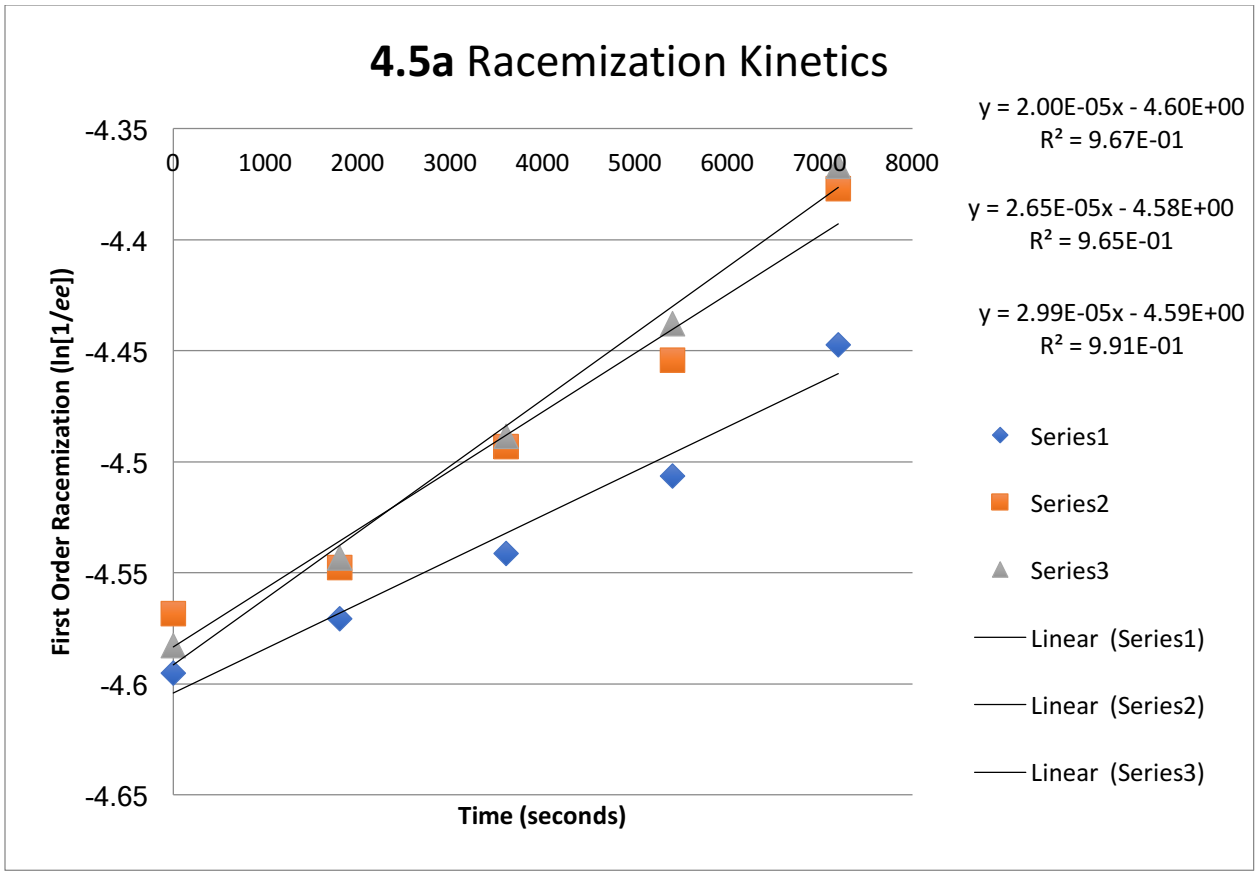

Figure 4.4.228. 4.5a Racemization Kinetics

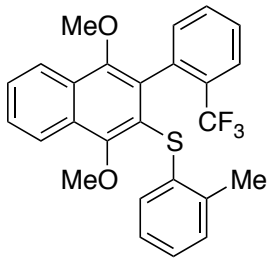

Figure 4.4.229. Structure of 4.2b

(1,4-dimethoxy-3-(2-(trifluoromethyl)phenyl)naphthalen-2-yl)(*o*-tolyl)sulfane (**4.2b**):

Barrier to rotation (ΔG) = 38.4 kcal/mol

Enantioenriched material was stirred in diphenyl ether @ 207 ^{o}C and monitored by chiral HPLC

Experiment was run in triplicate.

Timepoint	Trial 1 (e.r.)	Trial 2 (e.r.)	Trial 3 (e.r.)
0 minutes	88.6:11.4	95.9:4.1	92.0:8.0
60 minutes	80.9:19.1	84.9:15.1	81.8:18.2
120 minutes	72.7:27.3	76.5:23.5	74.0:26.0
180 minutes	68.4:31.6	69.5:30.5	66.0:34.0
240 minutes	66.3:33.7	65.7:34.3	63.8:36.2

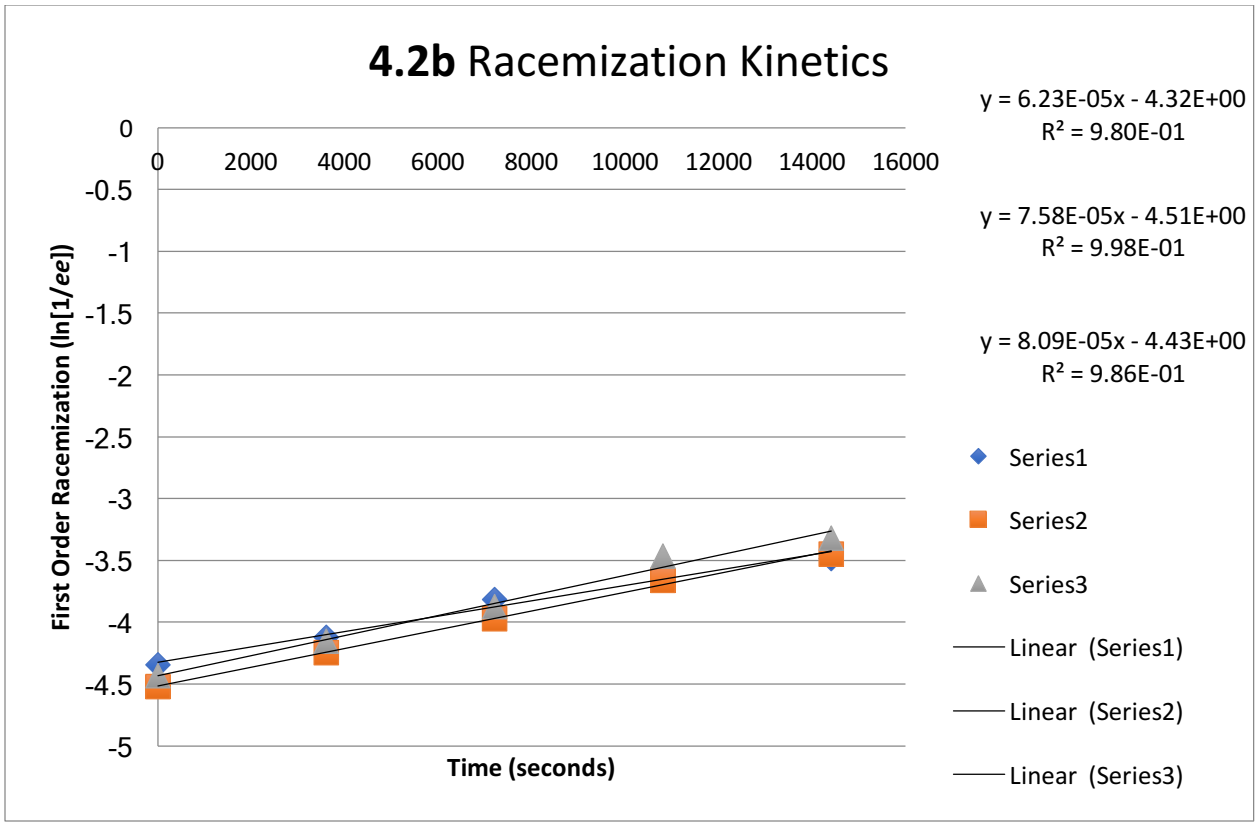

Figure 4.4.230. 4.2b Racemization Kinetics

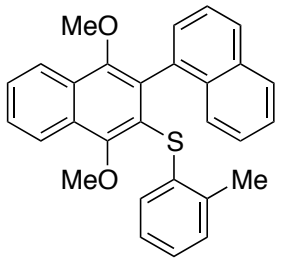

Figure 4.4.231. Structure of 4.2t

(1',4'-dimethoxy-[1,2'-binaphthalen]-3'-yl)(*o*-tolyl)sulfane (**4.2t**):

Barrier to rotation (ΔG) = 34.1 kcal/mol

Enantioenriched material was stirred in diphenyl ether @ 168 ^{o}C and monitored by chiral HPLC

Experiment was run in triplicate.

Timepoint	Trial 1 (e.r.)	Trial 2 (e.r.)	Trial 3 (e.r.)
0 minutes	86.8:13.2	86.5:13.6	86.7:13.7
20 minutes	80.0:20.0	76.3:23.7	78.8:21.2
40 minutes	72.9:27.1	68.5:31.5	75.4:24.6
60 minutes	70.2:29.8	62.9:37.1	61.5:38.5
80 minutes	62.6:37.4	60.3:39.7	62.2:37.8

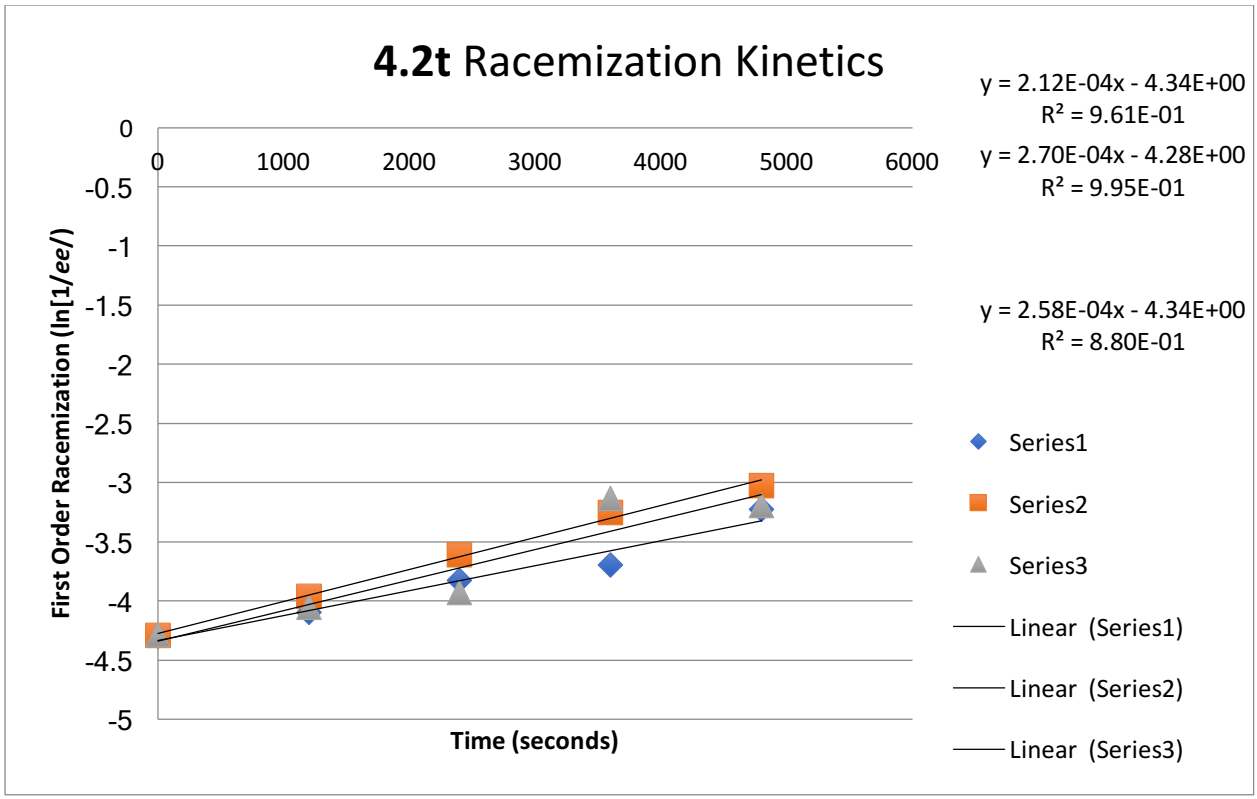

Figure 4.4.232. 4.2t Racemization Kinetics

Quinone Scaffold Redox Characterization:

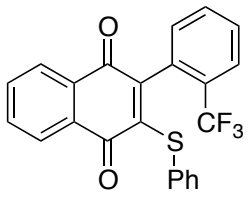

Figure 4.4.233. Product 4.3a

2-(phenylthio)-3-(2-(trifluoromethyl)phenyl)naphthalene-1,4-dione (**4.3a**): **4.2a** (30mg, 0.1mmol, 1.0 equiv) is added to a 20mL scintillation vial equipped with a stir bar, followed by the addition of 1mL of MeCN. A solution of CAN (137mg, 0.25mmol, 2.5 equiv) in deionized water (1mL) was then added to the stirring solution of **4.2a**. A quick color change of the acetonitrile solution occurred from clear → black → orange. After reaction completion by TLC (less than 1 hour), the mixture was diluted with EtOAc, washed with water, washed with brine, dried over sodium sulfate, and concentrated on the rotovap. The crude oil was filtered thru a silica plug with hexanes/EtOAc (90/10) to afford 37mg of **4.3a** as an orange amorphous solid containing minor impurities. This material was moved on without further purification.

^{1}H NMR (400 MHz, $CDCl_3$) δ 8.13 - 8.11 (m, 1H), 8.06 – 8.04 (m, 1H), 7.78 – 7.71 (m, 3H), 7.58 (t, *J* = 7.16 Hz, 1H), 7.52 (t, *J* = 7.72 Hz, 1H), 7.30 – 7.27 (m, 2H), 7.24 – 7.18 (m, 4H)

^{13}C NMR (126 MHz, $CDCl_3$) δ 181.57, 180.55, 148.12, 146.89, 134.13, 133.81, 132.70, 132.66, 132.18, 131.91 (q, *J* = 2.1 Hz), 131.85, 131.73, 130.39, 129.08, 129.05, 128.44 (q, *J* = 31 Hz), 127.91, 127.16, 126.94, 126.63 (q, *J* = 4.7 Hz), 123.90 (q, *J* = 274 Hz).

^{19}F NMR (470 MHz, $CDCl_3$) δ -58.61.

MS (APCI) Calculated for $C_{23}H_{14}F_3O_2S$ $[M+H]^+$: 411.1; Found: 411.4 m/z

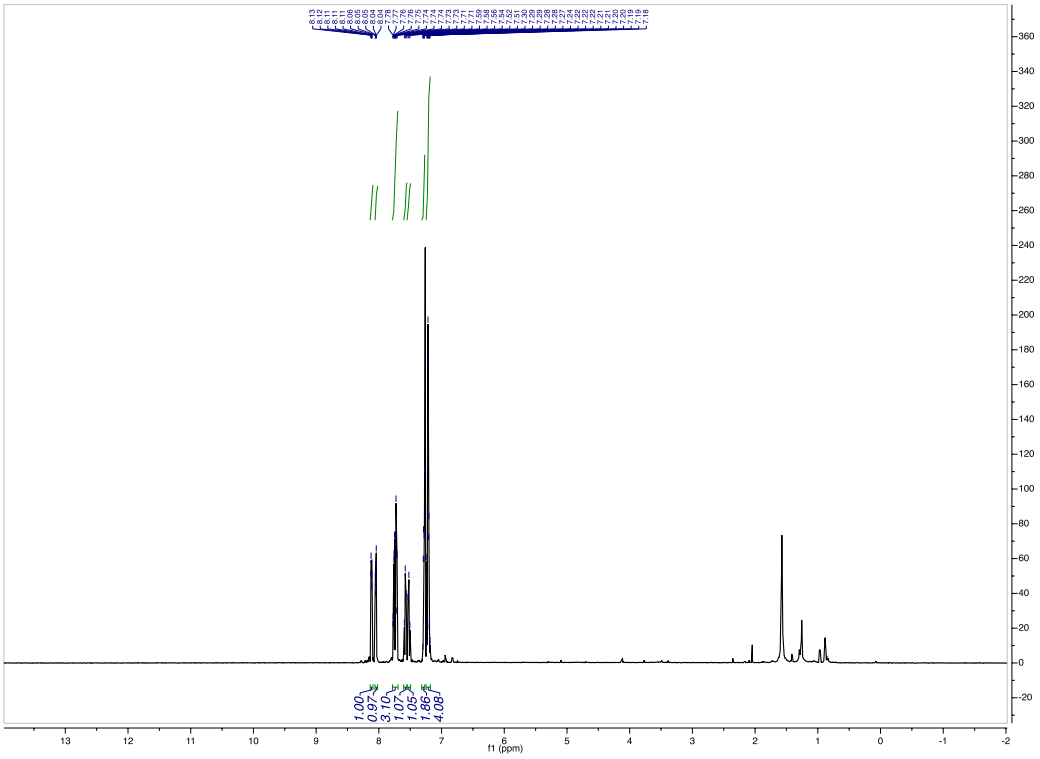

Figure 4.4.234. ^{1}H of 4.3a

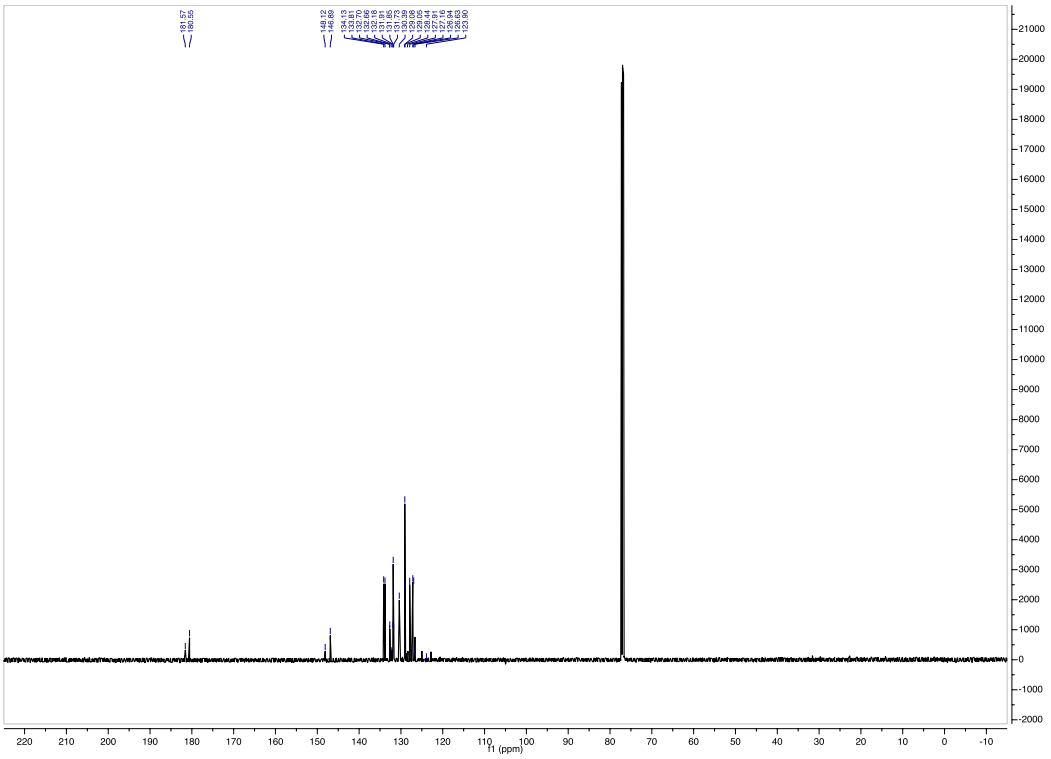

Figure 4.4.235. ^{13}C of 4.3a

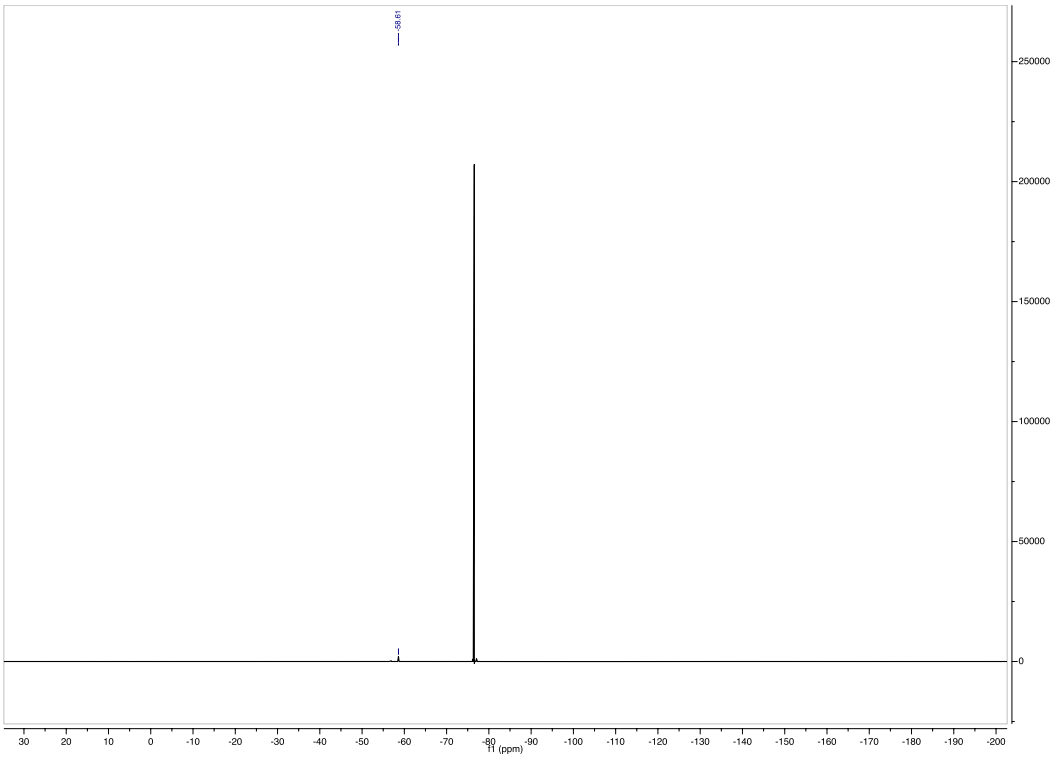

Figure 4.4.236. ^{19}F of 4.3a

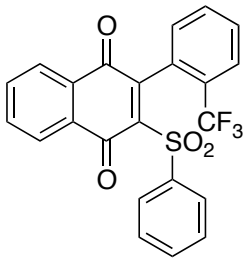

Figure 4.4.237. Product 4.4a

2-(phenylsulfonyl)-3-(2-(trifluoromethyl)phenyl)naphthalene-1,4-dione (**4.4a**): **4.3a** (400mg, 0.97mmol, 1.0 equiv) was dissolved in 5mL DCM in a 20 mL scintillation vial equipped with a stir bar. The vial was placed in a water/ice bath, and let stir for 30 minutes followed by the addition of mCPBA (600mg, 2.4mmol, 2.5 equiv, ~30% water content). The solution was let stir at 0^0 C for 12 hours. The reaction was not complete by TLC, however in an effort to retain enantioenrichment in the product, the reaction was stopped early. The reaction mixture was extracted with DCM (20mL, 2x), and the combined organic layer were washed with 4M $NaOH_{(aq)}$, washed with brine, dried over sodium sulfate, and concentrated on rotovap @ r.t.. The resulting crude oil was purified by FCC eluting with hexanes/EtOAc (95/5 → 90/10 → 85/15) to obtained 170mg (40% yield) **4.4a** as a yellow oil.

^{1}H NMR (500 MHz, $CDCl_3$) δ 8.12 – 8.01 (m, 4H), 7.84 (dd, *J* = 7.8, 1.4 Hz, 1H), 7.82 – 7.75 (m, 2H), 7.73 – 7.60 (m, 3H), 7.58 – 7.51 (m, 2H), 7.35 (dd, *J* = 7.6, 1.3 Hz, 1H).

^{13}C NMR (126 MHz, $CDCl_3$) δ 183.21, 179.79, 149.83, 143.31, 140.65, 135.16, 134.86, 134.21, 131.54, 131.31, 131.25, 129.68, 129.66 (q, *J* = 2.3 Hz), 129.42, 129.27, 128.98, 128.04 (q, *J* = 31 Hz), 127.30, 127.17, 126.70 (q, *J* = 4.3 Hz), 124.22 (q, *J* = 274 Hz).

^{19}F NMR (470 MHz, $CDCl_3$) δ -57.37.

MS (APCI) Calculated for $C_{23}H_{14}F_3O_4S$ $[M+H]^+$: 443.1; Found: 443.0 m/z

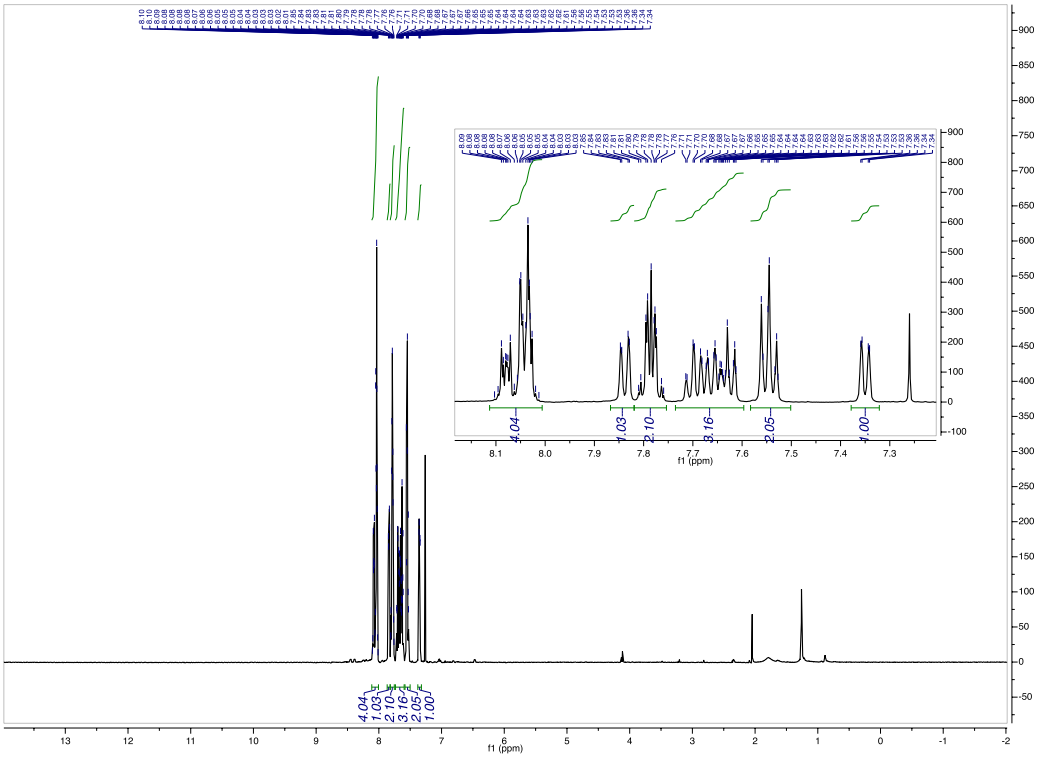

Figure 4.4.238. ^{1}H of 4.4a

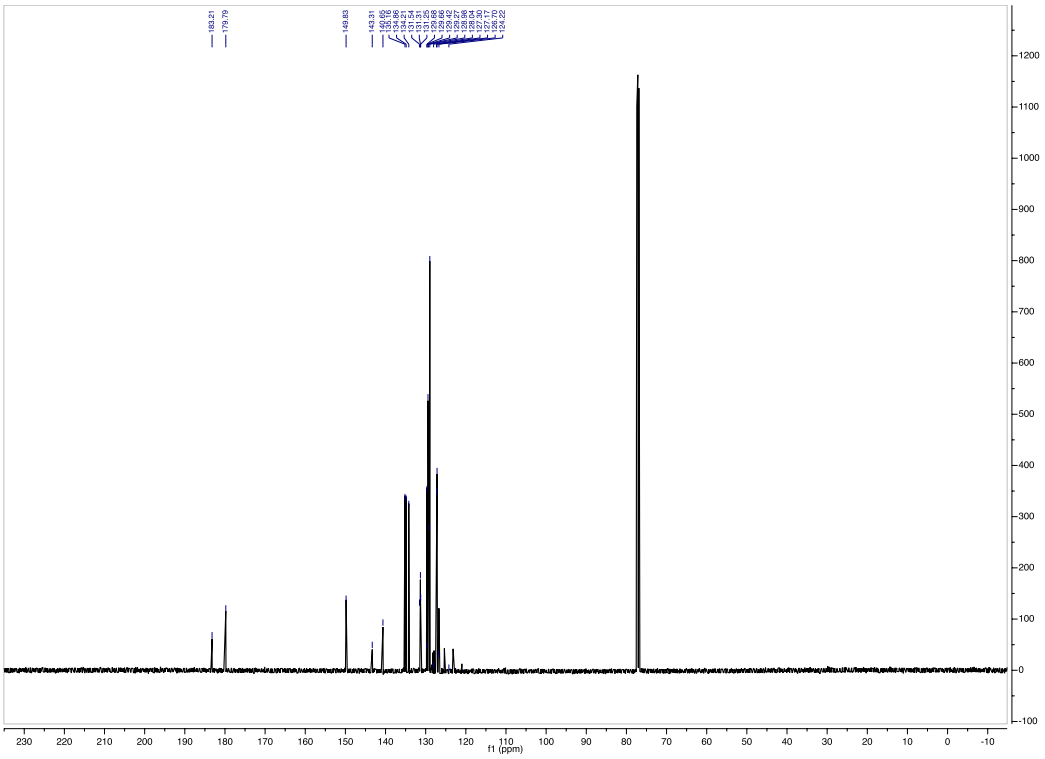

Figure 4.4.239. ^{13}C of 4.4a

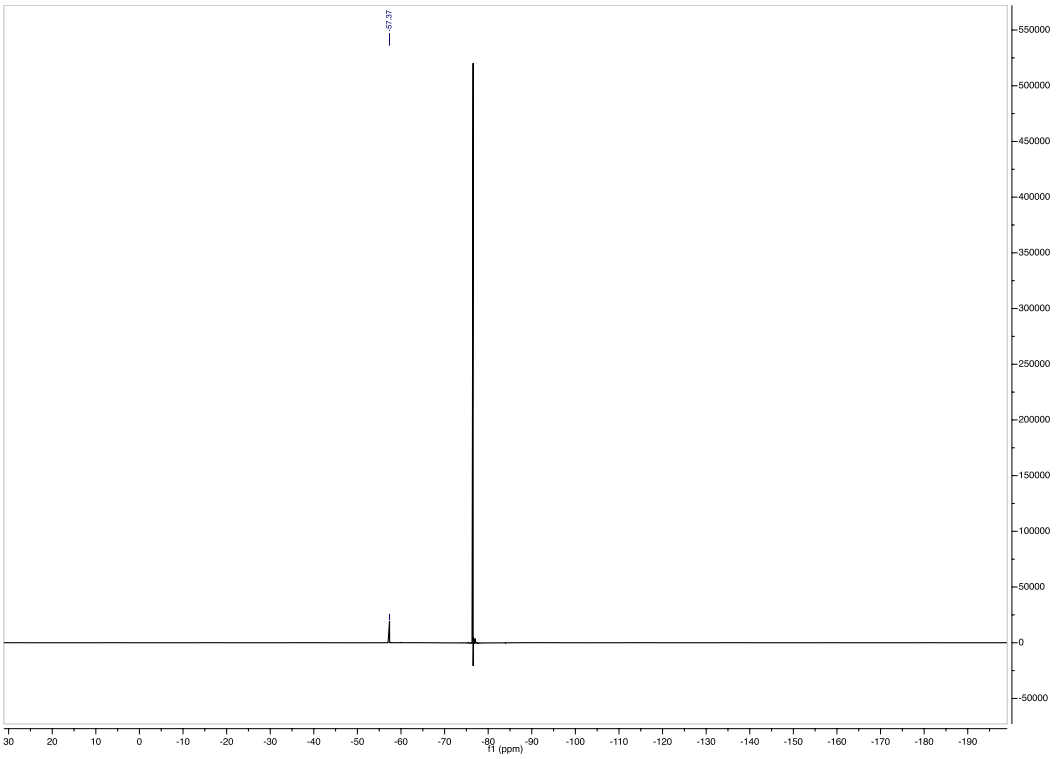

Figure 4.4.240. ^{19}F of 4.4a

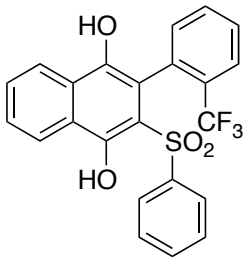

Figure 4.4.241. Product 4.5a

2-(phenylsulfonyl)-3-(2-(trifluoromethyl)phenyl)naphthalene-1,4-diol (**4.5a**): **4.4a** (150mg, 0.34mmol, 1.0 equiv) was dissolved in THF (2mL) in a 20 mL scintillation vial, followed by the addition a solution of $Na_2S_2O_4$ (472mg, 2.7mmol, 8.0 equiv) in DI water (2mL) with rigorous stirring at r.t.. The mixture was let stir for 1 hour at r.t., then it was extracted with EtOAc. The organic layer was washed with brine, dried over sodium sulfate, and concentrated on the rotovap. The resulting crude oil was recrystallized from EtOAc/hexanes to afford (30mg, 20% yield) **4.5a** as transparent crystals. The obtained crystals were >95% pure, and were used for barrier to rotation studies without further purification.

^{1}H NMR (500 MHz, $CDCl_3$) δ 11.11 (s, 1H), 8.55 – 8.53 (m, 1H), 8.19 – 8.17 (m, 1H), 7.75 – 7.67 (m, 3H), 7.60 (t, *J* = 7.7 Hz, 1H), 7.55 – 7.51 (m, 1H), 7.46 (t, *J* = 7.5 Hz, 1H), 7.40 – 7.33 (m, 4H), 6.86 (d, *J* = 7.7 Hz, 1H), 4.41 (bs, 1H).

^{13}C NMR (126 MHz, $CDCl_3$) δ 151.13, 142.19, 134.23, 133.66, 132.13 (q, *J* = 30 Hz), 131.73, 130.17, 130.02 (q, *J* = 1.9 Hz), 129.78, 128.93, 128.01, 127.69, 127.34 (q, *J* = 4.9 Hz), 127.06, 126.29, 124.48, 123.42 (q, *J* = 274 Hz), 122.60, 113.54, 113.17.

^{19}F NMR (470 MHz, $CDCl_3$) δ -59.14.

MS (APCI) Calculated for $C_{23}H_{16}F_3O_4S$ $[M+H]^+$: 445.1; Found: 445.0 m/z

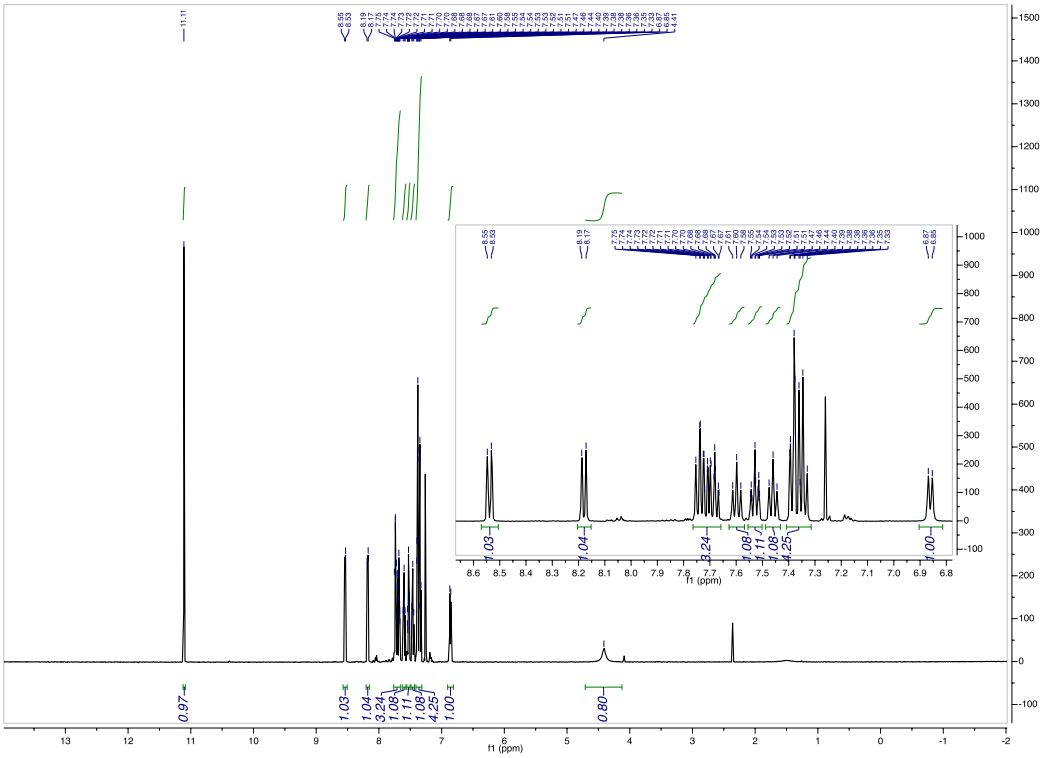

Figure 4.4.242. ^{1}H of 4.5a

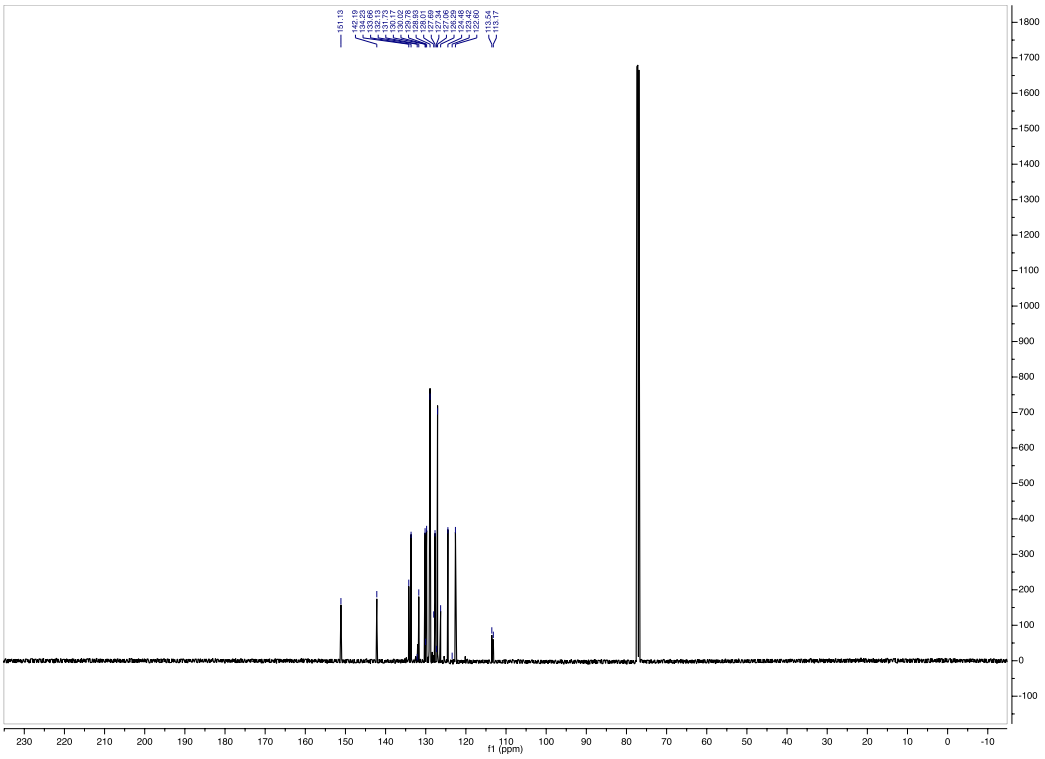

Figure 4.4.243. ^{13}C of 4.5a

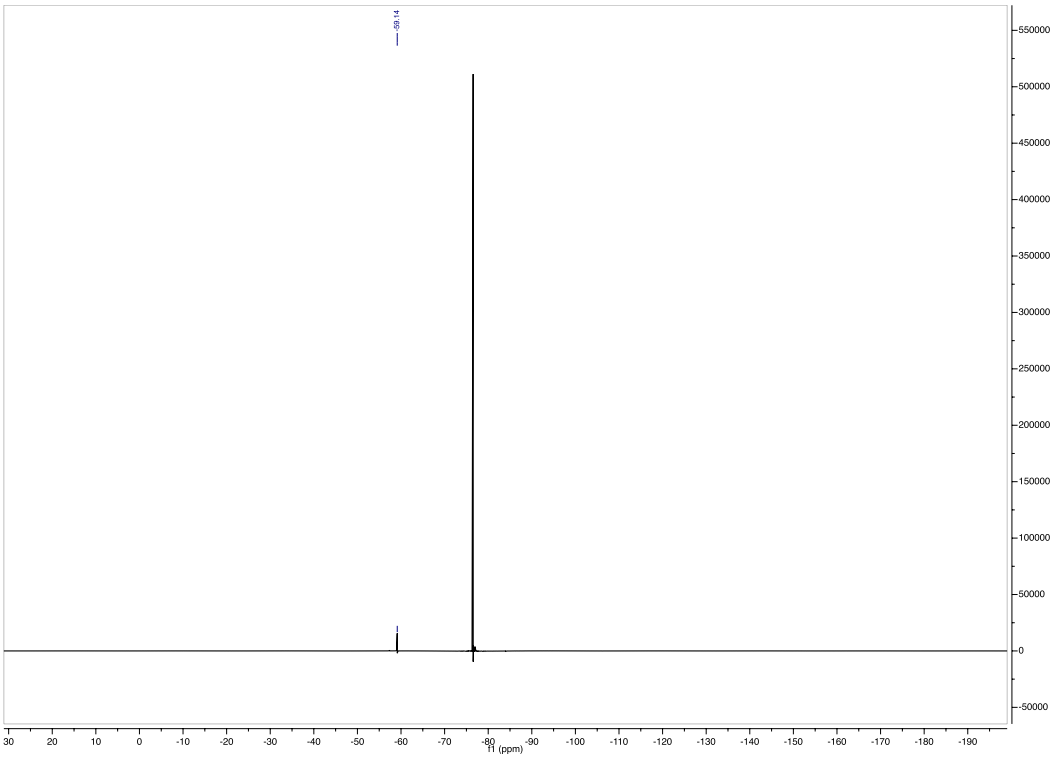

Figure 4.4.244. ^{19}F of 4.5a

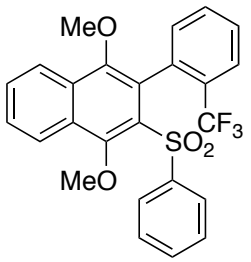

Figure 4.4.245. Product 4.6a

1,4-dimethoxy-2-(phenylsulfonyl)-3-(2-(trifluoromethyl)phenyl)naphthalene (**4.6a**): **4.2a** (50mg, 0.11mmol, 1.0 equiv) was dissolved in 5mL DCM in a 20mL scintillation vial equipped with a stir bar. mCPBA (70mg, 0.28mmol, 2.5 equiv, ~30 water content) was added to the stirring solution at r.t., and the reaction was let stir at r.t. for 24 hours. The reaction was then diluted with DCM, washed with 4M $NaOH_{(aq)}$, washed with brine, dried over sodium sulfate, and concentrated on rotovap. The resulting crude oil was purified by FCC, eluting with hexanes/EtOAc (94/6 → 90/10 → 85/15) to obtain 47mg (91% yield) **4.6a** as a white amorphous solid.

^{1}H NMR (500 MHz, $CDCl_3$) δ 8.15 – 8.11 (m, 1H), 8.10 – 8.07 (m, 1H), 7.90 – 7.86 (m, 2H), 7.85 – 7.82 (m, 1H), 7.70 – 7.55 (m, 4H), 7.54 – 7.50 (m, 1H), 7.47 – 7.42 (m, 3H), 4.12 (s, 3H), 3.57 (s, 3H).

^{13}C NMR (126 MHz, $CDCl_3$) δ 153.65, 150.73, 143.99, 134.14 (q, J = 2.2 Hz), 132.78, 131.59, 131.31, 130.65, 130.33, 129.53 (q, J = 30 Hz), 129.51, 128.83, 128.47, 127.98, 127.63, 127.42, 126.46 (q, J = 4.7 Hz), 124.53 (q, J = 274 Hz), 124.19, 123.61, 64.56, 61.99.

^{19}F NMR (470 MHz, $CDCl_3$) δ -57.67.

MS (APCI) Calculated for $C_{25}H_{20}F_3O_4S$ $[M+H]^+$: 473.1; Found: 473.0 m/z

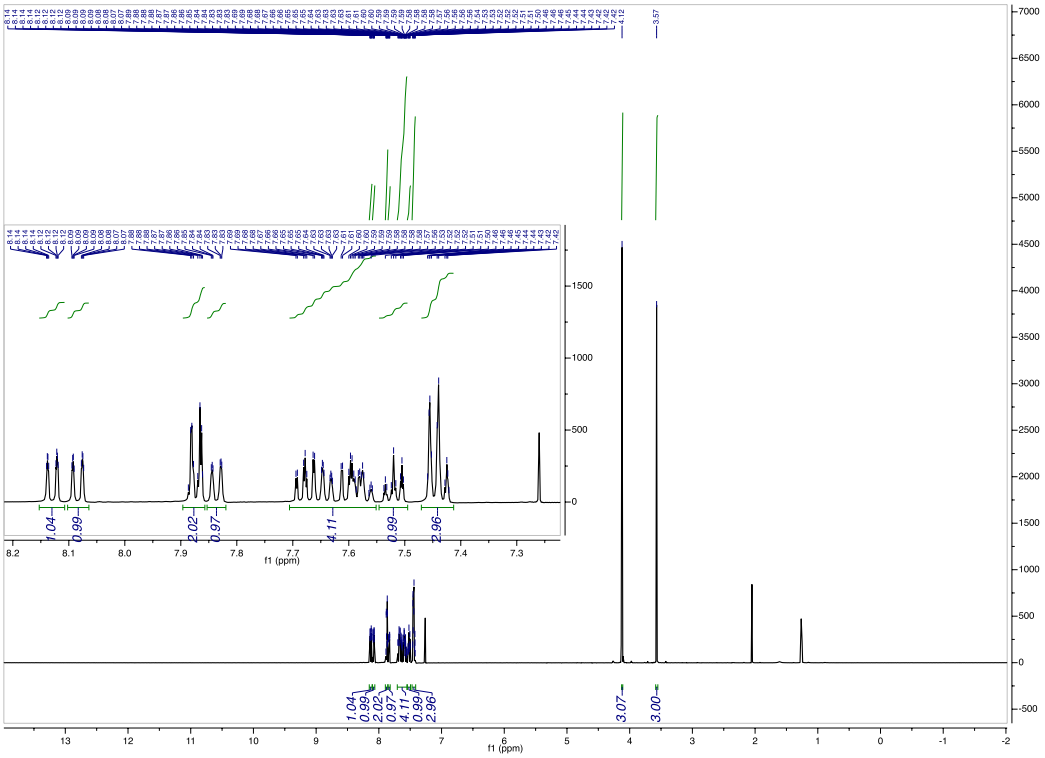

Figure 4.4.246. ^{1}H of 4.6a

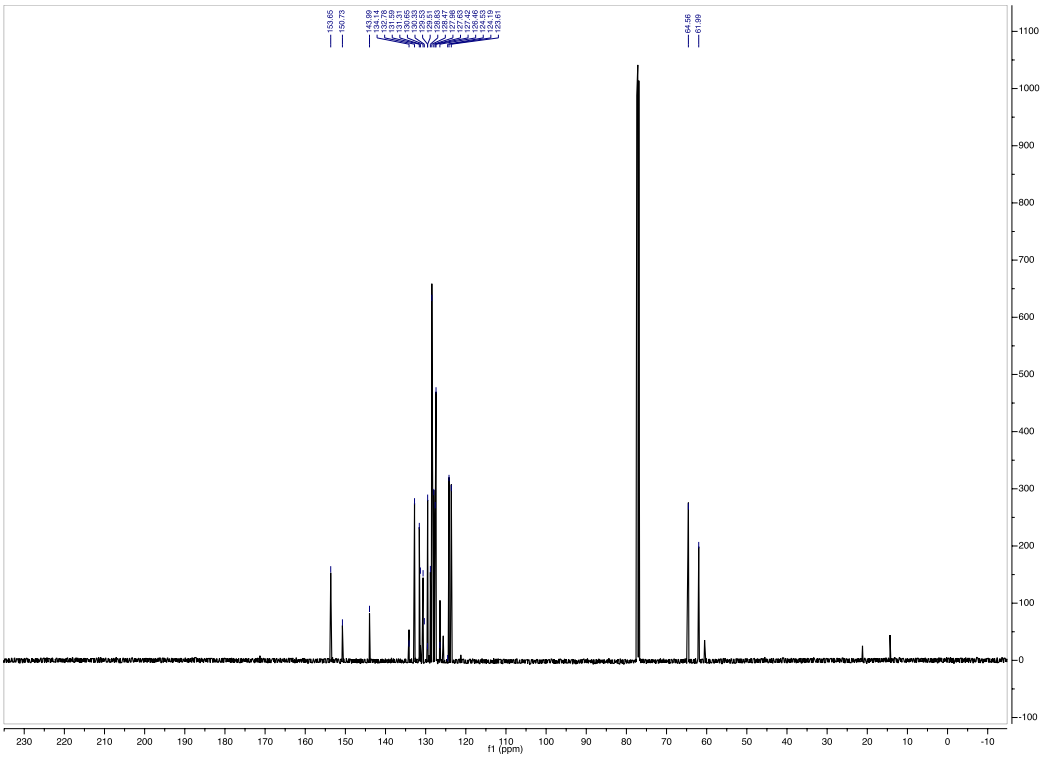

Figure 4.4.247. ^{13}C of 4.6a

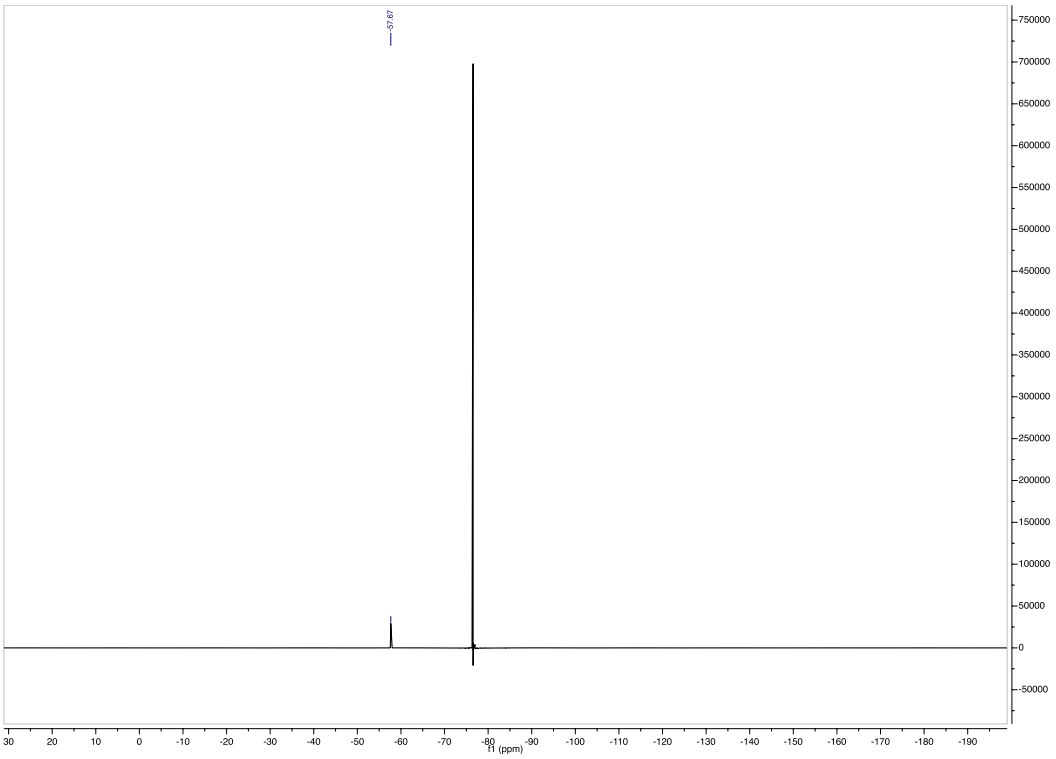

Figure 4.4.248. ^{19}F of 4.6a

4.4.7 "Net S_NAr" Reaction Sequences

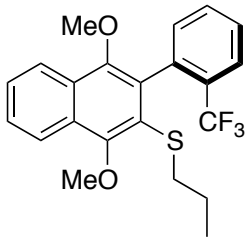

Figure 4.4.249. Product 4.2h

(1,4-dimethoxy-3-(2-(trifluoromethyl)phenyl)naphthalen-2-yl)(propyl)sulfane (**4.2h**): Similar to the procedure for the synthesis of **4.6a**, sulfane **4.2b** (1.09g, 2.41mmol, 96:4 e.r.) was oxidized using *m*-CPBA (603mg, 6.03mmol) in 45 mL DCM, to afford 1,4-dimethoxy-2-(*o*-tolylsulfonyl)-3-(2-(trifluoromethyl)phenyl)naphthalene in quantitative yield. The resulting 1,4-dimethoxy-2-(*o*-tolylsulfonyl)-3-(2-(trifluoromethyl)phenyl)naphthalene (1.17g, 2.41mmol, 95:5 e.r.) was dissolved in 12mL of MeCN in a 50mL round bottom flask equipped with a stir bar and cooled to 0 ^oC with stirring. A solution of CAN (3.30g, 6.03mmol) in 12mL of DI water was slowly added over 2 minutes. The reaction mixture was allowed to warm to r.t. and let stir until no more remaining starting material was detectable by TLC (4 hours on this scale). The resultant orange/yellow mixture was then diluted with 100mL of EtOAc and washed with water, brine, then dried over Na_2SO_4. The organic layer was then rotovapped in a 25 ^oC water bath until near dryness. The crude material was then dissolved in 10 mL of DCM and ran thru a short silica plug and rotovapped to dryness in a 25 ^oC water bath to give crude **4.4b**, which was used without further purification.

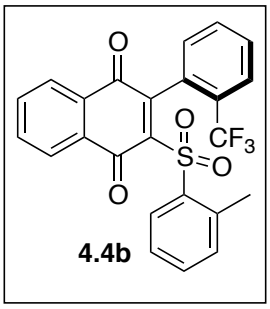

Figure 4.4.250. Intermediate 4.4b

Once **4.4b** is in hand, it should be moved on to the following reaction quickly as to avoid significant racemization

The crude **4.4b** was dissolved in 25mL of THF in a 250mL round bottom flask equipped with a stir bar, and the solution was brought to 0 ^{o}C with stirring. 1-propanethiol (450μL, 2.0 equiv) was added to the stirring solution, followed by the addition of DBU (330μL, 1.0 equiv). The reaction quickly turned dark, and after 10 minutes, the starting material was no longer present by TLC. TBAB (120mg, 15mol%) was then added to the solution, followed by the addition of a solution of sodium dithionite (4.2g, 10 equiv) in 24mL of DI water, keeping the reaction at 0 ^{o}C. Methanol (20mL), was added to the vigorously stirring reaction. Then reaction changed color from dark orange to clear in a short period of time, with vigorous stirring. A solution of potassium hydroxide (4.8g, 35 equiv) in 24mL DI water was then added at 0 ^{o}C (reaction darkened significantly), followed by the addition of dimethyl sulfate (8.3mL, 36 equiv). The reaction was let warm to room temperature with vigorous stirring. Over the course of the reaction, the mixture turned from a very dark orange mixture to a cloudy white/clear biphasic mixture. After 2 hours of stirring, the reaction was diluted with EtOAc and washed with water, brine, and dried over Na_2SO_4. The crude oil was purified by FCC (hexanes/EtOAc = 97:3 → 90:10) to afford 695mg (71% yield,

95:5 e.r.) of (1,4-dimethoxy-3-(2-(trifluoromethyl)phenyl)naphthalen-2-yl)(propyl)sulfane as a white solid.

^{1}H NMR (500 MHz, $CDCl_3$) δ 8.23 – 8.17 (m, 1H), 8.14 – 8.09 (m, 1H), 7.82 (d, *J* = 7.1 Hz, 1H), 7.66 – 7.53 (m, 4H), 7.33 (d, *J* = 7.6 Hz, 1H), 4.06 (s, 3H), 3.60 (s, 3H), 2.92 (ddd, *J* = 12.2, 7.9, 6.6 Hz, 1H), 2.69 (ddd, *J* = 12.2, 7.9, 6.9 Hz, 1H), 1.52 – 1.37 (m, 2H), 0.86 (t, *J* = 7.3 Hz, 3H).

^{13}C NMR (126 MHz, $CDCl_3$) δ 154.24, 149.66, 136.26 (q, *J* = 2.2 Hz), 132.87, 132.35, 130.98, 129.73 (q, *J* = 30 Hz), 129.30, 128.47, 127.92, 126.89, 126.81, 126.54 (q, *J* = 4.8 Hz), 125.18, 124.28 (q, *J* = 274 Hz), 123.03, 122.75, 61.72, 60.93, 37.25, 23.09, 13.51.

^{19}F NMR (470 MHz, $CDCl_3$) δ -58.21.

MS (APCI) Calculated for $C_{22}H_{22}F_3O_2S$ $[M+H]^+$: 407.1; Found: 407.2 m/z

HPLC trace: Chiralpak IA (hexanes/2-propanol = 90/10, 1.0 mL/min, t_{ent1} = 4.0 min, t_{ent2} = 5.0 min)

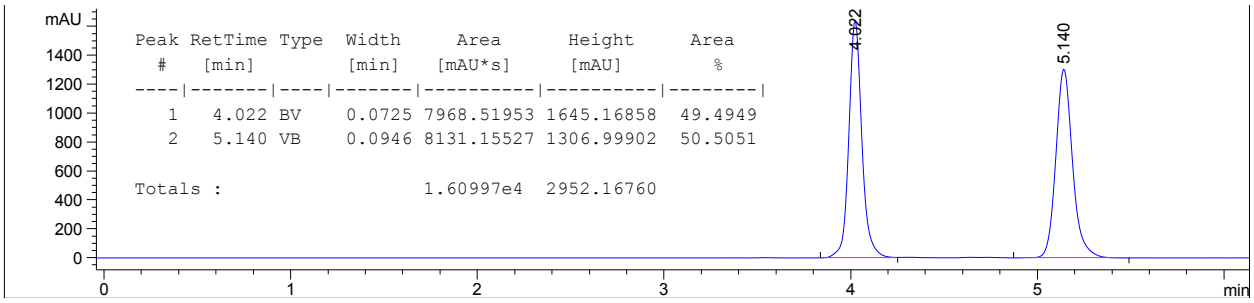

Figure 4.4.251. Racemic HPLC trace of 4.2h

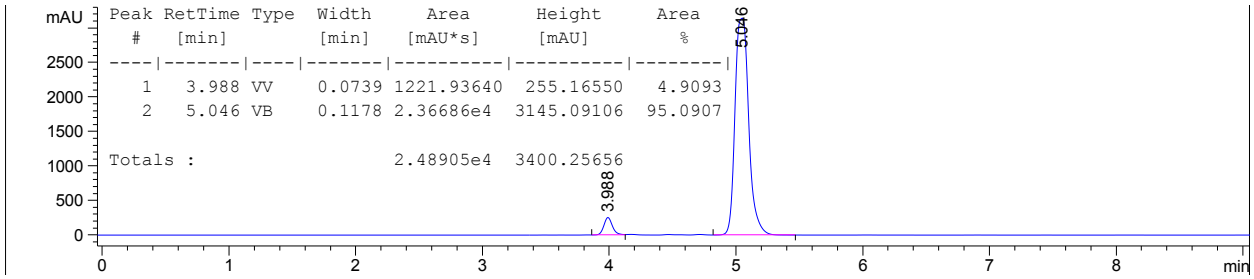

Figure 4.4.252. Asymmetric HPLC trace of 4.2h

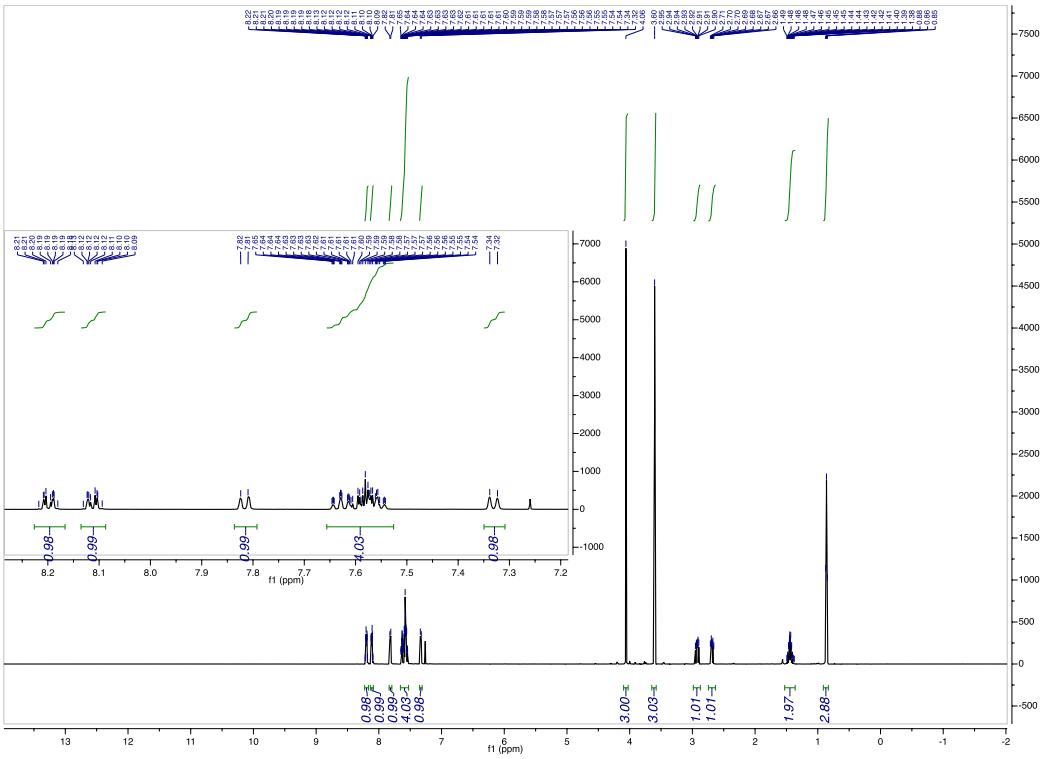

Figure 4.4.253. ^{1}H of 4.2h

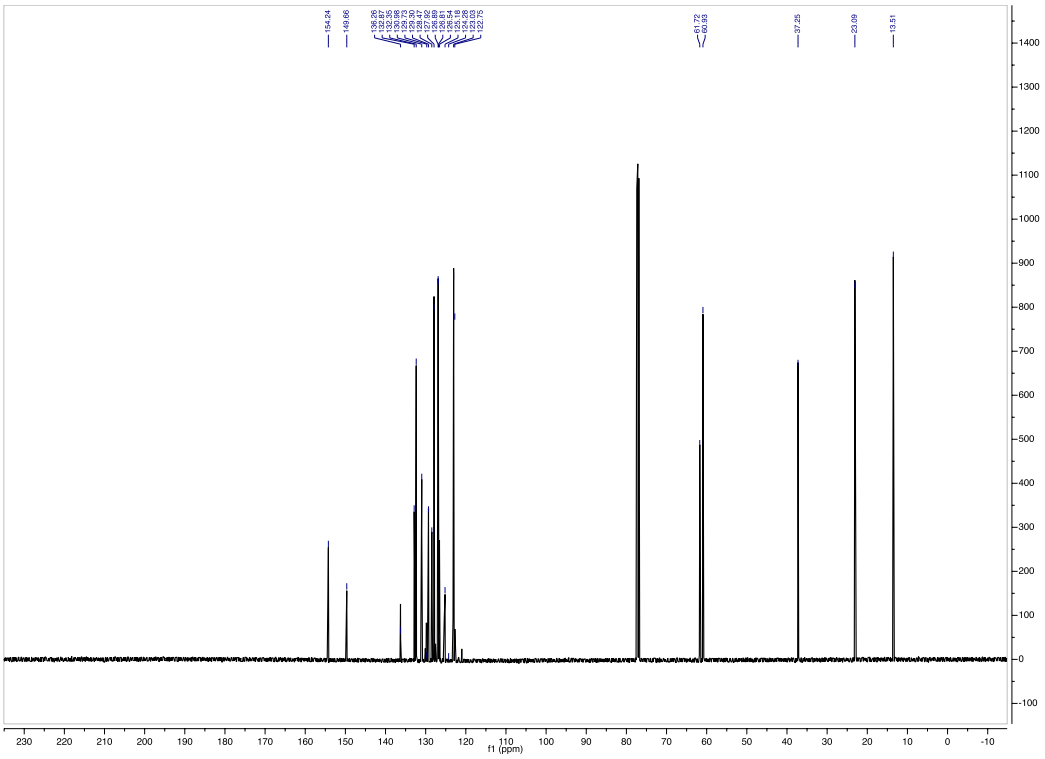

Figure 4.4.254. ^{13}C of 4.2h

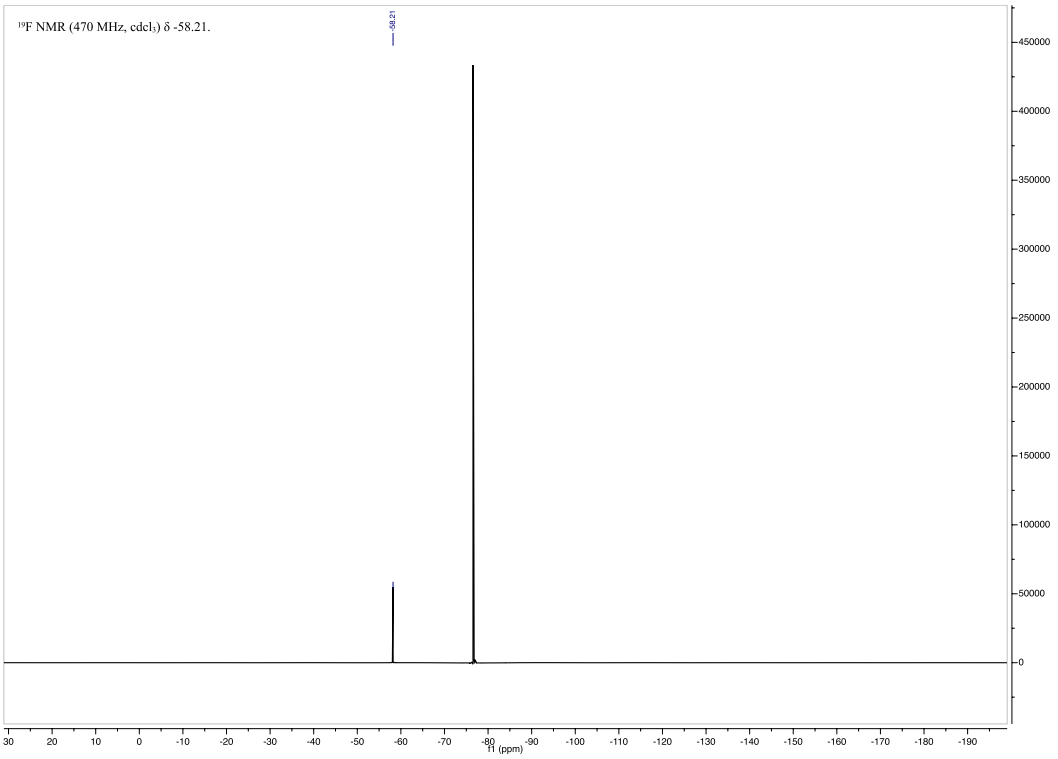

Figure 4.4.255. ^{19}F of 4.2h

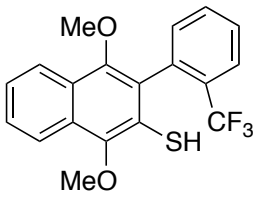

Figure 4.4.256. Product 4.2ab

1,4-dimethoxy-3-(2-(trifluoromethyl)phenyl)naphthalene-2-thiol (**4.2ab**): The entire reaction sequence for the synthesis of **4.2h** was repeated using 50 mg (0.109 mmol, 1.0 equiv) of sulfane **4.2b** and the appropriate equivalents of all reagents to account for the lower reaction scale. Otherwise, the following changes were made: 2-methyl-2-propanethiol (4.0 equiv) and DBU (2.0 equiv) were added to the stirring mixture of **4.4b** at room temperature, and the resulting mixture was let stir at room temperature for only 5 minutes before beginning the reductive methylation quench. The resulting mixture containing the corresponding *tert*-butyl sulfane was worked up in EtOAc and brine, dried over sodium sulfate, and filtered thru or short pad of silica gel, eluting with 10% EtOAc in hexanes. The resulting filtrate was rotovapped and taken up in toluene (2 mL), followed by the addition of $AlCl_3$ (11 mg, 0.082 mmol, 0.75 equiv). The mixture was let stir for 2 hours at room temperature. Upon reaction completion by TLC, the reaction was poured into a separation funnel with EtOAc and sat. $NaHCO_{3(aq)}$. The organic layer was also washed with brine, dried over sodium sulfate, and rotovapped. The resulting crude oil was purified by FCC eluting with hexanes/EtOAc (98/2 → 95/5) to obtain 23mg (58% overall yield) of **4.2ab** as a white solid. **^{1}H NMR** (500 MHz, C_6D_6) δ 8.06 (ddd, *J* = 8.4, 1.3, 0.7 Hz, 1H), 8.01 (ddd, *J* = 8.4, 1.3, 0.7 Hz, 1H), 7.56 (dt, *J* = 7.8, 0.8 Hz, 1H), 7.30 (ddd, *J* = 8.4, 6.8, 1.3 Hz, 1H), 7.23 (ddd, *J* = 8.2, 6.8, 1.3 Hz, 1H), 7.13 – 7.08 (m, 2H), 6.99 – 6.94 (m, 1H), 3.81 (s, 1H), 3.56 (s, 3H), 3.28 (s, 3H).

^{1}H NMR (500 MHz, $(CD_3)_2SO$) δ 8.04 – 8.00 (m, 2H), 7.92 – 7.88 (m, 1H), 7.82 (tdd, *J* = 7.5, 1.4, 0.7 Hz, 1H), 7.72 (tt, *J* = 7.7, 1.1 Hz, 1H), 7.65 (ddd, *J* = 8.4, 6.9, 1.2 Hz, 1H), 7.56 (ddd, *J* = 8.2, 6.8, 1.2 Hz, 1H), 7.53 – 7.50 (m, 1H), 4.51 (s, 1H), 3.87 (s, 3H), 3.52 (s, 3H).

^{13}C NMR (126 MHz, $(CD_3)_2SO$) δ 149.72, 146.14, 134.32 (q, *J* = 2 Hz), 132.44, 132.41, 129.12, 128.31 (q, *J* = 30 Hz), 127.85, 127.62, 127.43, 126.60 (q, *J* = 5 Hz), 125.81, 125.68, 123.85 (q, *J* = 274 Hz), 123.59, 122.84, 121.47, 61.68, 60.18.

The ^{13}C NMR signals of **4.2ab** in deuterated benzene were overwhelmed by the residual solvent peaks. Therefore, we opted to reported the ^{13}C spectrum in deuterated DMSO. Hence, we've tabulated ^{1}H spectra in both deuterated benzene and deuterated DMSO.

^{19}F NMR (470 MHz, (C_6D_6) δ -58.63.

MS (APCI) Calculated for $C_{19}H_{16}F_3O_2S$ $[M+H]^+$: 365.1; Found: 364.9 m/z

HPLC trace: Chiralpak IA (hexanes/2-propanol = 90/10, 1.0 mL/min, t_{ent1} = 4.7 min, t_{ent2} = 5.6 min)

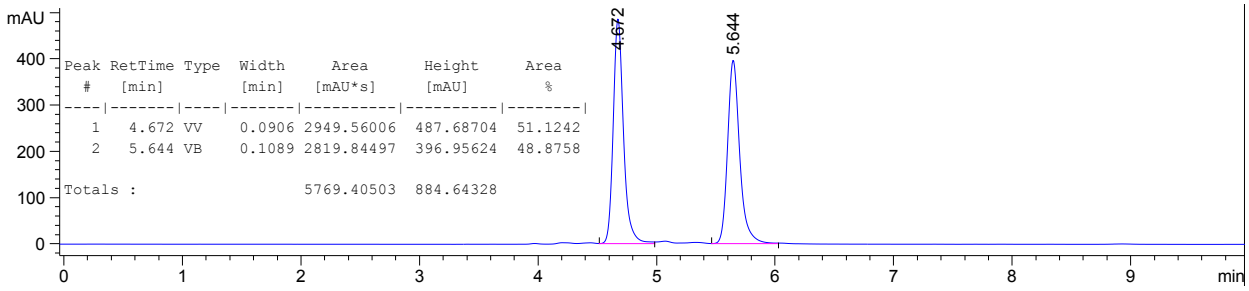

Figure 4.4.257. Racemic HPLC trace of 4.2ab

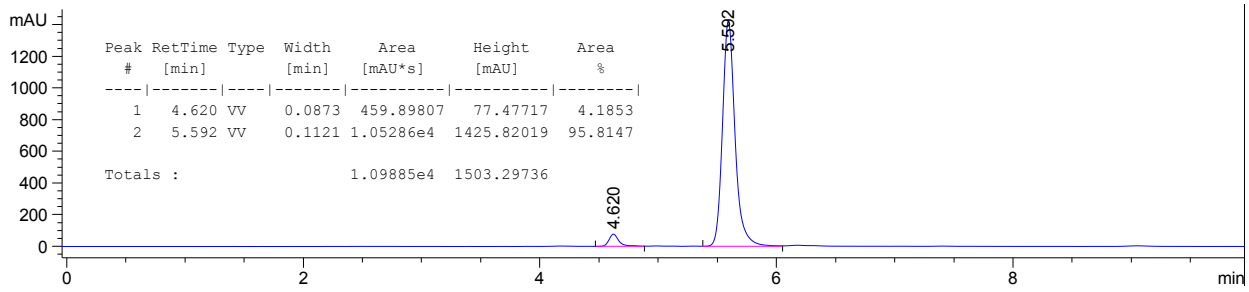

Figure 4.4.258. Asymmetric HPLC trace of 4.2ab

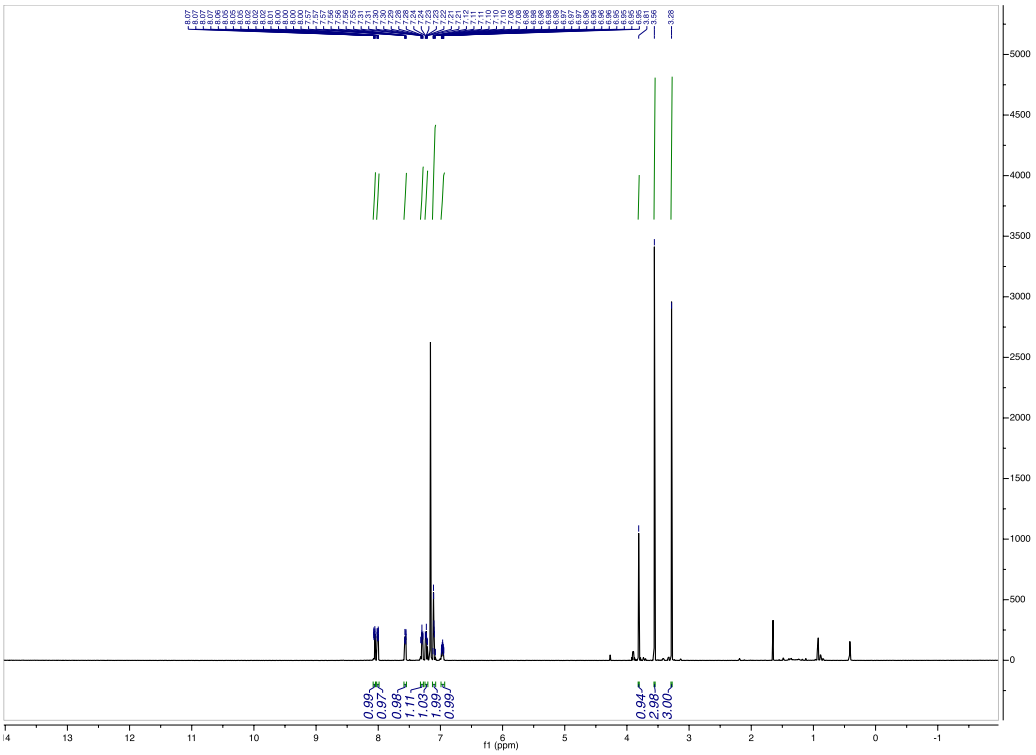

Figure 4.4.259. ^{1}H of 4.2ab in C_6D_6

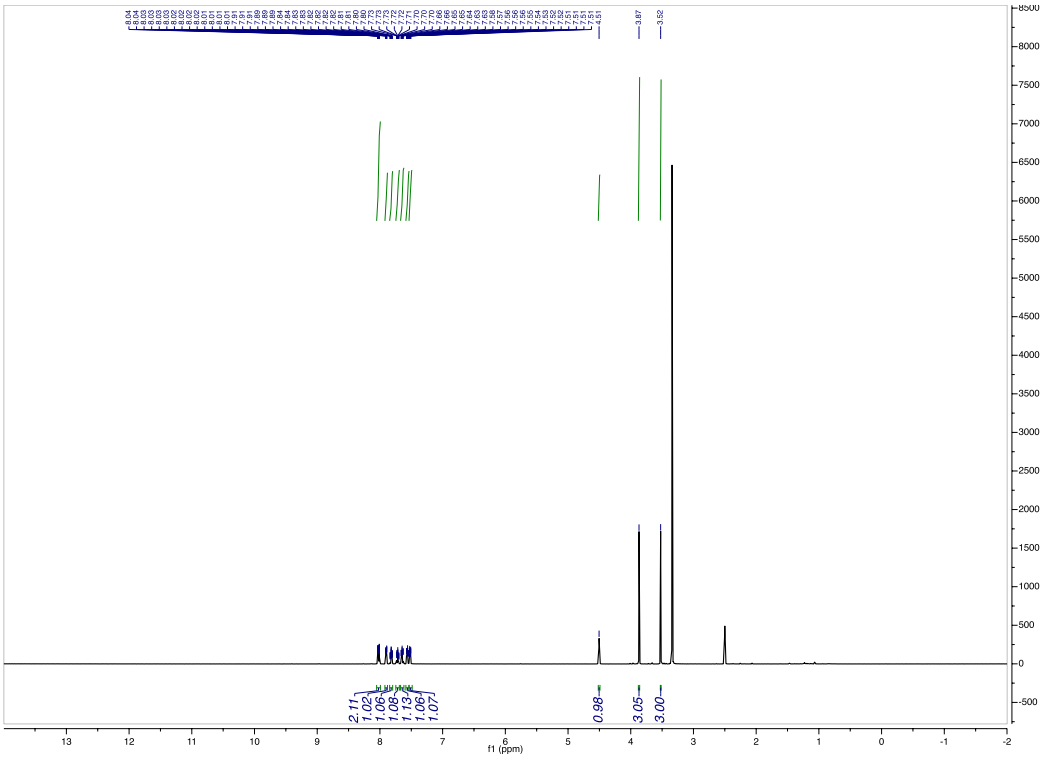

Figure 4.4.260. ^{1}H of 4.2ab in $(CH_3)_2SO$

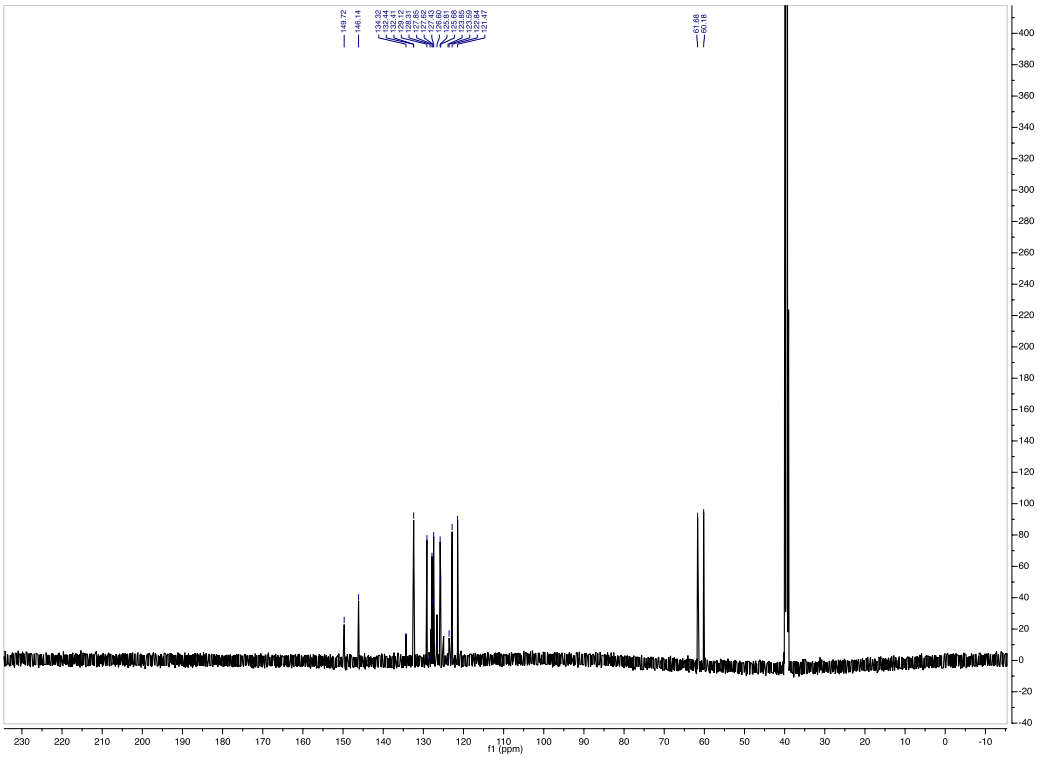

Figure 4.4.261. ^{13}C of 4.2ab in $(CH_3)_2SO$

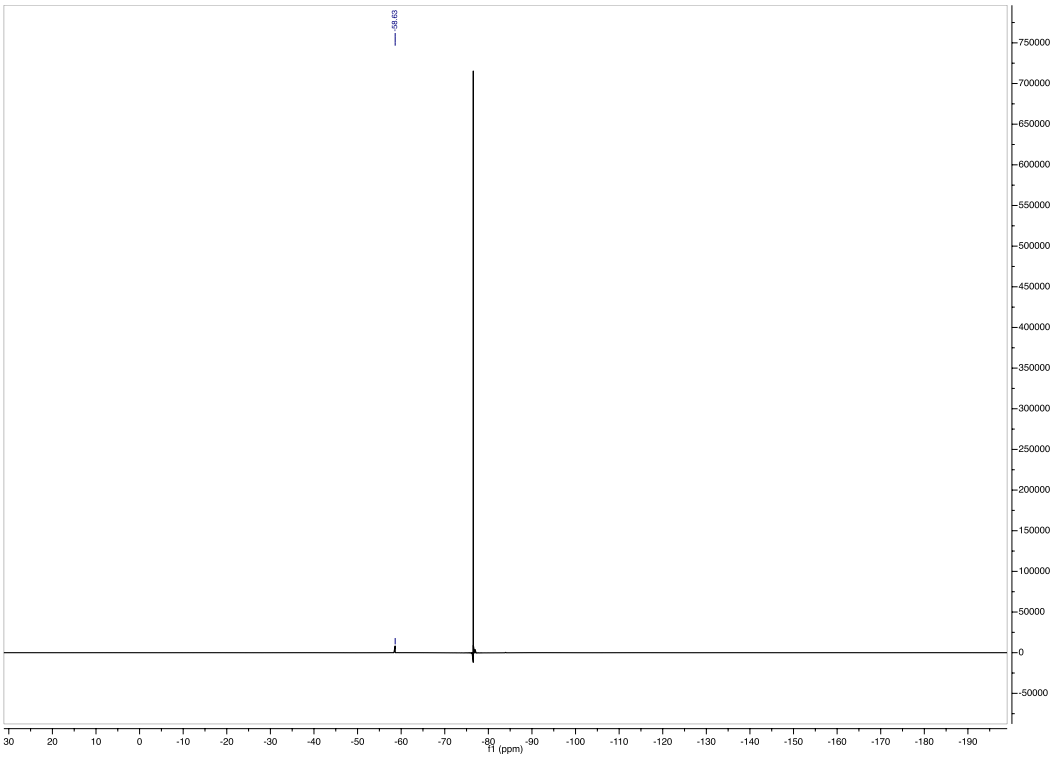

Figure 4.4.262. ^{19}F of 4.2ab in (C_6D_6)

4.4.8 Enantioselective Addition of Thiophenol into Cyclohexenone

Scheme 4.4.1. Asymmetric addition of thiophenol into cyclohexenone using 4.C7

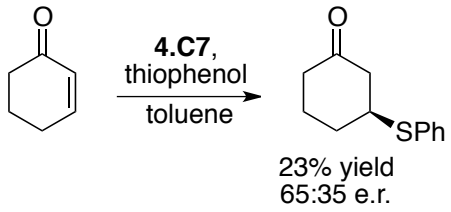

(*S*)-3-(phenylthio)cyclohexanone: Cycloxenone (0.1 mmol, 1.0 equiv) was added to a 20mL scintillation vial equipped with a stir bar followed by the addition of 2mL toluene and 4.C7 (0.005 mmol, 0.05 equiv). The reaction was brought to 0 ^{o}C followed by the addition of thiophenol (0.2 mmol, 2.0 equiv). The reaction was then transferred to a temperature-controlled facility and let stir for 20 hours at 4 ^{o}C. Afterwards, the reaction was concentrated by rotovap and purified by FCC to afford (*S*)-3-(phenylthio)cyclohexanone in 23% yield and 65:35 e.r.. NMR and HPLC data matches those previously reported in literature.[4]

4.4.9 NMR Kinetics study

4.1a (12mg, 0.04mmol, 1.0 equiv) was placed in a J. Young tube, followed by the addition of **4.C7** (0.94mg, 0.002mmol, 0.05 equiv), tetrakis(trimethylsilyl)methane (0.5mg), and toluene-D8 (800μL). The NMR was controlled to a temperature of 4 ^{o}C. The sample was then place in the NMR and let equilibrate for 30 minutes. An initial 1H spectra was obtained to represent the zero time-point. 41 ^{1}H NMR spectra were obtained directly after the addition of 4-methylthiophenol (9.9mg, 0.08mmol, 2.0 equiv). The following variables were adjusted in the ^{1}H experiment to obtain adequate baseline resolution with an overall interval of 30 minutes between the start of each experiment (Bruker Avance III 600 MHz spectrometer / 5mm TXI H-C-N liquids NMR probe w/ Z-axis gradient):

Acquisition Parameters:

NS (number of scans): 124

D20 (time between experiments): 1800 [sec]

DS (dummy scans): 4

TD (time domain size): 65536

D1 (relaxation delay): 10 [sec]

Acquisition Time: 2.5 [sec]

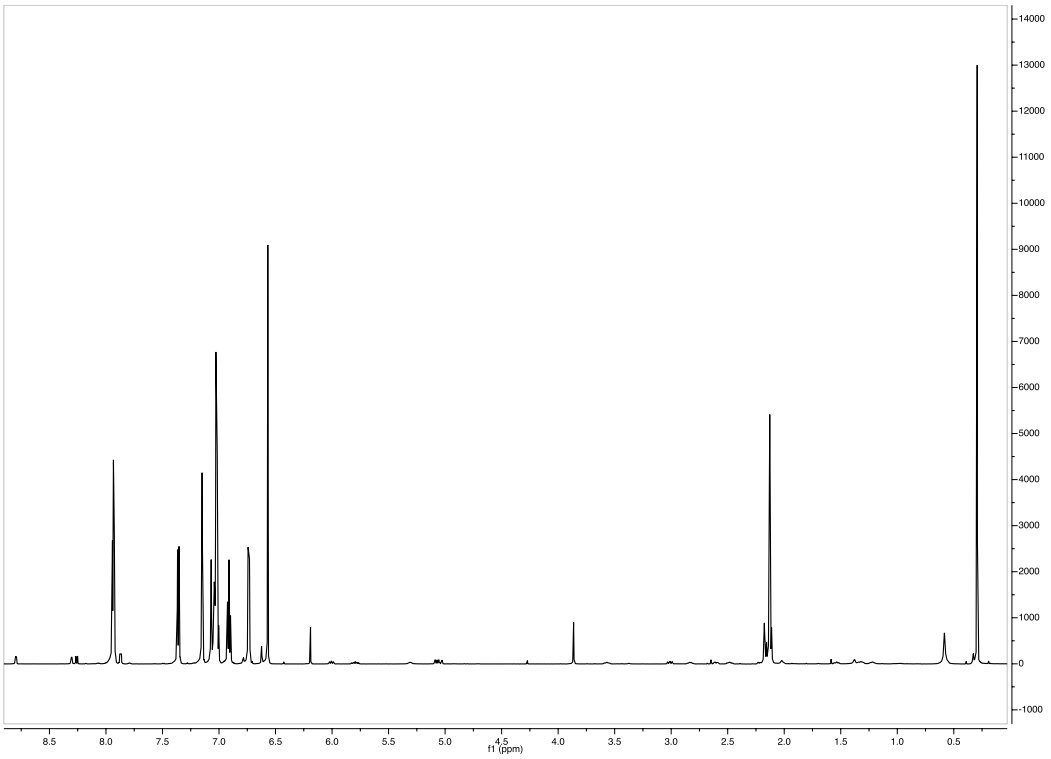

Figure 4.4.263. ^{1}H of 4.1a and 4.C7 in toluene-D_8 (T_0 time-point)

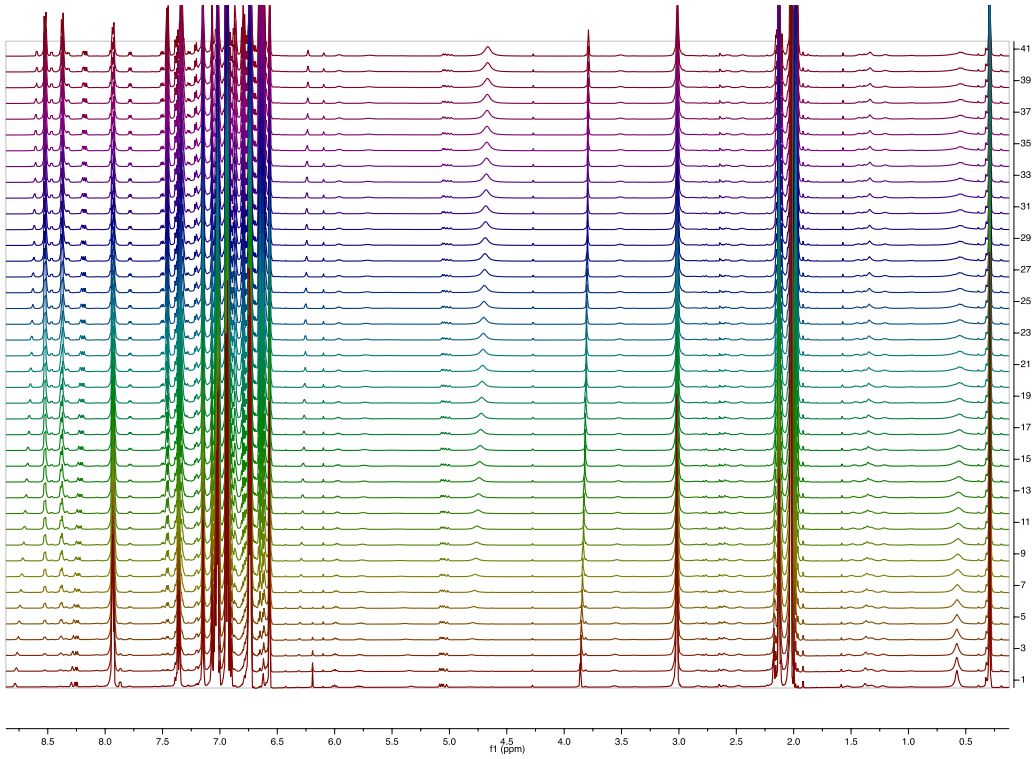

Figure 4.4.264. NMR kinetics study of 4.1a with 4.C7 (^{1}H x 41 in 30 minute intervals)

Discussion:

We quantified the Signal:Noise ratio of the peak between 6.5ppm and 6.6ppm to be >40,000:1. As the NMR acquisition time is on the order of seconds (2.5 seconds), the majority of the signal would be obtained within the first second of the acquisition. In order for **Int-4.1** to outcompete the noise (Signal:Noise at least 5:1), its lifetime would need to exceed 0.000125 seconds (one second divided by the quotient of 40,000/5).

Example Calculation: $\frac{1\,second}{40{,}000/5} = 0.000125\,seconds$

No quantifiable peaks that could unambiguously correspond to **Int-4.1** were observed. Thus we postulate that the lifetime of **Int-4.1** is <125 microseconds.

4.4.10 Int-4.1 Barrier to Rotation Calculations

Both diastereomers of **Int-4.1** were optimized in the gas phase using density functional theory (RB3LYP)[I] with the 6-31+G(d,p)I[II] basis set as implemented in the Gaussian 09[III] suite of programs. Single point energy calculations were performed on both minimized structures using M06-2X[IV] level of theory and 6-31+G(d,p) basis set as implemented in Gaussian 09. An initial rotational landscape scan (Figure S9) was performed using RB3LYP/6-31+G(d,p); the dihedral angle was frozen every 10 degrees while the rest of the structure was minimized (Figure S10). The two highest energy minimizations corresponding to the planarization of the atropisomer were recorded (**TS 4.1** and **TS 4.2**). The dihedral angle was then set to each of these conformational maxima and frozen every 2 degrees (and -2 degrees), sweeping 10 degrees in both directions while the rest of the structure was minimized {RB3LYP/6-31+G(d,p)} to arrive at a local maximum for each transition state. The highest energy minimization from each sweep corresponding to the atropisomers eclipsing each other (the local maxima) were recorded (**>TS 4.1** and **>TS 4.2**). Single point energy calculations were performed on the minimized structures using M06-2X/6-31+G(d,p) as implemented in Gaussian 09. All energies are reported in kcal/mol with respect to the lowest energy pseudo-perpendicular structure.

Sources cited:

(I) Becke, A. D. J. Chem. Phys.1993, 98, 5648. (b) Becke, A. D. J. Chem. Phys.1993, 98, 1372. (c) Lee, C.; Yang, W.; Parr, R. G. Phys. Rev. B, 1988, 37, 785. (d) Vosko, S. H.; Wilk, L.; Nusair, M. Can. J. Phys. 1980, 58, 1200

(II) (a) R. Ditchfield, W. J. Hehre, and J. A. Pople *J. Chem. Phys.*, **54** (1971) 724. (b) W. J. Hehre, R. Ditchfield, and J. A. Pople *J. Chem. Phys.*, **56** (1972) 2257. (c) P. C. Hariharan and J. A. Pople *Mol. Phys.*, **27** (1974) 209-14. (d) M. S. Gordon *Chem. Phys. Lett.*, **76** (1980) 163-68. (e) M. M. Francl, W. J. Pietro, W. J. Hehre, J. S. Binkley, D. J. DeFrees, J. A. Pople, and M. S. Gordon *J. Chem. Phys.*, **77** (1982) 3654-65. (f) R. C. Binning Jr. and L. A. Curtiss *J. Comp. Chem.*, **11** (1990) 1206-16. (g) J.-P. Blaudeau, M. P. McGrath, L. A. Curtiss, and L. Radom *J. Chem. Phys.*, **107** (1997) 5016-21. (h) V. A. Rassolov, M. A. Ratner, J. A.

Pople, P. C. Redfern, and L. A. Curtiss *J. Comp. Chem.*, **22** (2001) 976-84. (i) T. Clark, J. Chandrasekhar, G. W. Spitznagel, and P. v. R. Schleyer *J. Comp. Chem.*, **4** (1983) 294-301. (j) M. J. Frisch, J. A. Pople, and J. S. Binkley *J. Chem. Phys.*, **80** (1984) 3265-69.

(III) Gaussian 09, Revision D.01, M. J. Frisch, G. W. Trucks, H. B. Schlegel, G. E. Scuseria, M. A. Robb, J. R. Cheeseman, G. Scalmani, V. Barone, G. A. Petersson, H. Nakatsuji, X. Li, M. Caricato, A. Marenich, J. Bloino, B. G. Janesko, R. Gomperts, B. Mennucci, H. P. Hratchian, J. V. Ortiz, A. F. Izmaylov, J. L. Sonnenberg, D. Williams-Young, F. Ding, F. Lipparini, F. Egidi, J. Goings, B. Peng, A. Petrone, T. Henderson, D. Ranasinghe, V. G. Zakrzewski, J. Gao, N. Rega, G. Zheng, W. Liang, M. Hada, M. Ehara, K. Toyota, R. Fukuda, J. Hasegawa, M. Ishida, T. Nakajima, Y. Honda, O. Kitao, H. Nakai, T. Vreven, K. Throssell, J. A. Montgomery, Jr., J. E. Peralta, F. Ogliaro, M. Bearpark, J. J. Heyd, E. Brothers, K. N. Kudin, V. N. Staroverov, T. Keith, R. Kobayashi, J. Normand, K. Raghavachari, A. Rendell, J. C. Burant, S. S. Iyengar, J. Tomasi, M. Cossi, J. M. Millam, M. Klene, C. Adamo, R. Cammi, J. W. Ochterski, R. L. Martin, K. Morokuma, O. Farkas, J. B. Foresman, and D. J. Fox, Gaussian, Inc., Wallingford CT, 2013.

(IV) Zhao, Y.; Truhlar, D.G. *Theor. Chem. Acc.*, **120** (2008) 215-41

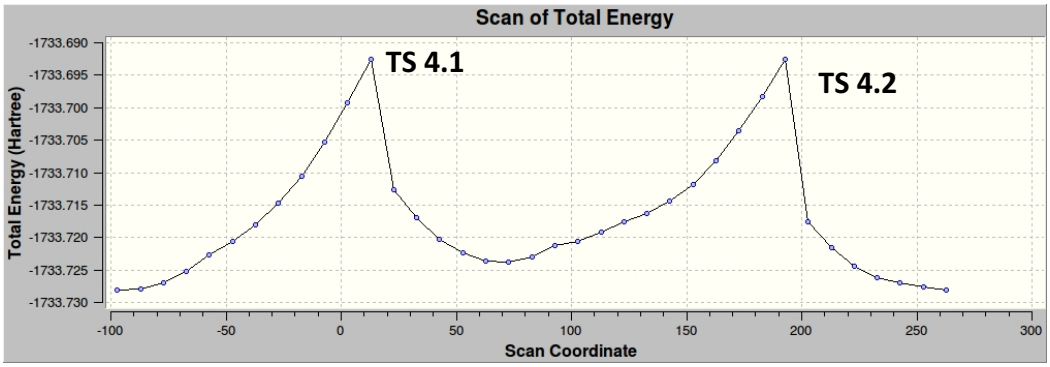

Figure 4.4.265. Rotational landscape of Int-4.1 with atropisomeric axis dihedral scanned 36 times in 10^{o} increments (Scan 1) {RB3LYP/6-31+G(d,p)}

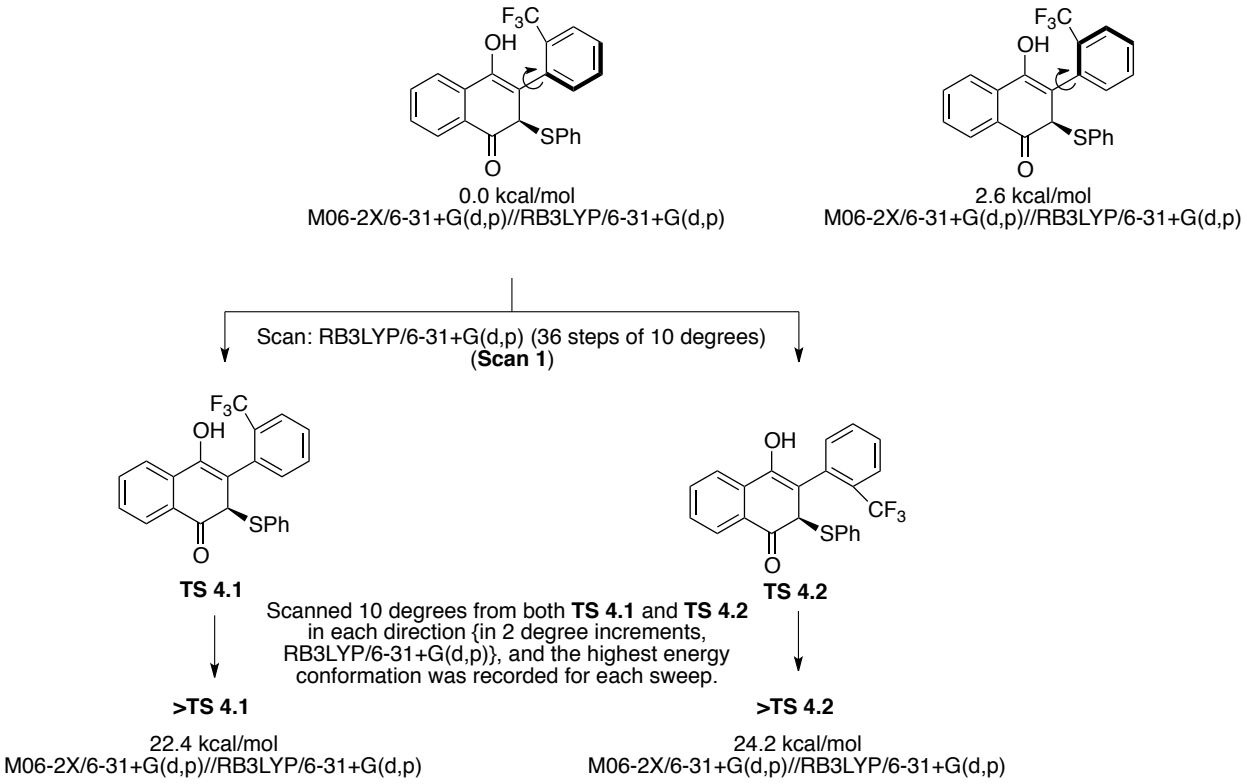

Figure 4.4.266. Graphical representation to computationally determine barrier to rotation of Int-4.1

4.4.11 Explanation for Missing Carbon Peaks in Several 13C NMR Spectra

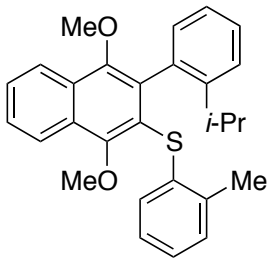

Figure 4.4.267. Structure of 4.2p

In the ^{13}C NMR spectrum of **4.2p**, only 27 signals are detected by the 500 MHz NMR spectrometer, however there are 28 carbons in the molecule. We observed the same number of signals in different deuterated solvents as well (e.g. MeOH-d4, DMSO-d6). We then performed ^{13}C inversion-recovery experiments for the ^{13}C NMR spectrum of **4.2p** in $CDCl_3$. Peak intensities were measured and plotted in Topspin's T1 (spin-lattice relaxation time) fitting software. The T1 was determined for the following signals.

Shift (ppm)	T1 (sec)	Carbon Type
128.9	3.39	sp2 quat
129.7	1.427	sp2 quat AND sp2 tert
130.3	0.739	sp2 tert
136	3.865	sp2 quat

Aromatic carbons with attached protons were all in the 800 ms range, while aromatic quaternary carbons were in the 3-4 second range. The T1 fit result of 1.4 seconds is an average of 2 components, therefore the corresponding signal at 129.7ppm is 2 unresolved carbon signals. Due to structural similarity, we expect the following atropisomers with missing peaks is a result of the same phenomenon:

4.2e, **4.2i**, **4.2j**, **4.2l**, **4.2m**, **4.2p**, **4.2v**, **4.2w**

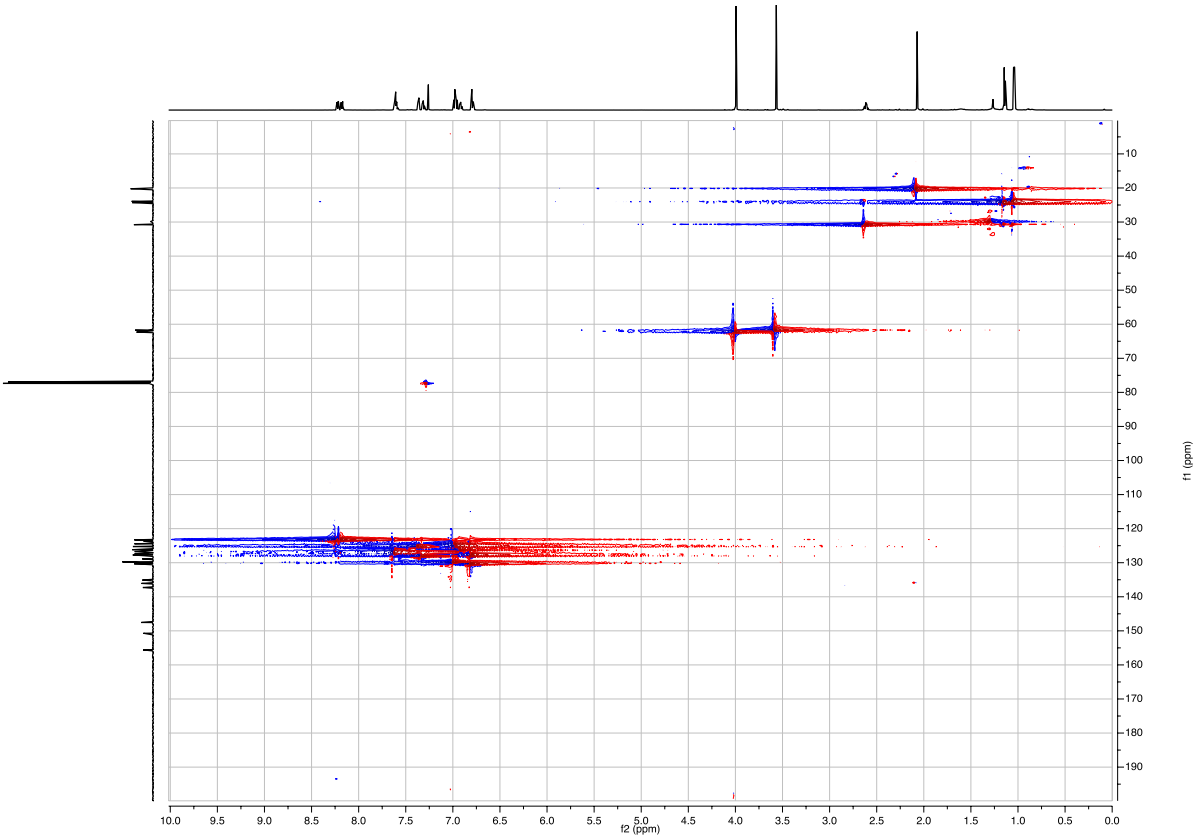

Figure 4.4.268. HSQC ($^{1}H/^{13}C$) of 4.2p

^{13}C Inversion Recovery Data

Dataset :
D:/My Documents/NMR_Data/SDSU_NMRF/Temp/smaddo-20170609_N6_SMM_9_176_C13_inv-rec/11/pdata/1
INTENSITY fit :
I[t]=I[0]+P*exp(-t/T1)

13 points for Peak 1, Peak Point at 155.476 ppm
Results Comp. 1

I[0] = 9.605e-001
P = -1.891e+000
T1 = 5.557s
SD = 4.210e-002

tau	ppm	integral	intensity
100.000m	155.477	-7.2003e+007	-2.3621e+007

200.000m	155.478	-8.232e+007	-2.4687e+007
300.000m	155.477	-6.5848e+007	-2.1873e+007
400.000m	155.478	-7.0845e+007	-2.1985e+007
500.000m	155.478	-6.4479e+007	-2.1709e+007
700.000m	155.477	-6.3059e+007	-1.934e+007
900.000m	155.477	-5.217e+007	-1.7121e+007
1.000s	155.477	-4.6487e+007	-1.5143e+007
2.000s	155.478	-3.2e+007	-8.745e+006
3.000s	155.476	-9.442e+006	eliminated
4.000s	155.476	4.3983e+006	eliminated
5.000s	155.476	1.3413e+007	eliminated
10.000s	155.479	6.4002e+007	1.6013e+007
15.000s	155.479	8.7104e+007	2.1705e+007
20.000s	155.479	1.1656e+008	2.6944e+007
30.000s	155.479	1.0228e+008	2.4748e+007

14 points for Peak 2, Peak Point at 150.592 ppm
Results Comp. 1

I[0] = 9.500e-001
P = -1.996e+000
T1 = 5.850s
SD = 2.655e-002

tau	ppm	integral	intensity
100.000m	150.593	-7.9332e+007	-2.8087e+007
200.000m	150.593	-7.6361e+007	-2.7807e+007
300.000m	150.592	-7.8175e+007	-2.7587e+007
400.000m	150.593	-7.1963e+007	-2.5099e+007
500.000m	150.593	-7.2659e+007	-2.4677e+007
700.000m	150.592	-6.7592e+007	-2.411e+007
900.000m	150.593	-6.1603e+007	-2.206e+007
1.000s	150.593	-5.6536e+007	-1.9102e+007
2.000s	150.593	-4.0892e+007	-1.2601e+007
3.000s	150.594	-2.131e+007	-6.2535e+006
4.000s	150.592	-1.6684e+006	eliminated
5.000s	150.592	1.0284e+007	eliminated
10.000s	150.593	5.9703e+007	1.5468e+007
15.000s	150.593	8.2493e+007	2.1961e+007
20.000s	150.593	9.8977e+007	2.5518e+007
30.000s	150.594	1.0154e+008	2.6528e+007

15 points for Peak 3, Peak Point at 147.422 ppm
Results Comp. 1

I[0] = 9.804e-001
P = -2.038e+000
T1 = 2.609s
SD = 3.925e-002

tau	ppm	integral	intensity
100.000m	147.423	-8.5607e+007	-2.9364e+007
200.000m	147.423	-7.9377e+007	-2.5394e+007
300.000m	147.423	-7.5228e+007	-2.5409e+007
400.000m	147.423	-6.8267e+007	-2.2493e+007
500.000m	147.423	-7.3051e+007	-2.3747e+007
700.000m	147.423	-5.4775e+007	-1.6401e+007
900.000m	147.422	-5.2832e+007	-1.4926e+007
1.000s	147.422	-4.3455e+007	-1.3146e+007
2.000s	147.422	5.9331e+006	eliminated
3.000s	147.423	4.3338e+007	1.1074e+007
4.000s	147.423	6.5857e+007	1.67e+007
5.000s	147.423	7.9298e+007	1.9752e+007
10.000s	147.423	1.2216e+008	3.0099e+007
15.000s	147.423	1.1595e+008	2.9519e+007
20.000s	147.423	1.1909e+008	2.8412e+007
30.000s	147.423	1.1467e+008	2.865e+007

14 points for Peak 4, Peak Point at 137.160 ppm
Results Comp. 1

I[0] = 8.150e-001
P = -1.838e+000
T1 = 4.531s
SD = 2.931e-002

tau	ppm	integral	intensity
100.000m	137.160	-9.8496e+007	-3.4093e+007
200.000m	137.161	-9.13e+007	-3.1872e+007

300.000m	137.160	-9.1245e+007	-3.0939e+007
400.000m	137.161	-8.2886e+007	-2.901e+007
500.000m	137.160	-8.6197e+007	-2.9487e+007
700.000m	137.160	-7.6638e+007	-2.4172e+007
900.000m	137.161	-7.5537e+007	-2.3939e+007
1.000s	137.161	-7.4002e+007	-2.2104e+007
2.000s	137.160	-5.5816e+007	-1.3878e+007
3.000s	137.160	-1.6761e+007	eliminated
4.000s	137.160	4.0467e+006	eliminated
5.000s	137.161	2.88e+007	7.6196e+006
10.000s	137.161	7.5058e+007	2.1431e+007
15.000s	137.161	9.2695e+007	2.5017e+007
20.000s	137.161	9.8594e+007	2.5245e+007
30.000s	137.161	1.1694e+008	2.9336e+007

15 points for Peak 5, Peak Point at 135.956 ppm
Results Comp. 1

I[0] = 9.015e-001
P = -1.968e+000
T1 = 3.865s
SD = 2.958e-002

tau	ppm	integral	intensity
100.000m	135.958	-9.3306e+007	-3.3192e+007
200.000m	135.959	-9.7272e+007	-3.3116e+007
300.000m	135.959	-9.6767e+007	-3.1738e+007
400.000m	135.958	-8.6161e+007	-2.8157e+007
500.000m	135.958	-8.6943e+007	-2.921e+007
700.000m	135.958	-6.8167e+007	-2.368e+007
900.000m	135.959	-6.2546e+007	-2.1032e+007
1.000s	135.958	-5.7648e+007	-1.8632e+007
2.000s	135.958	-3.126e+007	-9.4326e+006
3.000s	135.956	1.293e+006	eliminated
4.000s	135.959	2.4793e+007	6.6448e+006
5.000s	135.959	4.4234e+007	1.0789e+007
10.000s	135.958	9.49e+007	2.5618e+007
15.000s	135.959	1.1333e+008	2.9356e+007
20.000s	135.959	1.1304e+008	2.8965e+007
30.000s	135.958	1.1113e+008	2.9757e+007

15 points for Peak 6, Peak Point at 134.966 ppm
Results Comp. 1

I[0] = 8.238e-001
P = -1.864e+000
T1 = 3.378s
SD = 2.464e-002

tau	ppm	integral	intensity
100.000m	134.966	-9.1875e+007	-3.1951e+007
200.000m	134.967	-8.6621e+007	-2.9919e+007
300.000m	134.966	-8.4863e+007	-2.8018e+007
400.000m	134.967	-7.8139e+007	-2.7046e+007
500.000m	134.966	-7.5191e+007	-2.5473e+007
700.000m	134.966	-6.0996e+007	-2.1224e+007
900.000m	134.966	-5.1807e+007	-1.8456e+007
1.000s	134.967	-5.9963e+007	-1.7788e+007
2.000s	134.967	-2.1523e+007	-6.7688e+006
3.000s	134.966	4.4942e+006	eliminated
4.000s	134.966	3.1797e+007	7.7409e+006
5.000s	134.967	4.5651e+007	1.1687e+007
10.000s	134.967	9.6385e+007	2.5416e+007
15.000s	134.967	9.3336e+007	2.4632e+007
20.000s	134.967	1.0736e+008	2.6237e+007
30.000s	134.967	1.0535e+008	2.5988e+007

15 points for Peak 7, Peak Point at 134.881 ppm
Results Comp. 1

I[0] = 8.478e-001
P = -1.878e+000
T1 = 4.845s
SD = 3.316e-002

tau	ppm	integral	intensity
100.000m	134.883	-9.33e+007	-3.0196e+007
200.000m	134.883	-8.4023e+007	-2.8411e+007
300.000m	134.883	-8.8896e+007	-2.8335e+007

400.000m	134.883	-7.9992e+007	-2.6298e+007
500.000m	134.883	-7.2513e+007	-2.3665e+007
700.000m	134.883	-8.7181e+007	-2.5446e+007
900.000m	134.882	-7.1311e+007	-2.2585e+007
1.000s	134.883	-6.4024e+007	-1.9624e+007
2.000s	134.883	-3.3878e+007	-1.0786e+007
3.000s	134.884	-1.8782e+007	-6.3622e+006
4.000s	134.881	1.2391e+007	eliminated
5.000s	134.883	1.8772e+007	6.2811e+006
10.000s	134.883	7.366e+007	1.8137e+007
15.000s	134.884	9.0926e+007	2.2639e+007
20.000s	134.883	1.0592e+008	2.5358e+007
30.000s	134.884	1.023e+008	2.5218e+007

15 points for Peak 8, Peak Point at 130.196 ppm
Results Comp. 1

I[0] = 9.501e-001
P = -2.018e+000
T1 = 738.927m
SD = 5.075e-002

tau	ppm	integral	intensity
100.000m	130.195	-1.463e+008	-4.2715e+007
200.000m	130.195	-1.0711e+008	-3.1038e+007
300.000m	130.195	-6.875e+007	-2.0278e+007
400.000m	130.195	-4.8876e+007	-1.2865e+007
500.000m	130.196	-1.9482e+007	eliminated
700.000m	130.196	2.2993e+007	6.2149e+006
900.000m	130.196	6.0263e+007	1.746e+007
1.000s	130.195	8.8622e+007	2.3898e+007
2.000s	130.195	1.7536e+008	4.7365e+007
3.000s	130.196	2.0821e+008	5.3106e+007
4.000s	130.196	2.025e+008	5.1144e+007
5.000s	130.196	2.1782e+008	5.3338e+007
10.000s	130.196	2.1279e+008	5.2689e+007
15.000s	130.196	2.0746e+008	4.8599e+007
20.000s	130.196	2.1028e+008	4.612e+007
30.000s	130.197	2.0601e+008	4.5536e+007

16 points for Peak 9, Peak Point at 129.627 ppm
Results Comp. 1

I[0] = 9.623e-001
P = -2.084e+000
T1 = 1.437s
SD = 2.543e-002

tau	ppm	integral	intensity
100.000m	129.630	-2.6113e+008	-7.8352e+007
200.000m	129.631	-2.2553e+008	-6.6362e+007
300.000m	129.631	-1.8829e+008	-5.5615e+007
400.000m	129.631	-1.6446e+008	-4.7758e+007
500.000m	129.631	-1.3347e+008	-3.9948e+007
700.000m	129.632	-7.4394e+007	-2.4276e+007
900.000m	129.633	-3.9796e+007	-1.4174e+007
1.000s	129.634	-1.5813e+006	-6.959e+006
2.000s	129.628	1.319e+008	3.8929e+007
3.000s	129.629	2.0773e+008	5.4272e+007
4.000s	129.630	2.5018e+008	6.2863e+007
5.000s	129.630	2.788e+008	6.8326e+007
10.000s	129.631	3.3402e+008	7.8198e+007
15.000s	129.631	3.3961e+008	7.807e+007
20.000s	129.631	3.3468e+008	7.5531e+007
30.000s	129.631	3.3527e+008	7.2483e+007

15 points for Peak 10, Peak Point at 128.736 ppm
Results Comp. 1

I[0] = 8.521e-001
P = -1.919e+000
T1 = 3.391s
SD = 3.366e-002

tau	ppm	integral	intensity
100.000m	128.735	-9.889e+007	-3.2206e+007
200.000m	128.735	-9.0109e+007	-2.9774e+007
300.000m	128.735	-9.2949e+007	-2.9906e+007
400.000m	128.735	-9.1679e+007	-2.9914e+007

500.000m	128.735	-7.2977e+007	-2.5066e+007
700.000m	128.735	-7.2609e+007	-2.3032e+007
900.000m	128.735	-5.3929e+007	-1.8784e+007
1.000s	128.736	-6.1509e+007	-1.7871e+007
2.000s	128.736	-2.7284e+007	-7.7034e+006
3.000s	128.736	2.3322e+007	eliminated
4.000s	128.735	3.4193e+007	9.2107e+006
5.000s	128.735	5.2476e+007	1.204e+007
10.000s	128.736	1.0033e+008	2.5167e+007
15.000s	128.736	1.1097e+008	2.8054e+007
20.000s	128.736	1.0989e+008	2.6723e+007
30.000s	128.736	1.1057e+008	2.6287e+007

15 points for Peak 11, Peak Point at 127.837 ppm
Results Comp. 1

I[0] = 9.213e-001
P = -1.999e+000
T1 = 651.930m
SD = 5.384e-002

tau	ppm	integral	intensity
100.000m	127.837	-1.3844e+008	-4.117e+007
200.000m	127.837	-9.3972e+007	-2.9731e+007
300.000m	127.837	-7.643e+007	-2.1244e+007
400.000m	127.837	-4.1411e+007	-1.0562e+007
500.000m	127.837	-6.1944e+006	eliminated
700.000m	127.836	5.2786e+007	1.3515e+007
900.000m	127.837	8.3414e+007	2.3027e+007
1.000s	127.837	9.8054e+007	2.6954e+007
2.000s	127.837	1.7765e+008	4.8412e+007
3.000s	127.837	2.0938e+008	5.4763e+007
4.000s	127.837	2.103e+008	5.2817e+007
5.000s	127.837	2.1215e+008	5.3056e+007
10.000s	127.837	2.1306e+008	5.0275e+007
15.000s	127.837	2.156e+008	4.8364e+007
20.000s	127.837	2.0683e+008	4.6804e+007
30.000s	127.837	2.0105e+008	4.3751e+007

15 points for Peak 12, Peak Point at 127.598 ppm
Results Comp. 1

I[0] = 9.797e-001
P = -2.110e+000
T1 = 935.878m
SD = 4.272e-002

tau	ppm	integral	intensity
100.000m	127.597	-1.5073e+008	-4.7111e+007
200.000m	127.597	-1.3753e+008	-4.0462e+007
300.000m	127.598	-9.759e+007	-3.0921e+007
400.000m	127.597	-6.601e+007	-2.1549e+007
500.000m	127.597	-4.9086e+007	-1.6087e+007
700.000m	127.598	-9.0473e+006	eliminated
900.000m	127.598	3.6862e+007	9.6964e+006
1.000s	127.597	4.3854e+007	1.202e+007
2.000s	127.597	1.5556e+008	4.2398e+007
3.000s	127.598	2.0157e+008	5.2632e+007
4.000s	127.598	2.1128e+008	5.4074e+007
5.000s	127.598	2.1977e+008	5.4566e+007
10.000s	127.598	2.1535e+008	5.3133e+007
15.000s	127.598	2.2169e+008	5.3674e+007
20.000s	127.598	2.243e+008	5.1344e+007
30.000s	127.599	2.1297e+008	4.796e+007

15 points for Peak 13, Peak Point at 127.213 ppm
Results Comp. 1

I[0] = 9.406e-001
P = -2.005e+000
T1 = 690.152m
SD = 4.614e-002

tau	ppm	integral	intensity
100.000m	127.213	-1.3843e+008	-4.1034e+007
200.000m	127.213	-1.0244e+008	-3.1786e+007
300.000m	127.213	-7.3421e+007	-2.053e+007
400.000m	127.214	-3.569e+007	-1.0501e+007
500.000m	127.213	-6.8037e+006	eliminated

700.000m	127.213	3.8716e+007	1.1353e+007
900.000m	127.213	7.9677e+007	2.1361e+007
1.000s	127.213	8.6281e+007	2.5497e+007
2.000s	127.213	1.738e+008	4.7512e+007
3.000s	127.213	2.1362e+008	5.4473e+007
4.000s	127.213	2.1066e+008	5.3853e+007
5.000s	127.213	2.0446e+008	5.1721e+007
10.000s	127.213	2.1678e+008	5.202e+007
15.000s	127.213	2.1762e+008	5.0853e+007
20.000s	127.214	2.0924e+008	4.7826e+007
30.000s	127.213	2.014e+008	4.5046e+007

15 points for Peak 14, Peak Point at 126.600 ppm
Results Comp. 1

I[0] = 9.509e-001
P = -2.043e+000
T1 = 652.333m
SD = 4.265e-002

tau	ppm	integral	intensity
100.000m	126.602	-1.372e+008	-4.0536e+007
200.000m	126.602	-1.0723e+008	-3.0935e+007
300.000m	126.602	-6.3842e+007	-1.822e+007
400.000m	126.603	-3.1329e+007	-9.2529e+006
500.000m	126.600	-6.0667e+006	eliminated
700.000m	126.602	4.3767e+007	1.2172e+007
900.000m	126.602	8.3893e+007	2.4192e+007
1.000s	126.602	9.6886e+007	2.7367e+007
2.000s	126.602	1.7667e+008	4.8185e+007
3.000s	126.602	1.8962e+008	5.1331e+007
4.000s	126.602	2.0422e+008	5.3189e+007
5.000s	126.602	2.0298e+008	5.2049e+007
10.000s	126.602	2.0833e+008	5.2392e+007
15.000s	126.603	2.0354e+008	4.975e+007
20.000s	126.602	1.9365e+008	4.6043e+007
30.000s	126.602	1.9754e+008	4.5958e+007

15 points for Peak 15, Peak Point at 126.050 ppm

Results Comp. 1

I[0] = 9.511e-001
P = -2.050e+000
T1 = 820.800m
SD = 4.816e-002

tau	ppm	integral	intensity
100.000m	126.052	-1.5416e+008	-4.7545e+007
200.000m	126.052	-1.1172e+008	-3.5978e+007
300.000m	126.052	-8.9973e+007	-2.8849e+007
400.000m	126.052	-6.603e+007	-1.9737e+007
500.000m	126.053	-3.5283e+007	-1.1134e+007
700.000m	126.050	1.5144e+006	eliminated
900.000m	126.052	5.8415e+007	1.6291e+007
1.000s	126.052	6.8231e+007	1.9668e+007
2.000s	126.052	1.675e+008	4.6061e+007
3.000s	126.052	1.9696e+008	5.4274e+007
4.000s	126.052	2.1075e+008	5.7287e+007
5.000s	126.053	2.1777e+008	5.6171e+007
10.000s	126.053	2.1602e+008	5.5599e+007
15.000s	126.053	2.1795e+008	5.4703e+007
20.000s	126.053	2.113e+008	5.1728e+007
30.000s	126.053	1.9352e+008	4.6856e+007

15 points for Peak 16, Peak Point at 125.129 ppm
Results Comp. 1

I[0] = 9.551e-001
P = -2.041e+000
T1 = 738.241m
SD = 3.935e-002

tau	ppm	integral	intensity
100.000m	125.129	-1.5384e+008	-4.5021e+007
200.000m	125.129	-1.1077e+008	-3.224e+007
300.000m	125.129	-7.9133e+007	-2.3249e+007
400.000m	125.129	-4.9087e+007	-1.3808e+007
500.000m	125.129	-1.275e+007	eliminated
700.000m	125.129	3.1206e+007	8.9135e+006

900.000m	125.129	6.9186e+007	1.904e+007
1.000s	125.129	8.6785e+007	2.3346e+007
2.000s	125.129	1.7551e+008	4.6961e+007
3.000s	125.129	2.0732e+008	5.3941e+007
4.000s	125.129	2.1859e+008	5.4233e+007
5.000s	125.129	2.3148e+008	5.5195e+007
10.000s	125.129	2.3435e+008	5.3277e+007
15.000s	125.129	2.3468e+008	5.2557e+007
20.000s	125.129	2.1981e+008	4.9954e+007
30.000s	125.129	2.208e+008	4.6765e+007

15 points for Peak 17, Peak Point at 125.092 ppm
Results Comp. 1

I[0] = 9.505e-001
P = -2.019e+000
T1 = 796.117m
SD = 4.653e-002

tau	ppm	integral	intensity
100.000m	125.094	-1.6113e+008	-4.7789e+007
200.000m	125.094	-1.148e+008	-3.4823e+007
300.000m	125.094	-8.2926e+007	-2.5009e+007
400.000m	125.094	-6.6718e+007	-1.8894e+007
500.000m	125.094	-2.9204e+007	-8.1563e+006
700.000m	125.092	2.2267e+007	eliminated
900.000m	125.093	6.4137e+007	1.8175e+007
1.000s	125.093	7.4648e+007	2.0301e+007
2.000s	125.093	1.8181e+008	4.8763e+007
3.000s	125.094	2.1009e+008	5.6744e+007
4.000s	125.094	2.2307e+008	5.7216e+007
5.000s	125.094	2.2998e+008	5.8496e+007
10.000s	125.094	2.2961e+008	5.6901e+007
15.000s	125.094	2.2587e+008	5.4625e+007
20.000s	125.094	2.1154e+008	5.0131e+007
30.000s	125.094	2.1306e+008	5.0625e+007

15 points for Peak 18, Peak Point at 124.322 ppm
Results Comp. 1

I[0] = 9.537e-001
P = -2.049e+000
T1 = 736.931m
SD = 4.845e-002

tau	ppm	integral	intensity
100.000m	124.323	-1.389e+008	-4.2653e+007
200.000m	124.323	-1.1745e+008	-3.4959e+007
300.000m	124.323	-7.5705e+007	-2.4326e+007
400.000m	124.323	-4.6659e+007	-1.3944e+007
500.000m	124.322	-1.4773e+007	eliminated
700.000m	124.323	2.7796e+007	7.4005e+006
900.000m	124.323	7.244e+007	2.0114e+007
1.000s	124.323	7.7539e+007	2.3405e+007
2.000s	124.323	1.7352e+008	4.8583e+007
3.000s	124.323	1.93e+008	5.3141e+007
4.000s	124.323	2.0452e+008	5.4252e+007
5.000s	124.323	2.1204e+008	5.4977e+007
10.000s	124.323	2.0806e+008	5.331e+007
15.000s	124.323	2.1236e+008	5.162e+007
20.000s	124.324	1.9768e+008	4.9016e+007
30.000s	124.324	1.9262e+008	4.6037e+007

14 points for Peak 19, Peak Point at 123.581 ppm
Results Comp. 1

I[0] = 7.667e-001
P = -1.762e+000
T1 = 5.682s
SD = 2.309e-002

tau	ppm	integral	intensity
100.000m	123.584	-1.0951e+008	-3.4402e+007
200.000m	123.584	-1.0763e+008	-3.2347e+007
300.000m	123.584	-9.8444e+007	-3.216e+007
400.000m	123.584	-9.5042e+007	-3.0416e+007
500.000m	123.584	-8.6848e+007	-2.7255e+007
700.000m	123.584	-8.526e+007	-2.6737e+007
900.000m	123.584	-7.7619e+007	-2.4469e+007

1.000s	123.584	-7.4526e+007	-2.4161e+007
2.000s	123.584	-5.9403e+007	-1.6349e+007
3.000s	123.584	-3.8349e+007	-9.8456e+006
4.000s	123.581	-2.0161e+007	eliminated
5.000s	123.581	4.8112e+006	eliminated
10.000s	123.584	6.3584e+007	1.5154e+007
15.000s	123.584	9.3356e+007	2.2809e+007
20.000s	123.584	1.0802e+008	2.4707e+007
30.000s	123.584	1.1757e+008	2.5834e+007

15 points for Peak 20, Peak Point at 123.170 ppm
Results Comp. 1

I[0] = 9.347e-001
P = -2.054e+000
T1 = 690.041m
SD = 4.795e-002

tau	ppm	integral	intensity
100.000m	123.170	-1.4682e+008	-4.5814e+007
200.000m	123.170	-9.8664e+007	-3.1981e+007
300.000m	123.170	-7.1042e+007	-2.192e+007
400.000m	123.170	-5.285e+007	-1.5625e+007
500.000m	123.170	-1.3365e+007	eliminated
700.000m	123.169	3.7777e+007	1.042e+007
900.000m	123.170	7.4329e+007	2.0917e+007
1.000s	123.170	8.5371e+007	2.4972e+007
2.000s	123.170	1.7461e+008	4.9085e+007
3.000s	123.170	2.0087e+008	5.4177e+007
4.000s	123.170	2.0469e+008	5.3832e+007
5.000s	123.170	2.1485e+008	5.5455e+007
10.000s	123.170	1.9816e+008	4.9902e+007
15.000s	123.171	2.073e+008	5.0406e+007
20.000s	123.171	1.956e+008	4.6707e+007
30.000s	123.171	2.0489e+008	4.8442e+007

15 points for Peak 21, Peak Point at 123.086 ppm
Results Comp. 1

I[0] = 9.597e-001
P = -2.138e+000
T1 = 681.544m
SD = 4.506e-002

tau	ppm	integral	intensity
100.000m	123.086	-1.5072e+008	-4.7194e+007
200.000m	123.086	-1.0771e+008	-3.3844e+007
300.000m	123.086	-8.2298e+007	-2.3865e+007
400.000m	123.086	-4.7412e+007	-1.4036e+007
500.000m	123.086	-7.4753e+006	eliminated
700.000m	123.085	3.774e+007	1.0504e+007
900.000m	123.085	7.2016e+007	2.1325e+007
1.000s	123.086	8.1538e+007	2.4354e+007
2.000s	123.086	1.806e+008	5.0185e+007
3.000s	123.086	1.9612e+008	5.4541e+007
4.000s	123.086	2.0799e+008	5.4457e+007
5.000s	123.086	2.0568e+008	5.3671e+007
10.000s	123.086	2.0722e+008	5.2443e+007
15.000s	123.086	2.1269e+008	5.1495e+007
20.000s	123.086	2.0457e+008	4.9554e+007
30.000s	123.086	1.9249e+008	4.619e+007

15 points for Peak 22, Peak Point at 62.180 ppm
Results Comp. 1

I[0] = 9.667e-001
P = -1.936e+000
T1 = 2.486s
SD = 3.360e-002

tau	ppm	integral	intensity
100.000m	62.179	-1.3827e+008	-4.1488e+007
200.000m	62.179	-1.3222e+008	-4.0709e+007
300.000m	62.179	-1.1843e+008	-3.669e+007
400.000m	62.179	-1.0654e+008	-3.2376e+007
500.000m	62.179	-1.0439e+008	-3.1075e+007
700.000m	62.179	-8.3326e+007	-2.4148e+007
900.000m	62.178	-4.7307e+007	-1.5302e+007
1.000s	62.179	-5.0608e+007	-1.4289e+007

2.000s	62.180	1.2939e+007	eliminated
3.000s	62.179	6.4462e+007	1.7929e+007
4.000s	62.179	9.9603e+007	2.6532e+007
5.000s	62.179	1.2683e+008	3.2834e+007
10.000s	62.179	1.8856e+008	4.7455e+007
15.000s	62.180	1.9012e+008	4.7809e+007
20.000s	62.180	1.9269e+008	4.5299e+007
30.000s	62.180	1.8989e+008	4.3841e+007

15 points for Peak 23, Peak Point at 61.615 ppm
Results Comp. 1

I[0] = 9.879e-001
P = -2.020e+000
T1 = 2.860s
SD = 2.688e-002

tau	ppm	integral	intensity
100.000m	61.615	-1.477e+008	-4.9562e+007
200.000m	61.615	-1.2876e+008	-4.269e+007
300.000m	61.615	-1.2183e+008	-4.0352e+007
400.000m	61.615	-1.2224e+008	-3.9105e+007
500.000m	61.614	-1.1735e+008	-3.6638e+007
700.000m	61.614	-8.8197e+007	-2.8197e+007
900.000m	61.614	-7.6991e+007	-2.4231e+007
1.000s	61.614	-6.5076e+007	-2.0766e+007
2.000s	61.615	5.0565e+006	eliminated
3.000s	61.614	5.7447e+007	1.5442e+007
4.000s	61.615	8.7757e+007	2.3131e+007
5.000s	61.615	1.073e+008	2.9497e+007
10.000s	61.615	1.7733e+008	4.7625e+007
15.000s	61.615	1.9654e+008	4.9581e+007
20.000s	61.615	2.0088e+008	4.8812e+007
30.000s	61.615	2.0526e+008	4.7534e+007

14 points for Peak 24, Peak Point at 30.633 ppm
Results Comp. 1

I[0] = 9.376e-001

P = -1.543e+000
T1 = 956.980m
SD = 4.042e-002

tau	ppm	integral	intensity
100.000m	30.635	-9.1664e+007	-2.4917e+007
200.000m	30.636	-6.107e+007	-1.7537e+007
300.000m	30.635	-3.777e+007	-1.1176e+007
400.000m	30.633	-7.5893e+006	eliminated
500.000m	30.633	6.4863e+006	eliminated
700.000m	30.635	3.684e+007	1.0468e+007
900.000m	30.635	6.4236e+007	1.8606e+007
1.000s	30.635	8.5781e+007	2.1711e+007
2.000s	30.635	1.6265e+008	4.188e+007
3.000s	30.635	2.0399e+008	5.1363e+007
4.000s	30.636	2.2644e+008	5.6578e+007
5.000s	30.636	2.2891e+008	5.4312e+007
10.000s	30.636	2.3316e+008	5.4149e+007
15.000s	30.636	2.3505e+008	5.3475e+007
20.000s	30.637	2.317e+008	4.8532e+007
30.000s	30.637	2.2323e+008	4.8737e+007

14 points for Peak 25, Peak Point at 24.165 ppm
Results Comp. 1

I[0] = 9.591e-001
P = -1.517e+000
T1 = 671.233m
SD = 4.941e-002

tau	ppm	integral	intensity
100.000m	24.165	-6.7766e+007	-2.046e+007
200.000m	24.165	-3.3977e+007	-9.7086e+006
300.000m	24.165	-1.0649e+007	eliminated
400.000m	24.165	1.5742e+007	eliminated
500.000m	24.164	4.0628e+007	1.2999e+007
700.000m	24.164	7.6466e+007	2.3242e+007
900.000m	24.164	1.1773e+008	3.4289e+007
1.000s	24.165	1.3352e+008	3.9517e+007
2.000s	24.164	2.0665e+008	5.9107e+007

3.000s	24.165	2.2016e+008	6.1475e+007
4.000s	24.165	2.324e+008	6.0702e+007
5.000s	24.165	2.3436e+008	6.1289e+007
10.000s	24.165	2.375e+008	6.0932e+007
15.000s	24.165	2.3094e+008	5.6696e+007
20.000s	24.165	2.2932e+008	5.4233e+007
30.000s	24.166	2.2492e+008	5.2894e+007

15 points for Peak 26, Peak Point at 23.798 ppm
Results Comp. 1

I[0] = 9.596e-001
P = -1.507e+000
T1 = 709.662m
SD = 3.423e-002

tau	ppm	integral	intensity
100.000m	23.798	-6.5403e+007	-2.0251e+007
200.000m	23.798	-4.2017e+007	-1.1542e+007
300.000m	23.798	-2.7836e+006	eliminated
400.000m	23.798	1.9939e+007	5.6332e+006
500.000m	23.797	4.1769e+007	1.2001e+007
700.000m	23.797	8.6284e+007	2.5031e+007
900.000m	23.797	1.2218e+008	3.3476e+007
1.000s	23.798	1.3329e+008	3.6246e+007
2.000s	23.798	2.1396e+008	5.7461e+007
3.000s	23.798	2.3859e+008	6.2091e+007
4.000s	23.798	2.5362e+008	6.2449e+007
5.000s	23.798	2.4619e+008	6.041e+007
10.000s	23.798	2.5138e+008	5.9945e+007
15.000s	23.798	2.541e+008	5.896e+007
20.000s	23.798	2.501e+008	5.7199e+007
30.000s	23.798	2.5089e+008	5.5076e+007

14 points for Peak 27, Peak Point at 20.092 ppm
Results Comp. 1

I[0] = 9.750e-001
P = -1.500e+000

T1 = 2.833s
SD = 2.156e-002

tau	ppm	integral	intensity
100.000m	20.095	-7.7169e+007	-2.794e+007
200.000m	20.094	-8.0854e+007	-2.5714e+007
300.000m	20.094	-6.7349e+007	-2.2359e+007
400.000m	20.094	-6.4743e+007	-2.0463e+007
500.000m	20.094	-5.0085e+007	-1.604e+007
700.000m	20.093	-3.3876e+007	-1.1735e+007
900.000m	20.092	-1.2229e+007	eliminated
1.000s	20.092	-8.7148e+006	eliminated
2.000s	20.094	4.8198e+007	1.3522e+007
3.000s	20.094	9.8188e+007	2.7798e+007
4.000s	20.095	1.223e+008	3.4163e+007
5.000s	20.095	1.6164e+008	4.5097e+007
10.000s	20.095	2.0868e+008	5.7601e+007
15.000s	20.095	2.0705e+008	5.6673e+007
20.000s	20.095	2.2697e+008	5.9968e+007
30.000s	20.095	2.1707e+008	5.6516e+007

4.4.12 ORTEP Drawings of X-ray Crystal Structures

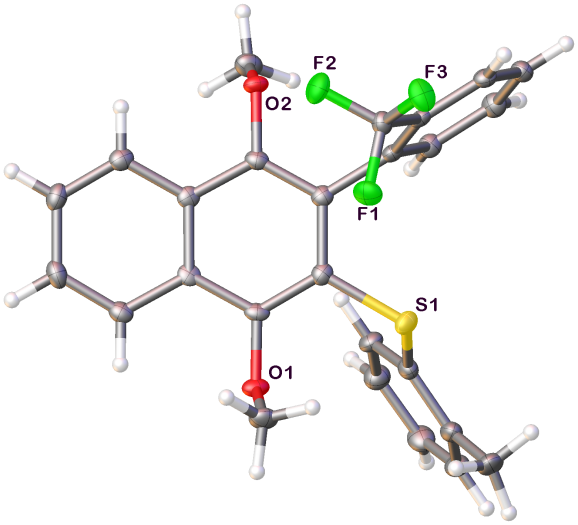

Figure 4.4.269. X-Ray crystal structure of 4.2b (ellipsoids at 50% probability level)

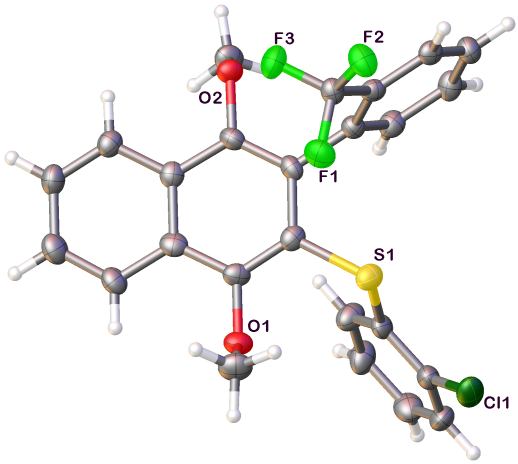

Figure 4.4.270. X-ray crystal structure of 4.2f (ellipsoids at 50% probability level)

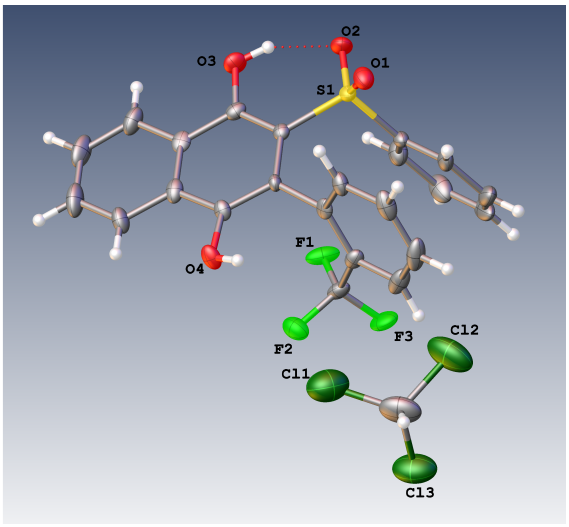

Figure 4.4.271. X-ray crystal structure of 4.5a (ellipsoids at 50% probability level)

4.5. Acknowledgements

The contents in Chapter 4 are a reformatted reprint of the following manuscript, with permission from the American Chemical Society: Maddox, S. M.; Dawson, G. A.; Rochester, N. C.; Ayonon, A. B.; Moore, C. E.; Rheingold, A. L.; Gustafson, J. L. "Atroposelective Dynamic Kinetic Resolution of Aryl-Naphthoquinones via the Addition of Thiophenols" *ACS Catal.* **2018**, *8*, 5443. The dissertation author was the primary researcher for the data presented. Support of this work by the National Institute of General Medical Sciences is acknowledged (R35GM124637).

References

(1) Kelsey, F. O. Thalidomide Update: Regulatory Aspects. *Teratology* **1988**, *38*, 221–226.

(2) Department of Health & Human Services, Food and Drug Administration: FDA's Policy Statement for the Development of New Stereoisomeric Drugs http://www.fda.gov/drugs/GuidanceComplianceRegulatoryInformation/Guidances/ucm122883.htm.

(3) Teo, S. K.; Colburn, W. A.; Tracewell, W. G.; Kook, K. A.; Stirling, D. I.; Jaworsky, M. S.; Scheffler, M. A.; Thomas, S. D.; Laskin, O. L. Clinical Pharmacokinetics of Thalidomide. *Clin. Pharmacokinet.* **2004**, *43*, 311–327.

(4) Eriksson, T.; Björkman, S.; Roth, B.; Höglund, P. Intravenous Formulations of the Enantiomers of Thalidomide: Pharmacokinetic and Initial Pharmacodynamic Characterization in Man. *J. Pharm. Pharmacol.* **2000**, *52*, 807–817.

(5) Eriksson, T.; Björkman, S.; Roth, B.; Fyge, Å.; Höglund, P. Enantiomers of Thalidomide: Blood Distribution and the Influence of Serum Albumin on Chiral Inversion and Hydrolysis. *Chirality* **1998**, *10*, 223–228.

(6) Jacques, V.; Czarnik, A. W.; Judge, T. M.; Ploeg, L. H. T. Van Der; Dewitt, S. H.; Jacques, V.; Czarnik, A. W.; Judge, T. M.; Ploeg, L. H. T. Van Der; Dewitt, S. H. Differentiation of Antiinflammatory and Antitumorigenic Properties of Stabilized Enantiomers of Thalidomide Analogs: Fig. 1. *Proc. Natl. Acad. Sci.* **2015**, *112*, E1471–E1479.

(7) Yoon, T. P.; Jacobsen, E. N. Privileged Chiral Catalysts. *Science* **2003**, *299*, 1691–1693.

(8) Hughes, Chambers, C.; Kauffman, C. A.; Jensen, P. R.; Fenical, W. Structures, Reactivities, and Antibiotic Properties of the Marinopyrroles A-F. *J. Org. Chem.* **2010**, *75*, 3240–3250.

(9) LaPlante, S. R.; Edwards, P. J.; Fader, L. D.; Jakalian, A.; Hucke, O. Revealing Atropisomer Axial Chirality in Drug Discovery. *ChemMedChem* **2011**, *6*, 505–513.

(10) Toenjes, S. T.; Gustafson, J. L. Atropisomerism in Medicinal Chemistry : Challenges and Opportunities. *Future Med. Chem.* **2018**, *10*, 409–422.

(11) Brown, D. G.; Boström, J. Analysis of Past and Present Synthetic Methodologies on Medicinal Chemistry: Where Have All the New Reactions Gone? *J. Med. Chem.* **2016**, *59*, 4443–4458.

(12) Zask, A.; Murphy, J.; Ellestad, G. A. Biological Stereoselectivity of Atropisomeric Natural Products and Drugs. *Chirality* **2013**, *25*, 265–274.

(13) Cohen, P. Protein Kinases--the Major Drug Targets of the Twenty-First Century? *Nat. Rev.*

Drug Discov. **2002**, *1*, 309–315.

(14) Liu, Y.; Bishop, A.; Witucki, L.; Kraybill, B.; Shimizu, E.; Tsien, J.; Ubersax, J.; Blethrow, J.; Morgan, D. O.; Shokat, K. M. Structural Basis for Selective Inhibition of Src Family Kinases by PP1. *Chem. Biol.* **1999**, *6*, 671–678.

(15) Smith, D. E.; Marquez, I.; Lokensgard, M. E.; Rheingold, A. L.; Hecht, D. A.; Gustafson, J. L. Exploiting Atropisomerism to Increase the Target Selectivity of Kinase Inhibitors. *Angew. Chem, Int. Ed.* **2015**, *54*, 11754–11759.

(16) Liu, Q.; Sabnis, Y.; Zhao, Z.; Zhang, T.; Buhrlage, S. J.; Jones, L. H.; Gray, N. S. Developing Irreversible Inhibitors of the Protein Kinase Cysteinome. *Chem. Biol.* **2013**, *20*, 146–159.

(17) Honigberg, L. a; Smith, A. M.; Sirisawad, M.; Verner, E.; Loury, D.; Chang, B.; Li, S.; Pan, Z.; Thamm, D. H.; Miller, R. a; Buggy, J. J. The Bruton Tyrosine Kinase Inhibitor PCI-32765 Blocks B-Cell Activation and Is Efficacious in Models of Autoimmune Disease and B-Cell Malignancy. *Proc. Natl. Acad. Sci. U. S. A.* **2010**, *107*, 13075–13080.

(18) Woyach, J. A.; Furman, R. R.; Liu, T.-M.; Ozer, H. G.; Zapatka, M.; Ruppert, A. S.; Xue, L.; Li, D. H.-H.; Steggerda, S. M.; Versele, M.; Dave, S. S.; Zhang, J.; Yilmaz, A. S.; Jaglowski, S. M.; Blum, K. A.; Lozanski, A.; Lozanski, G.; James, D. F.; Barrientos, J. C.; Lichter, P.; Stilgenbauer, S.; Buggy, J. J.; Chang, B. Y.; Johnson, A. J.; Byrd, J. C. Resistance Mechanisms for the Bruton's Tyrosine Kinase Inhibitor Ibrutinib. *N. Engl. J. Med.* **2014**, *370*, 2286–2294.

(19) Huang, D.; Zhou, T.; Lafleur, K.; Nevado, C.; Caflisch, A. Kinase Selectivity Potential for Inhibitors Targeting the ATP Binding Site: A Network Analysis. *Bioinformatics* **2010**, *26*, 198–204.

(20) Clayden, J.; Moran, W. J.; Edwards, P. J.; LaPlante, S. R. The Challenge of Atropisomerism in Drug Discovery. *Angew. Chem, Int. Ed.* **2009**, *48*, 6398–6401.

(21) Watterson, S. H.; De Lucca, G. V.; Shi, Q.; Langevine, C. M.; Liu, Q.; Batt, D. G.; Beaudoin Bertrand, M.; Gong, H.; Dai, J.; Yip, S.; Li, P.; Sun, D.; Wu, D. R.; Wang, C.; Zhang, Y.; Traeger, S. C.; Pattoli, M. A.; Skala, S.; Cheng, L.; Obermeier, M. T.; Vickery, R.; Discenza, L. N.; D'Arienzo, C. J.; Zhang, Y.; Heimrich, E.; Gillooly, K. M.; Taylor, T. L.; Pulicicchio, C.; McIntyre, K. W.; Galella, M. A.; Tebben, A. J.; Muckelbauer, J. K.; Chang, C.; Rampulla, R.; Mathur, A.; Salter-Cid, L.; Barrish, J. C.; Carter, P. H.; Fura, A.; Burke, J. R.; Tino, J. A. Discovery of 6-Fluoro-5-(R)-(3-(S)-(8-Fluoro-1-Methyl-2,4-Dioxo-1,2-Dihydroquinazolin-3(4H)-Yl)-2-Methylphenyl)-2-(S)-(2-Hydroxypropan-2-Yl)-2,3,4,9-Tetrahydro-1H-Carbazole-8-Carboxamide (BMS-986142): A Reversible Inhibitor of Bruton's Tyrosine Kinase (BT. *J. Med. Chem.* **2016**, *59*, 9173–9200.

(22) Wang, J.; Zeng, W.; Li, S.; Shen, L.; Gu, Z.; Zhang, Y.; Li, J.; Chen, S.; Jia, X. Discovery and Assessment of Atropisomers of (±)-Lesinurad. *ACS Med. Chem. Lett.* **2017**, *8*, 299–303.

(23) Blakemore, D. C.; Castro, L.; Churcher, I.; Rees, D. C.; Thomas, A. W.; Wilson, D. M.; Wood, A. Organic Synthesis Provides Opportunities to Transform Drug Discovery. *Nat. Chem.* **2018**, *10*.

(24) Cernak, T.; Dykstra, K. D.; Tyagarajan, S.; Vachal, P.; Krska, S. W. The Medicinal Chemist's Toolbox for Late Stage Functionalization of Drug-like Molecules. *Chem. Soc. Rev.* **2016**, *45*, 546.

(25) Voth, A. R.; Ho, P. S. The Role of Halogen Bonding in Inhibitor Recognition and Binding by Protein Kinases. *Current Topics in Medicinal Chemistry*, 2007, *7*, 1336–1348.

(26) Wilcken, R.; Zimmermann, M. O.; Lange, A.; Joerger, A. C.; Boeckler, F. M. Principles and Applications of Halogen Bonding in Medicinal Chemistry and Chemical Biology. *J. Med. Chem.* **2013**, *56*, 1363–1388.

(27) Auffinger, P.; Hays, F. A.; Westhof, E.; Ho, P. S. Halogen Bonds in Biological Molecules. *Proc. Natl. Acad. Sci. U. S. A.* **2004**, *101*, 16789–16794.

(28) McGrath, N. A.; Brichacek, M.; Njardarson, J. T. A Graphical Journey of Innovative Organic Architectures That Have Improved Our Lives. *J. Chem. Educ.* **2010**, *87*, 1348–1349.

(29) Flick, A. C.; Ding, H. X.; Leverett, C. A.; Kyne, R. E.; Liu, K. K. C.; Fink, S. J.; O'Donnell, C. J. Synthetic Approaches to the New Drugs Approved During 2015. *J. Med. Chem.* **2017**, *60*, 6480–6515.

(30) Surry, D. S.; Buchwald, S. L. Dialkylbiaryl Phosphines in Pd-Catalyzed Amination: A User's Guide. *Chem. Sci.* **2011**, *2*, 27.

(31) Martin, R.; Buchwald, S. L. Palladium-Catalyzed Suzuki− Miyaura Cross-Coupling Reactions Employing Dialkylbiaryl Phosphine Ligands. *Acc. Chem. Res.* **2008**, *41*, 1461–1473.

(32) Cho, E. J.; Senecal, T. D.; Kinzel, T.; Zhang, Y.; Watson, D. a; Buchwald, S. L. The Palladium-Catalyzed Trifluoromethylation of Aryl Chlorides. *Science* **2010**, *328*, 1679–1681.

(33) Fu, G. C. Transition-Metal Catalysis of Nucleophilic Substitution Reactions: A Radical Alternative to S N 1 and S N 2 Processes. *ACS Cent. Sci.* **2017**, *3*, 692–700.

(34) Choi, J.; Fu, G. C. Transition Metal–Catalyzed Alkyl-Alkyl Bond Formation: Another Dimension in Cross-Coupling Chemistry. *Science* **2017**, *356*, 152–160.

(35) Zapf, A.; Beller, M. The Development of Efficient Catalysts for Palladium-Catalyzed Coupling Reactions of Aryl Halides. *Chem. Commun.* **2005**, 431.

(36) Düfert, M. A.; Billingsley, K. L.; Buchwald, S. L. Suzuki-Miyaura Cross-Coupling of Unprotected, Nitrogen-Rich Heterocycles: Substrate Scope and Mechanistic Investigation.

J. Am. Chem. Soc. **2013**, *135*, 12877–12885.

(37) Park, N. H.; Vinogradova, E. V.; Surry, D. S.; Buchwald, S. L. Design of New Ligands for the Palladium-Catalyzed Arylation of α-Branched Secondary Amines. *Angew. Chemie, Int. Ed.* **2015**, *54*, 8259–8262.

(38) Shi, L.; Zhang, D.; Lin, R.; Zhang, C.; Li, X.; Jiao, N. The Direct C-H Halogenations of Indoles. *Tetrahedron Lett.* **2014**, *55*, 2243–2245.

(39) Prebil, R.; Laali, K. K.; Stavber, S. Metal and H2O2 Free Aerobic Oxidative Aromatic Halogenation with [RNH3(+)] [NO3(-)]/HX and [BMIM(SO3H)][NO3)x(X)y] (X = Br, Cl) as Multifunctional Ionic Liquids. *Org. Lett.* **2013**, *15*, 2108–2111.

(40) Payne, J. T.; Andorfer, M. C.; Lewis, J. C. Regioselective Arene Halogenation Using the FAD-Dependent Halogenase RebH. *Angew. Chem. Int. Ed. Engl.* **2013**, *52*, 5271–5274.

(41) Andorfer, M. C.; Park, H. J.; Vergara-Coll, J.; Lewis, J. C. Directed Evolution of RebH for Catalyst-Controlled Halogenation of Indole C–H Bonds. *Chem. Sci.* **2016**, *7*, 3720–3729.

(42) Payne, J. T.; Lewis, J. C. Upgrading Nature's Tools: Expression Enhancement and Preparative Utility of the Halogenase RebH. *Synlett* **2014**, *25*, 1345–1349.

(43) Mitchell, R. H.; Lai, Y.-H.; Williams, R. V. N-Bromosuccinimide-Dimethylformamide: A Mild, Selective Nuclear Monobromination Reagent for Reactive Aromatic Compounds. *J. Org. Chem.* **1979**, *44*, 4733–4735.

(44) Gilow, H. M.; Burton, D. E. Bromination and Chlorination of Pyrrole and Some Reactive 1-Substituted Pyrroles. *J. Org. Chem.* **1981**, *46*, 2221–2225.

(45) Gruter, G. J. M.; Akkerman, O. S.; Bickelhaupt, F. Nuclear versus Side-Chain Bromination of Methyl-Substituted Anisoles by N-Bromosuccinimide. *J. Org. Chem.* **1994**, *59*, 4473–4481.

(46) Lambert, F. L.; Ellis, W. D.; Parry, R. J. Halogenation of Aromatic Compounds by N-Bromo- and N-Chlorosuccinimide under Ionic Conditions. *J. Org. Chem.* **1965**, *30*, 304–306.

(47) Prakash, G. K. S.; Mathew, T.; Hoole, D.; Esteves, P. M.; Wang, Q.; Rasul, G.; Olah, G. A. *N* -Halosuccinimide/BF_3 −H_2O, Efficient Electrophilic Halogenating Systems for Aromatics. *J. Am. Chem. Soc.* **2004**, *126*, 15770–15776.

(48) Zhang, Y.; Shibatomi, K.; Yamamoto, H. Lewis Acid Catalyzed Highly Selective Halogenation of Aromatic Compounds. *Synlett* **2005**, 2837–2842.

(49) Zhang, R.; Huang, L.; Zhang, Y.; Chen, X.; Xing, W.; Huang, J. Silver Catalyzed Bromination of Aromatics with N-Bromosuccinimide. *Catal. Letters* **2012**, *142*, 378–383.

(50) Al-Zoubi, R. M.; Hall, D. G. Mild Silver (I)-Mediated Regioselective Iodination and

Bromination of Arylboronic Acids. *Org. Lett.* **2010**, *12*, 2480–2483.

(51) Mori, K.; Ichikawa, Y.; Kobayashi, M.; Shibata, Y.; Yamanaka, M.; Akiyama, T. Enantioselective Synthesis of Multisubstituted Biaryl Skeleton by Chiral Phosphoric Acid Catalyzed Desymmetrization/Kinetic Resolution Sequence. *J. Am. Chem. Soc.* **2013**, *135*, 3964–3970.

(52) Mo, F.; Yan, J. M.; Qiu, D.; Li, F.; Zhang, Y.; Wang, J. Gold-Catalyzed Halogenation of Aromatics by N-Halosuccinimides. *Angew. Chem. Int. Ed. Engl.* **2010**, *49*, 2028–2032.

(53) Chan, K. S. L.; Wasa, M.; Wang, X.; Yu, J. Q. Palladium(II)-Catalyzed Selective Monofluorination of Benzoic Acids Using a Practical Auxiliary: A Weak-Coordination Approach. *Angew. Chem, Int. Ed.* **2011**, *50*, 9081–9084.

(54) Chu, L.; Wang, X. C.; Moore, C. E.; Rheingold, A. L.; Yu, J. Q. Pd-Catalyzed Enantioselective C-H Iodination: Asymmetric Synthesis of Chiral Diarylmethylamines. *J. Am. Chem. Soc.* **2013**, *135*, 16344–16347.

(55) Kalyani, D.; Dick, A. R.; Anani, W. Q.; Sanford, M. S. A Simple Catalytic Method for the Regioselective Halogenation of Arenes. *Org. Lett.* **2006**, *8*, 2523–2526.

(56) Du, Z. J.; Gao, L. X.; Lin, Y. J.; Han, F. S. Cu-Mediated Direct Aryl C - H Halogenation: A Strategy to Control Mono- and Di-Selectivity. *ChemCatChem* **2014**, *6*, 123–126.

(57) Tian, Q.; Chen, X.; Liu, W.; Wang, Z.; Shi, S.; Kuang, C. Regioselective Halogenation of 2-Substituted-1,2,3-Triazoles via Sp2 C–H Activation. *Org. Biomol. Chem.* **2013**, *11*, 7830.

(58) Rodriguez, R. A.; Pan, C.-M.; Yabe, Y.; Kawamata, Y.; Eastgate, M. D.; Baran, P. S. Palau'chlor: A Practical and Reactive Chlorinating Reagent. *J. Am. Chem. Soc.* **2014**, *136*, 6908–6911.

(59) Wang, M.; Zhang, Y.; Wang, T.; Wang, C.; Xue, D.; Xiao, J. Story of an Age-Old Reagent: An Electrophilic Chlorination of Arenes and Heterocycles by 1‐Chloro-1,2-Benziodoxol-3-One. *Org. Lett.* **2016**, *18*, 1976–1979.

(60) Denmark, S. E.; Beutner, G. L. Lewis Base Catalysis in Organic Synthesis. *Angew. Chem, Int. Ed.* **2008**, *47*, 1560–1638.

(61) Gutmann, V. Empirical Approach to Molecular Interactions. *Coord. Chem. Rev.* **1975**, *15*, 207–237.

(62) Denmark, S. E.; Kuester, W. E.; Burk, M. T. Catalytic, Asymmetric Halofunctionalization of Alkenes--a Critical Perspective. *Angew. Chem. Int. Ed. Engl.* **2012**, *51*, 10938–10953.

(63) Denmark, S. E.; Burk, M. T. Lewis Base Catalysis of Bromo- and Iodolactonization, and Cycloetherification. *Proc. Natl. Acad. Sci.* **2010**, *107*, 20655–20660.

(64) Snyder, S. a; Treitler, D. S.; Brucks, A. P. Simple Reagents for Direct Halonium-Induced

Polyene Cyclizations. *J. Am. Chem. Soc.* **2010**, *132*, 14303–14314.

(65) Ke, Z.; Tan, C. K.; Chen, F.; Yeung, Y.-Y. Catalytic Asymmetric Bromoetherification and Desymmetrization of Olefinic 1,3-Diols with C2-Symmetric Sulfides. *J. Am. Chem. Soc.* **2014**, *136*, 5627–5630.

(66) Tay, D. W.; Leung, G. Y. C.; Yeung, Y.-Y. Desymmetrization of Diolefinic Diols by Enantioselective Amino-Thiocarbamate-Catalyzed Bromoetherification: Synthesis of Chiral Spirocycles. *Angew. Chem, Int. Ed.* **2014**, *53*, 5161–5164.

(67) Tay, D. W.; Tsoi, I. T.; Er, J. C.; Leung, G. Y. C.; Yeung, Y. Y. Lewis Basic Selenium Catalyzed Chloroamidation of Olefins Using Nitriles as the Nucleophiles. *Org. Lett.* **2013**, *15*, 1310–1313.

(68) Cohen, M. S.; Zhang, C.; Shokat, K. M.; Taunton, J. Structural Bioinformatics-Based Design of Selective, Irreversible Kinase Inhibitors. *Science (80-.).* **2005**, *308*, 1318–1321.

(69) Rafferty, P.; Twigger, H. L.; Johnston, D. N.; Arnold, L.; Calderwood, D. J. Pyrrolo[2,3]Pyrimidines and Their Uses as Tyrosine Kinase Inhibitors. WO98/41525, 1998.

(70) Welsch, M. E.; Snyder, S. A.; Stockwell, B. R. Privileged Scaffolds for Library Design and Drug Discovery. *Curr. Opin. Chem. Biol.* **2010**, *14*, 347–361.

(71) Smith, J. R. L.; McKeer, L. C. High Site-Selectivity in the Chlorination of Electron-Rich Aromatic Compounds by N-Chloroammonium Salts. *Tetrahedron Lett.* **1983**, *24*, 3117–3120.

(72) Watson, W. D. Regioselective Para-Chlorination of Activated Aromatic Compounds. *J. Org. Chem.* **1985**, *50*, 2145–2148.

(73) Gnaim, J. M.; Sheldon, R. A. Highly Regioselective Ortho-Chlorination of Phenol with Sulfuryl Chloride in the Presence of Amines. *Tetrahedron Lett.* **1995**, *36*, 3893–3896.

(74) Qian, G.; Hong, X.; Liu, B.; Mao, H.; Xu, B. Rhodium-Catalyzed Regioselective C − H Chlorination of 7‐Azaindoles Using 1,2-Dichloroethane. *Org. Lett.* **2014**, *16*, 5294–5297.

(75) Guo, H.; Chen, M.; Jiang, P.; Chen, J.; Pan, L.; Wang, M.; Xie, C.; Zhang, Y. Copper and Palladium Mediated C–H Chlorination on 8-Acylaminoquinoline Scaffolds. *Tetrahedron* **2015**, *71*, 70–76.

(76) Neufeldt, S. R.; Sanford, M. S. Controlling Site Selectivity in Palladium- Catalyzed C-H Bond Functionalization. *Acc. Chem. Res.* **2012**, *45*, 936–946.

(77) Maddox, S. M.; Nalbandian, C. J.; Smith, D. E.; Gustafson, J. L. A Practical Lewis Base Catalyzed Electrophilic Chlorination of Arenes and Heterocycles. *Org. Lett.* **2015**, *17*, 1042–1045.

(78) Bovonsombat, P.; Sophanpanichkul, P.; Pandey, A.; Tungsirisurp, S.; Limthavornlit, P.;

Chobtumskul, K.; Kuhataparuk, P.; Sathityatiwat, S.; Teecomegaet, P. Novel Regioselective Aromatic Chlorination via Catalytic Thiourea Activation of N-Chlorosuccinimide. *Tetrahedron Lett.* **2015**, *56*, 2193–2196.

(79) Samanta, R. C.; Yamamoto, H. Selective Halogenation Using an Aniline Catalyst. *Chem. - Eur. J.* **2015**, *21*, 11976–11979.

(80) Pathak, T. P.; Miller, S. J. Site-Selective Bromination of Vancomycin. *J. Am. Chem. Soc.* **2012**, *134*, 6120–6123.

(81) Giuliano, M. W.; Miller, S. J. Site-Selective Reactions with Peptide-Based Catalysts. In *Site-Selective Catalysis*; Kawabata, T., Ed.; Springer International Publishing: Cham, 2016; pp. 157–201.

(82) Lyons, T. W.; Sanford, M. S. Palladium-Catalyzed Ligand-Directed C-H Functionalization Reactions. *Chem. Rev.* **2010**, *110*, 1147–1169.

(83) Yang, Y. F.; Chen, G.; Hong, X.; Yu, J. Q.; Houk, K. N. The Origins of Dramatic Differences in Five-Membered vs Six-Membered Chelation of Pd(II) on Efficiency of C(Sp3)-H Bond Activation. *J. Am. Chem. Soc.* **2017**, *139*, 8514–8521.

(84) O'Duill, M. L.; Matsuura, R.; Wang, Y.; Turnbull, J. L.; Gurak, J. A.; Gao, D. W.; Lu, G.; Liu, P.; Engle, K. M. Tridentate Directing Groups Stabilize 6-Membered Palladacycles in Catalytic Alkene Hydrofunctionalization. *J. Am. Chem. Soc.* **2017**, *139*, 15576–15579.

(85) Mei, T. S.; Giri, R.; Maugel, N.; Yu, J. Q. PdII-Catalyzed Monoselective Ortho Halogenation of C-H Bonds Assisted by Counter Cations: A Complementary Method to Directed Ortho Lithiation. *Angew. Chem, Int. Ed.* **2008**, *47*, 5215–5219.

(86) Wang, L.; Chen, W.; Shao, Z.; Liu, S.; Yu, Y. Selective Halogenation of Arylurea Derivatives by Pd-Catalyzed C-H Activation. *Curr. Org. Chem.* **2013**, *17*, 3092–3096.

(87) Engle, K. M.; Mei, T.; Wasa, M.; Yu, J. Developing Broadly Useful C-H Functionalization Reactions. *Acc. Chem. Res.* **2012**, *45*, 788–802.

(88) Leow, D.; Li, G.; Mei, T.-S.; Yu, J.-Q. Activation of Remote Meta-C–H Bonds Assisted by an End-on Template. *Nature* **2012**, *486*, 518–522.

(89) Tang, R.-Y.; Li, G.; Yu, J.-Q. Conformation-Induced Remote Meta-C–H Activation of Amines. *Nature* **2014**, *507*, 215–220.

(90) Zhang, Z.; Tanaka, K.; Yu, J.-Q. Remote Site-Selective C–H Activation Directed by a Catalytic Bifunctional Template. *Nature* **2017**, *543*, 538–542.

(91) Xu, H.; Shang, M.; Dai, H. X.; Yu, J. Q. Ligand-Controlled Para-Selective C-H Arylation of Monosubstituted Arenes. *Org. Lett.* **2015**, *17*, 3830–3833.

(92) Tan, C. K.; Yeung, Y.-Y. Recent Advances in Stereoselective Bromofunctionalization of

Alkenes Using N-Bromoamide Reagents. *Chem. Commun. (Camb).* **2013**, *49*, 7985–7996.

(93) Wong, Y. C.; Ke, Z.; Yeung, Y.-Y. Lewis Basic Sulfide Catalyzed Electrophilic Bromocyclization of Cyclopropylmethyl Amide. *Org. Lett.* **2015**, *17*, 4944–4947.

(94) Ke, Z.; Wong, Y. C.; See, J. Y.; Yeung, Y.-Y. Electrophilic Bromolactonization of Cyclopropyl Carboxylic Acids Using Lewis Basic Sulfide Catalyst. *Adv. Synth. Catal.* **2016**, *358*, 1719–1724.

(95) Quin, L. D.; Williams, A. *Practical Interpretation of P-31 NMR Spectra and Computer AssistedStructure Verification*; Advanced Chemistry Development, Inc., 2004.

(96) Ashtekar, K. D.; Marzijarani, N. S.; Jaganathan, A.; Holmes, D.; Jackson, J. E.; Borhan, B. A New Tool To Guide Halofunctionalization Reactions: The Halenium Affinity (HalA) Scale. *J. Am. Chem. Soc.* **2014**, *136*, 13355–13362.

(97) Gnaim, J. M.; Sheldon, R. A. Selective Ortho-Chlorination of Phenol Using Sulfuryl Chloride in the Presence of t-Butylaminomethyl Polystyrene as a Heterogeneous Amine Catalyst. *Tetrahedron Lett.* **2004**, *45*, 8471–8473.

(98) Yu, M.; Snider, B. B. Syntheses of Chloroisosulochrin and Isosulochrin and Biomimetic Elaboration to Maldoxin, Maldoxone, Dihydromaldoxin, and Dechlorodihydromaldoxin. *Org. Lett.* **2011**, *13*, 4224–4227.

(99) Xiong, X.; Yeung, Y.-Y. Ammonium Salt-Catalyzed Highly Practical Ortho -Selective Monohalogenation and Phenylselenation of Phenols: Scope and Applications. *ACS Catal.* **2018**, *8*, 4033–4043.

(100) Ohkubo, K.; Hirose, K.; Fukuzumi, S. Solvent-Free One-Step Photochemical Hydroxylation of Benzene Derivatives by the Singlet Excited State of 2,3-Dichloro-5,6-Dicyano-p-Benzoquinone Acting as a Super Oxidant. *Chem. - Eur. J.* **2015**, *21*, 2855–2861.

(101) Kotoučová, H.; Strnadová, I.; Kovandová, M.; Chudoba, J.; Dvořáková, H.; Cibulka, R. Biomimetic Aerobic Oxidative Hydroxylation of Arylboronic Acids to Phenols Catalysed by a Flavin Derivative. *Org. Biomol. Chem.* **2014**, *12*, 2137–2142.

(102) Dong, Z.; Le, X.; Liu, Y.; Dong, C.; Ma, J. Metal Organic Framework Derived Magnetic Porous Carbon Composite Supported Gold and Palladium Nanoparticles as Highly Efficient and Recyclable Catalysts for Reduction of 4-Nitrophenol and Hydrodechlorination of 4-Chlorophenol. *J. Mater. Chem. A* **2014**, *2*, 18775–18785.

(103) Keane, M. A.; Gomez-Quero, S.; Cardenas-Lizana, F.; Shen, W. Alumina-Supported Ni-Au: Surface Synergistic Effects in Catalytic Hydrodechlorination. *ChemCatChem* **2009**, *1*, 270–278.

(104) Marzi, E.; Mongin, F.; Spitaleri, A.; Schlosser, M. Fluorophenols and (Trifluoromethyl)Phenols as Substrates of Site-Selective Metalation Reactions: To Protect or Not to Protect. *European J. Org. Chem.* **2001**, 2911–2915.

(105) Townsend, C. A.; Davis, S. G.; Christensen, S. B.; Link, J. C.; Lewis, C. P. Methoxymethyl-Directed Aryl Metalation. Total Synthesis of (.+-.)-Averufin. *J. Am. Chem. Soc.* **1981**, *103*, 6885–6888.

(106) Zhang, Z.; Schreiner, P. R. (Thio)Urea Organocatalysis--What Can Be Learnt from Anion Recognition? *Chem. Soc. Rev.* **2009**, *38*, 1187–1198.

(107) Schreiner, P. R.; Wittkopp, A. H-Bonding Additives Act like Lewis Acid Catalysts. *Org. Lett.* **2002**, *4*, 217–220.

(108) Sohtome, Y.; Tanatani, A.; Hashimoto, Y.; Nagasawa, K. Development of Bis-Thiourea-Type Organocatalyst for Asymmetric Baylis–Hillman Reaction. *Tetrahedron Lett.* **2004**, *45*, 5589–5592.

(109) Mittal, N.; Lippert, K. M.; De, C. K.; Klauber, E. G.; Emge, T. J.; Schreiner, P. R.; Seidel, D. A Dual-Catalysis Anion-Binding Approach to the Kinetic Resolution of Amines: Insights into the Mechanism via a Combined Experimental and Computational Study. *J. Am. Chem. Soc.* **2015**, *137*, 5748–5758.

(110) Busschaert, N.; Kirby, I. L.; Young, S.; Coles, S. J.; Horton, P. N.; Light, M. E.; Gale, P. A. Squaramides as Potent Transmembrane Anion Transporters. *Angew. Chemie - Int. Ed.* **2012**, *51*, 4426–4430.

(111) Ghosh, D.; Gupta, N.; Abdi, S. H. R.; Nandi, S.; Khan, N. U. H.; Kureshy, R. I.; Bajaj, H. C. Organocatalyzed Enantioselective Allylation of Isatins by Using a Chiral Amino Alcohol Derived Squaramide as Catalyst. *Eur. J. Org. Chem.* **2015**, *2015*, 2801–2806.

(112) Xu, H. J.; Liang, Y. F.; Cai, Z. Y.; Qi, H. X.; Yang, C. Y.; Feng, Y. S. CuI-Nanoparticles-Catalyzed Selective Synthesis of Phenols, Anilines, and Thiophenols from Aryl Halides in Aqueous Solution. *J. Org. Chem.* **2011**, *76*, 2296–2300.

(113) Magano, J.; Chen, M. H.; Clark, J. D.; Nussbaumer, T. 2-(Diethylamino)Ethanethiol, a New Reagent for the Odorless Deprotection of Aromatic Methyl Ethers. *J. Org. Chem.* **2006**, *71*, 7103–7105.

(114) Pallavicini, M.; Fumagalli, L.; Gobbi, M.; Bolchi, C.; Colleoni, S.; Moroni, B.; Pedretti, a; Rusconi, C.; Vistoli, G.; Valoti, E. QSAR Study for a Novel Series of Ortho Disubstituted Phenoxy Analogues of Alpha1-Adrenoceptor Antagonist WB4101. *Eur. J. Med. Chem.* **2006**, *41*, 1025–1040.

(115) Nagata, R.; Maruta, K.; Iwai, K.; Kitoh, M.; Ushiroda, K.; Yoshida, K. Pyrrole Derivative, EP1386913.

(116) Glunz, P. W. Recent Encounters with Atropisomerism in Drug Discovery. *Bioorg. Med. Chem. Lett.* **2017**, *28*, 53–60.

(117) Bencivenni, G. Organocatalytic Strategies for the Synthesis of Axially Chiral Compounds. *Synlett* **2015**, *26*, 1915–1922.

(118) Bringmann, G.; Menche, D. Atroposelective Total Synthesis of Axially Chiral Biaryl Natural Products. *Chem. Rev.* **2001**, *34*, 615–624.

(119) Bringmann, G.; Price Mortimer, A. J.; Keller, P. A.; Gresser, M. J.; Garner, J.; Breuning, M. Atroposelective Synthesis of Axially Chiral Biaryl Compounds. *Angew. Chem, Int. Ed.* **2005**, *44*, 5384–5427.

(120) Shen, X.; Jones, G. O.; Watson, D. a; Bhayana, B.; Buchwald, S. L. Enantioselective Synthesis of Axially Chiral Biaryls by the Pd-Catalyzed Suzuki-Miyaura Reaction: Substrate Scope and Quantum Mechanical Investigations. *J. Am. Chem. Soc.* **2010**, *132*, 11278–11287.

(121) Hayashi, T.; Hayashizaki, K.; Kiyoi, T.; Ito, Y. Asymmetric Synthesis Catalyzed by Chiral Ferrocenylphosphine-Transition-Metal Complexes. 6. Practical Asymmetric Synthesis of 1,1'-Binaphthyls via Asymmetric Cross-Coupling with a Chiral [(Alkoxyalkyl)Ferrocenyl]Monophosphine/Nickel Catalyst. *J. Am. Chem. Soc.* **1988**, *110*, 8153–8156.

(122) Nicolaou, K. C.; Li, H.; Boddy, C. N. C.; Ramanjulu, J. M.; Yue, T.-Y.; Natarajan, S.; Chu, X.-J.; Bräse, S.; Rübsam, F. Total Synthesis of Vancomycin—Part 1: Design and Development of Methodology. *Chem. Eur. J.* **1999**, *5*, 2584–2601.

(123) Link, A.; Sparr, C. Organocatalytic Atroposelective Aldol Condensation: Synthesis of Axially Chiral Biaryls by Arene Formation. *Angew. Chem, Int. Ed.* **2014**, *53*, 5458–5461.

(124) Fäseke, V. C.; Sparr, C. Stereoselective Arene-Forming Aldol Condensation: Synthesis of Axially Chiral Aromatic Amides. *Angew. Chem, Int. Ed.* **2016**, *55*, 7261–7264.

(125) Jolliffe, J. D.; Armstrong, R. J.; Smith, M. D. Catalytic Enantioselective Synthesis of Atropisomeric Biaryls by a Cation-Directed O-Alkylation. *Nat. Chem.* **2017**, *9*, 558–562.

(126) Gustafson, J. L.; Lim, D.; Miller, S. J. Dynamic Kinetic Resolution of Biaryl Atropisomers via Peptide-Catalyzed Asymmetric Bromination. *Science* **2010**, *328*, 1251–1255.

(127) Barrett, K. T.; Miller, S. J. Enantioselective Synthesis of Atropisomeric Benzamides through Peptide-Catalyzed Bromination. *J. Am. Chem. Soc.* **2013**, *135*, 2963–2966.

(128) Diener, M. E.; Metrano, A. J.; Kusano, S.; Miller, S. J. Enantioselective Synthesis of 3-Arylquinazolin-4(3H)-Ones via Peptide-Catalyzed Atroposelective Bromination. *J. Am. Chem. Soc.* **2015**, *137*, 12369–12377.

(129) Bringmann, G.; Hartung, T. First Atropo-Enantioselective Ring Opening of Achiral Biaryls Containing Lactone Bridges with Chiral Hydride-Transfer Reagents Derived from Borane. *Angew. Chemie, Int. Ed.* **1992**, *31*, 761–762.

(130) Mori, K.; Itakura, T.; Akiyama, T. Enantiodivergent Atroposelective Synthesis of Chiral Biaryls by Asymmetric Transfer Hydrogenation: Chiral Phosphoric Acid Catalyzed Dynamic Kinetic Resolution. *Angew. Chem, Int. Ed.* **2016**, *55*, 11642–11646.

(131) Bhat, V.; Wang, S.; Stoltz, B. M.; Virgil, S. C. Asymmetric Synthesis of QUINAP via Dynamic Kinetic Resolution. *J. Am. Chem. Soc.* **2013**, *135*, 16829–16832.

(132) Verrax, J.; Delvaux, M.; Beghein, N.; Taper, H.; Gallez, B.; Calderon, P. B. Enhancement of Quinone Redox Cycling by Ascorbate Induces a Caspase-3 Independent Cell Death in Human Leukemia Cells. An in Vitro Comparative Study. *Free Radic. Res.* **2005**, *39*, 649–657.

(133) Wang, Y.; Gray, J. P.; Mishin, V.; Heck, D. E.; Laskin, D. L.; Laskin, J. D. Distinct Roles of Cytochrome P450 Reductase in Mitomycin C Redox Cycling and Cytotoxicity. *Mol. Cancer Ther.* **2010**, *9*, 1852–1863.

(134) Chen, Y. H.; Cheng, D. J.; Zhang, J.; Wang, Y.; Liu, X. Y.; Tan, B. Atroposelective Synthesis of Axially Chiral Biaryldiols via Organocatalytic Arylation of 2-Naphthols. *J. Am. Chem. Soc.* **2015**, *137*, 15062–15065.

(135) Moliterno, M.; Cari, R.; Puglisi, A.; Antenucci, A.; Sperandio, C.; Moretti, E.; Di Sabato, A.; Salvio, R.; Bella, M. Quinine-Catalyzed Asymmetric Synthesis of 2,2'-Binaphthol-Type Biaryls Under Mild Reaction Conditions. *Angew. Chem, Int. Ed.* **2016**, *55*, 6525–6529.

(136) Wang, J.-Z.; Zhou, J.; Xu, C.; Sun, H.; Kürti, L.; Xu, Q.-L. Symmetry in Cascade Chirality-Transfer Processes: A Catalytic Atroposelective Direct Arylation Approach to BINOL Derivatives. *J. Am. Chem. Soc.* **2016**, *138*, 5202–5205.

(137) Chen, Y. H.; Qi, L. W.; Fang, F.; Tan, B. Organocatalytic Atroposelective Arylation of 2-Naphthylamines as a Practical Approach to Axially Chiral Biaryl Amino Alcohols. *Angew. Chem, Int. Ed.* **2017**, *56*, 16308–16312.

(138) Mellah, M.; Voituriez, A.; Schulz, E. Chiral Sulfur Ligands for Asymmetric Catalysis. *Chem. Rev.* **2007**, *107*, 5133–5209.

(139) Pan, F.; Shi, Z. J. Recent Advances in Transition-Metal-Catalyzed C-S Activation: From Thioester to (Hetero)Aryl Thioether. *ACS Catal.* **2014**, *4*, 280–288.

(140) Liu, J.; Robins, M. J. SNAr Displacements with 6-(Fluoro, Chloro, Bromo, Iodo, and Alkylsulfonyl)Purine Nucleosides: Synthesis, Kinetics, and Mechanism. *J. Am. Chem. Soc.* **2007**, *129*, 5962–5968.

(141) Chauhan, P.; Mahajan, S.; Enders, D. Organocatalytic Carbon-Sulfur Bond-Forming Reactions. *Chem. Rev.* **2014**, *114*, 8807–8864.

(142) Helder, R.; Arends, R.; Bolt, W.; Hiemstra, H.; Wynberg, H. Alkaloid Catalyzed Asymmetric Synthesis III the Addition of Mercaptans to 2-Cyclohexene-1-One; Determination of Enantiomeric Excess Using 13C NMR. *Tertrahedron Lett.* **1977**, *25*, 2181–2182.

(143) Hiemstra, H.; Wynberg, H. Addition of Aromatic Thiols to Conjugated Cycloalkenones,

Catalyzed by Chiral β-Hydroxy Amines. A Mechanistic Study on Homogeneous Catalytic Asymmetric Synthesis. *J. Am. Chem. Soc.* **1981**, *103*, 417–430.

(144) Armstrong, R. J.; Smith, M. D. Catalytic Enantioselective Synthesis of Atropisomeric Biaryls: A Cation-Directed Nucleophilic Aromatic Substitution Reaction. *Angew. Chemie, Int. Ed.* **2014**, *53*, 12822–12826.

(145) Cardenas, M. M.; Toenjes, S. T.; Nalbandian, C. J.; Gustafson, J. L. Enantioselective Synthesis of Pyrrolopyrimidine Scaffolds through Cation-Directed Nucleophilic Aromatic Substitution. *Org. Lett.* **2018**, *20*, 2037–2041.

(146) Schönherr, H.; Cernak, T. Profound Methyl Effects in Drug Discovery and a Call for New C-H Methylation Reactions. *Angew. Chem, Int. Ed.* **2013**, *52*, 12256–12267.

(147) Konkol, L. C.; Guo, F.; Sarjeant, A. A.; Thomson, R. J. Enantioselective Total Synthesis and Studies into the Configurational Stability of Bismurrayaquinone A. *Angew. Chemie, Int. Ed.* **2011**, *50*, 9931–9934.

(148) Sugahara, T.; Murakami, K.; Yorimitsu, H.; Osuka, A. Palladium-Catalyzed Amination of Aryl Sulfides with Anilines. *Angew. Chem, Int. Ed.* **2014**, *53*, 9329–9333.

(149) Dubbaka, S. R.; Vogel, P. Organosulfur Compounds: Electrophilic Reagents in Transition-Metal- Catalyzed Carbon-Carbon Bond-Forming Reactions. *Angew. Chem, Int. Ed.* **2005**, *44*, 7674–7684.

(150) Yang, J.; Xiao, J.; Chen, T.; Yin, S. F.; Han, L. B. Efficient Nickel-Catalyzed Phosphinylation of C-S Bonds Forming C-P Bonds. *Chem. Commun. (Cambridge, U.K.)* **2016**, *52*, 12233–12236.

(151) Bhanuchandra, M.; Baralle, A.; Otsuka, S.; Nogi, K.; Yorimitsu, H.; Osuka, A. Palladium-Catalyzed Ipso-Borylation of Aryl Sulfides with Diborons. *Org. Lett.* **2016**, *18*, 2966–2969.

(152) Grayson, M. N.; Houk, K. N. Cinchona Alkaloid-Catalyzed Asymmetric Conjugate Additions: The Bifunctional Brønsted Acid-Hydrogen Bonding Model. *J. Am. Chem. Soc.* **2016**, *138*, 1170–1173.

(153) Grayson, M. N.; Houk, K. N. Cinchona Urea-Catalyzed Asymmetric Sulfa-Michael Reactions: The Brønsted Acid-Hydrogen Bonding Model. *J. Am. Chem. Soc.* **2016**, *138*, 9041–9044.

(154) Vakulya, B.; Varga, S.; Csámpai, A.; Soós, T. Highly Enantioselective Conjugate Addition of Nitromethane to Chalcones Using Bifunctional Cinchona Organocatalysts. *Org. Lett.* **2005**, *7*, 1967–1969.

(155) Molnár, I. G.; Gilmour, R. Catalytic Difluorination of Olefins. *J. Am. Chem. Soc.* **2016**, *138*, 5004–5007.

(156) Wu, J. L.; He, Y. B.; Wei, L. H.; Liu, S. Y.; Xu, K. X.; Meng, L. Z. Two Multi-Armed

Neutral Receptors for α,ω-Dicarboxylate Anions. *Chinese J. Chem.* **2006**, *24*, 527–532.